



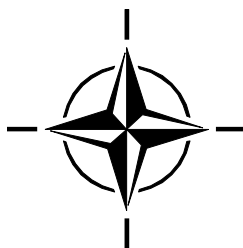
RTO AGARDograph

AG-AVT-140

Corrosion Fatigue and Environmentally Assisted Cracking in Aging Military Vehicles

(La fatigue-corrosion et la fissuration en milieu ambiant
des véhicules militaires vieillissants)

This AGARDograph has been sponsored by the
Applied Vehicle Technology Panel of RTO.



Published March 2011





RTO AGARDograph

AG-AVT-140

Corrosion Fatigue and Environmentally Assisted Cracking in Aging Military Vehicles

(La fatigue-corrosion et la fissuration en milieu ambiant
des véhicules militaires vieillissants)

This AGARDograph has been sponsored by the
Applied Vehicle Technology Panel of RTO.

The Research and Technology Organisation (RTO) of NATO

RTO is the single focus in NATO for Defence Research and Technology activities. Its mission is to conduct and promote co-operative research and information exchange. The objective is to support the development and effective use of national defence research and technology and to meet the military needs of the Alliance, to maintain a technological lead, and to provide advice to NATO and national decision makers. The RTO performs its mission with the support of an extensive network of national experts. It also ensures effective co-ordination with other NATO bodies involved in R&T activities.

RTO reports both to the Military Committee of NATO and to the Conference of National Armament Directors. It comprises a Research and Technology Board (RTB) as the highest level of national representation and the Research and Technology Agency (RTA), a dedicated staff with its headquarters in Neuilly, near Paris, France. In order to facilitate contacts with the military users and other NATO activities, a small part of the RTA staff is located in NATO Headquarters in Brussels. The Brussels staff also co-ordinates RTO's co-operation with nations in Middle and Eastern Europe, to which RTO attaches particular importance especially as working together in the field of research is one of the more promising areas of co-operation.

The total spectrum of R&T activities is covered by the following 7 bodies:

- AVT Applied Vehicle Technology Panel
- HFM Human Factors and Medicine Panel
- IST Information Systems Technology Panel
- NMSG NATO Modelling and Simulation Group
- SAS System Analysis and Studies Panel
- SCI Systems Concepts and Integration Panel
- SET Sensors and Electronics Technology Panel

These bodies are made up of national representatives as well as generally recognised 'world class' scientists. They also provide a communication link to military users and other NATO bodies. RTO's scientific and technological work is carried out by Technical Teams, created for specific activities and with a specific duration. Such Technical Teams can organise workshops, symposia, field trials, lecture series and training courses. An important function of these Technical Teams is to ensure the continuity of the expert networks.

RTO builds upon earlier co-operation in defence research and technology as set-up under the Advisory Group for Aerospace Research and Development (AGARD) and the Defence Research Group (DRG). AGARD and the DRG share common roots in that they were both established at the initiative of Dr Theodore von Kármán, a leading aerospace scientist, who early on recognised the importance of scientific support for the Allied Armed Forces. RTO is capitalising on these common roots in order to provide the Alliance and the NATO nations with a strong scientific and technological basis that will guarantee a solid base for the future.

The content of this publication has been reproduced directly from material supplied by RTO or the authors.

Published March 2011

Copyright © RTO/NATO 2011
All Rights Reserved

ISBN 978-92-837-0125-5

Single copies of this publication or of a part of it may be made for individual use only. The approval of the RTA Information Management Systems Branch is required for more than one copy to be made or an extract included in another publication. Requests to do so should be sent to the address on the back cover.

Table of Contents

	Page
List of Figures	xii
List of Tables	xxii
Theme	xxiii
List of Contributing Authors	xxiv
Executive Summary and Synthèse	ES-1
Chapter 1 – Introduction	1-1
1.1 Introduction	1-1
1.2 The Last 25 Years	1-1
1.3 References	1-3
Chapter 2 – Terms and Definitions Describing Corrosion Fatigue and Environmentally Assisted Cracking	2-1
2.1 Introduction	2-1
2.2 Terms and Definitions	2-2
2.3 List of Definitions Related to Corrosion Fatigue and Stress Corrosion Cracking	2-7
2.4 Acknowledgements	2-8
2.5 References	2-8
Appendix 2-1: Additional Definitions	2-9
Chapter 3 – Analysis and Comparison of Cost of Corrosion Maintenance Results	3-1
3.1 Introduction	3-1
3.2 Analysis of USAF Direct Corrosion Maintenance Cost	3-1
3.3 Specific Cost Analysis	3-4
3.3.1 Developing a Cost Analysis Methodology	3-4
3.3.1.1 Aspects of Corrosion Maintenance	3-5
3.3.1.2 Capturing All Related Costs	3-5
3.3.1.3 Corrosion Maintenance Definition	3-7
3.3.1.4 Obtaining Data to Complete the Studies	3-8
3.3.2 Fleet Corrosion Costs	3-8
3.3.3 Per Aircraft Corrosion Cost Comparisons	3-12
3.3.4 USAF Depot Costs	3-12
3.4 Examination of Cost Drivers	3-14
3.4.1 Examination of Depot Cost Drivers	3-15
3.4.2 Paint	3-16
3.4.3 Repair	3-16

3.4.4	Labor Rates	3-17
3.5	Conclusions	3-18
3.6	Acknowledgements	3-19
3.7	References	3-19
Chapter 4 – Corrosion Morphology: Documenting Corrosion		4-1
4.1	Introduction	4-1
4.2	Optical Methods	4-1
4.3	X-Ray Characterization	4-3
4.4	References	4-4
Chapter 5 – Pitting Corrosion: Morphology and Characterization		5-1
5.1	Introduction	5-1
5.2	Pitting Corrosion	5-1
5.2.1	Pit Characterization	5-3
5.2.2	Examples of Pitting Encountered in Components	5-6
5.3	Concluding Remarks	5-12
5.4	References	5-13
Chapter 6 – Corrosion Morphology: Intergranular Corrosion and Exfoliation		6-1
6.1	Introduction	6-1
6.2	Characteristics and Documentation	6-1
6.3	References	6-6
Chapter 7 – Corrosion Morphology: Corrosion Pillowing and Cracking		7-1
7.1	Introduction	7-1
7.2	The Pillowing Phenomenon	7-1
7.2.1	Mathematical Model of Pillowing	7-3
7.3	Pillowing Cracks	7-4
7.4	References	7-8
Chapter 8 – Fretting Corrosion and Fatigue		8-1
8.1	Introduction	8-1
8.2	Mechanisms of Fretting	8-2
8.3	Fretting Fatigue in Aircraft Joints	8-3
8.4	Reduction or Prevention Methods	8-4
8.5	Summary	8-6
8.6	References	8-6
8.7	General Bibliography of Important References on Fretting Fatigue	8-7
Chapter 9 – Environmentally Assisted Crack Growth of Metallic Alloys		9-1
9.1	Introduction	9-1

9.2	Phenomenological Aspects of EAC	9-1
9.2.1	EAC Under Sustained Loading	9-1
9.2.2	EAC Under Cyclic Loading	9-2
9.2.3	Sources of Information	9-4
9.3	The Holistic Approach to EAC	9-4
9.4	Implications for Aircraft Structural Integrity	9-5
9.5	Concluding Remarks	9-9
9.6	References	9-10

Chapter 10 – Simulating Corrosion Damage: Exfoliation **10-1**

10.1	Introduction	10-1
10.2	Methodology	10-1
10.3	Results	10-2
10.4	References	10-4

Chapter 11 – Simulating Pillowing Corrosion Damage **11-1**

11.1	Introduction	11-1
11.2	Surface Deformation	11-1
11.2.1	Mechanically Controlled Deformation	11-3
11.2.2	Hydraulic Pillowing	11-5
11.3	Pillowing Damage Internal Simulation	11-8
11.3.1	Pillowing Measurement	11-10
11.3.2	Machined Simulation	11-12
11.3.3	Pillowing Cracks	11-14
11.3.4	Wing Plank Simulated Corrosion Damage Calibration Standard	11-16
11.4	Conclusions	11-18
11.5	References	11-18

Chapter 12 – Surface Topography Influences on Structural Life Prediction **12-1**

12.1	What is Surface Topography? An Introduction	12-1
12.2	The Importance of Topography	12-1
12.3	Measuring Surface Topography	12-2
12.4	Topography and Fatigue Analysis	12-4
12.5	Topography Influences on Fatigue Life Calculations	12-9
12.6	References	12-10

Chapter 13 – Modeling Pitting Corrosion Fatigue: Pit Growth and Pit/Crack Transition Issues **13-1**

13.1	Introduction	13-1
13.2	Effects of Corrosion on Structural Integrity of Aircraft	13-3
13.3	Examples of Pitting Corrosion Incidents	13-4
13.4	Pitting Corrosion Fatigue Models	13-7
13.5	The Validity of Pitting Corrosion Fatigue (PCF) Models	13-10

13.5.1	Pit-to-Crack Transition	13-12
13.5.2	Estimation of Fatigue Cycles to Failure	13-12
13.6	Case Study	13-13
13.6.1	Background Information	13-13
13.6.2	Calculation of Critical Stress Intensity Factor at Fracture	13-15
13.6.3	Estimation of Pit to Crack-Transition Length	13-15
13.6.4	Estimation of Fatigue Cycles to Failure	13-15
13.6.5	Estimation of the Allowable Stress	13-16
13.7	Summary and Conclusions	13-16
13.8	Acknowledgements	13-17
13.9	References	13-17
 Chapter 14 – Modeling Corrosion Structural Impact: Pillowing		14-1
14.1	Introduction	14-1
14.2	Model Development	14-1
14.3	Results	14-2
14.4	References	14-5
 Chapter 15 – Exfoliation Corrosion and Fatigue Modeling		15-1
15.1	Introduction	15-1
15.2	DSTO Process Zone Model	15-2
15.2.1	Original DSTO Research	15-2
15.2.2	Studies of the Process Zone Model at APES	15-5
15.2.3	Studies of the Process Zone Model at NRC	15-6
15.3	NRC Exfoliation Model	15-8
15.3.1	Finite Element Model	15-8
15.3.2	Fatigue Model for Rivet Specimens	15-10
15.4	Summary	15-14
15.5	References	15-15
 Chapter 16 – Model Validation: Fuselage Lap Joints		16-1
16.1	Introduction	16-1
16.2	Experimental Procedures	16-2
16.2.1	Description of Lap Splice Specimen	16-2
16.2.2	Preparation of Corroded Specimens	16-3
16.2.3	Fatigue Testing	16-4
16.2.4	Measurement of Corrosion Damage	16-4
16.3	Results and Discussion	16-7
16.3.1	Failure Modes	16-7
16.3.2	Empirical Modelling of the Effects of Corrosion on MSD Crack Growth and Fatigue Life	16-7
16.4	Conclusions	16-13
16.5	Acknowledgements	16-14
16.6	References	16-14

Chapter 17 – Corrosion Fatigue Analysis of an F-18 Longeron	17-1
17.1 Introduction	17-1
17.2 Corrosion Fatigue Modeling Fundamentals	17-1
17.3 Inputs for Corrosion Fatigue Analysis	17-3
17.3.1 Cracking Scenario	17-3
17.3.2 Material Models (da/dN and IDS Crack)	17-3
17.3.3 Corrosion Growth Rate and Topography ID	17-4
17.3.4 Thickness Loss	17-5
17.3.5 Loading Spectrum	17-5
17.4 Results	17-6
17.5 Conclusion	17-7
17.6 References	17-8
Chapter 18 – Holistic Structural Integrity Analysis for Corrosion in a Hub on a Transport Aircraft Frame	18-1
18.1 Introduction	18-1
18.2 Fracture Analysis	18-1
18.3 Holistic Structural Integrity Analyses	18-2
18.4 Discussion	18-3
Chapter 19 – Holistic Structural Integrity Analysis of Corrosion in a Dynamic Helicopter Component	19-1
19.1 Introduction	19-1
19.2 Fracture Analysis	19-1
19.3 Holistic Life Assessment	19-3
19.3.1 Disposition	19-4
19.4 Summary	19-4
19.5 References	19-5
Chapter 20 – Prevention of Hydrogen Embrittlement in High Strength Steels, with Emphasis on Reconditioned Aircraft Components	20-1
20.1 Introduction	20-1
20.2 Basic Aspects of HE	20-2
20.2.1 Types of HE	20-2
20.2.2 Susceptibility of Materials to IHE	20-2
20.2.3 Important Variables for IHE	20-3
20.2.4 Sources of Internal Hydrogen	20-3
20.2.5 Sites and Traps for Hydrogen in Steels	20-3
20.2.6 IHE and Hydrogen Diffusivity	20-4
20.2.7 Minimising Hydrogen Contents	20-4
20.2.8 Characteristics of IHE Cracking	20-5
20.3 Distinguishing IHE from Other Intergranular Fracture Modes	20-7
20.4 Testing Procedures for Assessing the Degree of IHE	20-8
20.4.1 ASTM Standard Test Method F 519-06	20-8

20.4.1.1	Evaluating Plating Process IHE	20-8
20.4.1.2	Evaluating Service Environment IHE	20-9
20.4.2	National Aerospace Standard NASM1312-5	20-9
20.4.3	Proof Test Duration: The “No Failure in 200 Hours” Criterion	20-9
20.4.4	Problems Not Covered by Proof Testing	20-10
20.4.5	Incremental Step Load (ISL) Tests	20-11
20.4.6	Slow Strain Rate Tensile (SSRT) Tests	20-11
20.5	Case Histories: Reconditioned Components	20-13
20.5.1	Propeller Blade Retaining Bolts	20-13
20.5.1.1	Introduction	20-13
20.5.1.2	Investigation	20-14
20.5.1.3	Conclusions	20-20
20.5.1.4	Remedial Actions	20-21
20.5.2	Main Undercarriage Half-Fork Assemblies	20-21
20.5.2.1	Introduction	20-21
20.5.2.2	Investigation	20-22
20.5.2.3	Conclusions	20-25
20.5.2.4	Remedial Actions	20-25
20.5.3	Flap Carriage Assembly	20-26
20.5.3.1	Failure Investigation by the Operator	20-26
20.5.3.2	Review of the Operator’s Investigation	20-36
20.5.3.3	Remedial Actions and Final Conclusions	20-37
20.5.4	Wing Attachment Fitting Bolts	20-37
20.5.4.1	Introduction	20-37
20.5.4.2	Examination	20-38
20.5.4.3	Conclusions	20-46
20.5.4.4	Remedial Actions	20-46
20.5.5	Flap Tracks	20-47
20.5.5.1	Introduction	20-47
20.5.5.2	SSRT Testing and Fractography	20-47
20.5.5.3	Results	20-47
20.5.5.4	Conclusions and Recommendations	20-48
20.5.6	<i>In Situ</i> Brush-Plating Repair of Worn Flap and Slat Tracks	20-48
20.5.6.1	Introduction	20-48
20.5.6.2	Experimental Details	20-48
20.5.6.3	Results and Discussion	20-48
20.5.6.4	Conclusions and Recommendation	20-50
20.6	Concluding Remarks	20-50
20.7	Acknowledgements	20-51
20.8	References	20-51
	Chapter 21 – Non-Destructive Testing for Corrosion	21-1
21.1	Introduction	21-1
21.2	Non-Destructive Testing Methods	21-1
21.2.1	Visual NDT	21-2
21.2.2	Enhanced Visual/Optical NDT	21-2

21.2.3	Ultrasonic NDT	21-2
21.2.4	Eddy Current NDT	21-2
21.2.5	Thermographic NDT	21-3
21.2.6	Radiographic NDT	21-3
21.2.7	Additional NDT Methods	21-3
21.3	Data Fusion	21-3
21.4	Reliability of NDT for Corrosion	21-4
21.5	Case Studies	21-7
21.5.1	Intergranular Corrosion in Thick Section Aluminium Structure	21-7
21.6	References	21-10

Chapter 22 – Inspection of Helicopter Rotor Blades by Neutron- and X-Ray Radiography 22-1

22.1	Introduction	22-1
22.2	Methods	22-1
22.3	Investigated Objects	22-4
22.3.1	Metal Composite Structure	22-4
22.3.2	Plastic Fiber-Glass Structure	22-4
22.4	Experimental Facilities	22-5
22.5	Characterisation of the Defects	22-7
22.6	Measurements	22-8
22.7	Results	22-9
22.7.1	Metal Composite Structure	22-9
22.7.2	Plastic Fiber-Glass Structure	22-12
22.8	Conclusions	22-15
22.9	References	22-15

Chapter 23 – Replacing Cadmium and Chromium 23-1

23.1	Introduction	23-1
23.2	Environmental Legislation	23-2
23.2.1	Canada	23-2
23.2.2	U.S.A.	23-2
23.2.3	Europe	23-2
23.2.4	Other Countries	23-3
23.3	Cadmium Alternatives	23-3
23.3.1	ED Zinc-Based Coatings	23-5
23.3.2	ED Aluminum-Based Coatings	23-6
23.3.3	Vacuum-Deposited Aluminum and Aluminum Alloys	23-6
23.3.4	Spray Deposited Cadmium Alternatives	23-7
23.3.5	Alternative Substrate Materials	23-8
23.3.6	Summary on Cadmium Alternatives	23-8
23.4	Hard Chromium Alternatives	23-11
23.4.1	Spray Deposited Hard Chromium Alternatives	23-12
23.4.2	Electrolytic Hard Chromium Alternatives	23-12
23.4.3	Other “Dry” Alternatives	23-13

23.4.4	Summary on Hard Chromium Alternatives	23-14
23.5	Conclusions	23-17
23.6	References	23-17
23.7	Additional References	23-20
Chapter 24 – Materials Replacement for Aging Aircraft		24-1
24.1	Introduction	24-1
24.2	Aging (Legacy) Aluminum Alloys	24-2
24.2.1	Heat Treatment	24-2
24.2.2	Particles	24-4
24.2.3	Cladding/Anodizing	24-7
24.3	New Replacement Materials	24-9
24.4	Lessons Learned	24-12
24.5	Composite Materials	24-16
24.6	Processing Technologies	24-17
24.7	Conclusions	24-17
24.8	References	24-18
Chapter 25 – Corrosion Control Using Retrogression and Re-Aging (RRA)		25-1
	Abstract	25-1
25.1	Introduction	25-1
25.2	Kinetics Modelling of the Precipitation Process in 7000 Series Aluminum Alloys	25-2
25.3	Material Test Program	25-4
25.4	RRA Process Development	25-4
25.5	Certification Requirements	25-5
25.6	C-130 Sloping Longerons	25-5
25.6.1	Sloping Longerons Corrosion Results	25-6
25.6.2	Sloping Longerons Tensile Test Results	25-7
25.6.3	Sloping Longerons Electrical Conductivity Results	25-8
25.7	C-130 Paratrooper Door Longerons	25-8
25.7.1	PDL Test Results	25-9
25.8	Conclusions	25-9
25.9	Acknowledgements	25-10
25.10	References	25-10
Chapter 26 – Environmental Severity Assessment and Aircraft Wash Optimization		26-1
26.1	Introduction	26-1
26.2	Environmental Severity Assessment	26-2
26.2.1	USAF Environmental Severity Index (ESI)	26-2
26.2.2	International Organization for Standardization (ISO) Classification Scheme	26-6
26.2.3	Seasonal and Local Variations	26-7
26.3	Wash Costs Optimization	26-8

26.4	Summary	26-16
26.5	References	26-17

Chapter 27 – Repairing Corrosion Damage **27-1**

27.1	Introduction	27-1
27.2	Repairing Corrosion Damage	27-1
27.2.1	Standard Practice	27-1
27.2.2	Inspection Methods and Examples	27-2
27.2.2.1	D Sight Aircraft Inspection System (DAIS)	27-2
27.2.2.2	X-Ray Inspection	27-3
27.2.2.3	Examples of Damage Undetectable Without Detailed Inspections	27-4
27.2.2.4	Corrosion Pillowing and Cracked Rivets	27-7
27.2.3	Repair Philosophy	27-7
27.2.4	Repair and Repair Problems	27-8
27.2.4.1	Faying Surface Grinding Around Rivet Holes	27-8
27.2.4.2	FAA and Airbus Guidelines for Corrosion Removal	27-11
27.2.4.3	Exterior Grinding	27-11
27.2.4.4	Exfoliation Corrosion Removal	27-13
27.2.5	Post-Repair Inspection	27-14
27.2.5.1	Inside Surface Corrosion	27-15
27.2.5.2	Widespread Inside Corrosion	27-15
27.2.5.3	Exfoliation Corrosion	27-16
27.2.5.4	Other Problems with Sealants	27-17
27.2.6	Issues Related to New Materials and Techniques	27-18
27.2.6.1	Composite Patching	27-19
27.2.6.2	Fiber-Metal Laminates	27-19
27.2.6.3	Welding	27-20
27.2.6.4	Friction-Stir Welding (FSW)	27-21
27.2.6.5	Laser Welding	27-23
27.3	Corrosion Teardown Methods	27-23
27.3.1	Pre-Teardown	27-24
27.3.1.1	Initial Assessment and Records	27-24
27.3.1.2	Paint and Sealant Removal	27-26
27.3.1.3	Alloys and Coatings	27-27
27.3.1.4	Non-Destructive Inspection	27-28
27.3.2	Teardown	27-30
27.3.2.1	Fasteners	27-30
27.3.2.2	Adhesives and Sealants	27-31
27.3.2.3	Corrosion Removal	27-31
27.3.2.4	Thickness Loss	27-32
27.3.3	Post-Teardown	27-34
27.3.3.1	When It All Goes Wrong – C141 “Corroded” Joint	27-34
27.4	Corroded Components Availability	27-35
27.5	References	27-40

List of Figures

Figure		Page
Figure 3-1	Role of Direct Corrosion Maintenance in the AF O&M Budget (in Millions)	3-4
Figure 3-2	Three-Dimensional Data Base Illustration	3-6
Figure 3-3	Methodology Illustration	3-7
Figure 3-4	Total Costs for Fleets in '04 Dollars (in Thousands)	3-9
Figure 3-5	Per Aircraft Cost Comparison, '04 Dollars (in Thousands)	3-12
Figure 3-6	Depot Costs in '04 Dollars (in Thousands)	3-13
Figure 3-7	Paint Man-Hours	3-15
Figure 3-8	Repair Labor	3-16
Figure 3-9	Corrosion Percentage of Depot Maintenance	3-17
Figure 3-10	Depot Sales Rates Trend Over Time	3-18
Figure 4-1	Optical Micrographs Showing the Modified Discontinuity States from Naturally Corroded Components that were Progressively Polished	4-1
Figure 4-2	Corrosion Pit Sizes Measurements from Optical Micrographs of Naturally Corroded Components Progressively Polished	4-2
Figure 4-3	Difference in Pit Depth and Width Due to Presence of Intergranular Cracks	4-3
Figure 4-4	Histogram Plot of Thickness Loss of Different Coupons	4-4
Figure 5-1	Schematic Diagram Showing the Relationship Between Penetration Depth and Exposure Time	5-3
Figure 5-2	ASTM Standard G46 Showing Means of Characterizing Pit Density, Size, and Depth	5-5
Figure 5-3	ASTM Standard G46 Portion Showing Variation of Pit Character	5-6
Figure 5-4	Fracture Surface of C130 "Porkchop" Fitting that Unexpectedly Failed from Pitting that Transitioned into Cracks	5-8
Figure 5-5	A Second View of the Fracture Surface of C130 "Porkchop" Fitting that Unexpectedly Failed from Pitting that Transitioned into Cracks	5-8
Figure 5-6	View Showing Corrosion Pits Nucleating Cracks	5-9
Figure 5-7	View Showing Other Pits with Fatigue Cracks Propagating Between Them	5-9
Figure 5-8	Views in the Notch of Corrosion Fatigue Specimens Tested in the QIDEC Laboratory at the University of Utah (2000)	5-10
Figure 5-9	Post Corrosion Exposure of 30 Hours, d~0.0012" (30 mm) of Pit	5-11
Figure 5-10	SEM Photos Showing Pits Developed Under Corrosion Fatigue Conditions	5-12
Figure 6-1	Results from the Progressive Polishing Carried Out on Specimen 362-B-S4-1 that Contained Visible Exfoliation	6-2
Figure 6-2	Results from the Progressive Polishing Carried Out on Specimen 362-B-S4-2 that Contained both Visible Exfoliation and a Repaired (Ground-Out) Area	6-3

Figure 6-3	Results from the Progressive Polishing Carried Out on Section B Taken from Specimen 362-B-S4-1 that did Not Contain any Visible Exfoliation	6-4
Figure 6-4	Exfoliation Present Along S-T Direction 7075-T6 Upper Wing Skin	6-5
Figure 6-5	Exfoliation Present Along S-T Direction of Section Taken from 7075-T6 Upper Wing Skin	6-6
Figure 7-1	Schematic of Typical Longitudinal Boeing Lap Joint	7-1
Figure 7-2	Enhanced Visual Inspection Results (D-Sight™) of Fuselage Lap Joints	7-2
Figure 7-3	Various D-Sight™ Images Showing Degree of Pillowing for Different Level of Material Thickness Loss (ML)	7-3
Figure 7-4	D-Sight™ Images Showing Pillowing Caused by Corrosion Products	7-3
Figure 7-5	Effect of Rivet Spacing Ratio on Pillowing Ratio	7-4
Figure 7-6	Various Images Showing the Typical Star-Shape Pattern Associated with Pillowing Cracks	7-6
Figure 7-7	Micrographs Showing the Intergranular Cracking with Numerous Secondary Cracks	7-7
Figure 7-8	Micrographs Showing Multiple Crack Nucleation Sites	7-7
Figure 7-9	Optical Image of Pillowing Crack Showing Angled Crack Growth	7-8
Figure 7-10	Scanning Electron Micrographs Showing Fatigue Striations that were Found on the Fracture Surfaces on Some Pillowing Cracks	7-8
Figure 8-1	A Depiction of the Large Number of Parameters that may be Involved in Fretting Fatigue	8-1
Figure 8-2	Historical Perspective of Approaches to Fretting Fatigue Design Studies	8-2
Figure 8-3	An Illustration of an Approach that has been Used to Design for Fretting Fatigue Resistant Aircraft Joints	8-4
Figure 9-1	Plot of Applied Stress or Stress Intensity versus Time at Sustained Load in a Given Environment for a Given Material	9-2
Figure 9-2	Basic Diagram for Presentation of Fatigue Response	9-3
Figure 9-3	The Systems View of Corrosion Fatigue	9-4
Figure 9-4	Similar to Figure 9-1 Except the Effect of a Deleterious Environment is Shown	9-6
Figure 9-5	Diagram Depicting the Potential Effect of a Deleterious Chemical Environment on Fatigue Crack Propagation	9-7
Figure 9-6	A Depiction of Fatigue Crack Propagation Data Plotted on da/dN versus ΔK Axes	9-8
Figure 10-1	Configuration of Compression Rig Set-Up and an Example of the Exfoliation Damage Produced	10-2
Figure 10-2	Optical Micrographs Showing Large Pits Generated by EXCO Solution	10-3
Figure 10-3	Examples of ANCIT Generated Artificial Exfoliation and Natural Exfoliation	10-3
Figure 10-4	Modification Made to Steel Fastener to Introduce Exfoliation at Different Locations Along the Countersink	10-4
Figure 10-5	Typical Set-Up for Accelerated Exfoliation Protocol	10-4
Figure 11-1	Modeling (Ray Tracings) of Corrosion Pillowing at 2, 5, 10 and 15 % Thickness Loss	11-2

Figure 11-2	FEM Models of Varying Fastener and Row Spacings and Sample DAIS Images	11-3
Figure 11-3	Schematic View of Dual-Ramp Pin-Pressure Pillowing Simulator	11-4
Figure 11-4	Top View of Mechanical Pillowing Simulator	11-4
Figure 11-5	Side View of Mechanical Pillowing Simulator	11-4
Figure 11-6	Close-Up Side-View of Pin Contact with Underside of Skin Sheet	11-5
Figure 11-7	Sketch of Lap-Joint with Hydraulic Pillowing Bladder	11-5
Figure 11-8	Overall View of Rear Surface of Hydraulic Pillowing Lap-Joint with Stringer	11-6
Figure 11-9(a)	Close-Up of Bladder	11-6
Figure 11-9(b)	Close-Up of Vacuum/Hydraulic Port	11-6
Figure 11-10	DAIS Images of One Pressure Cycle on a Hydraulic Pillowing Lap Joint	11-7
Figure 11-11	Schematic of 7075-T6 Lap Joint NDI Calibration Standard for Eddy Current with Machined Thickness Loss Simulating Crevice Corrosion Damage	11-8
Figure 11-12	Baseline Absolute Eddy Current Scan of NDI Calibration Standard Joint at 7 kHz	11-9
Figure 11-13	DAIS Image of Accelerated Corrosion Pillowing Following 387 Days (9288 Hours) of Salt Fog Exposure	11-9
Figure 11-14	Absolute Eddy Current Scan of Accelerated Corrosion Panel at 7 kHz After 387 Days (9288 Hours) of Salt Fog Exposure to Faying Surfaces	11-10
Figure 11-15	Lap Joint Panel (2024 T3, 0.040 inch, 1.016 mm Thick Skins)	11-11
Figure 11-16	Faying Surface of One 2024-T3 Skin for a Simulation of Crevice Corrosion and Pillowing	11-12
Figure 11-17	CNC Machined Corrosion Damage Thickness Loss to Three Depths (30, 50 and 10 %)	11-13
Figure 11-18(a)	Machined Areas Hand-Ground	11-13
Figure 11-18(b)	Surface Sandblasted	11-13
Figure 11-19	Assembled Joint	11-14
Figure 11-20	DAIS Image of Machined Simulation Panel with Corrosion Product Included	11-14
Figure 11-21	Al/acrylic Hybrid Lap Joint After 15 Days Exposure to EXCO Solution	11-15
Figure 11-22	DAIS Images of Aluminum Outer Skin Front Surface	11-15
Figure 11-23	Cracks in Acrylic Inner Skin Caused by the Force of Corrosion Product Accumulation	11-16
Figure 11-24	Wing Planks	11-16
Figure 11-25	Location of Damage Sites	11-17
Figure 11-26	Typical “Area” Damage Site Preparation Prior to Corrosion Solution Application	11-17
Figure 11-27(a)	Corroded SCOS Damage Site	11-18
Figure 11-27(b)	Corroded Pit	11-18
Figure 12-1	Line Profile of Aluminum Surface that has Suffered from General Attack	12-2
Figure 12-2	Line Profile of Aluminum Surface that has Suffered from Pitting Attack	12-2
Figure 12-3	Eddy-Current Line Scan Compared with Laser Profile for Same Location	12-3
Figure 12-4	Surface Roughness Related to Corrosion Thickness Loss	12-4
Figure 12-5	Sample Correction Factors for Corroded Surfaces as a Function of Crack Length	12-5

Figure 12-6	Family of Beta Corrections for Corrosion for Various Cracks Along a Line of Surface Topography	12-6
Figure 12-7	(a) Shows the Von Mises Stress Contours for the Wide Pit with a 0.001 Inch Pit at the Base; and (b) Shows How the SIFs Compare Between FEA and the Analytic 2D-PC Model	12-7
Figure 12-8	(a) Shows the Von Mises Stress Contours for the Narrow Pit with a 0.001 Inch Pit at the Base; and (b) Shows How the SIFs Compare Between FEA and the Analytic 2D-PC Model	12-8
Figure 12-9	Comparison of Sample 3D and 2D Beta Correction Factors for Pitting	12-9
Figure 12-10	Cycles to Failure vs. % Thickness Loss for Exfoliated Coupons	12-10
Figure 13-1	A Depiction of the Degradation Process	13-2
Figure 13-2	Methods for Each Life Phase	13-3
Figure 13-3	Fracture Along the Parting Plane of 7075-T73 Shock-Strut Cylinder	13-14
Figure 13-4	A Transverse Section of a Pit on the Inner Surface of the Shock-Strut Cylinder	13-14
Figure 13-5	A Semi-Circular Crack Originated from a Pit that was Found on the Inner Surface of the Shock-Strut Cylinder	13-14
Figure 14-1	Effect of Increased Corrosion Pillowing on Critical Rivet Row of Respective Skins	14-2
Figure 14-2	Effect on Stress Caused by Reduction of Outer Skin Thickness as Compared to Pillowing (10% Thickness Loss)	14-3
Figure 14-3	Stress Plot for Non-Corroded and Corroded Lap Joints	14-3
Figure 14-4	Non-Dimensional Stress Intensity Plot of Outer Surface	14-4
Figure 14-5	Suggested Shape of Cracks in the Presence of Pillowing	14-4
Figure 15-1	Schematic of the Process Zone Model; and Variation of the Process Zone with Exposure Time to EXCO	15-3
Figure 15-2	Pitting and Exfoliation at Crack Nucleation Site in Specimen Exposed 48 Hours to EXCO	15-3
Figure 15-3	Predicted 7075-T6 Fatigue Life vs. ASTM EXCO Corrosion Time Using the 'Process Zone' Model and FASTRAN	15-4
Figure 15-4	Cycles to Failure vs. Percent Thickness Loss for Exfoliated Coupons	15-6
Figure 15-5	Predicted 7075-T6 Fatigue Life vs. Exfoliation Depth Using the 'Process Zone' Model and AFGROW	15-7
Figure 15-6	FE Modeling Process Using NDI Inputs and Modeling Results	15-9
Figure 15-7	3D FE Mesh with Soft Inclusion for Specimen 1 (362-A-S3-1)	15-9
Figure 15-8	Crack Nucleation Site and 3D FE Analysis Results	15-10
Figure 15-9	An Example FE Model Generated by NRC Automation Technique	15-10
Figure 15-10	Crack Nucleation Site at a Colony of Corrosion Pits on Countersunk Surface	15-11
Figure 15-11	Crack Model for Crack Growth Analysis	15-12
Figure 15-12	Cracking Model and Life Estimation Using Simplified Fatigue Model	15-13
Figure 15-13	Probabilistic Fatigue Modeling Based on a Grind-Out Database	15-14
Figure 16-1	Lap Splice Specimen with Clamping Plates and Loading Pins	16-3

Figure 16-2	D Sight Aircraft Inspection System (DAIS) Images of a Lap Splice Specimen Before Corrosion and After Corrosion	16-4
Figure 16-3	Faying Surface of the Countersunk Sheet of Specimen #037 Before and After the Removal of Corrosion Products	16-5
Figure 16-4	Pseudo-Colored Digitized X-Ray (DXR) Thickness Maps Showing Corrosion Distribution in Countersunk and Driven Sheets of Specimen #035	16-6
Figure 16-5	Example Sets of Individual Crack Growth Curves for Non-Corroded and Corroded Specimens	16-7
Figure 16-6	Aggregate Crack Growth Curves for Corroded and Non-Corroded Specimens	16-8
Figure 16-7	Mean Life to 0.5 in. Aggregate Crack with 90% Confidence Intervals	16-9
Figure 16-8	Empirical Models of Life to an Aggregate Crack Length of 0.5 in. (12.7 mm)	16-10
Figure 16-9	Illustration of the Relationship Between Aggregate Crack Growth Rate and Aggregate Crack Length in Non-Corroded and Corroded Specimens	16-10
Figure 16-10	Distribution of Exponent 'm' in Equation $da/dN = Q \cdot a^m$	16-11
Figure 16-11	Distribution of Constant 'Q' in Equation $da/dN = Q \cdot a^m$	16-12
Figure 16-12	Graph of Mean Whole Life to an Aggregate Crack Length of 6 in. (152.4 mm), Showing the Relative Contributions of the Hidden and Detectable Periods of Crack Growth	16-13
Figure 17-1	Fatigue Crack on the Right UOL of F-18 Central Fuselage	17-1
Figure 17-2	Corrosion Fatigue Analysis Procedure in HOLSIP/ECLIPSE	17-3
Figure 17-3	Corrosion Pits and Cracking Scenario	17-3
Figure 17-4	Corrosion Pit Growth Rate	17-4
Figure 17-5	Topography ID Used in ECLIPSE	17-5
Figure 17-6	Loading Spectrum Obtained from Strain Gauges	17-6
Figure 17-7	Life Comparison Between Corroded and Non-Corroded UOL	17-7
Figure 18-1	Drawing of Main Frame Landing Gear Hub	18-1
Figure 18-2	Load Spectrum Used in Analysis	18-2
Figure 18-3	Crack Growth Analysis of Main Landing Gear Hub Showing Traditional and HOLSIP Analyses	18-3
Figure 19-1	Optical Micrograph of Fracture Face Showing Beach Marks	19-1
Figure 19-2	Optical Micrograph Showing Pitting at Origin and River Marks Emanating from Region	19-2
Figure 19-3	Optical Micrograph of Surface Perpendicular to Fracture Plane Showing Clusters of Corrosion Pits	19-2
Figure 19-4	Plot of Normalized Life versus Normalized Crack Length for a Helicopter Main Rotor Component With and Without Corrosion Pitting	19-4
Figure 20-1	Sites and Traps for Hydrogen, Especially in Steels	20-4
Figure 20-2	Characteristics of Internal Hydrogen Embrittlement (IHE) in High Strength Steels – I	20-6
Figure 20-3	Characteristics of Internal Hydrogen Embrittlement (IHE) in High Strength Steels – II	20-7

Figure 20-4	Delayed Failure Curves for Cadmium-Plated AISI 4340 Steel Containing Various Hydrogen Concentrations Corresponding to Different Baking Times at 300°F (149°C)	20-10
Figure 20-5	Slow Strain Rate Tensile (SSRT) Test Rigs and Example Test Specimen	20-12
Figure 20-6	Comparison of SSRT and Sustained Load Test (SLT) Notched Fracture Stress Data for SAE E4340 Steel Specimens Cadmium Plated and Baked at 50°C for 0 – 13 Hours	20-13
Figure 20-7	Case History 20.5.1 – The Cracked Blade-Retaining Bolt	20-14
Figure 20-8	Case History 20.5.1 – Fracture Surface of the Blade-Retaining Bolt	20-15
Figure 20-9	Case History 20.5.1 – Example of Clean Intergranular Fracture	20-16
Figure 20-10	Case History 20.5.1 – Overview of Initiation Site O	20-16
Figure 20-11	Case History 20.5.1 – Detail from Figure 20-10 Showing Deposits on the Intergranular Fracture	20-17
Figure 20-12	Case History 20.5.1 – Nital-Etched Metallographic Section Through Crack A, Showing Tempered Martensite and the Intergranular Crack Path, Including Crack Branching	20-18
Figure 20-13	Case History 20.5.1 – Results of the Notched Tensile Tests and Hydrogen Analysis	20-20
Figure 20-14	Case History 20.5.2 – Main Undercarriage Half-Fork Assembly Sent for Examination	20-22
Figure 20-15	Case History 20.5.2 – Example of Helically Banded Cracking in the Hard-Chromium Plate	20-23
Figure 20-16	Case History 20.5.2 – Helical Dark Etching Bands Indicating Grinding Damage of the Steel Surface of the Lower Part of the Cylindrical Section	20-24
Figure 20-17	Case History 20.5.2 – Typical Cross-Section Through a Non-Stripped Area Containing Grinding Damage	20-24
Figure 20-18	Case History 20.5.2 – A Broken-Open Crack Showing Intergranular Fracture Followed by Transgranular Fatigue Fracture and Overload Fracture	20-25
Figure 20-19	Case History 20.5.3 – Broken Inboard Carriage Assembly <i>In Situ</i>	20-27
Figure 20-20	Case History 20.5.3 – Overview of the Fractured Spindle and Fork Assembly	20-28
Figure 20-21	Case History 20.5.3 – Spindle-Side Fracture Surface	20-30
Figure 20-22	Case History 20.5.3 – Fork-Side Fracture Surface	20-31
Figure 20-23	Case History 20.5.3 – Side Surface Around Fork-Side Crack Initiation Region	20-32
Figure 20-24	Case History 20.5.3 – Metallographic Cross-Section Through the Spindle-Side Crack Initiation Region	20-33
Figure 20-25	Case History 20.5.3 – Metallographic Cross-Section Through the Fork-Side Crack Initiation Region	20-34
Figure 20-26	Case History 20.5.3 – Summary of the Metallographic Observation	20-35
Figure 20-27	Case History 20.5.4 – Example of a Surface-Rusted WAF Bolt	20-38
Figure 20-28	Case History 20.5.4 – Fracture Characteristics of the Non-Suspect Used D12 Bolt from the Pilot Tensile Tests	20-40
Figure 20-29	Case History 20.5.4 – Histogram of the Definitive Tensile Test Data	20-41
Figure 20-30	Case History 20.5.4 – Normal Fit for the Bolt-Break Failure Load Data from the Definitive Tensile Tests	20-42

Figure 20-31	Case History 20.5.4 – Normal Fit for the Thread-Stripped Failure Load Data from the Definitive Tensile Tests	20-42
Figure 20-32	Case History 20.5.4 – Cumulative Distribution Function (CDF) for the Bolt-Break Failure Load Data from the Definitive Tensile Tests	20-43
Figure 20-33	Case History 20.5.4 – Simplified E – pH Diagram for the Iron-Water System at 25°C	20-44
Figure 20-34	Case History 20.5.4 – E – pH Diagram for Open Circuit Potentials of 4340 Steel and Galvanic Couple Potentials for Cadmium and 4340 Steel in Paint Strippers	20-45
Figure 20-35	The Effect of Current Density in the Range Suggested by the Manufacturer on the Notched Fracture Stress of SAE E4340 Steel Specimens	20-49
Figure 20-36	The Effect of Anode Speed on the Notched Fracture Stress of SAE E4340 Steel Specimens	20-49
Figure 21-1	An Example of a POD Curve, from the Ultrasonic Inspection of Welds in Aluminum for Cracks	21-5
Figure 21-2	Data from Experiment, Showing Contours of POD Values as a Function of Both Area and Thickness Loss of Damage	21-6
Figure 21-3	A Graph of the Effect of NDT Error on the Level of Damage and Subsequent Maintenance Actions	21-7
Figure 21-4	Metallographic Section Around a Fastener Hole in a Boeing 707 Wing Skin Plank, Showing Multiple Layers of Intergranular Attack from Pits in the Countersink	21-8
Figure 21-5	A Photograph, a UT Image, and an IR Image of a Section of Wing Plank from a Boeing 707, Showing Exfoliation Damage and Grinding Marks from Repairs	21-9
Figure 22-1	General Principle of Radiography	22-2
Figure 22-2	Attenuation Coefficient of Elements for Neutrons, for 1 MeV Gamma-Ray, for 150 kV X-Ray and for 60 kV X-Ray	22-3
Figure 22-3	The Inner Structure of the Rotor Blade	22-4
Figure 22-4	The Inner Structure of the Ka-26 Rotor Blade	22-5
Figure 22-5	Arrangement of the Imaging System	22-6
Figure 22-6	Mi-8 Rotor Blade Undergoing Moisture Conditioning	22-6
Figure 22-7	Mi-8 Type Rotor Blade Undergoing X-Ray Radiography	22-7
Figure 22-8	Radiography Pictures of a Mi-8 Type Helicopter Rotor Blade	22-9
Figure 22-9	Dry NR Image of the Honeycomb Structure with Resin-Rich Areas	22-10
Figure 22-10	Fiber Breakage and Slicing of Honeycomb and the Adhesive Material Revealed by NR; and Fiber Breakage and Slicing of Honeycomb and the Adhesive Material Revealed by XR	22-10
Figure 22-11	De-Bond in the Adhesive Material Between the Honeycomb and the Aluminium	22-11
Figure 22-12	Water Percolation in the Honeycomb Structures by NR	22-11
Figure 22-13	NR Picture of the Repaired Area; and XR Picture of the Repaired Area	22-11
Figure 22-14	NR Picture of the Corrosion Product in the Tail of the Rotor Blade	22-12
Figure 22-15	Corroded Heating Elements of the Anti-Ice Heater System Revealed by X-Ray Radiography	22-12
Figure 22-16	End Element of the Ka-26 Helicopter Rotor Blade by XR	22-13

Figure 22-17	End Element of the Ka-26 Helicopter Rotor Blade Revealed by NR	22-13
Figure 22-18	Front Edge of the Ka-26 Helicopter Rotor Blade Revealed by XR	22-13
Figure 22-19	Front Edge of the Ka-26 Helicopter Rotor Blade Revealed by NR with Corrosion Products on the Anti-Flutter Weight	22-14
Figure 22-20	Spar in the Middle Part of the Ka-26 Helicopter Rotor Blade Revealed by XR	22-14
Figure 22-21	Spar in the Middle Part of the Ka-26 Helicopter Rotor Blade Revealed by NR with De-Bonds Between the Spar and the Sections	22-15
Figure 23-1	Corrosion Potentials of Selected Metals in Reference to Saturated Calomel Electrode	23-3
Figure 23-2	Cadmium Alternative Coatings and Materials	23-5
Figure 23-3	Chromium Alternative Coatings	23-11
Figure 24-1	The Top Skin of a Severely In-Service Corroded B727 Lap Splice (Faying Surface) Made from One-Side Clad 2024-T3	24-3
Figure 24-2	Localized Corrosion (Pitting) Due to Discontinuity at the Surface of an Unclad 1.6 mm 2024-T351 Sheet which Acted as Fatigue Crack Nucleation Site	24-4
Figure 24-3	SEM Micrographs of Fracture Surfaces of Fatigue Coupons of 2024-T3 and 7075-T6 Sheets, Indicating Constituent Particles as Crack Origins	24-5
Figure 24-4	SEM Micrograph of Typical Constituent Particles in a 2024-T3 Alloy	24-6
Figure 24-5	Constituent Particles	24-7
Figure 24-6	The Thin Clad Layer Corrodes Rather Mildly and Uniformly to Protect the Core Alloy	24-8
Figure 24-7	Fatigue Fracture Surface of Coupons Made of Anodized 1.6 mm Thick 7079-T6 Alloy	24-9
Figure 24-8	SCC Failures During Service at Mid Thickness of a Sheet Made of Alloy 7079-T6	24-14
Figure 24-9	Typical Fracture Feature Found During Maintenance Inspection of the CH149 Cormorant at the Secondary Structures (Under-Floor Z-Stiffeners) After Only a Few Years of Service	24-15
Figure 25-1	Schematic of the Retrogression and Re-Aging Process	25-2
Figure 25-2	Comparison of Heat-Up and Retrogression Times for C-130 Sloping Longerons in Three Different Air-Recirculating Furnaces	25-3
Figure 25-3	<i>In Situ</i> RRA Process on C-141 Landing Gear Main Frame and C-130 Sloping Longerons Using Zimac Heater Cells	25-4
Figure 25-4	C-130 Showing Location of 26 ft Long Sloping Longerons and Heat Treatment Zone	25-6
Figure 25-5	C-Ring SCC Comparison with 54 ksi (372 MPa) Pre-Stress Level	25-6
Figure 25-6	Breaking Load SCC Test Results Using Box-Cox Metric (ASTM G 139)	25-7
Figure 25-7	UTS vs. Conductivity Data for Sloping Longerons Material	25-8
Figure 26-1	A C-130J Hercules is Cleaned Up in the New “Bird-Bath” System at Keesler Air Force Base, Biloxi, Mississippi	26-1
Figure 26-2	Section of the Corrosion Damage Algorithm that Considers Distance to Salt Water, Leading Either to the Very Severe AA Rating or a Consideration of Moisture	26-2
Figure 26-3	Section of the Corrosion Damage Algorithm for Planning a Washing Schedule	26-3

Figure 26-4	Metal Coupons in a Plastic Test Rack Exposed at the Kennedy Space Center Beach Corrosion Test Site Besides a CLIMAT Coupon	26-4
Figure 26-5	Metal Coupons Before Exposure to the Environment and After a Three Month Exposure in a Rural Environment	26-5
Figure 26-6	Maintenance Costs for Various Aircraft as a Function of the Corrosivity of Air Force Base Environments Towards the Corrosion of Aluminum	26-6
Figure 26-7	Average Corrosion Index for the Copper Rods Exposed on the Rooftop and the Average Wind Speed Recorded at the Local Weather Station as a Function of the Sixteen Points of the Compass	26-8
Figure 26-8	Schematic of Cumulative Corrosion Damage on Aircraft as a Function of Time	26-10
Figure 26-9	Monthly Corrosivity at Canadian Forces Base (CFB) Greenwood, Nova Scotia, as Mass Loss of CLIMAT Coupons Between 2002 and 2006	26-13
Figure 26-10	Geographical Position of CFB Greenwood in Nova Scotia and in Relation to the Sea	26-13
Figure 26-11	Predicted Wash Interval as Function of Corrosivity as Measured by CLIMATs Within Reasonable Limits for k_M	26-16
Figure 27-1	Lap Joint Corrosion and Repairs	27-3
Figure 27-2	Corrosion-Induced Pillowing Cracks	27-4
Figure 27-3	X-Ray Inspection Results for Intact and Disassembled Joint	27-4
Figure 27-4	X-Ray Inspection Results for Intact and Disassembled Joint	27-5
Figure 27-5	DAIS and X-Ray Images of Left End of Joint Showing Failed Rivets <i>In Situ</i>	27-6
Figure 27-6	Corrosion Pillowing Induced Failure-in-Place of Rivets Discovered by Tape Peel	27-7
Figure 27-7	Elongated Holes from Rivet Removal and Skin Thinned by Corrosion Removal	27-8
Figure 27-8	Scenario Showing how Grinding Could Remove Excessive Amounts of Material from Around Rivet Holes	27-9
Figure 27-9	Evidence of Grinding on Re-Assembled and Disassembled Joints	27-10
Figure 27-10	Digitized and Colorized X-Ray Thickness Loss Map for Outer Skin	27-11
Figure 27-11	Exterior Spot Grinding	27-12
Figure 27-12	DAIS View of Pillowed Skin Suffering Surface Grinding	27-12
Figure 27-13	Close-Up of Grinding Damage to Rivet Head, Middle Row Rivet, Joint Shown in Figure 27-12	27-13
Figure 27-14	Upper Wing Skin with Exfoliation Corrosion Damage at Fastener Holes	27-13
Figure 27-15	Upper Wing Skin with Multiple Sites Ground for Exfoliation Corrosion	27-14
Figure 27-16	View of Surface Corrosion on INBD Side of Upper Skin at Lap Joint	27-15
Figure 27-17	Rivet Shop Head and Stringer Edge Sealant Applications	27-16
Figure 27-18	Views of Exfoliated Frame Treated with Sealant	27-17
Figure 27-19	Surface Deformations from Excess Sealant in Laboratory Test Lap Joint (Non-Aerospace Fasteners)	27-18
Figure 27-20	Surface Deformations from Excess Sealant in Repaired On-Aircraft Lap Joint	27-18
Figure 27-21	Graphite to Aluminum Connection Produces Corrosion	27-19
Figure 27-22	Corrosion Damage on Outer Surface of Glare Lap Joint	27-20
Figure 27-23	Corroded KC-135 Spot Welded Lap Joint with 4 Fractured Welds	27-21

Figure 27-24	Friction Stir Welded Stringer and Skin	27-22
Figure 27-25	FSW Joint Structure and Corrosion Damage	27-22
Figure 27-26	Laser Welded Skin Butt Joint	27-23
Figure 27-27	Replicas on Rigid Foam Backing of Damaged Fuselage Joints	27-25
Figure 27-28	Fracture Surface Replica Analysis	27-26
Figure 27-29	Bilge Areas Below Cargo Floor (Floor Panels and Insulation Blankets Removed)	27-28
Figure 27-30	Three Views of Inner Surface of a Chemically Cleaned Corroded Skin Exhibiting Pillowing Cracks	27-29
Figure 27-31	Corrosion Pillowing Induced Cracks in a Rivet	27-30
Figure 27-32	Ultrasonic Immersion Corrosion Cleaning Tank	27-31
Figure 27-33	Views of Skin Surface Before and During Long Exposure Chemical/Ultrasonic Corrosion Cleaning for Corrosion Removal	27-32
Figure 27-34	DAIS Lap Inspections on the Intact Joint	27-32
Figure 27-35	Rear Surface of Outer Skin	27-33
Figure 27-36	X-Ray Thickness Loss Map	27-33
Figure 27-37	Thickness Measurement Map	27-33
Figure 27-38	A Visual Inspection of the Exterior Surface Indicated Corrosion Pillowing While the Interior Showed Sealant Added Indicating Maintenance for Same	27-34
Figure 27-39	Laboratory Inspections Preceding Teardown Both DAIS and UT Indicated Damage in the Upper Skin of the Butt Joint	27-35
Figure 27-40	A 0.080 Inch (2.03 mm) Thick Shim <i>In-Situ</i> , Enlarged	27-35
Figure 27-41	Aircraft Graveyards have been Valuable Sources of Corrosion Samples	27-36
Figure 27-42	Cut-Outs Show where Fuselage Structure was Harvested from WFU Airframes	27-37
Figure 27-43	Stringer and Frame Corrosion in the Crown of a Stored Fuselage Due to Moisture Remaining in Insulation Blankets (Removed)	27-37
Figure 27-44	Lower Window Frame Corrosion Due to Moisture Accumulating Between Seal and Structure of Stored Airframe	27-38
Figure 27-45	NRC/IAR Aircraft Specimen Library Database	27-39
Figure 27-46	Upper Wing Section Being Harvested for Corroded and Undamaged Material	27-40

List of Tables

Table		Page
Table 3-1	Total Annual Costs of Direct Corrosion in Then Year Dollars and '04 Dollars (in Millions)	3-2
Table 3-2	Total Corrosion Costs vs. USAF O&M Budget, in '04 Dollars (in Millions)	3-3
Table 3-3	Total Corrosion Costs by Weapon Fleet, in '04 Dollars (in Thousands)	3-10
Table 3-4	Per Aircraft Costs for All Aircraft Types in '04 Dollars (in Thousands)	3-11
Table 3-5	Total Depot Costs in '04 Dollars (in Thousands)	3-13
Table 3-6	Detailed Depot Costs in '04 Dollars (in Thousands)	3-14
Table 7-1	Recorded Incidences of Pillowing Cracks	7-5
Table 11-1	Pillowing Measurements of the Two-Layer Lap Joint Shown in Figure 11-15	11-11
Table 13-1	Pitting Corrosion Incidents of Aircraft and Helicopters	13-5
Table 13-2	Pitting Corrosion Fatigue Models	13-8
Table 13-3	Fatigue Life Estimation for the Shock-Strut Cylinder	13-16
Table 20-1	Bolt Elemental Compositions in wt. %	20-18
Table 20-2	Aircraft and Suspect Bolt Assembly Information	20-39
Table 20-3	Pilot Tensile Test Results	20-39
Table 20-4	SSRT Fracture Stress Results for Flap Track Steel Specimens	20-47
Table 22-1	Descriptions of Defects in Composite Structures	22-8
Table 23-1	General Requirements for Cadmium Alternative Coatings	23-9
Table 23-2	Key Technical Requirements for Cadmium Alternative Coatings	23-10
Table 23-3	General Requirements for Hard Chromium Alternative Processes and Coatings	23-15
Table 23-4	Technical Requirements for Hard Chromium Alternative Processes and Coatings	23-16
Table 24-1	Chemical Composition of Alternative Materials	24-10
Table 24-2	Mechanical Properties of Alternative Materials	24-11
Table 24-3	Al-Li Alloys Used in the CH149 Cormorant	24-16
Table 25-1	C-130 Sloping Longeron Tensile Strength Results	25-7
Table 25-2	C-130 PDL Tensile Strength Results	25-9
Table 25-3	C-130 PDL Stress Corrosion Cracking Results (ASTM G 38)	25-9
Table 26-1	ISO 9223 Corrosion Rates After One Year of Exposure Predicted for Different Corrosivity Classes	26-7
Table 26-2	Wash Periods Assigned to Sample of Bases According to Environmental Severity	26-9
Table 26-3	Periodic Inspection and Repair Records for Marine Air Patrol Fleet	26-11
Table 26-4	Estimates for Time Averaged k_M Based on Periodic Inspection and Repair Records in Table 26-3 and Equation (3)	26-14

Theme

Corrosion, corrosion fatigue and many other forms of environmentally assisted cracking continue to be major cost drivers for the operators and maintenance organizations responsible for military aircraft. This document reviews some of the developments in understanding of corrosion and corrosion related problems that have occurred since NATO, through its Advisory Group for Aerospace Research and Development (AGARD), published one of its last major works on the topic in 1985 (AGARD-AG-278, Volume 1). Several other organizations have made major contributions in the field since 1985, and both AGARD and later the RTO have looked at a variety of problems related to aging aircraft and their engines. This particular publication focuses on aging aircraft and provides some of the latest information on corrosion covering costs, detection, characterization, assessment of damage, repair and avoidance. But perhaps the major development over the past 25 years has been an improved understanding of how corrosion related issues affect aircraft structural integrity and safety, and how these effects can be modelled and managed. The present publication places particular emphasis on developments in these areas. While the focus is on aging aircraft many of the issues addressed will be applicable to some degree to other types of military vehicle in use today.

List of Contributing Authors

AVT-140 Chair

Dr. Mario Colavita
Agenzia Nazionale per la Sicurezza del Volo (ANSV)
Italian Air Safety Board
Via Attilio Benigni, 53
00156 Rome
ITALY
email: mario.colavita@ansv.it

AUSTRALIA

Dr. S.A. Barter
Defence Science and Technology Organization
506 Lorimer Street
Fishermans Bend, Victoria 3207
email: barter@dsto.gov.au

Dr. D.R. Gerrard
Defence Science and Technology Organization
506 Lorimer Street
Fishermans Bend, Victoria 3207
email: gerrard@dsto.gov.au

Dr. S.P. Lynch
Defence Science and Technology Organization
506 Lorimer Street
Fishermans Bend, Victoria 3207
email: lynchs@dsto.gov.au

CANADA

Mr. N.C. Bellinger
Research Officer
Institute for Aerospace
National Research Council Canada
1200 Montreal Road
Ottawa, Ontario K1A 0R6
email: nick.bellinger@nrc-cnrc.gc.ca

Dr. M. Bielewski
Research Officer
Institute for Aerospace
National Research Council Canada
1200 Montreal Road
Ottawa, Ontario K1A 0R6
email: bielewski@nrc-cnrc.gc.ca

Mr. G.F. Eastaugh
Research Officer, Institute for Aerospace
National Research Council Canada
Building M-14, 1200 Montreal Road
Ottawa, Ontario K1A 0R6
email: graeme.eastaugh@nrc-cnrc.gc.ca

Mr. R.W. Gould
Technical Officer
Structures and Materials Performance Laboratory
Institute for Aerospace
National Research Council Canada
1200 Montreal Road
Ottawa, Ontario K1A 0R6
email: gouldrw@nrc-cnrc.gc.ca

Mr. J.P. Komorowski
Research Officer, Institute for Aerospace Research
National Research Council Canada
Building M-13, 1200 Montreal Road
Ottawa, Ontario K1A 0R6
email: jerzy.komorowski@nrc-cnrc.gc.ca

Dr. M. Liao
Research Officer, Institute for Aerospace Research
National Research Council Canada
Building M-14, 1200 Montreal Road
Ottawa, Ontario K1A 0R6
email: min.liao@nrc-cnrc.gc.ca

Dr. A.A. Merati
Research Officer, Institute for Aerospace
Structures and Materials Performance Laboratory
National Research Council Canada
Building M-13, 1200 Montreal Road
Ottawa, Ontario K1A 0R6
email: ali.merati@nrc-cnrc.gc.ca

CANADA (cont'd)

Mr. D. Raizenne
Research Officer
Institute for Aerospace
National Research Council Canada
Building M-14, 1200 Montreal Road
Ottawa, Ontario K1A 0R6
email: don.raizenne@nrc-cnrc.gc.ca

Dr. Pierre R. Roberge
Royal Military College of Canada
Department of Mechanical Engineering
Department of National Defence
P.O. Box 17000, Station Forces
Kingston, Ontario K7K 7B4

Dr. P.V. Straznicky
Department of Mechanical and Aerospace
Engineering
Carleton University
M7AE 112E Colonel By Drive
Ottawa, Ontario K1S 5B6
email: pstrazni@mae.carleton.ca

Dr. W. Wallace
AMS Consulting Inc.
38 Regiment Road, RR4
Kemptville, Ontario K0G 1J0
email: wallace@ams.ca

Dr. X. Wu
Research Officer
Institute for Aerospace
National Research Council Canada
Building M-13, 1200 Montreal Road
Ottawa, Ontario K1A 0R6
email: xijia.wu@nrc-cnrc.gc.ca

HUNGARY

Dr. M. Balaskó
MTA KFKI Atomic Energy Research Institute
P.O. Box 49
H-1525 Budapest
email: balasko@aeki.kfki.hu

Dr. L. Horváth
MTA KFKI Atomic Energy Research Institute
P.O. Box 49
H-1525 Budapest
email: horvath6969@rta.nato.int

NETHERLANDS

Dr. R.J.H. Wanhill
Gas Turbine and Structural Integrity Department
Aerospace Vehicles Division
National Aerospace Laboratory, NLR
P.O. Box 153
8300 AD Emmeloord
email: wanhill@nlr.nl

UNITED STATES

Mr. G. Cooke
C² Technology, Inc.
3055 Rodenbeck Drive
Beavercreek, Ohio 45432

Mr. G. Cooke Jr.
C² Technology, Inc.
3055 Rodenbeck Drive
Beavercreek, Ohio 45432

Mr. D.S. Forsyth
Texas Research International
TRI/Austin
NDE Division Manager
9063 Bee Caves Road
Austin, Texas 78735
email: dforsyth@tri-austin.com

Professor D.W. Hoepfner
Professor and Director
Quality and Integrity Design Engineering Center
(QIDEC), Mechanical Engineering Department
University of Utah
Room 2202, 50 S Central Campus Drive
Salt Lake City, Utah 84112
email: dhoepfner@comcast.net

Dr. K.T. Honeycutt
Analytical Processes / Engineered Solutions, Inc.
Saint Louis, Missouri 63139
email: honeycutt@ap.us

Dr. S. Kuhlman
University of Dayton Research Institute
300 College Park
Dayton, Ohio 45469-0135
email: kuhlmans@rta.nato.int

Dr. T.B. Mills
Analytical Processes / Engineered Solutions, Inc.
Saint Louis, Missouri 63139
email: tmills@apesolutions.com

UNITED STATES (cont'd)

Dr. R. Rondeau
University of Dayton Research Institute
300 College Park
Dayton, Ohio 45469-0135
email: rondeau@rta.nato.int

Ms. A. Taylor
Research Engineer, FASIDE International Inc.
1146 S. Oak Hills Way
Salt Lake City, Utah 84108-2026
email: taylor@rta.nato.int

Dr. P. Sjöblom
University of Dayton Research Institute
Materials Engineering Division
Building KL, Room 161
300 College Park
Dayton, Ohio 45469-0135
email: sjoblom@rta.nato.int

Panel Mentor

Dr. P. Patnaik
Inst. for Aerospace Research
Building M-13, 1200 Montreal Road
Ottawa, Ontario K1A 0R6
CANADA
email: prakash.patnaik@nrc-cnrc.gc.ca

Corrosion Fatigue and Environmentally Assisted Cracking in Aging Military Vehicles

(RTO-AG-AVT-140)

Executive Summary

Damage to metallic aircraft structures due to corrosion is a continuing problem to operators, giving rise to high maintenance costs and loss of aircraft availability. Traditionally viewed as an economic issue, recent work has made a strong case that corrosion is also a threat to flight safety.

There is no universal solution to the problem of corrosion and thus it must be addressed at all stages of the equipment life cycle from initial design through careful selection of structural materials, corrosion protection systems, joint design and assembly, in-service inspection, maintenance and finally repair and refurbishment. In this report the Applied Vehicles Technology Panel of the NATO-RTO reviews progress in these areas occurring over the past twenty five years and with particular emphasis on the impact of corrosion on structural integrity and safety. Typically in built-up aircraft structures, corrosion occurs by pitting action in areas that are difficult to inspect visually without some degree of disassembly. These sites include faying surfaces between fasteners and skin and between the faying surfaces of lap joints. Damage in such areas may be exacerbated by fretting action caused by low amplitude sliding displacements between rubbing surfaces.

As corrosion pits grow stresses at their tips magnify and eventually cracks appear and also grow under the combined action of corrosion and stress that likely includes both static and cyclic components. Stresses arise from the usual sources; the effects of "weight on wheels", residual manufacturing or heat treatment stresses, assembly stresses, and take-off, landing and manoeuvre loads experienced during ground operations and flight. But in the presence of chemically aggressive environments that trigger corrosion, stresses are magnified further due to the thinning of sheet and due to the bulging action and plastic deformation at faying surfaces as corrosion products accumulate between them.

Cracks grow either intergranularly or transgranularly, influenced by electrochemical and stress conditions at crack tips at grain boundaries, and give rise to common forms of damage such as exfoliation, stress corrosion cracking, hydrogen assisted cracking and corrosion fatigue. Many challenges exist to the designer, operator and maintainer, and these challenges are being compounded by the growing awareness of the health, safety and environmental concerns associated with some of the corrosion protection systems that have traditionally been used. Thus all materials, including cadmium and chromium and their compounds, that have played such an important role in protective coatings, primers, paints, corrosion inhibitors and water displacing fluids in the past are being challenged. This report reviews some of the alternative systems that are available and also identifies recent publications that provide detailed and authoritative accounts of relevant work. In this publication a total of 27 chapters are provided covering the detection and characterization of corrosion damage, its impact on costs and structural integrity, its control in aircraft structures and its repair.

La fatigue-corrosion et la fissuration en milieu ambiant des véhicules militaires vieillissants

(RTO-AG-AVT-140)

Synthèse

Les dommages causés par la corrosion aux structures métalliques des aéronefs confrontent les opérateurs à un problème permanent, générant des coûts de maintenance élevés et rendant les appareils indisponibles. Des recherches récentes ont démontré que la corrosion, traditionnellement considérée comme un problème purement économique, représentait également une menace pour la sécurité des vols.

Il n'existe aucune solution universelle au problème de la corrosion, et il doit donc être combattu à chaque étape du cycle de vie du matériel, depuis la conception initiale via la sélection minutieuse des matériaux structurels, en passant par les systèmes de protection contre la corrosion, la conception et l'assemblage des joints, l'inspection en service, la maintenance, jusqu'aux réparations et à la remise à neuf. Dans ce rapport, la commission Technologie appliquée aux véhicules (AVT) de la RTO de l'OTAN a étudié les progrès accomplis en ce domaine au cours des vingt-cinq dernières années, insistant particulièrement sur l'impact de la corrosion sur la sécurité et l'intégrité des structures. Généralement, dans les structures d'aéronefs assemblées, la corrosion se produit par action de piquage à des endroits difficiles à inspecter visuellement sans procéder à un minimum de démontage. Ces zones comprennent notamment les surfaces de contact entre les pièces de fixation et le revêtement, ainsi que les surfaces de contact entre les joints à recouvrement. Les dommages occasionnés à ces emplacements peuvent être aggravés sous l'action du frottement causé par les glissements de faible amplitude entre les surfaces en friction.

Lorsque les piqûres de corrosion s'étendent, les contraintes pesant sur leurs extrémités s'accroissent et des craquelures finissent par apparaître et grandissent sous l'action combinée de la corrosion et des contraintes, ces dernières incluant vraisemblablement des composantes à la fois statiques et cycliques. Les contraintes proviennent des sources habituelles : les conséquences du « délestage », les contraintes résiduelles issues de la fabrication ou d'un traitement thermique, les contraintes d'assemblage et les charges au décollage, à l'atterrissage et lors des manœuvres, subies au cours des opérations au sol et en vol. Mais en présence d'un milieu chimiquement agressif déclenchant la corrosion, les contraintes sont amplifiées du fait de l'amincissement des tôles, ainsi que de la déformation du plastique et du gonflement au niveau des surfaces de contact lorsque les produits de la corrosion s'accumulent entre elles.

Les craquelures s'étendent de manière soit intergranulaire, soit transgranulaire, sous l'influence des conditions électrochimiques et de l'état des contraintes aux extrémités des fissures aux joints de grains, engendrant des formes classiques de dommages : corrosion exfoliante, corrosion sous contrainte, fissuration induite par l'hydrogène ou fatigue-corrosion. Le concepteur, l'opérateur et le responsable de la maintenance sont confrontés à de nombreux défis, qui viennent s'ajouter à la prise de conscience accrue des préoccupations liées à la santé, à la sécurité et à l'environnement associées à certains systèmes de protection contre la corrosion habituellement utilisés. En conséquence, l'usage de tous les matériaux (y compris le cadmium et le chrome et leurs composés) qui ont joué un rôle si important par le passé dans les enduits protecteurs, les couches de fond, les peintures, les inhibiteurs de corrosion et les fluides hydrophobes, est désormais contesté. Le présent rapport passe en revue certains des autres systèmes disponibles et identifie également les publications récentes qui rendent compte, de manière détaillée et digne de foi, des recherches sur ce sujet. Dans cette publication, 27 chapitres au total couvrent la détection et la caractérisation des dommages causés par la corrosion, leur impact sur les coûts et l'intégrité des structures, leur contrôle au niveau des structures des aéronefs et les moyens d'y remédier.

Chapter 1 – INTRODUCTION

W. Wallace and Jerzy P. Komorowski

Institute for Aerospace Research
National Research Council Canada
Ottawa, Ontario
CANADA

1.1 INTRODUCTION

Corrosion and corrosion fatigue in aircraft structures have been around for as long as the aircraft themselves. Various agencies of NATO have recognized this for almost as long, and interest has grown as recognition of the consequences of corrosion has increased. Corrosion was a major preoccupation of AGARD (Advisory Group for Aerospace Research and Development) since at least the mid-1970s and a major effort was made by the Structures and Materials Panel in the early 1980s. In 1985 the first of several publications appeared in the form of AG-278, AGARD Corrosion Handbook Volume 1, Aircraft Corrosion: Causes and Case Histories [1]. It was assembled by authors from Canada, The Netherlands and the United States but virtually all NATO member nations of the day contributed to the contents. However, the major credit for it should go to Mr. Tom Kearns of the United States since he understood, better than most, the enormous cost of corrosion in terms of operability and availability of equipment as well as direct financial outlays associated with repair and maintenance. He also understood the scientific and engineering complexities associated with the chemistry and physics of corrosion, as well as the challenges related to detection and quantification of damage, corrosion control and fleet management, damage repair and design for avoidance. He was the driving force for most of the early effort.

1.2 THE LAST 25 YEARS

While there was widespread recognition of the challenges posed by aircraft corrosion in 1980, there were few systematic programs in the NATO member nations designed to deal with the many problems associated with it. AG-278 had one primary goal and that was to alert those involved with the operation and maintenance of aircraft to the dangers of corrosion. Most member nations shared their experiences by providing practical case histories of corrosion related structural failures, and they explained the corrective measures that had been taken to return equipment to service. The authors of that publication would like to think that it has assisted maintenance personnel to recognize and address similar problems over the ensuing 25 years. In addition to the case histories, this early publication provides simple descriptions of the common airframe structural alloys in use at that time as well as the main forms of corrosion affecting them, namely; uniform corrosion and erosion, galvanic corrosion, pitting, crevice and filiform corrosion, intergranular and exfoliation corrosion, fretting corrosion, hydrogen embrittlement, stress corrosion cracking, corrosion fatigue, and microbiological corrosion.

The handbook may have done more than was expected since it is clear that the past 25 years have seen a dramatic increase in activity leading to a much better understanding of corrosion and particularly of the ways it contributes to the nucleation and growth of cracks, and how it interacts with mechanically induced cracks to pose threats to aircraft structural integrity. The very earliest thoughts on corrosion revolved around the simplistic recognition that it would cause thinning of structural materials, and that this thinning would cause increases in stresses on a macroscopic scale, thus contributing to instabilities in the form of buckling, crack nucleation and accelerated crack growth. As understanding increased and the mechanisms and consequences of pitting were better elucidated it was recognized that pits themselves would act as stress concentration sites and would behave as cracks. Indeed at some point they would be better described as cracks and would continue to grow by purely mechanical means as opposed to growth by dissolution of

INTRODUCTION

metal at their tips. This would happen even in the unlikely event that all environmental drivers to crack growth could be excluded.

Basic research on fatigue, in both inert and corrosive environments, soon showed that fatigue crack growth rates would be accelerated by the presence of chemically aggressive species, and thus the challenging field of corrosion fatigue emerged. The influence of these mechanical and environmental interactions on structural integrity was clearly a concern, but how to manage them in any aircraft structural integrity program remained uncertain. The dilemma gave rise to much debate on whether corrosion was strictly an economic issue or also a safety issue, and if the latter, how to deal with it.

Through years of practical operating experience and a few disasters it became clear that general and localized corrosion, corrosion pitting, exfoliation and crack nucleation and growth were frequently found on or below the hidden faying surfaces of lap joints and most often at fastener holes in built-up structures. The challenges of detection and quantification of damage rapidly became apparent. Also, it was soon realized that stresses would not only increase due to metal thinning and concentration effects at the base of pits, but also because the conversion of metal to metal oxides or hydroxides would involve substantial volumetric increases. The growing corrosion products would force sheet metal in faying surfaces apart, constrained only by the rivets or bolts holding the sheets together. Distortions between the fasteners would be plastic and therefore permanent. Thus complex stress distributions would arise that certainly had not been taken into account in any early airworthiness assessments.

Corrosion in aircraft structures is clearly a complex process and the more is learned about it the more we realize that understanding how to manage it to ensure flight safety is a challenge of enormous proportions. A widespread view has emerged that corrosion cannot be dealt with in isolation, but must be considered as part of a complex set of issues affecting structural integrity and safety. Several groups have explored the concepts of holistic structural integrity processes or HOLSIP, and have reached the point where it is being applied as a logical extension of ASIP. Here, knowledge gained of the way environmental variables interact with mechanical variables to drive the nucleation and growth of cracks is being combined with conventional elastic and plastic fracture mechanics and the concepts of damage tolerance in both deterministic and probabilistic approaches.

This present document reviews some of these developments with particular attention to work carried out since the publication of AGARD AG-278, and with emphasis on how to keep aircraft flying safely when exposed to aggressive environments. No attempt has been made to provide a complete and comprehensive description of aircraft corrosion but the report provides examples of some of the main forms of corrosion found in aircraft structures and it provides examples of best practices in detection, inspection, repair and avoidance. The opening chapter (Chapter 2) provides a summary of terminology and definitions in current use related to corrosion with emphasis on the types of discontinuity present in aircraft materials as well as those created by corrosion. It also covers the concepts of crack nucleation and propagation and crack instability. It draws heavily on the work of the American Society for Testing and Materials (ASTM), an organization that has provided leadership on an international basis. The third chapter provides an indication of the costs of corrosion obtained through a systematic survey carried out over several years in the United States, but many readers will find the methodology used in the study to be at least as useful as the results themselves. However, the main focus of the report is the application of holistic methods of life assessment of aircraft structures affected by both mechanical and environmental damage, and it reviews all the related technologies needed to apply these methods both in laboratory studies as well as operational aircraft.

Several chapters have been provided in groups to focus on common themes; thus several contributions are included dealing with each of the following:

- The morphology of corrosion as it appears in aircraft structures.
- Methods of simulating corrosion damage in materials and built-up structure typical of aircraft design.

- Impact of corrosion on aircraft structural integrity.
- Practical case histories of corrosion in aircraft components and structures and particularly of the application of holistic methods in the assessment of structural integrity in the presence of corrosion.
- Means of detecting corrosion non-destructively, including one chapter that deals with radiometric methods for detection of damage, including ingress of moisture into the cavities of composite honeycomb structure.
- Corrosion prevention or avoidance.

In short, the report covers many of the practical aspects of corrosion that have been discussed above but some important topics have been passed over. For example, corrosion preventative compounds are vital in the fight to impede corrosion but an excellent review has been published fairly recently and its contents are still very much applicable today. This is TTCP Technical Report, “Effective Use of Corrosion Preventative Compounds (CPCs) on Military Systems” [2]. It considers how to use CPCs effectively and assesses the range of commercially available CPCs of the participating countries in different environments. A related report on Chemical Inhibitors has also been published recently by TTCP as MAT-TP6, TR MAT-TP-6-4-2008. These reports are readily available to Canada, the United Kingdom and the United States and they might possibly be available to other NATO member nations through appropriate channels. Also, nothing has been provided in the present report on corrosion sensors and these are clearly important in at least two ways. Firstly, sensors are needed to detect the onset and growth of corrosion damage in structures while others are important in terms of characterizing and monitoring the severity of the corrosive environment that individual aircraft see. The latter are likely to become increasingly important as HOLSIP concepts become more firmly established and require accurate descriptions of the environments to which individual aircraft have been exposed.

1.3 REFERENCES

- [1] Wallace, W., Hoepfner, D.W. and Kandachar, P.V., “AGARD Corrosion Handbook Volume 1, Aircraft Corrosion: Causes and Case Histories”, AGARDograph No.278, Neuilly-sur-Seine, France, July 1985.
- [2] Beatty, J., Placzankis, B., Martin, B.J., Purdie, T. and Shaw, P., “Effective Use of Corrosion Preventative Compounds on Military Systems”, TTCP Technical Report, Operating Assignment 37, The Technical Cooperation Program, MAT-TP-1-5-2008.



Chapter 2 – TERMS AND DEFINITIONS DESCRIBING CORROSION FATIGUE AND ENVIRONMENTALLY ASSISTED CRACKING

David W. Hoepfner

Professor and Director, Quality and Integrity Design Engineering Center (QIDEC)
Mechanical Engineering Department, University of Utah
Salt Lake City, Utah
USA

2.1 INTRODUCTION

For several years the author and his colleagues have explored and promoted a holistic approach to life assessment of corroded and non-corroded structural components. The philosophy considers the structural integrity of parts in a broad – cradle to grave – approach where all impacting factors are taken into account. Along this journey it has been found that established terms and definitions do not always adequately describe the conditions being considered, and for this reason some new and some modified concepts have been developed. This chapter presents the authors latest thinking on this topic, but before tackling the many intricacies of corrosion fatigue and environmentally assisted cracking of structures it would be informative to review the origins of holistics. Some of the early concepts have been described by Reference [1] where many of the following ideas have been formulated.

“Ironically, scientific insights into the brain’s holistic talents – its right-hemisphere capacity to comprehend wholes – raise serious questions about the scientific method itself. Science has always tried to understand nature by breaking things into their parts. Now it is overwhelmingly clear that wholes cannot be understood by analysis. This is one of those logical boomerangs, like the mathematical proof that no mathematical system can be truly coherent in itself.”

“The Greek prefix syn (“together with”), as in synthesis, synergy, syntropy, becomes increasingly meaningful. When things come together something new happens. In relationship there is novelty, creativity, and richer complexity. Whether we are talking about chemical reactions or human societies, molecules or international treaties, there are qualities that cannot be predicted by looking at the individual components.”

“Half a century ago in Holism and Evolution, Ian Smuts tried to synthesize Darwin’s evolutionary theory, Einstein’s physics, and his own insights to account for the evolution of mind as well as matter.”

“Wholeness, Smuts said, is a fundamental characteristic of the universe – the product of nature’s drive to synthesize. “Holism is self-creative, and its final structures are more holistic than its initial structures.” These wholes – in effect, these unions – are dynamic, evolutionary, and creative. They thrust toward ever-higher orders of complexity and integration. “Evolution,” Smuts said, “has an ever deepening, inward spiritual character.”

“As we’ll see shortly, modern science has verified the quality of whole-making, the characteristic of nature to put things together in an ever-more synergistic, meaningful pattern. General Systems Theory, a related modern concept, says that each variable in any system interacts with the other variables so thoroughly that cause and effect cannot be separated. A single variable can be both cause and effect. Reality will not be still. Similarly, it cannot be taken apart! One cannot understand a cell, a rat, a brain structure, a family, or a culture if one isolates it from its context. Relationship is everything.”

“Ludwig von Bertalanffy said that General Systems Theory aims to understand the principles of wholeness and self-organization at all levels. Its applications range from the biophysics of cellular processes to the

dynamics of populations, from the problems of physics to those of psychiatry and those of political and cultural units.”

“General Systems Theory is symptomatic of a change in our worldview. No longer do we see the world in a blind play of atoms, but rather a great organization.”

“This theory says that history, while interesting and instructive, may not predict the future at all. Who can say what the dance of variables will produce tomorrow... next month.... next year? Surprise is inherent in nature.”

2.2 TERMS AND DEFINITIONS

ADP-Age Degradation Process: Any one of or combination of physical or chemical degradation processes such as fatigue, environmental effects (corrosion on metals and joints), creep, wear, and synergisms of these.

Anomalous: From Merriam Webster computer dictionary. This word was recently used by Bob Eastin to refer to corrosion, etc. Continuing discussions about the use of this term or the following terms for corrosion, fretting, creep, etc., in conjunction with fatigue have led to the notion of inconsistency, of deviation from what is usual, normal, or expected: IRREGULAR, UNUSUAL. Similarly it introduces the notion of uncertainty in nature or classification. The meaning is characterized by incongruity or contradiction: for synonyms see IRREGULAR

Extraneous: From Merriam Webster computer dictionary. This term was one the author used in papers to describe the extrinsic influences that should often be considered either concurrently with cyclic loading or sequentially. However, he has never considered any of the following to be anomalous:

- 1) Existing on or coming from the outside.
- 2) Not forming an essential or vital part.
- 3) Being a number obtained in solving an equation that is not a solution of the equation *extraneous roots* (synonyms see EXTRINSIC).

CLD – Crack Like Discontinuity: A discontinuity that meets the criteria for a crack. A stress singularity exists near or at the tip of the discontinuity; no “traction forces” exist on the surfaces of the discontinuity.

DADTA – Durability And Damage Tolerance Analysis: The procedure of performing an analysis of durability and damage tolerance. This is an analysis of the ability of the airframe or component to resist damage (including fatigue cracking, environmentally assisted cracking, hydrogen induced cracking, corrosion, thermal degradation, delamination, wear, and the effects of foreign objects), and failure due to the presence of damage, for a specified period of unrepaired usage.

Defect – (various definitions exist): The most common definition is any feature that is outside the boundary conditions of a given component/product design that will make the component/product incapable of meeting its requirements when it is needed. Defects are also defined related to product manufacturing and also related to representation of the product.

Examples are:

- **Manufacturing Defects** – When the product departs from its intended design, even if all possible care has been exercised.
- **Design Defects** – When the foreseeable risks of harm posed by the product could have been reduced or avoided by the adoption of a reasonable alternative design, and failure to use the alternative design renders the product not reasonably safe.

- **Inadequate Instructions or Warnings Defects** – When the foreseeable risks of harm posed by the product could have been reduced or avoided by reasonable instructions or warnings, and their omission renders the product not reasonably safe.

DEP – Discontinuity Evolution Process: The specific process by which a population of discontinuities evolves.

DNP – Discontinuity Nucleation Process: Any specific physical or chemical processes that may nucleate or form a discontinuity not inherent to a material. For example, in some materials fatigue deformation occurs by both dislocation movement and the production of slip bands on external or internal surfaces or by grain or twin boundary decohesion. The slip band mentioned is thus a nucleated discontinuity. Furthermore in some aluminum, titanium, and steel alloys (as well as others) intrinsic particles are known to nucleate corrosion pits if the Pitting Potential for nucleation is achieved. The pit is formed by a DNP.

DS – Discontinuity State: See IDS, EDS, and MDS below.

DSEP – Discontinuity State Evolution Process: The specific physical or chemical processes by which the discontinuity state evolves. The major forms of time dependent or related phenomena by which the state is changed are corrosion (more generally environmental degradation), creep, fatigue, wear and sequential combinations and synergisms of them. See EDS below.

DSER – Discontinuity State Evolution Response: Any change in state of an IDS population.

EAC – Environmentally Assisted Cracking: May occur under sustained load from either applied load or “residual stresses” EAC_{sl} . It may also occur under either constant amplitude cyclic forces or variable amplitude cyclic forces $EAC_{fatigue}$.

ECD – Equivalent Corrosion Damage: A Modified Discontinuity State (**MDS**) at some specific time that is made equivalent to a crack size often referred to as a “flaw” to start a residual life assessment by sub-critical crack growth analysis.

EDS – Evolving Discontinuity State: The description of the evolution of the discontinuity and the progression of changes to the discontinuity or population of discontinuities over time and cyclic load exposures. (Subsequent to either the nucleation of a discontinuity or the activation of an IDS by a specific physical or chemical process acting alone or conjointly the resultant discontinuity or population of them may evolve in state with time or cyclic load exposure. Various metrics are used to describe the EDS).

EIFS – Equivalent Initial Flaw Size: A term used to describe a discontinuity size usually determined by extrapolation from a set of fatigue data. The EIFS has no direct relationship to any specific IDS.

FCP – Fatigue Crack Propagation: Extension of a crack under cyclic or repeated loads. The stages of crack propagation are divided into four phases, viz.; 1) small or short crack propagation, long crack propagation in the linear elastic regime, and long crack propagation in either the elastic-plastic or fully plastic regime.

The following definitions related to fretting are from Reference [2].

Fretting, *n* – in tribology: Small amplitude oscillatory motion, usually tangential, between two solid surfaces in contact. Here the term *fretting* refers only to the nature of the motion without reference to the wear, corrosion, or other damage that may ensue. The term *fretting* is often used to denote *fretting corrosion* and other forms of *fretting wear*. Usage in this sense is discouraged due to the ambiguity that may arise.

Fretting Corrosion, *n*: A form of fretting wear in which corrosion plays a significant role.

Fretting Wear, *n*: Wear arising as a result of fretting (see **Fretting**).

See later part of this document for fretting fatigue, fretting plus fatigue, etc., which are non-standard definitions.

HOLISTIC: The whole and not fragmented actions in the structural integrity design process. See introductory remarks above and items below.

IDS – Initial Discontinuity State: The initial (intrinsic) population of discontinuities that are in a structure made of a given material as it was manufactured in a given geometric form. The IDS is a geometric and material characteristic that is a function of composition, microstructure, phases and phase morphology, and the manufacturing process used to process the material. The geometric and material discontinuities can be modeled separately. Examples of material IDS types include constitutive particles, inclusions, grain boundaries, segregated phases, phase boundaries, voids (vacancies, micro-porosity, and porosity) and intrinsic cracks, etc. Manufacturing processes such as machining and assembly can introduce additional discontinuities at fasteners, fillets, etc., that extend the tail (larger discontinuity sizes) of the IDS distribution.

IDS_{mat} – Initial Discontinuity State associated with a material: The initial population of intrinsic material discontinuities. See IDS.

IDS_{mfg} – Initial Discontinuity State associated with manufacturing of a given type: The resultant effect on the population of discontinuities from a given manufacturing process or sequence of manufacturing processes including joining of the three major types (viz. mechanical joining, thermal joining and adhesive bonding).

IDS_{geo} – Initial geometric discontinuity: The initial geometric discontinuities in a product. These often are generally referred to as a “notch”.

Integrity: Three concepts provide the basis of integrity, namely:

- 1) Firm adherence to a code of especially moral or artistic values: INCORRUPTIBILITY.
- 2) An unimpaired condition: SOUNDNESS.
- 3) The quality or state of being complete or undivided: COMPLETENESS.

Material Behavior: Response of a material to various factors such as chemical environment, forces, thermal environment, etc. Appropriate units must be used. Examples are fatigue behavior, environmentally assisted crack propagation.

Material Property Designators: See Mil Handbook 5, Section 9.2.2, Data Basis, T, S, A, B.

“Section 9.2.2.1, Data Basis – There are four types of room-temperature mechanical properties included in MIL HDBK-5. They are listed here, in order, from that having the least statistical confidence to that having the highest statistical confidence, as follows:

- **Typical Basis:** A-typical property value is an average value and has no statistical assurance associated with it.
- **S-Basis:** This designation represents the specification minimum value established by the governing industry specification (as issued by standardization groups such as SAE Aerospace Materials Division, ASTM, etc.) or federal or military standards for the material. (See MIL-Sm-970 for order of preference of specifications.) For certain products heat treated by the user (for example, steels

hardened and tempered to a designated F_{tu}), the S-value may reflect a specified quality-control requirement. Statistical assurance associated with this value is not known.

- **B-Basis:** This designation indicates that at least 90 percent of the population of values is expected to equal or exceed the statistically calculated mechanical property value, with a confidence of 95 percent.
- **A-Basis:** The lower value of either a statistically calculated number, or the specification minimum (S-basis). The statistically calculated number indicates that at least 99 percent of the population is expected to equal or exceed the statistically calculated mechanical property value with a confidence of 95 percent.

Material Response Characteristic: The manner in which a material behaves when subjected to a set of external parameters in a given condition of manufacture and geometry and joint. External parameters are cyclic forces (fatigue), different rates of force application, chemical environments, thermal environments, neutron environments, irradiation environments, contact conditions, wear conditions, and synergisms of these.

MDS – Modified Discontinuity State: This is described as the physical state of a discontinuity or damage state at any given time in its evolution. Various metrics may be used to describe the state. Example 1 – A crack has grown to a given size and is an MDS at a specific time and thus size. Example 2 – A corrosion pit has grown to a state at some point in time. The IDS may progress (EDS) to various MDS values through the mechanisms of corrosion, creep, fatigue, wear or combinations of these over time.

MSD and MED: “Multiple Site Damage (MSD) is a source of WFD characterized by the simultaneous presence of fatigue cracks in the same structural element (e.g., fatigue cracks that may coalesce with or without other damage leading to the loss of the residual strength). **Multiple Element Damage (MED)** is a source of WFD characterized by the simultaneous presence of fatigue cracks in similar adjacent structural elements. The development of cracks at multiple locations (both MED and MSD) may result in strong interactions that can affect subsequent crack growth, in which case the predictions for local cracking would no longer apply. An example of this situation may occur at a fuselage skin lap joint. Simultaneous cracking at many fasteners along a common rivet line may reduce the residual strength of the joint below required levels before the cracks are readily detectable during routine maintenance.” From FAA AC 91-56.

Prognosis: The prospect of recovery as anticipated from the usual course of disease or peculiarities of the case. “MOD policy for the development and exploitation of prognostic technology”, Author CTS REL1B, Squadron Leader-Fergus Hawkins, UK-MOD. “The process of using one or more parameters to predict the condition of a system at a defined point in its future operation”. These parameters may be data measured by in-line sensors, derived from off-line monitoring processes, empirical observations or any appropriate combination of these. From Dr. J. Cook, AHM Group, ES (Air), 24/3/03.

PSE – Principal Structural Element

Safe Life: A term usually taken to mean structural design based on ideal continuum mechanics assumptions and practices without consideration of cracks or crack like discontinuities and based on the assumptions of homogeneity and continuity. In traditional safe life design toughness, sub-critical crack growth, directed inspection and inspection intervals are not dealt with for fatigue, corrosion and related items.

Structure: “1: The action of building, as in CONSTRUCTION. 2a: Something (as a building) that is constructed. 2b: Something arranged in a definite pattern of organization (a rigid totalitarian structure, leaves and other plant structures). 3: Manner of construction, (MAKEUP, Gothic in structure). 4a: The arrangement of particles or parts in a substance or body (soil structure, molecular structure). 4b: Organization of parts as dominated by the general character of the whole (economic structure, personality structure). 5: The aggregate of elements of an entity in their relationships to each other.”

SSL – Structurally Significant Location: The significant locations on a structure determined by the potential behavior and changes in state that may occur in the structure related to its use under conditions of interest.

SSI – Structurally Significant Item: See Appendix 2-1.

Surface Morphology:

Morphology – From Merriam Webster computer dictionary:

“1a: A branch of biology that deals with the form and structure of animals and plants. 1b: The form and structure of an organism or any of its parts. 2a: A study and description of word formation (as inflection, derivation, and compounding) in language. 2b: The system of word-forming elements and processes in a language. 3a: A study of structure or form. 3b: STRUCTURE, FORM. 4: The external structure of rocks in relation to the development of erosional forms or topographic features.”

Surface Topography:

Topography – From Merriam Webster computer dictionary:

“1a: The art or practice of graphic delineation in detail usually on maps or charts of natural and man-made features of a place or region especially in a way to show their relative positions and elevations. 1b: Topographical surveying. 2a: The configuration of a surface including its relief and the position of its natural and man-made features. 2b: The physical or natural features of an object or entity and their structural relationships.”

Surface Topology:

Topology – From Merriam Webster computer dictionary:

1: Topographic study of a particular place; specifically the history of a region as indicated by its topography. 2a (1): A branch of mathematics concerned with those properties of geometric configurations (as point sets) which are unaltered by elastic deformations (as a stretching or a twisting) that are homeomorphisms, (2): the set of all open sub-sets of a topological feature.

Validate: 1a: To make legally valid. 1b: To grant official sanction to by marking. 1c: To confirm the validity of (an election); and also to declare (a person) elected. 2: To support or corroborate on a sound or authoritative basis experiments designed to validate the hypothesis.

Verify: 1: To confirm or substantiate in law by oath. 2: To establish the truth, accuracy, or reality of.

Widespread Corrosion Damage: Corrosion damage that is global on either a PSE or SSI or both and damage that may extend to one or more structural elements.

WFD – Widespread Fatigue Damage: Uniformly loaded structure may develop cracks in adjacent fasteners, or in adjacent similar structural details, which interact to reduce the damage tolerance of the structure in a manner which may not be readily detectable. Widespread Fatigue Damage (WFD) is characterized by the simultaneous presence of cracks at multiple structural details that are of sufficient size and density whereby the structure will no longer meet its damage tolerance requirement, § 25.571 (e.g., not maintaining required residual strength after partial structural failure). Multiple Site Damage (MSD) is a source of WFD characterized by the simultaneous presence of fatigue cracks in the same structural element (e.g., fatigue cracks that may coalesce with or without other damage leading to the loss of the residual strength). Multiple Element Damage (MED) is a source of WFD characterized by the simultaneous presence of fatigue cracks in similar adjacent structural elements. The development of cracks at multiple locations (both MED and MSD) may result in strong interactions that can affect subsequent crack growth, in which case the predictions for local cracking would no longer apply. An example of this situation

may occur at a fuselage skin lap joint. Simultaneous cracking at many fasteners along a common rivet line may reduce the residual strength of the joint below required levels before the cracks are readily detectable during routine maintenance. From FAA AC 91-56A 4/29/98.

2.3 LIST OF DEFINITIONS RELATED TO CORROSION FATIGUE AND STRESS CORROSION CRACKING

The following definitions are taken from Reference [3].

Corrosion Fatigue: The process in which a metal fractures prematurely under conditions of simultaneous corrosion and repeated cyclic loading at lower levels or fewer cycles than would be required in the absence of the corrosive environment. See for example G15-99B, Page 69.

Corrosion Fatigue Strength: The maximum repeated stress that can be endured by a metal without failure under definite conditions of corrosion and fatigue and for a specific number of stress cycles and a specified period of time. See for example G15-99B, Page 69.

Exfoliation Corrosion: Corrosion that proceeds laterally from the sites of nucleation along planes parallel to the surface, generally at grain boundaries, forming corrosion products that force metal away from the body of the material and giving rise to a layered appearance. See for example G15-99B.

Pitting: Corrosion of a metal surface, confined to a point or small area that takes the form of small cavities.

Stress-Corrosion Cracking: A cracking process that requires the simultaneous action of a corrodent and sustained tensile stress. (This excludes corrosion-reduced sections which fail by fast fracture. It also excludes intercrystalline or transcrystalline corrosion which can disintegrate an alloy without either applied or residual stress.)

The following definitions are taken from Reference [4].

Corrosion Fatigue: The process by which fracture occurs prematurely under conditions of simultaneous corrosion and repeated cyclic loading at lower stress levels or fewer cycles than would be required in the absence of the corrosive environment. See for example E1823-96, Page 1016.

EAC – Environment Assisted Cracking: A cracking process in which the environment promotes crack growth or higher crack growth rates than would occur without the presence of the environment. See for example E1823-96, page 1028. The same definition appears in E 1681-95, Page 944 (see below).

Fatigue: The process of progressive localized permanent structural change occurring in a material subjected to conditions that produce fluctuating stresses and strains at some point or points and that may culminate in cracks or complete fracture after a sufficient number of fluctuations. See for example E1823-96, Page 1019.

The following definition is taken from Reference [5].

Stress-Corrosion Crack: A crack which may be intergranular or transgranular depending on the material, resulting from the combined action of corrosion and stress, either external (applied) or internal (residual). See for example E7-97a, Page 52.

The following definitions are taken from Reference [6].

SCC – Stress-Corrosion Cracking: A cracking process that requires the simultaneous action of a corrodent and sustained tensile stress. See for example E1681-95, Page 943.

EAC – Environment-Assisted Cracking: Same as above in E1823 – 96 and E1681 – 95, Page 944.

The author has found no standard definitions for either corrosion – fatigue or corrosion/fatigue. Thus, unless one can be found or suggested for our work the author suggests using only standard terminology. Also, some other definitions have been added in the following appendix. These terms are all often used at conferences and our various team meetings.

Additional definitions are given in Appendix 2-1.

2.4 ACKNOWLEDGEMENTS

Significant input into the preparation of this document has been made by the following colleagues; Nick Bellinger, Graeme Eastaugh, Jerzy Komorowski, all of the Institute for Aerospace Research, National Research Council Canada, Ottawa, Ontario, and Dr. Charles Elliott, Ms. Amy Taylor of the University of Utah and FASIDE International Inc.

2.5 REFERENCES

- [1] Ferguson, M., “Holism and System Theory”, in *The Aquarian Conspiracy*, St. Martin’s Press, p. 156, 1980.
- [2] *Standard Terminology Relating to Wear and Erosion*”, ASTM G40-99, American Society for Testing and Materials, 100 Barr Harbor Dr., West Conshohocken, PA, USA, 1999.
- [3] *ASTM Standards Volume 03.02 – Wear and Erosion; Metal Corrosion, G15-97a – Standard Terminology Relating to Corrosion and Corrosion Testing*, ASTM, Philadelphia, PA, USA, 1994.
- [4] *ASTM Standards Volume 03.01 – Metals-Mechanical Testing; Elevated and Low Temperature Tests; Metallography, E1823 – 96, Standard Terminology Relating to Fatigue and Fracture Testing*, ASTM, Philadelphia, PA, USA, 1998.
- [5] *ASTM Standards Volume 03.01 – Metals-Mechanical Testing; Elevated and Low Temperature Tests; Metallography, E7-97a: Standard Terminology Relating to Metallography*, ASTM, Philadelphia, PA, USA, 1998.
- [6] *ASTM Standards Volume 03.01 – Metals-Mechanical Testing; Elevated and Low Temperature Tests; Metallography, E1681-95: Standard Test Method for Determining a Threshold Stress Intensity Factor for Environment-Assisted Cracking of Metallic Materials Under Constant Load*, ASTM, Philadelphia, PA, USA, 1998.

Appendix 2-1: ADDITIONAL DEFINITIONS

The definitions in this section are not standard definitions.

Corrosion + Fatigue: Fatigue occurs in a material/structure that has undergone corrosion. The fatigue may occur as either pure fatigue or corrosion fatigue. See ASTM definitions previously supplied.

Corrosion – Fatigue: Fatigue occurs in a material/structure that has undergone corrosion. The fatigue may occur as either pure fatigue or corrosion fatigue. See ASTM definitions previously supplied.

Corrosion/Fatigue: Fatigue occurs in a material/structure that has undergone corrosion. The fatigue may occur as either pure fatigue or corrosion fatigue. See ASTM definitions previously supplied.

Fretting Fatigue: Fatigue occurs in the presence of fretting. Thus, the action is concomitant. This situation occurs in many holes with fasteners moving in the holes or on faying surfaces in splice joints. It is also a significant challenge in many joints of helicopters (both airframes and rotor system components), engines, landing gears, wire cables and many other components.

Fretting + Fatigue: Fatigue occurs on a material/structure that has undergone fretting. The fatigue may occur as either pure fatigue or corrosion fatigue.

Fretting/Fatigue: Fatigue occurs on a material/structure that has undergone fretting. The fatigue may occur as either pure fatigue or corrosion fatigue.

(Prior Corrosion) + Fatigue: Fatigue occurs in a material/structure that has undergone corrosion. The fatigue may occur as either pure fatigue or corrosion fatigue. See ASTM definitions previously supplied.

(Prior Corrosion) / Fatigue: Fatigue occurs in a material/structure that has undergone corrosion. The fatigue may occur as either pure fatigue or corrosion fatigue. See ASTM definitions previously supplied.

Mechanism Overlap: The interaction of more than one degradation mechanism in generation of the degradation condition in a material/structure.

Missed Corrosion + Fatigue: Fatigue occurs in a material/structure that has undergone corrosion. The fatigue may occur as either pure fatigue or corrosion fatigue. See ASTM definitions previously supplied.

Missed Corrosion / Fatigue: Fatigue occurs in a material/structure that has undergone corrosion. The fatigue may occur as either pure fatigue or corrosion fatigue. See ASTM definitions previously supplied.

SSI/Corrosion: A structurally significant item designated by its propensity to become a critical item based on the potential for corrosion degradation of any type.

SSI / Corrosion Fatigue: A structurally significant item designated by its propensity to become a critical item based on the potential for corrosion fatigue degradation.

SSI/Fatigue: A structurally significant item designated by its propensity to become a critical item based on the potential for fatigue degradation. These sites are usually determined by durability and/or damage tolerance assessment.

SSI/Fatigue/Durability: A structurally significant item designated by its propensity to become a critical item based on the potential for fatigue degradation as determined by the durability assessment.

SSI / Fatigue / Damage Tolerance: A structurally significant item designated by its propensity to become a critical item based on the potential for fatigue degradation as determined by the damage tolerance assessment.

SSI / Fretting Fatigue: A structurally significant item designated by its propensity to become a critical item based on the potential for fretting fatigue degradation.

SSI/SCC: A structurally significant item based on its propensity to undergo the degradation mechanism of stress corrosion cracking. See the ASTM standard previously supplied on stress corrosion cracking.

SSL/Corrosion: A structurally significant location designated by its propensity to become a critical location based on the potential for corrosion degradation of any type.

SSL / Corrosion Fatigue: A structurally significant location designated by its propensity to become a critical location based on the potential for corrosion fatigue degradation.

SSL/Fatigue/Durability: A structurally significant location designated by its propensity to become a critical location based on the potential for fatigue degradation as determined by the durability assessment.

SSL / Fatigue / Damage Tolerance: A structurally significant item designated by its propensity to become a critical location based on the potential for fatigue degradation as determined by the damage tolerance assessment.

SSL / Fretting Fatigue: A structurally significant item designated by its propensity to become a critical location based on the potential for fretting fatigue degradation.

SSL/SCC: A structurally significant location based on its propensity to undergo the degradation mechanism of stress corrosion cracking. See the ASTM standard previously supplied on stress corrosion cracking.

Local Corrosion: Corrosion of a skin or web (wing, fuselage, empennage, or strut) not exceeding one frame, stinger, or stiffener bay) or corrosion of a single frame, chord, stringer, or stiffener, or corrosion of more than one frame, chord, stringer, or stiffener but, no corrosion on two adjacent members on each side of the corroded member.

Widespread Corrosion: Corrosion of two or more adjacent skin or web bays defined by frame, stringer or stiffener spacing. Or corrosion of two or more adjacent frames, chords, stringers, or stiffeners.

Level 1 Corrosion: Corrosion damage occurring between successive inspections that is LOCAL and can be re-worked/blended out within allowable limits as defined by the manufacturer. Or Corrosion damage that is local but exceeds allowable limits and can be attributed to an event not typical of the operator's usage of other airplane's in the same fleet. Or Operator experience over several years has demonstrated only light corrosion between successive inspections but latest inspection and cumulative blend-out now exceed allowable limits.

Level 2 Corrosion: Corrosion occurring between successive inspections that require re-work/blend-out which exceeds allowable limits, requiring a repair or complete or partial replacement of a principal structural element as defined by the original equipment manufacturer's structural repair manual. Or corrosion occurring between successive inspections that is widespread and requires blend-out approaching the allowable re-work limits.

Level 3 Corrosion: Corrosion found during the first or subsequent inspections, which is determined (normally by the operator) to be a potential urgent airworthiness concern requiring expeditious action.

The above are taken from Boeing Commercial Airplane Company and FAA documents.

Chapter 3 – ANALYSIS AND COMPARISON OF COST OF CORROSION MAINTENANCE RESULTS

Garth Cooke and Garth Cooke Jr.
C² Technology, Inc.
Beavercreek, Ohio
USA

3.1 INTRODUCTION

For the USAF, and most other western nations, new aircraft are becoming very rare and extremely expensive to acquire. As a result, nations of the NATO alliance have the choice of fulfilling their missions with increasingly older aircraft, or reducing the military commitments. Given that military commitments are generally a political decision of the civilian governments, only one option remains open to military planners. Corrosion control maintenance is an important driver of the costs of maintaining aircraft and an ever more important component of maintenance as air vehicles become older. This chapter is a compilation and analysis of results from Cost of Corrosion Studies conducted in 1990, 1997, 2001 and 2004 [1],[2],[3],[4],[10]. (*References [1],[2], [4], and [10] can be found at the Documents tab at <http://c2techinc.com/>.*) Each of those studies was conducted for the US Air Force Corrosion Prevention and Control Office, and the primary authors of those studies were Garth Cooke and Rob Cooke. Back in the 1988/89 time frame corrosion was a recognized driver of maintenance actions and costs, but there was no way to quantify the level of corrosion control activities throughout the USAF. Several databases existed that purported to offer a partial picture, but many activities, and generally the most expensive and important at that, fell well outside any accessible system. The authors of this chapter, whose members include a former director of the USAF Corrosion Program Office, undertook the task of quantifying the total cost of corrosion maintenance to the USAF. The definition and methodology developed in that first study were primary drivers of all subsequent Cost of Corrosion Studies. Each of the individual studies addressed only direct corrosion maintenance costs, and excluded from consideration classified systems, indirect costs, corrosion costs for classified systems, and real property costs such as those associated with corrosion control facilities. The first study was conducted to obtain the total costs of corrosion control activities throughout the USAF, and underlying data were used for study only subsequent to the original collection. The information obtained proved extremely useful for planning purposes and for directing R&D efforts effectively. As the detailed costs underlying the total cost of corrosion maintenance proved to be useful and important, the subsequent studies were conducted to obtain more complete underlying data, particularly those that could prove useful for comparison of costs over time. References 1 through 4 can be consulted for a complete enumeration of maintenance actions included or excluded from the corrosion cost studies. Bearing in mind its dependence on the data generated by the four studies, this chapter is a stand-alone analysis of the data from those studies.

3.2 ANALYSIS OF USAF DIRECT CORROSION MAINTENANCE COST

The purpose of the four Cost of Corrosion Studies (2004, 2001, 1997 and 1990) was to quantify the total annual cost of direct corrosion maintenance to the US Air Force. Each of the studies was performed by the same people and followed largely the same methodology, thus the results from the different studies are directly comparable, particularly the three most recent studies. Wherever any question of the comparable methodology is known, that instance is documented and this article attempts to present the associated costs from both the new methodology and the costs which would have resulted under a previous methodology. Given that the goal of each study was to determine the total annual costs of direct corrosion maintenance, it naturally follows that the first element to be analyzed is the total annual costs for all of the four study years. In this section, it is to be emphasized that these studies were an examination of the total USAF

corrosion maintenance cost not just that for aircraft related corrosion. They were an attempt to look at all USAF weapon systems, sub-systems, and support equipment and included aircraft, munitions, support equipment, and communications/electronics equipment; in fact, everything except Real Property and Real Property Installed Equipment (air conditioning equipment, back-up generators, etc.).

The following table, Table 3-1, presents the total annual costs of direct corrosion maintenance in then-year dollars (the costs as reported in the respective studies) and then presents the costs in (the more appropriate for comparison) constant 2004 dollars.

Table 3-1: Total Annual Costs of Direct Corrosion in Then Year Dollars and '04 Dollars (in Millions).

Total Costs, Then Yr Dollars, in Millions			
1990	1997	2001	2004
\$720	\$795	\$1,139	\$1,497
Total Costs, Adjusted to Constant 2004 Dollars			
1990	1997	2001	2004
\$926	\$857	\$1,175	\$1,497

As Table 3-1 clearly demonstrates, costs have not remained constant, neither in absolute dollar terms, nor in constant dollar terms. From 1990 to 1997 the total annual cost of corrosion maintenance increased slightly in absolute dollars, but actually decreased in constant dollars. The total costs for 2001, however, showed a sharp increase in both absolute as well as constant dollars, and 2004 again showed a sharp increase in costs. In fact, from 1990 to 2001 the annual cost of direct corrosion maintenance increased 27% faster than the inflation rate (using the O&M, non-pay, non-fuel, inflation indices), and the 2004 report shows that the increase was even greater – with corrosion costs increasing 60% in constant dollars from 1990 to 2004. From 1997 to 2001 the annual cost of direct corrosion maintenance increased 37% faster than the inflation rate, and the cost from 2001 to 2004 showed an increase that was 27% greater than the inflation rate. The inflation adjusted costs for corrosion maintenance decreased from 1990 to 1997, but this decrease was related more to force structure changes than to a decrease in the expenses of direct corrosion maintenance (see the 1997 corrosion report [2], for further discussions on this subject).

Perhaps of more interest than simply comparing the changes in total annual corrosion costs from study year to study year, is a comparison of the change in direct corrosion maintenance costs as an element in the overall Air Force Operations and Maintenance (O&M) budget. Table 3-2 provides both the total annual costs for direct corrosion maintenance as presented in Table 3-1, and the relative role of corrosion in the respective O&M budgets. As the table indicates, the AF O&M budget was reduced, in constant dollars, from 1990 through the 2001 study, but increased substantially in the three years leading up to 2004. Table 3-2 also indicates that the corrosion maintenance costs have grown sharply since 1997, rising 27% since 2001, after a slight decline in total constant costs between 1990 and 1997. In fact, even when the corrosion costs were shrinking in constant dollars (-7%) the reduction was far less than the reduction in the AF O&M budget (-24%). Therefore, direct corrosion maintenance has required a growing share relative to the AF O&M budget. Even in 1997, when the cost of corrosion maintenance decreased in constant dollars, the proportion of the O&M budget required for corrosion maintenance increased. Between the 1990 Cost of Corrosion study and the 2001 study, the corrosion maintenance share of the AF O&M budget grew from 2.86% of the budget to 3.88%. For the current study, the corrosion maintenance portion of the overall O&M budget remains 3.88%. The steady corrosion maintenance proportion does not, however, reflect a static situation over the past three years, rather the costs of corrosion maintenance and the overall USAF O&M budget have

both increased dramatically in recent years with the O&M budget rising from \$29B to \$38B in just three years between 2001 and 2004.

Table 3-2: Total Corrosion Costs vs. USAF O&M Budget, in '04 Dollars (in Millions).

Total Costs, Then Yr Dollars				AF O&M Budget, Then Yr Dollars			
1990	1997	2001	2004	1990	1997	2001	2004
\$720	\$795	\$1,139	\$1,497	\$25,160	\$22,728	\$29,328	\$38,406
Total Costs, Adjusted to 2004 \$'s				AF O&M Budget, Adjusted to '04 \$'s			
1990	1997	2001	2004	1990	1997	2001	2004
\$926	\$857	\$1,175	\$1,497	\$32,342	\$24,512	\$30,246	\$38,406
Percentage Change in Adjusted Costs (Growth in Total Corrosion Costs Above Inflation)				Percentage Change in Adjusted AF O&M Budget			
90 to 04	97 to 04	01 to 04		90 to 04	97 to 04	01 to 04	
61.0%	73.8%	27.4%		18.7%	56.7%	27.0%	
Depot Corrosion Maintenance Dollars in Constant 2004 \$'s (in Millions)				Corrosion Proportion of AF O&M Budget			
1990	1997	2001	2004	1990	1997	2001	2004
\$736	\$713	\$854	\$1,053	2.86%	3.50%	3.88%	3.90%
90 to 04	97 to 04	01 to 04		90 to 04	97 to 04	01 to 04	
36.1%	40.4%	17.2%		36%	11%	0%	
Fleet Size During Study Year				Corrosion Cost Growth '90 to 04 as a Constant Compounding Annual Rate			
8,722	5,991	6,075	6,066	5.23%			

Figure 3-1, Role of Direct Corrosion Maintenance in AF O&M Budget, graphically illustrates the impact of corrosion maintenance on the budget. It shows quite clearly that the reduction in corrosion maintenance expenditures in the 1990 – 1997 period of shrinking defence budgets was slower than the drop in the overall budget, and once the budgets started to recover, the corrosion maintenance costs grew quickly and have remained a cost driver within the O&M Budget.

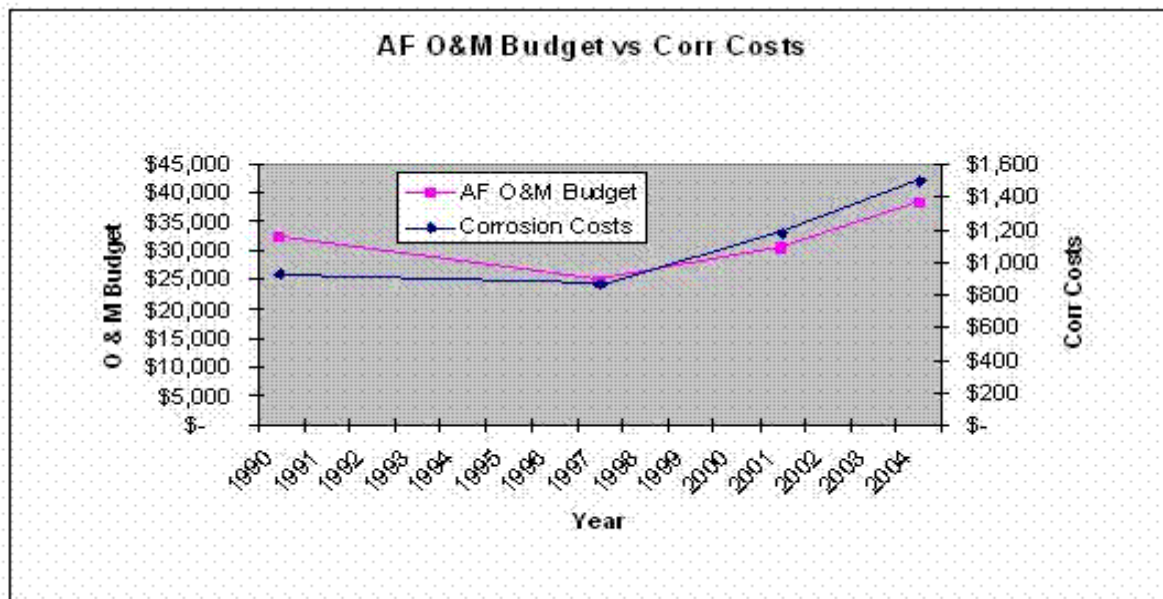


Figure 3-1: Role of Direct Corrosion Maintenance in the AF O&M Budget (in Millions).

3.3 SPECIFIC COST ANALYSIS

Whereas the previous section provided total USAF direct corrosion maintenance costs for everything except Real Property and Real Property Installed Equipment and its impact within the total USAF budget, the remainder of this paper addresses aircraft related corrosion maintenance, the main driver of corrosion costs and the main concern of the Air Force. First, we shall discuss methodologies and results for each of the individual studies, specifically examining the reasoning supporting certain key decisions in establishing methodologies and the results achieved. Then, we shall focus on two means of evaluating the costs of aircraft corrosion maintenance:

- Overall (aggregate) weapon system wide (fleet) corrosion maintenance costs; and
- The per-aircraft corrosion maintenance costs within a weapon system type.

3.3.1 Developing a Cost Analysis Methodology

In developing a cost analysis methodology, it was apparent that two key goals had to be met. First, we had to capture costs associated with all aspects of corrosion maintenance; and second, we had to ensure that we captured all of the costs associated with each aspect consistently across the entire USAF. (The discussion which follows applies, in most part, to all of the different systems and sub-systems considered throughout the four studies, but for the purposes of this chapter we shall limit the discussion to aircraft.) Since we were limited to examination of “direct corrosion maintenance” the corrosion prevention activities and their costs which have to be considered so carefully and thoroughly during the design and manufacturing phases of an aircraft’s life were not considered during these cost studies. Nor were the engineering and management activities involved in ensuring that a thorough and effective corrosion prevention and control program is in effect for each weapon system in the USAF. Finally, the Real Property and Real Property Installed Equipment which are needed to establish effective corrosion prevention and control programs were excluded from these studies because the Military Construction Program and the Civil Engineering programs that create these entities are totally separate from the aircraft maintenance communities.

3.3.1.1 Aspects of Corrosion Maintenance

Corrosion maintenance whether performed at the depot or the field level, can be considered as a cyclic process, and can be visualized as a continual circle containing three essential elements: Clean, Inspect, and Repair.

The clean aspect is essentially concerned with two crucial elements of a corrosion program. The first is to periodically remove atmospheric or environmental contaminants – which are frequently hygroscopic – from the surface thus hoping to prevent the formation of an electrolyte which is essential to creation of a corrosion cell. The second is to provide a clean surface so as to enhance the ability to perform the next essential element, inspection. In some instances, this cleaning process may include the removal of protective coating systems so that the inspection can take place.

The inspection requirement for corrosion control is simply to ensure, via whichever inspection method is most appropriate to the problem at hand, that corrosion is (or is not) present in or on the surface of interest.

Finally, the third aspect of the maintenance program is repair of corrosion damage. This is easily the most complex of the three. It includes rectification of the corrosion damage through either replacement of the corroded part or removal of the corrosion from the metal part. If necessary, faying surface sealant or sealant for wet installation of fasteners or some similar method for isolation of dissimilar metals must be applied. Then the protective coating system (which probably includes surface etch, primer, and top-coat application) must be renewed.

All of the above assume that one has gained access to the surface under consideration, so that a final step is required in that the aircraft must be returned to an operational configuration after the maintenance is completed.

3.3.1.2 Capturing All Related Costs

This section describes the analysis process employed to ensure that all appropriate data were collected and analyzed properly. A multi-dimensional cost database was built, as the data for these studies were collected. The dimensions were weapons system, cost category, and location. This allowed the database to be used to answer corrosion cost questions for specific weapons systems, locations, or cost categories. The cost categories included on-equipment maintenance, off-equipment maintenance, washing, painting, spares, inspections, hazardous material handling and disposal, and special facilities and processes. Figure 3-2 is a graphic representation of this database. The multi-dimensional database was used to develop the cost model matrix. Along the system axis are shown the weapons systems or sub-systems that are accumulating corrosion-related maintenance costs. Along the location axis are the geographic or functional places where the costs are accrued, and along the cost category axis are the corrosion-related maintenance process elements that account for the cost.

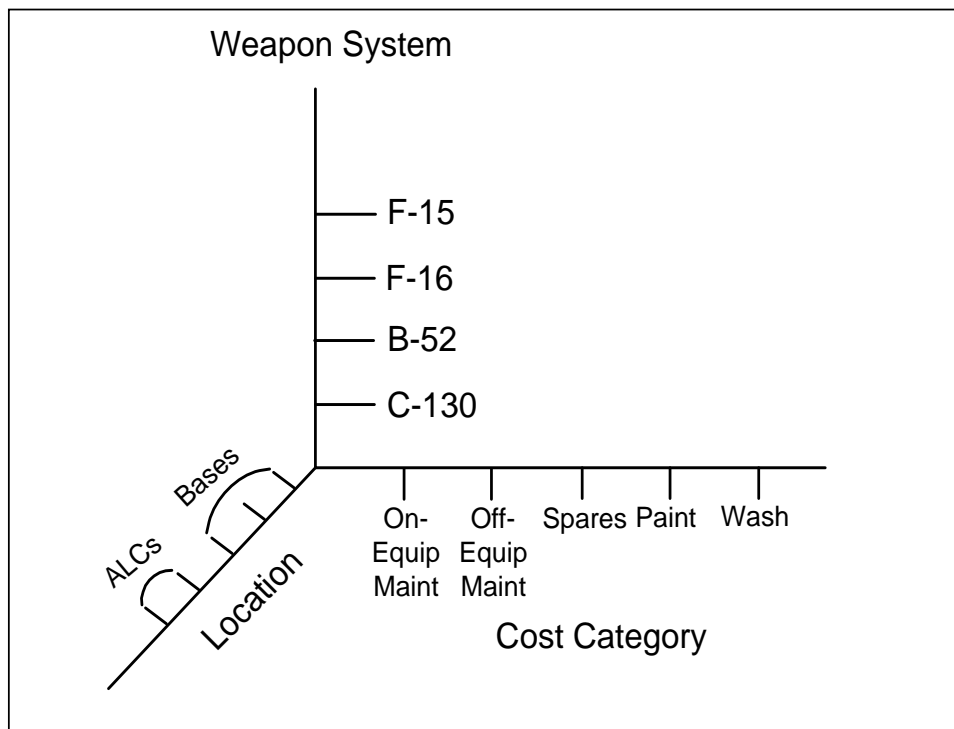


Figure 3-2: Three-Dimensional Data Base Illustration.

Figure 3-3 (below) illustrates the methodologies that were used to fill the individual cells of the cost model matrix. Starting at the bottom of the figure, the man-hours consumed in painting F-16 aircraft in each of the commands that operate F-16s are collected from each base. The man-hour total for each base is multiplied by the appropriate dollars per man-hour figure, obtained from AFI 65-503, U.S. Air Force Cost and Planning Factors, and placed in the cell for that base. We used the summary cost for all grades from Table A33-1 for extracting the labor hour costs from AFI 65-503. When all bases have been analyzed for all operating commands, the figure will be entered in the F-16 “command” cell of the slice in the matrix labeled “paint hours”. When the costs of painting for F-16s at depot and contractor repair facilities are calculated, they will also be added to the appropriate cells. After all paint hours accumulators are entered, the total labor cost associated with painting F-16s can be obtained from summing the three location axis cells for F-16 paint hours.

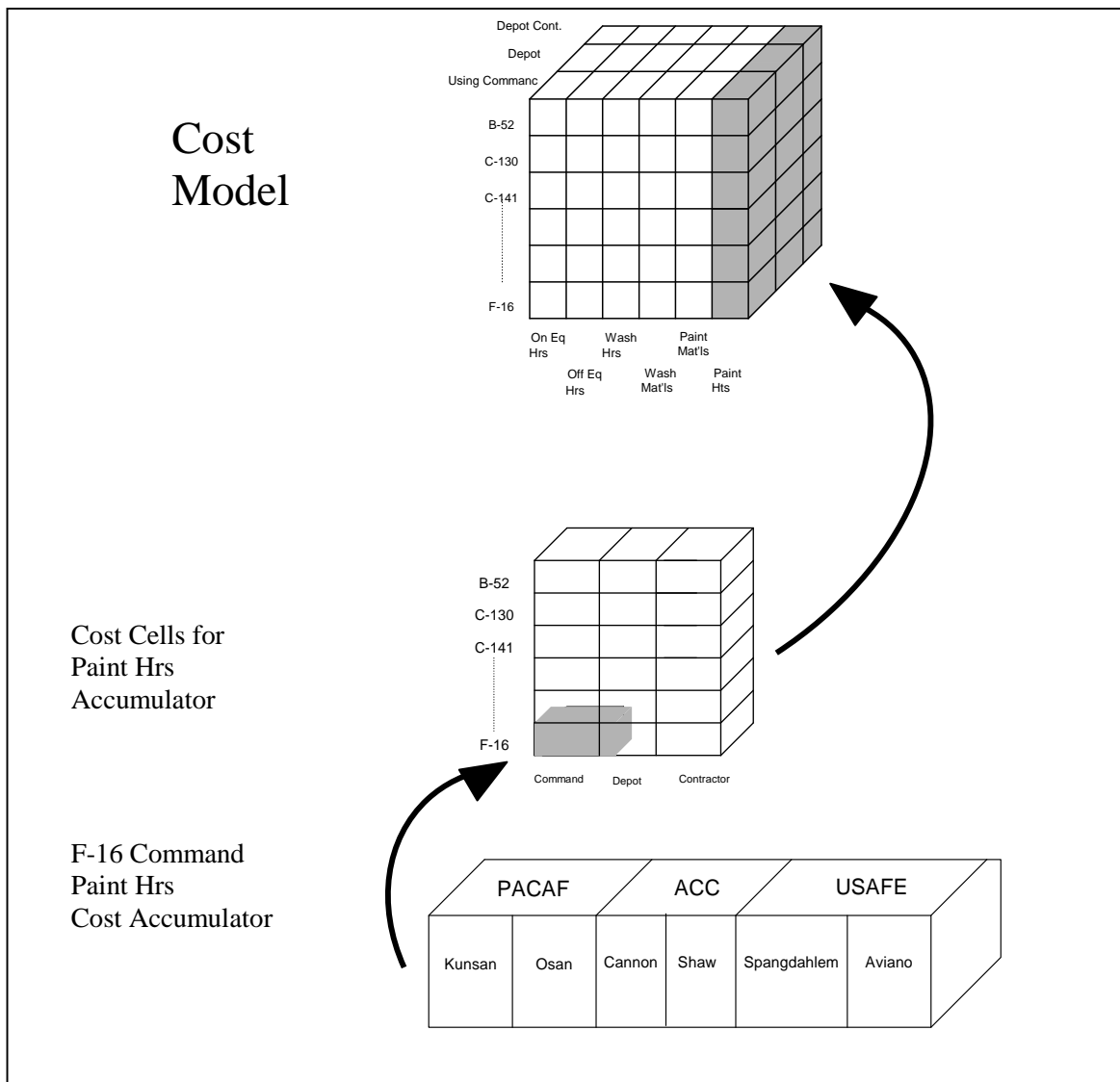


Figure 3-3: Methodology Illustration.

The cost matrix developed for these studies lends itself to ready feedback to the data collection system. If any cell in the matrix is empty, that cell must be individually analyzed to determine what pre-planned cost element has not been completed. It is entirely possible that some of the cost elements will be empty; however, this methodology ensures that only cost elements that are appropriately empty will be so. That is, no cost element cell can inadvertently be left empty. Additionally, any element of the cost of corrosion that is gathered by some methodology not directly recorded in dollars will be an empty cell until it has been analyzed and an appropriate dollar figure applied. This methodology ensures that man-hour figures or number of spares, for instance, are not entered inadvertently instead of the applicable dollar figure.

3.3.1.3 Corrosion Maintenance Definition

In establishing the data collection methodologies for the four studies, it was apparent that everyone responding to a request for data had to consider the same elements in the corrosion process as had been agreed to. Accordingly, the following definition of the elements of the USAF corrosion prevention and control program were adopted and employed in all four of the Cost of Corrosion studies:

- Cleaning to remove surface contaminants or to facilitate inspection.
- Stripping of protective coatings (regardless of purpose).
- Inspection to detect corrosion or corrosion related damage.
- Treatment of corrosion damage (corrosion removal, sheet metal or machinist work, replacement, etc.).
- Application of surface treatment (Alodine, other surface etch).
- Application of faying surface sealant (or similar sealing for corrosion protection).
- Application of protective coatings (regardless of reason).
- Time spent gaining access to and closure from parts requiring any of the above activities.
- Preparation and clean-up activities associated with any of the above.

All time and materials consumed in performing any of these activities were considered to be “direct corrosion maintenance” for the purposes of the Cost of Corrosion studies.

3.3.1.4 Obtaining Data to Complete the Studies

Virtually all of the data required to complete the studies were obtained through interviews with appropriate personnel at the various bases, depots, and contractor sites where USAF equipment is maintained.

The field level maintenance data were collected in a worksheet that was sent to every field maintenance base (except Air National Guard bases which were handled in a different way due to the exceptionally large number of such bases) by their respective major command corrosion manager. We had an amazing response rate of almost 100% on the questionnaires prepared and sent out in this manner (the actual questionnaire used in the 2004 study is available at an appendix to Reference [1]). In the 1990 study, we had not used the questionnaire – instead attempting to rely on REMIS data as the source of field level data. Subsequent studies used the questionnaire, and it was shown that this resulted in data at least twice as extensive as had been collected with the automated system.

Depot data were collected solely by interviews. Most of these data were based on discussions with depot engineers regarding the Maintenance Requirements Review Board (MRRB) documentation for their weapon system. The MRRB documents are based on an annual review of all of the actions completed on a particular aircraft type during the preceding year. The actions are then recorded in the brochure and, for the most part, projected as the requirements for the next review. This analysis, as it becomes the basis for all of the approved actions for the upcoming year within the depot maintenance community, contains the best possible identification of all of the actions completed during the immediately prior year. The discussions with the depot engineers then became one of identifying the tasks which involved corrosion maintenance. Obviously, there was more to it than that, but these reviews identified the majority of the costs associated with depot corrosion maintenance on aircraft.

3.3.2 Fleet Corrosion Costs

Figure 3-4 presents the total fleet costs for various weapon systems for each of the four Cost of Corrosion Studies. The aircraft fleets are grouped by the managing Air Logistics Center.

4 Study Fleet Cost Comparison, in 04 \$'s (in thousands)

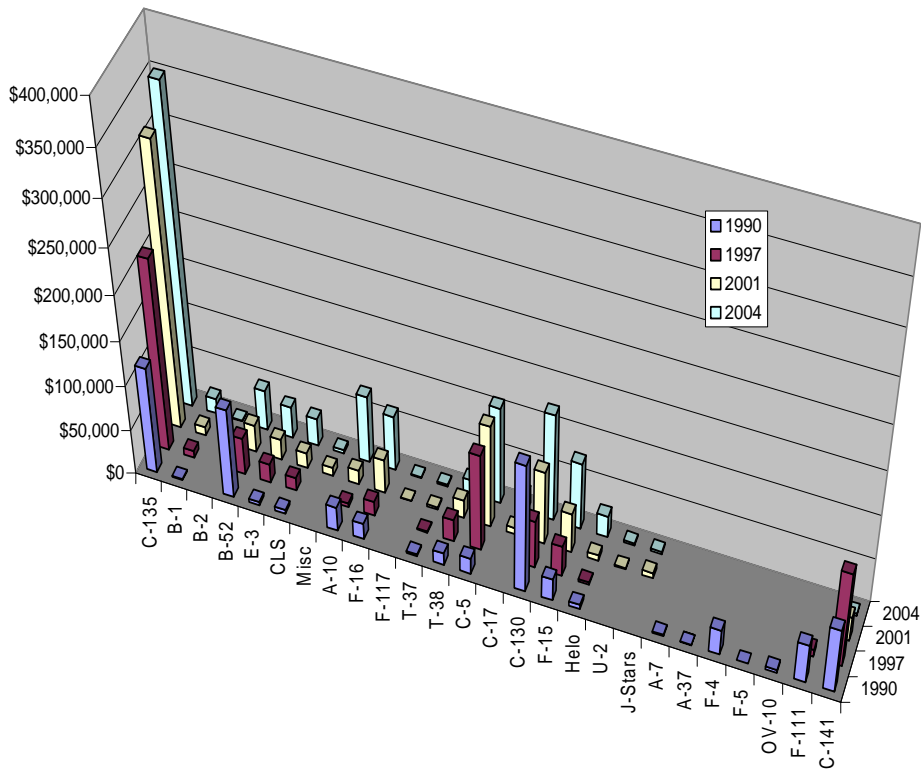


Figure 3-4: Total Costs for Fleets in '04 Dollars (in Thousands).

Obviously, when examining the corrosion costs of a particular weapon system fleet there are two driving factors, namely the corrosion maintenance cost per aircraft, and the size of the aircraft fleet. Table 3-3, Total Aircraft Costs by Weapon Systems Fleet, on the following page, presents the data from Figure 3-4 in table format and presents not just the total fleet cost for each study but also the fleet size for each study [5],[6],[7],[8].

Six of the bottom seven aircraft on the list have been retired from the USAF operational fleet altogether, and the C-141 costs had dropped so dramatically with the curtailment of Programmed Depot Maintenance due to its ongoing retirement, that the corrosion maintenance costs have essentially gone to zero. It is important and useful to examine the changes in the total corrosion maintenance costs of the weapon system fleets that are still active within the Air Force. It is very clear that the costs for corrosion maintenance on the C-135 fleet are the most important driver of total costs, making up 35% of the total costs attributable to aircraft. This is actually a drop from the 2001 study, where the C-135 fleet accounted for 40% of the total costs. Even with the portion down to 35%, this at first seems an extremely high percentage of the overall aircraft corrosion costs. However, the C-135 is in fact the oldest fleet in the Air Force, which as of September 2003 had an average age of 42.4 years, and the C-135 fleet is six times the size of the B-52 fleet, the next oldest fleet, at an average age of 41.8 years.

It is of note, however, that, because the B-52 fleet is still operated by the USAF, the corrosion costs associated with it are included in Table 3-4, which suggests that the B-52 is essentially unchanged from study to study after 1990. However, the B-52 fleet has experienced significant change in the force structure. That is, the B-52 fleet was dramatically reduced in size after the 1990 study; and the retired aircraft were, in fact, the oldest and most expensive to maintain.

**ANALYSIS AND COMPARISON OF
COST OF CORROSION MAINTENANCE RESULTS**



Table 3-3: Total Corrosion Costs by Weapon Fleet, in '04 Dollars (in Thousands).

In 04 \$'s, in Thousands								
Aircraft Type	Total Costs by Fleet				Fleet Size by Year			
	1990	1997	2001	2004	1990	1997	2001	2004
C-135	\$122,459	\$220,670	\$324,334	\$351,070	731	602	582	576
B-1	1,366	7,870	10,106	17,047	96	95	93	67
B-2			1,805	1,016			21	21
B-52	103,221	42,453	31,502	45,174	254	94	94	94
E-3	3,988	21,307	24,001	35,096	34	32	32	32
CLS	4,263	14,911	17,428	31,070	180	380	236	199
Misc			9,827	3,872			343	530
A-10	27,619	4,655	16,476	75,365	644	375	366	359
F-16	18,345	16,899	39,371	61,885	1433	1513	1381	1361
F-117			498	1,202			55	55
T-37	2,457	1,431	2,466	1,907	606	420	415	333
T-38	14,133	25,653	21,073	16,401	807	451	490	489
C-5	18,354	112,294	118,738	109,215	127	126	126	126
C-17			7,351	19,662			76	109
C-130	148,781	55,117	84,985	120,388	737	694	691	672
F-15	25,154	35,560	45,896	74,999	877	737	737	734
Helo's	5,235	2,709	6,666	24,086	233	215	205	200
U-2			1,381	2,540			35	34
J-Stars			5,850	2,765			9	16
A-7	1,726				365			
A-37	372				67			
F-4	28,974				906			
F-5	78				7			
OV-10	3,709				78			
F-111	45,054	8,339			270	37		
C-141	74,002	110,134	28,413	2,622	270	220	102	59
Totals with Retired Fleets	\$649,292	\$680,002	\$792,318	\$997,382				
Totals '04 Active Fleets	\$495,376	\$561,529	\$763,905	\$991,995	8722	5991	6075	6007

Table 3-4: Per Aircraft Costs for All Aircraft Types in '04 Dollars (in Thousands).

In 04 \$'s, in Thousands								
	Per AC Costs				Fleet Size by Year			
	1990	1997	2001	2004	1990	1997	2001	2004
C-135	\$168	\$367	\$557	\$609	731	602	582	576
B-1	14	83	109	254	96	95	93	67
B-2			86	48			21	21
B-52	406	426	335	481	254	94	94	94
E-3	117	666	750	1,097	34	32	32	32
CLS	24	39	74	156	180	380	236	199
Misc			29	7			343	530
A-10	43	12	45	210	644	375	366	359
F-16	13	11	29	45	1,433	1,513	1,381	1,361
F-117			9	22			55	55
T-37	4	3	6	6	606	420	415	333
T-38	18	57	43	34	807	451	490	489
C-5	145	891	942	867	127	126	126	126
C-17			97	180			76	109
C-130	202	79	123	179	737	694	691	672
F-15	29	48	62	102	877	737	737	734
Helo's	22	13	33	120	233	215	205	200
U-2			39	75			35	34
J-Stars			670	173			9	16
A-7	5				365			
A-37	6				67			
F-4	32				906			
F-5	11				7			
OV-10	48				78			
F-111	167	225			270	37		
C-141	274	501	279	44	270	220	102	59
All Fleets	\$74	\$114	\$131	\$164				
'04 Active Fleets	\$57	\$94	\$126	\$164	8,722	5,991	6,075	6,007

3.3.3 Per Aircraft Corrosion Cost Comparisons

The section that follows further develops the costs of corrosion maintenance related to aircraft, and examines the corrosion maintenance costs on an individual aircraft basis. As can be seen from the figure below (Figure 3-5), there is a significant difference in the costs for bomber, cargo, and tanker aircraft types and for the attack and fighter aircraft types. When data is presented in table format all the data is included, but when the costs per aircraft are presented in chart formats, they will often be separated into these groupings.

Per Aircraft Cost Comparison

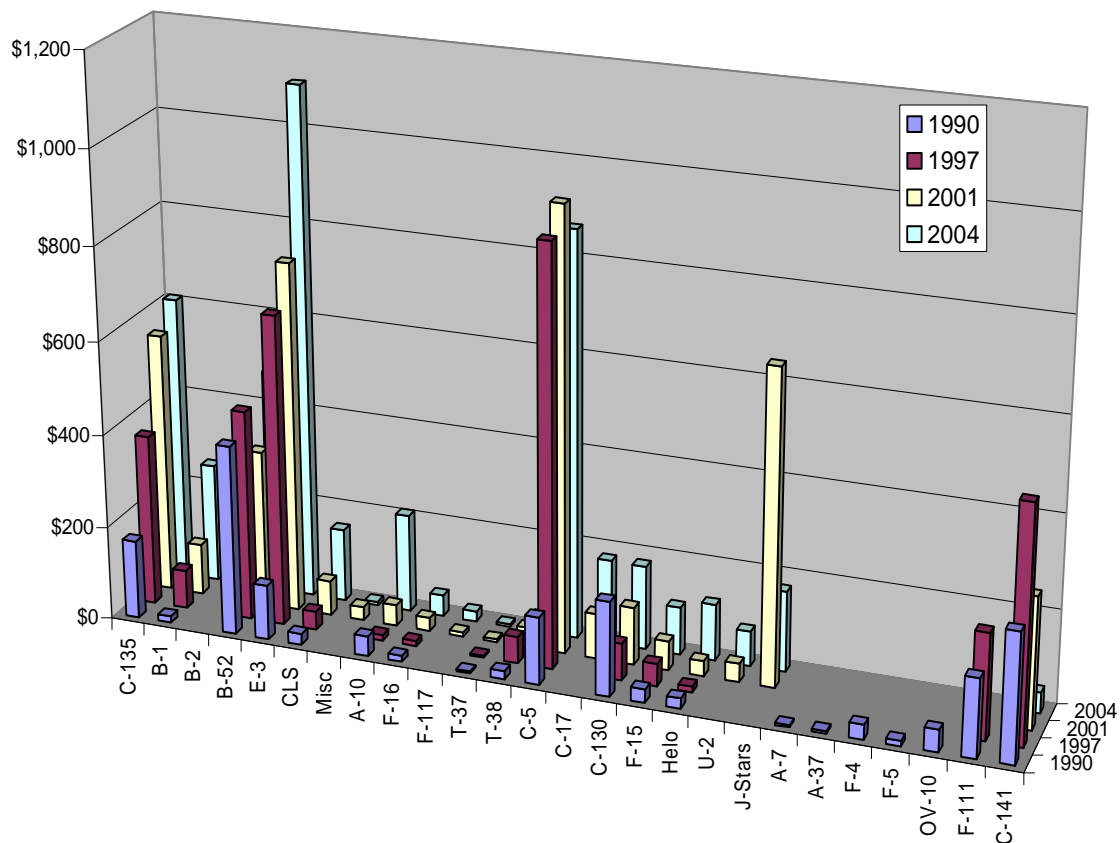


Figure 3-5: Per Aircraft Cost Comparison, '04 Dollars (in Thousands).

It is worth noting that while the C-135 fleet accounts for roughly 35% of the total USAF aircraft fleet corrosion costs, it is not the most expensive aircraft to maintain on a per aircraft basis. The most expensive to maintain on a per aircraft basis is the E-3, followed by the C-5. The E-3 fleet is much younger than the C-135, at an average age of 23.8 years, but as a 707 airframe, it has many of the problems associated with the C-135, plus the added burden of the large radome attached, and while the C-5, like the E-3, is about half the age of the C-135, at an average age of 23.56 years, it is also the larger aircraft with an empty weight over 3.5 times that of the C-135.

3.3.4 USAF Depot Costs

Table 3-5 presents total depot costs by study year. The first column is an identifier for each of the USAF aircraft major maintenance depots (OC – Oklahoma City, OK; OO – Ogden, UT; SM – Sacramento, CA; SA – San Antonio, TX; and WR – Warner Robins, GA. Due to internal USAF reorganizations, depot

operations at San Antonio and Sacramento were closed after the 1997 study). It is quite obvious from the magnitude of these numbers that the cost of corrosion maintenance at the depots is the main driver for corrosion maintenance costs overall and in particular for aircraft.

Table 3-5: Total Depot Costs in '04 Dollars (in Thousands).

Total Depot Costs				
	1990	1997	2001	2004
OC	\$220,441	\$295,539	\$398,297	\$454,765
OO	92,809	44,107	158,076	323,018
SM	130,205	28,639		
SA	46,773	129,697		
WR	221,603	191,936	271,583	249,182
Totals	\$711,832	\$689,917	\$827,955	\$1,026,965

The figure below (Figure 3-6) makes very plain in a graphical format the changes, not only in overall cost, but also in the structure of the depot maintenance. The Air Force has gone from five depots to only three, but the corrosion work requirements remain, and despite dropping from five ALCs to three, the overall costs have increased.

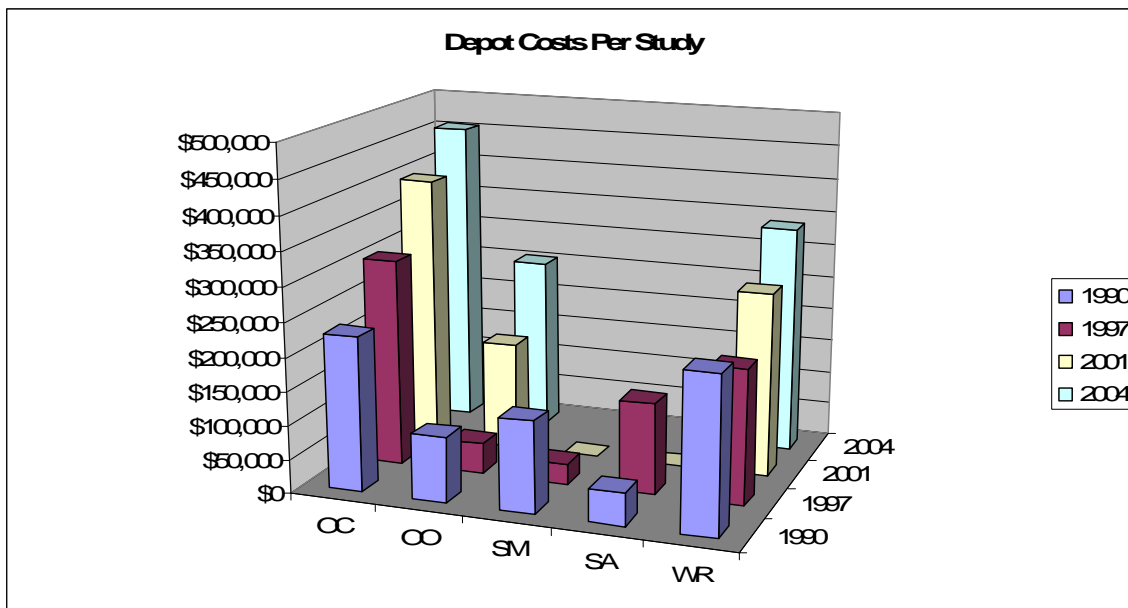


Figure 3-6: Depot Costs in '04 Dollars (in Thousands).

The following table, Table 3-6 Detailed Depot Costs, provides the depot costs by more detailed cost elements from study to study. Overall these costs have increased 43% since 1990 – that despite significant decreases in forces. Costs have increased 23% at the depots between 2001 and 2004. Most of the increase from the previous study has been in depot paint costs. See Section 3.4 for a discussion of why costs have increased as they have.

Table 3-6: Detailed Depot Costs in '04 Dollars (in Thousands).

Depot Cost, Detailed 1990, 1997							
	1990			1997			
	Repair	Paint	Total	Repair	Paint	Other	Total
OC	\$179,674	\$40,767	\$220,441	\$220,482	\$67,290	\$7,766	\$295,539
OO	90,283	2,526	92,809	7,001	9,569	27,537	44,107
SM	122,318	7,888	130,205	4,438	1,652	22,549	28,639
SA	43,497	3,276	46,773	80,035	46,868	2,795	129,697
WR	203,573	18,030	221,603	148,187	15,064	28,685	191,936
Total	\$639,334	\$72,488	\$711,832	\$460,143	\$140,441	\$89,332	\$689,917

Depot Cost, Detailed 2001, 2004						
	2001			2004		
	Repair	Paint	Total	Repair	Paint	Total
OC	\$305,2691	\$93,036	\$398,297	\$132,788	\$321,977	\$454,765
OO	143,190	14,885	158,076	65,780	257,237	323,018
WR	299,688	41,895	271,583	43,953	205,229	249,182
Total	\$678,138	\$19,816	\$827,955	\$242,521	\$784,444	\$1,026,965

The non-depot costs increased 38% from 2001 to 2004, and part of that increase in maintenance cost can be attributed to improvements in data collection methodologies and command personnel cooperation. However, unlike the changes in methodology between 1997 and 2001 when the study changed from using on-line databases as a data source for organizational maintenance costs, to command generated responses, there were very few changes in methodology between the current study and the 2001 study. The majority of the vast increase in costs can be attributed to the sharp increase in labor costs for Blue Suit maintenance, which increased from roughly \$25 per hour to \$37 per hour. (See the 2004 Cost of Corrosion Final Report, [1], for a discussion of the source of these rates.)

3.4 EXAMINATION OF COST DRIVERS

The data collected over the course of four Cost of Corrosion Studies and the results presented in this report, have painted a largely unambiguous picture of rapidly increasing corrosion maintenance costs. In fact, a fortune teller would have a clear picture of future cost growth based on the data thus far presented. However, to thoroughly cloud the clarity, one need only attempt to explain why corrosion maintenance costs have grown as rapidly as they have. Namely, have the costs for corrosion maintenance grown due to an increased need for the maintenance itself, driven perhaps by the effects of age and environment, or are other explanations required? Has the need for corrosion maintenance grown? It is reasonable to observe the clearly increasing costs for corrosion maintenance and conclude that age and use and environment have led to an ever increasing need for corrosion control maintenance, and the ever increasing level of maintenance required has led to the observed increasing costs. But, does the data collected support this interpretation? As the previous sections have made clear, the majority of the costs for corrosion maintenance are related to

Programmed Depot Maintenance (PDM) costs, thus, answers to the nature of the increasing costs will be sought via an examination of depot aircraft corrosion maintenance costs.

3.4.1 Examination of Depot Cost Drivers

The data collected over the three most recent Cost of Corrosion Studies were examined to determine if it were possible to identify an increasing maintenance requirement. This set of data was chosen because:

- 1) The 1990 study did not provide the same level of detail as the subsequent studies (the goal of determining the total cost of corrosion maintenance for the first time ever rather than developing the detailed cost elements in a consistent manner); and
- 2) The vast change in force structure between 1990 and 1997 would skew the examination.

Two maintenance elements were examined, addressing the main cost drivers in every corrosion cost study – depot level paint and repair. The following figures, Figure 3-7 and Figure 3-8, present the work load associated with painting and repairing aircraft at the depots for the years 1997, 2001, and 2004.

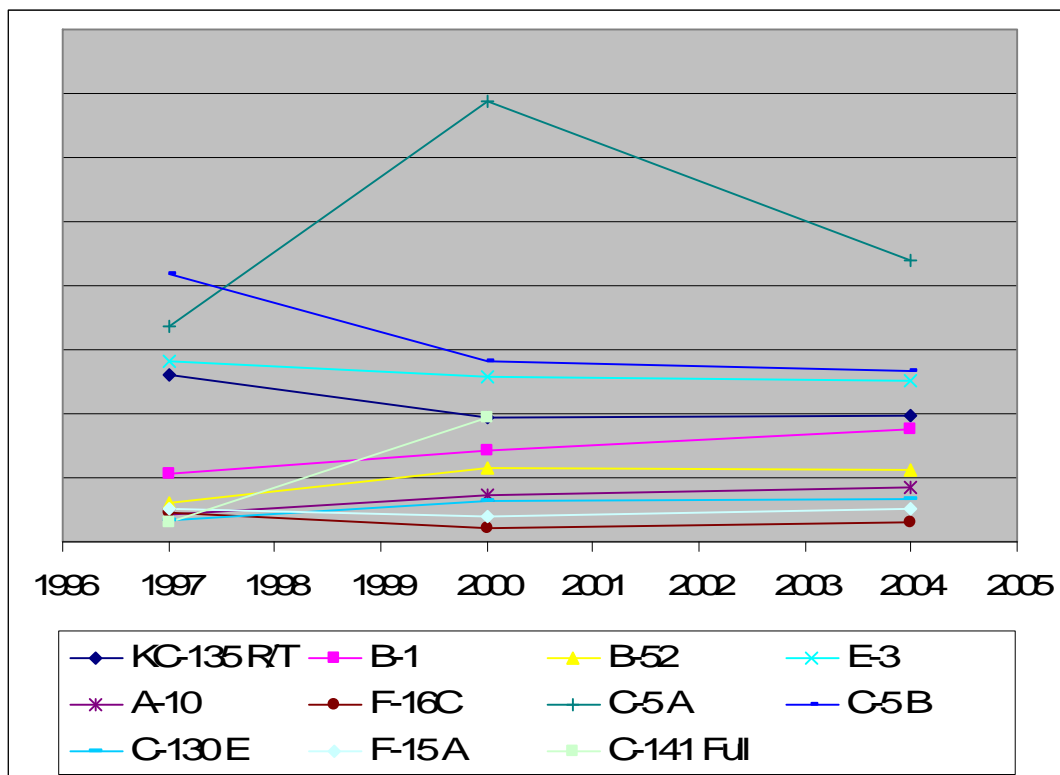


Figure 3-7: Paint Man-Hours.

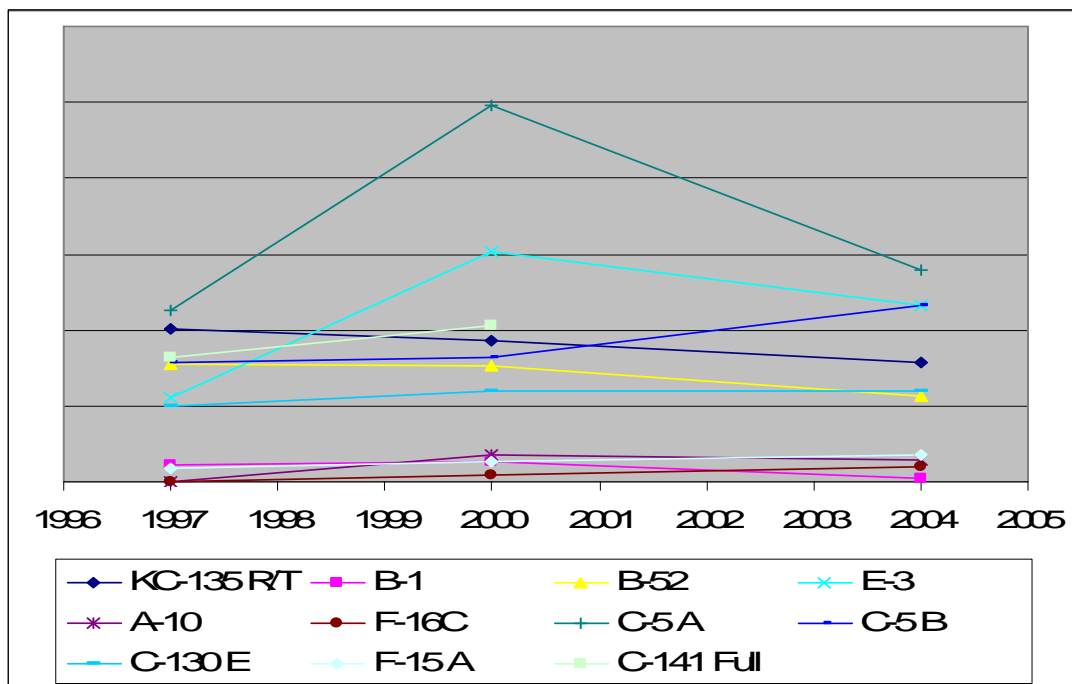


Figure 3-8: Repair Labor.

3.4.2 Paint

The following figure presents an examination of depot paint man-hours – that is the hours for the “strip and repaint” or the “scuff sand and repaint” tasks for each aircraft type. The conclusion to this chart is that there is no obvious growth in the level of effort necessary to paint aircraft at the depots over the course of the past three studies, but in fact the labor requirements for painting has remained amazingly stable.

3.4.3 Repair

The steady labor requirement for painting aircraft at the depots is perhaps not a surprise, once the requirement to strip and repaint most aircraft has been levied and a process developed, there is no real requirement for increasing labor hours to accomplish this activity. If there is an age, mission, and environmental driver for rapidly growing corrosion maintenance, it should appear in the repair aspect of depot maintenance. The following figure presents the labor associated with corrosion repair.

Again, Figure 3-8 appears to present a picture of fairly consistent corrosion repair labor requirements. Figure 3-9 below presents the reported/calculated corrosion percentage of depot effort over time, again suggesting a picture of steady corrosion work requirements, rather than a continuously growing proportion of the overall depot maintenance requirement.

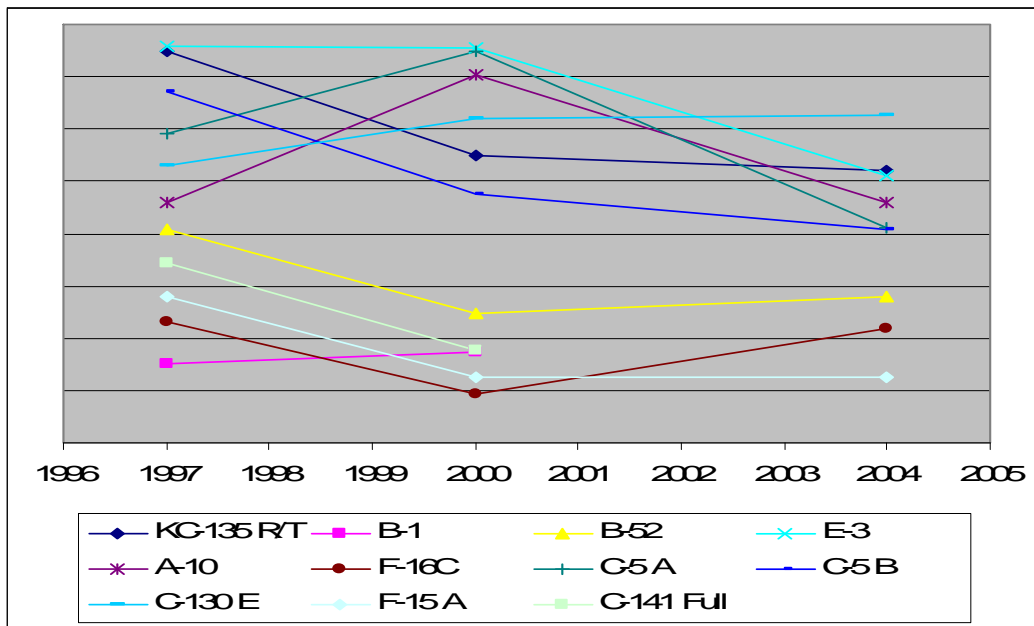


Figure 3-9: Corrosion Percentage of Depot Maintenance.

3.4.4 Labor Rates

What then explains the rapid increase in corrosion maintenance costs, if the amount of actual labor fails to explain the rapid cost growth? The following chart presents the changes in the depot labor rates from study to study, and a clear upward trend in the rates is very evident.

It is clear from Figure 3-10, that depot labor rates are increasing sharply, while corrosion maintenance measure in hours is largely constant. The increase in labor rates is clearly the major driver of the sharp increase in corrosion maintenance costs.

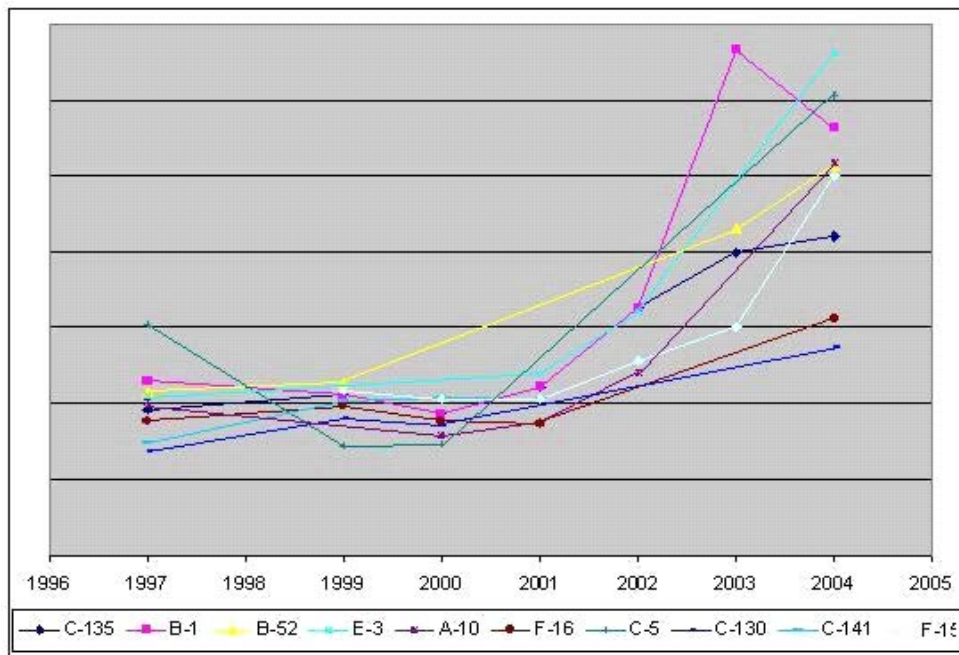


Figure 3-10: Depot Sales Rates Trend Over Time.

The fact that costs have risen sharply, not due to increased workload, but due to increasing depot sales rates, **does not preclude an aging and environmental corrosion effect on costs**. The depot sales rate includes the costs for materials and supplies, and the nature of aging aircraft – old parts with changing manufacturers, etc., can mean that at least part of the increase in rates is a function of the aging fleets.

A further concern is the methodology of the study and the effect rising rates can have. That is, the depot costs for the studies are dependent on the hours allocated to tasks via the MRRB process. With the Depot Sales Rates rising rapidly, it is reasonable to expect pressure to control the hours for repairs. It is further possible to envision greater hours being necessary to accomplish a task on the depot floor than are approved, but with the increasing rates making up the difference between the hours expended and the hours charged. As very anecdotal evidence, at least one corrosion manager was told by a contractor (off the record) that they (the aircraft management) can scrutinize the package of hours, but if the hours are cut the rates will rise to compensate. Thus, in contradiction to much of this section, it is possible, despite the evidence to the contrary, that corrosion work is increasing and that that work is reflected in the costs, and the interaction between rates and hours yields a true cost picture; but a confusing one when either is examined independently. On the other hand, the increasing sales rate might be driven by health care costs, previous year cost overruns, etc. – all beyond the purview of the corrosion maintenance costs study.

3.5 CONCLUSIONS

Having now had four separate cost of corrosion studies accomplished over a fourteen year span and performed using essentially the same techniques has allowed the generation of a number of comparative analyses [9],[10]. The more significant among these were:

- Over the fourteen-year period, the cost of corrosion maintenance has grown more than 25% above the cost of inflation. Most of this cost growth has occurred in the aging aircraft fleets.
- Corrosion maintenance has consumed an ever-increasing amount of the USAF O&M budget (2.86% – 3.88%).

- For corrosion cost trends to be most meaningful, Force Structure changes must be considered.
- Corrosion prevention activities consumed 27% of corrosion maintenance dollars.
- The depot level Paint and Repair man hours have remained essentially constant over the timeframe 1997 – 2004.
- The corrosion percentage of the total depot repair hours has remained essentially constant over the last seven years.
- The depot labor rate has escalated dramatically since 1997, and especially since 2001.
- The depot labor rate increase is not a result of a dramatic increase in direct labor cost; rather it appears to be a result of greatly increased overhead costs. Causes of these increases were not a specific data collection goal of the present study; however, the authors would speculate that there are two significant causes of this growth. The cost of replacement parts for aging aircraft has increased a great deal as the Original Equipment Manufacturers have moved on to other projects, and the parts now have to be provided by second tier suppliers at greatly increased cost. In addition, the costs of processes of corrosion maintenance have increased dramatically with the advent of increased demand for environmental and OSHA compliance.

3.6 ACKNOWLEDGEMENTS

The authors acknowledge significant contributions from several sources. Funding for accomplishment of each of these studies was provided by the USAF Corrosion Prevention and Control Office, located at Warner Robins Air Logistics Center, Georgia. Throughout the extended period covered by these studies, they were sponsored, guided, and directed by Mr. Richard Kinzie, since retired from government service. Without his active assistance in surmounting the many roadblocks that threatened each of these studies, we could never have completed any of them. The contributions from the engineers at each of the depots cannot be overemphasized. Responding to questions and providing detailed deconstruction of MRRB brochures takes a great deal of time out of otherwise very busy days, and we simply could not have completed these studies without their involvement. Finally, the cooperation of the corrosion managers at each of the USAF Major Commands was crucial to success in obtaining accurate and complete field level data. With this level of cooperation and assistance in providing all the data we asked for, or could possibly need, any errors or oversights were the fault of the authors, not of the active Air Force personnel (military and civilian) who assisted so ably in these cost studies.

3.7 REFERENCES

- [1] “Cost of Corrosion”, Final Report, C² Technology, Inc., February 2005.
- [2] “Collection/Assessment of United States Air Force Corrosion Costs”, Systems Exploration, Inc., April 1992.
- [3] “A Study to Determine the Annual Direct Cost of Corrosion Maintenance for Weapon Systems and Equipment in the United States Air Force”, NCI Information Systems, Inc., 26 June 1998.
- [4] “Cost of Corrosion”, NCI Information Systems Inc., May 2003.
- [5] “Air Force Space Digest”, Air Force Association, May 2004.
- [6] “Air Force Space Digest”, Air Force Association, May 1991.
- [7] “Air Force Space Digest”, Air Force Association, May 1998.

- [8] “Air Force Space Digest”, Air Force Association, May 2000.
- [9] “Cost of Corrosion Follow-up Analysis”, Systems Exploration Inc., 1989 – 1990.
- [10] “Analysis and Comparison of Cost of Corrosion Maintenance Results”, C² Technology, Inc., February 2005.

Chapter 4 – CORROSION MORPHOLOGY: DOCUMENTING CORROSION

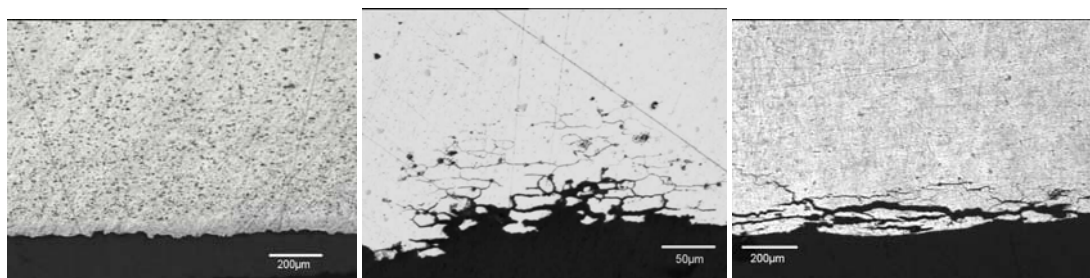
Nicholas C. Bellinger
Institute for Aerospace Research
National Research Council Canada
Ottawa, Ontario
CANADA

4.1 INTRODUCTION

Since corrosion can evolve from initial discontinuity states (e.g., constituent particles) present within metallic materials, these modified states have to be taken into account when carrying out a structural life assessment since they can affect both crack nucleation and growth. Therefore, it is necessary to carry out a damage characterization on naturally corroded components. Thus once a corroded aircraft component is disassembled and the corrosion products removed (depending on the type of corrosion), the damage that is present can be determined using a number of different techniques; optical microscopy, laser scanning confocal microscopy, scanning electron microscopy and x-ray. This section reviews the methods typically used in this characterization work and illustrates the type of information that can be obtained.

4.2 OPTICAL METHODS

The only technique that is capable of characterizing the different damage states present for all types of corrosion (pitting, exfoliation, intergranular, etc.) is optical microscopy [1],[2]. To document the damage, sections should be taken from the affected areas, cold mounted and progressively polished using standard metallurgical practices, examples of which are shown in Figure 4-1. It is essential to mount the sections for polishing using a cold resin in order not to affect the corrosion damage.



(a) Images from naturally corroded 2024-T3 fuselage lap joints.



(b) Image from exfoliated 7178-T6 upper wing skins.

Figure 4-1: Optical Micrographs Showing the Modified Discontinuity States from Naturally Corroded Components that were Progressively Polished.

From this type of study, the growth of different types of damage can be estimated, which could then be used to more accurately predict the life of components that are susceptible to corrosion. For example, a damage characterization study was carried out on corroded lap joints in which sections were taken and progressively polished [1]. From the different images, corrosion pit sizes were measured taking into account the presence of intergranular attack. The results, shown in Figure 4-2, indicated that as the thickness loss increased the pit shape tended to become elongated (shallow but long). As can be seen from this figure, as the thickness loss increased, the pit shapes tended to take on a high aspect ratio, shallow but long. The exception to this trend was the pits that were present at the base of environmentally assisted cracks, which occurred in the presence of a sustained stress, EAC_{ss} , and have been referred to as pillowing cracks. Previous studies have shown that these cracks usually occurred in areas where the thickness loss was small and only a small pit was present at the faying surfaces. Since the material thinning was high in the area examined during this study, it is assumed that these large pits developed over time after the environmentally assisted crack had nucleated.

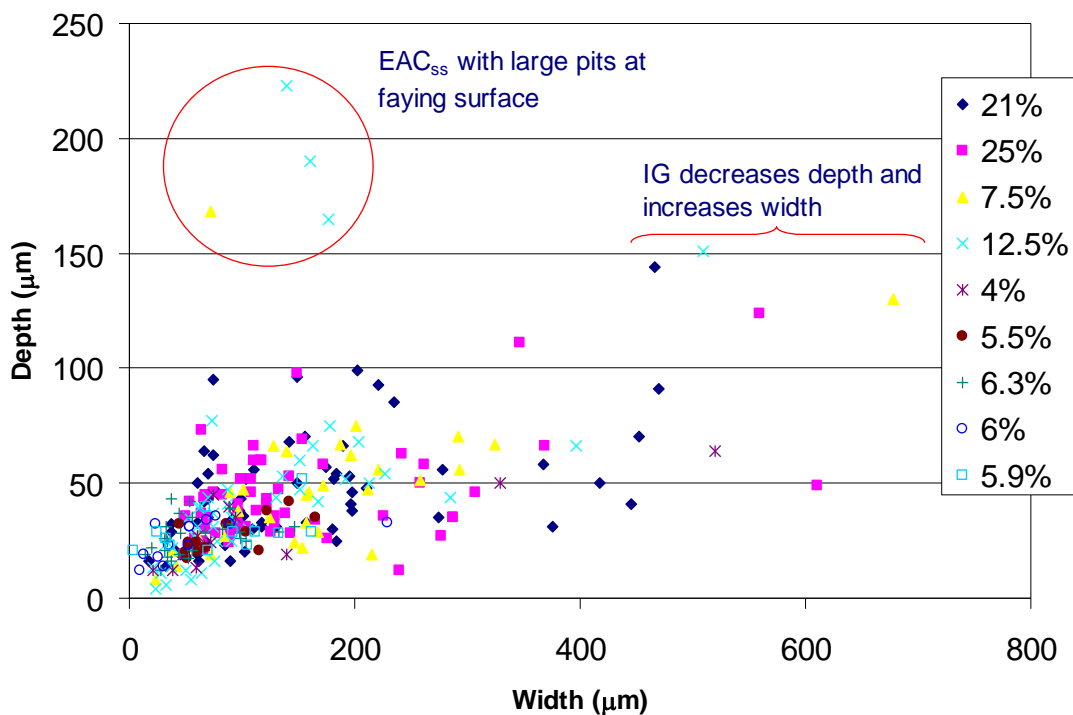
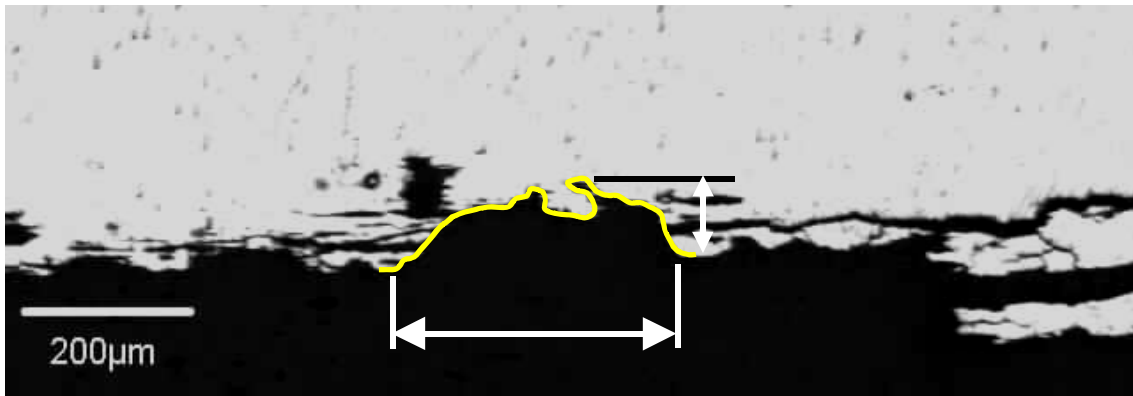
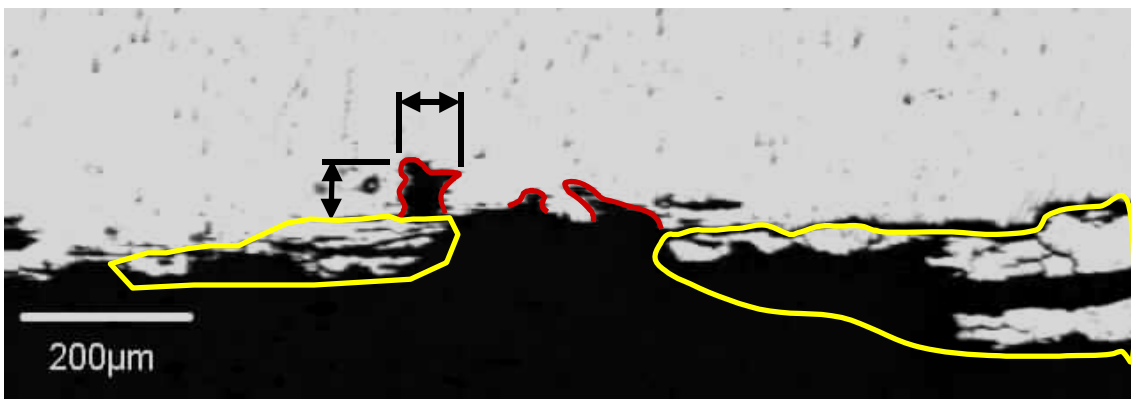


Figure 4-2: Corrosion Pit Sizes Measurements from Optical Micrographs of Naturally Corroded Components Progressively Polished.

The other microscopic techniques, laser scanning confocal microscopy and scanning electron microscopy are capable of determining small changes in the surface topography. However one disadvantage to using these techniques is that the damage that is present must be on a direct line of sight in order to measure its size, which means intergranular cracking or corrosion cannot be detected. This type of cracking must be taken into account since the material affected by it is incapable of carrying any stress. Therefore this material would not have an influence on any pits in the immediate vicinity of the intergranular cracking and thus the stress concentration at the base of each pit would be lower than if the material surrounding the pit was undamaged. For example, as can be seen from Figure 4-3, if the intergranular crack is not taken into account the pit width and depth would be 346 µm (0.0136 inch) and 159 µm (0.00626 inch), respectively. However, the presence of the intergranular crack would increase the number of pits from one to three and the dimensions of the largest of these “new” pits would be 74 µm (0.00291 inch) wide and 64 µm (0.00252 inch) deep, which is a significant decrease. This decrease would tend to delay the onset of cracking by reducing the stress concentration at the base of the pit.



(a)

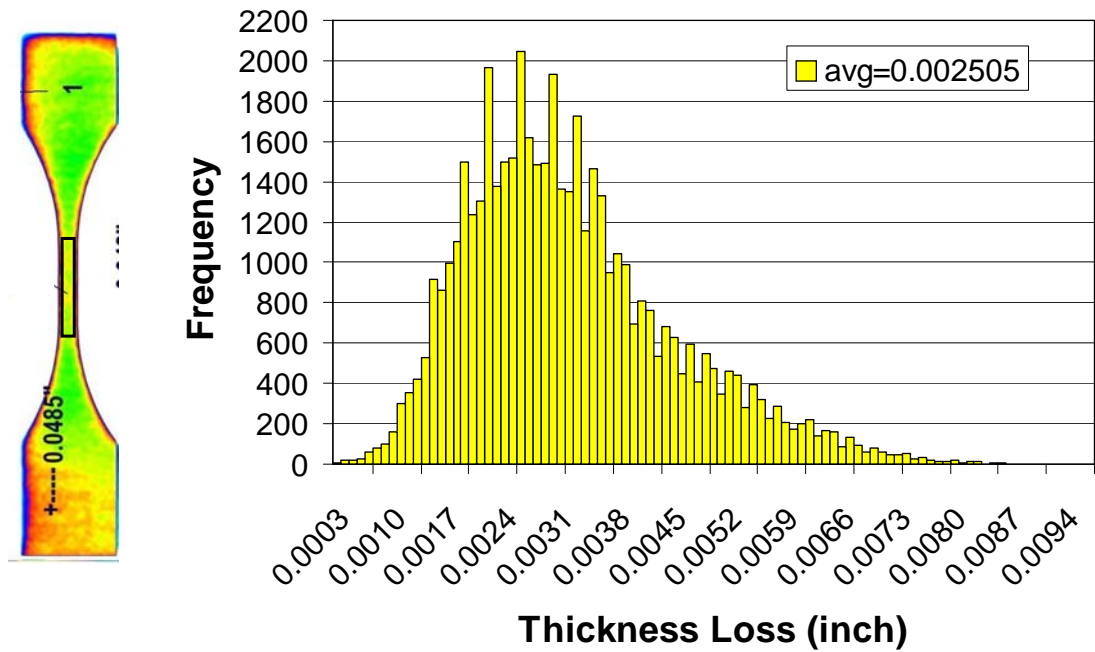


(b)

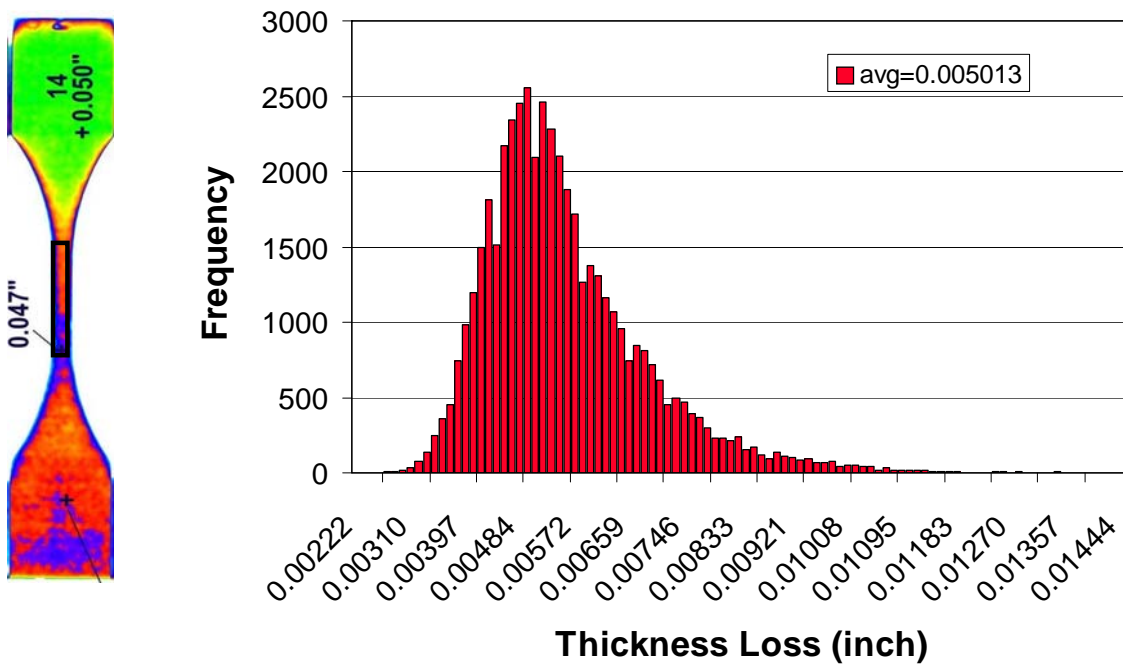
Figure 4-3: Difference in Pit Depth and Width Due to Presence of Intergranular Cracks – (a) Shape of pit if intergranular cracks ignored (pit shape determined by laser scanning confocal); (b) Shape of pits when intergranular cracks are taken into account (assume the material circled has been removed either by flaking or dissolution).

4.3 X-RAY CHARACTERIZATION

The final technique, x-ray, can only be used to document the surface topography and thickness loss associated with corrosion pitting. By using the cleaning process mentioned above to ensure that the corrosion products are removed from the pits in the affected areas, x-ray techniques can accurately document the surface topography present. After digitizing the radiographs and with the aid of the appropriate software, the average and maximum thickness loss can be determined in the affected area as well as the pit distribution, as shown in Figure 4-4. From these types of plots, trends can be determined for the mode of pit growth. For example, the pit distributions shown in Figure 4-4, obtained from 2024-T3 corroded lap joints, demonstrate that as the average thickness loss within an aluminum skin increases, the scatter in pit size decreases, indicating that the pit shape becomes more uniform.



(a) Average thickness loss on gauge length of 4.85% in a 0.0516 inch thick skin.



(b) Average thickness loss on gauge length of 7.60% in a 0.0516 inch thick skin.

Figure 4-4: Histogram Plot of Thickness Loss of Different Coupons.

4.4 REFERENCES

[1] Bellinger, N.C., Forsyth, D.S. and Komorowski, J.P., “Damage Characterization of Corroded 2024-T3 Fuselage Lap Joints”, Proceedings of the 5th Joint NASA/FAA/DoD Conference on Aging Aircraft, Kissimmee, FL, USA, 10-13 September 2001.

- [2] Bellinger, N.C., Komorowski, J.P., Liao, M., Carmody, D., Foland, T. and Peeler, D., “Preliminary Study into the Effect of Exfoliation Corrosion on Aircraft Structural Integrity”, Proceedings of 6th Joint FAA/DoD/NASA Conference on Aging Aircraft, San Francisco, CA, USA, 16-19 September 2002.



Chapter 5 – PITTING CORROSION: MORPHOLOGY AND CHARACTERIZATION

David W. Hoepfner

Professor and Director, Quality and Integrity Design Engineering Center (QIDEC)
Mechanical Engineering Department, University of Utah
Salt Lake City, Utah
USA

5.1 INTRODUCTION

Pit formation is a concern for integrity of components of aircraft for many reasons as cited in Chapter 13. Pits not only form local discontinuities (MDS – Modified Discontinuity States) but also serve as the nucleus of cracks under both sustained loading and cyclic loading of structural components.

In corrosion fatigue conditions, several studies have shown greater increase in fatigue crack growth rates compared to “baseline” fatigue conditions. Although major efforts have been expended to understand the crack propagation behavior of materials, a few studies have focused on the crack nucleation stage in the overall fatigue process. McAdam first suggested that corrosion induced pits might act as stress concentrators from which cracks could form [1]-[3]. A large number of chemical or electrochemical factors such as potential, passive film, pH, and composition of environment are found to affect the pitting corrosion fatigue process. As well, mechanical factors such as stress range, frequency, stress ratio (R), load waveform and metallurgical factors such as material composition, microstructure, heat treatment, and grain orientation can influence pitting corrosion fatigue processes. Nucleation of cracks from corrosion pits was observed by many researchers [1]-[19] including the works of Hoepfner [20]-[21], McAdam [22], and Goto [23] in heat-treated carbon steel, and Muller [24] in several steels. As well, in NaCl environment, lowering of the fatigue life due to the generation of pits in carbon steel [21],[22] and 7075-T6 Aluminum alloy [6],[21] was observed under corrosion fatigue conditions.

Once the pit forms, the rate of pit growth is dependent mainly on the chemical composition of the material, the microstructure of the material, temperature, duration of attack, local solution conditions, and the state of stress. Cracks have been observed to form from pits under cyclic loading conditions. Therefore, to estimate the total corrosion fatigue life of a structural component made of a given material it is of great importance to develop some realistic models to establish the relationship between pit propagation rate and the state of stress. This will also be discussed in Chapter 13. Furthermore, pitting corrosion in conjunction with externally applied mechanical stresses, for example, cyclic stresses, has been shown to severely affect the integrity of the oxide film as well as the fatigue life of a metal alloy. To understand and estimate the effects of pitting as well as to formulate repair procedures on components where pitting corrosion has been detected it is necessary to be able to characterize the pits.

5.2 PITTING CORROSION

Pitting is a form of localized corrosion that proceeds because of local cell action once the pitting potential has been attained under a given set of conditions for a given material in a given chemical environment. It is involved in causing serious integrity concerns related to several of the items noted above.

The autocatalytic reaction involved in pitting corrosion produces cavities/EDS (Evolving Discontinuity States) beginning at the surface and taking a myriad of shapes and sizes depending on both the microstructure of the material and the electrolyte and various electrochemical factors. One of the items to be dealt with in this chapter is the importance of attempting to characterize pitting corrosion. This needs to

be done in order to evaluate the requirement for removal of pitting once it is discovered, to analyze the significance of it in a corrosion and corrosion fatigue design system and to assure safety can be maintained even if pits of a certain character are present but not found in non-destructive inspection for one reason or another.

Temperature and time of exposure are critical parameters involved in the thermodynamics and kinetics of pitting corrosion. The cavities/EDS that form may or may not become filled with corrosion products. Pitting processes often proceed in growth by a combination of both intergranular attack and dissolution of the pit “walls”. As the pits are evolving they are referred to as Evolving Discontinuity States (EDS). If the process is fixed at time t the state is referred to as a Modified Discontinuity State (MDS). The characterization of both the EDS and the MDS has been of concern to scientists and engineers since the study of pitting corrosion began.

Pitting occurs when an electrolyte begins to allow the transport of ions between an anode and cathode. Only a small amount of metal is corroded and this is usually referred to as localized attack. The anticipation of pitting on structural members is a critical factor in maintaining component integrity and safety in some cases.

Inspection and characterization of pits in laboratories and in field applications is a challenging endeavor. This is done to establish the shape and general morphology of pits and to establish their surface dimensions and shape. Pit depths can be measured using a calibrated microscope focused first on the top of the pit and then on the bottom of the pit. More discussion of characterization of pits will follow.

Efforts have been made to treat the rate of corrosion pitting penetration into materials statistically. All the models known to date involve expressions for depth or area of pits, thus emphasizing the need for characterization. For example, equations have been developed to predict the perforation of boiler tubes, buried steel pipelines, critical components of aircraft and related areas. There is much work underway on pitting in both power plants and pipelines at present. The characterization of pitting has been of major concern to various types of power plants for many years.

In the airframe (both fixed wing and rotary wing) and aero-engine industry pitting has been recognized as a potential safety issue for some time and produces obvious maintenance concerns. Until recently both USAF and the USA FAA did not consider pitting or other mechanisms of corrosion as safety concerns. Since the Aloha Airlines accident of 1988 this has changed and in 1998 the FAA started requiring design for corrosion as a threat to structural integrity. However, most companies and government agencies are still in the embryonic stage with regard to design for pitting corrosion and similar threats. In addition, the USAF is in the process of modifying Mil Handbook 1530 to include corrosion as a consideration in design for structural integrity.

The efforts of Bob Jeal and David Hoepfner in moving toward a HOLISTIC Structural Integrity design framework (1985) [25],[26] has influenced some companies and government agencies to move toward a HOLSIP framework. The Canadian Department of National Defence (DND), led by efforts at NRC-IAR, has done an extensive amount of work to establish methods for characterizing corrosion and developing models to validate its prediction on aircraft structures. In addition, the British Royal Navy and Air Force through their ESVRE (Establish, Sustain, Validate, Recover, Exploit; ES<Air> Structures Support Group – UK) has implemented tools to design for corrosion effects in structural integrity and to maintain aircraft structures through their program. JAXA (the Japanese Aerospace Laboratory) and the Japanese equivalent to the USA Occupational Health and Safety efforts have begun implanting design for corrosion. Many of the activities mentioned are discussed in annual HOLSIP (Holistic Structural Integrity Processes) meetings that have been held since 2002. (See www.holsip.com). These organizations as well as AP/ES, and the University of Utah have done much research on attempting to characterize pits and incorporate them into models.

It has been shown that the rate of penetration of pits in aluminum exposed to water follows a cube root curve. The following equation represents Godard's model:

$$d_{\max.} = C(t)^{1/3} \tag{1}$$

where: d = maximum pitting depth

t = time

C = a parameter related to the combination of material and environment

The importance of an expression such as that above is that it provides a means of estimating the depth of pits from knowledge of the time of exposure. Thus it is very useful in models to estimate the significance of corrosion pits in affecting structural integrity. The use of this expression is discussed more in Chapter 13. A diagram depicting how this equation usually plots from data is shown below in Figure 5-1.

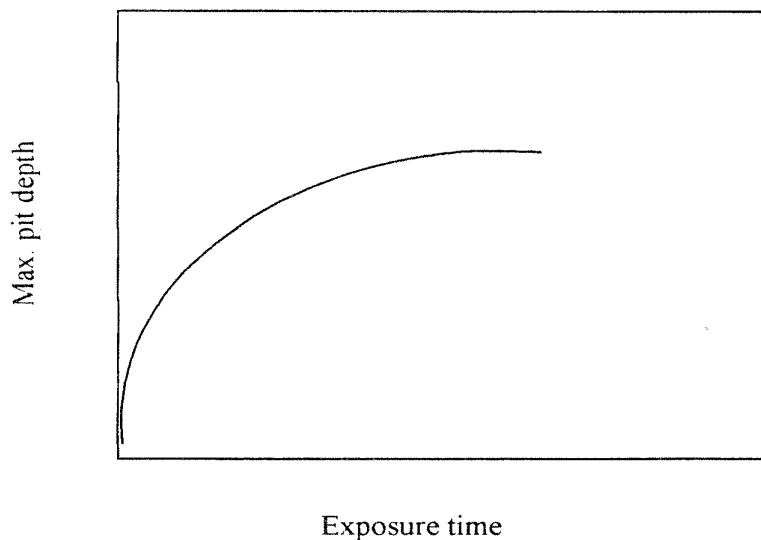


Figure 5-1: Schematic Diagram Showing the Relationship Between Penetration Depth and Exposure Time.

Equations incorporating the model above have been used extensively in models for pitting corrosion fatigue as will be discussed in a later section of this report. The greatest challenge in using the expression above, or similar ones, is in determining the pit depth. A brief discussion of how this pit characterization has been attempted is presented below. In attempting to detect corrosion pits and characterize their size and shape many approaches have been used.

5.2.1 Pit Characterization

Early workers studying pitting used various optical techniques to attempt to characterize pits. It became clear that this was not acceptable since it was virtually impossible to capture the depth and complex shape of pits below a surface. Optical techniques did prove useful for area determination related to surface area. But it was recognized by most researchers that the most important parameter related to assessing pit criticality was the depth. This dimension also is used extensively in maintenance for corrosion and rework considerations. Thus, in recent years more emphasis has been placed on developing methods of determining pit depth and shape. The following methods have been more extensively used in recent years:

- 1) Sectioning;
- 2) Replication and examination in scanning electron microscopes;
- 3) Examination of pit profiles subsequent to fracture or sectioning;
- 4) Use of confocal microscopy; and
- 5) Eddy current probes of various types.

Obviously any destructive technique on actual components is not that useful. Thus some rework or “blend” methods suggest or require attempting to use visual or other NDI as corrosion pits are blended out and then specifying a depth for additional removal of material to assure any remaining pit induced degradation will also be removed.

In research at the University of Utah over the last 25 years confocal microscopy has proved the most useful to determine pit depth, and pit shape to some extent, but does require observation in a laboratory setting. Thus it is not useful for field use at present. Many challenges with respect to evaluation of the threat of pitting to structural integrity arise in the field after pits have either caused a major failure or have been detected in areas of components where they were not expected and were not considered in the original structural integrity evaluation. The determination of pit depth remains a great challenge in these situations.

The ASTM G46¹ Standard Guide for the “Examination and Evaluation of Pitting Corrosion” is one of the most advanced descriptions of how to characterize pitting. This is one of the major starting points for all those interested in characterizing, evaluating and modeling pitting corrosion. The ASTM standard G15² entitled “Standard Terminology Relating to Corrosion and Corrosion Testing” is important to obtain and use in characterizing pitting corrosion as well as all forms of corrosion. Figure 5-2 below shows how pits may be classified by density, shape and size in the standard. In addition, Figure 5-3 shows the cross-sections and the variation according to the standard G46. The Advisory Circular AC 43-4A also has a way to classify pits [27]. However it tends to be very qualitative in nature and tends to concentrate on repair of pitting as well as other corrosion mechanisms. The document classifies pitting as **light** when at a depth of 0.025 mm (0.001 inch) maximum. Moderate pitting is viewed as potentially 0.25 mm (0.010 inch) and notes this type of damage is usually removed by “extensive mechanical sanding”. It does little to clarify what “extensive mechanical sanding” is and how deep or extensive it must be done. Pages 124-5 of reference 27 do state some guidelines but don’t emphasize the issue of characterizing pitting corrosion [28]. One of their statements is that the “pit has been cleaned up to the extent that all loose corrosion products have been removed”. Of course they do not mention the important issue of tunneling often connected with pits and the issue of intergranular attack and cracking that occurs with pit formation. Thus, due diligence must be exercised when removing by blending and sanding to “eliminate” pits. Much more effort must be expended on characterizing pits by NDI methods such as eddy current techniques or others in order to assure all traces of corrosion pitting degradation have been eliminated.

¹ ASTM Standard G46, Guide for the Examination and Evaluation of Pitting Corrosion, AMERICAN SOCIETY FOR TESTING AND MATERIALS, 100 Barr Harbor Dr., West Conshohocken, PA, USA, Approved on a regular basis.

² ASTM Standard G15, Standard Terminology Relating to Corrosion and Corrosion Testing, AMERICAN SOCIETY FOR TESTING AND MATERIALS, 100 Barr Harbor Dr., West Conshohocken, PA, USA, Approved on a regular basis.

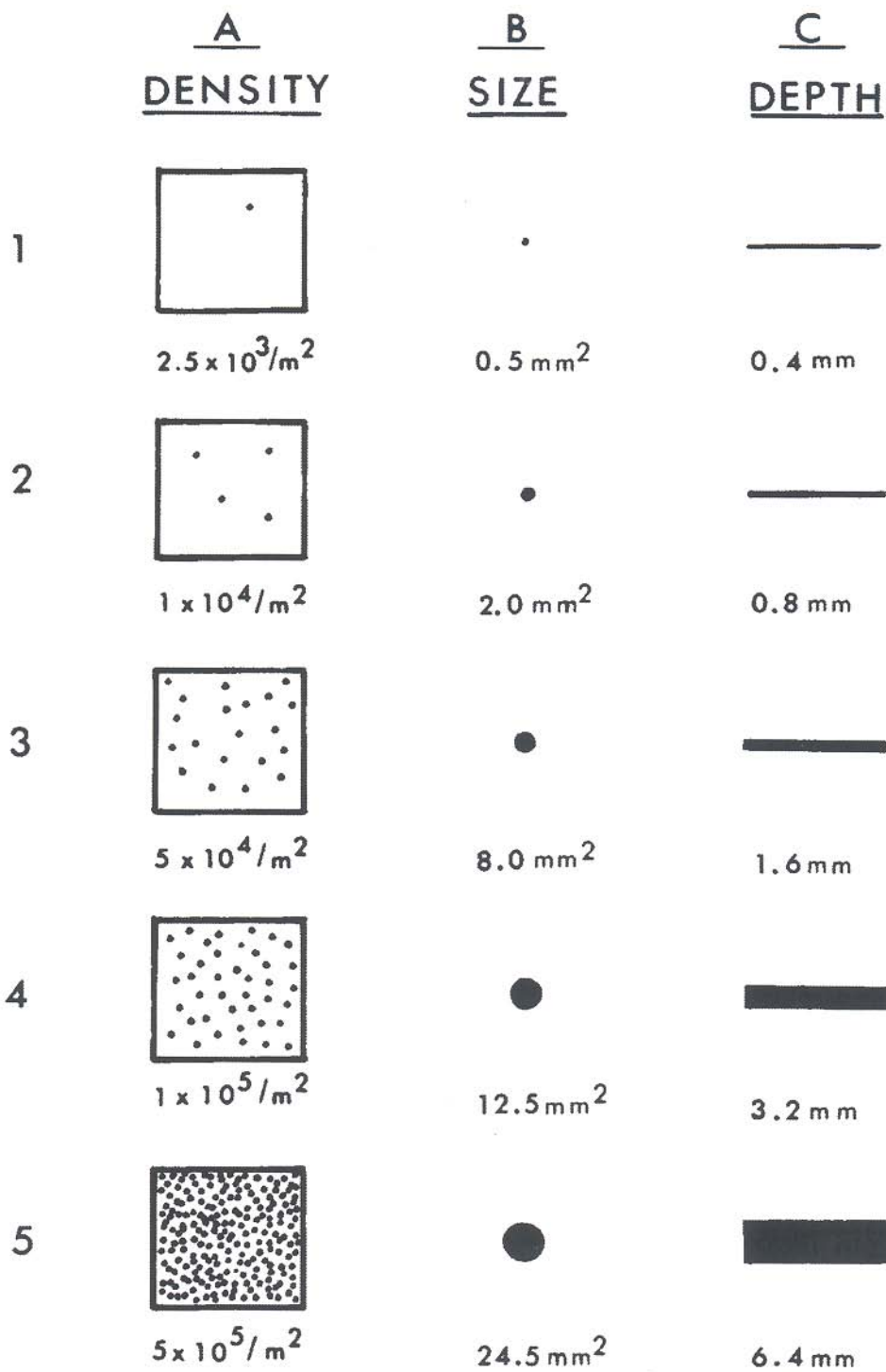
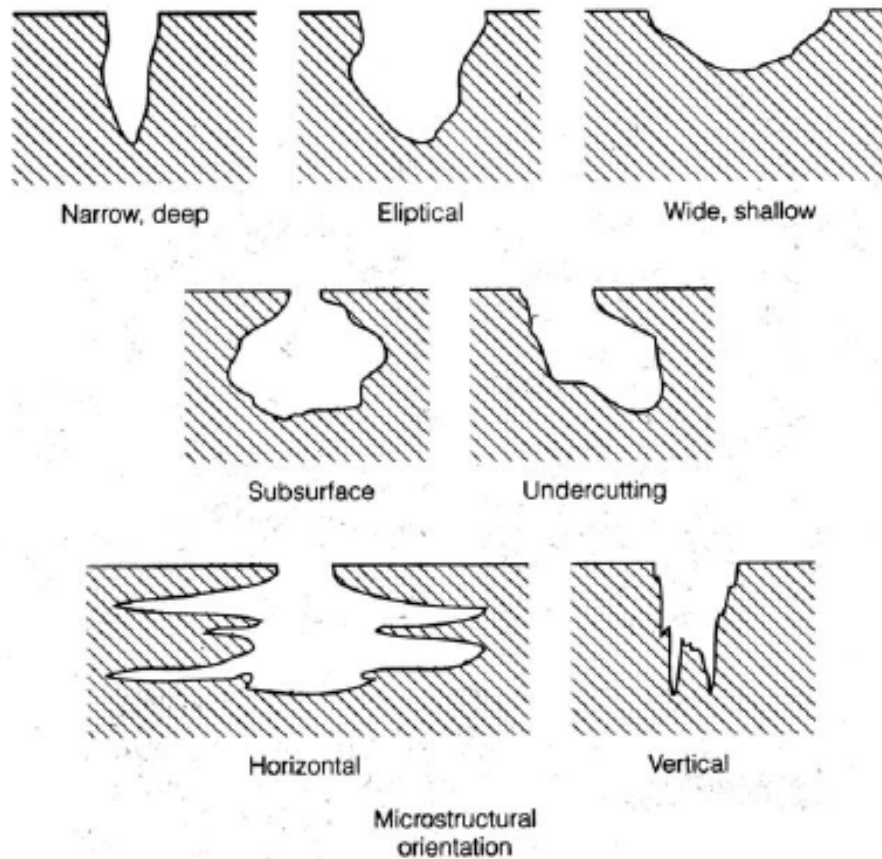


Figure 5-2: ASTM Standard G46 Showing Means of Characterizing Pit Density, Size, and Depth (Copyright ASTM).



Variations in cross sectional shape of pits. (ASTM G 46)

Figure 5-3: ASTM Standard G46 Portion Showing Variation of Pit Character (Copyright ASTM).

5.2.2 Examples of Pitting Encountered in Components

In the design of aircraft, damage due to corrosion mechanisms, and especially pitting, has not been considered as a criterion for determining either Structurally Significant Location (SSL) or Structurally Significant Items (SSI). Although most airframes, and power plants, have a Corrosion Prevention and Control Program (CPCP) they are designed for integrity under either the safe life or damage tolerant paradigms. Neither of these has considered corrosion in a critical way other than to use a CPCP. Thus stress or damage related allowables are generally not available for the various corrosion mechanisms. For example, if one were to query what the corrosion or corrosion fatigue pitting allowable is for a given component it would not likely be available. This is unfortunate since if corrosion pitting is found the only alternative becomes a repair to attempt to remove all of the pitting even though that is difficult on many occasions. The CPCP approach has provided some measure of protection and control but has proved to be inadequate. For this reason corrosion often is detected by diligent maintenance personnel or it becomes a recognized problem only when a failure has occurred in areas of components where it was not anticipated. Inspections often are “of opportunity” and neither quantified nor directed for corrosion. The issue of directed NDI (Non-Destructive Inspection) does occur after a problem has been identified by one means or another. In order to quantify and direct the inspections the following must be specified and placed in the maintenance manuals to some degree:

- 1) An indication of the **exact type of corrosion** being looked for should be specified. (What to look for!)

- 2) The **location** which is to be inspected must be clearly spelled out. (Where to look!)
- 3) The specific inspection **equipment** and **method** should be specified. (How to look!)
- 4) Either the **time of use or flight cycles** or both should be specified in order to specify when to look.
- 5) The **frequency** of inspections and time between inspections should be specified. (Repeat inspection interval for corrosion-how often to look)
- 6) The **detection threshold** for the type of corrosion should be specified.
- 7) The **Probability Of Detection (POD)** for the type of corrosion should be specified.

In the case of pitting corrosion the items above often are not defined until an accident, an incident, or an unexpected detection has occurred and is viewed as critical to safety. At that point the above often have been defined. In addition, detailed repair procedures often are developed at that point as well.

The following is an example of unexpected pitting corrosion on a “non-critical component” detected in service. The C130 aircraft, used in many countries throughout the world, was found to have cracking in a fitting that is in the rear of the aircraft and is referred to as either the “Porkchop” fitting or the “hockey stick fitting”. Which reference is used is a function of the country in which the problem was discovered. Some indicated the problem was due to stress corrosion. This is not viewed likely since the component experiences cyclic loads. When both DND, Canada, and the New Zealand forces were experiencing cracking of the component they decided to have competent failure analysis labs evaluate the cracked fittings further. Thus, the Aerospace and Maritime Research Laboratory (AMRL) in Melbourne, Australia and the Quality Engineering Test Establishment (QETE) in Gatineau, Quebec, Canada performed failure analyses on the subject components. Additional failure analysis was done by the University of Utah Quality and Integrity Design Laboratory (QIDEC) and IAR (Institute of Aerospace Research) in Ottawa, Ontario, Canada. Figure 5-4 and Figure 5-5 show two views of the pits that nucleated the fatigue cracks. In addition, growth rings typical of fatigue, in this case most likely environmentally assisted fatigue crack propagation, are also clearly apparent. AMRL and QETE were both helpful in identifying the true failure mode in this case. The subject component had not been identified as a structurally significant item. The cracking was found initially by diligent maintenance personnel. Subsequent to the discovery of the corrosion pitting as the source of the cracks a program was put into place to monitor the area in question for corrosion thereby preventing the rampant formation of both corrosion pits and fatigue cracking. This was a significant aid to all the forces flying this particular transport aircraft.

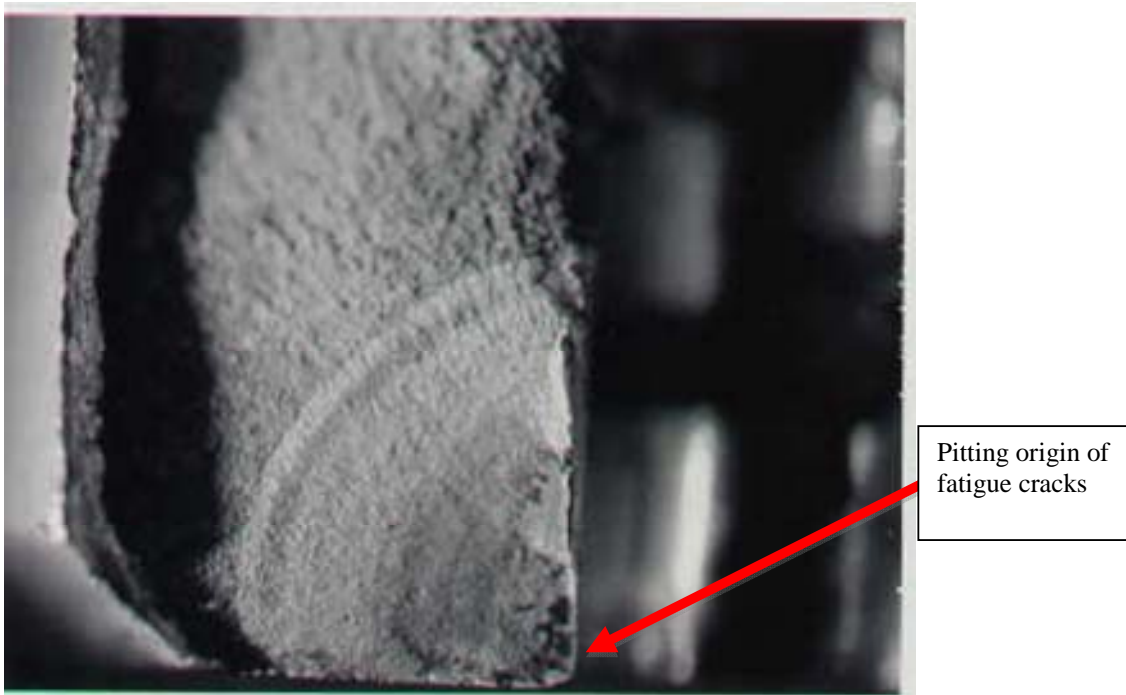


Figure 5-4: Fracture Surface of C130 “Porkchop” Fitting that Unexpectedly Failed from Pitting that Transitioned into Cracks.

(Photo by Ms. Amy Taylor, and David W. Hoepfner, University of Utah, 1999. Crack started at a pit at the lower right corner and propagated by corrosion fatigue mechanisms. This was commonly observed.)

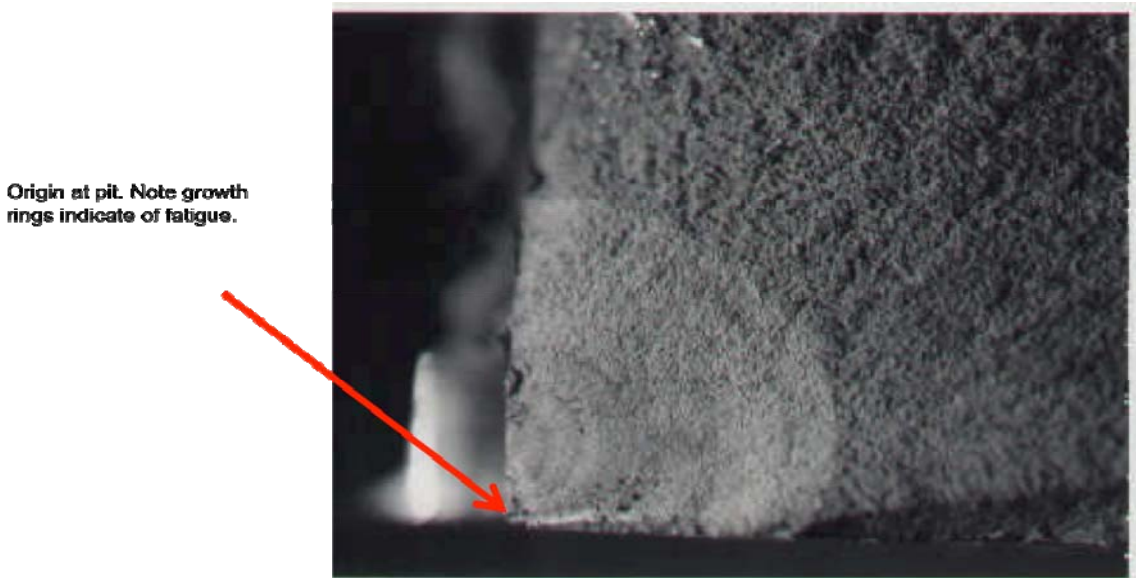


Figure 5-5: A Second View of the Fracture Surface of C130 “Porkchop” Fitting that Unexpectedly Failed from Pitting that Transitioned into Cracks.

(Photo by Ms. Amy Taylor, and David W. Hoepfner, University of Utah, 1999. In this view the crack nucleated at the lower left corner at a pit and propagated by corrosion fatigue. Note the growth rings as the crack propagates from the lower left toward the upper right corner of the photograph.)

Figure 5-6 and Figure 5-7 above show, respectively, the formation of fatigue cracks at corrosion pits and how fatigue cracks are observed to link pitting. It has been known for some time that both these occur. Thus, corrosion pitting often creates multiple site damage. The characterization studies done recently at the UU QIDEC laboratories have been instrumental in identifying features of pitting that are useful in modeling (see Chapter 7 and references [27]-[49]).

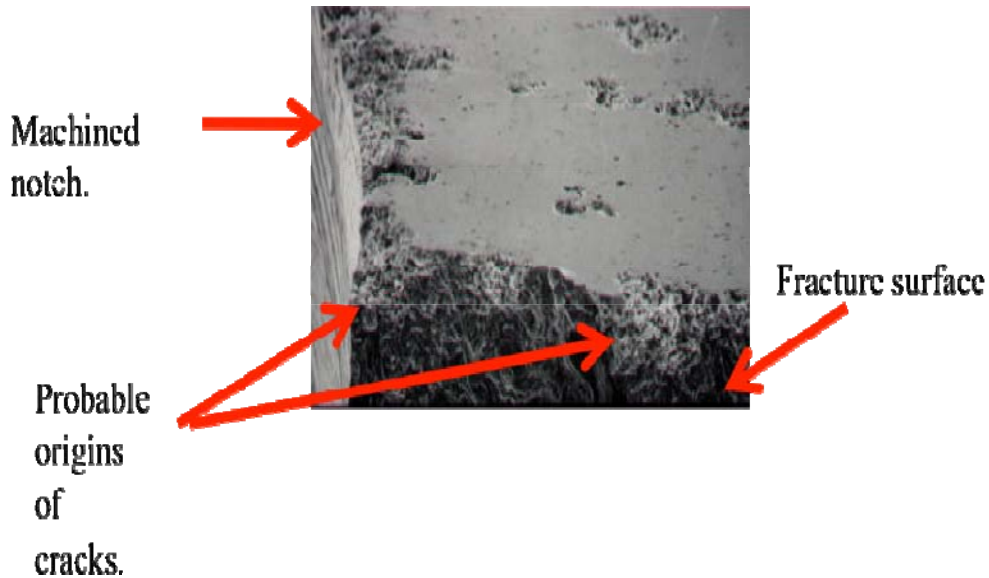


Figure 5-6: View Showing Corrosion Pits Nucleating Cracks.

Fatigue crack joining two pits. This is a common occurrence.

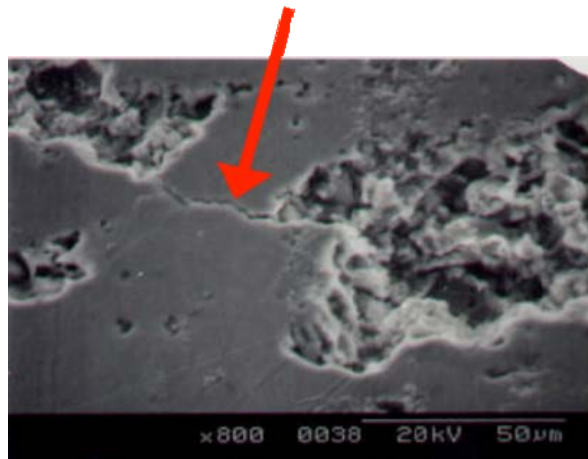


Figure 5-7: View Showing Other Pits with Fatigue Cracks Propagating Between Them.

Figure 5-8(a) below shows the frequently observed occurrence of either sustained load or cyclic load induced cracks forming and linking pits. This has significant implications in formulating repair practices and in developing accurate models to predict corrosion pit growth rates and incorporating them into

PITTING CORROSION: MORPHOLOGY AND CHARACTERIZATION

models. On the other hand Figure 5-8(b) shows a view of cracks in the bottom of pits. This observation was made quite frequently. (Although not visible in this photo cracks also were observed in pit walls. This too was frequently observed).

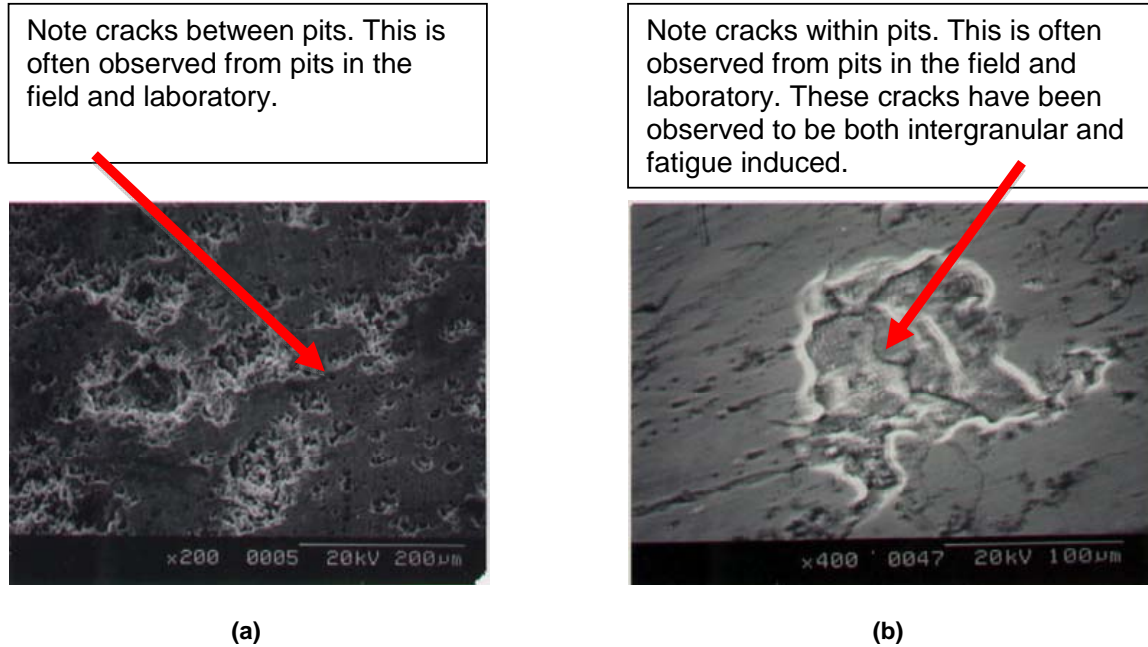


Figure 5-8: Views in the Notch of Corrosion Fatigue Specimens Tested in the QIDEC Laboratory at the University of Utah (2000). Alloy was 7075-T6 tested in 3.5% salt water.

Figure 5-9 below shows an example of an image of pits taken in a confocal microscope. The confocal microscope has been very successful in allowing the determination of pit depth and more clarity on the shape of pits as well (see Ref. [49] for more general descriptions of the use of the confocal microscope to characterize pits. This is in addition to many other references cited herein). Another example of the characterization of pits is shown in Figure 5-10. In this case the confocal microscope was used in conjunction with the SEM (Scanning Electron Microscope) to characterize the depth and shape of corrosion pits developing under corrosion fatigue test conditions. These tools proved invaluable in their ability to assist in characterizing the depth and shape for use in modeling efforts as described in Chapter 7 of this report.

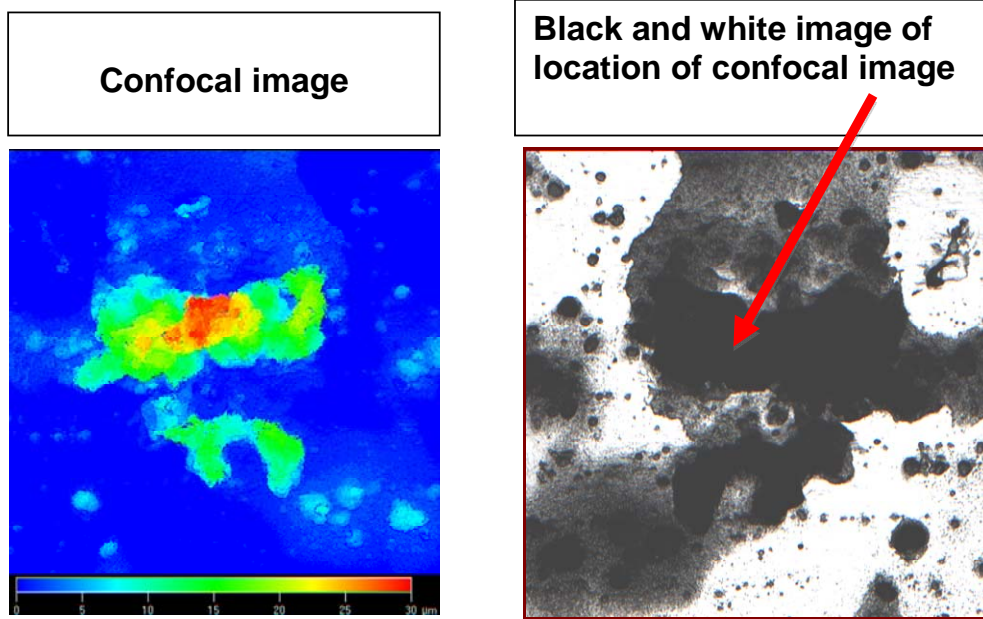
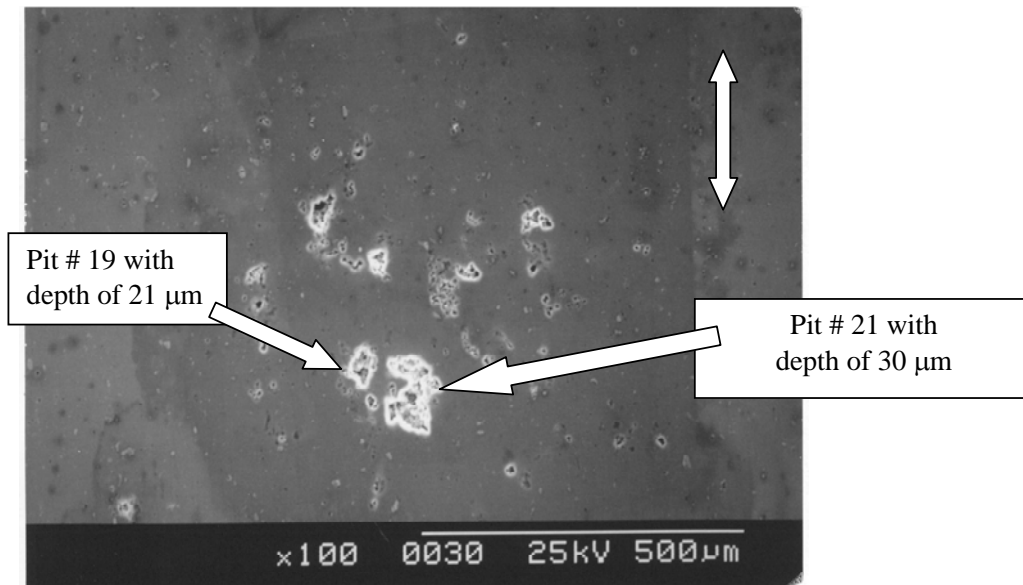
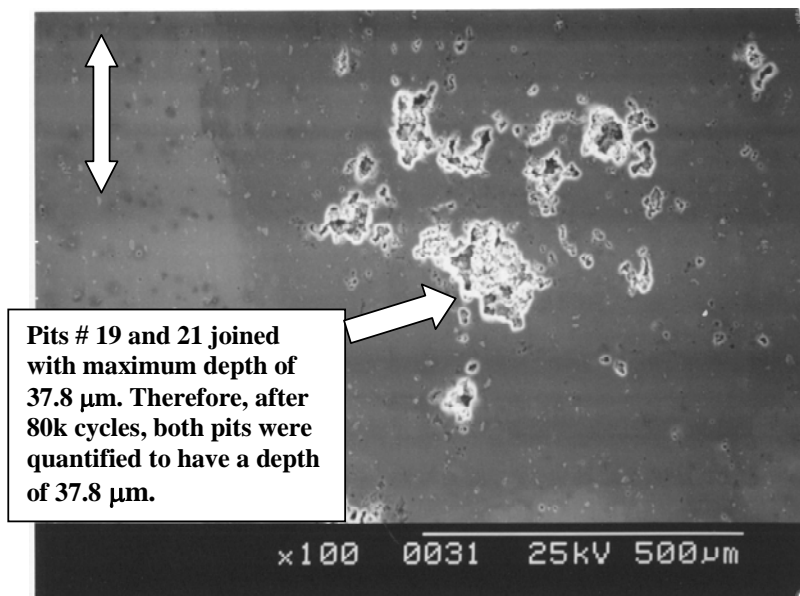


Figure 5-9: Post Corrosion Exposure of 30 Hours, $d \sim 0.0012''$ (30 μm) of Pit: Left image shows typical confocal image with variation in color showing depth – red indicates the deepest area of the pit; Image on right shows area where confocal image was taken.



(a)



(b)

Figure 5-10: SEM Photos Showing Pits Developed Under Corrosion Fatigue Conditions: (a) After 60,000 Cycles; and (b) After 80,000 Cycles. Vertical arrows indicate loading direction. Depth of pits determined by confocal microscopy. (Material was 7075-T6 tested in ASTM 3.5% NaCl solution).

5.3 CONCLUDING REMARKS

This chapter has described various techniques for characterizing pitting corrosion. Pitting has been observed to occur much more frequently than envisioned in early design of critical components of fixed wing and rotary wing aircraft. In some cases it has proved fatal due to lack of its consideration in the original design and lack of an ability to characterize it once it has been observed to occur. Some repair/

blend/sanding techniques are commonly used in maintenance to attempt to eliminate pitting. This in a sense has avoided the critical task of attempting to characterize pitting corrosion in terms of both depth and shape, and particularly shape below a surface. Thus, even though some NDI techniques have been used to attempt to assure that all detected pitting has been removed once it has been found in critical areas on critical components, much more work on quantification of NDI procedures to both detect pitting and completely characterize it are needed. In addition, much more exploration and quantification of NDI for pitting corrosion detection is needed. This included definition of the detection thresholds of various NDI practices for use in maintenance and original design. In addition, the probability of detection for various NDI practices employed to characterize pits also must be determined and included in both as well.

Another issue that is greatly needed in the future is the education of engineering students to deal with all types of corrosion on aircraft including pitting corrosion. This field has been sorrowfully neglected by the aviation industry in terms of going beyond the typical CPCP (Corrosion Prevention and Control Program). Some progress in this later area has been made but the engineering schools throughout the world still do not include enough education on corrosion and how to design for its occurrence (this is true of almost all designs and not just aircraft). The continued development of the HOLSIP concepts (Holistic Structural Integrity Design Processes) are providing much guidance on how to deal with all the issues mentioned.

5.4 REFERENCES

- [1] McAdam, Jr., D.J., "Stress-Strain-Cycle Relationship and Corrosion-Fatigue of Metals", Proceedings of the ASTM, Vol. 26 (II), pp. 224-280, 1926.
- [2] McAdam, Jr., D.J., "Corrosion-Fatigue of Non-Ferrous Metals", Proceedings of the ASTM, Vol. 27 (II), pp. 102-152, 1927.
- [3] McAdam, Jr., D.J., "Corrosion Fatigue of Metals Under Cyclic Stress", Proceedings of the ASTM, Vol. 29, No. 2, pp. 250-313, 1929.
- [4] Pettit, D., Ryder, J., Krupp, W. and Hoepfner, D., "Investigation of the Effects of Stress and Chemical Environments on the Prediction of Fracture in Aircraft Structural Materials", AFML-TR-74-183, Lockheed California Company, December 1974.
- [5] Aging of U.S. Air Force Aircraft, National Research Council (NRC) National Materials Advisory Board (NMAB) Report, National Academy Press, Washington, DC, USA, 1997.
- [6] Cole, G.K., Clark, G. and Sharp, P.K., "The Implications of Corrosion with Respect to Aircraft Structural Integrity", DSTO-RR-0102, DSTO, Melbourne, Victoria, Australia.
- [7] Groner, D.J., "US Air Force Aging Aircraft Corrosion", Current Awareness Bulletin, Structures Division, Wright Laboratory, Spring 1997.
- [8] Piascik, R.S., Kelly, R.G., Inman, M.E. and Willard, S.A., "Fuselage Lap Splice Corrosion", WL-TR-96-4094, Vol. II, ASIP, 1996.
- [9] Mills, T.B., "The Combined Effects of Prior Corrosion and Aggressive Chemical Environments on Fatigue Crack Growth Behavior in Aluminum Alloy 7075-T651", Ph.D. Dissertation, University of Utah, 1997.
- [10] Mills, T.B., "The Effects of Exfoliation Corrosion on the Fatigue Response of 7075-T651 Aluminum Plate", M.S. Thesis, University of Utah, 1994.

- [11] Chubb, J.P., Morad, T.A., Hockenhull, B.S. and Bristow, J.W., “The Effect of Exfoliation Corrosion on the Fatigue Behavior of Structural Aluminum Alloys”, in *Structural Integrity of Aging Airplanes*, pp. 87-97, 1991.
- [12] Pettit, D.E., Ryder, J.T., Krupp, W.E. and Hoepfner, D.W., “Investigation of the Effects of Stress and Chemical Environments on the Prediction of Fracture in Aircraft Structural Materials”, AFML-TR-74-183, 1974.
- [13] Swartz, D.D., Miller, M. and Hoepfner, D.W., “Chemical Environments in Commercial Transport Aircraft and Their Effect on Corrosion Fatigue Crack Propagation”, in *Estimation, Enhancement and Control of Aircraft Fatigue Performance*, Vol. I, J.M. Grandage and G.S. Jost, Eds., The proceedings of the 14th Symposium of the International Committee on Aeronautical Fatigue, Melbourne, Victoria, Australia, pp. 353-364, 3-5 May 1995.
- [14] Kramer, J. and Hoepfner, D.W., “Effects of Cyclic Immersion in 3.5% NaCl Solution on Fatigue Crack Propagation Rates in Aluminum 2024-T351”, *Proceedings of the 1995 USAF Structural Integrity Program Conference*, WL-TR-96-4093, Vol. II, pp. 1089-1112, 1995.
- [15] Mills, T.B., Magda, D.J., Kinyon, S.E. and Hoepfner, D.W., “Fatigue Crack Growth and Residual Strength Analyses of Service Corroded 2024-T3 Aluminum Fuselage Panels”, Report to Oklahoma City Air Logistics Center and Boeing Defense and Space Group, University of Utah, 1995.
- [16] Komorowski, J.P., Bellinger, N.C. and Gould, R.W., “The Role of Corrosion Pitting in NDI and in the Structural Integrity of Fuselage Joints”, in *Fatigue in New and Aging Aircraft*, Proceedings of the 19th Symposium of ICAF, 1997.
- [17] Op-cit Ref. 12.
- [18] Bellinger, N.C., Komorowski, J.P. and Gould, R.W., “Damage Tolerance Implications of Corrosion Pitting on Fuselage Lap Joints”, *Journal of Aircraft*, Vol. 35, No. 3, pp. 487-491, May – June 1998.
- [19] Bellinger, N.C. and Komorowski, J.P., “Corrosion Pitting Stresses in Fuselage Lap Joints”, *AIAA Journal*, Vol. 35, No. 3, 1997.
- [20] Hoepfner, D.W., Mann, D.S. and Weekes, J., “Fracture Mechanics Based Modeling of Corrosion Fatigue Process”, in *Corrosion Fatigue: Proceedings of the 52nd meeting of the AGARD Structures and Materials Panel held in Turkey*, 5-10 April 1981.
- [21] Hoepfner, D.W., “Corrosion Fatigue Considerations in Materials Selections and Engineering Design”, *Corrosion Fatigue: Chemistry, Mechanics, and Microstructure*, NACE, pp. 3-11, 1972.
- [22] McAdam, D.J. and Gell, G.W., “Pitting and its Effect on the Fatigue Limit of Steels Corroded Under Various Conditions”, *Journal of the Proceedings of the American Society for Testing Materials*, Vol. 41, pp. 696-732, 1928.
- [23] Goto, M. and Nisitani, H., “Crack Initiation and Propagation Behavior of a Heat Treated Carbon Steel in Corrosion Fatigue”, *Fatigue Fracture Engineering Material Structure*, Vol. 15, No. 4, pp. 353-363, 1992.
- [24] Muller, M., “Theoretical Considerations on Corrosion Fatigue Crack Initiation”, *Metallurgical Transactions*, Vol. 13A, pp. 649-655, 1982.
- [25] Jeal, R.H., “Damage Tolerance Concepts for Critical Engine Components”, Invited Keynote Paper, AGARD Conference, San Antonio, Texas, April 1985, Published in Conference Proceedings AGARD-

- CP-393, Damage Tolerance Concepts for Critical Engine Components, Invited Keynote Paper, pp. 1-1 to 1-12, October 1985.
- [26] Hoepfner, D.W., "Parameters that Input to Application of Damage Tolerance Concepts to Critical Engine Components", AGARD Conference, San Antonio, Texas, April 1985, Published in Conference Proceedings AGARD-CP 393, Damage Tolerance Concepts for Critical Engine Components, Invited Keynote Paper, pp. 4-1 to 4-16, NATO-AGARD, France, October 1985.
- [27] "Corrosion Control of Aircraft", AC 43-4A, U.S. Dept. of Transportation, Federal Aviation Administration, Washington, DC, USA, p. 151, 1991.
- [28] Op. Cit. Ref. 27, pp. 124-125.
- [29] Jones, K. and Hoepfner, D.W., "The Interaction Between Pitting Corrosion, Grain Boundaries, and Constituent Particles During Corrosion Fatigue of 7075-T6 Aluminum Alloy", International Journal of Fatigue, Vol. 31, pp. 686-692, February 2009.
- [30] Jones, K. and Hoepfner, D.W., "Prior Corrosion and Fatigue of 2024-T3 Aluminum Alloy", Corrosion Science, Vol. 48, No. 10, pp. 3109-3122, 2006.
- [31] Jones, K., Shinde, S.R., Clark, P.N. and Hoepfner, D.W., "Effect of Prior Corrosion on Short Crack Behavior in 2024-T3 Aluminum Alloy", Corrosion Science, Vol. 50, Issue 9, pp. 2588-2595, September 2008.
- [32] Clark, P.N., Jones, K., Huang, J.T. and Hoepfner, D.W., "Observations from the Inspection of an Aged Fuselage Panel", Journal of Aircraft, Vol. 42, No. 6, pp. 1403-1408, 2005.
- [33] Clark, P.N., Jones, K., Huang, J.T. and Hoepfner D.W., "Observations from the Inspection and Sectioning of an Aged Fuselage Panel", Proceedings, USAF Aircraft Structural Integrity Program (ASIP) Conference, December 2002.
- [34] Clark, P.N., Jones, K. and Hoepfner, D.W., "Pitting Behavior and Residual Fatigue Life of 7075-T6, Aluminum Extruded C-141 Wing", Proceeding, International Committee on Aeronautical Fatigue (ICAF) Lucerne, Switzerland, 2003.
- [35] Okada, T. and Hoepfner, D.W., "The Behavior of Short Cracks in Corrosive Environments for 7075 Al Alloy", Presented at ICAF 2005, Hamburg, Germany, 2005, ICAF 2005 – Structural Integrity of Advanced Aircraft and Life Extension for Current Fleets – Lessons Learned in 50 Years after the Comet Accidents, Vol. 2, Edited by Claudio Dalle Donne, Proceedings, 23rd Symposium of the International Committee on Aeronautical Fatigue, pp. 613-622, 2005.
- [36] Jones, K. and Hoepfner, D.W., "Pitting Corrosion, Grain Boundaries, and Constituent Particles: Which One Will Win the Crack Nucleation Race", Presented at the International Committee on Aeronautical Fatigue Meeting, Hamburg, Germany, ICAF 2005 – Structural Integrity of Advanced Aircraft and Life Extension for Current Fleets – Lessons Learned in 50 Years after the Comet Accidents, Vol. 2, Edited by Claudio Dalle Donne, Proceedings of the 23rd Symposium of the International Committee on Aeronautical Fatigue, June 2005.
- [37] Jones, K. and Hoepfner, D.W., "Pit-to-Crack Transition in Prior-corroded 2024-T3 Aluminum Alloy Under Cyclic Loading", Corrosion Science, pp. 2185-2198, 2005.
- [38] Jones, K. and Hoepfner, D.W., "Effect of Microstructure on Pit-to-Crack Transition of 7075 T6 Aluminum Alloy", Fatigue and Fracture Mechanics, ASTM STP 1480, R.E. Link and K.M. Nikbin

- (Eds.), American Society for Testing and Materials International, Mayfield, PA, USA, pp. 271-280, 2008.
- [39] Jones, K. and Hoepfner, D.W., "Pit-to-Crack Transition in Prior-Corroded 2024-T3 Aluminum Alloy under Cyclic Loading", *Corrosion Science*, Vol. 48/10, pp. 3109-3122, 2006.
- [40] Hoepfner, D.W., "A Review of Corrosion Fatigue and Corrosion/Fatigue Considerations in Aircraft Structural Design", Invited Paper Presented at International Conference on Fatigue of Aircraft, Lucerne, Switzerland, May, 2003, ICAF 2003 – Fatigue of Aeronautical Structures as an Engineering Challenge, Vol. 1, Edited by M. Guillaume, Proceedings of the 22nd Symposium of the International Committee of Aeronautical Fatigue, EMAS Publishing, Sheffield, England, pp. 425-438, 2004.
- [41] Jones, K., Clark, P.N. and Hoepfner, D.W., "Pitting Behavior and Residual Fatigue Life of 7075-T6 Aluminum Extruded C-141 Wing", Poster/Paper Presented at the International Committee on Aeronautical Fatigue (ICAF) Lucerne, Switzerland, 2003.
- [42] Clark, P.N., Jones, K., Huang, J.T. and Hoepfner, D.W., "Observations from the Inspection of an Aged Fuselage Panel", *Journal of Aircraft*, Vol. 42, No. 6, pp. 1403-1408, 2005.
- [43] Hoepfner, D.W., Restis, J. and Reid, L., "Fatigue Life Enhancement of Structure in the Presence of Corrosion Using Cold Expansion", Proceedings Tri-Service Conference on Corrosion, 2003.
- [44] Clark, P.N., Jones, K., Huang, J.T. and Hoepfner, D.W., "Observations from the Inspection and Sectioning of an Aged Fuselage Panel", Aircraft Structural Integrity Program, Conference 2002 Proceedings, Savannah, GA, USA, 2002.
- [45] Jones, K. and Hoepfner, D.W., "Effect of Microstructure on Pit-to-Crack Transition of 7075-T6 Aluminum Alloy", *Journal of ASTM International*, Vol. 3, No. 7, 2006.
- [46] Ma, Li and Hoepfner, D.W., "A Finite Element Model for Determining Stress Intensity Factors at Pits Formed by Pitting Corrosion Fatigue", Presented at the 12th. U.S. National Congress of Applied Mechanics, University of Washington-Seattle, Published in Conference Proceedings, p. 182, June 1994.
- [47] Bucci, R.J., Konish, H.J., Kulak, M. and Hoepfner, D.W., "A Protocol to Evaluate Consequences of Corrosion Damage in Aging Aircraft", Presented at the FAA/NASA International Symposium on Advanced Structural Integrity Methods for Airframe Durability and Damage Tolerance, Hampton, VA, USA, 4-6 May 1994.
- [48] Ma, Li and Hoepfner, D.W., "The Effects of Pitting on Fatigue Crack Nucleation in 7075-T6 Aluminum Alloy", Presented at the FAA/NASA International Symposium on Advanced Structural Integrity Methods for Airframe Durability and Damage Tolerance, Hampton, VA, May 4-6, NASA Conference Publication 3274 Part 1, September, pp. 425-440, 1994.
- [49] Grimes, L., "Corrosion Pitting Fatigue", M.S. Thesis, University of Utah (Ms. Grimes did the pioneering work on use of the confocal microscope to characterize the shape and depth of pits), 1995.

Chapter 6 – CORROSION MORPHOLOGY: INTERGRANULAR CORROSION AND EXFOLIATION

Nicholas C. Bellinger

Institute for Aerospace Research
National Research Council Canada
Ottawa, Ontario
CANADA

6.1 INTRODUCTION

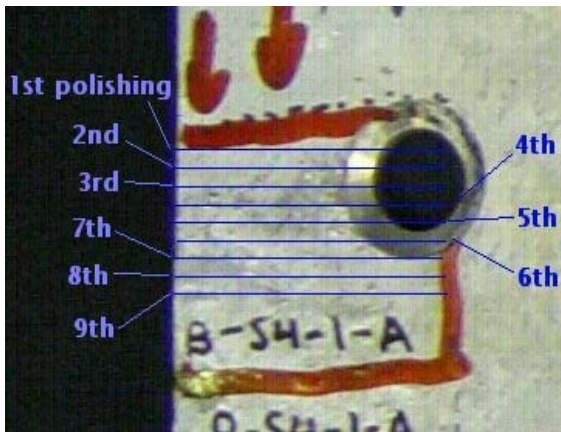
Intergranular corrosion in highly textured aluminum alloys, such as those used in aircraft structures, can cause severe flaking of the surface grains in a process commonly referred to as exfoliation. This chapter shows typical examples of this type of corrosion and describes investigations carried out at the National Research Council Canada to characterize the damage.

6.2 CHARACTERISTICS AND DOCUMENTATION

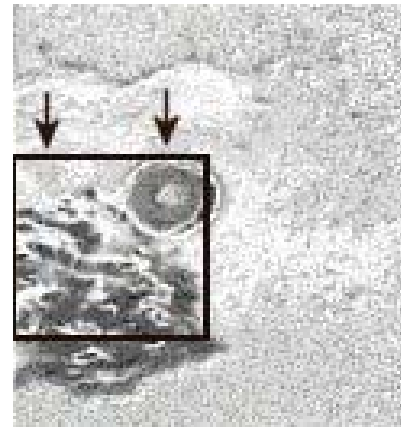
Exfoliation corrosion, or exfoliation, is defined as corrosion that proceeds laterally from the sites of “initiation” along planes parallel to the surface, generally at grain boundaries, forming corrosion products that force metal away from the body of the material, giving rise to a layered appearance [1]. In other words, exfoliation is a form of severe intergranular corrosion, which occurs at the boundaries of grains elongated in the rolling or extrusion direction. Generally, exfoliation corrosion occurs when there is a combination of three factors: a highly directional microstructure, a preferential anodic path and a specific type of corrosive environment. In aircraft materials exfoliation corrosion is most common in the heat-treatable Al-Zn-Mg-Cu (7000 series), Al-Cu-Mg (2000 series), and Al-Mg alloys, but it has also been observed in Al-Mg-Si alloys [2]. The generation of exfoliation corrosion products forces layers apart and causes the metal component to swell. Flakes of metal may be pushed up and may even peel from the surface. The results from this particular study also indicated that the depth of penetration for the exfoliation present was small and there was very little intergranular corrosion present below the main area of exfoliation.

To document the damage caused by exfoliation corrosion, sections were taken from service exposed 7178-T6 upper wing skins from retired Boeing 707 aircraft [3]. As outlined in Chapter 4, these sections were cold mounted and progressively polished to determine the damage state. An image of this section along with the NDI and polishing results are shown in Figure 6-1. It is interesting to note how the damage morphology substantially changed over a small distance, 1.067 mm (0.042 inches), from very little intergranular corrosion to considerable amounts of exfoliation. Although very little intergranular corrosion was present below the observed exfoliation, as can be seen from the arrows in Figure 6-1, the intergranular corrosion that was present was located very close to the maximum exfoliation depth. This suggests that if this area of the wing skin was repaired the intergranular corrosion would probably also be removed.

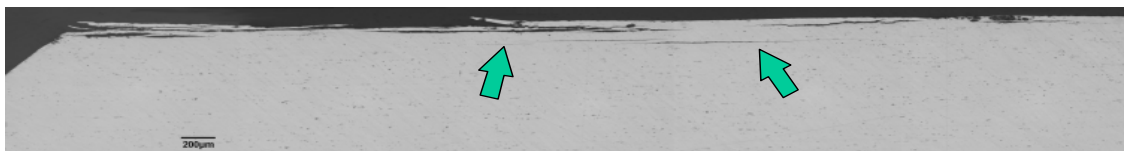
Another section that was taken from an upper wing skin contained both visible exfoliation and a repaired (ground-out) area. An image of this section along with the NDI and polishing results are shown in Figure 6-2. Although visible exfoliation was clearly present outside of the repaired area, no damage was detected within the area. It is interesting to note that as the polishing progressed the severity of the exfoliation decreased to intergranular corrosion, which extended into the repaired area. Whether the intergranular corrosion at this depth was present before the repair process was carried out could not be determined.



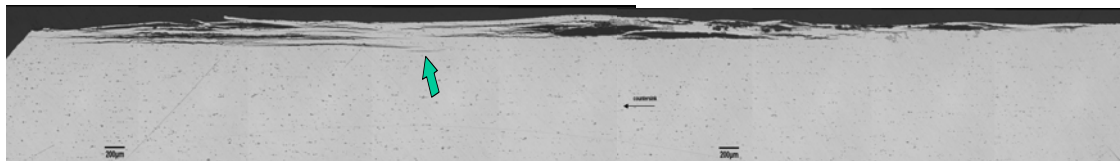
(a) Photograph of section showing locations of polishing.



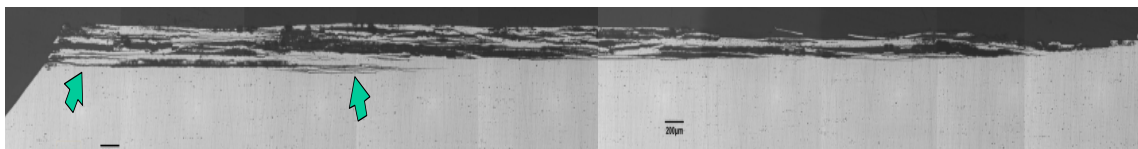
(b) Ultrasonic inspection results.



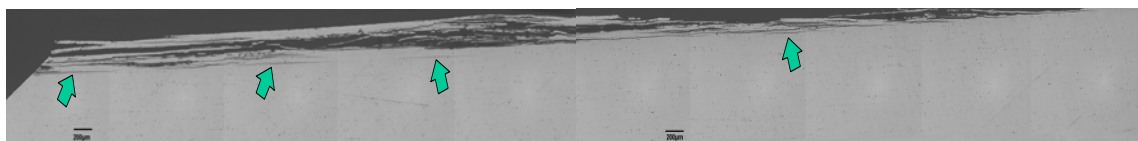
(c) Second polishing that removed 1.118 mm (0.044 inch) from the first polishing.



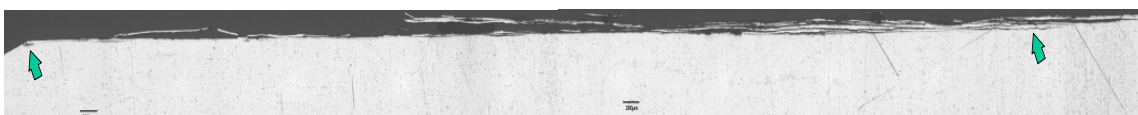
(d) Third polishing that removed 1.067 mm (0.042 inch) from the second polishing.



(e) Fourth polishing that removed 1.041 mm (0.041 inch) from the third polishing.

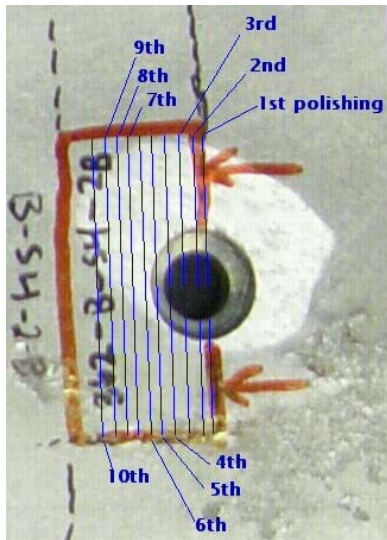


(f) Fifth polishing that removed 1.118 mm (0.044 inch) from the fourth polishing.

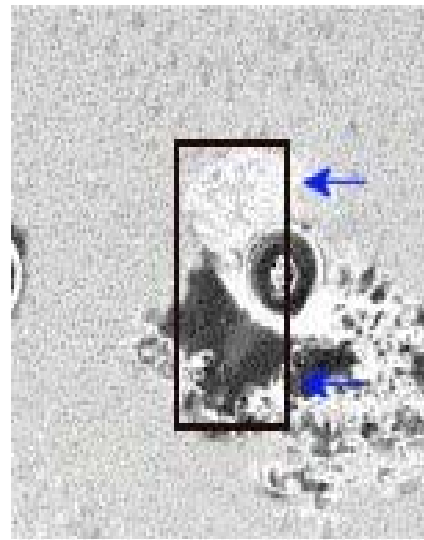


(h) Sixth polishing that removed 1.092 mm (0.043 inch) from the fifth polishing. It should be noted that additional polishing revealed similar damage to that found in the sixth polishing.

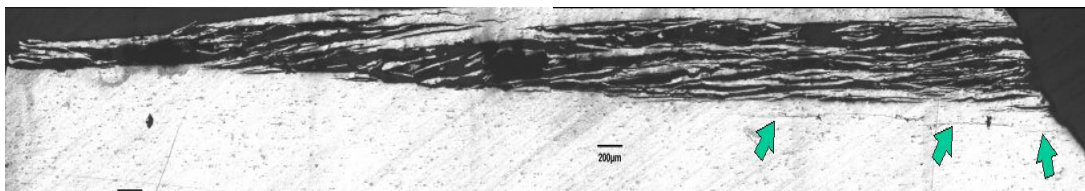
Figure 6-1: Results from the Progressive Polishing Carried Out on Specimen 362-B-S4-1 that Contained Visible Exfoliation (arrows indicate the location of the deepest intergranular attack).



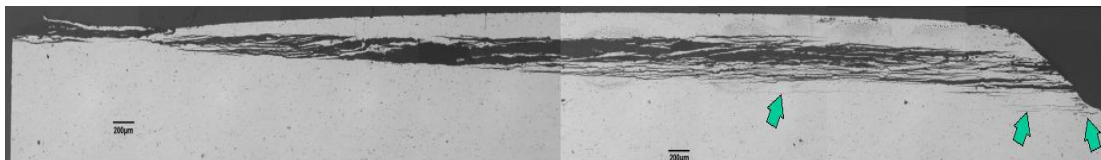
(a) Photograph of section showing locations of polishing.



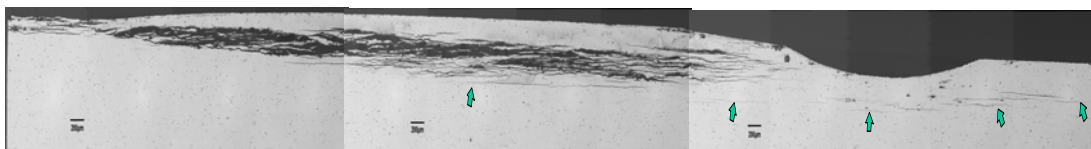
(b) Ultrasonic inspection results.



(c) First polishing.



(d) Fourth polishing that removed a total of 3.15 mm (0.124 inch) from the first polishing.



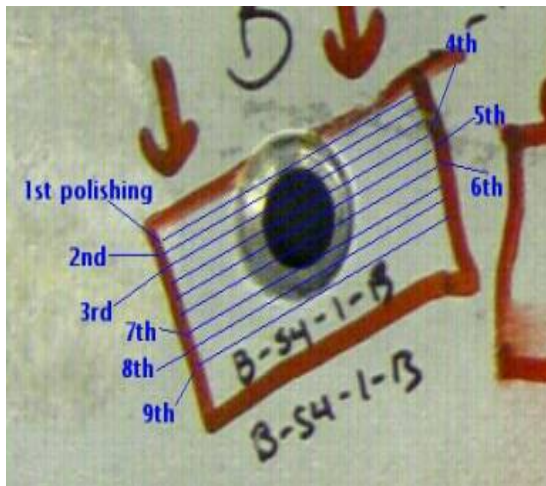
(e) Fifth polishing that removed a total of 1.189 mm (0.0468 inch) from the fourth polishing. The "indent" is the result of a repair procedure that was carried out to remove previous exfoliation damage. Note the intergranular corrosion that is present below the indent.



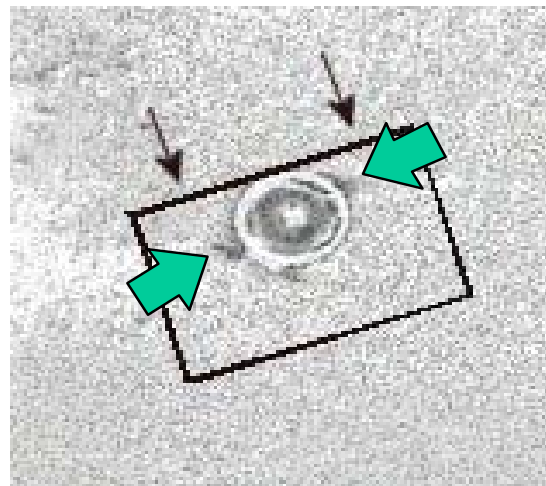
(f) Tenth polishing that removed a total of 4.902 mm (0.193 inch) from the fifth polishing.

Figure 6-2: Results from the Progressive Polishing Carried Out on Specimen 362-B-S4-2 that Contained both Visible Exfoliation and a Repaired (Ground-Out) Area (arrows indicate the location of the deepest intergranular attack).

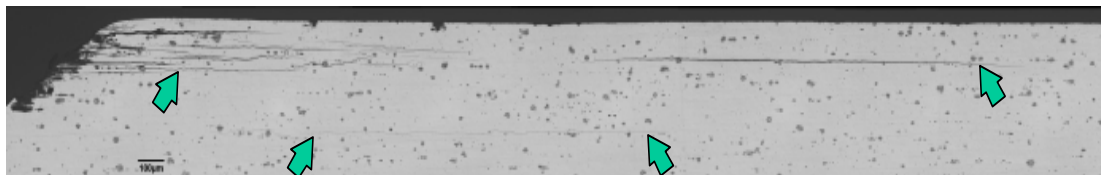
A section was taken from a 7178-T6 upper wing skin that did not contain any visible exfoliation, cold mounted and progressively polished, the results of which are shown in Figure 6-3. As can be seen from this figure, intergranular corrosion was present in the fastener area, which was detected by the ultrasonic inspection technique. This result demonstrated the sensitivity of the ultrasonic techniques to detect small levels of intergranular corrosion. It should also be mentioned that if a repair procedure were to be carried out in this area it is highly unlikely that all the intergranular corrosion would be removed, which is a requirement.



(a) Photograph of section showing locations of polishing.



(b) Ultrasonic inspection results.



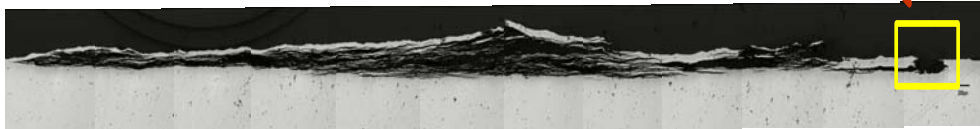
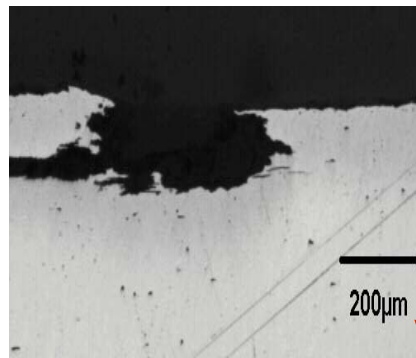
(c) Fourth polishing that removed a total of 2.59 mm (0.102 inch) from the first polishing.

Figure 6-3: Results from the Progressive Polishing Carried Out on Section B Taken from Specimen 362-B-S4-1 that did Not Contain any Visible Exfoliation (arrows in (c) indicate the location of the deepest intergranular attack).

Another study was carried out on exfoliated integrally stiffener extruded 7075-T6511 upper wing skins (that is fasteners were not present) [3]. Wing skins that were accidentally subjected to an age degradation process while in storage were used in this study. However it was determined that the damage sustained from this process was representative of the damage that occurred in service. Sections were taken from exfoliated areas; cold mounted and progressively polished using standard metallurgical techniques to determine the origin of the exfoliation as well as to characterize the damage present. Some of the results are shown in Figure 6-4 and Figure 6-5. From this characterization study it was found that the intergranular corrosion, which developed into exfoliation, originated at a modified discontinuity state (corrosion pit) that evolved from the age degradation process.



(a) Photograph of section SC3-1A.

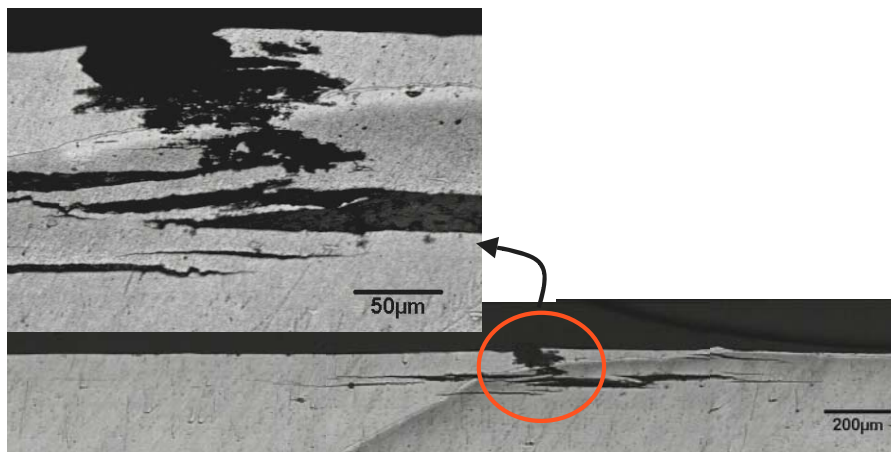


(b) Photomicrograph showing exfoliation present in section. Note corrosion pit (square) that was present, which may have started the intergranular corrosion.

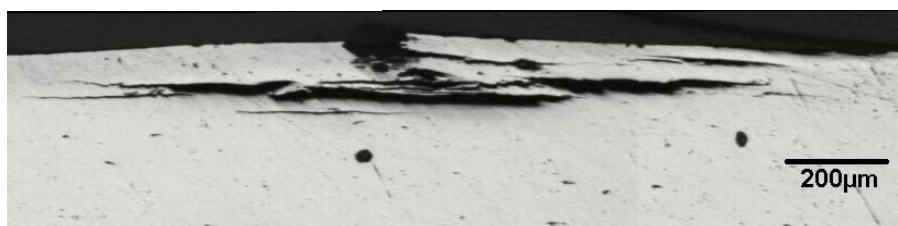
Figure 6-4: Exfoliation Present Along S-T Direction 7075-T6 Upper Wing Skin.



(a) Photograph of section SC5-3E.



(b) Photomicrograph of exfoliation present in section after first polish. Note presence of corrosion pit (circle).



(c) Photomicrograph of exfoliation present after second polish in same area as (b).

Figure 6-5: Exfoliation Present Along S-T Direction of Section Taken from 7075-T6 Upper Wing Skin.

6.3 REFERENCES

- [1] ASTM G15-97a, "Standard Terminology Relating to Corrosion and Corrosion Testing", 1997.
- [2] Speidel, M.O. and Hyatt, M.V., "Stress Corrosion Cracking of High-Strength Aluminum Alloys", Chapter 3 in "Advances in Corrosion Science and Technology", Vol. 2, Edited by M.G. Fontana and R.W. Staehle, Plenum Press, 1972.

- [3] Bellinger, N.C., Marincak, A., Harrison, M. and Reeb, T., “Effect of Exfoliation Corrosion on the Structural Integrity of 7075-T6 Upper Wing Skins”, Proceedings of the 2003 USAF Aircraft Structural Integrity Program Conference, Savannah, GA, USA, 2-4 December 2003.



Chapter 7 – CORROSION MORPHOLOGY: CORROSION PILLOWING AND CRACKING

Nicholas C. Bellinger

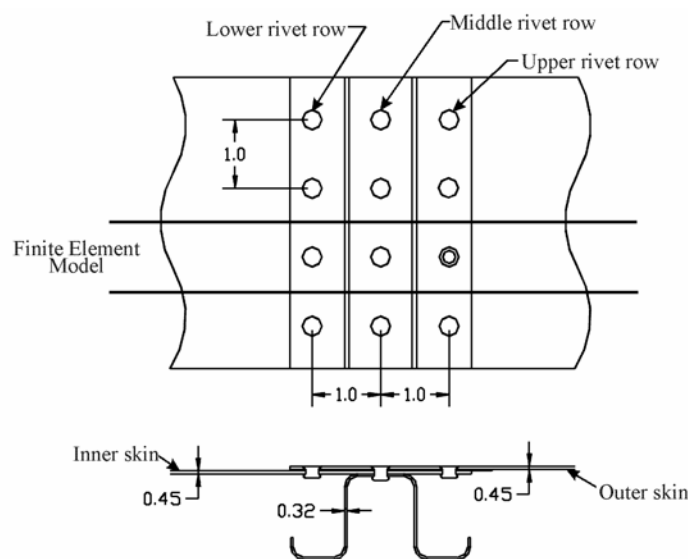
Institute for Aerospace Research
National Research Council Canada
Ottawa, Ontario
CANADA

7.1 INTRODUCTION

This section examines the corrosion induced distortion of aircraft skins commonly referred to as “Pillowing”, which involves plastic deformation and in extreme cases cracking in lap joints. Examples of pillowing and pillowing induced cracking in some typical commercial transport aircraft are shown. It is suggested that both the associated stresses and the cracking that arises due to these stresses should be taken into account during the assessment of structural integrity. References are provided to literature that explores these suggestions in more detail.

7.2 THE PILLOWING PHENOMENON

The majority of fuselage lap joints consist of an outer and inner skin fabricated from aluminum alloy 2024-T3 joined together with multiple rows of countersunk rivets, Figure 7-1, as well as an adhesive layer. During the operation of an aircraft the adhesive layer can deteriorate and disbond allowing moisture to migrate between the skins. This moisture can in turn, breakdown the material protective system resulting in the formation of crevice corrosion. As the corrosion forms, the skins between the rivets are forced apart due to the presence of the corrosion products. A chemical analysis on corrosion samples taken from service-exposed lap joints indicated that the insoluble product contained a mix of oxides, primarily aluminum oxide trihydrate, which has a molecular volume ratio of 6.454 times that of pure aluminum [1]. It is this high molecular volume ratio that is responsible for the deformation of the riveted skins in a joint resulting in the appearance commonly referred to as “pillowing”.



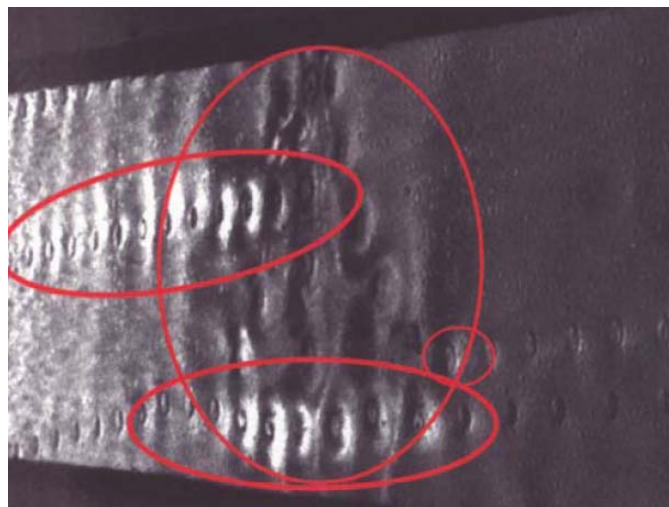
**Figure 7-1: Schematic of Typical Longitudinal Boeing Lap Joint
(Dimensions are in inches – 1 inch = 25.4 mm).**

CORROSION MORPHOLOGY: CORROSION PILLOWING AND CRACKING

The most common procedure is to inspect the fuselage joints visually from the aircraft exterior. Typically inspectors look at the lap joint surfaces for traces of corrosion products, and for corrosion pillowing deformation, most often with the aid of a flashlight. Figure 7-2, Figure 7-3 and Figure 7-4 show typical images of pillowing obtained using an optical inspection method, known as D-Sight™, designed to enhance the appearance of the surface perturbations. The fundamental assumption is that corrosion is not significant unless the inspector is able to see shadows cast by the deformed surface. Unfortunately, there is no data on the Probability Of Detection (POD) for corrosion pillowing using visual inspection.



(a) No corrosion indications.



(b) Corrosion is present within the joint which is indicated by a bright to dark change in an area of the grayscale image.

Figure 7-2: Enhanced Visual Inspection Results (D-Sight™) of Fuselage Lap Joints.

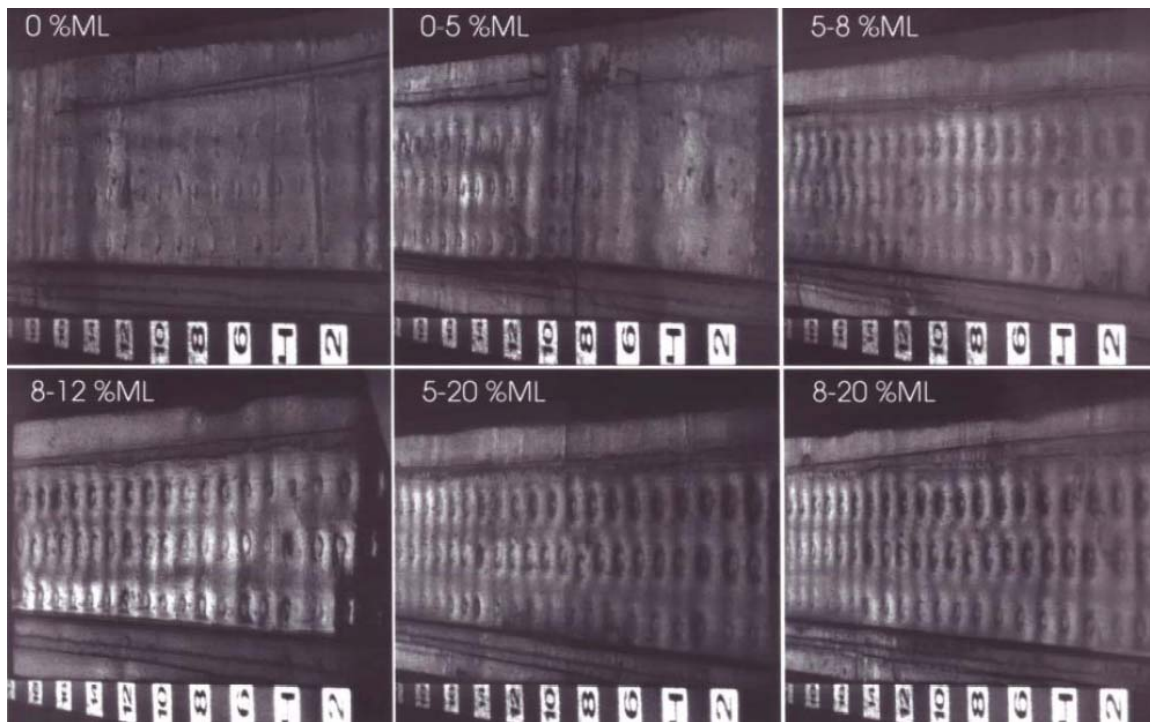


Figure 7-3: Various D-Sight™ Images Showing Degree of Pilling for Different Level of Material Thickness Loss (ML).

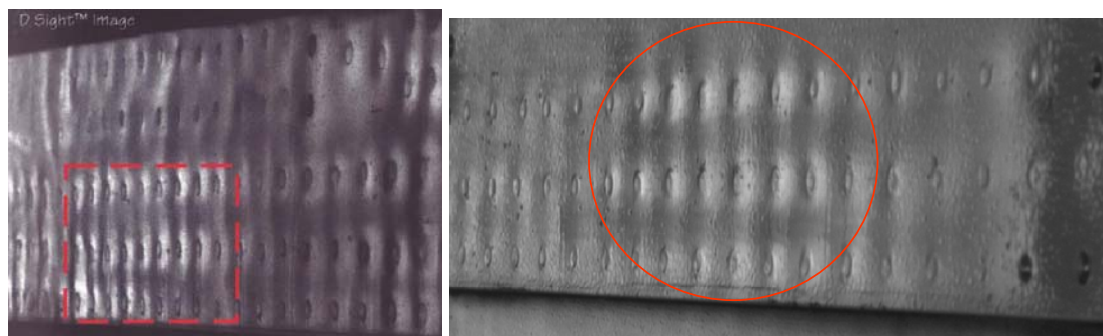
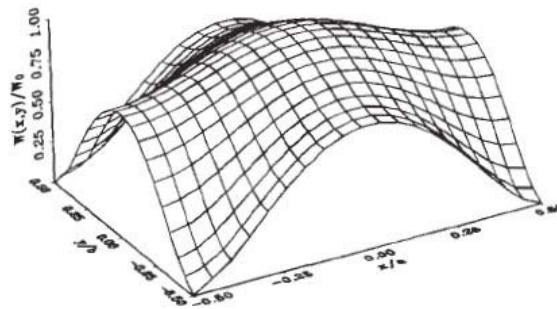


Figure 7-4: D-Sight™ Images Showing Pilling Caused by Corrosion Products.

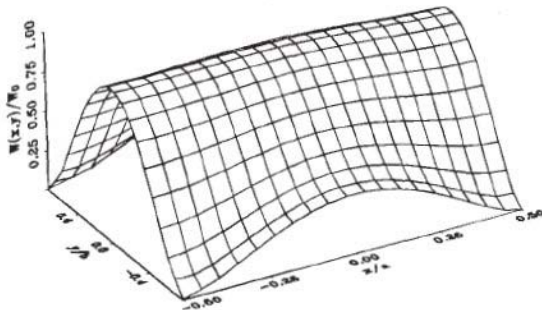
7.2.1 Mathematical Model of Pilling

The unaided visual non-destructive inspections used to detect corrosion pilling in fuselage lap joints are not capable of determining the level of corrosion within a joint. Therefore to determine if a correlation existed between the amplitude of the pilling deformation of the outer skin of a lap joint to the degree of corrosion inside the joint a mathematical model was developed [2]. The model assumed that the corrosion product was distributed within the joint so as to exert a uniform lateral pressure on the fuselage skins. It was also assumed that the joint was symmetrical about its mid-plane and thus only the outer skin was modeled. The closed-form classical plate theory of Timoshenko and Krieger was used to calculate the deformation of the outer skin supported by equidistant rivets and subjected to a uniform lateral pressure [3]. In order to better understand the effect that the rivet spacing ratio had on corrosion pilling, the deformed shapes of plates with various rivet spacing ratios were calculated and the results are plotted in Figure 7-5. The results showed that as the rivet spacing increased, the relative deflections at the shorter edges decreased while those at the longer edges increased, which can significantly reduce the probability

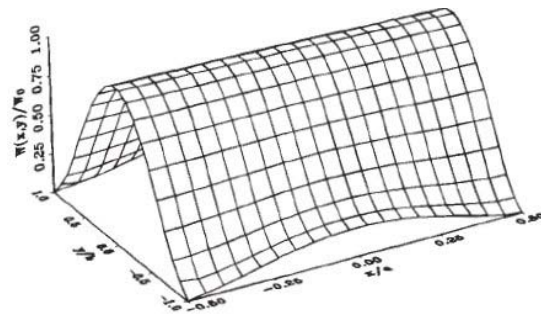
of detecting the corrosion visually. This suggests that the detection limit for joints with a high rivet spacing ratio may be significantly larger than the maximum allowed 10% thickness loss.



(a) Rivet spacing of 1.0.



(b) Rivet spacing of 1.5.



(c) Rivet spacing of 2.0.

Figure 7-5: Effect of Rivet Spacing Ratio on Pillowing Ratio [4].

It should be mentioned that although this section has concentrated on the effect that corrosion pillowing has on the stress state in fuselage lap joints, this phenomenon is present in any area of an aircraft where corrosion is contained between two fixed surfaces and the subsequent increase in stress occurs where the material is restricted from deforming.

7.3 PILLOWING CRACKS

Following the finite element analysis [4], non-surface breaking cracks were found in a number of naturally corroded joints removed from both retired and operational aircraft, Table 7-1. These cracks were identified using either x-ray non-destructive inspection techniques or when some of the joints were disassembled and the corrosion products removed. As can be seen from Table 7-1, cracks were found in a number of different locations on various aircraft with diverse operating lives. For the A300 incident a service bulletin was found that was issued in 1982 by Airbus Industrie [5]. The bulletin described the discovery of numerous cracks around the rivet holes of a corroded lap joint that resulted in a “star-shape” pattern.

Table 7-1: Recorded Incidences of Pillowing Cracks.

Type of Aircraft	Hours/Cycles	Location of Crack	Layer	WFU* / CUT**
L1011	38,040 / 31,370	33R / BS589-609	First	Dec. 92 / Sept. 93
B727-235	55,640 / 48,660	4R / BS1100	Second	Sept. 92 / May 93
B727-200	D Check	S30 / BS1090	First	In Service / Aug. 95
B727-100	61,890 / 54,150	S19R / BS600-640	Second	July 94 / July 96
B727-90C	72,400 / 56,700	S19-26L / BS440	First	In Service / Oct. 95
B727-235	56,870 / 49,530	S19R / BS700-720	First	Mar. 92 / Feb. 93
A300(AD)	10,400 / 6,940	S31L / FR26-31	First	In Service / Oct. 81
B727-295	61,854 / 55,465	S19R / BS660-680	First	Jan. 90 / Feb. 98
B727-295	63,349 / 55,676	S19R / BS720A-720B	First	Aug. 89 / Feb. 98
B707(Bueno)	–	Floor to Skin Joint	First	In Service
B707-3J6C	26,545 / 11,448	S20R / BS590-600H +10	–	Feb. 97 / Jan. 99

* WFU-Date aircraft was withdrawn from service.

** CUT-Date when lap joint was cut from aircraft.

The presence of these non-surface breaking cracks, referred to as pillowing cracks, has raised concerns into the effect they could have on the structural integrity of corroded fuselage lap joints [6]. Visual examinations of lap joint faying surfaces that were cleaned of corrosion products revealed that pillowing cracks could extend to approximately one-quarter to one-half the rivet pitch.

To determine the failure mode of these pillowing cracks, a number of cracks were examined using both optical and scanning electron microscopy [4],[7],[8]. The following observations were made:

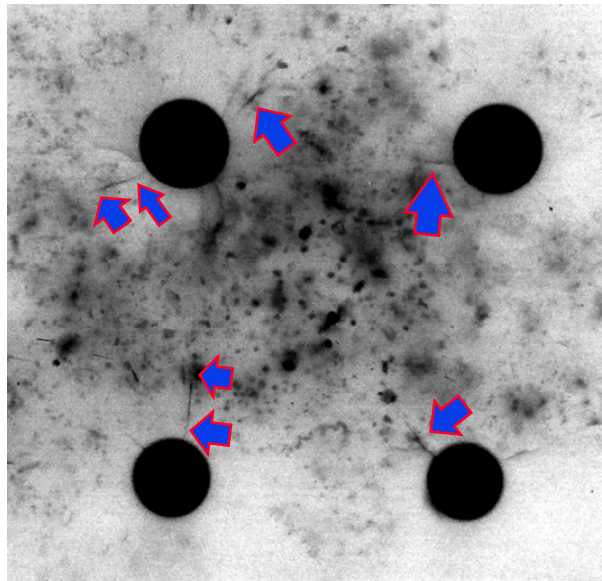
- Pillowing cracks tended to occur in groups (i.e., “star-shape” pattern cracks at more than one rivet hole), which did not normally penetrate through the thickness. The cracks always occurred on the side of the hole that was affected by the increased stress due to the pillowing and tended to propagate into the pillowed region Figure 7-6.
- The crack faces that were pried open contained corrosion products and showed extensive intergranular fracture with numerous secondary cracking, Figure 7-7.
- A number of the cracks had multiple nucleation sites. Although these sites could not be determined, they were evidently based on the different crack planes present, Figure 7-8.

CORROSION MORPHOLOGY: CORROSION PILLING AND CRACKING

- The crack growth through the thickness was not perpendicular to the faying and outer skin surfaces but occurred at an angle, Figure 7-9.
- Some of the fracture surfaces contained fatigue striations near the crack edge where the corrosion was light, Figure 7-10 and suggests that once these cracks form, they may continue to grow under fatigue loading.

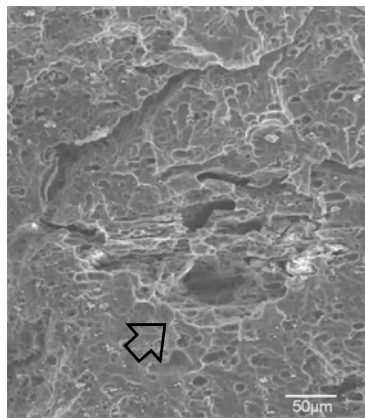


(a) Optical image of cracks in Boeing 707 longitudinal lap joints.

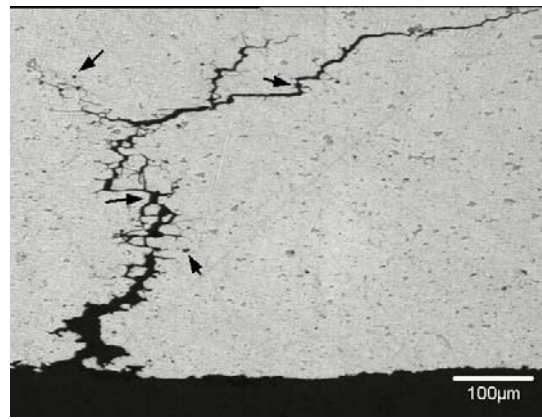


(b) X-ray micrograph showing cracks in L1011 lap joint.

Figure 7-6: Various Images Showing the Typical Star-Shape Pattern Associated with Pillowing Cracks.



(a) Scanning electron micrograph of crack face.



(b) Optical micrograph obtained from progressive polishing.

Figure 7-7: Micrographs Showing the Intergranular Cracking with Numerous Secondary Cracks.

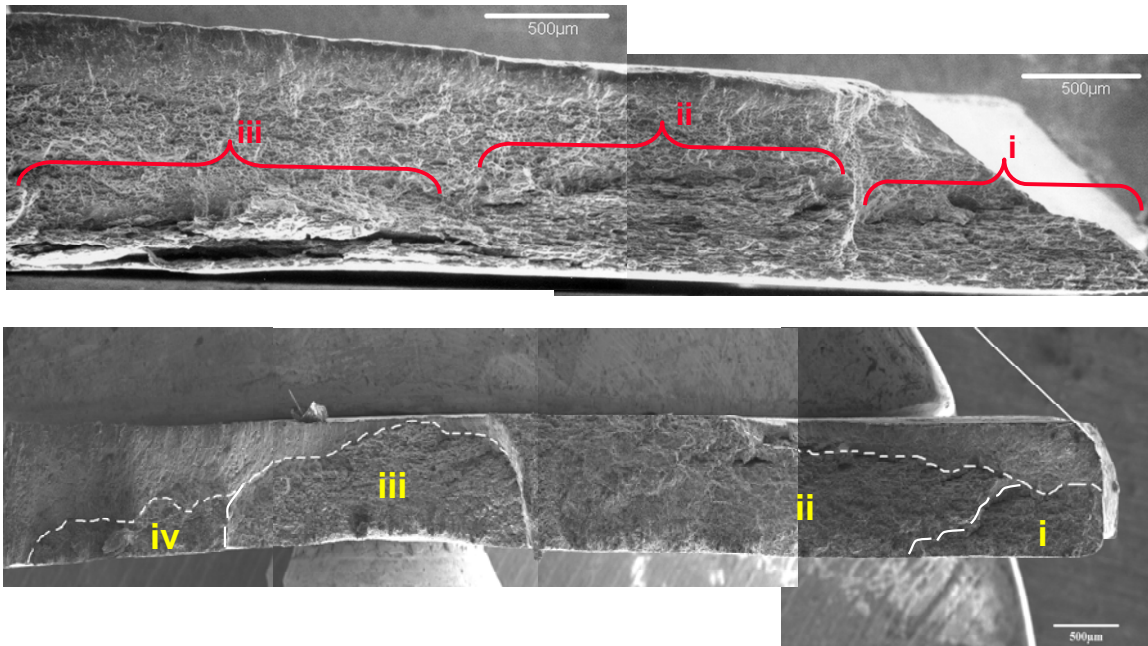


Figure 7-8: Micrographs Showing Multiple Crack Nucleation Sites.

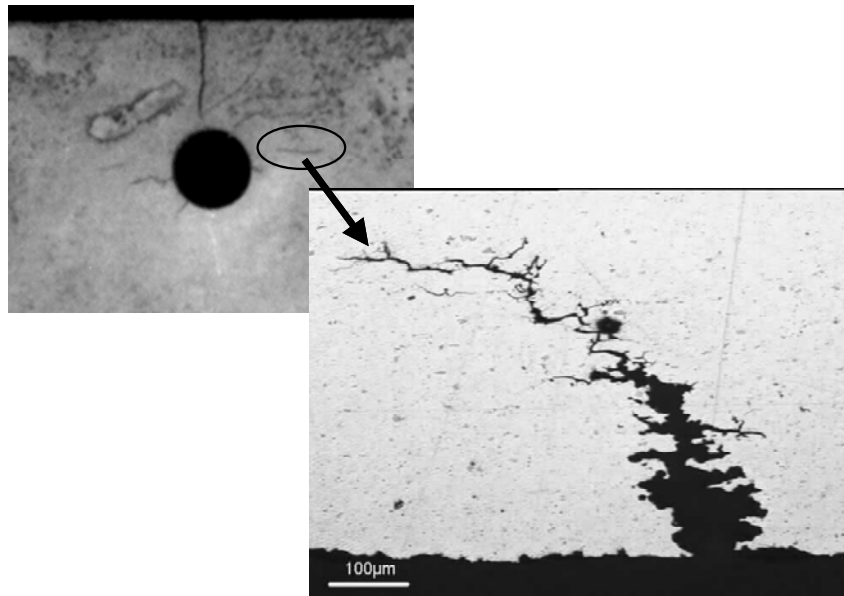


Figure 7-9: Optical Image of Pillowing Crack Showing Angled Crack Growth.
(Note that the crack occurred away from the edge of the hole but is still within the highly stressed area caused by the corrosion pilling.)

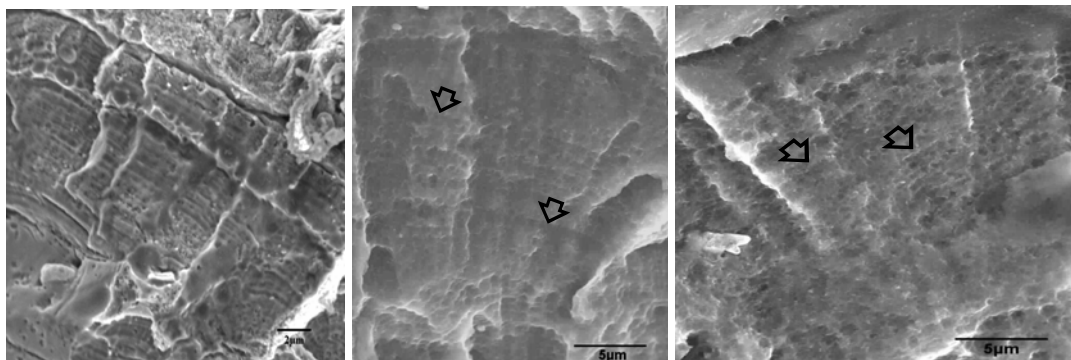


Figure 7-10: Scanning Electron Micrographs Showing Fatigue Striations that were Found on the Fracture Surfaces on Some Pillowing Cracks.

With the discovery of pillowing cracks and the fact that Wanhill discovered these cracks at every fastener hole in an area of about one bay length (500 mm) [9], it is proposed that the term Multi-Site Damage (MSD) should include corrosion, since the effect that pillowing cracks may have on structural integrity could be similar to fatigue crack MSD.

7.4 REFERENCES

- [1] Krishnakumar, S., Komorowski, J.P. and Sproule, I, "Chemical Characterization of Corrosion Products in Fuselage Lap Joints", LTR-ST-1952, November 1993.
- [2] Bellinger, N.C., Krishnakumar, S. and Komorowski, J.P., "Modelling of Pillowing Due to Corrosion in Fuselage Lap Joints", Canadian Aeronautics and Space Journal, Vol. 40, No. 3, pp. 125-130, September 1994.

- [3] Timoshenko, S. and Woinowsky-Krieger, S., “Theory of Plates and Shells” (2nd Ed.), McGraw-Hill Book Company, 1959.
- [4] Bellinger, N.C., Komorowski, J.P. and Gould, R.W., “Corrosion Pillowing Cracks in Fuselage Lap Joints”, Proceedings of the Second Joint NASA/FAA/DoD Conference on Aging Aircraft, NASA/CP-1999-208982/Part 2, Williamsburg, Virginia, pp. 535-544, 31 August – 3 September 1998.
- [5] “Airbus Service Bulletin”, A300-53-178, Revision, 19 September 1988.
- [6] Komorowski, J.P., Bellinger, N.C. and Gould, R.W., “The Role of Corrosion Pillowing in NDI and in the Structural Integrity of Fuselage Joints”, Proceedings of the 19th Symposium of the International Committee on Aeronautical Fatigue, Edinburgh, Scotland, 16-20 June 1997.
- [7] Komorowski, J.P., Bellinger, N.C., Gould, R.W., Forsyth, D. and Eastaugh, G., “Research in Corrosion of Ageing Transport Aircraft Structures at SMPL”, CAS Journal – Special Edition 50th Anniversary of IAR, Vol. 47, No. 3, pp. 289-299, September 2001.
- [8] Bellinger, N.C. and Komorowski, J.P., “Environmentally Assisted Cracks in 2024-T3 Fuselage Lap Joints”, Proceedings of the Third Joint FAA/DoD/NASA Conference on Aging Aircraft, Albuquerque, NM, USA, 20-23 September 1999.
- [9] Wanhill, R.J.H., “Corrosion and Fatigue Assessment of Aircraft Pressure Cabin Longitudinal Lap Splices”, 5th International Aerospace Corrosion Conference, November 1999.



Chapter 8 – FRETTING CORROSION AND FATIGUE

David W. Hoepfner

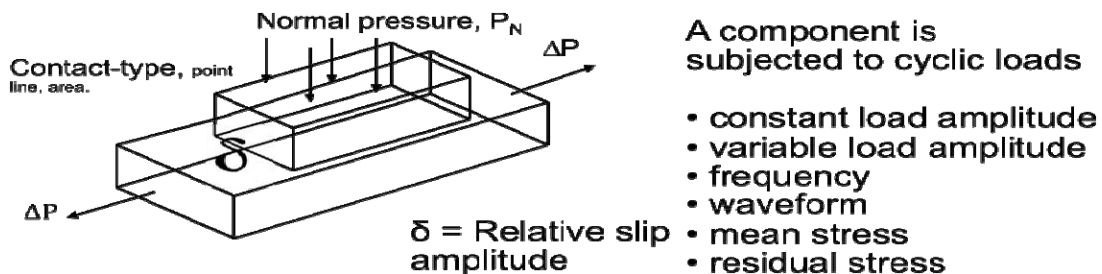
Professor and Director, Quality and Integrity Design Engineering Center (QIDEC)
 Mechanical Engineering Department, University of Utah
 Salt Lake City, Utah
 USA

8.1 INTRODUCTION

Virtually all mechanical joints of fixed wing aircraft, rotary wing aircraft, engine and propulsion systems, gearbox and other electrical and mechanical components of aircraft are susceptible to the occurrence of fretting fatigue. The complexities of fatigue design, either safe-life or damage tolerant or HOLSIP (Holistic Structural Integrity Processes), are enough to challenge the most talented technical personnel. Add to that the occurrence of fretting and truly complex phenomena occur that require a fully comprehensive structural integrity design policy.

Fretting fatigue was originally discovered in the early part of the 20th century. Since that time a great deal of work has been done to understand the mysteries of fretting fatigue. As well, engineers have devoted a significant effort to studying fretting fatigue to be able to cope with the potentially deleterious effects it may have on the life of engineering components.

Fretting is a phenomenon that involves both environmental effects (corrosion in metals) and wear. Thus, it is a complex phenomenon. Figure 8-1 shows some of the parameters involved in fretting fatigue. When it acts with cyclic loading on engineering components the result frequently is to either shorten the fatigue life or to lower the fatigue design allowable.



A component is subjected to cyclic loads

- constant load amplitude
- variable load amplitude
- frequency
- waveform
- mean stress
- residual stress

FRETTING FATIGUE OF A COMPONENT
 Obtain fatigue response for conditions of interest (COI)

- | | |
|----------------------------------------------------------------------------------------------------------------------------------------------------------------------------------------------------------------------|---------------------------------------------------------------------------------------------------------------------------------------------------------------------------|
| <ul style="list-style-type: none"> • δ, P_N - magnitude, frequency • material compatibility • friction • temperature • environment | <ul style="list-style-type: none"> • stress state • geometric detail • material • surface condition • failure criteria |
|----------------------------------------------------------------------------------------------------------------------------------------------------------------------------------------------------------------------|---------------------------------------------------------------------------------------------------------------------------------------------------------------------------|

Figure 8-1: A Depiction of the Large Number of Parameters that may be Involved in Fretting Fatigue (the view shown in the upper left depicts single sided contact but many contacts are double sided) – from Hoepfner, 1991.

Historically three approaches have been employed in fretting fatigue studies as shown in Figure 8-2 below. One approach is to perform fretting fatigue testing by simulating the contact or fastening conditions.

The fretting fatigue test results thus generated are used to determine the fretting fatigue life reduction factor K_{ff} . Although this approach has been to introduce a fretting fatigue life reduction factor into the fatigue design process this is not always a satisfactory procedure. A second approach is to develop the fatigue structural allowables by testing the mechanical joints and including fretting considerations in these tests including the alleviation or prevention schemes. Another approach is to use a fretting protection and control plan to focus on potentially blocking the occurrence of fretting or to prevent the propagation of cracks from fretting damage areas. This approach simulates fretting damage that will assist in developing greater understanding of the basic mechanisms of fretting which in turn will lead to the development of standardized fretting fatigue test methods. In addition, this approach will help to find some preventive systems to alleviate fretting fatigue problems on structural components. This mechanistic approach also will be useful to develop inspection systems. Some investigators are coupling damage tolerance concepts to fretting studies to assist in more accurate tracking of damage as well as setting more realistic inspection intervals. Therefore, one of the needs for improved fretting fatigue resistance is the development of adequate experimental procedures to simulate fretting fatigue phenomena.

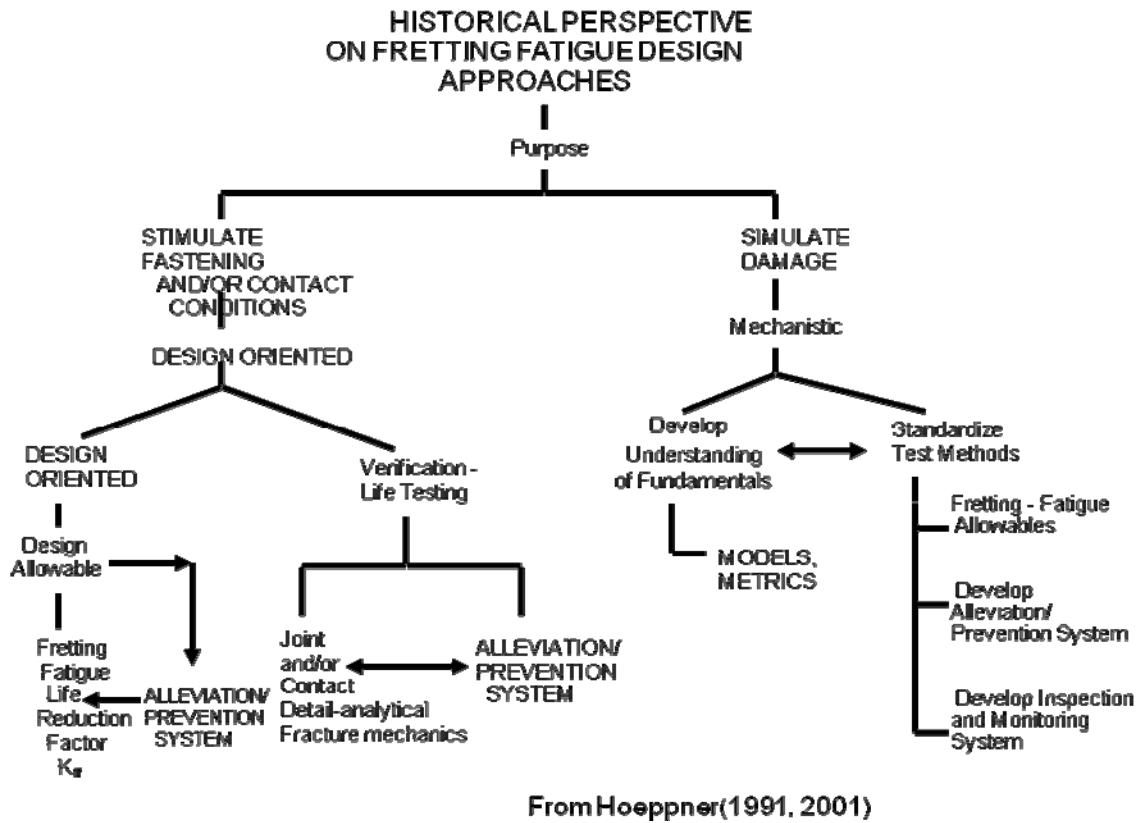


Figure 8-2: Historical Perspective of Approaches to Fretting Fatigue Design Studies.

8.2 MECHANISMS OF FRETTING

Fretting is believed to rupture the protective oxide films of the metal alloys that are in contact although the influence of oxide film is brief in the subsequent degradation mechanism of fretting. Therefore, it is commonly believed that the first stage of fretting is adhesive contact of the asperities on contact surfaces [1]. Microscopic plastic deformation of the contacting asperities in relative motion may result in the nucleation of cracks. In addition, metal transfer may occur from one surface to another depending on the hardness and the relative displacement of the contacting surfaces. The production of fretting debris and the

oxidation of the fresh surface may result in the build-up of oxides on the contacting surfaces. These may result in the formation of pits on the contacting surfaces. These damages may very well accelerate the nucleation of cracks. Depending on the contact stress state the nucleated cracks may result in early propagation in a rapid manner. Contact stresses are high enough to significantly influence crack propagation. The cracks may propagate at various rates and angles. Subsequent final propagation of cracks may depend on the bulk stress alone rather than on the contact stress. As the crack grows into the material, a depth is reached beyond which the contact stresses have little or no influence and the applied cyclic stresses play a dominant role. Therefore, the fretting process can be divided into four stages viz. nucleation of cracks, early propagation of cracks by contact stress state, final propagation of cracks by bulk stress and instability resulting in the decreased fatigue life. The aforementioned fretting process is dependent on many different variables such as material microstructure, stress state, environment, relative slip amplitude, and contact pressure.

The theories related to nucleation of fretting fatigue cracks are usually based on the adhesive contact of the asperities as well as the cracks that form sub-surface. Displacements that are “small” on a macroscopic scale are very large when acting on asperities. Relative movement of adhesively bonded asperities results in plastic or near-plastic strains around asperities. The importance of the formation of oxides may be based on their affect on adhesive contacts. Oxides usually prevent direct metal contact and reduce coefficient of friction by rolling. However, under certain conditions, such as the presence of discontinuities and/or sliding motion, cracks could nucleate sub-surface.

Dependent upon nucleation and contact stress state it has been observed that after a specific time, fretting contact no longer affects the fatigue life. This implies that nucleation occurs very early. In addition, it should be noted that fatigue life reduction occurs only after a specific amount of fretting damage and the nucleated crack must be large enough to propagate under bulk stress alone [2].

8.3 FRETTING FATIGUE IN AIRCRAFT JOINTS

Fretting fatigue has been observed as a potential degradation mechanism in aircraft structural components [3]. Many cracks have been found to originate at fasteners and on faying surfaces. Cracks may form due to fretting mechanisms from one or more rivet holes leading to the concept of multiple-site damage. Evidence supports that elimination of fretting with adhesives greatly increases fatigue life [4]. Also, it has been observed that cracks appear in lugs much sooner if fretting is present. In addition, failures observed originating at areas of fretting damage often occur away from fastener holes. Figure 8-3 shows a schematic of the design methods proposed in the past by Hoepfner [4],[5] to minimize the effect of fretting fatigue in aircraft joints. In addition, the methods to alleviate fretting fatigue challenge in aerospace components are provided in the next section.

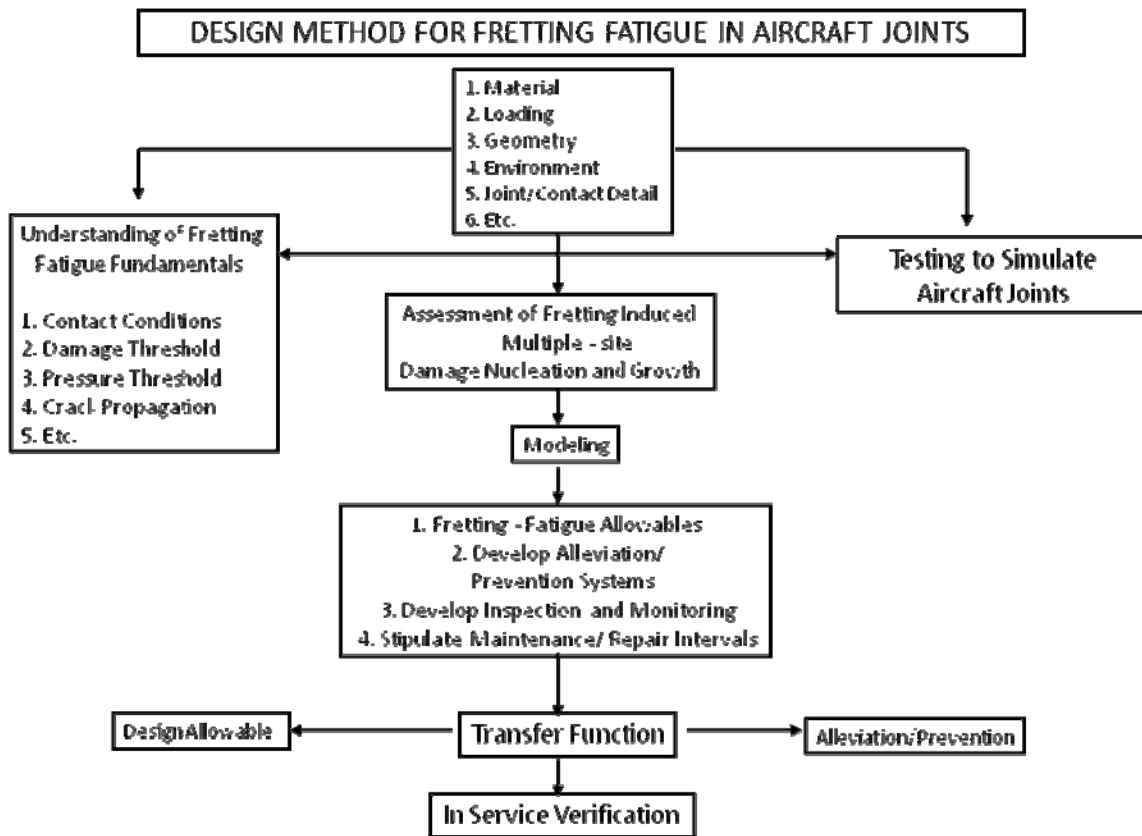


Figure 8-3: An Illustration of an Approach that has been Used to Design for Fretting Fatigue Resistant Aircraft Joints (4, 5).

8.4 REDUCTION OR PREVENTION METHODS

The following are some methods that can be employed to reduce the problem of fretting fatigue in aircraft joints [5]. It is important that a surface integrity engineering plan be developed to assure the integrity desired for fretting fatigue resistance. The items listed below will all fall within a typical surface integrity engineering plan.

I – Design

- a) Prevent all relative motion of the surfaces.
- b) Prevent the surfaces from contacting.
- c) Surface roughness changes that may involve either an increase or decrease in roughness depending on the conditions of interest.
- d) Surface hardness changes that may involve either an increase or decrease in hardness.

The most common approach appears to be to increase the hardness of the component whose life is being affected.

II – Mechanical Methods

- a) Shot peening.
- b) Vapour blasting.

- c) Bead blasting.
- d) Surface rolling.
- e) Dimpling of the surface.

These methods include processes that cold work the surface to increase hardness and introduce residual surface compressive stresses.

III – Coatings

- a) Hard metal coatings.
- b) Soft metal coatings.
- c) Polymer coatings.

There are multiple purposes to coatings. One is that they provide a separation of surfaces that are in contact. Another is that the coating may become sacrificial to the fretting fatigue loading such as in some shims or bushings. Coatings can be hard or soft depending on the overall purpose that is desired which varies with design application. On occasion the coating will be selected to provide a lower sliding frictional behavior. This usually involves extensive trial and error evaluation.

IV – Lubricants

- a) Solid lubricants.
- b) Greases.
- c) Oils.

In the case of lubricants they too have purposes that vary with the design application. In some cases they provide hydrodynamic lubrication and thus provide a film between the surfaces that actually maintains separation. In addition, even if hydrodynamic lubrication is not attained the lubricant may provide separation and a concomitant reduction in contact force which decreases the propensity for fretting. Lubricants also provide for significant reductions in dynamic or sliding friction which also has been noted to reduce fretting thereby reducing fretting fatigue life reduction. Some lubricants also assist in fretting debris removal which is important to aiding the reduction of fretting induced surface damage. In some cases it has been noted that a temperature reduction occurs by the use of lubricants thereby decreasing the fretting surface damage as well. Each case of lubrication provides it unique challenge and to date no general design rules have emerged that are reliable for all fretting fatigue cases.

V – Surface Treatments

- a) Anodization.
- b) Ion implants.
- c) Sulphidization.
- d) Phosphatization.

Surface treatments, similar to the discussions under III and IV above, can have varying beneficial effects based on the same general principals. They have the added potential benefit of providing, in some cases, compressive surface residual stresses that also can significantly enhance fretting fatigue resistance.

VI – Influence of Substances Used in Aircraft Joints

- a) Faying Surface Sealants:
 - ADHESIVE types can significantly increase fretting fatigue life.

FRETTING CORROSION AND FATIGUE

- FLEXIBLE sealants can decrease fretting fatigue life.
 - Increasing sealant thickness decreases fretting fatigue life.
- b) Adhesives:
- Can significantly improve fatigue life even if fretting does not occur.
 - Curing an adhesive, then assembling the joint can decrease fatigue life due to decreased friction.
- c) Penetrants:
- Usually reduce fatigue life but can have no affect or increase life.
 - Penetrants applied after joint assembly can easily enter joints depending upon the type of faying surface sealant.

VII – Palliatives Tested in Aircraft Joints

- a) Cold working can significantly improve joint fatigue life.
- b) Solid lubricants escape from the joint or are wiped away.
- c) Teflon usually decreases fatigue life due to load transfer to fastener shanks.

8.5 SUMMARY

In summary, adhesion based mechanisms of fretting fatigue appear to be most common and fretting contact significantly increases stress at and near the surface.

It should be noted that palliative effectiveness is extremely **CASE SPECIFIC** as noted in the above discussions and only methods which induce surface residual compressive stresses consistently increase fretting fatigue life. Moreover, evidence shows that fretting fatigue is a pervasive mode of failure with riveted aircraft joints and many contact related joints in gas turbine engines and helicopter applications. Furthermore, methods which reduce fretting in aircraft joints often do not increase the fatigue life as a reduction in coefficient of friction requires more load to be taken by the fastener shank in the case of mechanical fasteners. It is desirable that in time more specific design guidelines be established. Regrettably no extensive **long-term** studies of the phenomenon of fretting fatigue have been undertaken in any NATO or other country in which the efforts have been focused in fretting fatigue. There have been studies in some laboratories around the world where the focus has been on the general phenomenon of fretting fatigue. Many studies from these laboratories are reported in the general bibliography provided after the references. Those interested in the progress on this important subject should go to the entire series of publications of the International Symposia on Fretting Fatigue. Undoubtedly future meetings of that body will provide much continuing insight into fretting fatigue. Finally it is important to note that Japan assembled the first group of fretting fatigue workers to produce a fretting fatigue test standard. This too is mentioned in the general bibliography. In recent months the ASTM has produced a draft fretting fatigue standard that is currently being voted on by the ASTM E9 membership. Hopefully these recent developments will bode well for the future production of much more understanding of the fretting fatigue phenomenon, much more reliable data to allow comparison of fretting fatigue data between various laboratories, and effective design guidelines for the anticipation, elimination of and control of fretting fatigue of aircraft structures.

8.6 REFERENCES

- [1] Hoepfner, D.W., "Mechanisms of Fretting Fatigue", Keynote Invited Paper, in Fretting Fatigue, ESIS 18, Mechanical Engineering Publications, London, UK, pp. 3-19, 1994.

- [2] Hoepfner, D.W. and Goss, G.L., "A Fretting Fatigue Damage Threshold Concept", *Wear*, 27, pp. 61-70, 1974.
- [3] Hoepfner, D.W. and Adibnazari, S., "Fretting Fatigue in Aircraft Joints", in *Durability and Structural Integrity of Airframes S.*, International Committee of Aeronautical Fatigue (ICAF), pp. 191-207, 1993.
- [4] Hoepfner, D.W., "Fretting of Aircraft Control Surfaces", in *AGARD Conference Proceedings No. 161, Specialists Meeting on Fretting in Aircraft Systems*, pp. 1.1 – 1.7, 1974.
- [5] Hoepfner, D.W., Adibnazari, S. and Moesser, M.W., "Literature Review and Preliminary Studies of Fretting and Fretting Fatigue Including Special Applications to Aircraft Joints", DOT/FAA/CT-93/2, 1994.

8.7 GENERAL BIBLIOGRAPHY OF IMPORTANT REFERENCES ON FRETTING FATIGUE

- 1) Waterhouse, R.B., "Fretting Corrosion", Pergamon Press, USA, 1972.
- 2) Specialist Meeting on Fretting in Aircraft Systems, NATO-AGARD Conference Proceedings No. 161, Advisory Group for Aerospace Research & Development, Neuilly-sur-Seine, France, 1974.
- 3) Barrois, W.G., *Manual on Fatigue of Structures, II-Causes and Prevention of Structural Damage, 6. Fretting-Corrosion Damage in Aluminum Alloys*, NATO, AGARD MAN 9, Advisory Group for Aerospace Research & Development, Neuilly-sur-Seine, France, 1975.
- 4) "Control of Fretting Fatigue", Report of the Committee on Control of Fretting-Initiated Fatigue, NMAB, NRC, Publication NMAB-33, National Academy of Sciences, Washington, DC, USA, 1977.
- 5) Waterhouse, R.B. (Editor), "Fretting Fatigue", Applied Science Publishers, UK, 1981.
- 6) Attia, M.H. and Waterhouse, R.B. (Editors), "Standardization of Fretting Fatigue Test Methods and Equipment", ASTM STP 1159, American Society for Testing and Materials, West Conshohocken, Philadelphia, PA, USA, 1992.
- 7) Waterhouse, R.B. and Lindley, T.C. (Editors), "Fretting Fatigue", ESIS Publication 18, Mechanical Engineering Publications Ltd., London, England, 1994.
- 8) Hoepfner, D.W., Chandrasekaran, V. and Elliott, C. (Editors), "Fretting Fatigue-Current Technology and Practice", ASTM STP 1367, American Society for Testing and Materials, West Conshohocken, PA, USA, 2000.
- 9) Kinyon, S.E., Hoepfner, D.W. and Mutoh, Y. (Editors), "Fretting Fatigue: Advances in the Basic Understanding and Applications", ASTM STP 1425, American Society for Testing and Materials, West Conshohocken, PA, USA.



Chapter 9 – ENVIRONMENTALLY ASSISTED CRACK GROWTH OF METALLIC ALLOYS

David W. Hoeppe

Professor and Director, Quality and Integrity Design Engineering Center (QIDEC)
Mechanical Engineering Department, University of Utah
Salt Lake City, Utah
USA

9.1 INTRODUCTION

Environmentally Assisted Cracking (EAC) of metal alloys is one of the most fascinating and challenging time dependent mechanisms of degradation that may lead to failure of aircraft components in use today. The cause of environmentally assisted cracking is related to corrosion mechanisms. This effect is one of the four major time dependent or time related failure mechanisms. The other three being fatigue, creep, and wear. When combinations of the failure mechanisms occur the challenge for engineers and scientists becomes vexing. Corrosion, when combined with fatigue, produces a phenomenon that is called corrosion fatigue. It is defined as when corrosion and fatigue occur **simultaneously**. Note it does not define the sequential occurrence when corrosion may occur prior to fatigue or vice versa. The objective of this chapter is to present the key issues involved in environmentally assisted cracking and its relationship to the integrity of aircraft components.

9.2 PHENOMENOLOGICAL ASPECTS OF EAC

Environmentally assisted cracking of metal alloys used in aircraft occurs under two major conditions, viz.:

- 1) Sustained loading; and
- 2) Cyclic loading (fatigue).

For many years the former has been referred to as stress corrosion cracking. There is an effort underway throughout the technical community to refer to these as follows:

- 1) Environmentally assisted cracking under sustained loading; and
- 2) Environmentally assisted cracking under cyclic loading.

9.2.1 EAC Under Sustained Loading

The science of corrosion is very extensive and it is well known that thermodynamics and kinetics control this most interesting electrochemical phenomenon. See Roberge [1],[2],[3] and Fontana and Green [4] for detailed information about corrosion. Figure 9-1 shows a typical manner in which data are presented for environmental effects of crack growth under sustained loading. The plot represents time to failure for a defined failure condition for all conditions at a given temperature. The plot has often been referred to as the stress corrosion cracking plot, but hydrogen embrittlement data may also be presented in this manner. In the fields of both polymers and ceramics, data plotted in this manner is often referred to as “static fatigue” data but this is not recommended. The asymptote that may develop at the lower right is referred to as the stress corrosion cracking threshold. It is very important to mention that the effects are very sensitive to both chemical composition and grain orientation in most aircraft alloys. Thus, materials characterization programs must include extensive evaluation to both uncracked and precracked specimens of the alloy under consideration. In addition, evaluations of manufacturing in relation to orientation effects also must be considered. For example, when machining all care must be taken not to expose short transverse grain

boundaries or parting planes in either castings or forgings. It is imperative that chemical environment maps related to positions in aircraft be prepared. These will define the severity of the chemical environment and temperature related to the location in the aircraft. Some companies actually test materials in “severe” environments to attempt to assure a “conservative” approach. Some military agencies and companies have actually attempted to do environmental tracking with various types of environmental measuring devices. This is leading to much more precise definition of the actual environment at the location of interest.

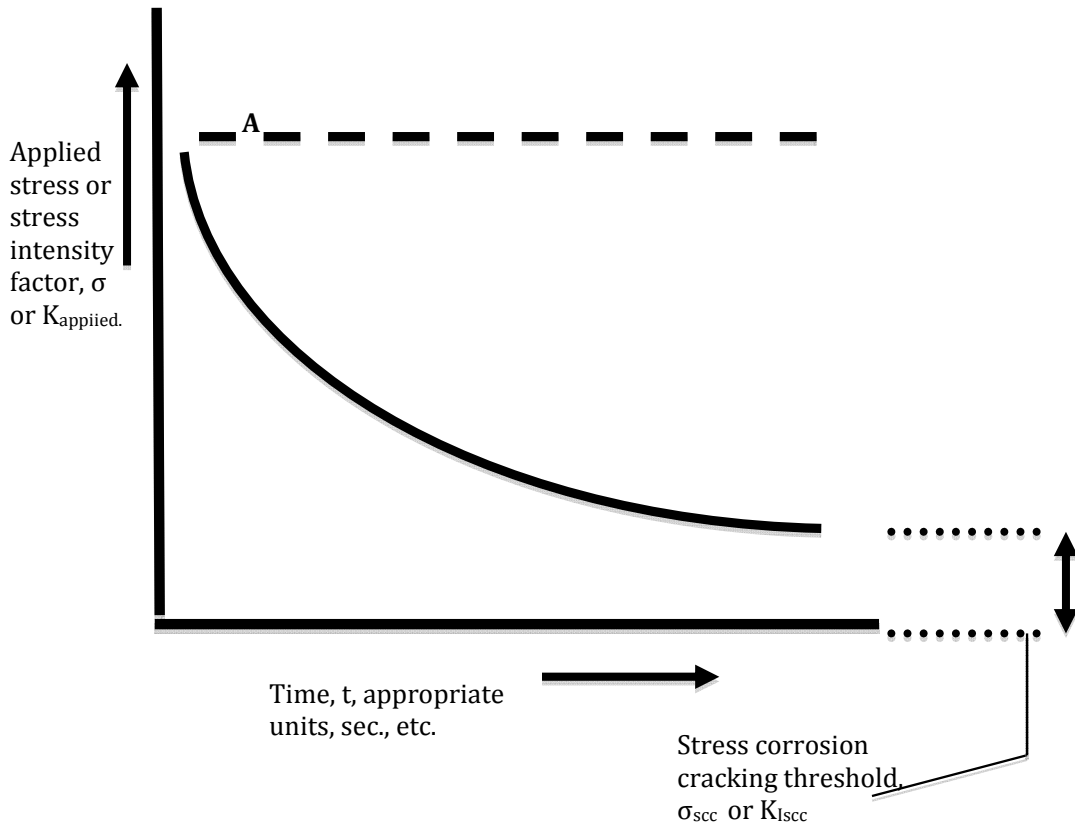


Figure 9-1: Plot of Applied Stress or Stress Intensity versus Time at Sustained Load in a Given Environment for a Given Material.

9.2.2 EAC Under Cyclic Loading

Fatigue has been studied since the early 1800 period and much of the activity has centered around mechanics applications of either stress or strain versus cycles or reversals to failure as depicted in Figure 9-2.

FATIGUE RESPONSE DIAGRAM

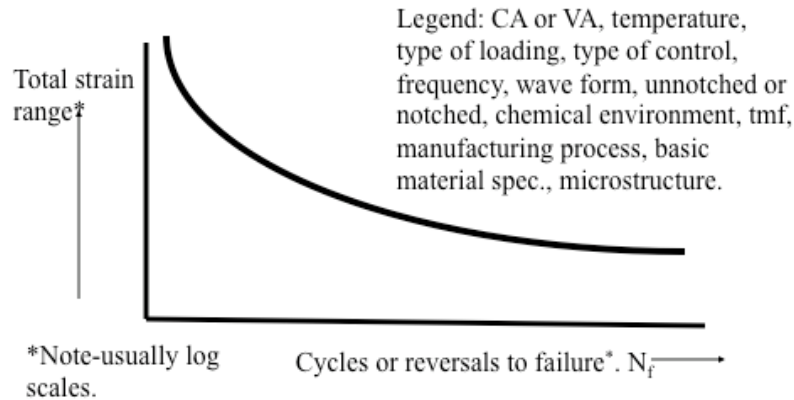


Figure 9-2: Basic Diagram for Presentation of Fatigue Response (see Hoepfner [5]).

ASTM defines corrosion fatigue in E1823 as follows:

“Corrosion fatigue is the process by which fracture occurs prematurely under conditions of simultaneous corrosion and repeated cyclic loading at lower stress levels or fewer cycles than would be required in the absence of the corrosive environment.” ASTM E1823 [6]. Note in the definition the application of corrosion and cyclic loading occurs simultaneously. Some recent studies reported in the literature actually do not apply to the process of corrosion fatigue in that they involve corrosion prior to the fatigue loading. The researchers who report this are evaluating what is often referred to as prior corrosion plus fatigue or corrosion + fatigue.

In 1972 Hoepfner [7] suggested the corrosion fatigue process needs to be evaluated in a systems framework such as shown in Figure 9-3. Later work suggested this might be referred to within a Holistic Structural Integrity Process Paradigm (HOLSIP – see www.holsip.com). The reason this is important for corrosion fatigue as well as other time dependent interactions of failure mechanisms is the complexity of the processes involved and the need to formulate methods of life estimation/prediction to establish structural integrity over the component life of interest. With corrosion this is particularly important due to the different types of corrosion that may occur on structures in the field and the insidious nature of the degradation. Furthermore, if the fatigue and corrosion fatigue processes are divided into four phases of nucleation, short crack propagation, long crack propagation, and final instability/failure as has been suggested by Hoepfner [8] then the types of corrosion important in nucleation can be different than those involved in propagation.

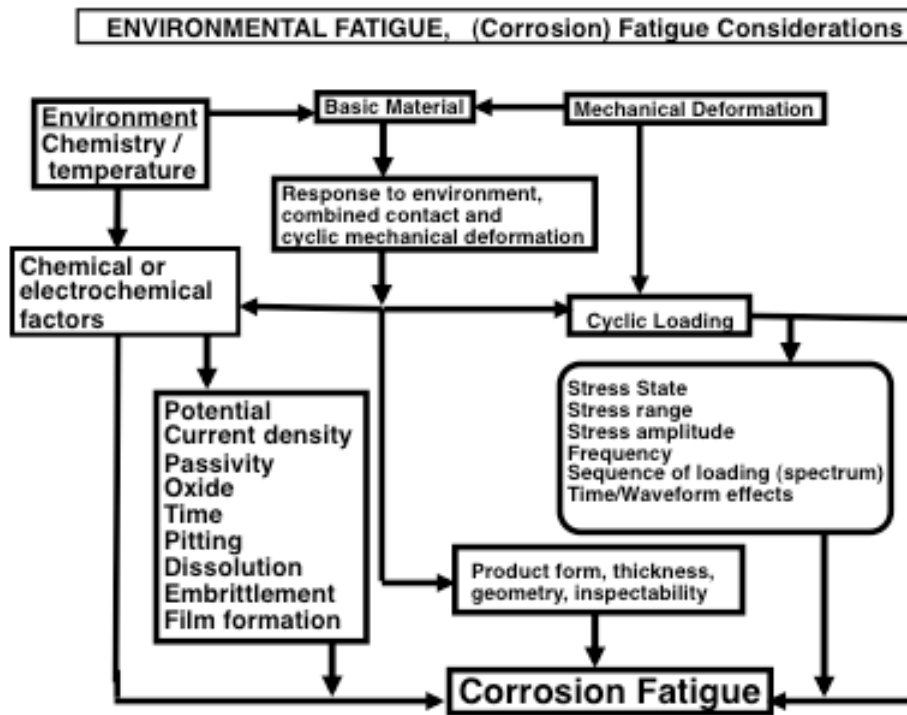


Figure 9-3: The Systems View of Corrosion Fatigue (see Hoepfner [5] and [7]).

9.2.3 Sources of Information

Corrosion fatigue studies were first reported by Haigh [9] in 1917 and followed by McAdam during 1926 – 1930 [10]-[13]. Gough and Sopwith [14]-[17] published extensively on the topic from 1932 – 1946. One of the first meetings devoted to environmental aspects of fatigue was the ASTM symposium entitled “the Effects of Complex Load Histories and Chemical Environments on Fatigue” [18]. In 1971 a major symposium sponsored by NACE was held on corrosion fatigue at the U. of Connecticut and the proceedings were published by NACE. The proceedings from that symposium contain many key papers on the work to that time [19]. Duquette provided an extensive review of corrosion in that volume [20]. In more recent years NACE has held another meeting on environmental effects and the proceedings of that symposium are noteworthy. In addition to the research work by Professor Pierre Roberge (e.g., Refs [1]-[3]) he also manages an important web site which is one of the most valuable resources on corrosion (www.corrosion-doctors.org).

9.3 THE HOLISTIC APPROACH TO EAC

The systems view, or more recently the HOLISTIC view, of corrosion fatigue [5],[7] can be viewed as shown in Figure 9-3. All of the basic elements of the fatigue systems view are included in this figure and the key issues of the chemical environment are added. It now becomes important for the engineer interested in designing a component to anticipate the chemical environments that the component will be exposed to along with the mechanical load/force spectra and these issues must be incorporated into the life estimation and all aspects related to it. In a manner similar to what the fatigue community has done to standardize load spectra for applications, and certainly as a minimum to define the force spectrum to the highest degree possible, so the chemical environmental spectrum must now be understood and defined as well. This is needed since the chemical environment composition, type of exposure, frequency of loading, and electrochemical parameters are all involved in determining the type of corrosion that will result and

the resultant detailed mechanism of corrosion fatigue. To complicate matters some components will experience chemical exposure and loading where corrosion mechanism overlap will occur. In other words, pitting may be a dominant nucleation mechanism and a bona fide Mode I crack may form from the pit growth and become either an environmentally accelerated short crack or a long crack.

Although there are some laboratories in the world that control the chemical environment for “baseline” or reference fatigue data for a given set of test parameters this is rare to this writer’s knowledge. Most laboratories use the term “lab air” or some equivalent without defining what lab air means. In the fatigue test community and corrosion community this has been known to be inadequate since it has been known for many years that the chemistry of the lab air can significantly alter the quality and reliability of the resultant data. Some laboratories take great care to maintain control over the standard environment in which they obtain their baseline fatigue data.

Part of the justification for the above relates to the fact that little work has been done to either characterize the chemical environments encountered by most aircraft components or to adopt rational methods to deal with those environments in their sustained loading and fatigue design methods. This has been markedly improving in recent years. The manner in which most companies and government agencies have tried to deal with corrosion fatigue is to use a CPCP (Corrosion Prevention and Control Program). However, it is well known in the structural design community that this has serious shortcomings since the corrosion protection systems may break down and must be replaced or repaired. In addition, where corrosion is detected either by astute maintenance personnel or by failures or both the damage caused by corrosion or corrosion fatigue degradation must now be repaired or the component must be replaced. This is often referred to as the “find it and fix it approach”. Many engineers rely on the detection of corrosion as part of a poorly defined and directed maintenance and inspection program to assure the integrity of components from the ravages of corrosion fatigue. This is not an acceptable design practice and today the knowledge base on corrosion and corrosion fatigue is such that a design approach of “anticipate and manage”, similar to fatigue and damage tolerance, can and should be used. This is part of the HOLSIP approach.

9.4 IMPLICATIONS FOR AIRCRAFT STRUCTURAL INTEGRITY

Most fatigue design has been done assuming that materials used are homogeneous, continuous and isotropic media. This allows engineers to apply principles of solid mechanics and makes the challenges of design tractable using stress and strain and fracture mechanics techniques. In addition, surfaces are often assumed to be perfect or to be in an ideal state and the materials are assumed to be free of all types of corrosion. Corrosion is often thus classed as a defect or a flaw. As indicated, when corrosion is found on critical components it must either be removed or the component must be replaced, or we operate the component at much higher risk in terms of integrity. Many aspects of this idealized paradigm have been discussed by Hoepfner and others in many past and relatively recent papers [7].

In a large body of work culminating in a paper at a recent ICAF meeting (International Committee on Aeronautical Fatigue) Hoepfner pointed out that corrosion / corrosion fatigue may cause any or all of the following conditions to occur when components are operating in corrosion producing conditions:

- 1) Reduction of section size with a concomitant increase in stress. *Global or local.*
- 2) Production of stress concentration. *Local.*
- 3) Nucleation of cracks. *Local, possibly global. Source of multiple-site cracking.*
- 4) Production of corrosion debris. This may result in surface pilling in some cases by various means, which may significantly change the stress state and structural behavior. *Local and global.*
- 5) Creation of a situation that causes the surfaces to malfunction. *Local and global.*

- 6) Cause Environmentally Assisted Crack Growth (EACG) under cyclic (Corrosion fatigue) or sustained loading (Stress Corrosion Cracking – SCC) conditions. *Local.*
- 7) Create a damage state that is missed in inspection when the inspection plan was not developed for corrosion or when corrosion is missed. *Local and global.*
- 8) Change the Structurally Significant Item (SSI) due to the creation of a damage state not envisioned in the structural damage analysis or fatigue and strength analysis. If the SSI is specified, for example, by location of maximum stress or strain, then the corrosion may cause another area(s) to become significant. *Local or global.*
- 9) Create an embrittlement condition in the material that subsequently affects behavior. *Local or global.*
- 10) Create a general aesthetic change from corrosion that creates maintenance to be done and does damage to the structure. *Local or global.*
- 11) Corrosion maintenance does not eliminate all the corrosion damage and cracking or the repair is specified improperly or executed improperly thus creating a damage state not accounted for in the design. *Local or global.*
- 12) Generation of a damage state that alters either the durability phase of life or the damage tolerant assessment of the structure or both.
- 13) Creation of a Widespread Corrosion Damage (WCD) state or a state of corrosion that impacts the occurrence of Widespread Fatigue Damage (WFD) and its concomitant effects. This has been observed in many applications from automobile frames to aircraft wings or fuselage segments, etc.

The types of corrosion vary widely and depending on which author you read and study it appears there are at least 8 and up to 14 types of corrosion. Thus, the thermodynamics vary widely and activation energies to nucleate a given mechanism have been found to vary with numerous input parameters. For this reason, in those cases where the attempts have been made to deal with the potential fatigue life reduction or fatigue allowable stress/strain reduction in a given environment the investigators often resort to response testing and produce results similar to those shown in Figure 9-4.

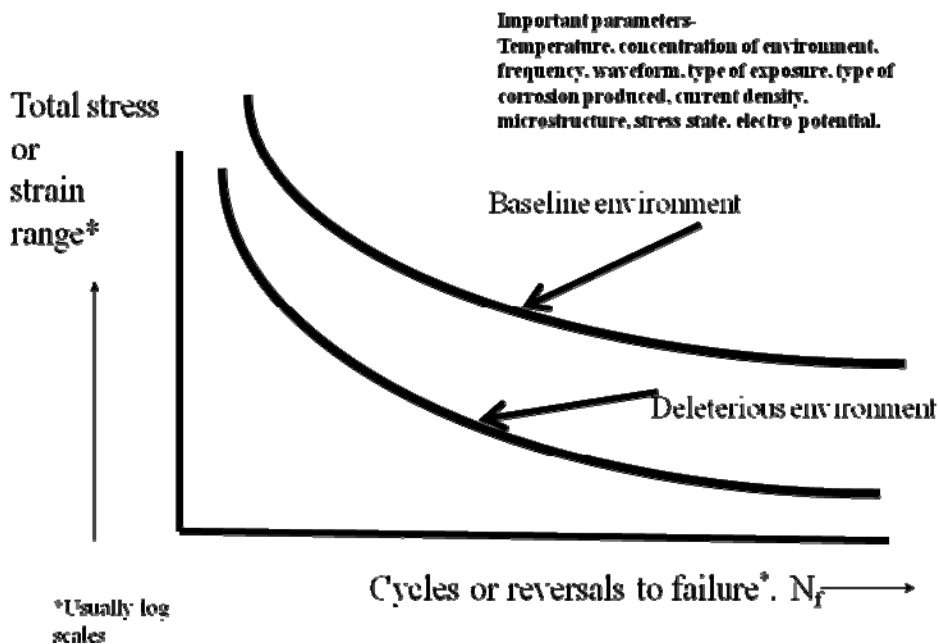


Figure 9-4: Similar to Figure 9-1 Except the Effect of a Deleterious Environment is Shown (see Hoepfner [7]).

The general effects first observed by Haigh, Gough et al., and McAdam and now many others [19]-[33] are as follows:

- The fatigue limit, if it truly existed in a baseline situation, is eliminated as depicted in Figure 9-4. The consequences of this are extremely significant if a component has been designed for “infinite life” since it now becomes a clearly finite life or limited life part.
- At a given stress or strain the expected life to failure is reduced.
- At a given life the stress or strain allowable is reduced.
- In the fatigue crack propagation realm the chemical environment accelerates fatigue crack propagation at a given stress intensity level.
- The fatigue crack propagation threshold is reduced and may not exist at all.
- Embrittlement occurs during crack nucleation and all phases of crack propagation. Thus, corrosion fatigue crack fracture surfaces take on a faceted appearance similar to Stress Corrosion Cracking (SCC). In many metallic alloys it is difficult if not impossible to determine a fractographic difference between environmentally assisted crack growth under cyclic loading and that which occurs under sustained static loading.
- The amount of scatter in data is potentially altered in various portions of the stress/strain versus cycles to failure diagram under corrosion fatigue conditions. The amount of the change has been noted to vary considerably but usually decreases.

Figure 9-5 shows the basic effect of a deleterious chemical environment on fatigue crack propagation. Extensive studies of the effect of environment and load spectra were undertaken in related to significant concern about aircraft structural integrity by Hoepfner et al. [32] and Hall et al. [22] on fatigue crack propagation in the early 1970 period. Many studies on the effect of chemical environments on fatigue crack propagation have been conducted since that time and data are now included in many handbooks.

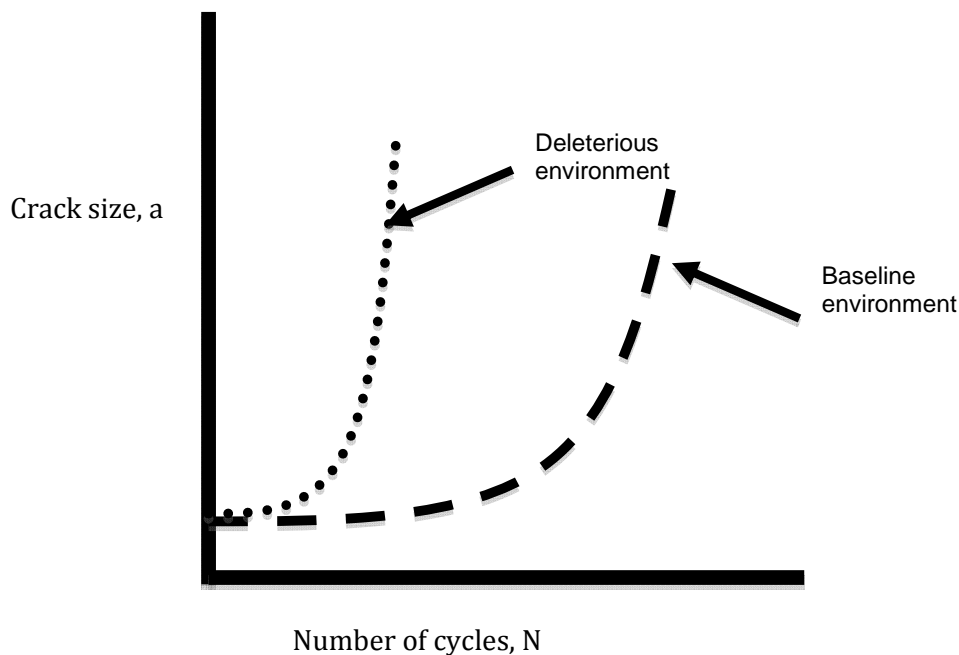
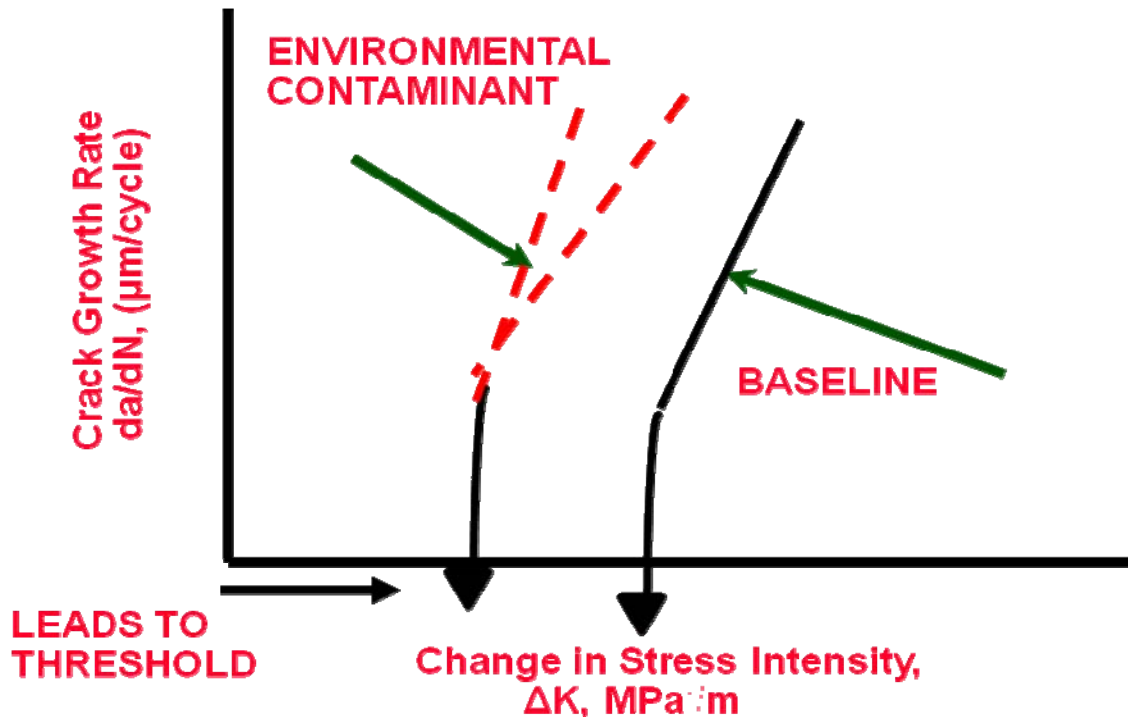


Figure 9-5: Diagram Depicting the Potential Effect of a Deleterious Chemical Environment on Fatigue Crack Propagation (the amount of the effect(s) is dependent on numerous parameters mentioned in Figure 9-4).

When fatigue crack propagation data such as shown in Figure 9-5 are evaluated using fracture mechanics concepts the data are usually plotted on a da/dN versus ΔK set of axes as shown in Figure 9-6 above.



**Figure 9-6: A Depiction of Fatigue Crack Propagation Data Plotted on da/dN versus ΔK Axes
(Note the potentially significant effect of a chemical environment is shown in the left dashed line).**

The figure shows the general trend when a chemical environment may influence the fatigue crack propagation behavior of a component in the field. The dashed red lines on the upper left of the figure indicate potential lines/bands of data from the environmental effects. In addition to the potential effects shown, the fatigue crack growth threshold also may be modified by the environment and generally lowered. Furthermore, significant effects of the environment have been observed on short crack propagation rates. This is very significant when attempting to assess the role of short cracks in Multiple Site Damage (MSD) and the potential for crack link up and the effects on structural integrity. It is clear from an observation of Figure 9-6 that a major impact from the acceleration of fatigue crack propagation may occur and alter the time or cycles between inspection intervals of components and thereby significantly alter the integrity assessment. Many ways have been proposed for assessing the potential impact of the environmental effects. Chapter 13 discusses more aspects of this.

In recent years the aviation industry has devoted much attention to introducing design and integrity practices into aircraft structural integrity programs. This is in part related to recognition of the significance of the problems of corrosion and corrosion fatigue as they relate to integrity after the Aloha Airlines Accident in 1988. The commercial and military aircraft fleet surveys subsequent to the event led to an understanding that these two degradation modes were much more serious than originally envisaged. Thus, all the structural integrity programs are being modified to deal with corrosion and corrosion fatigue along with fatigue, damage tolerance and residual strength issues.

The need to understand the potential for the occurrence of corrosion and corrosion fatigue on structural components is critical. Thus, to even begin the assessment of this potential the technical community needs to know the following:

- The chemical environment likely to be encountered on the structure of interest at the location of interest;
- The material from which the component is manufactured;
- The orientation of the critical forces (loads) applied externally and internally with respect to the critical directions in the material;
- The susceptibility of the material to occurrence of a given type of corrosion;
- The temperature of exposure of the component;
- The type of forces applied (i.e., sustained force {SCC} or cyclic force (constant force amplitude or variable force amplitude corrosion fatigue));
- The type of exposure to the chemical environment (i.e., constant, intermittent, concomitant with the forces (corrosion fatigue or stress corrosion cracking) or sequentially with force (corrosion/fatigue or corrosion-fatigue));
- The rates of corrosive attack;
- The potential influence of the effects of corrosion on fatigue crack nucleation and propagation;
- The impact of any related corrosion degradation on residual strength;
- The type(s) of corrosion encountered;
- The means of inspecting for corrosion at the locations of interest;
- Models to assist and guide the estimation of lives and lives between inspection and maintenance intervals where corrosion fatigue will be a major failure consideration;
- The potential for Widespread Corrosion Damage (WCD) to occur; and
- The potential impact of corrosion on the occurrence of Widespread Fatigue Damage (WFD) and its impact on structural integrity.

9.5 CONCLUDING REMARKS

Based on today's understanding of both corrosion and corrosion fatigue the technical community can effectively deal with these issues in a component integrity and reliability program. Some companies and government agencies are deeply immersed in this at present.

Obviously the above list is formidable but the assessment of these items is possible to some degree to make the estimation or prediction of the effects of corrosion more accurate than they have been to date. To assist in making Prevention and Control and Prediction and Management of corrosion fatigue more realistic in the future engineers will have to be educated with respect to the phenomenon. In addition more models will need to be developed. The issue of modeling has not been addressed extensively in this chapter but other papers by Hoepfner, Bellinger, Mills, Liao et al. and others (see Chapters 13, 14, 17, 18 and 19 of this document for more detailed descriptions of modeling and quantitative treatment of environmental effects on fatigue crack propagation) have focused on this issue.

At present few U.S. or Canadian Universities **require** a basic undergraduate class in corrosion and related electrochemistry principles for most undergraduate engineering students. Most engineers get a two to three day exposure in their basic material science class that is often the only requirement beyond inorganic chemistry dealing with either corrosion or wear. Of course chemical engineers tend to study more chemistry but many also do not study either electrochemistry or corrosion as a basic requirement. Various technical bodies have attempted to rectify this situation but to date have been unsuccessful. A part of the education must deal with the issues that impact structural integrity to enhance quality and reliability of components critical to many areas of industry and government. To this end there is no doubt that engineers

will have to learn much more about the physics of failure including as many aspects of corrosion and fatigue as possible. This, of course, must be coupled with the study of tribology and creep as well.

Corrosion fatigue is one of the major considerations now recognized as a major failure prevention issue on products. With energy issues becoming more and more important relative to the survival of the planet the issue of corrosion fatigue, along with other failure mechanisms, will become even more critical to the future integrity of products. The last 100 years or so have produced great strides in both understanding and designing for the anticipation and management of corrosion fatigue. The next 100 years will undoubtedly produce many more advances.

9.6 REFERENCES

- [1] Roberge, P.R., "Handbook of Corrosion Engineering", McGraw Hill Book Co., New York, NY, USA, 1999.
- [2] Roberge, P.R., "Corrosion Engineering: Principles and Practice", McGraw Hill Book Co., New York, NY, USA, 2008.
- [3] Roberge, P.R., "Corrosion Inspection and Monitoring", Wiley-Interscience, John Wiley and Sons, Hoboken, NJ, USA, 2007.
- [4] Fontana, M.G. and Greene, N.D., "Corrosion Engineering", McGraw Hill Book Co., New York, NY, USA, 1967, 1978, 1986.
- [5] Hoepfner, D.W., "Cyclic Loading and Fatigue", Tribology Encyclopedia, in press, 2010.
- [6] ATSM E 1823, Part 3, ASTM Standards, ASTM, New Conshohocken, PA, USA, Issued Yearly by ASTM.
- [7] Hoepfner, D.W., "Corrosion Fatigue Considerations in Materials Selection and Engineering Design", Lead Paper, Corrosion Fatigue: Chemistry, Mechanics, and Microstructure, Editors; Devereux, O., McEvily, A.J., Staehle, R.W., Proceedings of the Conference held at the University of Connecticut, 14-18 June 1971, NACE-2, National Association of Corrosion Engineers, Houston, TX, USA, pp. 3-11, 1973.
- [8] Hoepfner, D.W., "Estimation of Component Life by Application of Fatigue Crack Growth Knowledge", Fatigue, Creep of Pressure Vessels for Elevated Temperature Service, MPC 17, ASME, NY, USA, pp. 1-85, 1981.
- [9] Haigh, B.P., "Experiments on the Fatigue of Brasses", Journal of the Institute of Metals, Vol. 18, pp. 55-86, 1917.
- [10] McAdam, Jr., D.J., "Stress-Strain-Cycle Relationship and Corrosion-Fatigue of Metals", Proceedings of the ASTM, Vol. 26 (II), pp. 224-280, 1926.
- [11] McAdam, Jr., D.J., "Corrosion-Fatigue of Non-Ferrous Metals", Proceedings of the ASTM, Vol. 27, No. 2, pp. 102-152, 1927.
- [12] McAdam, Jr., D., "Stress-Strain-Cycle Relationship and Corrosion Fatigue of Metals", Proceedings of the ASTM, Vol. 26, No. 2, pp. 224-280, 1926.
- [13] McAdam, Jr., D.J., "Corrosion Fatigue of Metals Under Cyclic Stress", Proceedings of the ASTM, Vol. 29, No. 2, pp. 250-313, 1929.

- [14] Gough, H.J. and Sopwith, D.G., "Atmosphere Action as a Factor in Fatigue of Metals", Institute of Metals Journal, Vol. 49, pp. 93-122, 1932.
- [15] Gough, H.J. and Sopwith, D.G., "Some Further Experiments on Atmospheric Action in Fatigue", Journal of the Institute of Metals, Vol. 56, pp. 55-89, 1935.
- [16] Gough, H.J. and Sopwith, D.G., "Inert Environments as Fatigue Environments", Journal of the Institute of Metals, Vol. 72, pp. 415-421, 1946.
- [17] Gough, H.J. and Sopwith, D.G., "Some Further Experiments on Atmospheric Action in Fatigue", Journal of the Institute of Metals, Vol. 56, pp. 55-89, 1935.
- [18] "Effects of Environment and Complex Load History on Fatigue Life", ASTM STP 462, Proceedings of the Symposium on Effects of Environment and Complex Load History on Fatigue Life held in Atlanta, GA, 29 September – 4 October, 1968, Edited by M. Rosenfeld, D.W. Hoepfner, and R.I. Stephens, ASTM, Philadelphia, PA, USA, 1970.
- [19] "Corrosion Fatigue: Chemistry, Mechanics, and Microstructure", Editors: Devereux, O., McEvily, A.J., Staehle, R.W., Proceedings of the Conference held at the University of Connecticut, 14-18 June 1971, NACE-2, National Association of Corrosion Engineers, Houston, TX, USA, 1972.
- [20] Duquette, D.J., "A Review of Aqueous Corrosion Fatigue", in Corrosion Fatigue: Chemistry, Mechanics, and Microstructure, O.F. Devereux, A.J. McEvily and R.W. Staehle, Eds., NACE-2, pp. 12-24, 1972.
- [21] Pettit, D., Ryder, J., Krupp, W. and Hoepfner, D., "Investigation of the Effects of Stress and Chemical Environments on the Prediction of Fracture in Aircraft Structural Materials", AFML-TR-74-183, Lockheed California Company, December 1974.
- [22] Hall, L.R., Finger, R.W. and Spurr, W.F., "Corrosion Fatigue Crack Growth in Aircraft Structural Materials", AFML-TR-73-204, Boeing Company, September 1973.
- [23] "Corrosion-Fatigue Technology", ASTM STP 642, Proceedings of a Symposium held in Denver, CO, 14-19 November 1976, Edited by H.L. Craig, Jr., T.W. Crooker, and D.W. Hoepfner, ASTM, Philadelphia, PA, USA, 1978.
- [24] "Aircraft Corrosion", AGARD Conference Proceedings No. 315, Papers presented at the 52nd Meeting of the AGARD Structures and Materials Panel held in Cesme, Turkey, 5-10 April 1981, NATO-AGARD, 64 rue De Varenne, Paris, France, 1981.
- [25] "Corrosion Fatigue", AGARD Conference Proceedings No. 316, Papers presented at the 52nd Meeting of the AGARD Structures and Materials Panel Meeting held in Cesme, Turkey, 5-10 April 1981, NATO-AGARD, 64 rue De Varenne, Paris, France, 1981.
- [26] "Corrosion Fatigue", ASTM STP 801, Proceedings of the Symposium on Corrosion Fatigue: Mechanics, Metallurgy, Electrochemistry, and Engineering held in St. Louis, MO, 21-22 October 1981, Edited by T.W. Crooker, B.N. Leis, ASTM, Philadelphia, PA, USA, 1983.
- [27] Campbell, G.S. and Lahey, R., Int. J. Fatigue, Vol. 6, No. 1, pp. 25-30, 1984.
- [28] Metals Handbook, 9th Ed., Vol. 13, Corrosion, American Society for Metals, Metals Park, OH, USA, pp. 584-609, 1985.

- [29] Wallace, W., Hoepfner, D.W. and Kandachar, P.V., "Aircraft Corrosion: Causes and Case Histories", AGARD Corrosion Handbook, Vol. 1, AGARD-AG-278-Vol. 1, 1985.
- [30] Schütz, W., "Corrosion Fatigue-The Forgotten Factor in Assessing Durability", ICAF 95, Estimation, Enhancement and Control of Aircraft Fatigue Performance, Vol. 1, Edited by J.M. Grandage, G.S. Jost, Proceedings of the 18th Symposium on the International Committee on Aeronautical Fatigue, 3-5 May 1995, Melbourne, Victoria, Australia, EMAS, Warley, West Midlands, UK, pp. 1-52, 1995.
- [31] Swift, S.J., "The Aero Commander Chronicle", ICAF 95, Estimation, Enhancement and Control of Aircraft Fatigue Performance, Vol. 1, Edited by J.M. Grandage, G.S. Jost, Proceedings of the 18th Symposium on the International Committee of Aeronautical Fatigue, 3-5 May 1995, Melbourne, Victoria, Australia, EMAS, Warley, West Midlands, UK, pp. 507-530, 1995.
- [32] Hoepfner, D.W., Grimes, L., Hoepfner, A., Ledesma, J., Mills, T. and Shah, A., "Corrosion and Fretting as Critical Aviation Safety Issues", ICAF 95, Estimation, Enhancement and Control of Aircraft Fatigue Performance, Vol. 1, Edited by J.M. Grandage, G.S. Jost, Proceedings of the 18th Symposium on the International Committee of Aeronautical Fatigue, 3-5 May 1995, Melbourne, Victoria, Australia, EMAS, Warley, West Midlands, UK, pp. 87-106, 1995.
- [33] Cole, G.K., Clark, G. and Sharp, P.K., "Implications of Corrosion with Respect to Aircraft Structural Integrity", DSTO -RR-0102, AMRL, Melbourne, Victoria, Australia, March 1997.

Chapter 10 – SIMULATING CORROSION DAMAGE: EXFOLIATION

Nicholas C. Bellinger

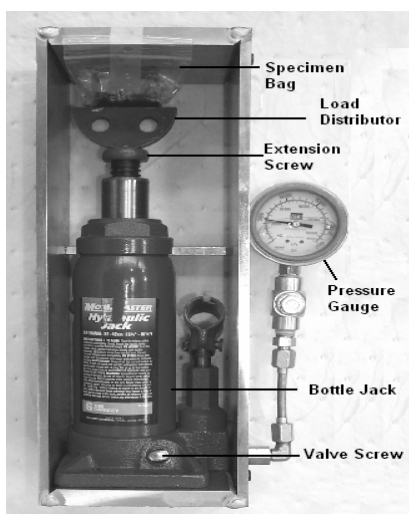
Institute for Aerospace Research
National Research Council Canada
Ottawa, Ontario
CANADA

10.1 INTRODUCTION

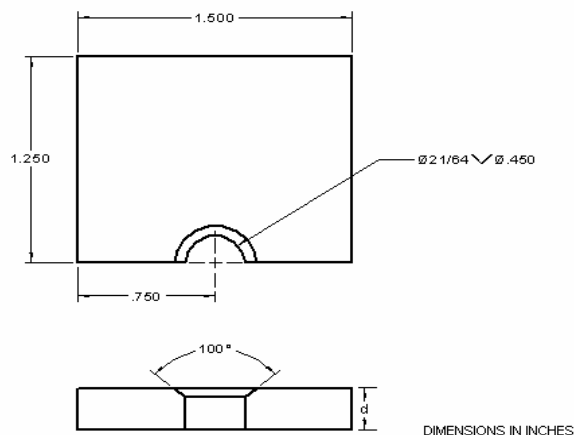
To determine the effect that exfoliation has on the fatigue strength of upper wing skins, fatigue tests need to be carried out on coupons that contain this type of damage. Since it is difficult to obtain naturally exfoliated wing skins because maintenance procedures require that exfoliated areas be ground out to remove the damage, an accelerated artificial exfoliation protocol is required to create the damage in specimens needed to carry out material testing. The methods developed by the National Research Council of Canada to simulate exfoliation damage in a controlled laboratory environment are briefly reviewed in this short note.

10.2 METHODOLOGY

The ASTM G34 EXCO Standard Test Method [1] was developed to determine the susceptibility of 7XXX and 2XXX series material to exfoliation. The EXCO solution has been successful in generating near surface exfoliation at holes that were originally machined in the wing skin material. However, the results were inconsistent when the process was applied to newly manufactured material as well as new holes machined in old material. In an effort to produce exfoliation more consistently, it was suggested that a compressive load, emulating the predominant upper wing skin flight loading, be applied to the specimens. It was proposed that due to the Poisson effect the induced compressive stress, which would occur along the LT direction, would cause a tensile stress in the ST direction making the exposed grain boundaries along a machined edge more susceptible to intergranular corrosion (i.e., exfoliation). A proof-of-concept rig [2] was designed to introduce a static compressive load into simple specimens, Figure 10-1, which would be sectioned and progressively polished to characterize the exfoliation damage generated.



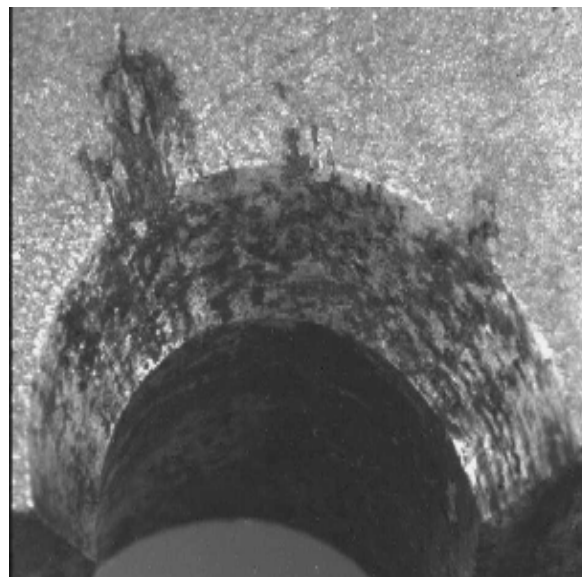
(a) Compression rig.



(b) Detailed specimen drawing.



(c) Specimen placement in compression rig.



(d) Exfoliation produced at countersink side of wing skin after 28 days of exposure to EXCO / compressive load combination for new hole / old material.

Figure 10-1: Configuration of Compression Rig Set-Up and an Example of the Exfoliation Damage Produced.

10.3 RESULTS

The polishing results showed the presence of large pits, which appeared prior to the formation of intergranular corrosion, Figure 10-2. These large pits, which are not normally found in natural exfoliation, have been attributed to the initial pH level of the EXCO solution [3]. During the first 24 hours of the EXCO test, the solution (234 g of NaCl, 50 g of KNO₃ in water, 6.3 mL of concentrated HNO₃, 70% and dilute to 1 L) is highly acidic, starting at a pH of 0.4 and gradually stabilizing at a pH of 3.2. To eliminate this initial acidity, the EXCO solution was modified to produce an initial pH level of 3.2, which would

remain constant over an extended period of time [3]. The new protocol, known as the Aluminum-Nitrate-Chloride Immersion Test (ANCIT) [3], was developed that consists of 235 g of NaCl, 60.6 g of KNO₃, 5.31 g of AlCl₃·6H₂O in water and diluted to 1 L.

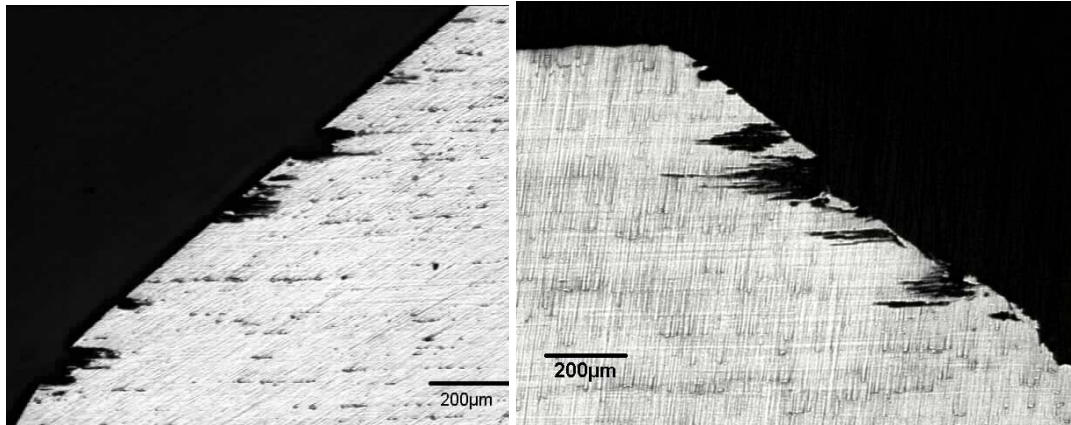
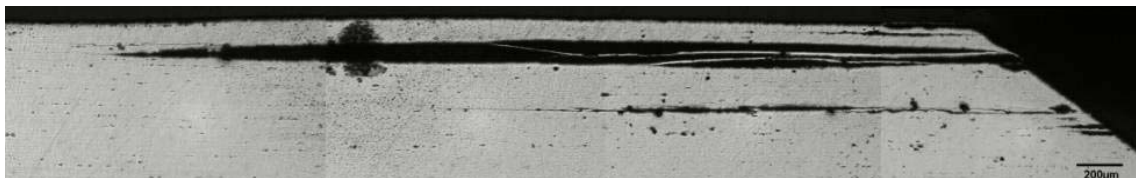
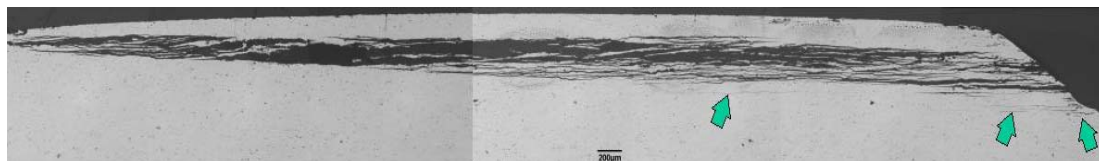


Figure 10-2: Optical Micrographs Showing Large Pits Generated by EXCO Solution.

When the ANCIT solution was used to generate exfoliation at the countersink of a hole in an upper wing skin, the damage produced was considered light, in that, the surface of the wing showed only a slight bulge. The results from the polishing showed the absence of the large pits that were present in the EXCO tests. The ANCIT tests resulted in similar damage to that present in naturally exfoliated wing skins, as shown in Figure 10-3.



(a) Artificial exfoliation (ANCIT).



(b) Natural exfoliation.

Figure 10-3: Examples of ANCIT Generated Artificial Exfoliation and Natural Exfoliation.

To artificially introduce exfoliation in undamaged wing skins, the surface of the test area within the hole was scratched with a probe to provide a nucleation site for the damage, after which the steel fastener was installed. In addition, the fastener can be modified according to Figure 10-4 in order to introduce exfoliation damage at specific locations along the countersink of a fastener hole. The top surface paint in the area of the fastener holes was removed and double sided-sealant tape was used to mask off the area that would be exposed. A syringe was then used to deliver the different solutions to the area of interest by moving the plunger periodically to force fresh solution into the test region. The double-sided tape was used to seal the syringe in order to prevent leakage of the solution. Figure 10-5 shows an image of the

SIMULATING CORROSION DAMAGE: EXFOLIATION

syringes in which one contained the EXCO solution while the other held the ANCIT solution and the sealant tape that was located at two fastener holes, which prevented leakage.

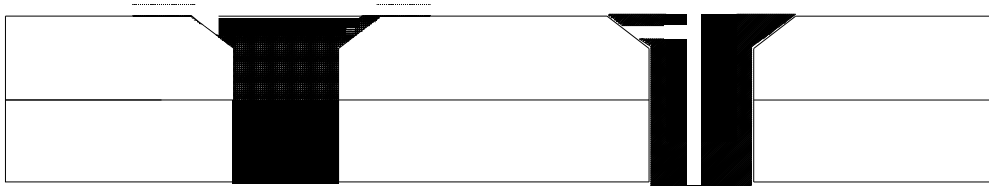


Figure 10-4: Modification Made to Steel Fastener to Introduce Exfoliation at Different Locations Along the Countersink.



Figure 10-5: Typical Set-Up for Accelerated Exfoliation Protocol.

During the development of the accelerated protocol, it was determined that the exfoliation damage that was generated could continue to grow after a solution is removed. To prevent this continuous growth, it is recommended that the specimens should be tested within a reasonable time frame. An alternative to this quick turn-around is to develop a protocol that would arrest the growth such as de-humidification and pH neutralization. It is also recommended that specimens be stored in a freezer to prevent further growth.

10.4 REFERENCES

- [1] ASTM G34 EXCO Standard Test Method, American Society for Testing and Materials, West Conshohocken, PA, USA, Copyright 1996.
- [2] Roe, P.W., Gould, R.W. and Bellinger, N.C., "Induced Exfoliation Compression Rig Experiment; Overview of Apparatus and Testing Procedure", LM-SMPL-2002-0084, Institute for Aerospace Research, National Research Council Canada, 2002.
- [3] Lee, S. and Lifka, B.W., "Modification of the EXCO Test Method for Exfoliation Corrosion Susceptibility in 7XXX, 2XXX and Aluminum-Lithium Alloys", New Methods for Corrosion Testing of Aluminum Alloys, ASTM STP 1134, pp. 1-19, 1992.

Chapter 11 – SIMULATING PILLOWING CORROSION DAMAGE

Ronald W. Gould

Structures and Materials Performance Laboratory, Institute for Aerospace Research
National Research Council Canada
Ottawa, Ontario
CANADA

11.1 INTRODUCTION

The ability to discover the accumulation of corrosion products hidden within a built-up structure is as important as being able to measure the damage so that appropriate repair and corrective actions can be determined.

Today's robotic assembly of aerospace structures tends to remove the surface deformations due to hand assembly resulting in very smooth surfaces and making the visualization of surface disturbances easier. Once located there remains the issue of determining where in the assembled layers the damage actually lies.

Hand-held eddy current devices are basic tools used to perform spot measurements to determine depth of corrosion damage. Machined blocks or sheets of the identical material are used to create calibration standards for setting up the eddy current device. The calibration standards are thus representing a machined thickness loss as corrosion damage. The issue is that the machining results in flat bottom circles or squares with straight edges which are not fully representative of real damage. When the standard consists of machined sheets assembled together into a multi-layered structure an air gap is created between the sheets at the machined sites which is also not realistic.

The simulation of corrosion pillowing will thus be divided into two parts:

- 1) Techniques to generate surface deformations that simulate pillowing; and
- 2) Those employed to artificially represent the internal damage to make the simulation sufficiently realistic.

It should be noted that to visualize the pillowing of the outer skin surface on some of the lap joint examples herein an enhanced optical technique has been employed. The D-Sight™ images were obtained through the use of a D Sight Aircraft Inspection System (DAIS) -250C (corrosion) inspection head. The DAIS are no longer available commercially but the technique remains a significant tool for visualizing subtle surface deformations characteristic of corrosion pillowing not normally detectable by un-aided close visual inspection techniques.

11.2 SURFACE DEFORMATION

Figure 11-1 shows the results of ray tracings depicting corrosion damage of increasing severity when a rivet-to-rivet and rivet row spacing ratio of 1.0 is modeled.

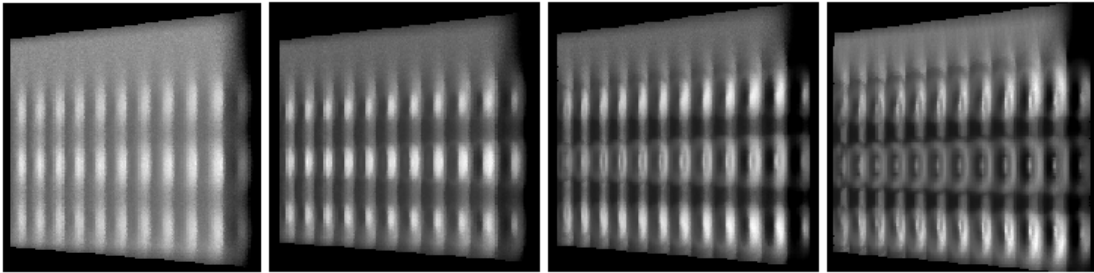
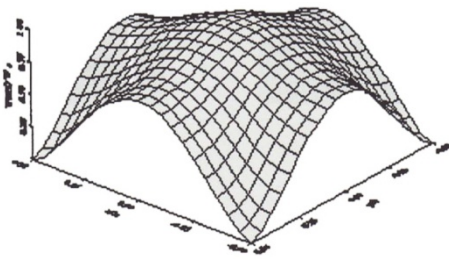
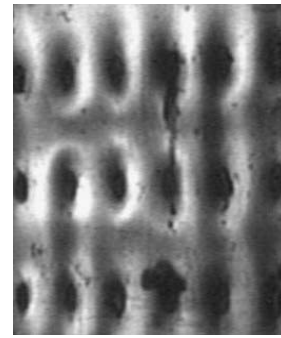


Figure 11-1: Modeling (Ray Tracings) of Corrosion Pilling at 2, 5, 10 and 15 % Thickness Loss.

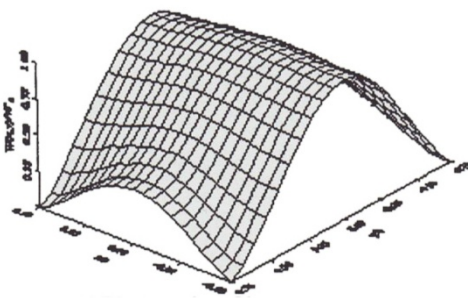
As manufacturers choose to construct joints with two or more rows of mechanical fasteners and then space them at varying intervals the characteristic deformation of these arrangements must be understood so that any simulation will be true to their response to the forces of corrosion damage. The Finite Element Models (FEM) shown in Figure 11-2 depict rivet to row spacing ratios from 1.0 to 2.0 and are accompanied by sample images of corroded joints. The rivets and rows in the Boeing 727 joint are nominally at 1.0 although the holes were drilled by hand not machine. This ratio results in the classic “pillow” with the sheet constrained at the four corners. The Lockheed L1011 joint top and middle row spacing is at 1.5 whereas the middle and bottom rows are at 1:1. This results in a “wave” when observed along the length of the joint. Both examples above are three-row joints. The McDonnell Douglas DC-9 joint is a two-row joint (the top row of rivets actually fastens separate internal “finger” doublers). The skin is very much constrained along the rivet rows and the result is that the skin must deform in a continuous wave that can only be observed when viewed perpendicular to the joint with the aid of optical means sensitive to very small displacements. It must be stated that such close rivet spacing makes the eddy current technique difficult if not impossible to apply between the rivets. Additionally, protruding head rivets can dramatically reduce the inspectable area even on a 1:1 ratio joint. Protruding head rivets also interfere with the normal practice of using grazing light to create shadows to detect pilling as they cast the dominant shadows and limit the unobstructed viewing area.



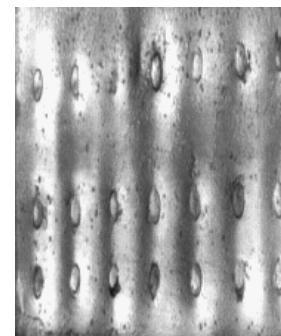
(a) Rivet Spacing 1.0



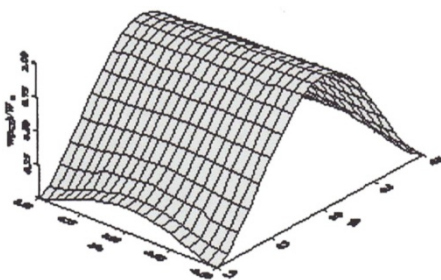
B727



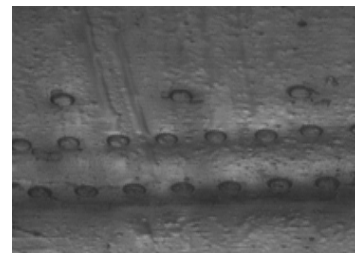
(b) Rivet Spacing 1.5



L1011



(c) Rivet Spacing 2.0



DC-9

Figure 11-2: FEM Models of Varying Fastener and Row Spacings and Sample DAIS Images.

With the above considerations in mind, methods were sought to allow the surface characteristics of early corrosion damage for various lap joint constructions to be quickly simulated and studied at the smallest damage levels.

11.2.1 Mechanically Controlled Deformation

Much like the recent developments in re-configurable discrete-die tooling that controls the displacement of a field of individual pins to form sheet materials for aerospace structures, devices have been built to mechanically deform joints to simulate varying levels of faying surface damage. The intention was to be able to control the deformation between fasteners and create reference masters for optical inspection techniques. The device illustrated in Figure 11-3, Figure 11-4, Figure 11-5 and Figure 11-6 relied on two screw-driven wedges moving equally (in opposite directions) against stationary wedges attached to an internal carriage that mounted an array of hemispherically shaped pins in contact with the inner surface of the skin sheet. The sheet was riveted to the top plate of the apparatus and the pins were located at holes

SIMULATING PILLOWING CORROSION DAMAGE

through the top plate that corresponded with the centroid between the evenly spaced rivets. Small amounts of displacement could be accommodated but obtaining an even deformation across the entire array proved impossible due to bending of the carriage and sticking of the wedges. Smaller areas were successfully deformed and employed to cast dimensionally stable silicone surface replicas that themselves were used as masters for evaluating the sensitivity of enhanced optical pillowing detection devices.

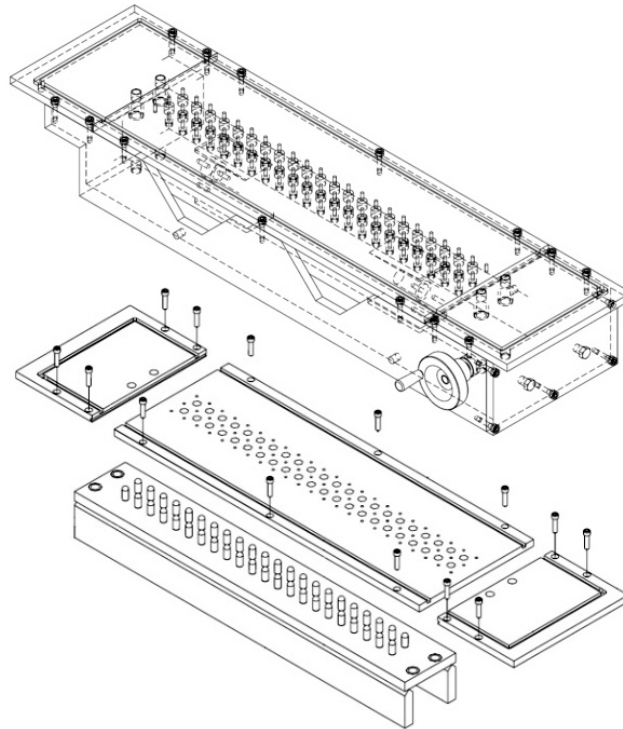


Figure 11-3: Schematic View of Dual-Ramp Pin-Pressure Pillowing Simulator.



Figure 11-4: Top View of Mechanical Pillowing Simulator.



Figure 11-5: Side View of Mechanical Pillowing Simulator.



Figure 11-6: Close-Up Side-View of Pin Contact with Underside of Skin Sheet

11.2.2 Hydraulic Pillowing

Another way of developing surface deformations to simulate corrosion pillowing is by fabricating the structure with an inflatable bladder located between the layers. Many fuselage joints are constructed with faying surface sealants or adhesive layers. The bladder was no thicker than these layers.

The bladder edges and perimeters around each fastener hole are sealed before lap joint assembly and a port is provided into the bladder. A vacuum is drawn through the port to remove all air before a liquid is introduced under pressure. Simple single-bladder lap joints were fabricated and pumped to various pressures/skin deflections using hydraulic fluid or water. To produce examples with permanent deformations at various simulated damage levels the bladder was pumped with a low temperature casting metal (i.e., Cerrobend which becomes a liquid at 70°C (158°F)) that was allowed to cool and solidify. Waxes were also liquefied, pumped and allowed to solidify.

More complex structures can also be fabricated with bladders between the skins and the stringer, tear straps, doublers and beauty strips. Therefore damage in all or only selected areas may be simulated and the external surface effects observed and recorded.

The sequence of images shown in Figure 11-10 illustrates one complete pressurization cycle for a lap joint fabricated with two 0.045 inch (1.14 mm) 2024-T3 skins and depicted in Figure 11-7, Figure 11-8 and Figure 11-9. The lap joint was hand riveted and thus not completely flat. After being deformed to a maximum fluid pressure of 80 psi (551 kilopascals) the outer surface returned to its original condition when the pressure was released.

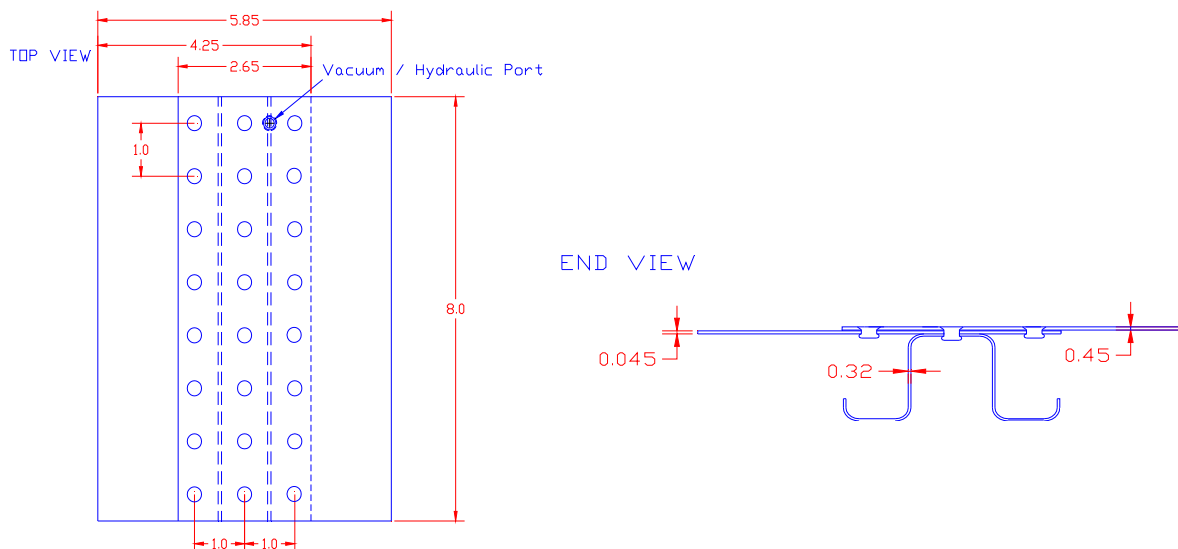


Figure 11-7: Sketch of Lap-Joint with Hydraulic Pillowing Bladder.

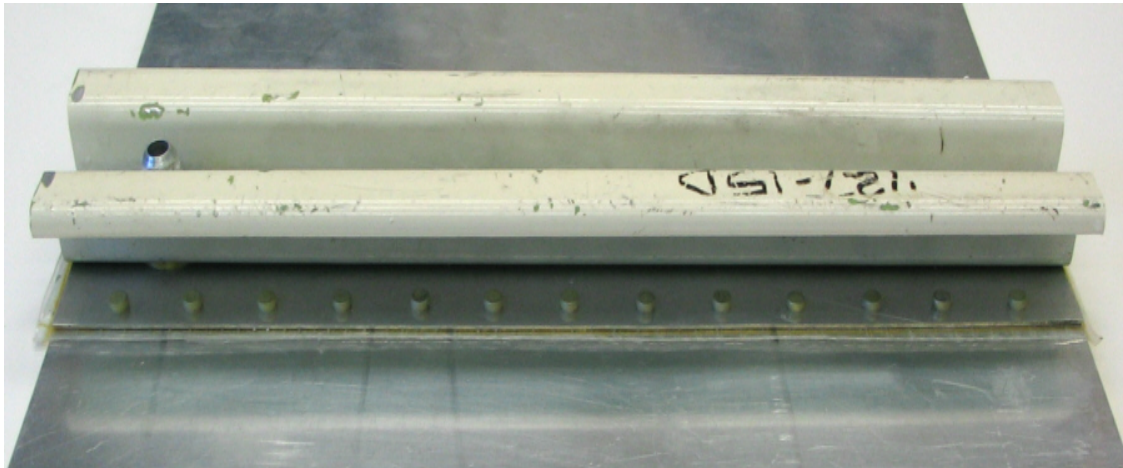


Figure 11-8: Overall View of Rear Surface of Hydraulic Pillowing Lap-Joint with Stringer.

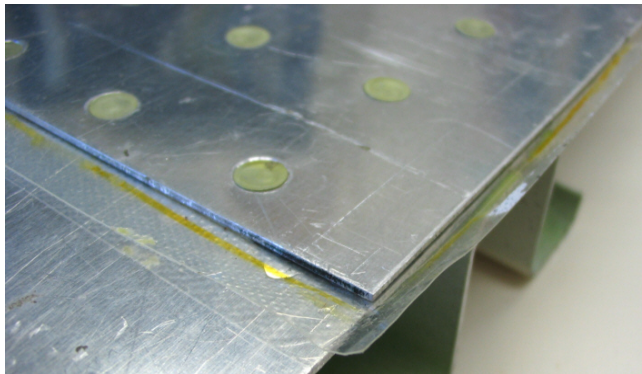


Figure 11-9(a): Close-Up of Bladder.

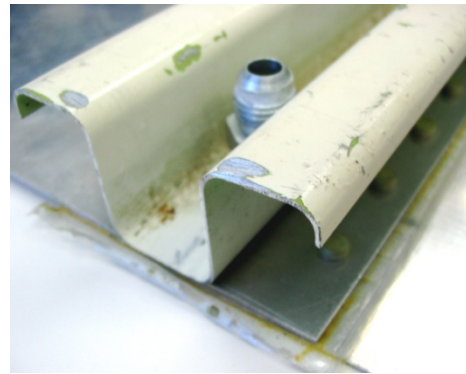


Figure 11-9(b): Close-Up of Vacuum/Hydraulic Port.

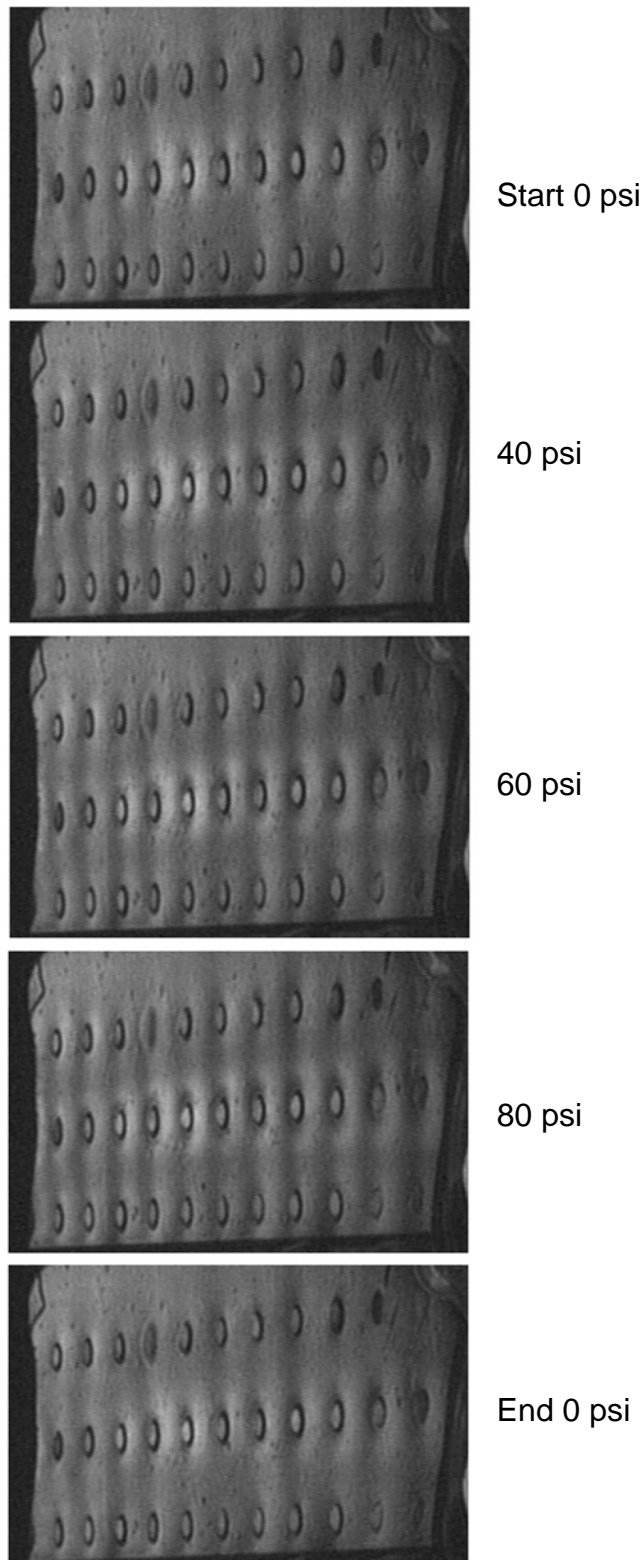


Figure 11-10: DAIS Images of One Pressure Cycle on a Hydraulic Pillowing Lap Joint.

It should be noted that the surface deformation of the hydraulic pillowing joint at 80 psi appears similar to the ray tracing model for 10% thickness loss shown in Figure 11-1.

11.3 PILLOWING DAMAGE INTERNAL SIMULATION

In-service damaged structure, if available, exhibits only the current level of corrosion pilling. Damage formation and progression are best understood by applying artificially accelerated corrosion processes to pristine original or purpose-built new structures. The advantage of using original structure is that the alloys, protective coatings and faying surface sealants are to the manufactures exact specifications. In either case the corrosion can be monitored from the beginning. With multiple samples some can be sacrificed to teardown analysis. It is the teardown and investigation of the damage that assists in the understanding of corrosion pilling, its simulation and its implications with respect to structural integrity.

Figure 11-11 shows a typical two-layer lap joint calibration standard with machined areas on the inner surfaces of the outer and inner skin. The circular areas were milled to specified depths to represent varying levels of corrosion damage as thickness losses. As stated in the introduction, this type of eddy current calibration standard suffers from being non-representative of the internal characteristics of the natural corrosion damage found on an aircraft. Direct comparison for damage assessment is therefore difficult.

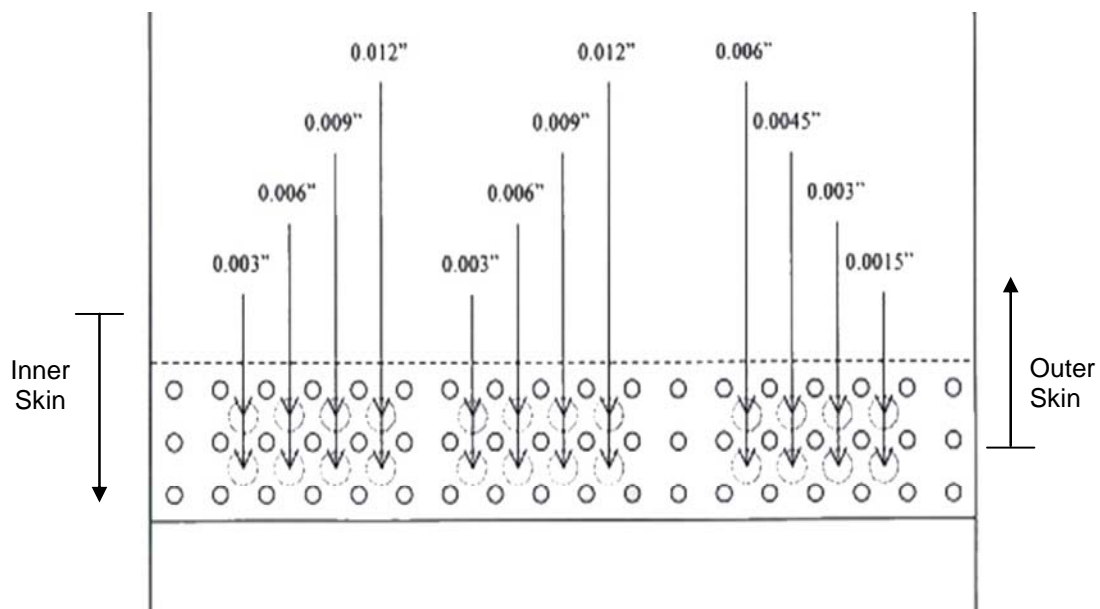


Figure 11-11: Schematic of 7075-T6 Lap Joint NDI Calibration Standard for Eddy Current with Machined Thickness Loss Simulating Crevice Corrosion Damage.

Figure 11-12 shows a robotized eddy current scan image of the entire joint area on the lap joint standard shown in Figure 11-11. A line (profile) has been taken from left to right through the area between the top and center rows of rivets. Such profiles are generated at each of four frequencies (2, 4, 7 and 12 kHz) used to scan both the standard and the suspect corroded structure. The calibration panel has machined areas of known material loss in both the front and back layers ranging from 0.0015" (0.038 mm) to a maximum of 0.012" (0.305 mm) which provide a distinctive profile related to the material loss. By comparing the deflections in the profile line from the corroded panels and from the calibration panel images it is possible to estimate the amount of material loss due to corrosion.

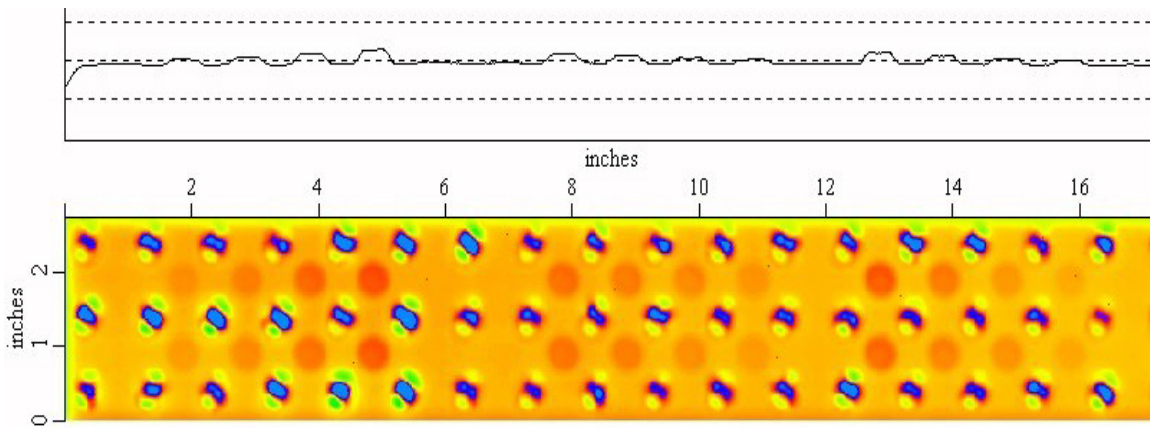


Figure 11-12: Baseline Absolute Eddy Current Scan of NDI Calibration Standard Joint at 7 kHz.

The technique described above is simple but problematic. The areas of machined thickness loss are easy to detect because they do not represent internal damage features such as corrosion product, surface topography, sealants or protective coatings. Also, the standard would not represent the external features of surface deformation or “pillowing” that result from corrosion product accumulation and volumetric increase of that product. Pillowing can cause “lift-off” difficulties with the eddy current probe contact with the surface. Figure 11-13 shows the outer surface of a lap joint undergoing accelerated corrosion where only the inner “faying” surfaces are being corroded. The outer surface is protected by a paint system. The damage is approaching 10% thickness loss yet the eddy current scan of this specimen, Figure 11-14, is not as easy to evaluate as the calibration standard.

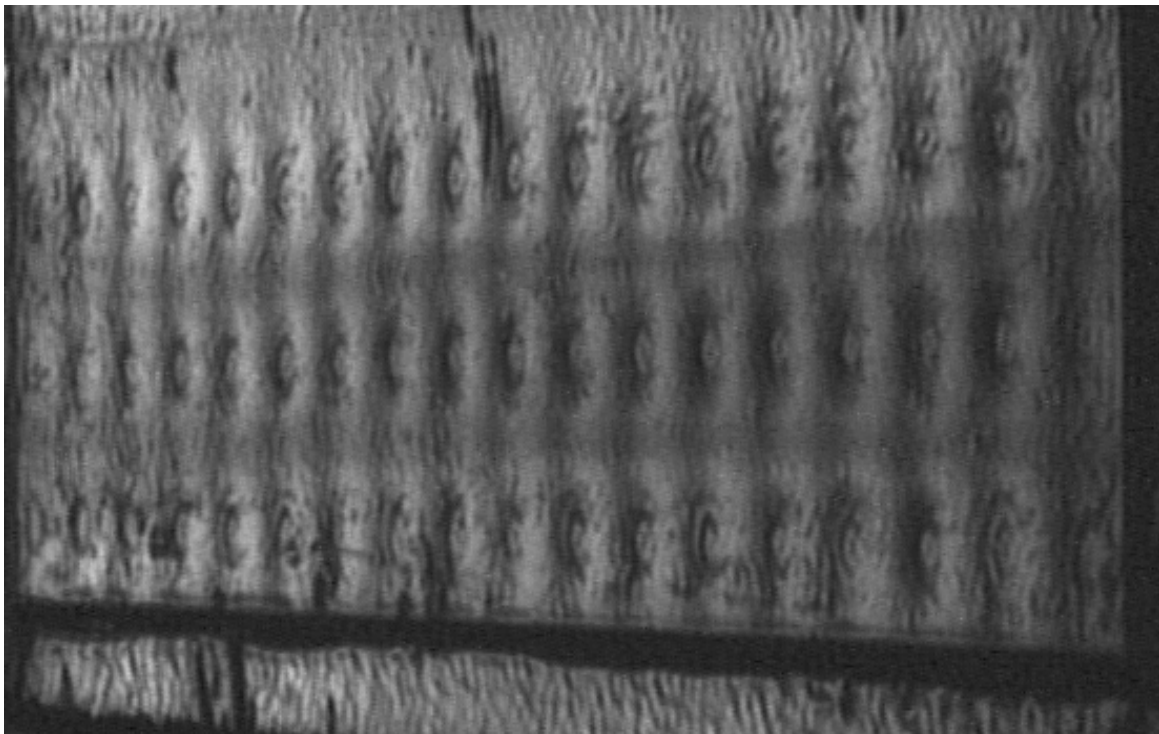


Figure 11-13: DAIS Image of Accelerated Corrosion Pillowing Following 387 Days (9288 Hours) of Salt Fog Exposure.

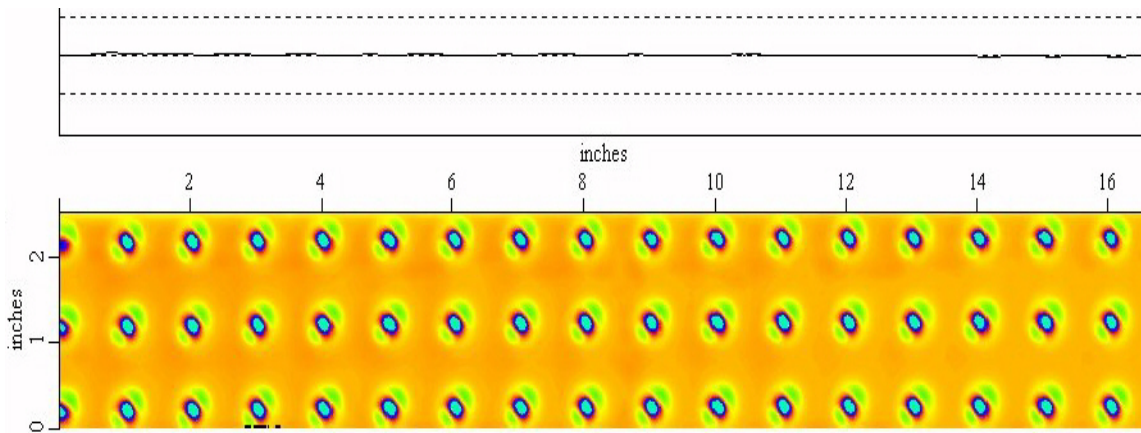


Figure 11-14: Absolute Eddy Current Scan of Accelerated Corrosion Panel at 7 kHz After 387 Days (9288 Hours) of Salt Fog Exposure to Faying Surfaces.

Note the effect of the stringer attached to the center row of rivets. This area of the outer skin is pillowed more than the upper and lower rivet rows because all the deformation (pillowing) must be outwards due to the stiffness supplied by the stringer. The inner skin at the upper and lower rivet rows can be deformed inwards and thus the outer surface deformation is less, when compared to the middle row, for the same damage level. Note also the similarity to the ray tracing model for 15% shown in Figure 11-1.

Figure 11-13 illustrates the ultimate method for simulating corrosion pillowing that being the accelerated corrosion of the subject joint design. The effort is very labour intensive and the results cannot be predicted. Protection of the surfaces that are not to be corroded is key while the specimen must be configured such that periodic inspections can be conducted to determine the presence and level of corrosion activity. Typically, months of continuous salt fog environmental conditioning are required to initiate internal damage and, as shown in Figure 11-13, more than a year was required to attain approximately 15% thickness loss damage.

11.3.1 Pillowing Measurement

Whereas the accelerated corrosion lap joint shown in Figure 11-13 shows uniform damage the simple two-layer lap shown in Figure 11-15 is more typical of natural damage found in service in that the damage is not uniform throughout. Prior to disassembly this corroded joint was measured to determine the skin deformation that upon teardown could be more directly related to the assessed internal damage.

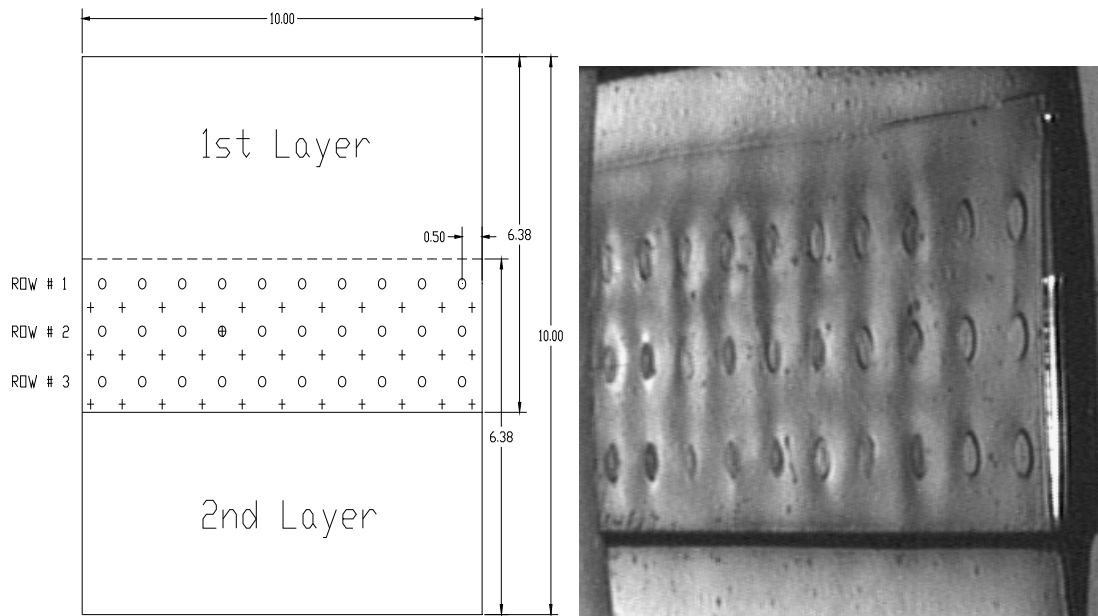


Figure 11-15: Lap Joint Panel (2024 T3, 0.040 inch, 1.016 mm Thick Skins).

The table of measurements below is in two parts. The measurements were taken with a deep throat micrometer and three measures were averaged for each result. The top group of measurements is of the total thickness measured at the locations shown in the drawing above, for the three rows. The bottom group of measurements is the pillowing (theoretical pristine lap thickness deducted from values in top table).

Table 11-1: Pillowing Measurements of the Two-Layer Lap Joint Shown in Figure 11-15.

		1st Layer 0.040											
	1	2	3	4	5	6	7	8	9	10	11		
a	0.108	0.097	0.098	0.096	0.104	0.095	0.096	0.095	0.094	0.089	0.092		
b	0.096	0.097	0.096	0.092	0.095	0.093	0.094	0.098	0.099	0.092	0.091		
c	0.092	0.096	0.094	0.092	0.093	0.100	0.097	0.105	0.095	0.091	0.092		
						2nd Layer 0.040						Zero 0.001	
	1	2	3	4	5	6	7	8	9	10	11		
a	0.027	0.016	0.017	0.015	0.023	0.014	0.015	0.014	0.013	0.008	0.011		
b	0.015	0.016	0.015	0.011	0.014	0.012	0.013	0.017	0.018	0.011	0.010		
c	0.011	0.015	0.013	0.011	0.012	0.019	0.016	0.024	0.014	0.010	0.011		

11.3.2 Machined Simulation

Careful teardown and corrosion product removal was applied to both natural and artificially corroded structures to enable the interrogation of the damaged area. The exposed corrosion product was removed by use of a chemical process to avoid further mechanically induced abrasive damage. The chemical cleaning process permitted a better appreciation for the surface topography on the remaining metal. The teardown and cleaning also pointed to the fact that the clamp-up provided by the rivets means that the last locations to suffer corrosion damage within the joint are those nearest the fasteners.

The objection to the flat-bottomed machined thickness loss areas used on the typical calibration standard (Figure 11-11) was first addressed by creating an Electric Discharge Machining (EDM) tool electrode that incorporated a rough face. When this rough-faced tool was worked to the desired depth the result would be a surface topography emulating the surface condition previously observed on the cleaned corroded specimens. A calibration standard prepared in this way would thus be more realistic [1].

The inner surface of a CNC machined sheet shown in Figure 11-16 incorporates the observations and thickness loss values from disassembled and cleaned corroded lap joint skins. The maximum thickness loss is in the zone between the fasteners and tapers towards the edges and fastener locations. The as-machined condition for various thickness loss or damage levels is shown in Figure 11-17. The CNC machined surfaces were then hand sculpted to give them unique surface topographies. These coarsely roughened areas were then lightly sandblasted to better represent corrosion surface damage, Figure 11-18. This technique is an improvement on the EDM method since the topographies are unique.

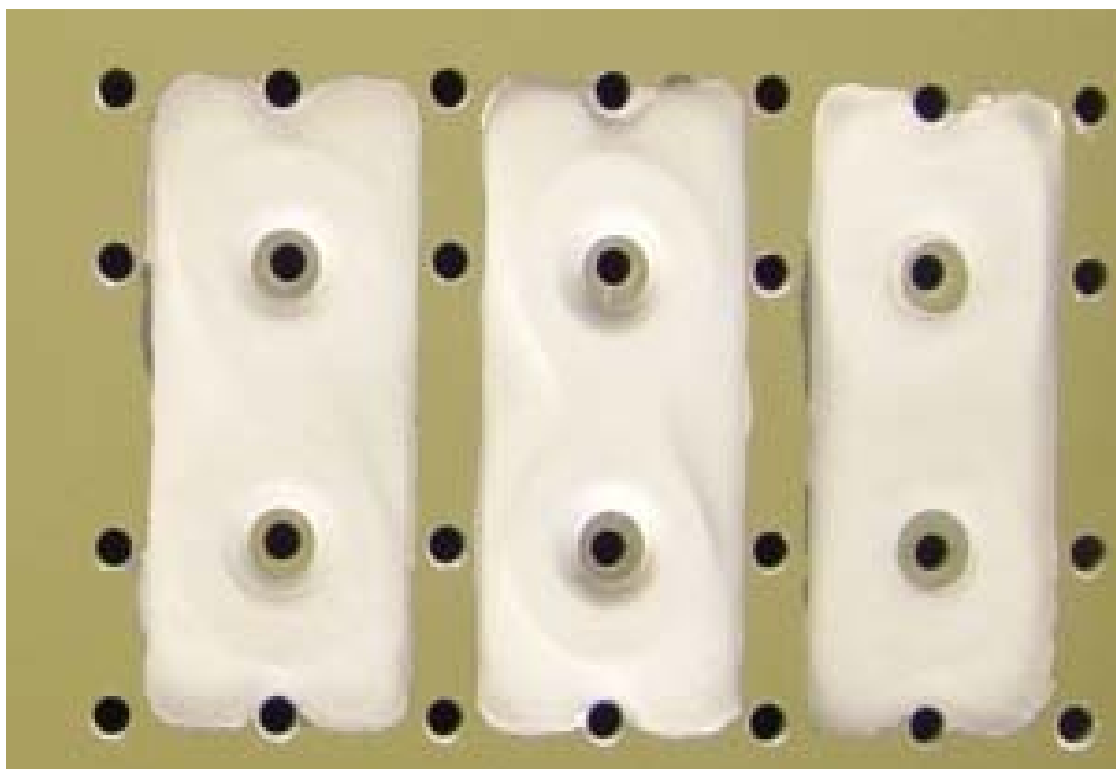


Figure 11-16: Faying Surface of One 2024-T3 Skin for a Simulation of Crevice Corrosion and Pillowing.

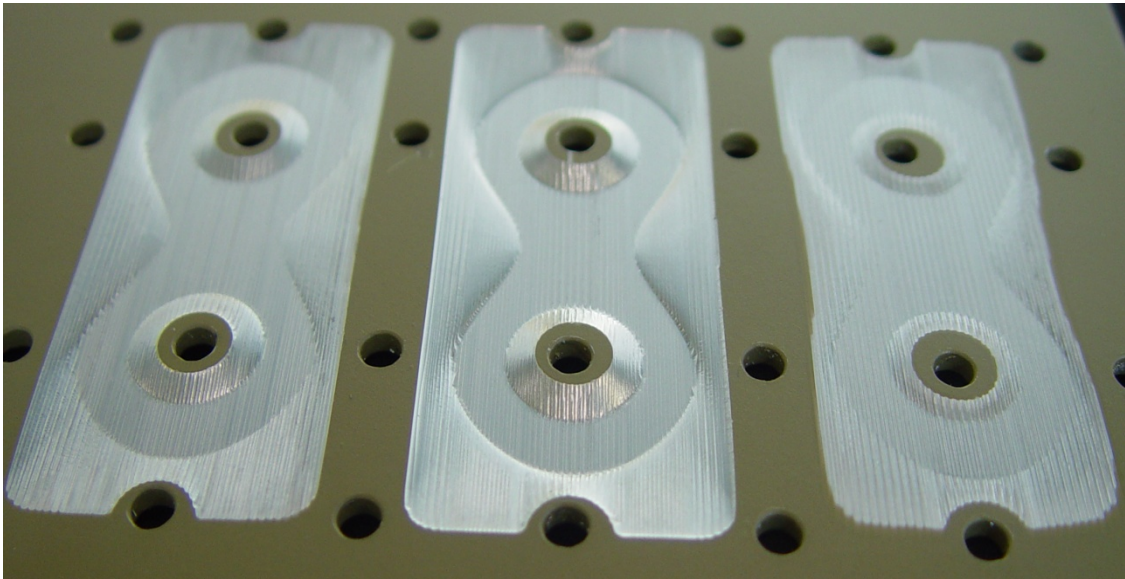


Figure 11-17: CNC Machined Corrosion Damage Thickness Loss to Three Depths (30, 50 and 10 %).

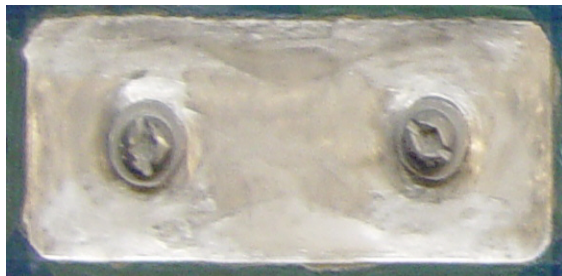


Figure 11-18(a): Machined Areas Hand-Ground.

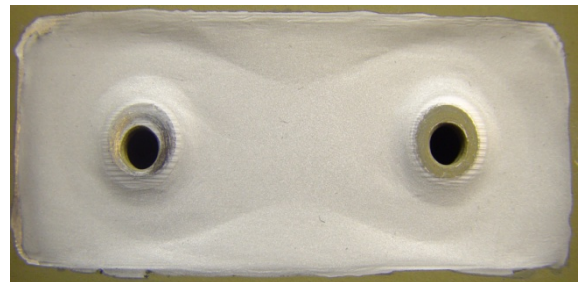


Figure 11-18(b): Surface Sandblasted.

The sandblasted surface offers more natural exposure to the aluminum grains and grain boundaries in comparison to the surface following the milling and grinding. Without sandblasting the corrosive attack would be more likely to advance along the small scratches remaining from the machining.

The machined and artfully sculpted surfaces were then subjected to a short period of accelerated corrosion. Although attack by both ANCIT and EXCO solutions was tried the best results were achieved through exposure to Copper Assisted Salt Fog (CASS).

Once the “corroded” areas were individually prepared the voids were packed with aluminium oxide to the volume required by the thickness loss and the calibration standard was assembled by attaching the inner sheet which was not machined. Assembly with the corrosion product *in situ* proved very difficult especially in the proper formation of the shop head of the rivets. Special tooling was devised to deform and squeeze the skins together so that successful riveting could be achieved. The loose aluminium oxide powder also posed a problem as it shifted during assembly. Figure 11-19 shows the assembled joint. Figure 11-20 shows a later more successful pillowing simulation joint.

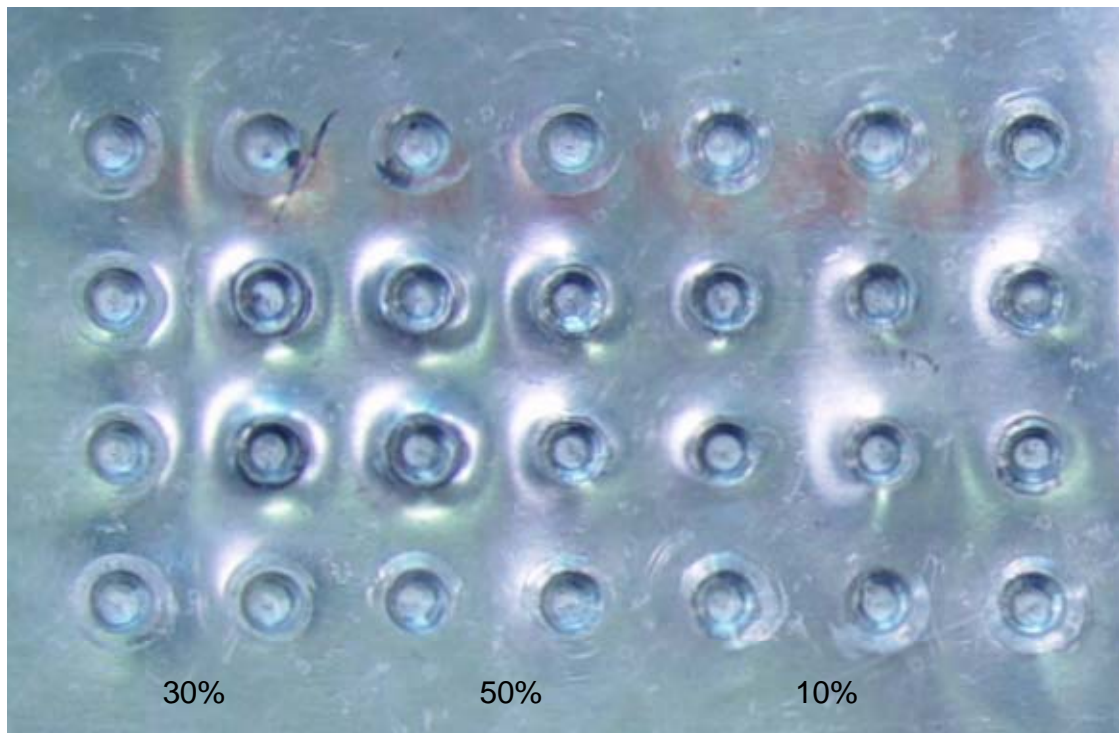


Figure 11-19: Assembled Joint.

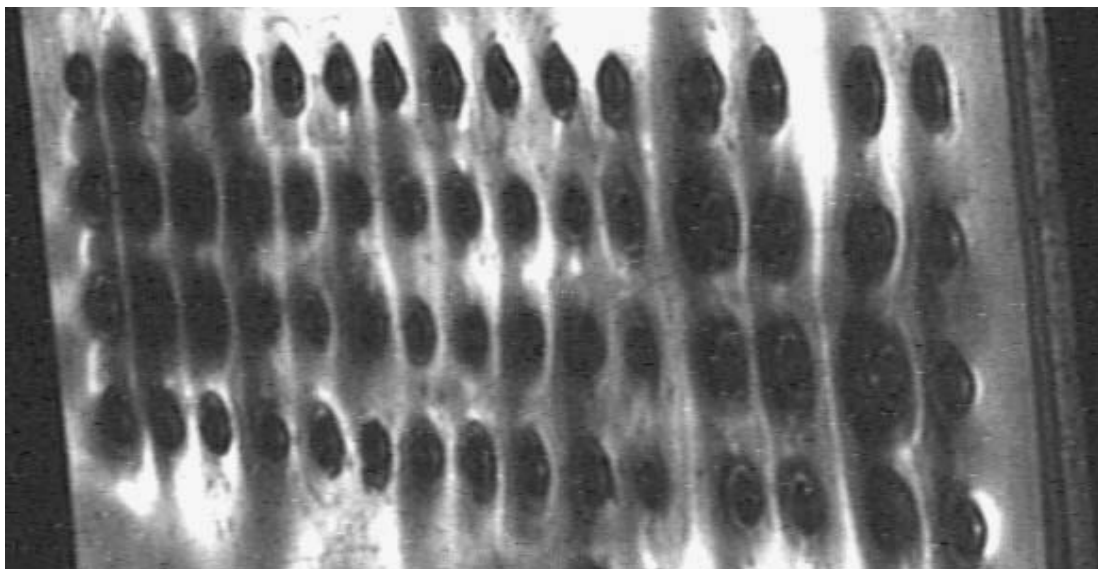


Figure 11-20: DAIS Image of Machined Simulation Panel with Corrosion Product Included.

11.3.3 Pillowing Cracks

One of the insidious effects of corrosion pillowing is the development of non-surface-breaking, high aspect ratio cracks originating on the faying surfaces (inner surfaces and thus not visually detectable). Whereas fatigue cracks may originate from fastener holes and run longitudinally due to hoop stresses under cyclic pressurization, these “pillowing cracks” are driven by tensile forces, originate away from the

fastener holes and they can grow in any direction. To date this feature has not been simulated in a lap joint calibration standard but the phenomenon has been demonstrated in an accelerated corrosion process.

The lap joint illustrated in Figure 11-21 was assembled with one aluminium and one clear acrylic skin. The two skins were assembled with screws not rivets and the assembly was exposed to a corrosive environment. The acrylic skin panel was intended to facilitate visualizing and documenting the damage onset and progress of the accelerated corrosion process.

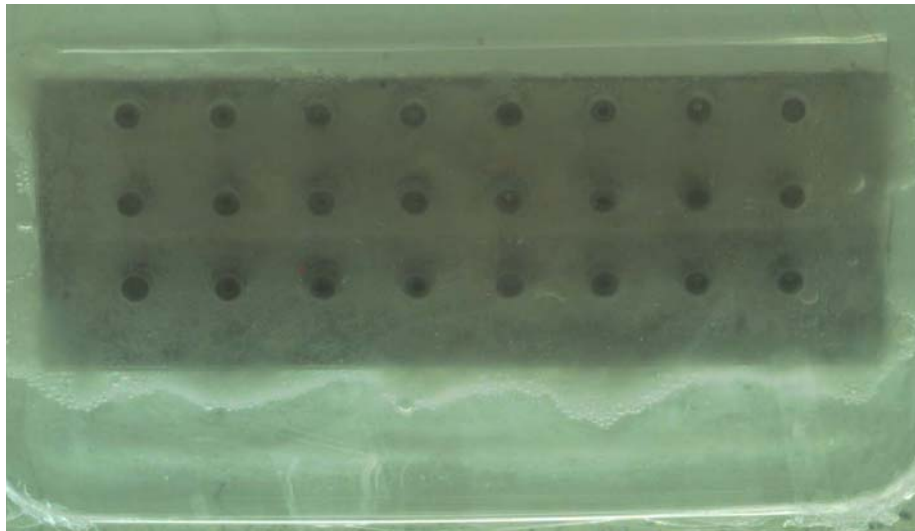
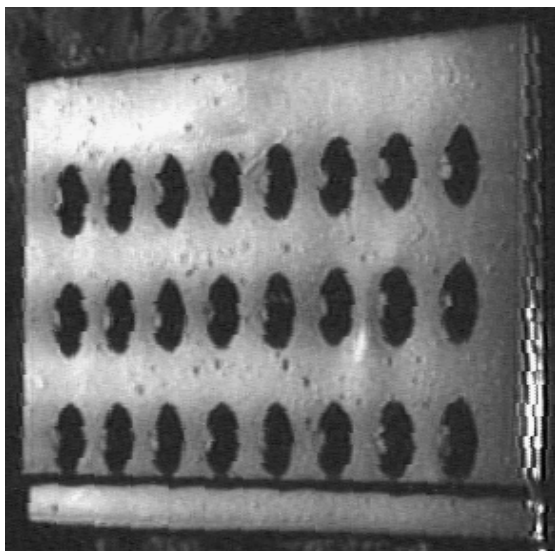
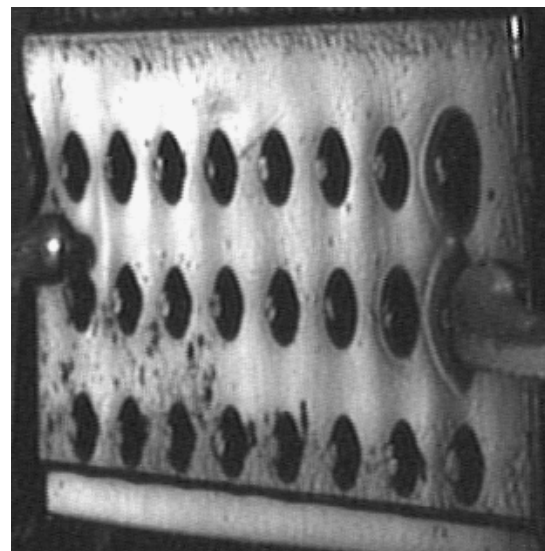


Figure 11-21: Al/acrylic Hybrid Lap Joint After 15 Days Exposure to EXCO Solution.

Figure 11-22 shows the outer surface of the aluminium skin before and after exposure to the corrosive environment. Unexpectedly this set-up helped in recognizing the formation of pillowing induced cracks, as shown in Figure 11-23.



(a)



(b)

Figure 11-22: DAIS Images of Aluminum Outer Skin Front Surface: (a) Before; and (b) After Corrosion.

SIMULATING PILLOWING CORROSION DAMAGE

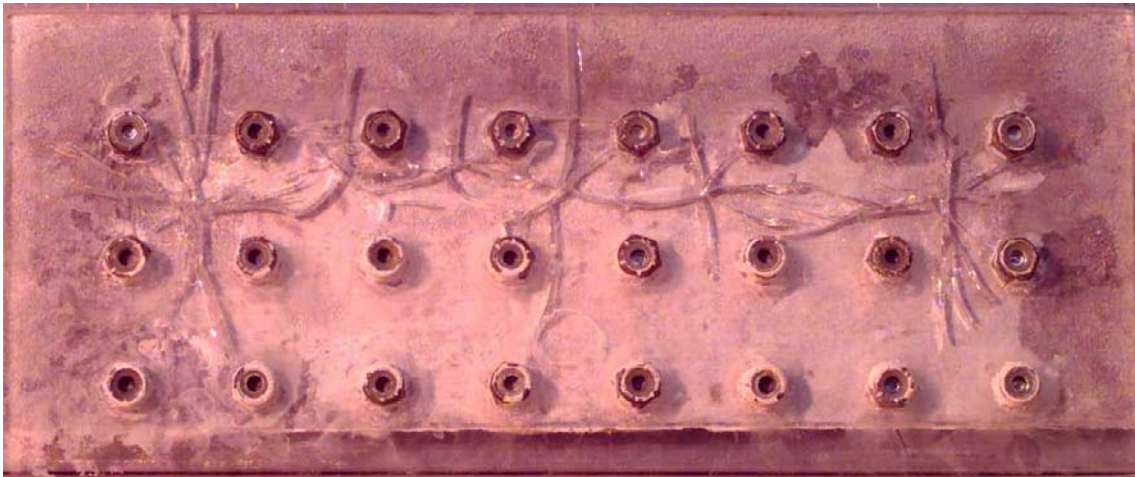


Figure 11-23: Cracks in Acrylic Inner Skin Caused by the Force of Corrosion Product Accumulation.

11.3.4 Wing Plank Simulated Corrosion Damage Calibration Standard

The lessons learned in modelling and teardown used to facilitate the fabrication of fuselage lap joint pillowing calibration standards were applied to thicker plate material to provide standards for general, spot and pitting corrosion in the machined step joint on wing skin material (7075-T6). Figure 11-24 shows the two adjacent 87-inch (221 cm) long wing planks. A sketch of the three locations for the various damage sites is shown in Figure 11-25. The Bottom Of Top (BOT) and Top Of Bottom (TOB) sites were assembled with the mandated sealant applied once the damage had been introduced. The Bottom Of Bottom (BOB) sites were unique in that the inserted corrosion product had to remain in place and this was achieved by using an adhesive.

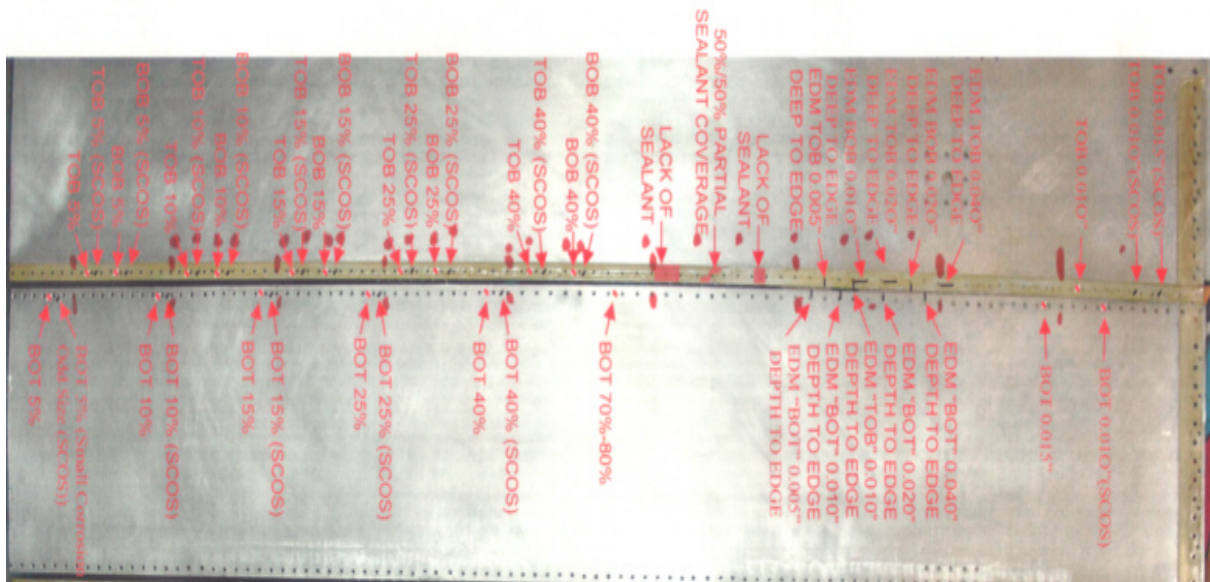


Figure 11-24: Wing Planks.

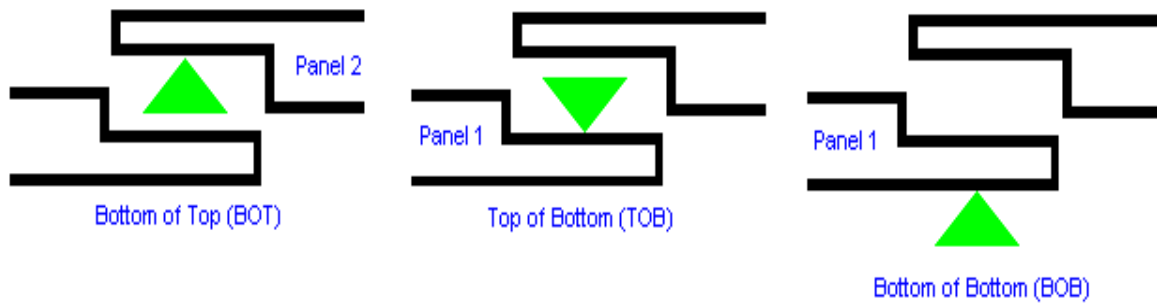
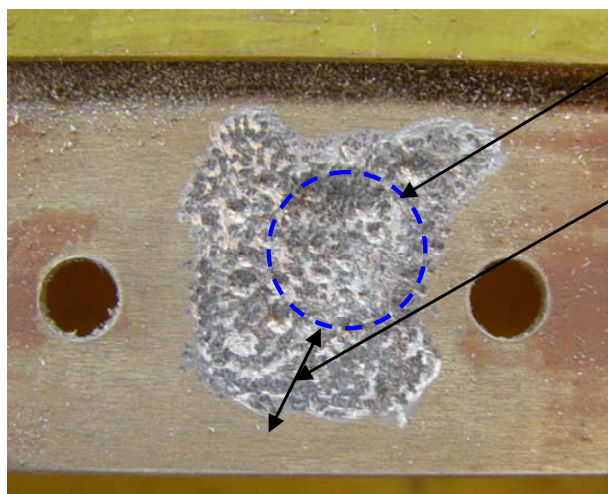


Figure 11-25: Location of Damage Sites.

The thickness of each plank was measured adjacent to each damage site and these local measurements were used to determine the amount of material to be removed. For “area” corrosion damage sites a 0.375 inch (9.5 mm) diameter end mill was used to remove material down to within a few thousandths of an inch from the final desired dimension. This small thickness was left so that the surface could include some gross topographical roughness without exceeding the desired mean thickness. Blending from the flat bottom of the milled site to the level of the surrounding undamaged surface was done by hand with a Dremel tool and high speed steel bits. Artificial corrosion of the surface was induced to provide the micro-roughness associated with natural corrosion damage and the period of exposure was controlled to match the severity of the thickness loss (Figure 11-26).



Area flat-bottom end milled to near full depth.

“Artistic” blend-out to full thickness.

Note also “Artistic” macro surface roughness features and less blending towards fasteners in appreciation of less damage due to clamp-up.

Figure 11-26: Typical “Area” Damage Site Preparation Prior to Corrosion Solution Application.

Smaller features were included such as minor Surface Corrosion (SCOS) and corrosion pits (Figure 11-27). Only the area and surface corrosion sites were back-filled with corrosion product. In this case the corrosion product used was harvested from naturally occurring corrosion of identical material.

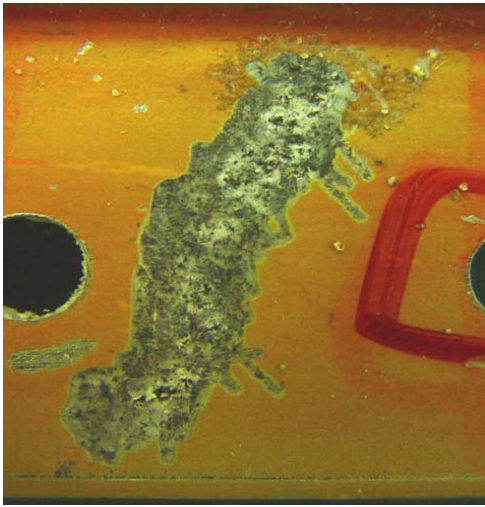


Figure 11-27(a): Corroded SCOS Damage Site.

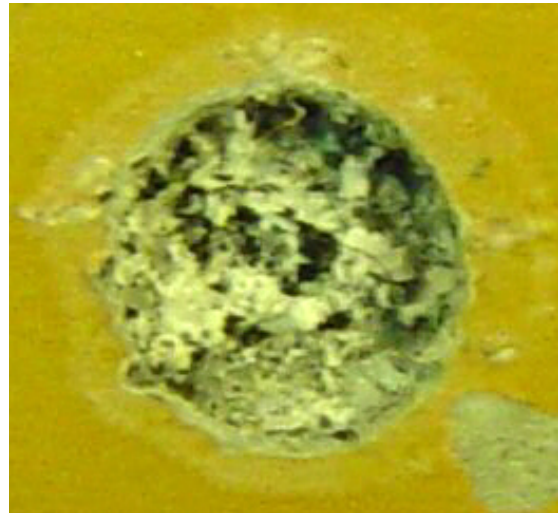


Figure 11-27(b): Corroded Pit.

The “SCOS” damage was machined entirely by hand and the depth measured by a dial gauge with a needle nose attachment. The “Pit” damage sites were counter-bored by hand and the depth measured by dial gauge.

As described above, the lessons earned in developing lap joint pillowing and corrosion simulation calibration masters has permitted the simulation of similar damage in wing plank joints.

As a complimentary development to the wing plank corrosion joint, a wing plank joint was prepared with induced cracks to challenge the current tools and techniques used to detect them. With special tooling, forced overload cracks could be inserted at any fastener hole, run in any direction and the length of the crack could be controlled. Ultimately both simulated corrosion and crack damage could be combined in one wing plank joint.

11.4 CONCLUSIONS

It has been demonstrated that corrosion occurring between the faying surfaces of aluminum aircraft structures introduces damaging stresses. These stresses are due in part to the loss of thickness of the structural skins and to the accumulation of high volume corrosion products between the skins. Both contribute to plastic deformation and cracking of the skins. This plastic deformation has been referred to as pillowing and it is usually most pronounced in the outer layer of skin where it is seen as an undulating surface profile. The amplitude of the undulations is a direct indication of the severity of corrosion and of the loss of thickness of the associated metal sheets. However, quantitative measurement of thickness loss requires that carefully prepared calibration standards be available. A number of methods have been developed to produce the standards and perform these calibrations, employing either optical or electromagnetic methods. These methods have been described and their merits and limitations have been explained. Of particular concern is that pillowing induced cracking often occurs on the inside surfaces of the skins and is therefore not seen during direct visual examination. This makes the assessment of corrosion severity of particular importance, and thus reinforces the need for accurate calibration of the available detection methods. It is also important to be able to simulate the corrosion that occurs in service in a well controlled laboratory environment.

11.5 REFERENCES

- [1] Chapman, C.E., National Research Council Canada, Private Communication.

Chapter 12 – SURFACE TOPOGRAPHY INFLUENCES ON STRUCTURAL LIFE PREDICTION

Thomas Mills

Analytical Processes / Engineered Solutions, Inc.
Saint Louis, Missouri
USA

12.1 WHAT IS SURFACE TOPOGRAPHY? AN INTRODUCTION

Topography describes the complex form of a surface--the undulations which make up its character. Topography comes in all shapes and forms; what is true for the surface of our planet is also true for the surfaces of engineered structures. If you have ever driven across the Flint Hills in south-eastern Kansas, you probably recognize that the only indicator you have that you are climbing a hill is that the engine rpm goes up ever so slightly. These hills have little in common with the hills of south-eastern Kentucky, yet on an ordinary road atlas, they are labeled “hills” just the same. It is not until you look at these regions on a topographic map that the differences become clear. In an engineered structure, sometimes topography is important, and other times it is not. When we produce, for example, a residual strength analysis, the assumption of a pristine surface is the norm. For many types of analyses and under many criteria, this is acceptable. However, surface integrity is often critical to proper function of a structure. Ignoring the form of a surface, or the deviation of a surface from its intended form, either from improper machining, accidental damage, wear, or corrosion, can have profound structural implications.

A cursory scan of basic fatigue design textbooks will reveal fatigue life “knock-down factors” that are a function of machined surface roughness. Sometimes you will even find “knock-down factors” for corrosion. What these two factors (machined surface roughness and corrosion) have in common is surface topography that casts aside any assumption of a perfectly flat surface.

To focus on corrosion, the impacts it can have on structural integrity are clear. Corrosion can greatly accelerate the time to fatigue crack nucleation; it can accelerate the propagation rates of fatigue cracks both chemically and mechanically; it can alter intended load paths. The place where the topography of a surface affected by corrosion is most important is in the nucleation phase of fatigue cracks (or EAC) and in the propagation of these cracks, particularly at smaller sizes (dimensions to come!). That is where the discussions for this section will be focused. This chapter will also address many questions, such as:

- Why is topography important to consider?
- How do we measure it?
- How do we use the information?
- What is the influence of topography on fatigue life calculations?

12.2 THE IMPORTANCE OF TOPOGRAPHY

High-fidelity fatigue analyses must take surface condition into account. To be able to model the physical processes of failure, and to become more holistic, we must understand complex interactions between surfaces and applied stress, both external and residual. The effects of corrosion morphology on fatigue have long been recognized. Studies of the geometric “stress riser” influence of corrosion on fatigue response started long ago, dating back to the 1920s for aluminum alloys [1],[2] and back to the mid-1800s on steels used in the railroad industry. These works continued in earnest through the 1960s [3],[4],[5], 1970s [6], 1980s [7],[8], 1990s [9],[10],[11],[12],[13] and into the 2000s [14],[15],[16],[17],[18],[19],[20]. The stress

risers related to corrosion damage are directly related to topography. If “uniform corrosion” was indeed uniform, there would be no topography, only constant removal of material that, from a fatigue analysis perspective, could conveniently be handled by assuming a uniform, wholesale increase in applied stress with no complex stress concentrations. But, as experience shows, even “general attack” of a surface in an aluminum alloy is characterized by roughness and waviness. Consider the profile below, which is a trace of an aluminum surface subject to general attack (Figure 12-1).

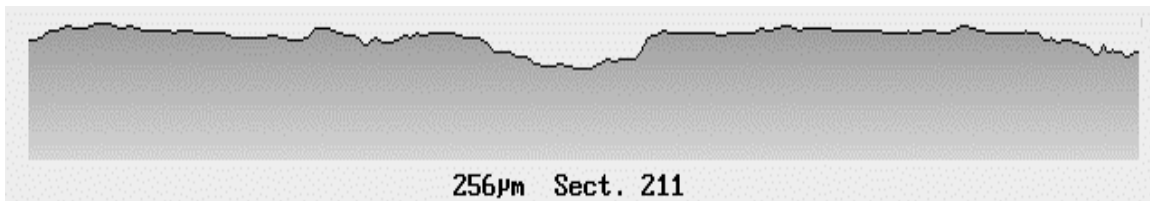


Figure 12-1: Line Profile of Aluminum Surface that has Suffered from General Attack.

The general attack profile has quite different characteristics than a surface subjected to pitting (see Figure 12-2). However, the structural implications can be similar, especially relative to a machined surface.

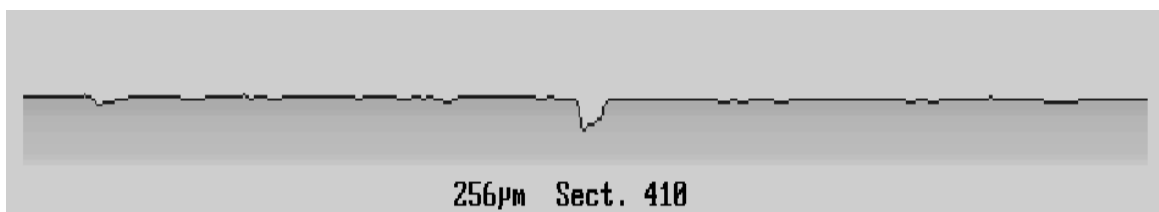


Figure 12-2: Line Profile of Aluminum Surface that has Suffered from Pitting Attack.

Even exfoliation, long considered a uniform material loss with no associated stress concentration, shows topographies that look very similar to general attack; in places, the exfoliation damage may also contain pitting. Regardless of the topography that is present, it is safe to say that in many cases, assuming a loss of material sans stress concentration (i.e., beyond that of net section stress increase) is inadequate, especially in fatigue assessments (see Chapters 6, 10 and 15) for detailed discussion regarding exfoliation).

12.3 MEASURING SURFACE TOPOGRAPHY

As with many technologies, one of the biggest hurdles one must overcome is the difference between being able to measure something in the laboratory versus measuring that same parameter in the field. For measuring surface topography in the laboratory, we might have laser confocal microscopes, or laser profilometers, or stylus profilometers. We might cross-section a sample and use some sort of image analysis software to define the surface profile. Clearly, we have many tools available to us to generate high fidelity surface profile information, in 2D and in 3D. Translating that capability into the field is much more difficult, however.

Using aircraft structure as an example, much of the corrosion in which we are interested is hidden, such as within lap joints or down the bore of fastener holes. In 2000, the USAF launched Phase II of the of Corrosion Fatigue Structural Demonstration program, and a portion of that program sought to understand the relationship between the outputs of conventional NDT methods, such as X-ray, ultrasound, and eddy current, and the surface topography information required to feed structural effects models. DSTO Australia went down a similar path in the same time frame when developing their ‘Process Zone Model’

for modeling exfoliation/fatigue interactions [21],[23]. The conclusion at that time was that although the ‘Process Zone’ was very successful at modeling the influence of exfoliation on fatigue response, the level of detail required for the corrosion damage morphology was well beyond what could be delivered by available NDT methods.

Figure 12-3 shows an example of data extracted from a field-supportable eddy-current scan of a lap joint compared with a scan down the same line using laser profilometry. The eddy-current scan has a 500-micron resolution, and the laser scan has a resolution of 25 microns. Although the eddy-current data is suitable for estimating basic thickness loss, it does not provide the spatial resolution necessary for high fidelity fatigue analyses (determined in this study to be 25 microns). The eddy-current data in this example would miss finer details associated with pitting, or instance. Keep in mind that not every analysis would require high-fidelity topography information.

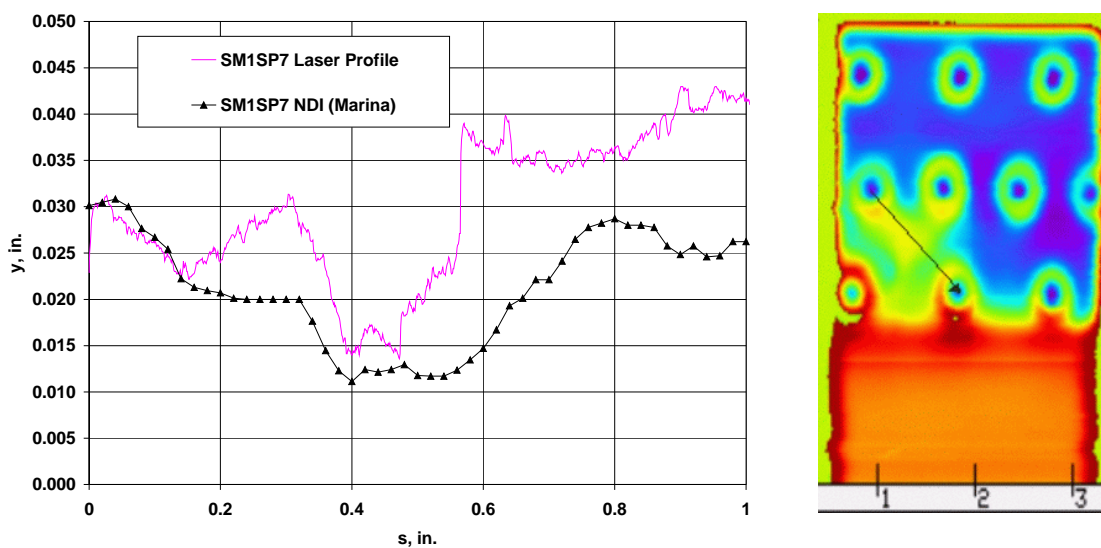


Figure 12-3: Eddy-Current Line Scan Compared with Laser Profile for Same Location.

To try and bridge the gap between NDT capability and structural analysis requirements for corrosion, studies have been undertaken to see if the parameters necessary for surface topography determination can be inferred from the global thickness loss determined by eddy-current. One example is shown in Figure 12-4, where the roughness of corroded samples does indeed correlate to global thickness loss. Note the roughness/thickness loss relationship also varies by product thickness, as one might expect.

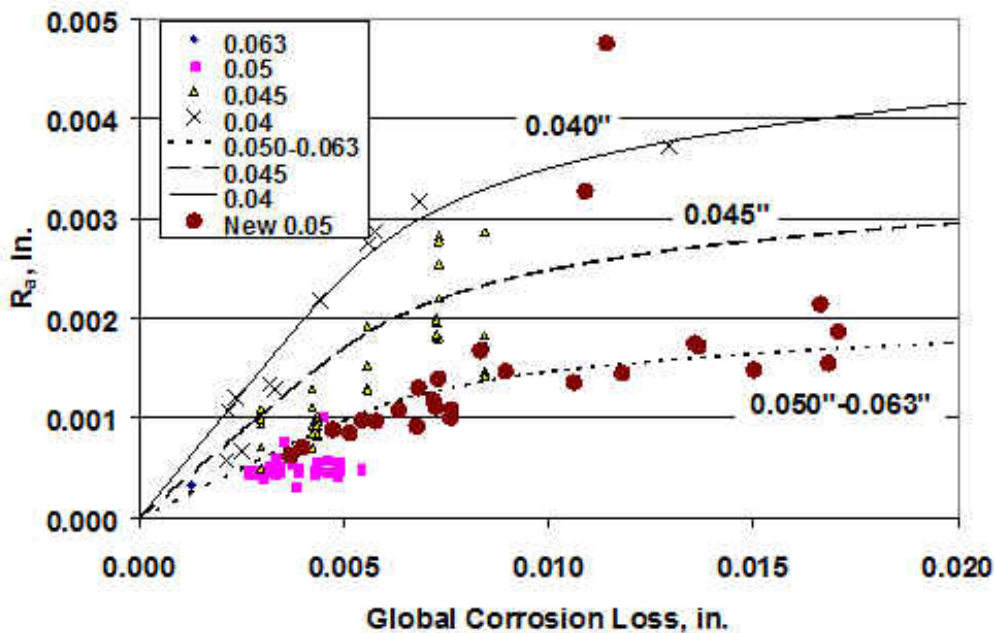


Figure 12-4: Surface Roughness Related to Corrosion Thickness Loss (the solid, dashed and dotted lines represent approximate power law curve fits for each initial product thickness, 0.040", 0.045" or 0.050 – 0.063").

As mentioned in the chapter on exfoliation/fatigue modeling, there is benefit to be gained from pursuing these types of relationships for common engineering materials. The ‘Process Zone Model’ fell victim to this lack of information. Time would be well spent trying to understand limit states of surface roughness and damage morphologies for various alloys in a variety of product forms and grain orientations.

12.4 TOPOGRAPHY AND FATIGUE ANALYSIS

As this section and countless case studies from field failures show, local topography of a surface can be critical to a structure’s fatigue resistance. At the same time, not every structure is fatigue critical or even corrosion fatigue critical. The ability to consider topography in fatigue analysis is another tool we can use to determine the susceptibility of structure to certain types of damage, either in the design stage or in the sustainment phase of a structure’s life.

In aircraft, many classification criteria exist for determining what is a primary structural element, a structurally significant item, a fracture critical component, etc. We can combine this knowledge with an understanding of stress levels, local details, and material properties to gain an understanding of which structure might be vulnerable to damage (typically cracking) and which will require inspection during use to ensure safety. This template clearly exists for fatigue, and the methods now exist to expand this capability to include corrosion (although the philosophy in the industry still seems to lag technical capability).

The first step – well before we figure out how much detailed corrosion topography we *can* gather – is to determine what we *need* to gather. This is a function of the structure’s susceptibility to corrosion/fatigue (surface topography is much more important to fatigue analysis than it is to residual strength analysis). Structural requirements should define the NDT requirements. At the design stage, if the NDT cannot provide what we need, or if the inspection requirement proves to be too burdensome, then a redesign would likely be in order. In the sustainment stage, a gap between NDT requirement and NDT capability

might force us into determining some sort of gap-filling algorithm that transforms NDT capability into the type of information we need with reasonable confidence (as shown earlier in Figure 12-4).

Determining what we need to gather (and the locations for which we need to gather the corrosion information) is part of corrosion criticality analyses and corrosion tolerance assessments. And as we stated above, the capability exists today to do this type of activity with far more fidelity than it is currently being practiced.

The methods put into practice at APES are centered on determining surface topography correction factors that are used in conjunction with conventional fatigue analyses. These essentially take the form of ‘beta corrections’ to the stress intensity solution for a crack growing from a flat surface. If the crack is emanating from a deep pit, for instance, the presence of that pit will amplify the stress intensity the crack sees. From an analytical standpoint, this increase in K translates into an increase in crack growth rate, which further translates into a decrease in fatigue life from that crack size to failure compared to the ‘un corroded’ baseline condition.

As with traditional beta solutions, finite element technology allows us to build families of beta correction curves for various ‘typical’ surface topography conditions from varying degrees of general attack to increasing depths and shapes of pitting. In addition, it is possible to develop these beta solutions for any structural detail if that level of fidelity is warranted. Figure 12-5 shows a simplified example of beta corrections for the two surface profiles shown earlier in this section (refer back to Figure 12-1 and Figure 12-2).

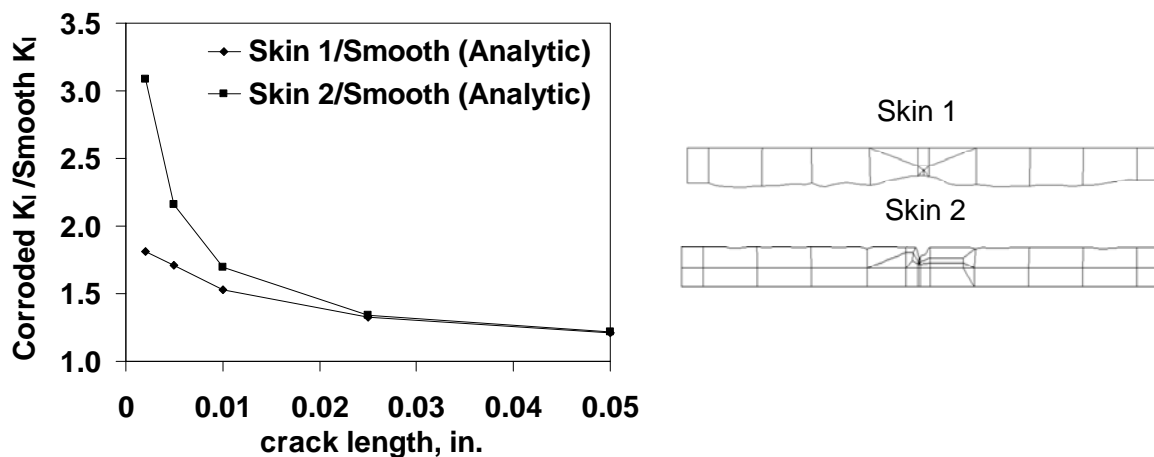


Figure 12-5: Sample Correction Factors for Corroded Surfaces as a Function of Crack Length.

The graph plots normalized stress intensity for the two profiles, the normalized value being the stress intensity of a crack emanating from a corroded surface divided by the stress intensity of the same crack emanating from a flat surface. Two things stand out from the figure – neither of which should be all that surprising. First of all, when the crack is small, the influence of the corrosion is quite large. This effect dissipates quite rapidly as the crack extends away from the surface, but the effect never really goes away (normalized value does not reach unity). Second, the ‘pitted’ surface (Skin 2) has a much more severe initial correction factor associated with it than does the general attack surface (Skin 1).

One can also examine these beta corrections from a probabilistic sense, wherein a family of corrections (Figure 12-6) for corrosion can be determined by placing cracks of varying sizes at different locations (x-coordinate along surface ‘S1_2’ in Figure 12-6) along a corroded surface.

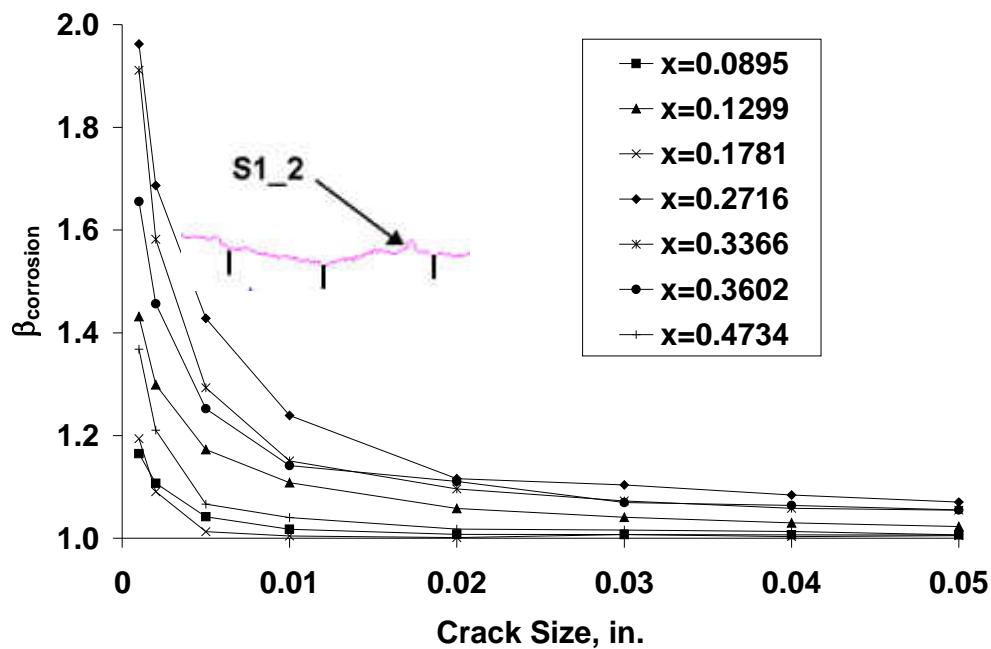
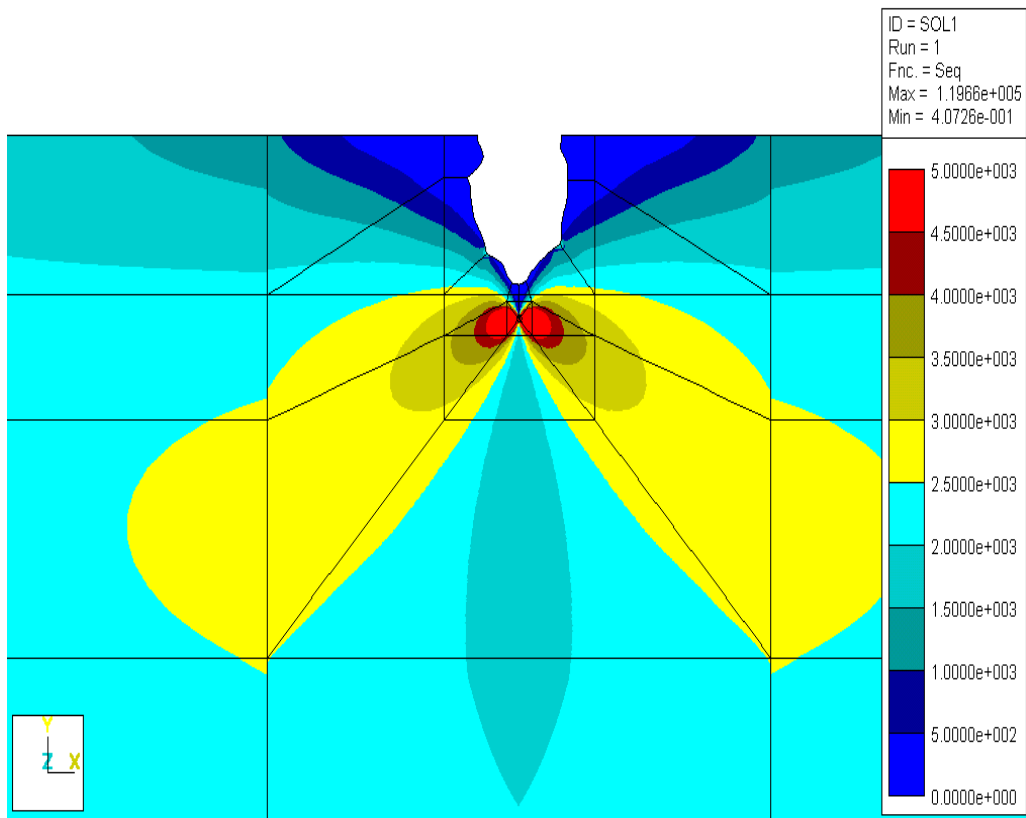


Figure 12-6: Family of Beta Corrections for Corrosion for Various Cracks Along a Line of Surface Topography.

More severe topography gives rise to higher beta correction factors, to the point in fact that very sharp pits (such as those which might attack the short-transverse grain direction of a structural aluminum alloy, for instance), can effectively be modeled as cracks of equivalent depth. This tends to be a slightly aggressive treatment of pitting effects on fatigue, but for certain pit morphologies, this assumption appears to work reasonably well.

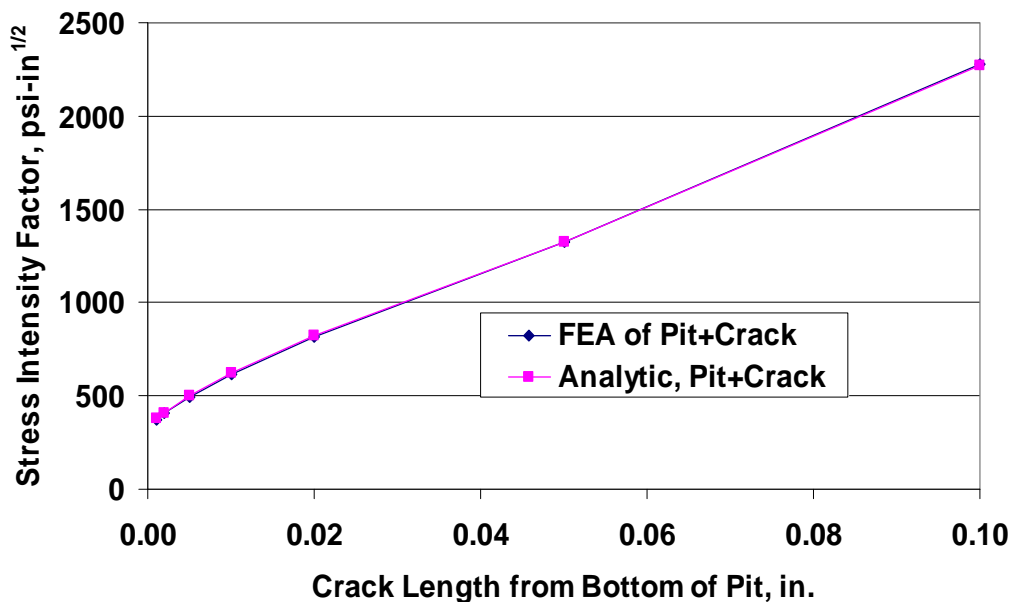
The original pitting model developed by APES, Inc. was based on a small study driven by DSTO/AMRL of Australia [23]. The work involved pitting/fatigue in 7050-T7451 aluminum alloy, a material common in their F/A-18 aircraft. In this limited study, planform views of two pits were lifted from fractographs, and these shapes were recreated using two-dimensional finite element analysis (2D-FEA). These analyses confirmed that sharp, deep pits could be modeled as cracks of equivalent depth.

As can be seen from Figure 12-7 and Figure 12-8, these planforms were of quite different shape, but they produced very similar stress states and stress intensity factors, which was a result of similar pit radii at the very tip (bottom) of the pit.



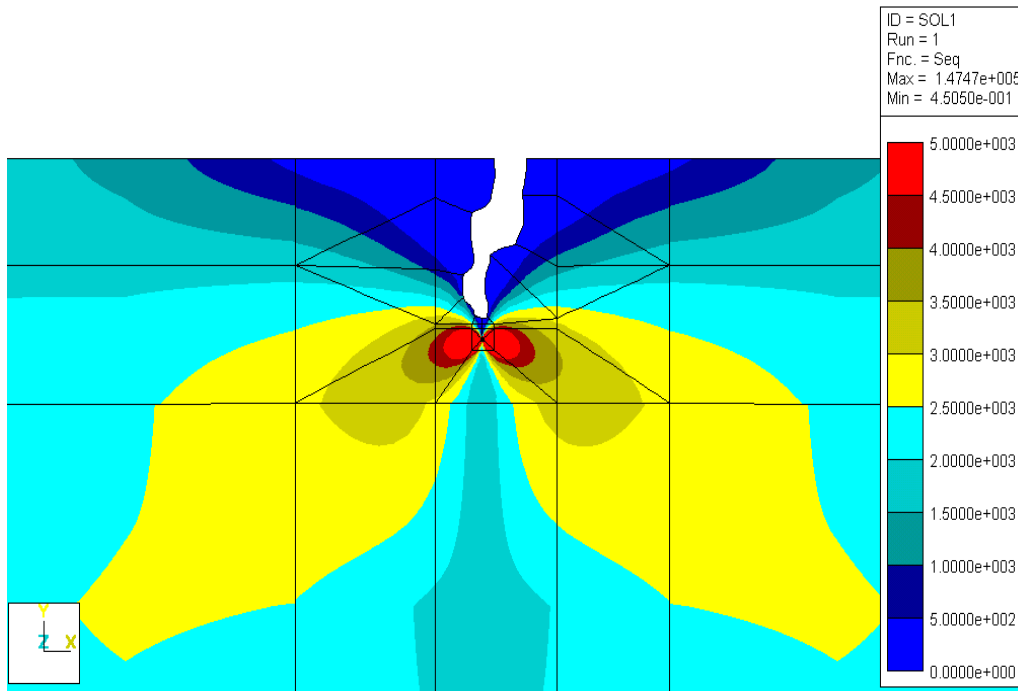
(a)

Shallow, Wide Pit



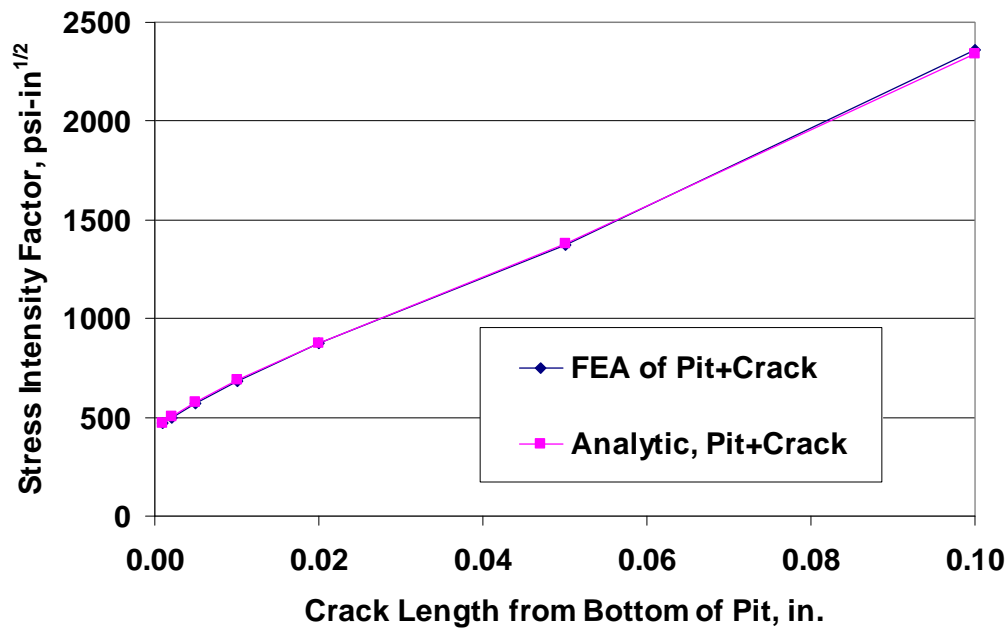
(b)

Figure 12-7: (a) Shows the Von Mises Stress Contours for the Wide Pit with a 0.001 Inch Pit at the Base; and (b) Shows How the SIFs Compare Between FEA and the Analytic 2D-PC Model.



(a)

Deep, Narrow Pit



(b)

Figure 12-8: (a) Shows the Von Mises Stress Contours for the Narrow Pit with a 0.001 Inch Pit at the Base; and (b) Shows How the SIFs Compare Between FEA and the Analytic 2D-PC Model.

In Figure 12-7, the Von Mises stress contours are shown for a wider ‘shallow’ 0.004 inch (100 micron) pit with a 0.001 inch (25 micron) crack at the base. Similar models were built which varied crack depth from

this same pit geometry, with crack lengths approaching 0.1 inch (250 microns). The stress intensity factors at the crack tip (which would be influenced by the pit) were compared with a simple model that treated the pit as a crack of equivalent depth to which the real crack was added. Figure 12-7 shows the comparison between the FEA model of the real pit + crack (labeled as FEA) and the assumption that the pit is simply an extension of a 2D crack (labeled as Analytic). The Stress Intensity Factors (SIFs) at all combinations of pit depth and crack length are within 1% of each other.

This exercise was repeated with a narrower and deeper pit (0.007 inch, 175 microns). Figure 12-8 shows similar plots for this other pit geometry. Again, the differences between FEA and simplified model were negligible, and so the original APES pitting model, which we now call the 2D Pit/Crack (2D-PC) model was born.

Later work with the US Air Force [24],[25] saw the pitting models expand and benefit from 3D Finite Element Analysis (3D-FEA), which generated beta correction factors for cracks next to hemispherical corrosion pits. In essence, the use of 3D-FEA created a less severe option to the pit-as-crack model developed using the 2D-FEA (see Figure 12-9).

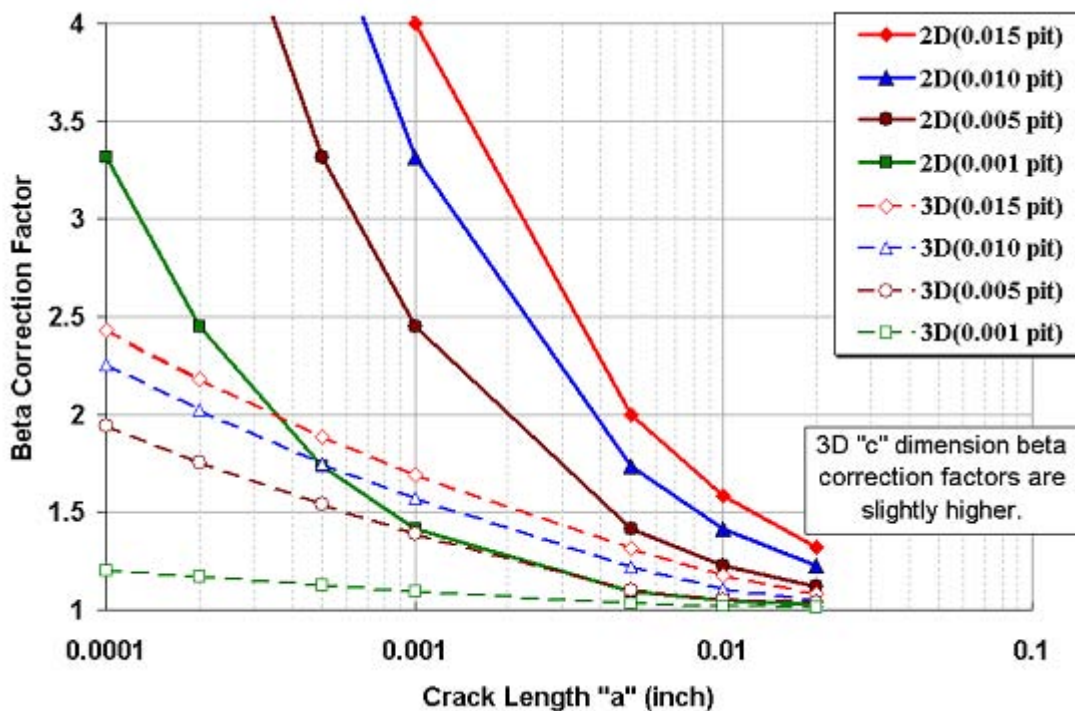


Figure 12-9: Comparison of Sample 3D and 2D Beta Correction Factors for Pitting.

12.5 TOPOGRAPHY INFLUENCES ON FATIGUE LIFE CALCULATIONS

No one clear cut answer exists for the effects of surface topography on fatigue life calculations. However, it is clear just from service failures alone that corrosion, for example, causes structures to fail much sooner than expected. Perhaps one of the most telling examples of the effects of surface topography on fatigue life calculations comes from the modeling of exfoliation corrosion. In the chapter on exfoliation fatigue modeling (see Chapter 15), the observation was made that exfoliation is typically just considered a material loss issue, wherein it can be modeled as a simple reduction in component thickness. This approach is reasonable for strength and stability calculations. And while the impact that this thinning has on fatigue life

computations is real and noticeable, the reduction in life arrived at by this modeling approach misses a very key physical interaction, namely: the surface is far from pristine. It is in fact quite tortuous with many pit-like discontinuities (referenced earlier). These pit-like discontinuities are what drive the often-dramatic life reductions seen in cases of exfoliation/fatigue interactions. It is worth presenting Figure 12-10 as part of this discussion, although it is repeated in Chapter 15. In this chart, experimental exfoliation fatigue data is plotted alongside three different modeling approaches:

- 1) Thickness loss only;
- 2) Thickness loss in conjunction with beta corrections from 2D-FEA; and
- 3) Thickness loss in conjunction with beta corrections from 3D-FEA.

The most important thing to recognize in this example is that when one considers thickness loss as the only influencing factor, then life capability is over-predicted by a factor of four, consistently, at all thickness loss levels examined. Only by including the effects of surface topography do the computed fatigue lives approach those of the experiment.

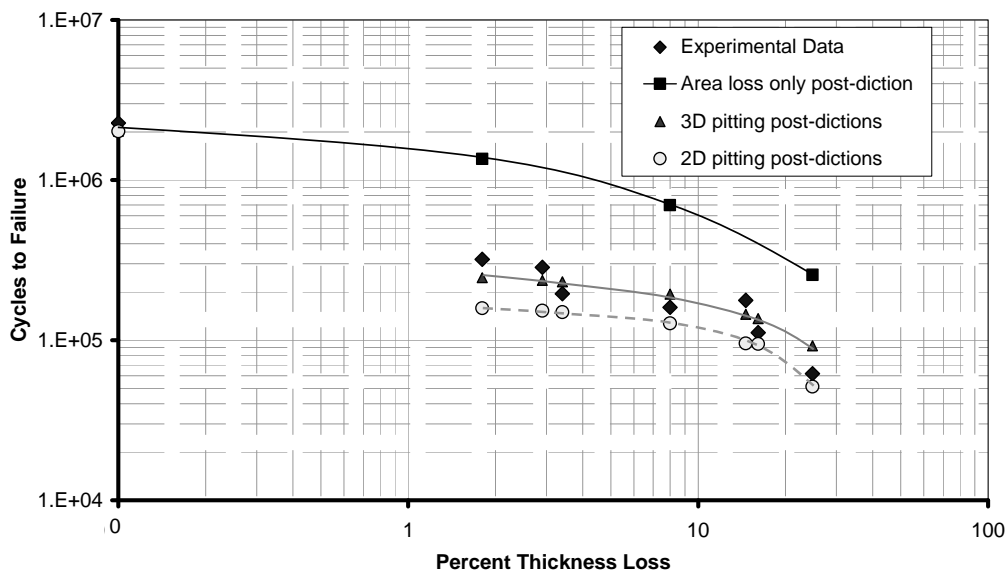


Figure 12-10: Cycles to Failure vs. % Thickness Loss for Exfoliated Coupons (Note that only by incorporating pitting into the model do the post-dicted fatigue lives approximate those of the coupons. Assuming area loss only is extremely unconservative (factor of four)).

12.6 REFERENCES

- [1] Moore, R., "Effect of Corrosion Upon the Fatigue Resistance of Thin Duralumin", Proceedings of the ASTM, Vol. 27 (2), pp. 128-152, 1927.
- [2] McAdam, Jr., D., "Corrosion-Fatigue of Non-Ferrous Metals", Proceedings of the ASTM, Vol. 27 (2), pp. 102-125, 1927.
- [3] Harmsworth, C., "Effect of Corrosion on the Fatigue Behavior of 2024-T4 Aluminum Alloy", ASD Technical Report, pp. 61-121, 1961.
- [4] Shaffer, I., Sebastian, J., Rosenfeld, M. and Ketcham, S., "Corrosion and Fatigue Studies of Extruded 7075-T6 Spar Caps", Journal of Materials, Vol. 3, (2), pp. 400-424, 1968.

- [5] Gruff, J. and Hutcheson, J., “Effects of Corrosive Environments on Fatigue Life of Aluminum Alloys Under Maneuver Spectrum Loading”, AFFDL Technical Report 70-144, pp. 521-537, 1969.
- [6] Hoepfner, D.W., “Corrosion Fatigue Considerations in Materials Selections and Engineering Design”, Corrosion Fatigue, NACE-2, pp. 3-11, 1971.
- [7] Lindley, T., McIntyre, P. and Trant, P., “Fatigue Crack Initiation at Corrosion Pits”, Metals Technology, Vol. 9, pp. 135-142, 1982.
- [8] Kawai, S. and Kasai K., “Considerations of Allowable Stress of Corrosion Fatigue (Focused on the Influence of Pitting)”, Fatigue & Fracture of Engineering Materials & Structures, 8 (2), pp. 115-127, 1985.
- [9] Chubb, J., Morad, T., Hockenull, B. and Bristow, J., “The Effect of Exfoliation Corrosion on the Fatigue Behavior of Structural Aluminum Alloys”, Structural Integrity of Aging Airplanes, pp. 87-97, 1991.
- [10] Koch, G., Hagerdorn, E. and Berens, A., “Effect of Preexisting Corrosion on Fatigue Cracking of Aluminum Alloys 2024-T3 and 7075-T6”, Final Report to Flight Dynamics Directorate, USAF Research Laboratory, August 1995.
- [11] De Luccia, J., “The Corrosion of Aging Aircraft and its Consequences”, AIAA-91-0953, AIAA 32nd Structures, Structural Dynamics, and Materials Conference, Baltimore, MD, USA, 1991.
- [12] Hahin, C., “Effects of Corrosion and Fatigue on the Load-Carrying Capacity of Structural and Reinforcing Steel”, IDOT Report FHWA/IL/PR-108, 1994.
- [13] Mills, T., “The Effects of Exfoliation Corrosion on the Fatigue Response of 7075-T651 Aluminum Plate”, Thesis, University of Utah, 1995.
- [14] Wei, R., “Corrosion and Corrosion Fatigue of Airframe Materials”, Final Report, DOT/FAA/AR - 00/22, Federal Aviation Administration, 2000.
- [15] Mills, T., Clark, G., Loader, C., Sharp, P. and Schmidt, R., “Review of F-111 Structural Materials”, DSTO-TR-1118, Defence Science and Technology Organization, Australia, 2001.
- [16] Mills, T., Sharp, P. and Loader, C., “The Incorporation of Pitting Corrosion Damage into F-111 Fatigue Life Modeling”, DSTO-RR-0237, Defence Science and Technology Organization, Australia, 2002.
- [17] Mills, T., Honeycutt, K., Brooks, C., Sharp, P., Loader, C. and Crawford, B., “Development and Demonstration of a Holistic Structural Integrity Process Using the Initial Discontinuity State Concept for 7050-T7451 Aluminum”, USAF Aircraft Structural Integrity Program Conference, Memphis, TN, USA, 2004.
- [18] Mills, T., Honeycutt, K. and Brooks, C., “Demonstration of a Holistic Structural Integrity Process using Corrosion/Fatigue Interactions from Laboratory Experiments and Field Experience”, Proceedings, 6th International Aircraft Corrosion Workshop, Solomon’s, MD, USA, 2004.
- [19] Crawford, B., Loader, C. and Sharp, P., “The Effect of Pitting Corrosion on the Position of Aircraft Structural Failures”, Proceedings, Structural Integrity and Fracture 2004, Brisbane, Queensland, Australia.

- [20] Quispitupa, A., Shafiq, B., Marcelo, O., Uwakweh, O. and Duque, N., “Corrosion Fatigue of High-Strength Aircraft Structural Alloys”, *Journal of Aircraft*, Vol. 43, No. 2, pp. 787-792, 2006.
- [21] Sharp, P., Mills, T. and Clark, G., “Modeling of Fatigue Crack Growth from Pitting and Exfoliation Corrosion”, *Proceedings, 21st Symposium of the International Committee on Aeronautical Fatigue, Toulouse, France*, pp. 485-498, 27-29 June 2001.
- [22] Sharp, P., Mills, T. and Clark, G., “Aircraft Structural Integrity: The Impact of Corrosion”, *Proceedings, 10th International Congress of Fracture (ICF 10), Honolulu, HI, USA, Elsevier Science*, 2001.
- [23] Sharp, P., “ECS Modeling of 7050 Aluminium Alloy Corrosion Pitting and its Implications for Aircraft Structural Integrity”, *DSTO Research Report, Australia*, 2007.
- [24] Brooks, C., Mills, T., Prost-Domasky, S., Honeycutt, K. and Young, N., “Advances in Holistic Life Prediction Methodology: Exfoliation Effects on Upper Wing Structure Subject to Fatigue and Static Loads”, *USAF Contract No. F09650-00-D-0018*, 2003.
- [25] Brooks, C., Mills, T., Prost-Domasky, S. and Honeycutt, K., “Development of a Holistic Structural Integrity Process”, *Dual Use Science & Technology Program, USAF Contract Number: F33615-03-C-3301*, 2006.

Chapter 13 – MODELING PITTING CORROSION FATIGUE: PIT GROWTH AND PIT/CRACK TRANSITION ISSUES

David W. Hoepfner

Professor and Director, Quality and Integrity Design Engineering Center (QIDEC)
Mechanical Engineering Department, University of Utah
Salt Lake City, Utah
USA

Amy Taylor

Research Engineer with FASIDE International Inc.
Salt Lake City, Utah
USA

13.1 INTRODUCTION

The combined effects of corrosion and cyclic loading have been shown to produce cracks from corrosion pits and pits have frequently been the source of cracks on components operating in fleets of aircraft. Once the pit, or group of pits form, the rate of pit growth is dependent mainly on the material, environmental conditions, temperature, and type and state of stress. Therefore, to estimate the total corrosion fatigue life of a component, it is of great importance to develop realistic models to establish the component life in these situations and to formulate methods by which designers and operators know likely sources of pitting early in the design and fleet operation. In this manner the structurally significant items can be classed by susceptibility to pitting corrosion fatigue as well as conventional fatigue criteria. Therefore, to understand this phenomenon, some models based on Pitting Corrosion Fatigue (PCF) mechanisms and understanding have been proposed in the past and new ones are emerging.

It is important to note that both pitting theory and crack growth theory have been used in pitting corrosion fatigue model development. The first known conceptual (notional) model was presented in 1971 (see the lead paper by Hoepfner in [6]) and subsequently the pit growth rate theory proposed by Godard was combined with fatigue crack growth concepts. Following this basic idea a few models have been proposed.

This chapter presents some examples of critical pitting corrosion fatigue situations in aircraft, discusses the framework of the PCF models to date, presents some applications of the models, and discusses current work underway. Additionally, some recommendations are made related to future work needed to enhance structural integrity and minimize degradation of aircraft due to this failure mechanism.

The phases of life of a structure may be classified as follows [1]:

- Formation or nucleation of damage by a specific, physical or corrosion damage process interacting with the fatigue process if appropriate. Corrosion and other processes may act alone to create the damage. A transition from the nucleation stage to the next phase must occur. *Phase L₁*.
- Microstructurally dominated crack linkup and propagation (“short” or “small” crack regime). *Phase L₂*.
- Crack propagation in the regime where either LEFM, EPFM, or FPFM may be applied both for analysis and material characterization (the “long” crack regime). *Phase L₃*.
- Final instability. *Phase L₄*.

Thus, the total life (L_T) of a structure is $L_T = L_1 + L_2 + L_3 + L_4$. Figure 13-1 presents a depiction of the degradation process. The regions shown, e.g., 1, 2, 3, and 4, illustrate the portion of life, on the abscissa,

and the corresponding growth in discontinuity size plotted schematically on the ordinate. This paper concentrates on the phases L_1 and L_2 . That is, the corrosion process that results in the generation of a specific form of corrosion generating a specific form of discontinuity that is not necessarily a crack like discontinuity, and the development of short cracks and their propagation. The requirement of the community to develop design methods to deal with corrosion or other degradation, fatigue, creep, and wear, is essential and some of the elements are depicted in Figure 13-2. This figure illustrates that most of the quantitative methods that have been developed used the concepts of mechanics of materials with an incorporation of fracture mechanics [2].

The degradation process

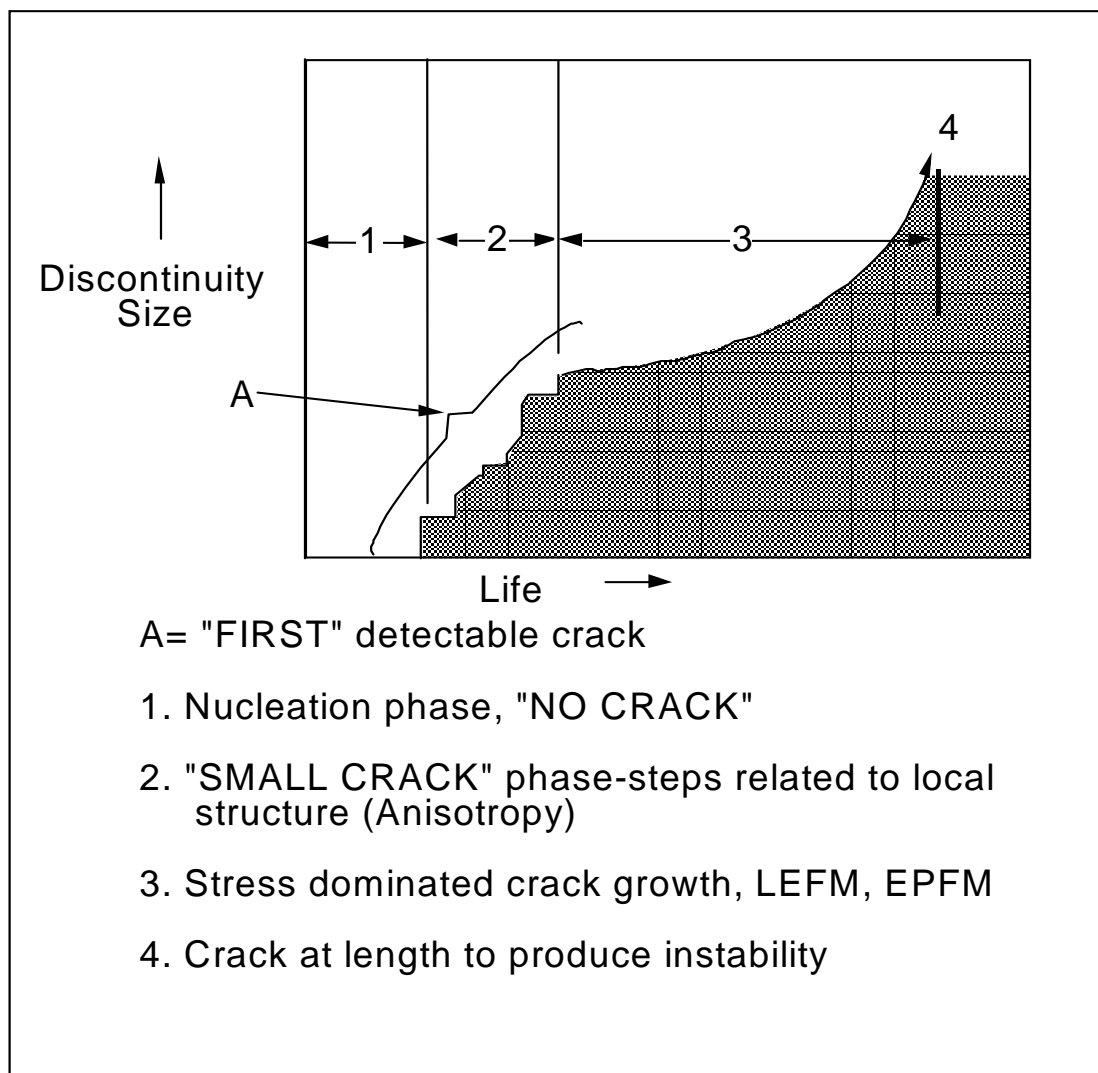


Figure 13-1: A Depiction of the Degradation Process (after Hoepfner [1], [40]).

METHODS FOR EACH LIFE PHASE

NUCLEATION	"SMALL CRACK" GROWTH	STRESS DOMINATED CRACK GROWTH	FAILURE (FRACTURE)
<p>Material failure mechanism with appropriate stress/strain life data</p>	<p>Crack Prop. threshold related to structure (micro)</p>	<p>Fracture mechanics •similitude •boundary cond.</p>	<p>K_{Ic} etc. C.O.D. Tensile/compressive buckling</p>
<p>Nucleated discontinuity (not inherent) type, size, location</p>	<p>Structure dominated crack growth</p>	<p>Data base** Appropriate stress intensity factor</p>	
<p>Presence of malignant D^*, H^*</p>	<p>Mechanisms, rate</p>	<p>Initial D^*, H^* size, location, type</p>	
<p>Possibility of extraneous effects •Corrosion •Fretting •Creep •Mechanical Damage</p>	<p>Onset of stress dominated crack growth</p> <p>Effects of •R ratio •Stress state •Environment •Spectrum -waveform</p>	<p>Effects of •R ratio •Stress state •Environment •Spectrum -waveform</p>	

Figure 13-2: Methods for Each Life Phase (after Hoepfner [1], [40]).

NOTE: Initiation as frequently used by the technical community is usually part of the nucleation (or formation), short crack growth, and stress dominated crack growth phase of life. One is never sure however how much of the life is taken up by the traditional use of the "initiation" concept. To avoid this we have used the term initiation herein only to refer to the beginning of a specific degradation process such as corrosion, fatigue, or initiation of crack propagation. As depicted in Figure 13-1 what often is referred to as "initiation" is life to a certain detectable crack size or damage size. This is a critical distinction in that use of "first" crack detection concepts, or related on condition evaluation terms, forces the designer to think about inspectability and detectability of specific forms of degradation. As well, it is imperative that the technical community develop an understanding of the nucleation and growth phases of degradation processes.

13.2 EFFECTS OF CORROSION ON STRUCTURAL INTEGRITY OF AIRCRAFT

The issue of the effects of corrosion on structural integrity of aircraft has been a question of concern for some time [3]-[38]. The potential effects are many and they can be categorized as follows. In the discussion below the use of the terms global and local refers to the likely extent of the corrosion on the surface of a component. Global means the corrosion would be found on much of the component whereas local means the corrosion may be localized to only small, local areas:

- 1) Reduce the section with a concomitant increase in stress. *Global or local.*
- 2) Produce a stress concentration. *Local.*
- 3) Nucleate cracks. *Local, possibly global. Source of multiple-site cracking.*

- 4) Produce corrosion debris. This may result in surface pilling by various means, which may significantly change the stress state and structural behavior. *Local and global.*
- 5) Create a situation that causes the surfaces to malfunction. *Local and global.*
- 6) Cause Environmentally Assisted Crack Growth (EACG) under cyclic (corrosion fatigue) or sustained loading (SCC) conditions. *Local.*
- 7) Create a damage state that is missed in inspection when the inspection plan was not developed for corrosion or when corrosion is missed. *Local and global.*
- 8) Change the structurally significant item due to the creation of a damage state not envisioned in the structural damage analysis or fatigue and strength analysis. If the SSI is specified, for example, by location of maximum stress or strain, then the corrosion may cause another area(s) to become significant. *Local or global.*
- 9) Create an embrittlement condition in the material that subsequently affects behavior. *Local or Global.*
- 10) Create a general aesthetic change from corrosion that creates maintenance to be done and does damage to the structure. *Local or global.*
- 11) Corrosion maintenance does not eliminate all the corrosion damage and cracking or the repair is specified improperly or executed improperly thus creating a damage state not accounted for in the design. *Local or global.*
- 12) Generate a damage state that alters either the durability phase of life or the damage tolerant assessment of the structure or both.
- 13) Create a Widespread Corrosion Damage (WCD) state or a state of corrosion that impacts the occurrence of Widespread Fatigue Damage (WFD) and its concomitant effects. (See References [3], [5], [6], [15], [17], [28], [29], [30], [34], [35], [36], [37], [38] for more information).

The question of whether corrosion, corrosion fatigue and stress corrosion cracking are safety concerns or just maintenance/economic concerns has been a point of discussion related to aircraft structural integrity for over 30 years. Nonetheless, a great deal of the aircraft structural integrity community believes that corrosion related degradation is just an economic concern. It was with this situation in mind that Campbell and Lahey [14] and Wallace, Hoepfner and Kandachar [15] pursued the presentation of technical facts and knowledge to illustrate the potential for a safety issue as well as a maintenance/economic issue. Finally, Hoepfner et al. [30] reviewed failure data obtained from the USAF, USN, US Army, FAA, and the NTSB related to aircraft incidents and accidents in the USA between 1975 and 1994. The review evaluated further the potential for corrosion and fretting related degradation to be significant safety issues. Recently, several instances of pitting corrosion in aircraft and helicopter components have been identified as critical safety issues as discussed in the following section.

13.3 EXAMPLES OF PITTING CORROSION INCIDENTS

A survey was performed of incidents and accidents of aircraft and helicopters caused by pitting corrosion, where an incident is any damage to the aircraft and/or injuries to passengers and crew and an accident is loss of the aircraft and/or fatal injuries to passengers and crew. Data were taken from the NTSB and FAA websites, which include their databases of all aircraft incidents and accidents since 1983. It was determined that of the 91 incidents and accidents found under corrosion, seven of them gave the cause of failure as pitting corrosion.

Unfortunately, it has been found that there are problems in reporting the causes of the incidents and accidents in the NTSB and FAA in that the real cause of an incident or accident is not reported properly

and, therefore, does not show up in the database. For example, in reading through some of the incidents and accidents caused by corrosion, it was found in the text that the real cause of failure was, more specifically, due to pitting corrosion or exfoliation. But those words were not highlighted so that incident or accident did not show up in a search of pitting corrosion or exfoliation. This makes the validity of numbers of incidents and accidents caused by pitting corrosion questionable due to the fact that additional incidents and accidents may be listed under different causes and/or more general causes. Also included in the survey were the three Embraer 120 incidents involving propeller blades, the Aero Commander 680 lower spar cap, and the F-18 trailing edge flap failure. These civilian and military incidents and accidents were all due to pitting corrosion as shown in Table 13-1. When these examples are taken with the general information cited in the previous references they clearly show that corrosion related degradation is a significant safety issue in the assurance of structural integrity of aircraft.

Table 13-1: Pitting Corrosion Incidents of Aircraft and Helicopters.

Aircraft	Location of Failure	Cause	Incident Severity	Place	Year	From
Bell Helicopter	Fuselage, longeron	Fatigue, corrosion and pitting present	Serious	AR, USA.	1997	NTSB
DC-6	Engine, master connecting rod	Corrosion pitting	Fatal	AK, USA.	1996	NTSB
Piper PA-23	Engine, cylinder	Corrosion pitting	Fatal	AL, USA.	1996	NTSB
Boeing 75	Rudder Control	Corrosion pitting	Substantial damage to plane	WI, USA.	1996	NTSB
Embraer 120	Propeller Blade	Corrosion pitting	Fatal and serious, loss of plane	GA, USA.	1995	NTSB
Gulfstream GA-681	Hydraulic Line	Corrosion pitting	Loss of plane, no injuries	AZ, USA.	1994	NTSB
L-1011	Engine, compressor assembly disk	Corrosion pitting	Loss of plane, no injuries	AK, USA.	1994	NTSB
Embraer 120	Propeller Blade	Corrosion pitting	Damage to plane, no injuries	Canada	1994	NTSB
Embraer 120	Propeller Blade	Corrosion pitting	Damage to plane, no injuries	Brazil	1994	NTSB
F/A-18	Trailing-Edge Flap (TEF) Outboard Hinge Lug	Corrosion pitting, fatigue	Loss of TEF	Australia	1993	AMRL
Mooney-Mooney 20	Engine, interior	Corrosion pitting, improper approach	Minor injuries	TX, USA.	1993	NTSB
Aero Commander 680	Lower Spar Cap	Corrosion pitting	Fatal	Sweden	1990	Swedish CAA

Therefore, the potential regrettable occurrence of accidents from corrosion related crack nucleation is a constant threat to aircraft safety. The following quote from the recent NATO RTO conference on fatigue in the presence of corrosion [38] adds some understanding to the need for greater effort to understand the potential role of the effects of corrosion on structural integrity.

“Some of the workshop papers discussed the significance of corrosion-fatigue as a safety issue or an economic issue. There is ample data to support the contention that it is definitely an economic issue. There is also ample data to support the contention that it has not been a significant safety problem. However, the problem is certainly a potential safety concern if maintenance does not perform their task diligently. In addition, management must continuously update established maintenance and inspection practices to address additional real-time degradation threats for aircraft operated well beyond their initial design certification life. The economic issue alone is sufficient to motivate the support of research and development that can reduce the maintenance burden. This research will also reduce the threat of catastrophic failure from the corrosion damage.” (Lincoln, J., Simpson, D., Introduction to Reference [38])

Another quote from a different reference also sheds further light on this issue (Reference [36], Page 1-1).

“At the present time, structural life assessments, inspection requirements, and inspection intervals, are determined by Durability and Damage Tolerance Assessments (DADTAs) using fracture mechanics crack growth techniques in accordance with the Aircraft Structural Integrity Program (ASIP). These techniques do not normally consider the effects of corrosion damage on crack initiation or crack growth rate behavior. Also, these techniques do not account for multiple fatigue cracks in the DADTAs of the structural components susceptible to WFD. For aircraft that are not expected to have significant fatigue damage for many years, such as the C/KC-135, this approach has severe limitations since it does not account for corrosion damage or WFD. The impact of corrosion damage and WFD on stress, fatigue life, and residual strength must be understood to ensure maintenance inspections and repair actions are developed and initiated before serious degradation of aircrew/aircraft safety occurs.”

Thus, the community now clearly recognizes the potential impact of corrosion related degradation on structural integrity of aircraft. The need to understand the potential for the occurrence of corrosion on aircraft components is critical. Thus, to even begin the assessment of this potential the community needs to know the following:

- The chemical environment likely to be encountered on the structure of interest at the location of interest;
- The material from which the component is manufactured;
- The orientation of the critical forces (loads) applied externally and internally with respect to the critical directions in the material;
- The susceptibility of the material to a given type of corrosion;
- The temperature of exposure of the component;
- The type of forces applied, i.e., sustained force or cyclic force (constant force amplitude or variable force amplitude);
- The type of exposure to the chemical environment, i.e., constant, intermittent, concomitant with the forces (corrosion fatigue or stress corrosion cracking) or sequentially with force (corrosion/fatigue or corrosion-fatigue);
- The rates of corrosion attack;
- The potential influence of the effects of corrosion on fatigue crack nucleation and propagation;
- The impact of any related corrosion degradation on residual strength;

- The potential for Widespread Corrosion Damage (WCD) to occur; and
- The potential impact of corrosion on the occurrence of Widespread Fatigue Damage (WFD) and its impact on structural integrity.

In corrosion fatigue conditions, several studies showed greater increase in fatigue crack growth rates compared to “baseline” fatigue conditions. Although major efforts were expended to understand the crack propagation behavior of materials, a few studies have focused on the crack nucleation stage in the overall fatigue process [39]-[41]. McAdam first suggested that corrosion induced pits might act as stress concentrators from which cracks could form [42]. A large number of chemical or electrochemical factors such as potential, passive film, pH, and composition of environment are found to affect the pitting corrosion fatigue process. As well, mechanical factors such as stress range, frequency, stress ratio (R), and load waveform and metallurgical factors such as material composition, microstructure, heat treatment, and orientation can influence pitting corrosion fatigue process. Nucleation of cracks from corrosion pits was observed by many researchers including Hoepfner [39]-[41], Goto [43] in heat-treated carbon steel, and Muller [44] in several steels. As well, in NaCl environment, lowering of the fatigue life due to the generation of pits in carbon steel [45] and 7075-T6 aluminum alloy [46] was observed under corrosion fatigue conditions.

Once the pit forms, the rate of pit growth is dependent mainly on the material, local solution conditions and the state of stress. Cracks have been observed to form from pits under cyclic loading conditions. Therefore, to estimate the total corrosion fatigue life of an alloy, it is of great importance to develop some realistic models to establish the relationship between pit propagation rate and the state of stress. Furthermore, pitting corrosion in conjunction with externally applied mechanical stresses, for example, cyclic stresses, has been shown to severely affect the integrity of the oxide film as well as the fatigue life of a metal or an alloy. Therefore, to understand this phenomenon, some models based on pitting corrosion fatigue mechanisms have been proposed as discussed below.

13.4 PITTING CORROSION FATIGUE MODELS

Linear Elastic Fracture Mechanics (LEFM) concepts are widely used to characterize the crack growth behavior of materials under cyclic stresses in different environmental conditions. It is important to note that both pitting theory and crack growth theory have been used in the model development as follows. Pit growth rate theory proposed by Godard is combined with the fatigue crack growth concepts. The time (or cycles or both) to nucleate a Mode I crack from a pit (under cyclic loading) could be modeled using LEFM concepts. Based on this idea, a few models [41], [47]-[49] were proposed. All of the models assume hemispherical geometry for the pit shape and the corresponding stress intensity relation is used to determine the critical pit depth using the crack growth threshold (ΔK_{th}) that is found empirically. For a hemispherical pit geometry, these models provide “a reasonable estimate” for the total corrosion fatigue life. Details of these models are presented in Table 13-2. The applicability of the proposed pitting corrosion fatigue models in practical cases is discussed in the next section.

Table 13-2: Pitting Corrosion Fatigue Models.

	Proposed By	Summary	Description	Advantages/ Limitations
1	Hoepfner (1971 – current)	<ul style="list-style-type: none"> Proposed a model to determine critical pit depth to nucleate a Mode I crack under pitting corrosion fatigue conditions. Combined with the pit growth rate theory as well as the fatigue crack growth curve fit in a corrosive environment, the cycles needed to develop a critical pit size that will form a Mode I fatigue crack can be estimated. 	<ul style="list-style-type: none"> Using a four parameter Weibull fit, fatigue crack growth threshold (ΔK_{th}) was found from corrosion fatigue experiments for the particular environment, material, frequency, and load spectrum. The stress intensity relation for surface discontinuity (half penny shaped crack) was used to simulate hemispherical pit, i.e., $K = 1.1 \sigma \sqrt{\pi \left(\frac{a}{Q} \right)}$ Where, σ is the applied stress, a is the pit length, and Q is the function of $a/2c$, S_{ty}. Using the threshold determined empirically, critical pit depth was found from the stress intensity relation mentioned above. Then, the time to attain the pit depth for the corresponding threshold value was found using: $t = \left(\frac{d}{c} \right)^3$ where, t is the time, d is the pit depth, and c is a material/environment parameter. 	<ul style="list-style-type: none"> This model provides a reasonable estimate for hemispherical geometry of the pits. This model is useful to estimate the total corrosion fatigue life with knowledge of the kinetics of pitting corrosion and fatigue crack growth. This model did not attempt to propose mechanisms of crack nucleation from corrosion pits. This model is valid only for the conditions in which LEFM concepts are applicable. Material dependent.
2	Lindley et al. (1982)	<ul style="list-style-type: none"> Similar to Hoepfner’s model, a method for determining the threshold at which fatigue cracks would grow from the pits was proposed. 	<ul style="list-style-type: none"> Pits were considered as semi-elliptical shaped sharp cracks. Used Irwin’s stress intensity solution for an elliptical crack in an infinite plate and came up with the relationship to estimate threshold stress intensity values related to fatigue crack nucleation at corrosion pits, i.e., $\Delta K_{th} = \frac{\Delta \sigma \sqrt{(\pi a) \left[1.13 - 0.07 \left(\frac{a}{c} \right)^2 \right]}}{\left[1 + 1.47 \left(\frac{a}{c} \right)^{1.64} \right]^{1/2}}$ 	<ul style="list-style-type: none"> The proposed stress intensity relation can be used in tension – tension loading situations where stress intensity for pits and cracks are similar.

	Proposed By	Summary	Description	Advantages/ Limitations
2	Lindley et al. (1982) (cont'd)		<p>where, $\Delta\sigma$ is the stress range, a is the minor axis, and c is the major axis of a semi-elliptical crack.</p> <ul style="list-style-type: none"> From the observed pit geometry, i.e., for a/c ratio, threshold stress intensity can be calculated. For the corresponding a/c ratio, critical pit depth can be estimated. 	<ul style="list-style-type: none"> Critical pit depths for cracked specimens can be estimated using the existing threshold stress intensity values. This model is valid only for the conditions in which LEFM concepts are applicable. Material dependent.
3	Kawai and Kasai (1985)	<ul style="list-style-type: none"> Proposed a model based on estimation of allowable stresses under corrosion fatigue conditions with emphasis on pitting. As corrosion is not usually considered in developing S-N fatigue curves, a model for allowable stress intensity threshold involving corrosion fatigue conditions was proposed. 	<ul style="list-style-type: none"> Considered corrosion pit as an elliptical crack. Based on experimental data generated on stainless steel, new allowable stresses based on allowable stress intensity threshold was proposed, i.e., $\Delta\sigma_{all} = \frac{\Delta k_{all}}{F\sqrt{\pi h_{max}}}$ <p>where, ΔK_{all} can be determined from a da/dN vs. ΔK plot for a material, h_{max} is the maximum pit depth, and F is a geometric factor.</p>	<ul style="list-style-type: none"> Using this model, allowable stress in relation to corrosion fatigue threshold as a function of time can be estimated. Material dependent. This model is valid only for the conditions in which LEFM concepts are applicable.
4	Kondo (1989)	<ul style="list-style-type: none"> Corrosion fatigue life of a material could be determined by estimating the critical pit condition using stress intensity factor relation as well as the pit growth rate relation. 	<ul style="list-style-type: none"> Pit diameter was measured intermittently during corrosion fatigue tests. From test results, corrosion pit growth law was expressed as $2c \propto C_p t^{1/3}$ <p>where, $2c$ is the pit diameter, t is the time, and C_p is an environment/material parameter.</p> <p>Then, critical pit condition (ΔK_p) in terms of stress intensity factor was proposed by assuming pit as a crack.</p>	<ul style="list-style-type: none"> The aspect ratio was assumed as constant. Material and environment dependent.

	Proposed By	Summary	Description	Advantages/ Limitations
4	Kondo (1989) (cont'd)		$\Delta K_p = 2.24 \sigma_a \sqrt{\pi c \alpha / Q}$ <p>where, σ_a is the stress amplitude, α is the aspect ratio, and Q is the shape factor.</p> <ul style="list-style-type: none"> Critical pit condition was determined by the relationship between the pit growth rate theory and fatigue crack growth rates. $c = c_p (N/f)^{1/3}$ <p>where, N is the number of stress cycles, f is the frequency, and $2c$ is the pit diameter.</p> <ul style="list-style-type: none"> The pit growth rate dc/dN was developed using ΔK relation as given below: $dc/dN = \left(\frac{1}{3}\right) C_p^3 f^{-1} \alpha^2 \pi^2 Q^{-2} (2.24 \sigma_a)^4 \Delta K^{-4}$ <p>dc/dN was determined using experimental parameter C_p.</p> <ul style="list-style-type: none"> Finally, the critical pit size $2C_{Cr}$ was calculated from the stress intensity factor relation, i.e., $2C_{Cr} = (2Q/\pi\alpha) (\Delta K_p / 2.24\sigma_a)^2$	

13.5 THE VALIDITY OF PITTING CORROSION FATIGUE (PCF) MODELS

In this section, two of the PCF models proposed in the past viz. Hoepfner [41], and Kawai and Kasai [48] are examined to illustrate the applicability of these models in practice. Hoepfner in 1979 proposed the first model to estimate the time or cycles for a pit to reach the critical pit depth to nucleate a Mode I crack under pitting corrosion fatigue conditions based on the conceptual framework presented in 1971. It was proposed that with the pit growth rate theory as well as data from fatigue crack growth experiments in a corrosive environment, the cycles needed to develop a critical pit size that will form a Mode I fatigue crack can be estimated. Using this model, the pit-to-crack transition length and cycles to failure for various stresses can be determined. However, currently, there are many unknowns for the analysis of an aircraft component to estimate accurately the fatigue life under PCF conditions. For example, for any material, no attempt has been made to date to determine the rate of pitting growth and the size of pits at various times. This is necessary to determine the *Phase I* life (L_1 , time or cycles to nucleate pits) of a component under PCF conditions. Once the pits are formed, it is necessary to estimate the time or cycles for the pits to reach a critical condition or critical depth to nucleate fatigue cracks from those pits (L_2). First, the transition of pits to “short” cracks occurs and then cracks will grow to “long” cracks [50]. Therefore, the time or cycles to form “short” cracks from fatigue nucleated pits and propagation to mode I cracks needs to be determined

to estimate the *Phase 2* life (L_2) of a component. To accurately estimate the PCF life of a component using the model proposed by Hoepfner, the following information is necessary to estimate the Phase 1 and the Phase 2 of the total fatigue life:

- The material;
- The geometry;
- The predicted maximum stress on the part;
- The realistic chemical environment around the part;
- The loading spectra;
- A reasonable value for maximum stress on the part;
- The time or cycles to nucleate pits (L_1) – can be estimated from pit growth rate experimental data at different stress levels including the predicted maximum stress on the part;
- Quantified depth of pits from either damage tracking or failure analysis or both;
- “Short” crack behavior of the material, such as fatigue crack growth rate data in the “short” crack regime and the “short” crack threshold stress intensity value;
- The Mode I fatigue crack growth rate data in a realistic corrosive environment including empirical parameters, C and n;
- Certain material parameters, such as the Mode I threshold stress intensity value as a function of frequency, environment, waveform, and R value; and
- Fatigue crack propagation data for evaluating the effect of prior corrosion on the fatigue crack propagation behavior of the component.

As mentioned in Table 13-2, Kawai and Kasai proposed a model to estimate allowable stresses based on the allowable stress intensity threshold. They recognized that large safety factors are often used in determining allowable stresses because considerations like corrosion are often neglected in S-N curves. Knowing the allowable stress intensity threshold (K_{all}) determined from corrosion fatigue experiments and the maximum pit depth (h_{max}) measured from corrosion pit growth rate experiments for a given “machine-material-environment system”, the allowable stress at which the particular component can be operated is determined using the following relation:

$$\Delta\sigma_{all} = \frac{\Delta K_{all}}{F\sqrt{\pi h_{max}}} \quad (1)$$

where ΔK_{all} can be determined from a da/dN vs. ΔK plot for a material, h_{max} is the maximum pit depth, and F is a geometric factor.

Combining these two models, two approaches are suggested to estimate the total fatigue life of a component under PCF conditions as discussed below.

The first approach needs data from either failure analysis or extensive experimentation on the design problem of interest. Both approaches are vital. Assuming that the failure analysis of a component revealed that the fatigue crack originated from a pit and because of it fracture occurred, then, the depth of the pit (a) could be measured. The quantified pit depth can be correlated to the pit growth rate curve for the material and the time or cycles to nucleate the size of the pit measured from failure analysis can be determined (Phase 1, L_1). From this, an estimate of the stress value for pit-to-crack transition corresponding to the measured pit depth (from fracture analysis) can be made. The critical crack size for instability (a_c) can be

calculated for the given value of K_{IC} for the material as well as the maximum applied stress for the component. Then, 'a' can be used in the calculation as the initial crack size and knowing the stress intensity threshold value, as well as a_c , the total number of cycles to failure can be estimated using the Paris relation as explained in the later part of this section.

The second approach involves determining the pit-to-crack transition length under various stresses using the stress intensity threshold value from fatigue crack growth experiments as explained in the following steps.

13.5.1 Pit-to-Crack Transition

This is performed to determine the critical size of pit in terms of pit depth that would transition to a crack (not necessarily a Mode I crack) for different stresses. The stress values that could be used in the calculation are:

- a) The estimated maximum applied stress that the component would be subjected to; and
- b) The ultimate stress for the material in question.

From Hoepfner's pitting corrosion fatigue model, the following equation can be used to determine the critical pit depth:

$$K_{sf} = 1.1\sigma \sqrt{\pi (a/Q)} \quad (2)$$

where:

K_{sf} = Stress intensity factor for a surface discontinuity (MPa \sqrt{m})

σ = Applied stress (MPa)

a = Size of the pit in terms of pit depth (μm or m)

Q = f [(a/2c, tensile yield stress (σ_{ty}))] (dimensionless)

In this calculation, it can be assumed that K_{sf} is equal to the "short" crack stress intensity threshold (ΔK_{scth}) for the material. It is recommended that the value of ΔK_{scth} be used because the pit-to-crack transition first would result in a non-Mode I crack, that is in the "short" crack region. It is important to note that there is no standard value for the ΔK_{scth} in the "short" crack region for a particular material as there is no standard test method to measure the fatigue crack growth rates in this regime. Therefore, this value can either be determined by conducting "short" fatigue crack growth experiments or determined from literature for a specific material. The shape parameter, Q, for a surface crack can be assumed depending on the pit morphology. For different stress levels, ranging from the estimated applied stress for the component to the ultimate stress of the material, the critical pit depth 'a' that would enable the transition of the pit to a "short" crack can be determined. The resultant value of 'a' can be compared with the measured depth of the pit from the failure analysis of a similar component, if there is any. Moreover, the calculated value of 'a' can be correlated to the experimentally generated pit growth rate curve to estimate the phase 1 life (L_1). Then, equation (1) can be used to determine the critical crack size for instability (a_c) given the value of K_{IC} for the material as well as the maximum applied stress for the component.

After this, the total cycles to failure under corrosion fatigue conditions can be estimated as discussed below.

13.5.2 Estimation of Fatigue Cycles to Failure

The total fatigue cycles to failure under corrosion fatigue conditions can be estimated using the well-known Paris relation as given below:

$$da/dN = C \Delta K^n \quad (3)$$

Where da/dN is the rate of crack growth per cycle (m/cycle), 'C' and 'n' are empirical parameters, and ΔK is the stress intensity range ($\text{MPa}\sqrt{\text{m}}$).

The fatigue crack growth data per ASTM 647 standard is needed for the component. From this, a plot of da/dN vs. ΔK can be made. Also, to estimate the fatigue life, the initial discontinuity size, in this case, the initial pit depth is needed. This is in fact the size of the pit-to-crack-transition as determined from step 1. This can be calculated for various stress values as discussed in step 1. Starting with the initial size of the pit-to-crack-transition that is considered as the initial crack size, first, K_{sf} (that is assumed to be equal to ΔK) can be calculated for equal change or increment of crack size (Δa) at a particular stress level using equation (2). Then, the plot of da/dN vs. ΔK for the component can be used to find the corresponding crack growth rate per cycle (da/dN) for each calculated ΔK . Knowing the value of da/dN , ΔN can be calculated from $[\Delta a/(da/dN)]$. This iterative process will be continued until the critical crack length (a_c) is reached. The critical crack size (a_c) can be calculated for different applied stresses for the given K_{IC} for the material using equation (2) as discussed in step 1. Then, the total number of fatigue cycles is added over all of the increments of Δa up to the critical crack size at a particular stress level. This procedure can be repeated for various stress levels and the total fatigue cycles to failure can be compared.

The accuracy of the estimation can be improved if fatigue crack growth rate data under realistic corrosive environments are used in calculating the total cycles to failure. As well, the data on the effect of prior corrosion on the fatigue crack propagation also can help in getting more accurate estimation. The following case study is provided to illustrate the applicability of the PCF models described above in estimating the fatigue life of a component.

13.6 CASE STUDY

13.6.1 Background Information [51]

A landing gear shock-strut cylinder was subjected to fatigue tests with an applied internal pressure of 41.4 MPa (6 Ksi) and an R-value of zero in the laboratory air environment. The cylinder (wall thickness 't' = 5.59 mm or 0.22 in. and inner radius = 44.5 mm or 1.75 in.) was made from a die forging of 7075-T73 aluminum alloy material. The K_{IC} value for 7075-T73 is about $32.6 \text{ MPa}\sqrt{\text{m}}$. After 30,000 cycles, fracture occurred along the parting plane as shown in Figure 13-3. Subsequent failure analysis revealed numerous pits on the internal surface of the cylinder. Figure 13-4 shows a transverse section through one of these pits. The depth of the pit was quantified at about 6 mils. or 0.15 mm. Also, as shown in Figure 13-5 the fracture surface revealed a semi-circular fatigue crack that originated from a pit on the internal surface of the cylinder. The crack depth (a) and crack width (2c) were found to be 4.32 mm (0.17 in.) and 9.65 mm (0.38 in.) respectively [52]. The nominal hoop stress at the fracture location was calculated at about 331.2 MPa (48 ksi). The calculated hoop stress was about 68% of the parent material ultimate strength and 80% of the nominal design stress (414 MPa or 60 ksi) for the component.

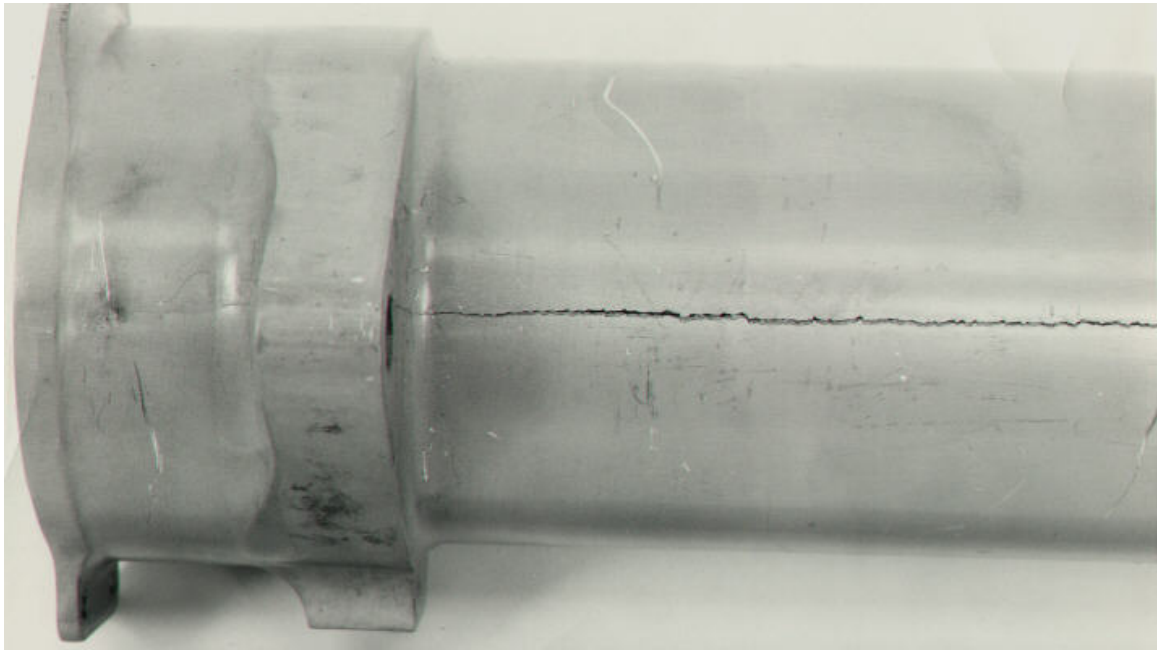


Figure 13-3: Fracture Along the Parting Plane of 7075-T73 Shock-Strut Cylinder.

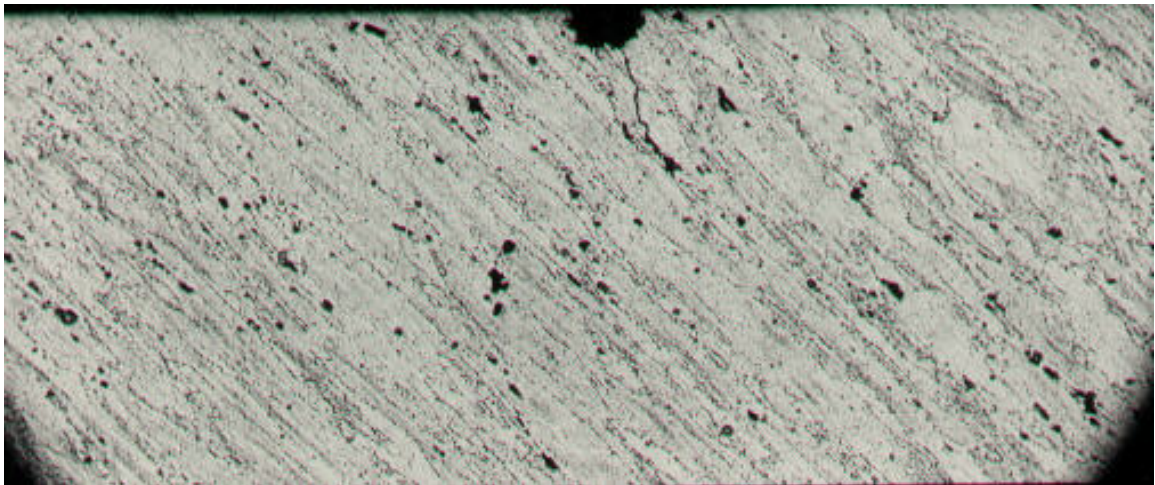


Figure 13-4: A Transverse Section of a Pit on the Inner Surface of the Shock-Strut Cylinder (Note a fatigue crack nucleated from the pit).

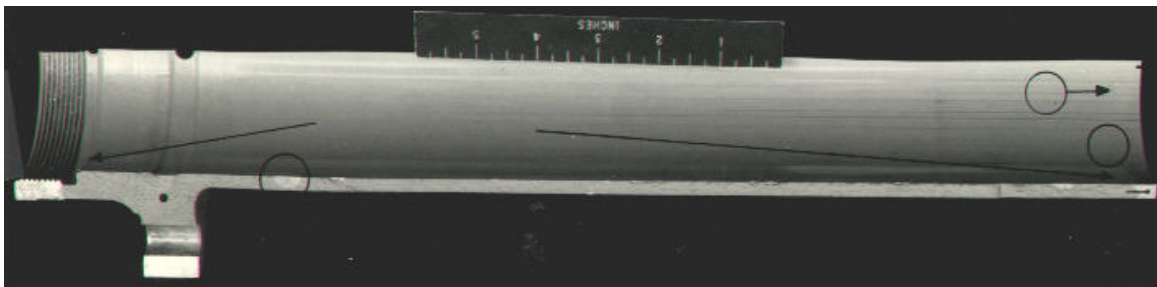


Figure 13-5: A Semi-Circular Crack Originated from a Pit that was Found on the Inner Surface of the Shock-Strut Cylinder (shown by an arrow pointing a circle).

As there is no data available with regard to the pit growth rate for 7075-T73, the *Phase 1* life, that is, the time or cycles to nucleate the pit, from which the crack formed resulting in fracture of the cylinder cannot be estimated. In addition, fatigue crack growth rate data for 7075-T73 in a realistic environment is not available to estimate the number of fatigue cycles for fracture of the cylinder. However, fatigue crack growth rate data for 7075-T73 in a laboratory environment will be used in the estimation. Therefore, with the available information from the failure analysis, the applicability of the PCF models proposed by Hoepfner [41] and Kawai and Kasai [48] to the shock-strut cylinder is demonstrated below.

13.6.2 Calculation of Critical Stress Intensity Factor at Fracture

From equation (2), the critical stress intensity factor at fracture can be calculated. Considering the measured crack depth value from the failure analysis as ‘a’, the calculated σ_{hoop} as σ and Q is assumed as 2.48, the critical stress intensity factor at fracture is found to be 26.95 MPa $\sqrt{\text{m}}$. However, as mentioned before, the K_{Ic} value for 7075-T73 was about 32 MPa $\sqrt{\text{m}}$. The lower K_{Ic} value at fracture could be attributed to numerous pits that were found on the surfaces of the cylinder.

13.6.3 Estimation of Pit to Crack-Transition Length

Using equation (2) from Hoepfner’s PCF model, the pit-to-crack transition can be estimated. For $\sigma = \sigma_{\text{hoop}} = 331.2$ MPa, $K_{\text{sf}} = \Delta K_{\text{scth}} = 0.75$ MPa $\sqrt{\text{m}}$ (for 7075-T6 from ref. 50), the pit-to-crack-transition length is determined to be 0.0035 mm.

13.6.4 Estimation of Fatigue Cycles to Failure

Considering the pit-to-crack-transition length (0.0035 mm) as the initial crack size and the measured crack depth from the failure analysis (4.32 mm) as the critical crack size, the number of fatigue cycles to failure once the pit is transitioned to a crack is determined as shown in Table 13-3. The procedure outlined in the previous section is used in estimating the number of cycles to failure. The fatigue crack growth rate data for 7075-T73 is used in determining da/dN for each calculated ΔK . As determined from Table 13-3, the estimated number of cycles to failure is 20,793. When it is compared to the actual cycles to fracture from testing, that is, 30,000 cycles, it is a reasonable estimate.

Table 13-3: Fatigue Life Estimation for the Shock-Strut Cylinder.

a	K = ΔK	Δa	da/dN***	Avg. da/dN	ΔN	N_{total}
m	MPa*m^{1/2}	m	m/cycle	m/cycle	cycles	cycles
3.35E-06*	0.75075**		2.54E-12			
5.03E-04	9.1996	0.0005	5.08E-08	2.5401E-08	19684	19684
1.00E-03	12.9885	0.0005	2.03E-06	1.0414E-06	480	20164
1.50E-03	15.8987	0.0005	5.08E-07	0.00000127	394	20558
2.00E-03	18.3532	0.0005	2.03E-05	1.0414E-05	48	20606
2.50E-03	20.5160	0.0005	1.65E-05	1.8415E-05	27	20633
3.00E-03	22.4717	0.0005	1.27E-05	1.4605E-05	34	20667
3.50E-03	24.2702	0.0005	1.02E-05	0.00001143	44	20711
4.00E-03	25.9444	0.0005	2.54E-06	0.00000635	79	20790
4.32E-03****	26.9614	0.00032	0.000216	0.00010922	3	20793

* The calculated pit-to-crack transition length based on Hoepfner's PCF model (considered as the initial crack length).

** The "short" crack stress intensity threshold (ΔK_{scth}) for 7075-T6 from reference (50).

*** Determined from the plot of da/dN vs. ΔK for 7075-T73.

**** The measured crack depth from the fracture surface of the shock-strut cylinder (considered as the critical crack length).

13.6.5 Estimation of the Allowable Stress

Using the model proposed by Kawai and Kasai, the allowable stress at which the shock-strut cylinder can be operated is determined using equation (1). In this equation, ΔK_{all} (allowable stress intensity threshold value) is considered equal to the "long" crack threshold stress intensity value for 7075-T73, that is, 5 MPa√m (from [51]). The geometric factor 'F' is assumed as 1. The quantified depth of pit (6 mils. or 1.5e-04 m) on the inner surface of the cylinder from failure analysis is considered as h_{max} , that is, the maximum pit depth. Substituting these values in equation (1), the estimated allowable stress at which the shock-strut cylinder can be operated is determined to be 230.3 MPa. It is about 30% lower when compared to the calculated hoop stress (331.2 MPa) at the fracture location of the shock-strut cylinder.

13.7 SUMMARY AND CONCLUSIONS

This chapter reviewed some PCF models and discussed their usefulness and limitations in estimating the total fatigue life of a component. The applicability of PCF models was demonstrated with a realistic case study involving the fatigue failure of a landing gear shock-strut cylinder. Some examples of critical pitting corrosion fatigue incidents in aircraft and helicopter components were provided to illustrate the significance of developing more realistic models to address this particular failure mechanism. To accomplish this, fatigue growth rate data in a realistic environment need to be generated. Also, the material's response to nucleation of pits and their growth rate under various stresses and environments should be studied. In recent years extensive research at the University of Utah has been performed by numerous students for their Ph.D. degrees and various post doctoral associates.

13.8 ACKNOWLEDGEMENTS

The authors would like to thank Dr. Chandrasekaran for contributions to portions of this summary over many years. We also are grateful to RR Aeroengine Co. for many years of support related to this activity as well as others related to modeling fatigue behavior of materials and structures. Mr. Robert Jeal has contributed much to these efforts over many years. As well, we are grateful to the University of Utah for use of facilities. FASIDE International Inc. provided support for this effort for which we are grateful. We also acknowledge the extensive discussions with Mr. Jerzy Komorowski and Mr. Nick Bellinger of NRC/IAR Canada over many years. Mr. Craig Brooks of AP/ES in St. Louis, MO also has made several suggestions to the modeling that are incorporated herein. We appreciate the interaction of all these persons.

13.9 REFERENCES

- [1] Hoepfner, D.W., "Parameters that Input to Application of Damage Tolerance Concepts to Critical Engine Components", AGARD Conference Proceedings No. 393, Damage Tolerance Concepts for Critical Engine Components, pp. 4-1 – 4-16, 1985.
- [2] Hoepfner, D.W. and Chandrasekaran, V., "Corrosion and Corrosion Fatigue Predictive Modeling – State of the Art Review", FASIDE Report to NCI Information Systems, Fairborn, OH, USA, 1998.
- [3] "Stress Corrosion Cracking in Aircraft Structural Materials", AGARD Conference Proceedings Series 18, Report of a two day Symposium held by the Structures and Materials Panel of AGARD in Turin, Italy, 18-19 April 1967, NATO-AGARD, 64 rue De Varenne, Paris, France, 1967.
- [4] "Fundamental Aspects of Stress Corrosion Cracking", Editors: Staehle, R.W., Forty, A.J., and van Rooyen, D., Proceedings of a Conference held at the Ohio State University, 11-15 September 1967, NACE-1, National Association of Corrosion Engineers, Houston, TX, USA, 1969.
- [5] "Effects of Environment and Complex Load History on Fatigue Life", ASTM STP 462, Proceedings of the Symposium on Effects of Environment and Complex Load History on Fatigue Life held in Atlanta, GA, USA, 29 September – 4 October 1968, Edited by Rosenfeld, M, Hoepfner, D.W, and Stephens, R.I., American Society for Testing and Materials, Philadelphia, PA, USA, 1970.
- [6] "Corrosion Fatigue: Chemistry, Mechanics, and Microstructure", Editors: Devereux, O., McEvily, A.J. and Staehle, R.W., Proceedings of the Conference held at the University of Connecticut, 14-18 June 1971, NACE-2, National Association of Corrosion Engineers, Houston, TX, USA, 1973.
- [7] Brown, B.F., "Stress-Corrosion Cracking in High Strength Steels and in Titanium and Aluminum Alloys", Naval Research Laboratory, Washington, DC, USA, 1972.
- [8] Hall, L.R., Finger, R.W. and Spurr, W.F., "Corrosion Fatigue Crack Growth in Aircraft Structural Materials", AFML-TR-73-204, Boeing Company, September 1973.
- [9] Pettit, D., Ryder, J., Krupp, W. and Hoepfner, D.W, "Investigation of the Effects of Stress and Chemical Environments on the Prediction of Fracture in Aircraft Structural Materials", AFML-TR-74-183, Lockheed California Company, December 1974.
- [10] "Corrosion-Fatigue Technology", ASTM STP 642, Proceedings of a Symposium held in Denver, CO, USA, 14-19 November 1976, Edited by Craig, Jr., H.L., Crooker, T.W. and Hoepfner, D.W., American Society for Testing and Materials, Philadelphia, PA, USA, 1978.
- [11] "Aircraft Corrosion", AGARD Conference Proceedings No. 315, Papers presented at the 52nd Meeting of the AGARD Structures and Materials Panel held in Cesme, Turkey, 5-10 April 1981, Advisory Group for Aerospace Research and Development, 64 rue de Varenne, Paris, France, 1981.

- [12] “Corrosion Fatigue”, AGARD Conference Proceedings No. 316, Papers presented at the 52nd Meeting of the AGARD Structures and Materials Panel held in Cesme, Turkey, 5-10 April 1981, Advisory Group for Aerospace Research and Development, 64 rue de Varenne, Paris, France, 1981.
- [13] “Corrosion Fatigue”, ASTM STP 801, Proceedings of the Symposium on Corrosion Fatigue: Mechanics, Metallurgy, Electrochemistry, and Engineering held in St. Louis, MO, 21-22 October 1981, Edited by Crooker, T.W., Leis, B.N., American Society for Testing and Materials, Philadelphia, PA., USA, 1983.
- [14] Campbell, G.S. and Lahey, R., “A Survey of Serious Aircraft Accidents Involving Fatigue”, Int. J. Fatigue, Vol. 6, No. 1, pp. 25-30, 1984.
- [15] Wallace, W., Hoeppe, D.W., and Kandachar, P.V., “Aircraft Corrosion: Causes and Case Histories”, AGARD Corrosion Handbook, Vol. 1, AGARD-AG-278, Advisory Group for Aerospace Research and Development, 1985.
- [16] ASM Metals Handbook, Vol. 13, “Corrosion”, ASM International, Metals Park, Ohio, USA, 1987.
- [17] The Boeing Company, “Corrosion Prevention and Control”, Manual for Training Operators of Boeing Commercial Aircraft, Seattle, WA, USA, 1988.
- [18] NTSB Metallurgist’s Report, “Aloha Airlines Flight 243”, Materials Laboratory Report 88-85, 1988.
- [19] “Environment Induced Cracking of Metals”, Editors: Gangloff, R.P. and Ives, M.B., Proceedings of the Conference held in Kohler, WI, 2-7 October 1988, NACE-10, National Association of Corrosion Engineers, Houston, TX, USA, 1990.
- [20] ASM Handbook, Volume 18, “Friction, Lubrication, and Wear Technology”, ASM International, Metals Park, Ohio, USA, 1992.
- [21] Naval Aviation Safety Program, US Navy, OPNAVINST 3750.6Q CH-1, OP-05F, March 1991.
- [22] Federal Aviation Administration, “Aircraft Accident and Incident Synopses Related to Corrosion, Fretting, and Fatigue for the Period 1976 – 1993”, obtained July 1994.
- [23] National Transportation Safety Board, “Aircraft Accident and Incident Synopses Related to Corrosion, Fretting, and Fatigue for the Period 1975 – 1993”, obtained July 1994.
- [24] Roberge, P., “Corrosion Engineering Principles and Practice”, McGraw Hill Book Co., New York, NY, USA, 2008.
- [25] Karpala, F. and Hageniers, O.L., “Characterization of Corrosion and Development of a Breadboard Model of a D-Sight Aircraft Inspection System”, Phase 1, Diffracto Ltd., Report to DOT, August 1994.
- [26] United States Air Force, Navy, and Army, Aircraft Accident and Incident Synopses Related to Corrosion, Fretting, and Fatigue, obtained June – August 1994.
- [27] Cooke, G., Vore, P.J., Gumienny, C. and Cooke, Jr., G., “A Study to Determine the Annual Direct Cost of Corrosion Maintenance for Weapon Systems and Equipment in the United States Air Force”, Final Report, Contract Number F09603-89-C-3016, September 1990.
- [28] Schutz, W., “Corrosion Fatigue – The Forgotten Factor in Assessing Durability”, ICAF 95, Estimation, Enhancement and Control of Aircraft Fatigue Performance, Vol. 1, Edited by J.M. Grandage and

- G.S. Jost, Proceedings of the 18th Symposium on the International Committee of Aeronautical Fatigue, 3-5 May 1995, Melbourne, Victoria, Australia, EMAS, Warley, West Midlands, UK, pp. 1-52, 1995.
- [29] Swift, S.J., "The Aero Commander Chronicle", ICAF 95, Estimation, Enhancement and Control of Aircraft Fatigue Performance, Vol. 1, Edited by Grandage, J.M. and Jost, G.S., Proceedings of the 18th Symposium on the International Committee of Aeronautical Fatigue, 3-5 May 1995, Melbourne, Victoria, Australia, EMAS, Warley, West Midlands, UK, pp. 507-530, 1995.
- [30] Hoepfner, D.W., Grimes, L., Hoepfner, A., Ledesma, J., Mills, T. and Shah, A., "Corrosion and Fretting as Critical Aviation Safety Issues", ICAF 95, Estimation, Enhancement and Control of Aircraft Fatigue Performance, Vol. 1, Edited by Grandage, J.M. and Jost, G.S., Proceedings of the 18th Symposium on the International Committee of Aeronautical Fatigue, 3-5 May 1995, Melbourne, Victoria, Australia, EMAS, Warley, West Midlands, UK, pp. 87-106, 1995.
- [31] Brooks, C.L., Liu, K. and Eastin, R.G., "Understanding Fatigue Failure Analyses Under Random Loading Using a C-17 Test Article", ICAF 95, Estimation, Enhancement and Control of Aircraft Fatigue Performance, Vol. 1, Edited by Grandage, J.M. and Jost, G.S., Proceedings of the 18th Symposium on the International Committee of Aeronautical Fatigue, 3-5 May 1995, Melbourne, Victoria, Australia, EMAS, Warley, West Midlands, UK, pp. 449-468, 1995.
- [32] ASM Handbook, Vol. 19, "Fatigue and Fracture", ASM International, Metals Park, OH, USA, 1996.
- [33] Schmidt, C.G., Crocker, J.E., Giovanola, J.H., Kanazawa, C.H. and Schockey, D. "Characterization of Early Stages of Corrosion Fatigue in Aircraft Skin", Final Report, Contract No. 93-G-065, SRI International Final Report to DOT, Menlo Park, CA, USA, Report No. DOT/FAA/AR-95/108, February 1996.
- [34] Cole, G.K., Clark, G. and Sharp, P.K., "Implications of Corrosion With Respect to Aircraft Structural Integrity", DSTO-RR-0102, AMRL, Melbourne, Victoria, Australia, March 1997.
- [35] "Aging of U.S. Air Force Aircraft", Report of the Committee on Aging of U.S. Air Force Aircraft, NMAB (National Materials Advisory Board), Commission on Engineering and Technical Systems, National Research Council, Publication NMAB-488-2, 1997.
- [36] Boeing, "Corrosion Damage Assessment Framework, Corrosion/Fatigue Effects on Structural Integrity", Report D500-13008-1, USAF Contract No. F9603-97-C-0349, 1998.
- [37] Paul, C. and Mills, T., "Corrosion/Fatigue", Presentation made at AeroMat, "A Study to Determine the Cost of Corrosion Maintenance for Weapon Systems and Equipment in the United States Air Force", Final Report, Contract Number F09603-95-D-0053, February 1998.
- [38] "Fatigue in the Presence of Corrosion", NATO-RTO Proceedings 18, Papers Presented at the Workshop of the NATO-RTO Applied Vehicle Technology (AVT) Panel, held in Corfu, Greece, 7-9 October, 1998, AC/323(AVT) TP/8, NATO, Research and Technology Organization, BP 25, 7 rue Ancelle, F-92201, Neuilly-Sur-Seine, Cedex, France, 1999.
- [39] Hoepfner, D.W., Mann, D. and Weekes, J., "Fracture Mechanics Based Modeling of Corrosion Fatigue Process", in Corrosion Fatigue: Proceedings of the 52nd Meeting of the AGARD Structures and Materials Panel, held in Turkey, 5-10 April 1981.
- [40] Hoepfner, D.W., "Corrosion Fatigue Considerations in Materials Selection and Engineering Design", Corrosion Fatigue: Chemistry, Mechanics, and Microstructure, NACE, pp. 3-11, 1972.

- [41] Hoepfner, D.W., "Model for Prediction of Fatigue Lives Based Upon a Pitting Corrosion Fatigue Process", *Fatigue Mechanisms, Proceedings of an ASTM-NBS-NSF Symposium*, Ed., Fong, J.T., ASTM STP 675, American Society for Testing and Materials, pp. 841-870, 1979.
- [42] McAdam, D.J. and Gell, G.W., "Pitting and Its Effect on the Fatigue Limit of Steels Corroded Under Various Conditions", *Journal of the Proceedings of the American Society for Testing Materials*, Vol. 41, pp. 696-732, 1928.
- [43] Goto, M. and Nisitani, H., "Crack Initiation and Propagation Behavior of a Heat Treated Carbon Steel in Corrosion Fatigue", *Fatigue Fracture Engineering Material Structure*, Vol. 15, No. 4, pp. 353-363, 1992.
- [44] Muller, M., "Theoretical Considerations on Corrosion Fatigue Crack Initiation", *Metallurgical Transactions*, Vol. 13A, pp. 649-655, 1982.
- [45] Mehdizadeh, P., et al., "Corrosion Fatigue Performance of a Carbon Steel in Brine Containing Air, H₂S, CO₂", *Corrosion*, Vol. 22, pp. 325-335, 1966.
- [46] Corsetti, L.V. and Duquette, D.J., "The Effect of Mean Stress and Environment on Corrosion Fatigue Behavior of 7075-T6 Aluminum", *Metallurgical Transactions*, Vol. 5, pp. 1087-1093, 1974.
- [47] Lindley, T.C., McIntyre, P. and Trant, P.J., "Fatigue Crack Initiation at Corrosion Pits", *Metals Technology*, Vol. 9, pp. 135-142, 1982.
- [48] Kawai, S. and Kasai, K., "Considerations of Allowable Stress of Corrosion Fatigue (Focused on the Influence of Pitting)", *Fatigue Fracture of Engineering Materials Structure*, Vol. 8, No. 2, pp. 115-127, 1985.
- [49] Kondo, Y., "Prediction of Fatigue Crack Initiation Life Based on Pit Growth", *Corrosion Science*, Vol. 45, No. 1, pp. 7-11, 1989.
- [50] Newman, Jr., J.C., Phillips, E.P., and Swain, M.H., "Fatigue-Life Prediction Methodology Using Small-Crack Theory", *International Journal of Fatigue*, 21, pp. 109-119, 1999.
- [51] Bowie, G.E., Van Orden, J.M., Besari, M.S., Pettit, D.E., Weber, K.E., Krupp, W.E., Fairchild, J. and Meyer, D.R., "Correlation of Failure Analysis Data: Pitting Corrosion", LR 27399, Lockheed California Company Report, 1975.
- [52] Hoepfner, D.W., "Applied Fracture Mechanics and Prevention of Fracture in Materials", Lockheed Continuing Education Course, Lockheed Engineering Extension Program (LEEP), Lockheed Aircraft Corporation, Burbank, CA, USA, 1970.

Chapter 14 – MODELING CORROSION STRUCTURAL IMPACT: PILLOWING

Nicholas C. Bellinger
Institute for Aerospace Research
National Research Council Canada
Ottawa, Ontario
CANADA

14.1 INTRODUCTION

Since actual lap joints contain free edges and stiffeners, which cannot be modeled using the closed-form solution, finite element techniques have been developed to model an actual aircraft lap joint. This model included the effects of the hoop stress from the pressurization of the fuselage, the rivet pre-stress caused by the rivet installation as well as the corrosion pillowing stress. The fuselage curvature was ignored for all the analyses that were performed during this program. Since it was assumed that a linear relationship existed between the different loads, three finite element models were generated for each load and the resultant stresses were added together.

14.2 MODEL DEVELOPMENT

All the finite element models were generated with first-order brick elements. It was assumed for the hoop stress model that some of the load transfer would be due to friction under the rivet heads, which was simulated by merging the nodes in these areas. Since lap joints contain stiffeners, the joints were not symmetrical about their mid-planes and thus both skins had to be modeled. Initially, a constant pressure of 6.89 kPa (1 psi) was applied to both the outer and inner skins of the joint. The resulting volume under the deformed shape, V_{fem} , was determined using an iterated integral:

$$V_{fem} = \int_c^d \left(\int_a^b f(x, y) dx \right) dy \quad (1)$$

where (a, b) and (c, d) are the intervals of integration along the x- and y-axes respectively, over the length of the joint for which the volume was to be calculated. In computing the iterated integrals, y was held constant while integrating with respect to x (vice-versa in the second case). Simpson's 1/3 and 3/8 rule [1] were used depending on the number of nodes to be evaluated. Then, assuming a thickness loss, t_{lo} , given a specific percentage of corrosion, the actual volume required by the corrosion products, V_{req} can be determined using Equation 2:

$$V_{req} = abt_{lo} \left[\frac{V_{mr}}{2} - 1 \right] \quad (2)$$

To obtain this volume, the pressure between the rivets in the initial finite element analysis was multiplied by the ratio, P_{req} , given in Equation 3:

$$P_{req} = \frac{V_{req}}{V_{fem}} \quad (3)$$

Since the free edges of a lap joint are usually sealed (either by paint or a sealant) to prevent moisture from entering the joint, the volume of corrosion products is less than that present around the rivet. Therefore, the pressure is decreased from the rivets to the free edge to simulate this reduction in corrosion products [2].

14.3 RESULTS

The results indicated that the stress in the vicinity of the upper rivet row in the outer skin and the lower rivet row in the inner skin, which are the critical locations in terms of cracking for the respective skins in a typical two layer aircraft joint, increases as the pillowing increased, as shown in Figure 14-1.

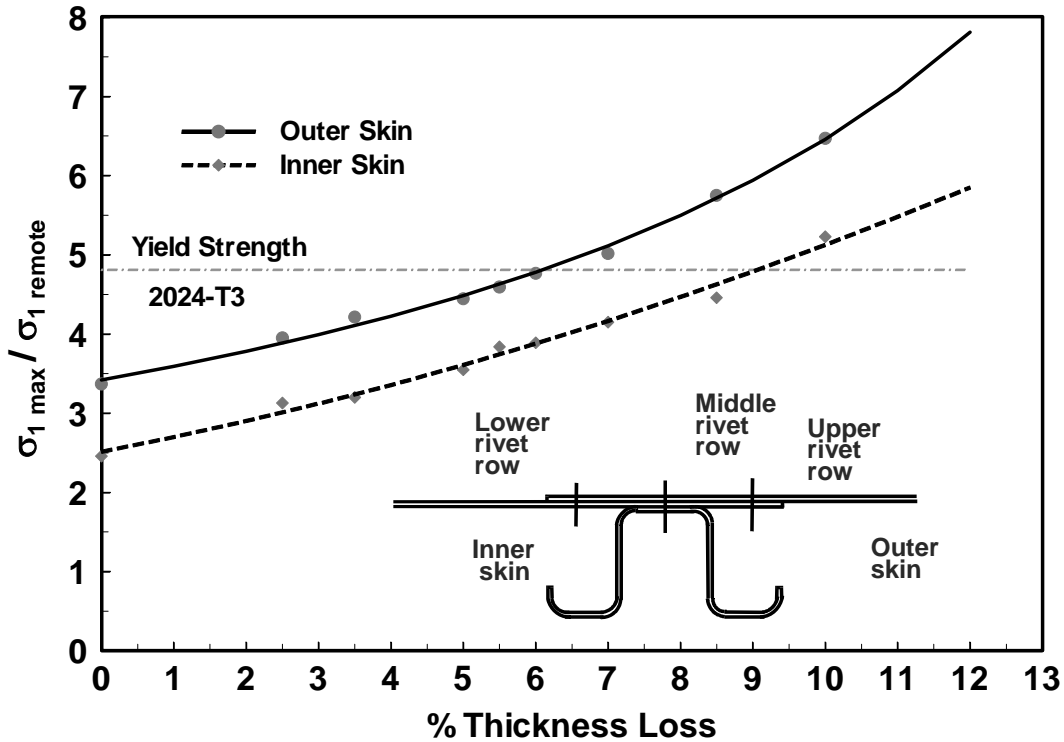


Figure 14-1: Effect of Increased Corrosion Pillowing on Critical Rivet Row of Respective Skins [1].

A comparison was also made between the increase in stress caused by an equivalent thinning of the outer skin and that caused by pillowing, Figure 14-2. The results showed that pillowing had a greater influence on the stress in a joint as compared to the effective thickness loss alone. This larger influence is a significant finding, since it has been previously assumed that by reducing the skin thickness and increasing the crack growth rate, the effect of corrosion on fuselage lap joints can be adequately taken into account. However, this simple assumption can result in non-conservative life estimates that can increase the risk of premature cracking. The finite element results also showed that pillowing could change the location of the maximum principal stress within a lap joint [2]. This finding has raised concerns since the new critical location could occur in an area that is not normally inspected for cracks, again increasing the risk that these cracks could remain undetected.

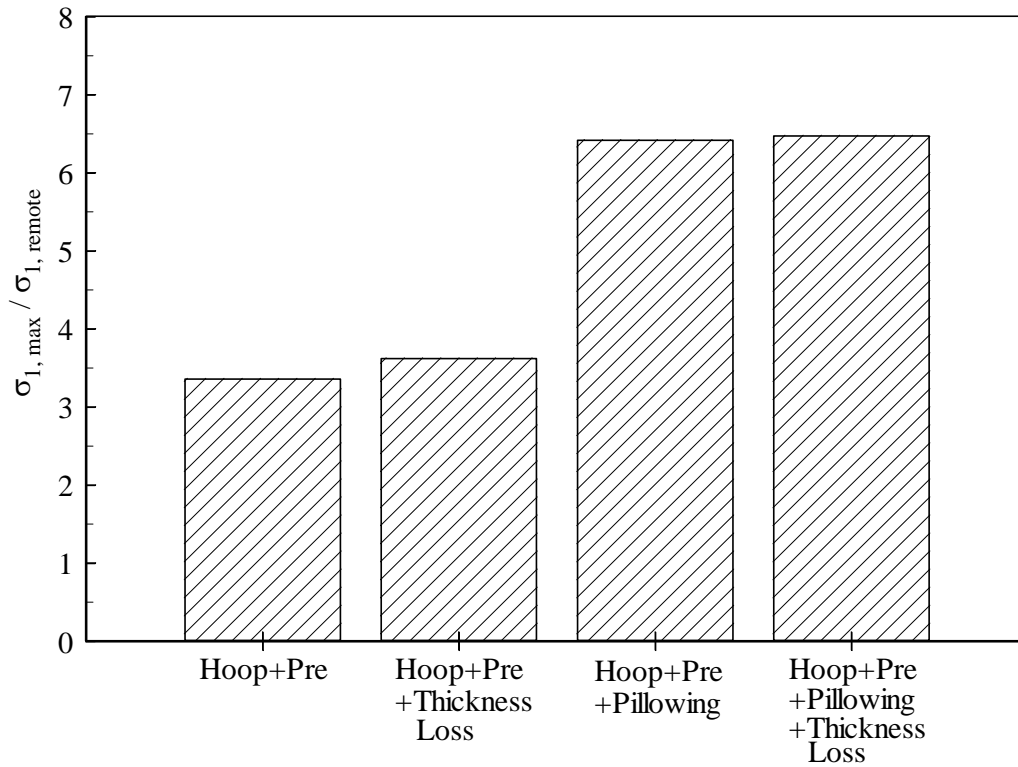
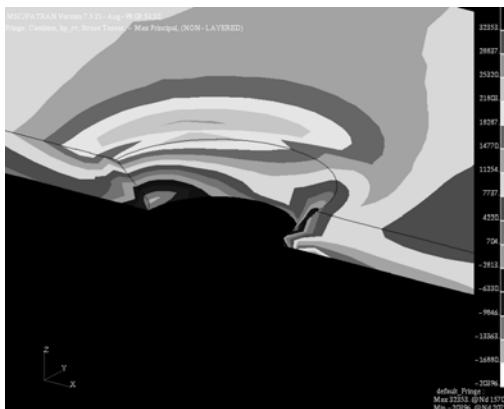
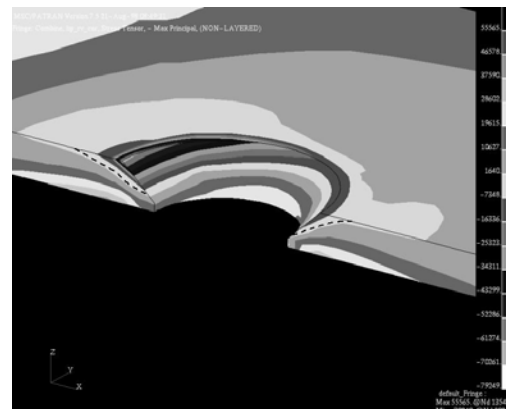


Figure 14-2: Effect on Stress Caused by Reduction of Outer Skin Thickness as Compared to Pillowing (10% Thickness Loss) [2].

The finite element results also showed that the stress along the outer surface of the outer skin in the vicinity of the critical rivet row could become compressive at the holes when the thickness loss in a corroded lap joint increased to above 10%, Figure 14-3 [3]. This smaller stress along the outer surface raised concerns about the nucleation and growth of cracks in the presence of corrosion pillowing.



(a) Non-corroded lap joint, includes hoop stress and rivet interference.



(b) Corroded lap joint showing approximate location of neutral axis (dashed line) for 10% thickness loss. Loading includes hoop stress, rivet interferences and corrosion pillowing.

Figure 14-3: Stress Plot for Non-Corroded and Corroded Lap Joints.

MODELING CORROSION STRUCTURAL IMPACT: PILLOWING

To examine this effect, a fracture mechanics analysis was carried out using finite element techniques [4]. A number of straight-fronted-through cracks were examined for joints containing two levels of corrosion, 5% and 10% thickness loss and with a crack located at the critical rivet row. The results showed that the stress intensity factors along the inner and outer surface of the outer skin diverged as the thickness loss increased, Figure 14-4. As can be seen from this figure, the stress intensity factor for the crack edge along the faying (inner) surface increased as the pillowing increased while that at the crack edge along the outer surface decreased. This difference in the two surfaces suggests that the crack edge located along the faying surface would grow more rapidly in the direction of the row of rivets than through the thickness resulting in a semi-elliptical crack front with a high aspect ratio as shown in Figure 14-5.

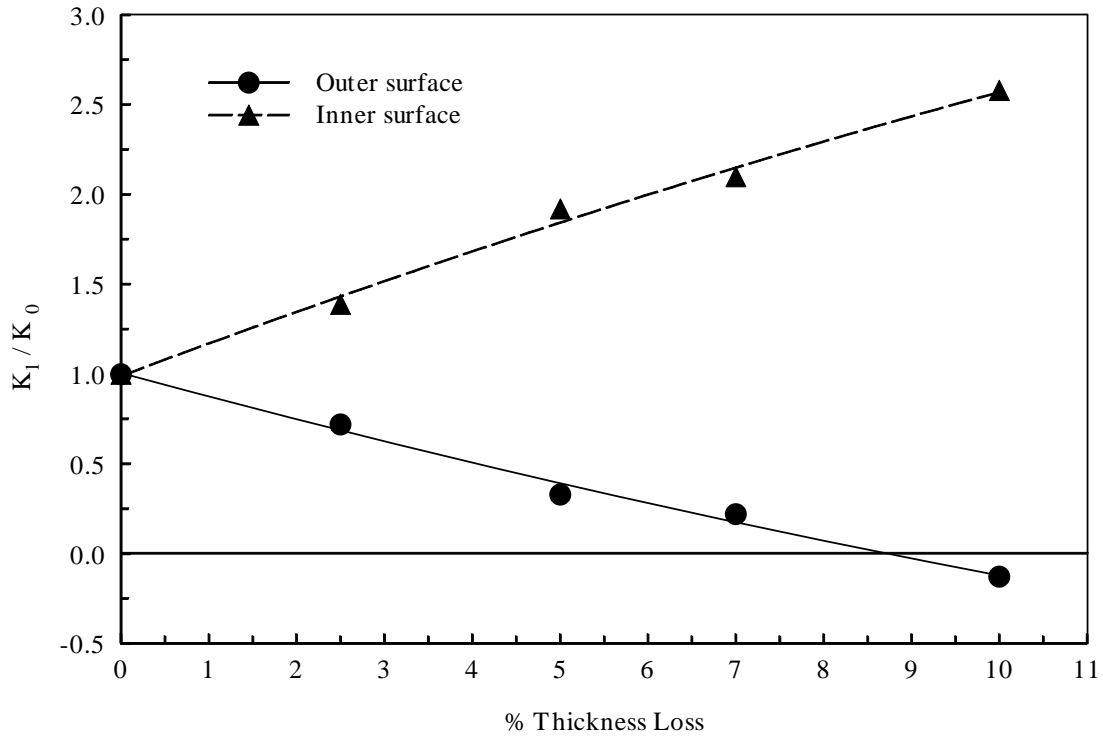


Figure 14-4: Non-Dimensional Stress Intensity Plot of Outer Surface, $z = 0.00$ and Inner (Faying) Surface, 1.14 mm (0.045 inch) of Outer Skin for Single Crack Length of, 3.84 mm (0.151 inch), where K_0 is the Stress Intensity Factor of a Through Crack Without Corrosion ($K_0 = \sigma\sqrt{\pi a}$) [4].

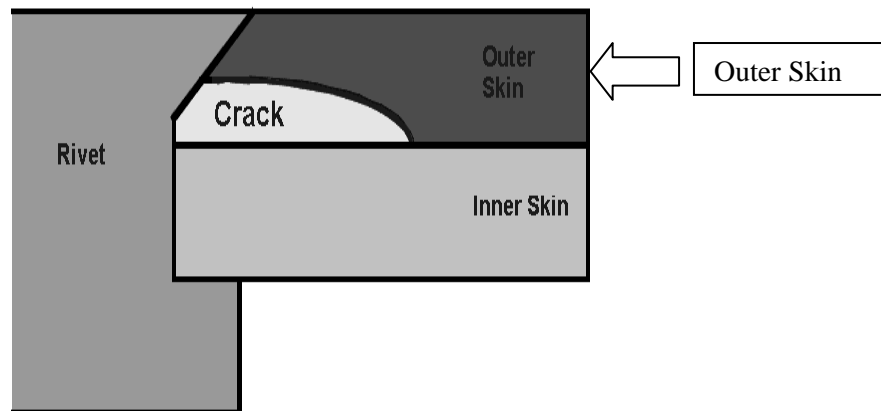


Figure 14-5: Suggested Shape of Cracks in the Presence of Pillowing [4].

14.4 REFERENCES

- [1] Gerald, C.F. and Whearley, P.O., “Applied Numerical Analysis”, 3rd Ed., Addison-Wesley Publishing Company, 1985.
- [2] Bellinger, N.C. and Komorowski, J.P., “Corrosion Pillowing Stresses in Fuselage Lap Joints”, AIAA Journal, Vol. 35, No. 2, pp. 317-320, February 1997.
- [3] Bellinger, N.C., Komorowski, J.P. and Gould, R.W., “Corrosion Pillowing Cracks in Fuselage Lap Joints”, Proceedings of the Second Joint NASA/FAA/DoD Conference on Aging Aircraft, NASA/CP-1999-208982/Part 2, Williamsburg, VA, USA, pp. 535-544, 31 August – 3 September 1998.
- [4] Bellinger, N.C., Komorowski, J.P. and Gould, R.W., “Damage Tolerance Implications of Corrosion Pillowing on Fuselage Lap Joints”, Journal of Aircraft, Vol. 35, No. 3, pp. 487-491, May – June 1998.



Chapter 15 – EXFOLIATION CORROSION AND FATIGUE MODELING

Min Liao

Institute for Aerospace Research
National Research Council Canada
Ottawa, Ontario
CANADA

Thomas Mills

Analytical Processes / Engineered Solutions, Inc.
Saint Louis, Missouri
USA

15.1 INTRODUCTION

Corrosion is a persistent threat to aircraft structural integrity, yet existing structural integrity methodologies tend to treat corrosion in a questionable manner. The safety factors employed in the safe life approach prove to be unreliable. The practice in the damage tolerance approach that large assumed crack sizes ‘cover’ the influence of corrosion might be valid in some cases, but there are many cases where that assumption is invalid or just unaffordable.

Thus, the aviation community needs methods that properly account for the physical effects of corrosion on a structure. Part of this need is driven by the desire to reduce maintenance costs and increase aircraft availability, and part of it is driven by emerging regulatory requirements, such as the recent US Federal Aviation Administration proposed rulemaking on Widespread Fatigue Damage (WFD) [1] and the recent notices for proposed rulemaking issued regarding damage tolerance for rotorcraft [2] and engine life-limited parts [3].

This chapter specifically studies the latest advances in the modeling of exfoliation/fatigue interactions using Finite Element Analysis (FEA) and fracture mechanics methods.

Exfoliation corrosion, defined as a severe Intergranular Corrosion (IGC) (ASTM G15-97a), is one of the most common corrosion forms found in aircraft structures [4],[5]; however, its significance has long been undermined as merely a warning of other insidious failure modes such as Stress Corrosion Cracking (SCC) or as only a threat to static strength or stability. To illustrate this perception, even the ASM Handbook on Corrosion [6] explains that exfoliation itself is not of concern because it is a surface phenomenon that is “easily detectable”, that “proceeds to only a limited depth”, and that “does not result in sudden failures” as does SCC. This view is unsatisfactory for a number of reasons:

- Aircraft structural members have been completely consumed by exfoliation corrosion thus nullifying the limited depth argument.
- Many aircraft structural components that suffer from exfoliation corrosion (such as stringers and internal surfaces of wing skins) are hidden from view and are, as a consequence, not readily inspectable.
- Exfoliation damage has been shown to cause sufficient stress concentrations to nucleate multiple fatigue cracks [7]-[9].
- Studies have shown that fatigue crack growth rates through exfoliated material can be higher than in uncorroded material [10]-[13].

The studies referenced above did much to explain the degree by which exfoliation affected the fatigue performance of aircraft structural aluminum alloys, but they did not delve into the modeling of exfoliation and fatigue interactions other than to account for increases in crack growth rate due to thickness loss.

In general, exfoliation effects on static properties, such as buckling, yielding, and bearing strength, can be conservatively modeled by simply considering exfoliation corrosion as a thickness loss. However, as illustrated by the following factors, the modeling of the exfoliation effect on the fatigue response is much more complicated:

- 1) Multiple cracking mechanisms – fractography has shown that fatigue cracks could start from:
 - a) Pits on the bottom of the exfoliated surface;
 - b) Tip of intergranular corrosion; and
 - c) A particle or grain denuded by IGC/exfoliation [14],[15].
- 2) Complex exfoliation morphology – particularly, when exfoliation occurs in a complicated geometry, like near or under a countersunk hole in a lap joint.
- 3) Loading spectrum – some tests showed that exfoliation had a benign effect on the fatigue life when the structure is under a compression-dominated spectrum loading, like a representative loading for upper wing skin [14]-[16]. Other tests showed that, under the severest constant amplitude loading, i.e., $R = -1$, the exfoliation dramatically reduced the fatigue life [17].

In addition, the difference between artificial and natural exfoliation is not completely understood. These differences, where they exist, may also affect the applicability of some models developed using the artificial corrosion data to a natural exfoliation situation.

This chapter introduces two types of exfoliation and fatigue models:

- 1) The Defence Science and Technology Organisation (DSTO) process zone model; and
- 2) The National Research Council Canada (NRC) exfoliation model.

15.2 DSTO PROCESS ZONE MODEL

15.2.1 Original DSTO Research

Clark, et al. [18] conceptualized the process zone model in 1998. Their hypotheses supported the view of Mills [8] that the discontinuities, which violate the surface integrity, are key fatigue-related concerns with exfoliation. Mills joined Clark and Sharp in 2000 – 2001 to further develop data to support the original process zone model presented in various publications [19]-[20].

The process zone in exfoliation and fatigue seeks to explain the rapid drop in fatigue life exhibited in the early stages of corrosion damage. The ‘zone’ was found to be a pit-like intrusion with intergranular cracking at the tip (see Figure 15-1(a)). This microscopic pit-plus-crack combination is at the base of the exfoliated region, and it travels with the exfoliation as the damage deepens to a severe level (see Figure 15-1(b)). The efforts at DSTO focused on determining how exfoliation attacked 2024-T351 and 7075-T651 alloys subjected to an ASTM EXCO environment (ASTM Standard G34).

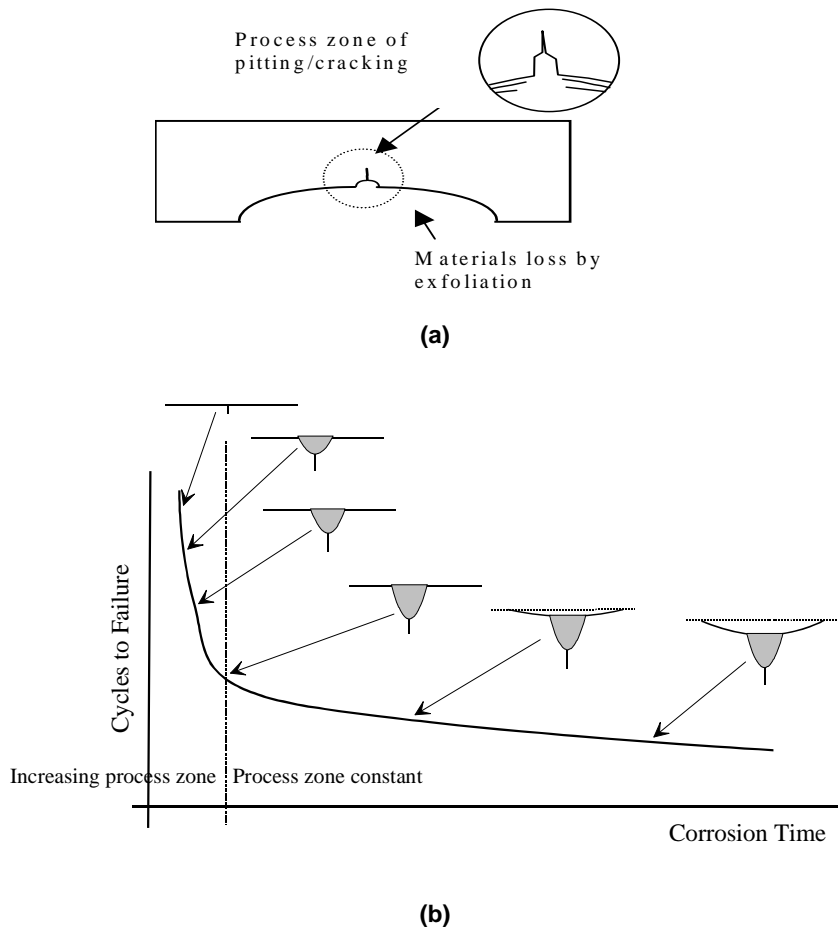


Figure 15-1: (a) Schematic of the Process Zone Model; and (b) Variation of the Process Zone with Exposure Time to EXCO (after [19]).

The pit-like intrusions were of particular interest because they, more than any other feature, supported the process zone model. Note the convincing image of the ‘process zone’ shown in Figure 15-2 [19]. This specimen, exposed for 48 hours, shows a classic pit-like fatigue crack origin along with the general thinning associated with advanced exfoliation.

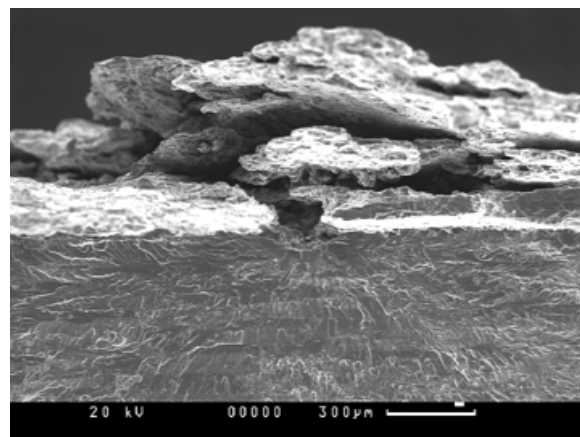


Figure 15-2 : Pitting and Exfoliation at Crack Nucleation Site in Specimen Exposed 48 Hours to EXCO (after [20]).

Pit sizes tended to reach a maximum of 100 microns (0.0039 inch) in the 2024 alloy [21]. Moreover, many of the pits showed small intergranular cracks (0.001 inch or 25 microns) at their bases, which is not at all surprising since exfoliation propagates along intergranular paths.

In the original work, DSTO conducted fatigue modeling of these experimental results using FASTRAN II. In FASTRAN II, the process zone was represented by a notch and crack combination with sizes derived from experimental observations of pit and intergranular crack sizes for various corrosion stages. For modeling the corrosion damage in 7075-T651 dogbone coupons, Clark et al. [19] examined cases where the process zone was represented by a pit ranging in depth from 20 – 100 μm and an intergranular crack ranging in depth from 10 – 30 μm emanating from the base. The corrosion damage was generated using the EXCO solution for 2 to 245 hours. The coupons were then subjected to a constant amplitude loading ($R = 0.1$, $\sigma_{\text{MAX}} = 240 \text{ MPa}$) until failure. Figure 15-3 displays experimental results together with those from the three FASTRAN based process zone models. Model (4a), which forms the upper bound, was based on an initial process zone made up of a notch (representing the pit) with a size between 20 – 100 μm and a 10 μm crack at the tip. Model (4b) varies notch (pit) size with a 20 μm crack, and Model (4c) varies notch (pit) size with a 30 μm crack. As can be seen from Figure 15-3, all models give slightly unconservative results, close to the experimental data.

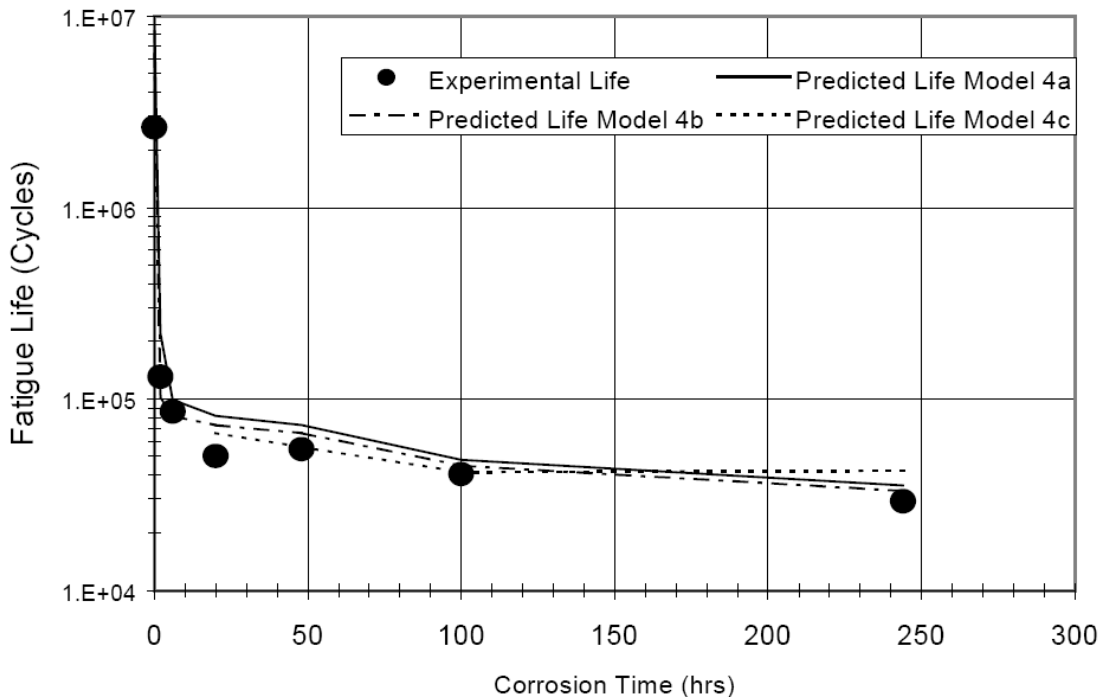


Figure 15-3: Predicted 7075-T6 Fatigue Life vs. ASTM EXCO Corrosion Time Using the 'Process Zone' Model and FASTRAN [19].

As part of these same studies [20], the authors also investigated other models for estimating the influence of exfoliation on fatigue response. These models included:

- 1) Treating exfoliation as a semi-elliptical crack with the same dimensions as the 2D slice through the corrosion.
- 2) Treating exfoliation as a semi-circular crack with depth equal to that of the exfoliation.
- 3) Treating the exfoliated region as a blended region. The model assumed the presence of a typical inclusion-sized starter crack ($a = 3 \mu\text{m}$ and $c = 9 \mu\text{m}$) at the base of the blended region.

As might be expected, the first two models produced extremely conservative results. The third model produced – as expected – seriously unconservative analytical results.

15.2.2 Studies of the Process Zone Model at APES

In 2003, APES began working with the DSTO Process Zone model, as it fit well within the surface integrity effects models that the company was developing to address corrosion and fatigue interactions. The primary difference between the activities at DSTO and APES was that DSTO attributed the crack-like discontinuities necessary for a fracture-mechanics based analysis to intergranular cracking at the tip of the exfoliation process zone, whereas APES modeled the failure scenario by assuming that the material Initial Discontinuity State (IDS) could be related to the second phase constituent particles present in high-strength aluminum alloys. These particles are often associated with fatigue failure of uncorroded material in the laboratory, and the hypothesis was that the distribution of the particle sizes provided a reasonable starting crack size distribution for crack growth analyses.

Also, where DSTO used a notch model in FASTRAN II, APES used beta correction capabilities in the crack growth code, AFGROW, to simulate the effect of a pit on the IDS (this now becomes the process zone).

So, for the APES analyses (conducted by Mills et al. [22]-[23]) the growth of the IDS was influenced by surface integrity effects models for pitting (solutions based on both 2D-FEA and 3D-FEA models of pits were used) and by the general thinning associated with gross exfoliation. This revised analytical approach was applied to the same data sets as the original DSTO work discussed previously.

For fatigue life post-dictions of the 2024-T351 data from DSTO ($R = 0.1$, $\sigma_{MAX} = 240$ MPa), the ninety percentile (90%) IDS from the size distribution was used (Note: derivation of the IDS distribution is beyond the scope of this chapter, but it has been presented in the literature in the past [22]-[23]). The 90% IDS value for 2024-T351 was found to be 25.4 microns (0.001 inch) and was selected because that value produced a life post-diction that correlated to one pristine fatigue life (2,268,668 cycles) data point within 10%.

This IDS size was then coupled with various models and levels of corrosion damage for each test specimen to produce post-dictions of the experimental fatigue lives. The corrosion damage for the specimens was modeled as a combination of a corrosion pit 60 microns (0.0027 inch) deep, which represented a typical size of the process zone from the DSTO fractography work discussed previously, and the corresponding thickness loss for that specimen. Three pitting models were selected for post-diction:

- None: Only thickness loss was taken into account (net section stress increase);
- 2D-FEA: Where (in addition to thickness loss) a process zone pit is treated as a sharp crack of equivalent depth and influences an adjoining IDS with an aspect ratio of 1.0; and
- 3D-FEA: Where (in addition to thickness loss) a hemispherical pit influences the stress intensity factors of an adjoining IDS.

These various initial states were modeled in AFGROW as general surface cracks using FEA-based beta corrections to account for the pits and higher stress multiplication factors and reduced thicknesses to account for the thickness loss to produce the fatigue life estimates.

The results are summarized in Figure 15-4 and show that by assuming only thickness loss, fatigue life is over-estimated by a factor of four. This clearly reinforces the DSTO conclusions that it is necessary to include the effects of surface integrity to capture the appropriate degradation in life. Figure 15-4 shows that the experimental results are bounded by the 3D-FEA estimates, which treat the pits as hemispherical notches, and the more severe 2D-FEA estimates, which treat the pits as sharp cracks. On average, the 3D-FEA estimates produce a ratio of computed life to experimental life of 1.08, and the 2D-FEA estimates

produce a computed to experimental life ratio of 0.69. Although the 3D-FEA produced the best results based on the average, only the 2D-FEA results captured the most aggressive cracking behavior.

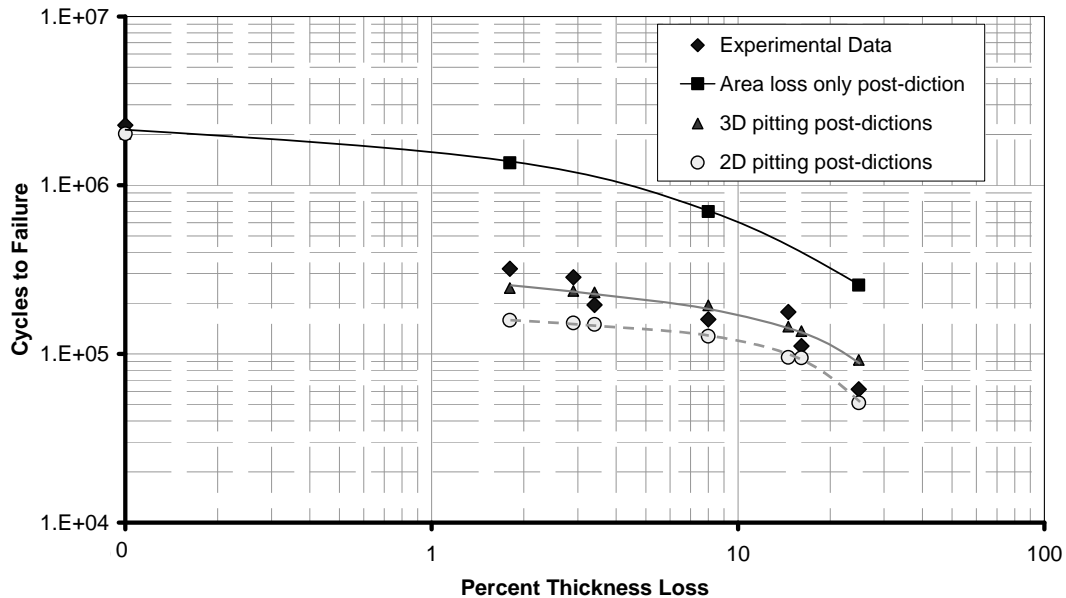


Figure 15-4: Cycles to Failure vs. Percent Thickness Loss for Exfoliated Coupons (Note that only by incorporating pitting into the models do the post-dicted fatigue lives approximate those of the coupons. Assuming area loss only is extremely unconservative (factor of 4)).

The most important message that can be derived from this effort is that if exfoliation is treated as simply a general thinning of material for analytical purposes, then expect the assessments to be dangerously unconservative. Exfoliation is closely related to corrosion pitting, and this fact should be exploited in modeling considerations. It was obvious from the laboratory experiments that even small levels of exfoliation damage, with barely any perceptible thickness loss, have profound effects on fatigue life in laboratory experiments. Therefore, susceptibility to exfoliation is not the same as structural vulnerability. ‘Mild’ exfoliation can be almost as damaging to structural fatigue performance as ‘severe’ exfoliation.

15.2.3 Studies of the Process Zone Model at NRC

Liao et al. also examined the ‘process zone’ concept using AFGROW [17]. Since AFGROW does not have a starter notch model, the ‘process zone’ was simplified as a semi-elliptical crack with a depth of 120 μm on the substrate material (i.e., similar to DSTO Model 4(b)), in which the exfoliation layer was removed and the net stress was increased correspondingly. Because the real aspect ratio of the corrosion pit was unknown, different crack aspect ratios were used in the analysis. The analytical results are presented in Figure 15-5(a), along with the DSTO test results. It is shown that the ‘process zone’ concept can be implemented using AFGROW to provide similar life estimations for the DSTO specimens, especially with aspect ratio of 1.0 to 2.0.

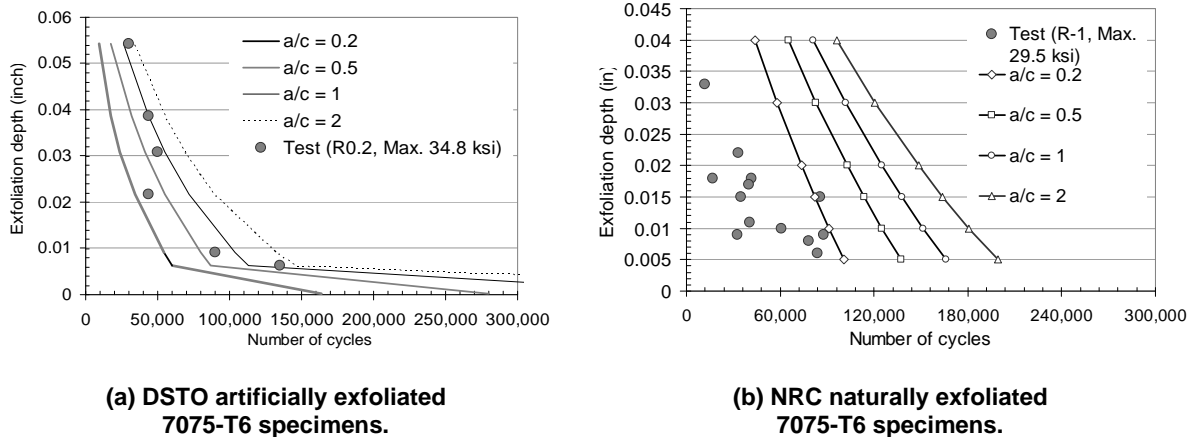


Figure 15-5: Predicted 7075-T6 Fatigue Life vs. Exfoliation Depth Using the 'Process Zone' Model and AFGROW [17].

However, in an example in [17], the 'process zone' model largely over-estimated the life of the naturally exfoliated 7075-T6511 coupons under a fully reversed cyclic load ($R = -1$) (test details are described in Section 3.3, Example 2), even with the upper limit of pit depth of $100 \mu\text{m}$, plus remote stress increased based on the maximum depth of exfoliation (determined by ultrasonic Non-Destructive Inspection (NDI)), the model still over-estimated the lives, Figure 15-5(b). The over-estimation might be caused by the following factors:

- Differences between natural and artificial corrosion such as:
 - a) The exfoliation area or volume in the naturally exfoliated NRC specimens were mostly larger than those in the DSTO EXCO specimens*; and
 - b) Natural and artificial corrosion may have produced different hydrogen embrittlement effects in the material, which could affect the crack nucleation and small crack growth.
- High compression loads may cause local buckling or delamination in the natural exfoliation damage, which in turn may affect the fatigue life. It is also difficult to model the fatigue crack growth behavior under the stress ratio $R = -1$ due to crack closure effects.

In general, the major limitation of the 'Process zone' model is that detailed fractography is needed to determine how the depth of exfoliation changes with time, and to determine when the growth of the 'process zone' stabilizes. For these reasons, DSTO abandoned the 'Process Zone' model around 2001. However, the disconnect between current NDI capabilities and the physical material features that are critical to fatigue response under corrosion conditions is not a new issue. The same argument could be made for trying to detect and assess pitting corrosion.

A large research program in the USAF from 2003 – 2006 (the Corrosion Effect on Structural Integrity) encountered this same difficulty. The proposed action at that time was to build a "library of damage", wherein the subtle damage details could be inferred from the macro "indications" derived from NDI and derived from the construction of an alloy's microstructure and grain orientation. This approach was

* The ASTM EXCO solution was found too corrosive for 7000 series aluminum alloys, which during the first 24 hours of the test, the EXCO solution is highly acidic, starting at pH 0.4 and gradually stabilizing at pH 3.2 [24]. This explains why the EXCO often produce extensive corrosion pits at the beginning, and then takes a long time to produce less IGC than natural exfoliation. An aluminum chloride modified EXCO solution, i.e., ANCIT [24], starts the corrosion test at pH 3.2 and creates more aggressive attack along grain boundaries. The ANCIT has been found to repeatedly produce more representative exfoliation to aluminum alloys [24],[25].

reasonable, and it is unfortunate that this work was not pursued in earnest. Regardless, it is still needed to develop high-fidelity corrosion structural effects models to understand the important aspects of the failure mechanisms. It is impossible to evolve towards more holistic assessment mechanisms without understanding the physics of failure.

Another apparent limitation is that for exfoliation corrosion around fastener/rivet holes. As originally presented in the literature, it is difficult to use the ‘Process Zone’ model where cracks nucleate from the countersink or bore surface. However, exfoliation at fastener holes often has attendant with it pitting down the bore of the holes. In these cases, it may be possible to analyze failure progression through a pitting analysis (at the bore of the hole) coupled with an increase in net section stress due to exfoliation.

15.3 NRC EXFOLIATION MODEL

15.3.1 Finite Element Model

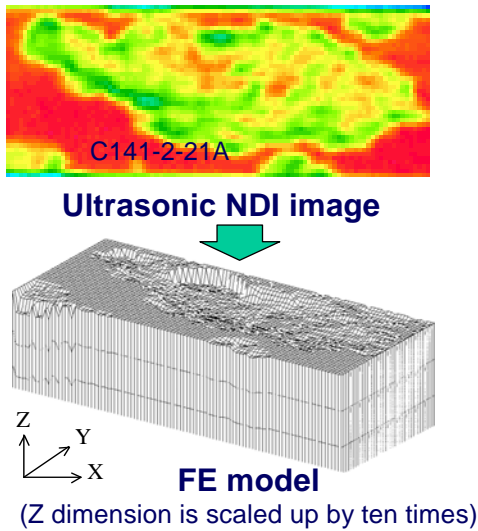
A three dimensional (3D) Finite Element (FE) model was developed to determine the local stress/strain distribution of fastener specimens. In the model, a “soft inclusion” technique, which was previously developed and verified at NRC to simulate Compression After Impact (CAI) in composite structures [26] was applied to simulate the exfoliation present in the specimen. The basic assumptions associated with the soft inclusion are:

- Exfoliated area, simulated by a soft inclusion with reduced stiffness, has some load carrying capability;
- Soft inclusion is an isotropic material; and
- Soft inclusion can have uniform depth or irregular geometry as corrosion.

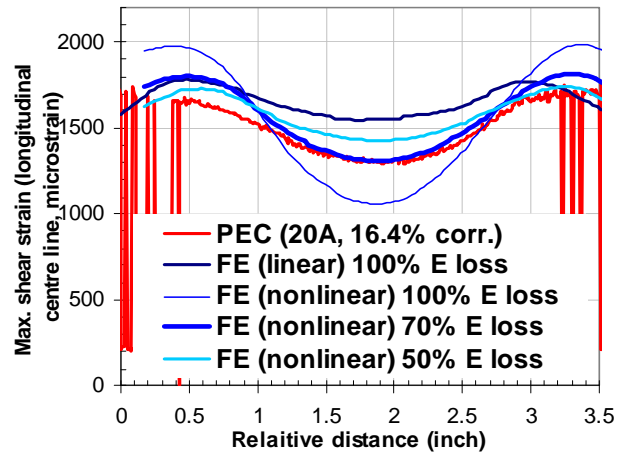
A calibration and validation for the ‘soft inclusion’ model was carried out using smooth coupon specimens and Photoelastic Correlation (PEC) measurements [27]. A technique to automatically generate the 3D geometry of the ‘soft inclusion’ (damage zone) from the NDI input was developed using the PATRAN Command Language (Figure 15-6(a)). Non-linear FE analysis was then performed to analyze the non-linear bending effect due to exfoliation [27]. The calibrated results, as shown in Figure 15-6(b), indicated that:

- 1) Different Young modulus (E) reduction should be used for different exfoliated area to match FE with the PEC; and
- 2) 70% E reduction led to numerical results that matched the test results.

After the calibration, the ‘soft inclusion’ based FE model was used to provide the local stress distribution for fatigue modeling. In addition, the ‘soft-inclusion’ model has been successfully applied for quantifying the effects of the exfoliation on the residual strength (yielding strength and buckling) [27].



(a) FE model based on NDI inputs.



Max. shear strain by nonlinear geometry FE for 20A (severe) at 5000 lb compression

(b) Calibration of soft-inclusion stiffness.

Figure 15-6: FE Modeling Process Using NDI Inputs and Modeling Results (Note: Young's modulus E loss was calibrated in between 50 – 70 % by non-linear FE analyses. The PEC measurements were performed on the back (non-corroded) surface of the coupon).

Figure 15-7 presents a 3D FE model generated for a corroded specimen with exfoliation damage. The exfoliation was simulated using a number of 3D elements with the calibrated Young's modulus (E). The thickness of the soft inclusion was set by the maximum depth of the exfoliation that was measured by ultrasonic inspection. The FE analyses were carried out using the commercial code MSC/MARC including contact analysis between the fastener to plate, plate to flange, and flange to fastener.

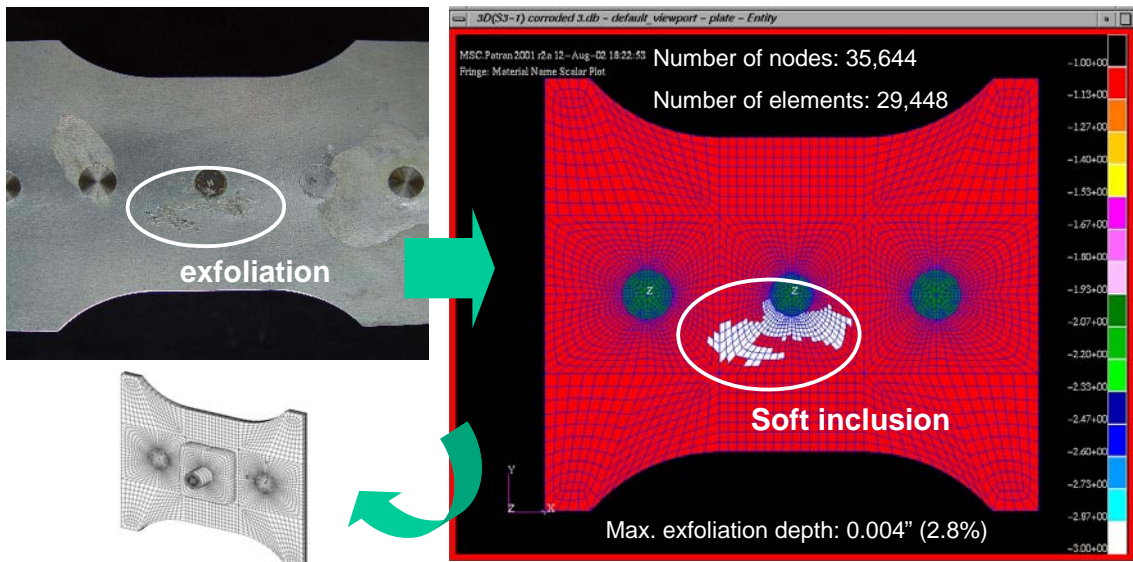


Figure 15-7: 3D FE Mesh with Soft Inclusion for Specimen 1 (362-A-S3-1).

A comparison between the crack nucleation sites in an exfoliated specimen with the location of the maximum principal stress ($\sigma_{1, \max}$) determined from the FE analysis for tension loading is shown in

Figure 15-8. The crack nucleation sites are located near the 1 o'clock and 5 o'clock positions. The FE analyses were carried out under both tension and compression loading in order to obtain the local stress results for fatigue analysis.

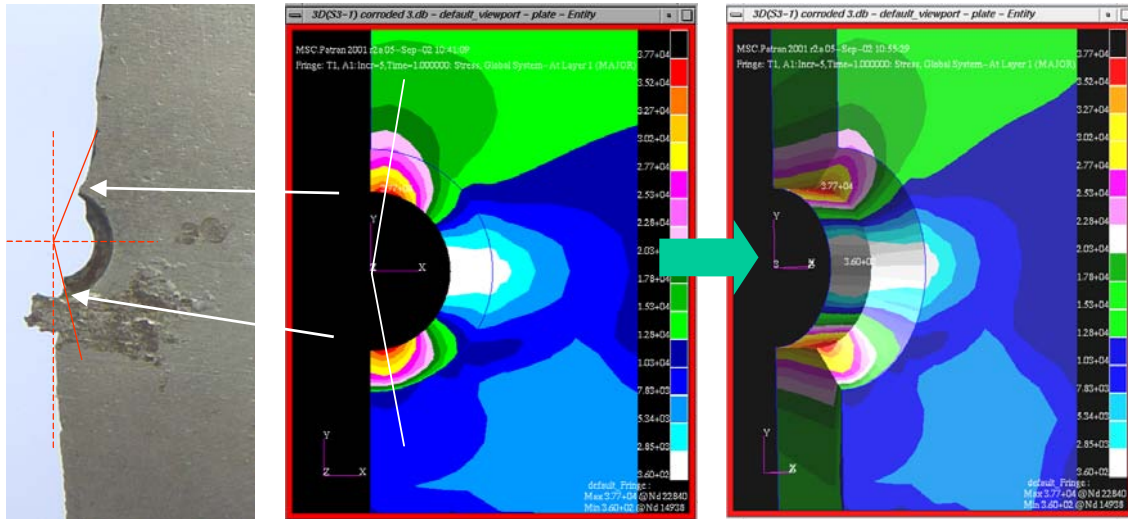
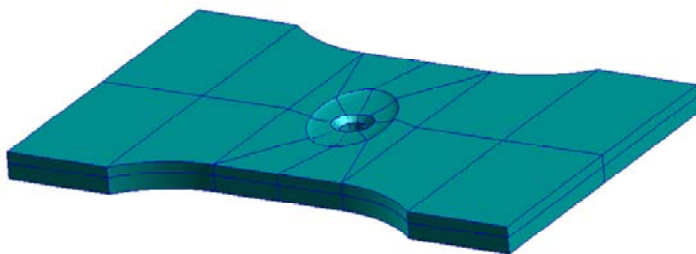


Figure 15-8: Crack Nucleation Site and 3D FE Analysis Results.

Recently, the MSC PCL based automation technique was further improved at NRC to quickly generate a soft-inclusion based FE model for different degrees of exfoliation corrosion found at aircraft rivet holes [28]. Figure 15-9 presents the modeling variables that can be changed for different rivet hole models.



User-defined geometric variables

- Damage zone:** ellipsoid short and long axes, max depth, angle, position
- Rivet hole:** radius, countersink depth, countersink angle
- Plate:** grip length, width, radius, grip length, tapered thickness

Figure 15-9: An Example FE Model Generated by NRC Automation Technique (the soft inclusion and rivet have been removed for clarity) [28].

15.3.2 Fatigue Model for Rivet Specimens

From the existing studies on exfoliation kinetics, the crack-nucleating pits, IGC, and particles or grain boundaries denuded by IGC are created by the local electrochemical cells of precipitates at grain boundaries [29]. From a mechanical point of view, the corrosion pit and denuded particle or grain could easily serve as local stress concentrations. The tip of IGC could also become a high stress site when the IGC dissolves precipitates or turns into the next layer of grains. Since upper layers of exfoliated materials would be pushed and flaked away, the pit/IGC discontinuities on the exfoliation sub-surface would remain of limited depth depending on the microstructure.

Due to the multiple cracking mechanisms in the exfoliation region [16],[17], it is difficult to use a single model to cover all of them. Also due to the complexity of the pit/IGC geometries, plus the chemical

effects on material properties, it is very difficult to accurately determine the local stress distribution for pit/IGC tips, and the stress intensity factors. Simplifications and assumptions are needed for developing an engineering model. A common simplification is to consider the pit/IGC as a pre-crack, then use a fracture mechanics model to estimate the remaining fatigue life with the prior corrosion. Two examples are presented as follows.

Example 1: Fatigue Life Analysis for Riveted Specimens

Fatigue tests were carried out on naturally exfoliated 7178-T6 coupons, using a constant amplitude loading ($R = -1.67$, $\sigma_{max} = 12$ ksi). The fractography found that a primary crack formed from a corrosion pit-like discontinuity on the countersunk surface of one coupon. This coupon was cut from a B707 wing panel, with 5.4% exfoliation (i.e., max. exfoliation depth/nominal thickness) at the fastener hole, Figure 15-10.

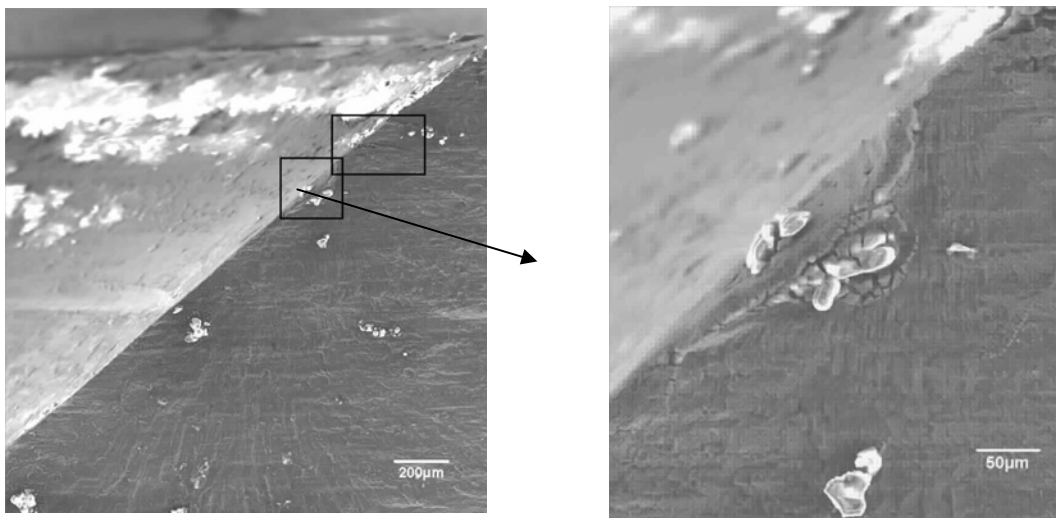


Figure 15-10: Crack Nucleation Site at a Colony of Corrosion Pits on Countersunk Surface.

A crack growth analysis starting from the pit-like discontinuity to final failure was first carried out using 3D FE analysis results and AFGROW [16]. The pit-like discontinuity was assumed to be a half-elliptical crack with dimensions of 262 x 98 µm, measured from the SEM image (Figure 15-10). Since the current version of AFGROW does not have a crack model for a countersink hole filled with a rivet, a straight open hole crack model was used for the crack growth analysis along with corrected beta factors from FE, see Figure 15-11(a). Based on a point load stress intensity solution, the beta correction factors were calculated by AFGROW using the normalized stress distribution. This stress distribution was determined by the following procedure. First, a 2D FE analysis was carried out on the straight open hole model and the stress distribution along the assumed crack path was obtained. For the countersink hole model (with fastener), the stress distribution along the assumed crack path was obtained from the 3D FE analysis previously described. Then the ratio of the stress distribution from the countersink hole to that of the straight hole model at various crack length intervals was determined. Finally, the normalized stress values along the assumed crack path were calculated by dividing each ratio by the ratio at the crack origin. The normalized stress values along the assumed crack path are presented in Figure 15-11(b).

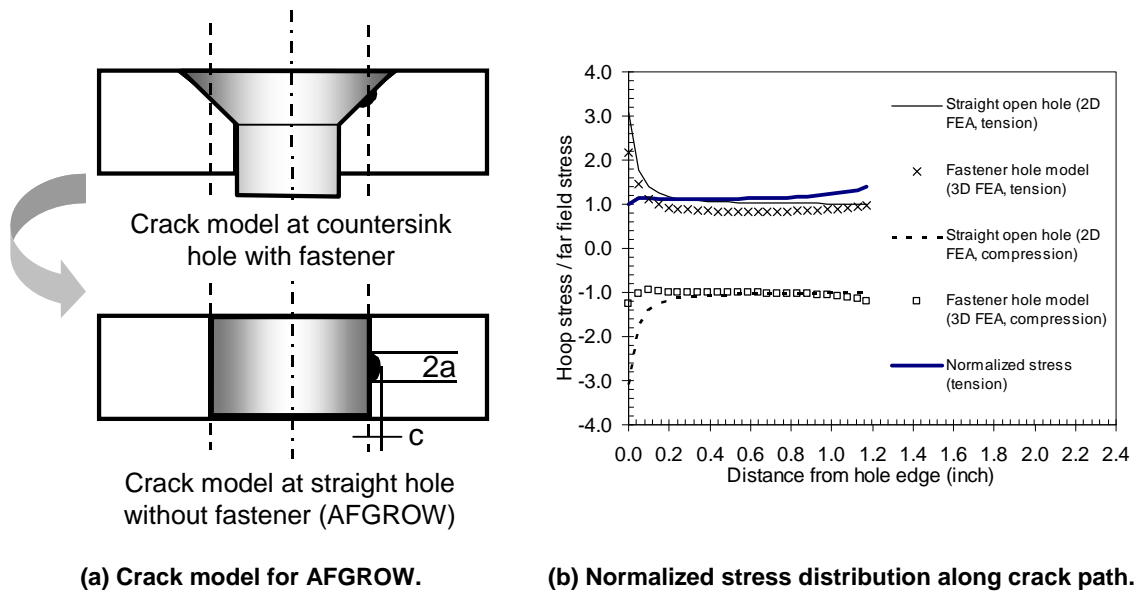


Figure 15-11: Crack Model for Crack Growth Analysis.

Using the NASGRO material model (i.e., 7178-T6 and T651 Al, [Plate and sheet; L-T; LA, HHA]), AFGROW calculated the crack growth life from the pit-like discontinuity to final failure as 179,217 cycles, which is about 33% less than the test results. This conservative prediction can be attributed to:

- 1) The pit to crack nucleation life was not included in the analysis; and
- 2) The fatigue life scatter including possible analytical errors due to the complex geometry and beta solutions.

Overall this example showed that assuming a pit to be a pre-crack could result in a reasonable, conservative fatigue life prediction.

Example 2: Fatigue Life Analysis for Smooth Specimens

In a previous NRC project, dog bone specimens were manufactured from the 7075-T6511 upper wing panels of C141 aircraft containing natural exfoliation. The maximum depth of the exfoliation damage was determined by ultrasonic NDI. A number of fatigue tests were carried out under fully reversed constant amplitude loading ($R = -1.0$), and fractographic analyses were performed to examine the cracking mechanisms in the exfoliation region.

As described in Section 15.2, the DSTO ‘process zone’ model was first used but largely overestimated the fatigue lives. A simplified fatigue model was proposed at NRC to estimate the remaining fatigue life of the corroded specimens [17]. In this model, the exfoliation damage was assumed as a surface crack with a depth that was presumably available from an NDI or grind-out database. The initial idea of the model was to treat the exfoliation damage as a semi-elliptical surface crack with a profile that would approximate the projection of the exfoliation zone onto the plane vertical to the tensile loading direction. Later a modified profile with reduced crack length (exfoliation width) was found to have almost the same stress intensity factor as the original profile. The model actually used a modified profile and was calibrated using different crack aspect ratios (i.e., same depth but varying length) with the intention to seek an ‘effective crack’ for providing a good life estimation. The calibrating process essentially made the model more ‘effective’, so the simplified model is also called the ‘effective crack’ model. A schematic of the model is shown in Figure 15-12(a). It should be noted that the remote stress is not increased by the material loss in the

‘effective crack’ model. In this way, the pristine/design stress can be used directly in this mode to predict the remaining life.

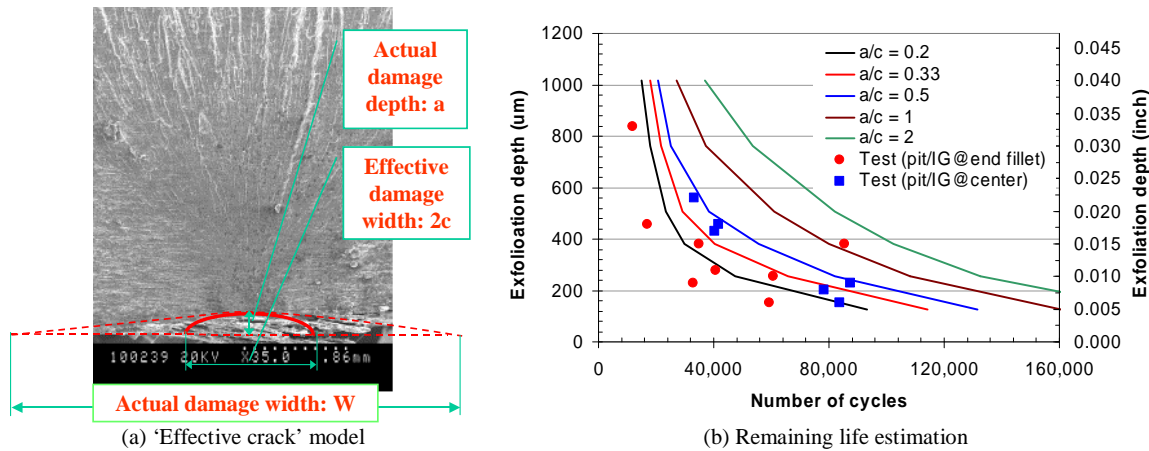
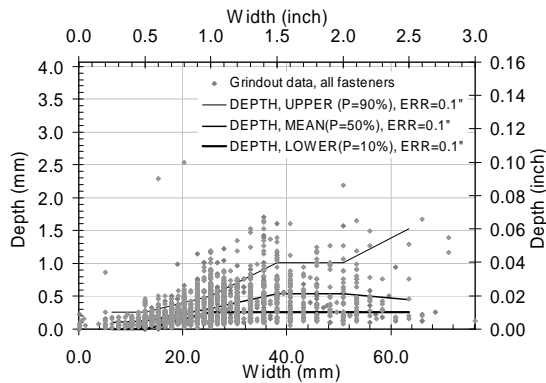


Figure 15-12: Cracking Model and Life Estimation Using Simplified Fatigue Model [17].

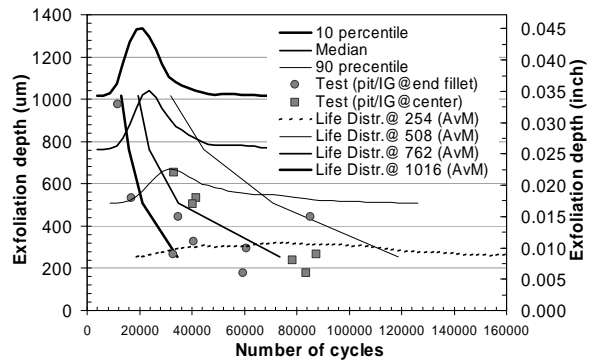
Along with the test results, the fatigue lives estimated by the ‘effective crack’ model are presented in Figure 15-12(b). This figure indicates that with crack aspect ratios (crack depth / half crack length, a/c) ranging from 0.2 – 2.0, the model gave good estimation of the range of the fatigue lives. Particularly, the aspect ratio $a/c = 0.33$ was found to give the best representation of the average test results. Therefore, the ratio $a/c = 0.33$ was considered as an ‘effective’ aspect ratio for the model to give good results on the average life. To apply the model to other structure applications, the ‘effective’ crack aspect ratio has to be calibrated using coupon tests, the representative spectrum loading, and the approach developed in this chapter.

Example 3: Probabilistic Fatigue Modeling

In practice, conventional NDI techniques still have difficulty in determining the exfoliation depth on the wing skin without disassembling the structures. Advanced NDI, such as angled ultrasonic, may be able to do so but it is still very time-consuming and needs further development. A grind-out database provides a practical option to estimate the exfoliation depth without disassembly. In this estimation, the grind-out area (width and depth) is assumed to be equal to the corrosion damage (width and depth). As an example, a grind-out database based on exfoliation repair records for some large transport aircraft is shown in Figure 15-13(a). This figure shows that a large scatter is associated with the depth or width data. To address this scatter, the simplified model was enhanced with probabilistic techniques in order to handle the exfoliation depth as a random variable.



(a) Grind-out database example.



(b) Fatigue life distribution vs. exfoliation depth.

Figure 15-13: Probabilistic Fatigue Modeling Based on a Grind-Out Database.

For demonstration purposes, the exfoliation depth estimated from the grind out database (Figure 15-13(a)) was assumed as a lognormal distribution with a Coefficient Of Variation (COV) of 54%. A MS Excel Visual Basic for Applications (VBA) program was developed to execute the Component Object Model (COM) version of AFGROW in a Monte Carlo simulation. For the naturally exfoliated specimens, the fatigue life distributions were obtained by the Monte Carlo AFGROW analysis using the random exfoliation depth and the ‘effective’ aspect ratio of 0.33 for the surface crack. The life distributions for different exfoliation depth and the life curves for the 10, 50, and 90 percentiles are presented in Figure 15-13(b). The Monte Carlo simulation used 1000 trials for determining each life distribution. If required, safety factor or risk analysis could be carried out using the life distributions, which are not available from the traditional fatigue or damage tolerance analysis without corrosion considerations.

15.4 SUMMARY

As the fractographic analysis revealed multiple cracking mechanisms from exfoliation, it also revealed the difficulties to develop an ‘accurate’ fatigue model. Simplifications and assumptions are needed for developing an engineering fatigue model.

The DSTO modeling showed that the ‘process zone’ model gave a good estimation on the fatigue life of artificially exfoliated specimens, but its applicability for fleet problems was limited to simple geometry and by lack of detailed fractography data in the field. A simplified ‘effective crack’ model was proposed at NRC with the motivation to estimate the fatigue life using the exfoliation depth available from either an NDI or grind-out database. It was shown that this model could give good life estimation for the naturally exfoliated specimens, under the severest constant amplitude loading ($R = -1$).

The NRC soft-inclusion model was originally developed to simulate the stiffness reduction and quantify the residual strength of exfoliated material, but it can also provide a better local stress distribution for fatigue modeling purpose. In particular, for complex geometry, such as fastener holes where the majority of exfoliation was found, the soft-inclusion based FE and fracture mechanics model provided reasonably well life estimation.

Overall, fracture mechanics based models could provide reasonable prediction of the remaining fatigue life of prior-exfoliated aluminum alloys. More fundamental work including characterization of exfoliation sub-surface topography could build-up a database for the topography of exfoliation corrosion. With such a database, a local pit/IGC model may be developed and integrated with the ‘Process Zone’ or ‘soft-inclusion’ model to provide better and practical life prediction for corroded structures.

15.5 REFERENCES

- [1] “Notice of Proposed Rulemaking”, Federal Register: April 18, 2006 (Vol. 71, No. 74), 14 CFR Parts 25, 121, and 129 (Docket No. FAA-2006-24281; Notice No. 06-04).
- [2] http://www.faa.gov/regulations_policies/rulemaking/committees/arac/media/r/R_MRS_T1.pdf.
- [3] Notice of Proposed Rulemaking, Federal Register: February 2, 2006 (Vol. 71, No. 22), 14 CFR Part 33, (Docket No. FAA-2006-23732; Notice No. 06-03).
- [4] Liao, M. and Komorowski, J.P., “Effect of Prior Exfoliation Corrosion on Fatigue and Fracture Behavior of Aging Aircraft Structures and Materials”, Technical Report, IAR-LTR-SMPL-2002-0136, National Research Council Canada, Ottawa, Ontario, Canada, 2002.
- [5] Wallace, W. and Hoepfner, D.W., “Aircraft Corrosion: Causes and Case Histories”, AGARD Corrosion Handbook, Vol. 1, AGARD-AG-278, p. 93, Neuilly-sur-Seine, France, 1985.
- [6] “Metals Handbook”, 9th Ed., Vol. 13, Corrosion, American Society for Metals, Metals Park, Ohio, USA, pp. 584-609, 1985.
- [7] Shaffer, I.S., Sebastian, J.C., Rosenfeld, M.S. and Ketcham, S.J., “Corrosion and Fatigue Studies of Extruded 7075-T6 Spar Caps”, Journal of Materials 3 (2), pp. 400-424, June 1968.
- [8] Mills, T.B., “The Effects of Exfoliation Corrosion on the Fatigue Response of 7075-T651 Aluminum Plate”, Ph.D. thesis, University of Utah, USA, June 1995.
- [9] Hubble, M.J. and Chubb, J.P., “The Effect of Corrosion on Fatigue Crack Initiation in 2024-T3 and 7075-T6 Aluminum Alloys”, Proceedings of 5th International Conference on Structural Airworthiness of New and Aging Aircraft, Hamburg, Germany, pp. 231-232, 1993.
- [10] Chubb, J.P., Morad, T.A., Hockenhull, B.S. and Bristow, J.W., “The Effect of Exfoliation Corrosion on the Fatigue Behavior of Structural Aluminum Alloys”, Structural Integrity of Aging Airplanes, pp. 87-97, 1991.
- [11] Chubb, J.P., Morad, T.A., Hockenhull, B.S. and Bristow, J.W., “The Effect of Exfoliation Corrosion on the Fracture and Fatigue Behavior of 7178-T6 Aluminum”, International Journal of Fatigue 17, (1), pp. 49-54, 1995.
- [12] Koch, G.H., Hagerdorn, E.L. and Berens, A.P., “Effect of Pre-existing Corrosion on Fatigue Cracking of Aluminum Alloys 2024-T3 and 7075-T6”, Final Report to Flight Dynamics Directorate, WPAFB, Dayton, OH, USA, August 1995.
- [13] Mills, T.B. and Paul, C.A., “Constant Stress Intensity Determination of Fatigue Crack Growth Rates in Exfoliated Panels of 7075-T651 Aluminum”, AFOSR Summer Research Program Report, USA, September 1996.
- [14] Bellinger, N.C., Komorowski, J.P., Liao, M., Carmody, D., Foland, T. and Peeler, D., “Preliminary Study into the Effect of Exfoliation Corrosion on Aircraft Structural Integrity”, Proceedings of 6th Joint FAA/DoD/NASA Conference on Aging Aircraft, San Francisco, CA, USA, 16-19 September 2002.
- [15] Bellinger, N.C., Foland, T. and Carmody, D., “Structural Integrity Impacts of Aircraft Upper Wing Exfoliation Corrosion and Repair Configurations”, Proceedings of the 7th Joint DoD/FAA/NASA Conference on Aging Aircraft, New Orleans, LA, USA, September 2003.

- [16] Liao, M., Bellinger, N.C. and Komorowski, J.P., “Modeling the Effects of Prior Exfoliation Corrosion on Fatigue Life of Aircraft Wing Skins”, *International Journal of Fatigue*, 2003:25 (9-11), pp. 1059-1067, 2003.
- [17] Liao, M., Renaud, G. and Bellinger, N.C., “Fatigue Modeling for Aircraft Structures Containing Natural Exfoliation Corrosion”, *International Journal of Fatigue*, 29/4, pp. 677-686, 2007.
- [18] Sharp, P.K., Cole, G., Clark, G. and Russo, S.G., “The Influence of Corrosion on Aircraft Structural Integrity”, *Proceedings, 21st Congress of the International Council Aeronautical Sciences*, Melbourne, Victoria, Australia, 13-18 September 1998.
- [19] Sharp, P.K., Mills, T. and Clark, G., “Modeling of Fatigue Crack Growth from Pitting and Exfoliation Corrosion”, *Proceedings, 21st Symposium of the International Committee on Aeronautical Fatigue*, Toulouse, France, pp. 485-498, 27-29 June 2001.
- [20] Sharp, P.K., Mills, T. and Clark, G., “Aircraft Structural Integrity: The Impact of Corrosion”, *Proceedings, 10th International Congress of Fracture (ICF 10)*, Honolulu, HI, USA, Elsevier Science, 3-7 December 2001.
- [21] Sharp, P.K., Mills, T., Russo, S., Clark, G. and Qianchu, L., “Effects of Exfoliation Corrosion on the Fatigue Life of Two High-Strength Aluminum Alloys”, *Proceedings, 4th Joint DoD/FAA/NASA Conference on Aging Aircraft*, St. Louis, MO, USA, Universal Technology Corporation, 15-18 May 2000.
- [22] Mills, T.B., Honeycutt, K.T. and Brooks, C.L., “Demonstration of an Holistic Structural Integrity Process Using Corrosion/Fatigue Interactions from Laboratory Experiments and Field Experience”, *Proceedings, 6th International Aircraft Corrosion Workshop*, Solomons, MD, USA, August 2004.
- [23] Mills, T.B., Honeycutt, K.T., Brooks, C.L., Sharp, P.K., Loader, C. and Crawford, B., “Development and Demonstration of an Holistic Structural Integrity Process using the Initial Discontinuity State Concept for 7050-T7451 Aluminum”, *USAF Aircraft Structural Integrity Program Conference*, Memphis, TN, USA, November 2004.
- [24] Lee, S. and Lifka, B.W., “Modification of the EXCO Test Method for Exfoliation Corrosion Susceptibility in 7XXX, 2XXX, and Aluminum-Lithium Alloys”, *ASTM STP 1134*, V.S. Agarwala and G.M. Ugiansky, Ed., American Society for Testing and Materials, Philadelphia, PA, USA, pp. 1-19, 1992.
- [25] Bellinger, N.C., Overton, J.M., Roe, P.W. and Gould, R.W., “Accelerated Exfoliation Protocol”, *IAR-LTR-SMPL-2002, 0083*, National Research Council Canada, Ottawa, Ontario, Canada, 2002.
- [26] Xiong, Y. and Poon, C., “Failure Prediction of Composite Laminates Containing Impact Damage”, *IAR-LTR-ST-1898*, National Research Council Canada, Ottawa, Ontario, Canada, 1992.
- [27] Liao, M., Renaud, G., Bellinger, N.C., Backman, D. and Forsyth, D.S., “Effects of Exfoliation Corrosion on Static and Fatigue Behavior of Aircraft Materials and Structures – Testing and Modeling Studies”, *The 8th Joint NASA/FAA/DoD Conference on Aging Aircraft*, Palm Springs, CA, USA, January 2005.
- [28] Renaud, G., Liao, M., Uebersax, A. and Huber, C., “Static and Fatigue Analysis of an Upper Wing Skin with Exfoliation Corrosion”, *Proceeding of the 26th International Congress of the Aeronautical Science (ICAS)*, Anchorage, AK, USA, 2008.

- [29] Speidel, M.O. and Hyatt, M.V., "Stress-Corrosion Cracking of High-Strength Aluminum Alloys", Chapter 3 in "Advances in Corrosion Science and Technology", Vol. 2, Edited by M.G. Fontana and R.W. Staehle, Plenum Press, 1972.



Chapter 16 – MODEL VALIDATION: FUSELAGE LAP JOINTS

Graeme F. Eastaugh and Ali Merati

Institute for Aerospace Research
National Research Council Canada
Ottawa, Ontario
CANADA

Paul V. Straznicky

Department of Mechanical and Aerospace Engineering, Carleton University
Ottawa, Ontario
CANADA

16.1 INTRODUCTION

While current design and maintenance guidelines and procurement specifications provide a good structural integrity framework for new aircraft and the reassessment of existing aircraft, there remains a risk that Corrosion Fatigue Interaction (CFI) can undermine the margins of safety in the durability or damage tolerance assessments as they are currently performed. This statement applies to all forms of corrosion, including pitting, stress corrosion cracking, crevice, galvanic, filiform, and exfoliation corrosion. It also applies to all forms of CFI, some of which may be dependent on the geometry and other features of the structural component in question. This risk is unquantified, because most manufacturers and operators treat corrosion and fatigue as separate issues during design, and they assume that the design and the maintenance program will obviate any serious interaction.

There might be several reasons why some people believe that corrosion fatigue interaction need not or cannot be taken into account. They are summed up as follows:

- a) In damage tolerant structure, fatigue cracks will be detected before they reach critical size, and so the cause of the fatigue cracks does not significantly influence the risk of structural failure.
- b) In safe life structure, the large safety margins (scatter factors) applied to the estimated fatigue life take into account unknowns such as corrosion.
- c) While corrosion is widespread on aircraft, no fatigue cracks are found at corrosion sites and no catastrophic failures have recently been attributed to corrosion. Hence corrosion is thought to be an economic problem but not a safety problem.
- d) There are no widely accepted models for predicting the onset and the effects of corrosion fatigue interaction and thereby estimating the associated risk.

The first three reasons are not considered to be valid. With regard to a), if corrosion fatigue interaction is not considered in damage tolerance analysis some potential failure modes of Structurally Significant Items (SSI) will be overlooked, and some components that should be regarded as SSI will not be analyzed. Consequently, insufficient components will be included in the targeted inspection program and some of those that are included will not be inspected in an appropriate manner.

With regard to b), the safety factors of between three and five currently in use for safe life structure derive primarily from the variability noted in accelerated fatigue tests in ambient air and the need to work with small sample sizes. They do not make a specific allowance for life reduction due to CFI under operating conditions. Much larger factors would be needed for this purpose, as proposed by Schütz [1].

With regard to c), the high annual cost of corrosion related maintenance – estimated to be over \$1B in the USAF [2] – is a testament to the underlying danger of premature structural failure due to corrosion fatigue interaction. Therefore, it is difficult to see how a general argument can be made that corrosion only presents an economic problem. Fortunately, catastrophic structural failures in aircraft are rare, and so catastrophic failures due to corrosion fatigue interaction are also rare. But they do occur. Furthermore, a thorough investigation (failure analysis) is needed to fully understand the degradation mechanisms. In most cases of corrosion, this is not necessary or cost-effective. Therefore, it is not possible to generalize that corrosion found in service on highly stressed components is not already interacting with fatigue.

The last reason, d), is valid. It is the justification for the considerable effort expended in the USA and Canada over many years to investigate ways of modeling corrosion fatigue interaction in aircraft structure. This effort has been driven by the high cost of corrosion related maintenance in terms of resources and aircraft down-time. Modeling of corrosion fatigue interaction is expected to help reduce maintenance costs and improve aircraft availability. If successful, it will provide the means to design structure with tolerance to this form of degradation, and it will allow alternative responses to a corrosion occurrence in service to be evaluated. The ways in which assessments of corrosion fatigue interaction can be included in the Aircraft Structural Integrity Programs (ASIP) followed by the USAF and other air forces were outlined in a landmark paper by Brooks and Simpson [3].

Unfortunately, the modeling of corrosion fatigue interaction is a difficult topic, even for simple components. It is important to study and model the fundamental mechanisms of such interaction, but it is also important to use traditional engineering methods to understand and model it at the component level. This section presents a study of the effects of corrosion on the fatigue characteristics of a riveted fuselage skin splice. This is a complex component with complex failure mechanisms, including a failure mode known as Multiple Site Damage (MSD). One of the aims of the study was to determine whether it might be feasible despite this complexity to construct a useful empirical model of the effects of prior corrosion on fatigue life and crack growth characteristics. If successful, the approach could be cost-effective to apply, since fuselage skin splices are one of the most widespread and corrosion-prone structural details on transport aircraft. The aim was achieved by manufacturing and fatigue testing a specially designed splice specimen under controlled conditions to produce statistically significant results. Fifty percent of the test specimens were pre-corroded. The test program is outlined, and a probabilistic model based on the test results is proposed that could be used in durability, damage tolerance, and risk analyses.

16.2 EXPERIMENTAL PROCEDURES

16.2.1 Description of Lap Splice Specimen

The splice element is a single shear lap splice 8.0 in. (203.2 mm) long with 3 rows of 5/32 in. (4.0 mm) diameter rivets at 1 in. (25.4 mm) pitch in the hoop and longitudinal directions. The spliced sheets are 0.040 in. (1.0 mm) thick 2024-T3 aluminum alloy clad both sides without any other surface treatments. Single shear lap splices of this approximate configuration are used in the fuselages of the KC-135, JSTARS, C-130, and P-3 aircraft. However, in this study, the results are intended for the development of a general modelling approach and should not be applied directly to any specific aircraft. For specific studies, the design of the specimen should be tailored to the aircraft splice in question, taking care to simulate correctly the out-of-plane bending stresses and the load transfer from cracked regions.

The specimen complete with the clamping plates and pins used to mount it in the load frame is shown in the drawing and photograph in Figure 16-1. In this figure, the specimen is shown with the splice oriented as though being viewed from outside an aircraft. The upper sheet in this view is the countersunk sheet. The lower sheet is referred to as the driven sheet. The specimen was designed to simulate the stress conditions and MSD failure mode experienced by fuselage skin splices. Back-to-back strain gauges were placed in rows 1 in. (25.4 mm) above and below the splice to record the nominal stress distribution across the

specimen. Additional detail on the specimen and the general procedure for adapting the MSD specimen concept to a specific aircraft splice are in [4].

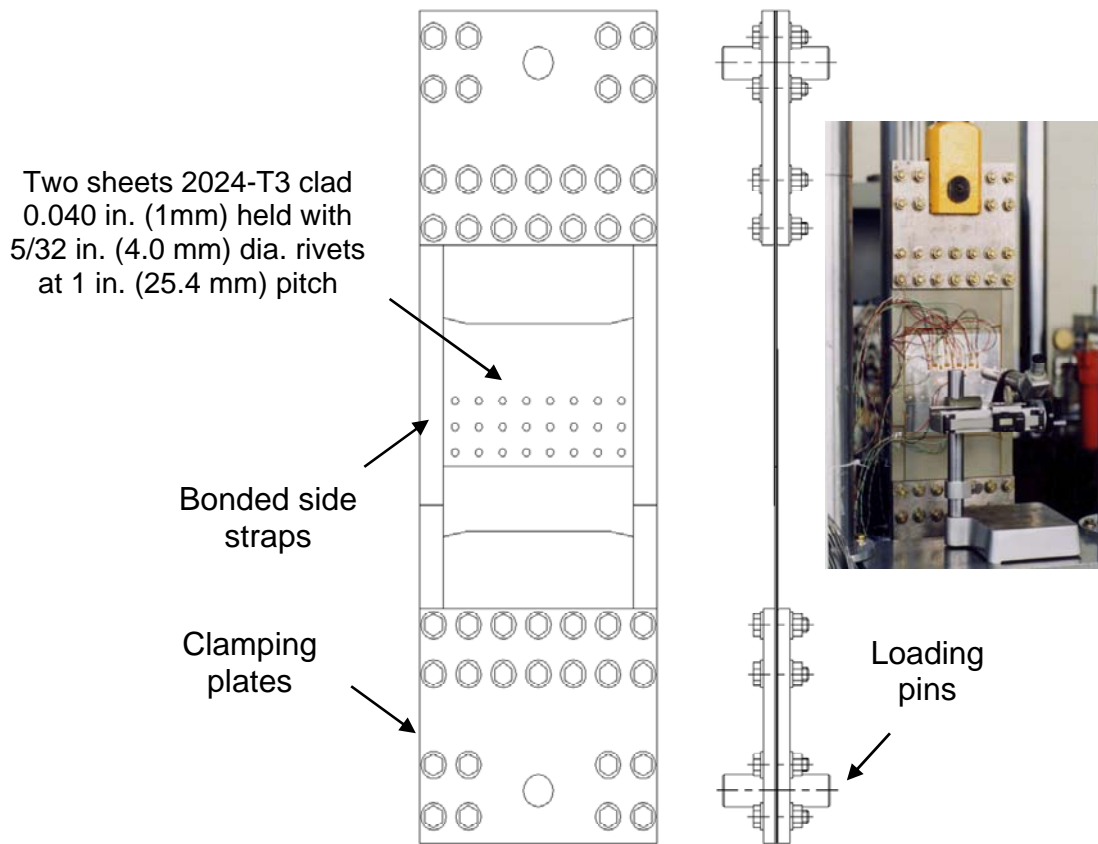


Figure 16-1: Lap Splice Specimen with Clamping Plates and Loading Pins
(the left-hand drawing shows the splice as it would appear from outside an aircraft).

16.2.2 Preparation of Corroded Specimens

The specimens to be corroded were selected randomly. The interior of the splice was corroded and dried prior to fatigue testing. The target range of corrosion severity had been observed in several lap splices from service aircraft. It was a moderate level that might go unnoticed during routine visual inspection for corrosion pillowing. The corrosion procedure was developed during a pilot test program. It was not expected to simulate accurately the iterative, mainly sequential process of corrosion and fatigue that occurs on aircraft over many years in service. However, it was expected to provide evidence of some of the mechanisms of interaction of corrosion and fatigue in service and to provide a statistically significant indication of the effect of typical corrosion on fatigue characteristics. More information on the corrosion procedure and its simulation of service corrosion can be found in [5].

The corrosion build-up inside the splice caused pillowing distortion. This distortion can be seen clearly in comparing the images of corroded and non-corroded specimens in Figure 16-2, which were obtained using the D Sight Aircraft Inspection System (DAIS). The distortion can significantly affect the stress distribution in a splice, and has been modeled in other work at the National Research Council (NRC) Canada [6]. Measurements of pillowing distortion were used to monitor the level of corrosion during the pre-corrosion process.

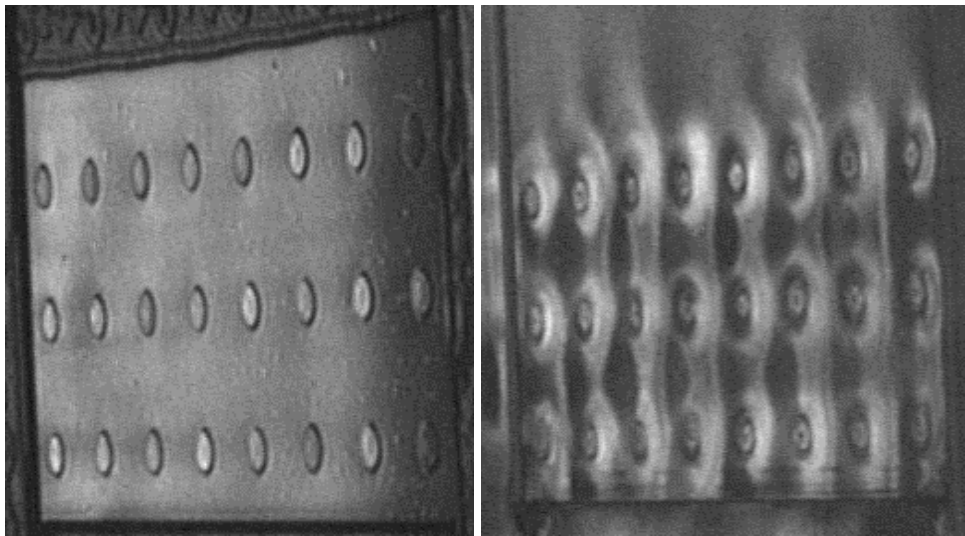


Figure 16-2: D Sight Aircraft Inspection System (DAIS) Images of a Lap Splice Specimen Before Corrosion (left) and After Corrosion (right).

16.2.3 Fatigue Testing

Nine non-corroded and nine corroded specimens were fatigue tested. The approach followed ASTM guidelines for a paired comparison test program [7] as far as practicable. Various other precautions were taken to minimize nuisance variables that might mask the effects of corrosion on fatigue characteristics.

All specimens were subjected to constant amplitude, uniaxial, cyclic loading at 4 Hz using a MTS servo hydraulic load frame. The fatigue test was load controlled, with a load ratio of 0.02. After cracks emerged from under the rivet heads they were measured using a travelling microscope. The tests were generally allowed to continue until cracks had developed and linked up across the full width of the splice. The specimen did not break apart at this point, because the side straps carried the maximum load. A few tests were terminated earlier for various reasons.

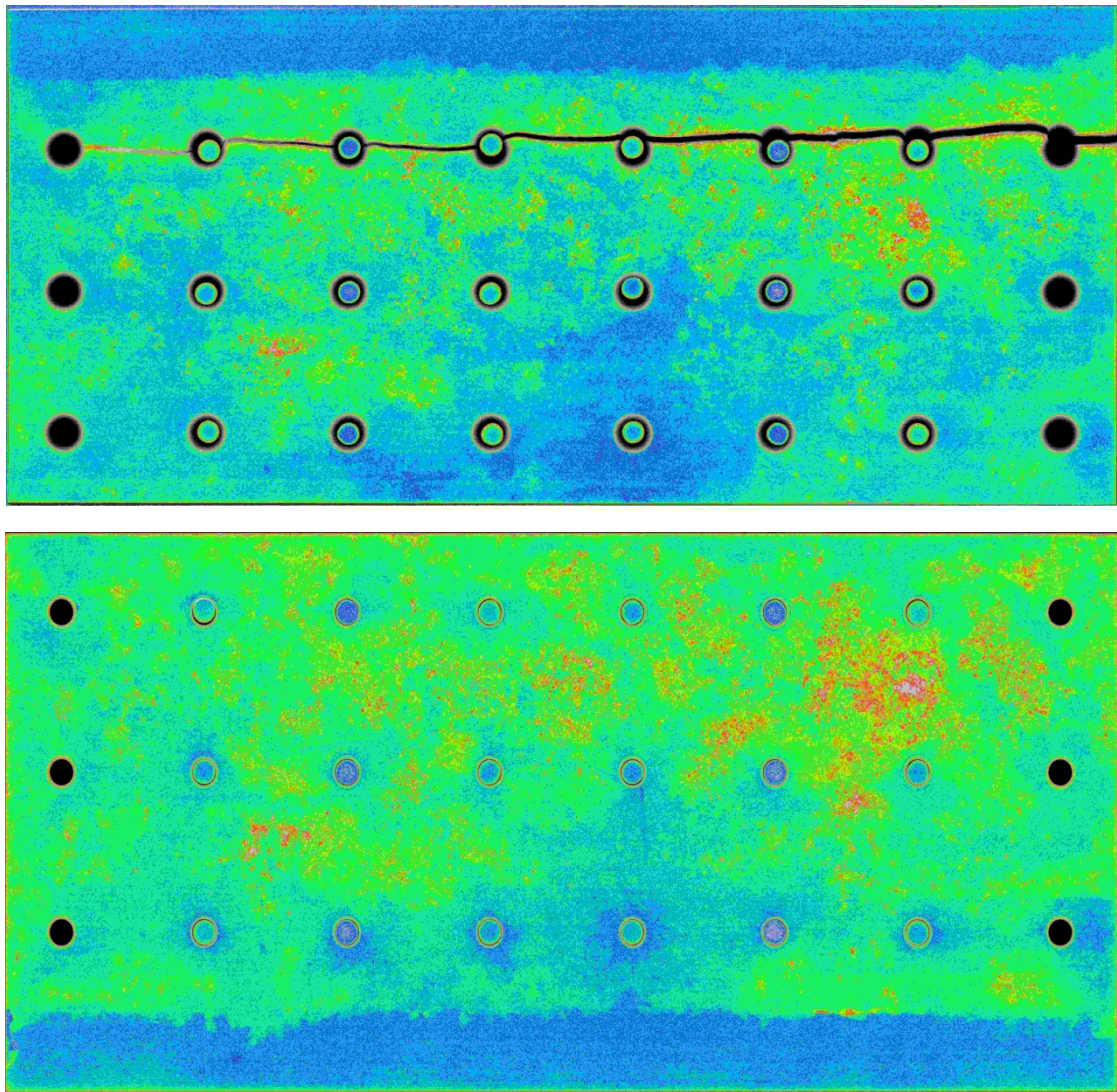
16.2.4 Measurement of Corrosion Damage

In the case of fuselage splices, it is currently difficult to measure the hidden corrosion damage at the faying surfaces, i.e., the internal contacting surfaces, accurately and with high resolution using Non-Destructive Inspection (NDI). Therefore, the corrosion damage was measured throughout each sheet after dismantling the splices. An efficient method of doing this over large areas was developed by the NRC several years ago, and procedures have been progressively improved. It involves dismantling the splice and removing the corrosion products chemically from each sheet (Figure 16-3). Then each sheet is radiographed using X-rays. Various calibration pieces of known thickness are included in the radiograph. The radiograph is digitized, calibrated, and analyzed using custom and commercial image processing software. Measurements of the average thickness loss in specific areas of interest were obtained from the grey scale versions of the radiographs. The grey scale radiographs were also colorized to provide calibrated thickness maps for general study and comparison with NDI (Figure 16-4). The X-ray images are presented in standard orientation for this work, i.e., as though being viewed from the exterior of an aircraft. Thus, if the images for the countersunk and driven sheets were overlaid, they would indicate the total distribution of corrosion damage at the faying surfaces of the splice.



Figure 16-3: Faying Surface of the Countersunk Sheet of Specimen #037 Before and After the Removal of Corrosion Products.

MODEL VALIDATION: FUSELAGE LAP JOINTS



Thickness range (in.)		Thickness loss range (in.)		Thickness loss range (%)		Pseudo-color
Min	Max	Min	Max	Min	Max	
0.041						Light Grey
0.04	0.041		0		0.00%	Dark Blue
0.039	0.04	0	0.001	0.00%	2.50%	Light Blue
0.038	0.039	0.001	0.002	2.50%	5.00%	Green-Blue
0.037	0.038	0.002	0.003	5.00%	7.50%	Green
0.036	0.037	0.003	0.004	7.50%	10.00%	Orange
0.035	0.036	0.004	0.005	10.00%	12.50%	Red
	0.035	0.005		12.50%		Mid-Grey

Figure 16-4: Pseudo-Colored Digitized X-Ray (DXR) Thickness Maps Showing Corrosion Distribution in Countersunk (upper image) and Driven (lower image) Sheets of Specimen #035 (higher resolution grey scale images are used for quantitative analysis).

The measurements obtained from radiographs indicated that the overall average thickness loss varied between specimens. The average thickness loss per sheet in the corroded specimens was estimated to be in

the range of 3% to 6%. The term “average thickness loss per sheet” is used to signify that the data is a combined average of both sheets in a given location, expressed as a percentage of the original thickness of one sheet. As can be seen from the example of an X-ray thickness map, the depth of the corrosion damage in some locations within a splice was much higher than this average value.

16.3 RESULTS AND DISCUSSION

16.3.1 Failure Modes

All non-corroded specimens failed by cracking in the countersunk sheet along the upper rivet row. The set of individual crack growth curves on the left in Figure 16-5 illustrates the typical MSD failure mode of the non-corroded specimens.

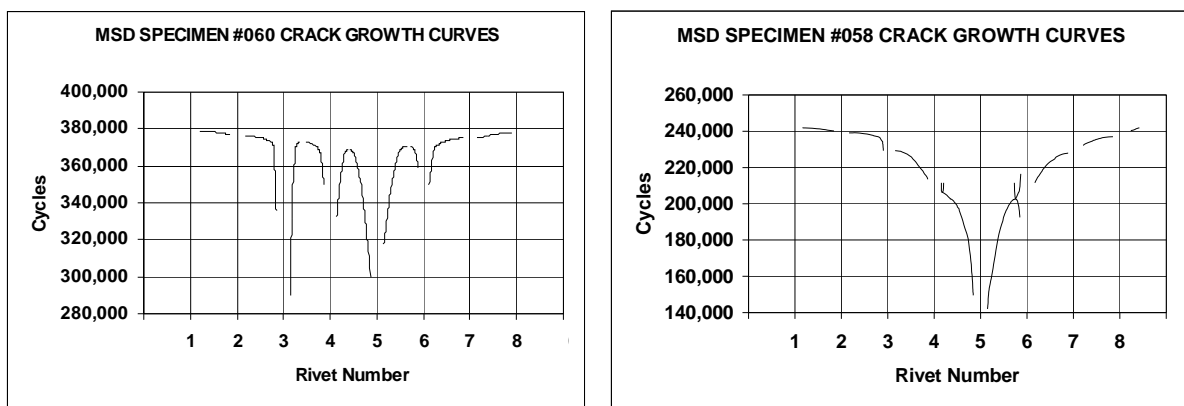


Figure 16-5: Example Sets of Individual Crack Growth Curves for Non-Corroded (left) and Corroded (right) Specimens.

Two general modes of failure were observed in the corroded specimens. Firstly, six out of nine specimens failed by cracking in the countersunk sheet along the upper rivet row. In these cases, the crack pattern was dominated by the early nucleation of cracks at one location. Thus a MSD pattern like the one in the non-corroded specimens did not develop. The right hand graph in Figure 16-5 illustrates this mode of failure. Secondly, three out of nine corroded specimens failed by cracking in the driven sheet, just below or along the lower rivet row. This mode of failure would be difficult to detect on an aircraft. Again, the crack pattern was dominated by the lead crack in each case. There were other, less obvious differences in the failure modes of the corroded and non-corroded specimens, but a discussion of these is outside the scope of this paper.

16.3.2 Empirical Modelling of the Effects of Corrosion on MSD Crack Growth and Fatigue Life

For the purpose of modeling the experimental data, the fatigue life of a specimen was divided into two parts: the life to the detection of the first crack, and the subsequent life to failure of the specimen. While MSD occurred in many cases, it was observed that the cracks invariably linked up progressively to form a single crack across the splice. A similar phenomenon has been observed in longitudinal fuselage skin splices on aircraft. Therefore, it was decided to investigate the possibility of characterizing the detectable crack growth in a splice by a single aggregate crack growth curve. Since the specimens were designed not to collapse when fully cracked, an aggregate crack length of 6 in. (152.4 mm) was defined as failure. If the test was terminated earlier, as was the case with some corroded specimens, the final crack length was used

MODEL VALIDATION: FUSELAGE LAP JOINTS

without adjustment. Since the actual length of the first crack at detection varied between tests, the criterion for first detection for analytical purposes was defined as an aggregate crack length of 0.5 in. (12.7 mm). This criterion encompassed the actual detection of the first crack in all specimens except one, and is consistent with the smallest crack in a splice that can reliably be detected in service using eddy current inspection.

To provide an overview of the fatigue test results, the aggregate crack growth curves for detectable crack growth are presented first. These are in Figure 16-6. The curves were constructed by summing the lengths of all detected cracks in the manner indicated in the sketch. Each curve starts at the length at which the crack was actually detected during the fatigue test. The single point is for a test that was terminated as soon as the first crack was detected. The aggregate crack growth curves for corroded and non-corroded specimens are fairly closely grouped, except for the curves for two corroded specimens. As yet, no reason has been found for treating these two specimens as statistical outliers, and so they have been included in all the statistics for Corroded Sample A. This sample excludes only the specimen with the single point plot. For interest, some graphs in this paper include comparative statistics for a Corroded Sample B that excludes the specimen with the longest life.

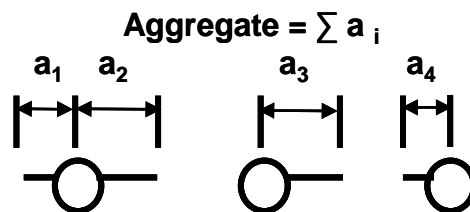
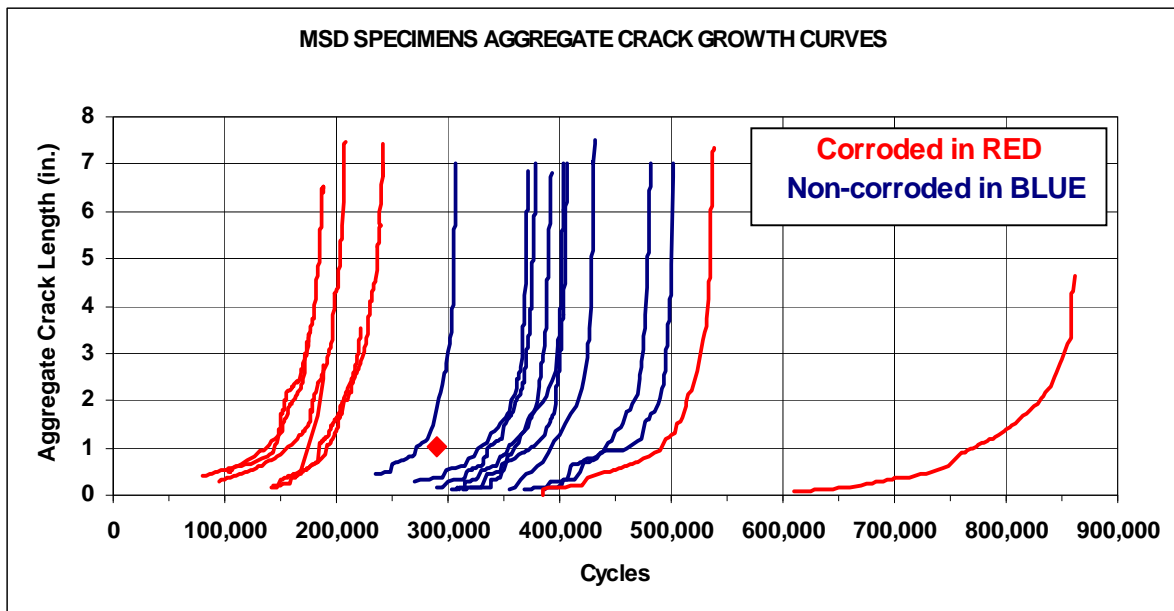


Figure 16-6: Aggregate Crack Growth Curves for Corroded and Non-Corroded Specimens.

The mean life to an aggregate crack length of 0.5 in. (12.7 mm) – i.e., to the first crack – is presented in Figure 16-7. In practice, an aggregate crack length of 0.5 in. (12.7 mm) implied two-sided cracking at one rivet, as illustrated in the sketch in the figure. The central bars represent the mean lives, while the accompanying pairs of bars represent the lower and upper bounds of the 90% confidence interval. The graph shows that pre-corrosion caused a statistically significant reduction in the life to the first crack.

The difference in mean lives indicates a 44% reduction in this portion of the life of the splice. The statistics for Corroded Sample B indicate a 54% reduction.

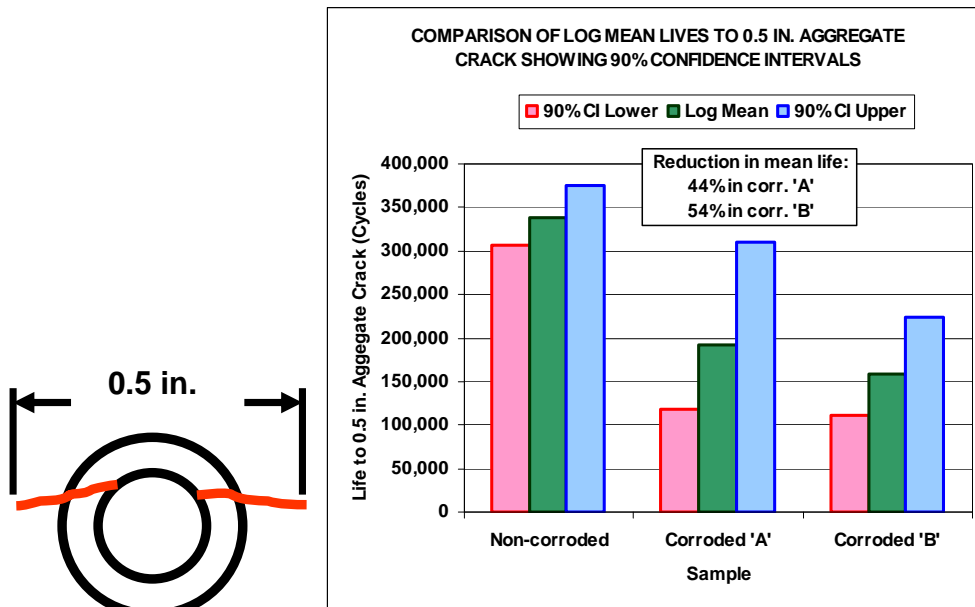


Figure 16-7: Mean Life to 0.5 in. Aggregate Crack with 90% Confidence Intervals.

The distribution of life to the first crack is presented in Figure 16-8. The graph shows the experimental data points plotted using a non-parametric distribution formula – i.e., one that does not require any prior assumption concerning the shape of the distribution. The graph superimposes the continuous curves obtained by fitting a Log Normal distribution to the data. These Log Normal curves are the probabilistic models of the life to the detection of the first crack for non-corroded and corroded specimens. The probability that the life to the first crack, N_1 , has a certain value can be represented mathematically as follows:

$$P(N_1 \leq x) = F_{N_1}(x) \quad (1)$$

where $F_{N_1}(x)$ is a Log Normal cumulative distribution function whose mean and standard deviation are estimated from the test data. $F_{N_1}(x)$ is different for corroded and non-corroded splices.

MODEL VALIDATION: FUSELAGE LAP JOINTS

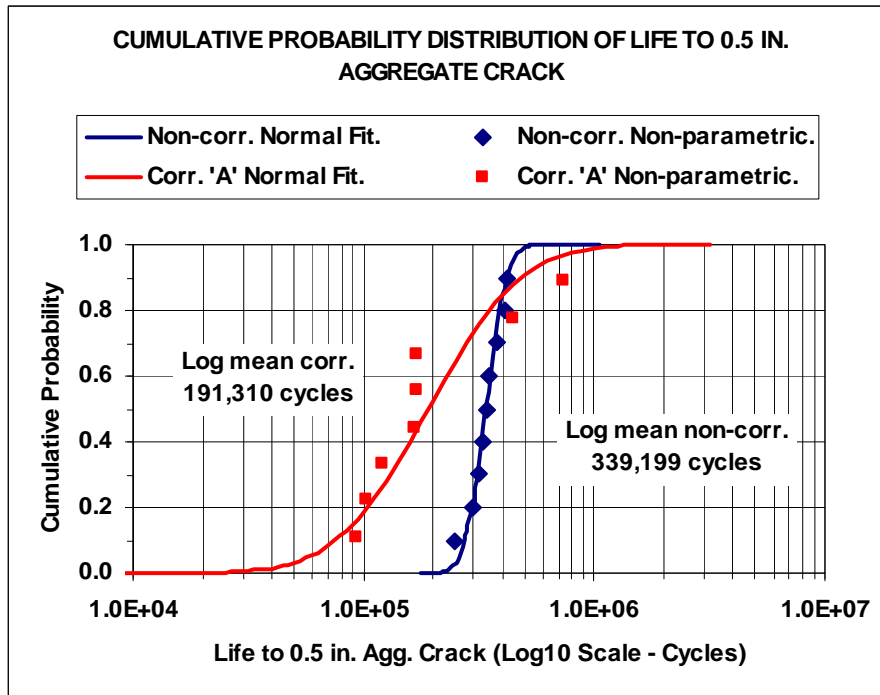


Figure 16-8: Empirical Models of Life to an Aggregate Crack Length of 0.5 in. (12.7 mm).

To model the subsequent period of detectable crack growth, the relationship between the aggregate crack growth rate per cycle, da/dN , and the aggregate crack length, a , was investigated and is presented in Figure 16-9. The left hand graph shows the relationship for a non-corroded specimen. The right hand graph shows the relationship for a corroded specimen. Similar analyses were performed for every specimen. Linear regression of the data for each specimen indicated that a relationship could be assumed of the form:

$$da/dN = Q.a^m \tag{2}$$

where m and Q are stochastic variables. This second phase model of multiple crack growth is comparable to the one proposed in [8] for a single crack in non-corroded structure. However, the analytical approach developed below is closer to the one used in [9] for the Paris-Erdogan equation.

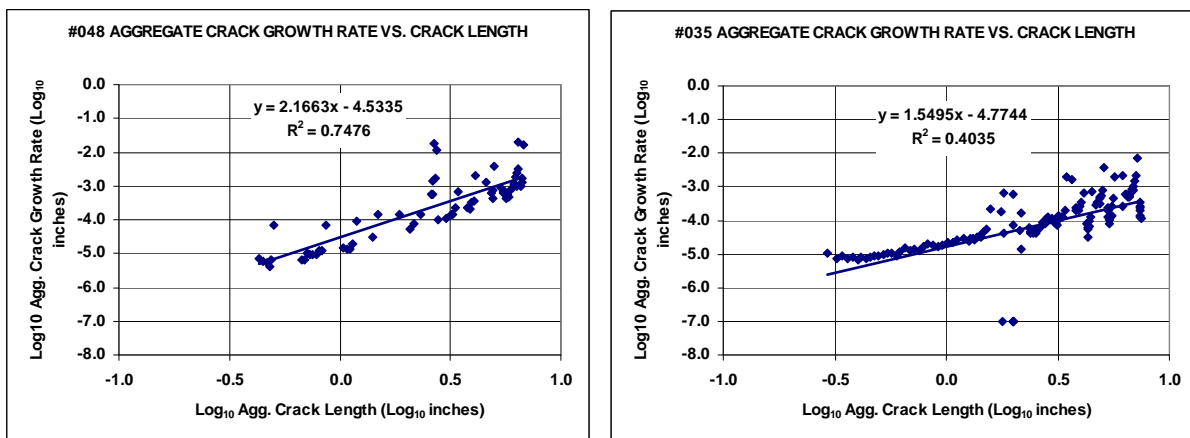


Figure 16-9: Illustration of the Relationship Between Aggregate Crack Growth Rate and Aggregate Crack Length in Non-Corroded (left) and Corroded Specimens (right).

From data of the kind illustrated in Figure 16-9, distributions for the exponent “m” were estimated for the corroded and non-corroded populations. The graph in Figure 16-10 shows the data points of the non-parametric analyses. The superimposed continuous curves are Normal distributions estimated from the experimental data. The Normal fits show reasonable agreement with the non-parametric analyses for both the corroded and the non-corroded populations. Similar distributions were developed for the parameter Q and are shown in Figure 16-11. Log Normal fits were assumed in this case. Based on these assumed curve fits, the probability that the parameters m and Q in Equation (2) have certain values can be represented by the following general equations:

$$P(m [x]) = F_m(x) \tag{3}$$

$$P(Q [x]) = F_Q(x) \tag{4}$$

where $F_m(x)$ is a Normal cumulative distribution function and $F_Q(x)$ is a Log Normal cumulative distribution function. The means and standard deviations of $F_m(x)$ and $F_Q(x)$ are estimated from test data. The functions will be different for non-corroded and corroded specimens.

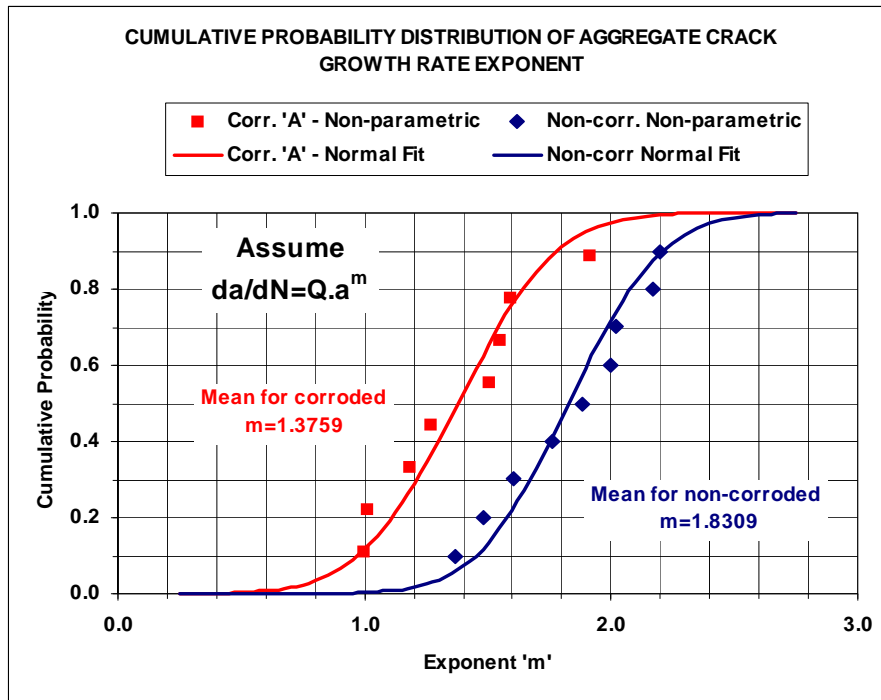


Figure 16-10: Distribution of Exponent ‘m’ in Equation $da/dN = Q.a^m$.

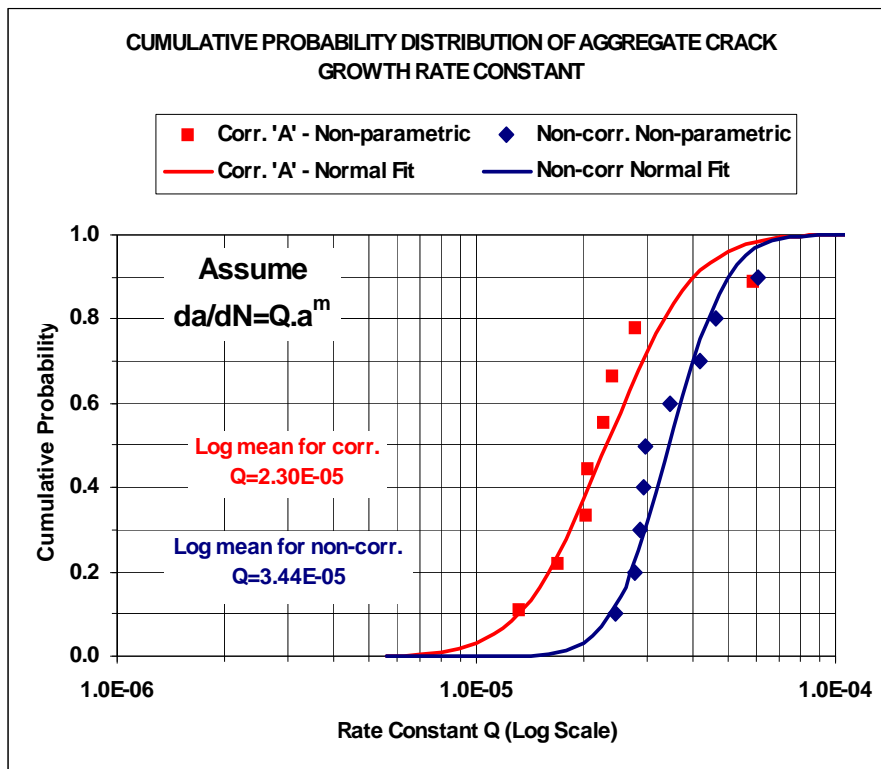


Figure 16-11: Distribution of Constant 'Q' in Equation $da/dN = Q.a^m$.

Equations (1) to (4) together represent a generalized probabilistic model of the whole fatigue life of a splice. The cumulative distribution functions of aggregate crack length at given values of the total life, $F_{a, N_{total}}(x)$, could be estimated from this model using a Monte Carlo simulation. This would involve repeated numerical integration of Equation (2) to generate a large sample of aggregate crack growth curves. For each simulation of a splice fatigue life, the parameters N_1 , m , and Q , would be sampled according to their respective distributions using a random number method. Assuming constant amplitude loading, the probability of failure of the splice after a certain number of fatigue cycles, N_{total} , would be the probability that the crack length had exceeded the failure criterion:

$$P(a > 6 \text{ in.}) = 1 - F_{a, N_{total}}(x = 6 \text{ in.}) \tag{5}$$

If any of the parameters N_1 , m , and Q were found to be related, the relationships could be used to reduce the variability in $F_{a, N_{total}}(x)$. In the tests reported here, there was statistically significant correlation between Q and m in the corroded sample. There was weaker correlation between Q and m in the non-corroded sample.

Damage tolerance inspections of a fuselage skin splice are costly. Equations (1) to (5) and the associated Monte Carlo simulation could be used to help in selecting an inspection threshold and interval that will provide an acceptably low risk of fatigue failure at minimum cost. This analysis would require knowledge of the probability of crack detection (POD) characteristics of the chosen method of non-destructive inspection.

For illustrative purposes, the model has been applied in a simplified way using the mean value of the parameters N_1 and m and the correlation between m and Q to estimate the mean whole life to failure. The results of this analysis are summarised in Figure 16-12. The reduction in mean whole life due to corrosion was 32%. The model predicted 29%. In Corroded Sample B the reduction was 42%. The model

predicted 40%. As mentioned earlier, some of the corroded tests were terminated early. If the test lives had been adjusted to compensate, it is estimated that these test and model statistics would have been closer. The relative contributions of the hidden and detectable periods of crack growth are shown in each bar. The graph serves to confirm that there are no major inconsistencies between the model and the test data. It also highlights the longer period of detectable crack growth in corroded specimens. This was probably due to the reduced tendency for MSD in the corroded specimens.

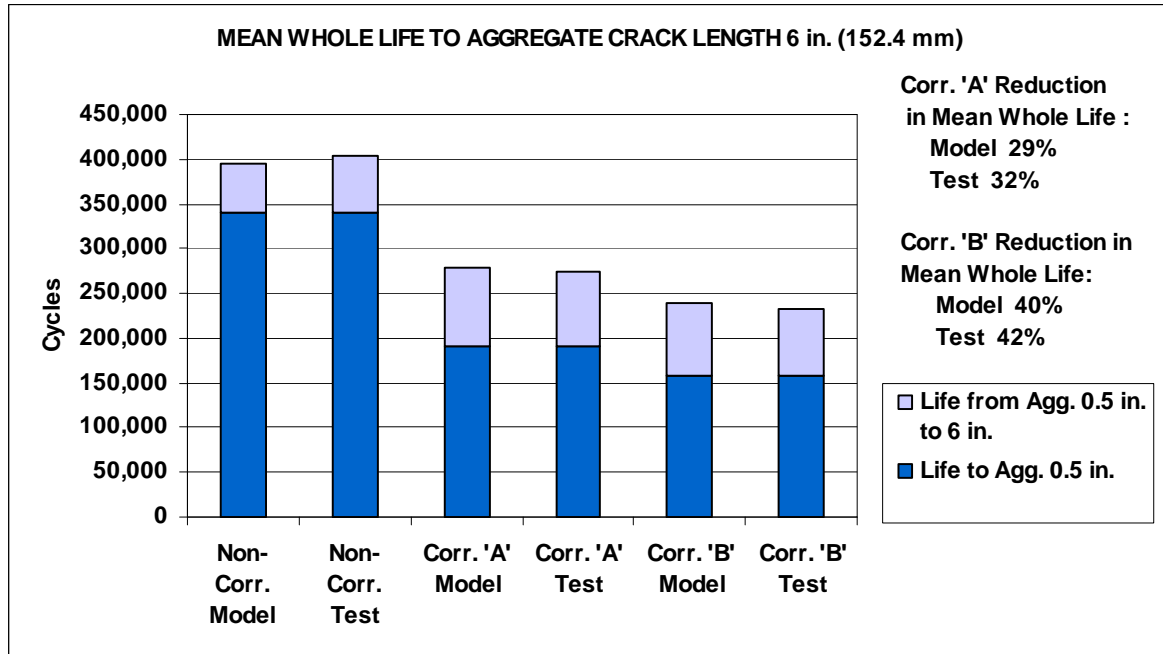


Figure 16-12: Graph of Mean Whole Life to an Aggregate Crack Length of 6 in. (152.4 mm), Showing the Relative Contributions of the Hidden and Detectable Periods of Crack Growth.

16.4 CONCLUSIONS

This section has described an experimental procedure that has been developed for evaluating the effect of prior corrosion on the fatigue characteristics of longitudinal fuselage skin splices in transport aircraft. The detailed design of the test specimen must be tailored to the aircraft splice to be studied.

It has been shown how the data from the experimental procedure can be used to construct a probabilistic model of fatigue life and crack growth in a splice where MSD is occurring. The model is applicable to non-corroded and corroded specimens.

The experimental procedure and the model have been demonstrated using a specimen design that is approximately representative of the types of single shear lap splices that are in use on several military and civil transport aircraft. Despite the complexity of the component and the variability of corrosion, statistically significant test results were obtained. These give confidence that the empirical modeling approach could have wide applicability.

The test data indicate that prior corrosion reduced the mean fatigue life to the detection of the first crack by 44%. The mean whole fatigue life was reduced by a lesser amount, 32%, because corrosion extended the period of detectable crack growth. This extension resulted mainly from a reduced tendency for MSD in corroded specimens.

The experimental procedure and model could be used to provide key input data for the durability and damage tolerance analysis of a fuselage skin splice. By taking corrosion fatigue interaction into account in this way, a more cost-effective design and maintenance policy might be achieved while maintaining or improving safety.

16.5 ACKNOWLEDGEMENTS

This work was a team effort involving many individuals at the NRC Institute for Aerospace Research, Carleton University, and Defence R&D Canada. In particular, Mr. D.V. Krizan and Mr. J.C. Cook of Carleton University and Mr. T.J. Benak of the NRC made a substantial contribution to the experimental work. Funding for the design, development, manufacture, and pre-corrosion of the test specimens, for the pilot test program (not described), and for part of the fatigue testing described in this paper was provided by the NRC and Defence R&D Canada. Part of the fatigue testing was supported by Lockheed Martin Aeronautics under the USAF Corrosion Fatigue Structural Demonstration (CFSD) Program (Contract RW26923, USAF prime contract F33165-97-C-3218).

16.6 REFERENCES

- [1] Schütz, W., “Corrosion Fatigue the Forgotten Factor”, Proceedings of the 18th Symposium of the International Committee on Aeronautical Fatigue, Melbourne, Victoria, Australia, 3-5 May 1995.
- [2] Kinzie, R., “Cost of Corrosion”, Proceedings of the 6th Joint FAA/DoD/NASA Conference on Aging Aircraft, San Francisco, CA, USA, 16-19 September 2002.
- [3] Brooks, C.L. and Simpson, D.L., “Integrating Real Time Age Degradation Into the Structural Integrity Process”, Proc. Conf. Fatigue in the Presence of Corrosion, RTO-MP-18, NATO/RTO, March 1999.
- [4] Eastaugh, G.F, Simpson, D.L., Straznicky, P.V. and Wakeman, R.B., “A Special Uniaxial Coupon Test Specimen for the Simulation of Multiple Site Fatigue Crack Growth and Link-Up in Fuselage Splices”, AGARD-CP-568, NATO/AGARD, pp. 2-1 – 2-19, December 1995.
- [5] Eastaugh, G.F., Merati, A.A., Simpson, D.L., Straznicky, P.V., Scott, J.P., Wakeman, R.B. and Krizan, D.V., “An Experimental Study of Corrosion/Fatigue Interaction in the Development of Multiple Site Damage in Longitudinal Fuselage Skin Splices”, Proc. Conf. Fatigue in the Presence of Corrosion, RTO-MP-18, NATO/RTO, March 1999.
- [6] Bellinger, N.C. and Komorowski, J.P., “Corrosion Pillowing Stresses in Fuselage Lap Joints”, AIAA Journal, Vol. 35, No. 2, pp. 317-320, February 1997.
- [7] Little, R.E. and Jebe, E.H., “Manual on Statistical Planning and Analysis for Fatigue Experiments”, ASTM STP 588, American Society for Testing and Materials, Philadelphia, PA, USA, 1975.
- [8] Manning, S.D. and Yang, J.N., “USAF Durability Design Handbook”, AFWAL-TR-88-3119, February 1989.
- [9] Liao, M. and Yang, Q.X., “A Probabilistic Model for Fatigue Crack Growth”, Engineering Fracture Mechanics, Vol. 43, No. 4, pp. 651-655, 1992.

Chapter 17 – CORROSION FATIGUE ANALYSIS OF AN F-18 LONGERON

Min Liao, Nicholas C. Bellinger and Jerzy P. Komorowski

Institute for Aerospace Research
National Research Council Canada
Ottawa, Ontario
CANADA

17.1 INTRODUCTION

A full scale F-18 wing test (FT245) was conducted at the National Research Council (NRC) Canada under the International Follow-On Structural Test Project (IFOSTP) supported by The Canadian Forces (CF) and The Royal Australian Air Force (RAAF). During the test, a long fatigue crack of 46 mm (1.81 inch) was discovered on the right hand upper Outboard Longeron (UOL) of the centre fuselage at 2932 Simulated Flight Hours (SFH), as shown in Figure 17-1. In this test, the fuselage was used as a transition structure, and was a retired United States Navy (USN) F-18 aircraft that had been in-service for ten years (1984 – 1994), Rutledge et al. [1]. Extensive corrosion was reported on the UOL by the US Navy (USN) during its service life, which was repaired (blended out) [1]. During the full scale wing test, the crack in the component was discovered after a fairing and sealant had been removed to perform a scheduled life enhancement procedure. Corrosion pits were found in the area near the apparent crack nucleation site. Since the full scale wing test was conducted in an environmentally controlled facility, it was reasonable to assume that these pits formed in-service and went undetected after the last maintenance cycle prior to the aircraft being retired. This cracking case was used to demonstrate and validate the applicability of a Holistic Structural Integrity Process (HOLSIP) based corrosion fatigue analysis methodology and tool.

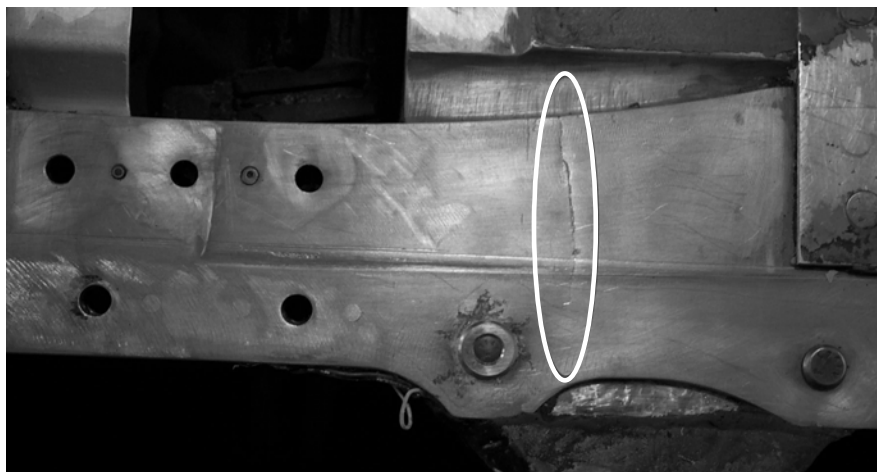


Figure 17-1: Fatigue Crack on the Right UOL of F18 Central Fuselage.

17.2 CORROSION FATIGUE MODELING FUNDAMENTALS

In HOLSIP, corrosion and fatigue can act not only *concurrently* but also *independently*. These effects are characterized by changes to the crack tip stress intensity. Based on the HOLSIP concept, a computer code ECLIPSE – Environmental and Cyclic Life Interaction Predictions for in-Service Evaluations has been developed by Analytical Process / Engineered Solutions (APES) Inc., Brooks et al. [2]-[3]. ECLIPSE uses fracture mechanics principles to formulate stress intensity factor solutions as follows, Brooks et al. [3]:

$$\Delta K_{cyclic} = \beta_T \Delta \sigma_{cyclic} \sqrt{\pi a / Q} \Psi(a, t, Env) \quad (1)$$

$$\Delta K_{time} = \beta_T \Delta E_{time} \sqrt{\pi a / Q} \Psi(a, t, Env) \quad (2)$$

where ΔK_{cyclic} and ΔK_{time} are driven by cyclic and time dependent mechanisms, respectively; β_T is the total geometry correction which is a function of geometry and crack length; $\Delta \sigma_{cyclic}$ represents the cyclic stress, and ΔE_{time} represents the environmental cyclic stress (environment spectrum) that is a function of time, sustained stress, environmental exposure, hydration cycles or potentially electro-chemical processes; Q is the crack shape parameter that is also a significant metric to accurately account for the aspect ratio of crack depth and width. $\Psi(a, t, Env)$ is the total correction, which is a function of crack length, time, and environment. This parameter represents the effects of corrosion or corrosion fatigue interaction on ΔK , such as corrosion related thickness loss, local geometric stress risers, topography change, corrosion induced sustained stress, and corrosion pillowing stress, etc. Therefore, $\Psi(a, t, Env)$ has different expressions for different corrosion mechanisms.

The total crack growth is determined through the summation of the cyclic damage and other time dependent damage, which is used to grow an Initial Discontinuity State (IDS, treated as a crack in any fracture mechanics model) to final instability. Incremental growth rates from both the operational stress cycles and the age degradation effects are used to determine a combined incremental growth. Therefore the total crack length is expressed as:

$$a_{Total} = a_{IDS} + \sum \Delta a \text{ and } \Delta a = \Delta a_{cyclic} + \Delta a_{time} \quad (3)$$

where a_{IDS} is the material, geometric or manufactured IDS that is simulated as an active crack in HOLSIP, and:

$$\Delta a_{cyclic} = \left(\frac{da}{dN} \right)_{cyclic} dN = f(\Delta K_{cyclic}) dN \text{ and } \Delta a_{time} = \left(\frac{da}{dt} \right)_{time} dt = g(\Delta K_{time}) dt \quad (4)$$

Note that Δa_{cyclic} is expressed in the cyclic domain while Δa_{time} is in the time domain. Since a relationship exists between cyclic and time domains for each increment of crack growth, the summation in Equation (3) could be performed on either cyclic or time domains. For the cyclic domain, Equation (3) can be solved using the following equation, Brooks et al. [3]:

$$\begin{aligned} a_{Total} &= a_{IDS} + \int \left(\frac{da}{dN} \right)_{cyclic} dN + \int \int \left(\frac{da}{dt} \right)_{time} dt dN \\ &= a_{IDS} + \int f(\Delta K_{cyclic}) dN + \int \int g(\Delta K_{time}) dt dN \end{aligned} \quad (5)$$

In ECLIPSE, age degradation is applied at each integration interval and the relationship between cyclic and time domains has to be specified to determine the cycles per integration interval. The corrosion fatigue analysis procedure of ECLIPSE is schematically presented in Figure 17-2. The USAF program, AFGROW, is linked to ECLIPSE as a crack growth analyzer. For each integration interval, β_T and $\Psi(a, t, Env)$ are determined and updated in ECLIPSE, and then the appropriate time-dependent ΔE_{time} parameters (stress, beta corrections, etc.) are passed to AFGROW to calculate the crack growth for the next integration interval. The input parameters required by ECLIPSE are also shown in Figure 17-2.

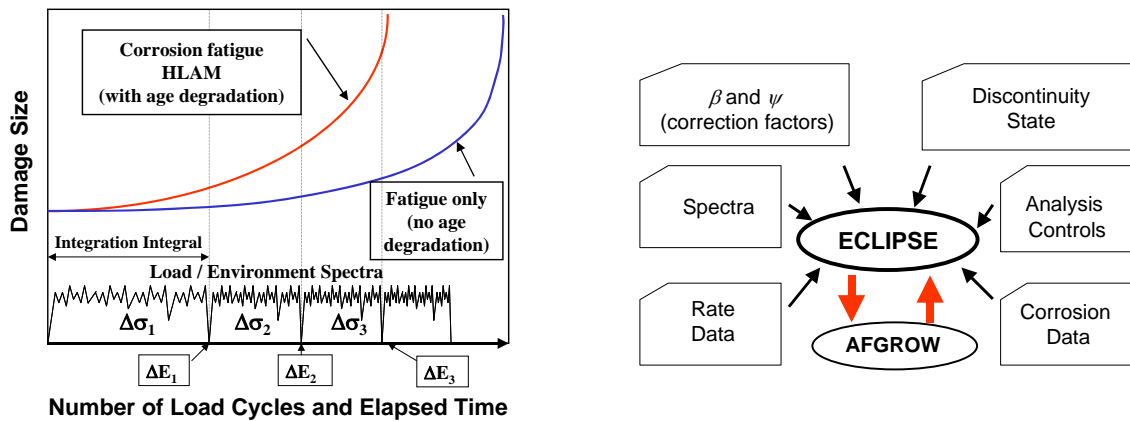


Figure 17-2: Corrosion Fatigue Analysis Procedure in HOLSIP/ECLIPSE [2]-[3].

17.3 INPUTS FOR CORROSION FATIGUE ANALYSIS

The input parameters for ECLIPSE were prepared based on the data and assumptions as follows.

17.3.1 Cracking Scenario

A replica was taken to verify that the crack nucleated from corrosion pits (see the dotted line in Figure 17-3) that were present at the round corner. A corner crack model was thus added to ECLIPSE in order to simulate this cracking scenario. The combined length of the pits along the thickness direction was approximately 0.63 mm (0.0248 inch), and the pit depth (shortest dimension), which occurred in the width direction was approximately 0.44 mm (0.0172 inch).

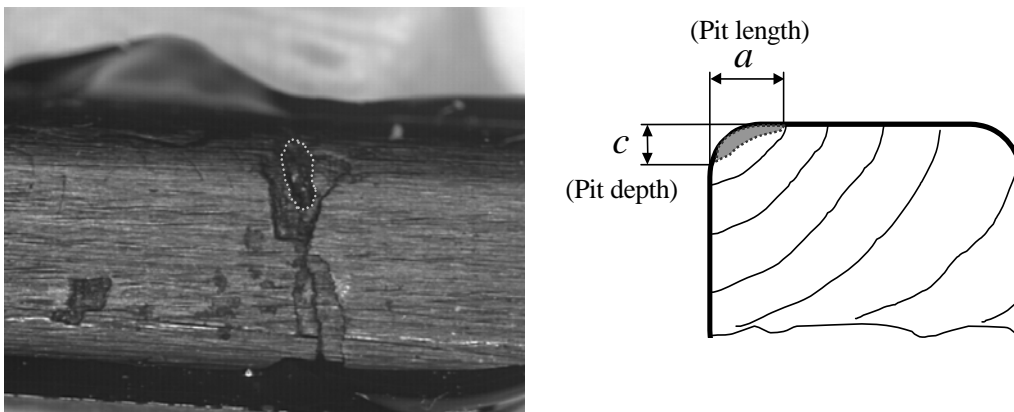


Figure 17-3: Corrosion Pits and Cracking Scenario.

17.3.2 Material Models (da/dN and IDS Crack)

The UOL material was 7149-T73511 aluminum extrusion (L-T). Ideally, HOLSIP would require physical measurements and a metallurgical study to determine the IDS distribution presented in the alloy. However, due to the unavailability of pristine material, it was decided to use the existing fatigue life data to estimate the IDS value, i.e., initial crack size, of this alloy. Crack growth data from the full scale CF-18 fuselage test (FT55) conducted at Bombardier Aerospace were used to estimate the initial crack size, in which a

fatigue crack nucleated at the same location of the UOL but in that case, no corrosion was present. The crack growth data from the FT55 test are presented in Figure 17-7. Revised Crack Growth Rate (CGR) data for this alloy, which were originally taken from the NASGRO material database and modified by APES to include the small crack growth regime using the method developed by Brooks et al. [4], was employed to estimate the IDS value. The *geometry* for the initial crack on the corner of the UOL was assumed to have a quarter circle shape.

To determine the loading spectrum, the readings from one strain gauge, which was placed on the UOL in the full scale fuselage test (FT55) and very close to the crack nucleation site, was used. One block of this spectrum contained 8,369 cycles, which represented 326 SFH. The analytical results, labeled as HOLSIP (non-corroded) are presented in Figure 17-7, which indicates that, if an initial crack size of 0.18 mm (0.0071 inches) was used, the non-corroded analytical results are very close to the test (FT55). This initial crack size was then employed for the following corrosion fatigue analysis.

17.3.3 Corrosion Growth Rate and Topography ID

The corrosion pits were assumed to have developed under service environments and cyclic loading during the ten years of service in the USN. It has been shown that a cube root power law can effectively describe the corrosion pit growth in aluminum alloys, Godard [5] and Hoepfner [6]. Also, Harlow and Wei [7], and Turnbull [8] demonstrated that this power law could be derived based on pit growth kinetics and Faraday’s law. Thus, the cube root power law was used in this work to describe the corrosion pit growth rates:

$$d = C(T)^{1/3} \tag{6}$$

where *d* is the maximum pit depth, *T* is the time, and *C* is a parameter related to the material/environment combination. Based on the pit depth and time information given previously, the corrosion pit growth curve was estimated (Figure 17-4). It has been demonstrated that the topography, i.e., surface roughness of a corroded surface, has an effect on the local stress states around a pit/crack, Brooks, et al. [2]. The effect was quantified using the StressCheck finite element model and converted to stress intensity factor beta factors library. The software ECLIPSE used what is termed the ‘Topography ID’ to represent different beta factors. The topography IDs are in increasing order of severity from 0 (0.0 mm pit in depth or no topography correction) to 9 (1.0 mm (0.040 inch) pit in depth). From the corrosion pit growth curve (Figure 17-4), the pit depth for every year was obtained, then the corresponding ID for this pit depth at this year was interpolated using the pre-defined IDs in ECLIPSE. The resulting topography ID used in ECLIPSE is shown in Figure 17-5.

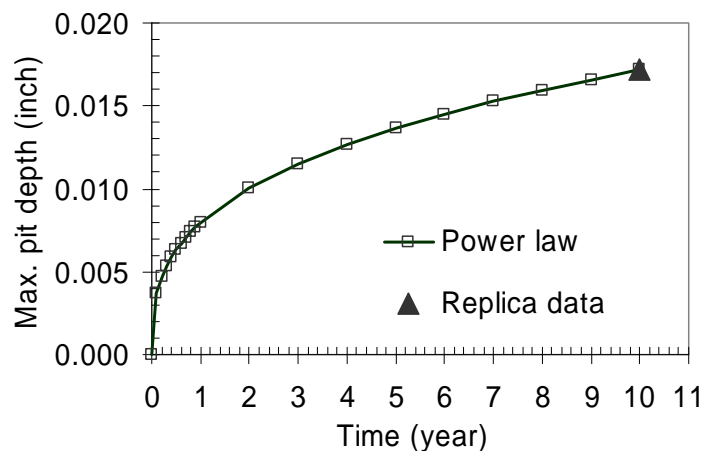


Figure 17-4: Corrosion Pit Growth Rate.

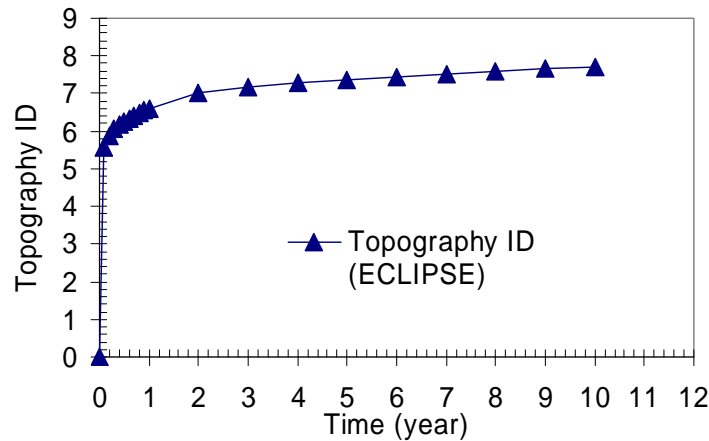


Figure 17-5: Topography ID Used in ECLIPSE.

17.3.4 Thickness Loss

The thickness loss effect is included in ECLIPSE through the time related correction, $\Psi(a,t,Env)$. Although the UOL surface had been blended out to remove damage (surface corrosion) during its service life, no blending marks were found along the crack path. It was thus decided that no thickness loss would be taken into account in the corrosion fatigue analysis. To accurately measure the thickness of the present UOL along the crack path, an ultrasonic technique was employed. The average thickness along the crack path was determined to be 3.12 mm (0.123 inch).

17.3.5 Loading Spectrum

During the NRC full scale test, two aluminum alloy (7075-T6) straps were used to repair the cracked UOL and the test resumed. The readings from two strain gauges, placed on the two straps, were then processed to determine the loading spectrum. A two step process was used:

- 1) The nominal stress level was first determined based on the total loads that by-passed the UOL, which can be calculated by assuming that the UOL was completely broken; and
- 2) The stress level at the fillet where the pits and crack nucleated was determined by applying a combined (tension and bending) stress concentration factor of 1.35 determined by Bombardier Aerospace during the repair disposition process.

Figure 17-6 illustrates one block of the loading spectrum, which includes 46,588 cycles that represent 326 SFH.

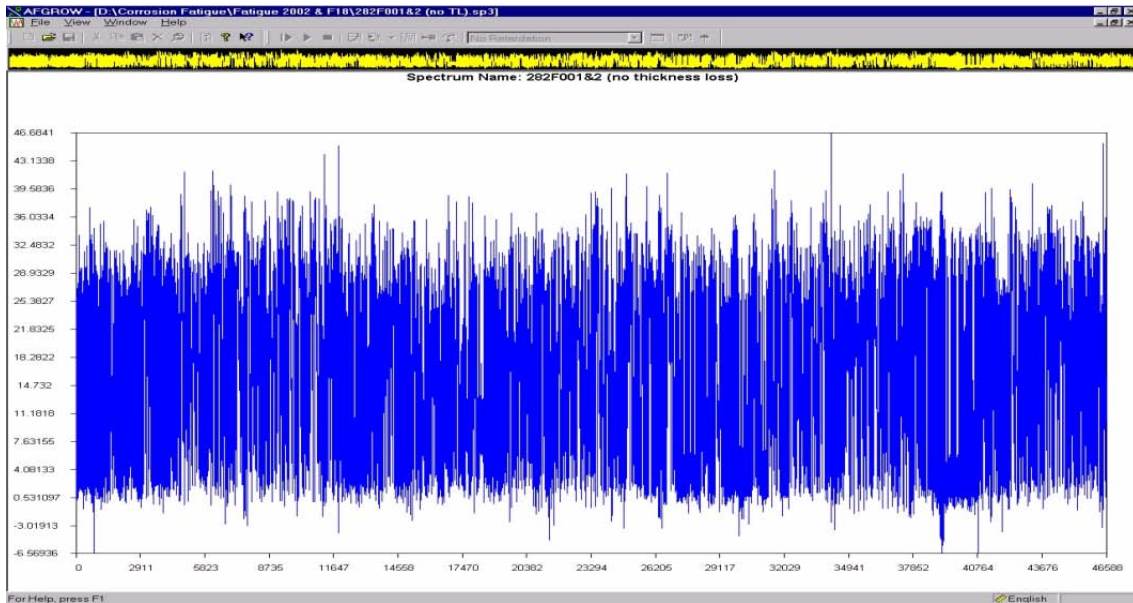


Figure 17-6: Loading Spectrum Obtained from Strain Gauges.

17.4 RESULTS

Using the estimated initial crack size (0.18 mm, 0.0071 inches) and other input parameters (corrosion growth, thickness loss, etc.) discussed in the previous section, the corrosion fatigue analysis was carried out for the corroded UOL using ECLIPSE. This analysis was carried out from the start of service life (1984) to when the crack was found during the wing test. It should be noted that this fuselage had previously accumulated 3,644 flight hours with a recorded FLEI (Fatigue Life Evaluation Index) of 0.309 in the USN, Rutledge et al. [1]. This usage converted to the full scale wing test hours is approximately 1,446 SFH. This reduction is due to more aggressive loading spectrum applied to the wing test. The results, labeled as HOLSIP (corroded), from the corrosion and fatigue analysis are shown in Figure 17-7, along with the test results for the corroded and non-corroded UOL. This figure shows that the analytical results for the corroded UOL are in close agreement with the NRC test results.

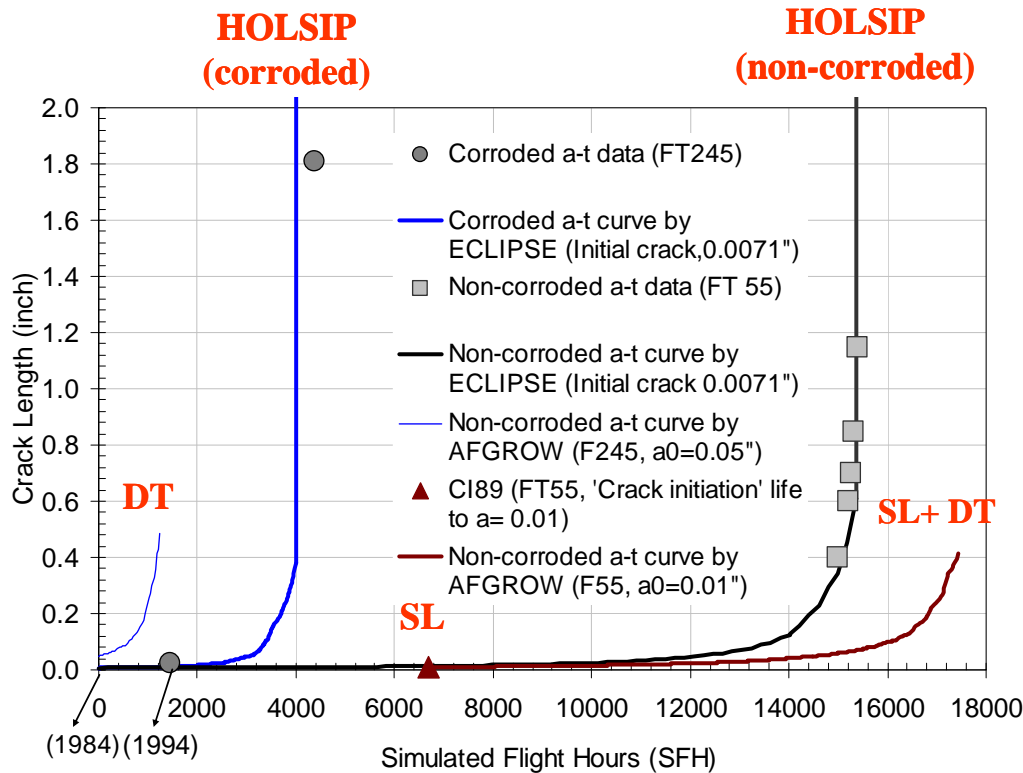


Figure 17-7: Life Comparison Between Corroded and Non-Corroded UOL.

In Figure 17-7, the result of a Damage Tolerance (DT) analysis is also presented. The DT analysis was carried out using AFGROW, and a typical initial crack size of 1.27 mm (0.050 inches). It is shown that the typical DT analysis clearly underestimated the life of the corroded UOL, without including the corrosion effect.

As the F-18 was originally designed based on the Safe Life (SL) approach, a “Crack Initiation” software (CI89) which was specifically calibrated for the CF-18 material and load spectra, was used to estimate the ‘crack initiation’ life (time to a crack size of 0.25 mm, or 0.010 inches). The CI89 results, labeled as SL, are presented in Figure 17-7. As can be seen, since the SL approach did not consider corrosion effects, its predicted life is longer than that of the corroded UOL, but less than the life of non-corroded UOL. Further analysis was performed to continue a DT analysis (AFGROW) from the 0.010-inch crack to failure, the total life (i.e., sum of CI89 and DT lives) is presented in Figure 17-7, labeled as SL+DT. It is shown that the SL+DT total life approach overestimated the life of the non-corroded UOL, while the HOLSIP approach provided a result close to that of the test.

In summary, both analytical and test results showed that the corrosion pits significantly decreased the life of the UOL. The HOLSIP/ECLIPSE analysis provided most reasonable results for both corroded and non-corroded cases.

17.5 CONCLUSION

A corrosion fatigue analysis using HOLSIP/ECLIPSE was carried out to assess the life of the corroded UOL of an F-18 aircraft, in which the concurrent interaction of corrosion and fatigue were quantitatively taken into account. The analytical results were compared to full scale test results. The good agreement

between the analytical and test results indicated that HOLSIP/ECLIPSE is a promising analytical tool for corrosion fatigue analysis of aircraft structures. The HOLSIP framework has potential to augment and enhance the safe life and damage tolerance approaches.

17.6 REFERENCES

- [1] Rutledge, R.S., Sullivan, A.B. and Lafleur, L.J., LM-ST-780, Institute for Aerospace Research of National Research Council Canada, 1996.
- [2] Brooks, C.L., Prost-Domasky, S. and Honeycutt, K., "Fatigue in the Presence of Corrosion", RTO-MP-18, NATO, Brussels, Belgium, 1998.
- [3] Brooks, C.L., Prost-Domasky, S. and Honeycutt, K., Proceeding of the 1999 USAF ASIP Conference, San Antonio, TX, USA, 1999.
- [4] Brooks, C.L., Honeycutt, K. and Prost-Domasky, S., Proceeding of the 2001 USAF ASIP Conference, Williamsburg, VA, USA, 2001.
- [5] Godard, H.P., Canadian J. of Chemical Eng., Vol. 38, pp. 167-173, 1960.
- [6] Hoepfner, D.W., ASTM STP 675, pp. 841-870, 1979.
- [7] Harlow, D.G. and Wei, R.P., "Engineering Fracture Mechanics", Vol. 59, No. 3, pp. 305-325, 1998.
- [8] Turnbull, A., British Corrosion J., Vol. 28, No. 4, pp. 297-308, 1962.

Chapter 18 – HOLISTIC STRUCTURAL INTEGRITY ANALYSIS FOR CORROSION IN A HUB ON A TRANSPORT AIRCRAFT FRAME

Thomas Mills and K.T. Honeycutt
Analytical Processes / Engineered Solutions, Inc.
Saint Louis, Missouri
USA

18.1 INTRODUCTION

This case study examines the failure of fuselage frames on the now-retired USAF C-141 aircraft. The component experiencing the problem was the frame at Fuselage Station (FS) 998. In particular, cracking was occurring in a hub for a main landing gear attachment point (Figure 18-1). Special concern was placed on this component because it was largely expected to be an ‘infinite life’ component, at least in the area where cracking was occurring. The discovery of cracks, not explained by any analyses, had the USAF confronting a very likely possibility of wholesale frame replacement throughout the fleet, which would have been a very costly option in terms of both dollars and asset availability. Replacing the FS 998 frame is major surgery.

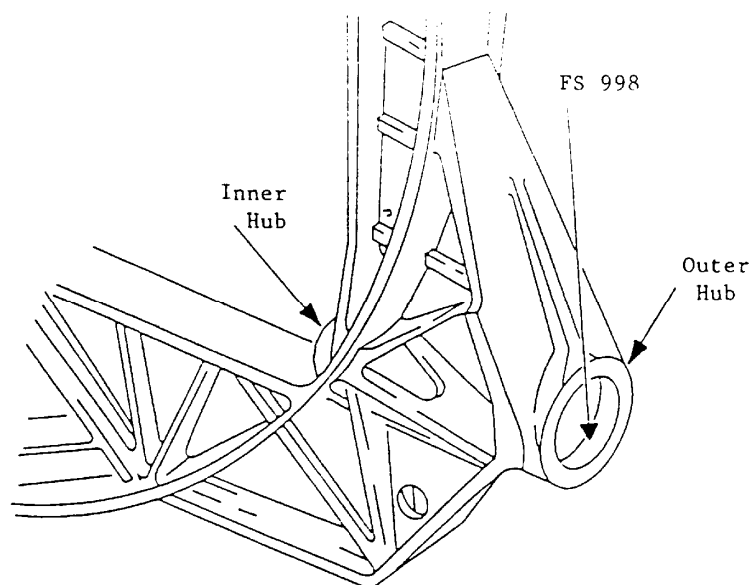


Figure 18-1: Drawing of Main Frame Landing Gear Hub.

In sight of the financial and logistical complexity of such a sizeable fleet-wide action, the decision was made to include analysis of this component in a 1997 USAF research and development program known as the Corrosion Fatigue Structural Demonstration Program (CFSD). Details follow.

18.2 FRACTURE ANALYSIS

As with any structural analysis, it is good to start with determining the root cause. As stated above, prior to the CFSD program, the cracking in this component was largely unexplained. Aircraft teardown and failure

analysis revealed corrosion pitting at the crack nucleation site of the failed frames. Beyond this, very little information was known about the nature of the pitting other than the fact that corrosion up to 250 microns (0.01 inch) deep was found on 20-year old components. This provided a target metric for the holistic structural integrity analyses discussed in the next section.

18.3 HOLISTIC STRUCTURAL INTEGRITY ANALYSES

As with any structural fatigue analysis, it is necessary to understand key aspects of the component, such as the material, geometry, and crack driving force. Beyond that, to practically implement a solution, we need to understand usage requirements, inspection capabilities, and other factors.

Fortunately, the frame was made from a common aerospace structural alloy, 7075-T6 aluminum. Geometry was easy to grasp, and the failure location in the hubs was in a region of mild stress gradient, so constant tension spectral stresses were an adequate representation of the component loading. Understanding the load spectrum itself, however, was more challenging, as the actual load spectrum was proprietary and not available. The best we could do, under direction of the C-141 Aircraft Structural Integrity Program (ASIP) manager, was to use the MIL-A-008866B specification for Nz exceedances during landing, and generate a blocked and randomized landing spectrum (see Figure 18-2) for 30,000 spectrum flight hours (one lifetime) of a C-141 aircraft.

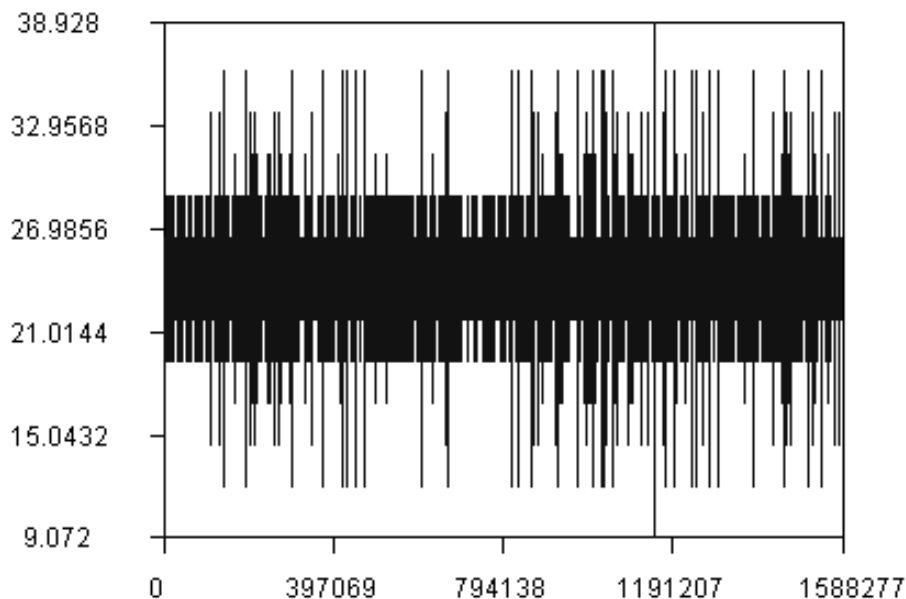


Figure 18-2: Load Spectrum Used in Analysis.

Fatigue analyses were then conducted using AFGROW (a publicly-available crack growth code) and two different starting crack sizes, specifically:

- 0.25 mm (0.01 inch) corner crack typical of ‘durability analyses’; and
- 1.25 mm (0.05 inch) corner crack typical of ‘damage tolerance analyses’.

These two cases provided ‘traditional’ bounds, wherein crack sizes typical of analyses in the industry were used. These two cases did not consider geometric corrosion effects on crack propagation, which is also typical of industry analyses.

The other critical aspect of the analysis, to trend it towards ‘holistic’, was to include pitting. In the models used, the presence of the pit amplifies the beta solution associated with the crack, which causes a shift in stress intensity, an increase in crack growth rate, and a decrease in fatigue life.

Additional complexities in the analysis had the pit grow according to a power law from time zero, with the end condition that the pit reached 250 microns (0.01 inch) in depth at 20 years (as determined by the teardown analysis from the fleet). This is a conservative approach, as pitting most likely did not occur until later in service after coating breakdown.

Figure 18-3 shows the results of the demonstration analyses. In practice, the fleet was experiencing failures in the range of 35,000 to 43,000 flight hours. Using traditional analysis techniques and the common durability crack size of 0.25 mm (0.01 inch), the hub showed flat crack growth (practically speaking, infinite life). On the other extreme, by assuming a damage tolerance crack size of 1.25 mm (0.05 inch), the component appeared to have an extremely short service life, which results in a heavy and expensive inspection burden.

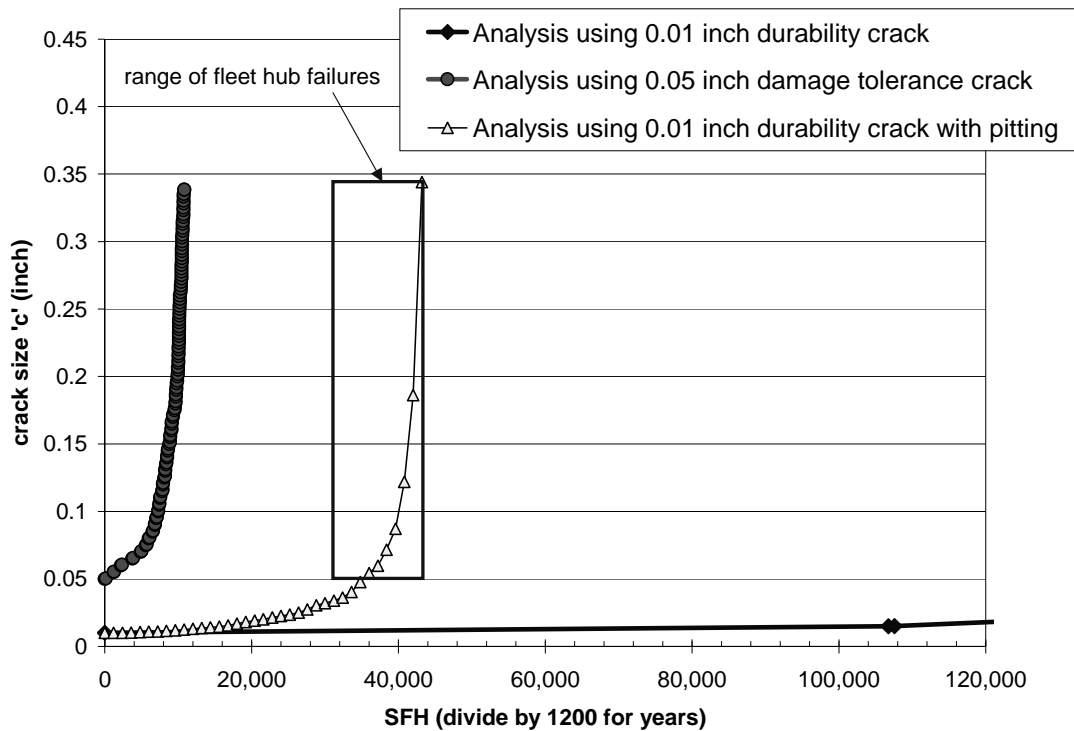


Figure 18-3: Crack Growth Analysis of Main Landing Gear Hub Showing Traditional and HOLSIP Analyses.

However, by including corrosion pitting in the traditional durability analysis, the life capability is reduced considerably but accurately (less than with damage tolerance assumptions) and estimates structural capability in the range of the fleet failures. The impact of corrosion is clear and further demonstrates the importance of holistic structural integrity considerations in aircraft maintenance, and also illustrates the power of these methods to identify corrosion-susceptible structure during design.

18.4 DISCUSSION

In the case of FS 998 frame, holistic structural integrity methods were able to correlate analysis life with field failures better than industry standard techniques. The inclusion of pitting in the life assessment

captured the general flavor of the fleet experience and provides an analytical path that was previously unavailable.

The lesser consequences of failure associated with this location on the frame precluded it being managed as a damage tolerance control point in practice. At the same time, the sensitivity of this area to pitting also meant that considering it to be an infinite life component was not effective either. Inspections for pitting in this location would be appropriate, since such violations of surface integrity appear to be a critical precursor to the evolution of fatigue failure.

This case study provided another example of a retrospective corrosion fatigue failure analysis to illustrate how information can be used to plan inspections for the appropriate types of damage in lieu of wholesale, major structural replacements across an entire fleet. The methods used were completely compatible with existing methodologies and ideologies, which also makes it possible to set inspection intervals, for instance, to guard against cracks that may form from previously undetected corrosion (Note: this is not a trivial location to access for the purposes of inspection, so we cannot look whenever we want).

An important lesson to learn from this case study is that the most efficient capability of these methods, from both safety and economic perspectives, will only be realized when quantitative evaluations of real-time degradation processes are proactively entrenched in the design requirements for new systems. In the same way that damage tolerance assessments can identify fracture critical structure, corrosion sensitivity analyses can identify corrosion critical structures and lead to more corrosion tolerant designs.

Chapter 19 – HOLISTIC STRUCTURAL INTEGRITY ANALYSIS OF CORROSION IN A DYNAMIC HELICOPTER COMPONENT

Thomas Mills and K.T. Honeycutt
Analytical Processes / Engineered Solutions, Inc.
Saint Louis, Missouri
USA

19.1 INTRODUCTION

A dynamic component in the main rotor system of a helicopter has had a recurrent cracking problem, where fracture is occurring at less than 10% of the part's rated 'safe life.' This problem is not unique to the operator for whom this assessment was conducted.

The component in question is made of a high strength aluminum alloy, and it is in contact with a stainless steel retaining ring. During this study, fractured parts were recovered from two different helicopters and were subjected to a detailed fractographic analysis and holistic structural integrity analysis. A synopsis of that effort has been provided here as a case study supporting the power of including corrosion effects in analyses not only for sustainment, but for design as well.

19.2 FRACTURE ANALYSIS

Fracture analysis was conducted using an optical stereoscope and an optical microscope. The fracture face revealed beach marks at lower magnification (Figure 19-1) and striae at higher magnification, which indicated fatigue was the primary crack propagation mechanism.

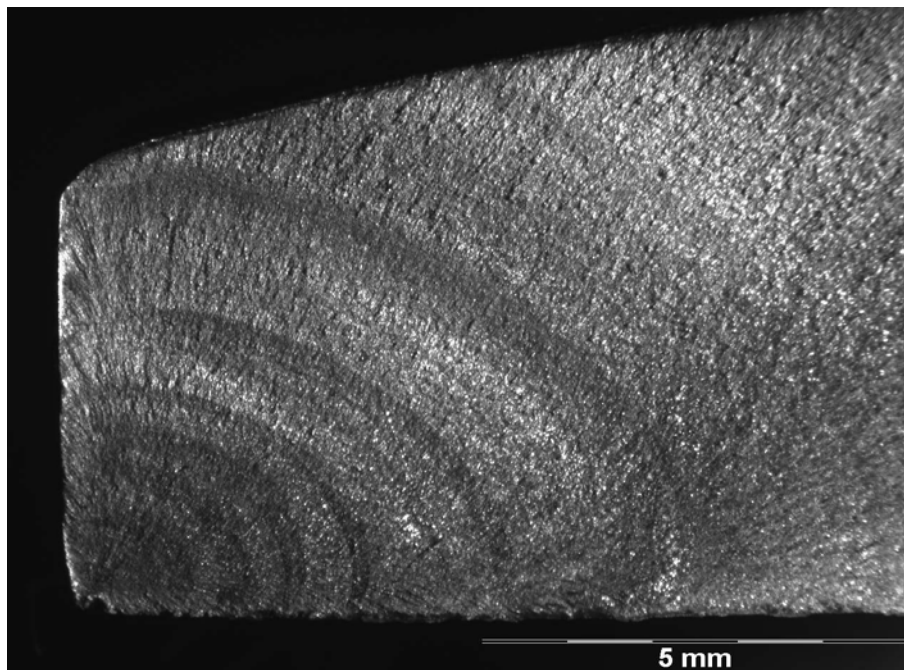


Figure 19-1: Optical Micrograph of Fracture Face Showing Beach Marks.

River marks on the fracture pointed back to a single origin at a corrosion pit (Figure 19-2) that was approximately 175 microns deep and hemispherical in nature. Other surface pitting was evident in areas adjacent to the failure location (Figure 19-3).

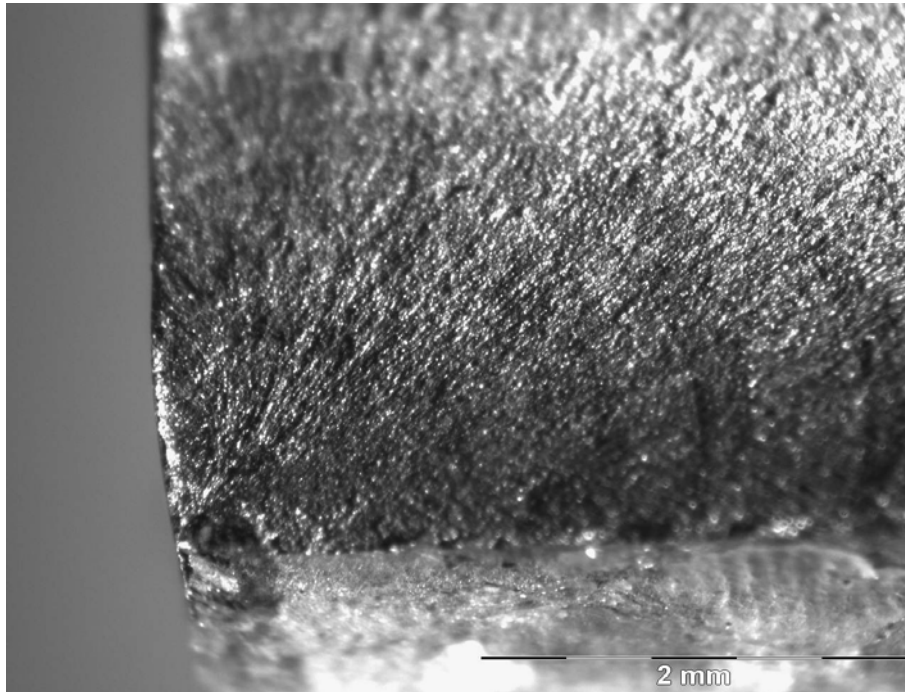


Figure 19-2: Optical Micrograph Showing Pitting at Origin and River Marks Emanating from Region.

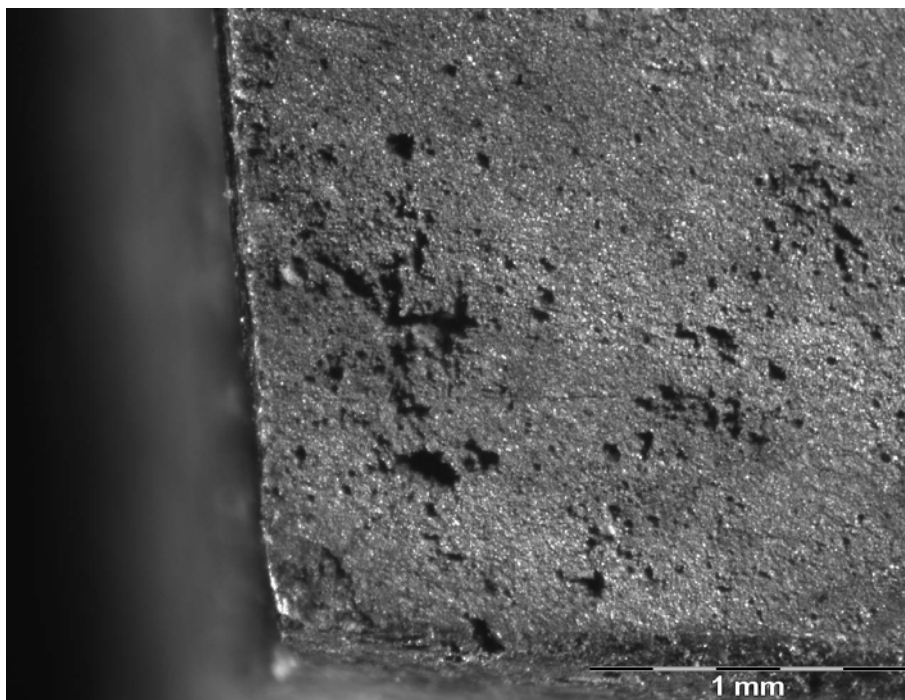


Figure 19-3: Optical Micrograph of Surface Perpendicular to Fracture Plane Showing Clusters of Corrosion Pits.

Although the components contained a corrosion protection coating in service, the contact of a stainless steel retaining ring against the aluminum, in combination with the dynamic operating environment, is believed to have damaged the coating. Unrelated maintenance activities on these components may also have adversely affected coating integrity. Once the coating was compromised, the presence of a crevice and galvanic couple (between the retaining ring and the component) and a harsh operating environment made the component very susceptible to pitting. The violation of surface integrity caused by the pitting then made the part susceptible to corrosion fatigue.

19.3 HOLISTIC LIFE ASSESSMENT

The fractographic study confirmed the failure mode to be corrosion-pitting fatigue. The next step was to conduct holistic life assessments to understand the nature of failure progression and to establish a recommended course of action for the operator.

Fortunately, the design load spectrum for the component was available for use in the analysis. This information was used in combination with a Finite Element Analysis (FEA) of the component to understand the nature of the crack driving force. The FEA accurately modeled the location of the fracture plane and also computed the nature of the stress distribution in the component, which was a combination of tension and bending.

An AFGROW (a publicly-available crack growth code) model of the component in the fracture plane was designed that accounted for the applied tension and resultant bending. The automation capability of AFGROW was used to model load shedding as the crack propagated.

From that point, several crack growth scenarios were executed assuming no corrosion. Initial crack sizes associated with the Initial Discontinuity State (IDS) for the material [1],[2] accurately reproduced a total component life that reflected the certified safe life of the component. Other larger crack sizes were also modeled to develop residual life curves (i.e., remaining life from various crack sizes).

This exercise was repeated assuming the presence of a 175-micron deep, hemispherical corrosion pit at the critical location on the component. In the models used, the presence of the pit amplifies the beta solution associated with the crack, which causes a shift in stress intensity, an increase in crack growth rate, and a decrease in fatigue life [3]. The results shown in Figure 19-4 illustrate the very severe influences of a corrosion pit in this scenario. If the pit had existed from time zero, the analysis shows that the part would only have about 1.5% of its original rated life capability. In reality, the components are failing at closer to 10% rated capability, but this is simply an indicator that the pits are not in the components at manufacture; rather, they form during operational usage. However, it is safe to say that once the coating is compromised, pitting is likely to follow, and once the pits form, failure of the component will follow shortly thereafter.

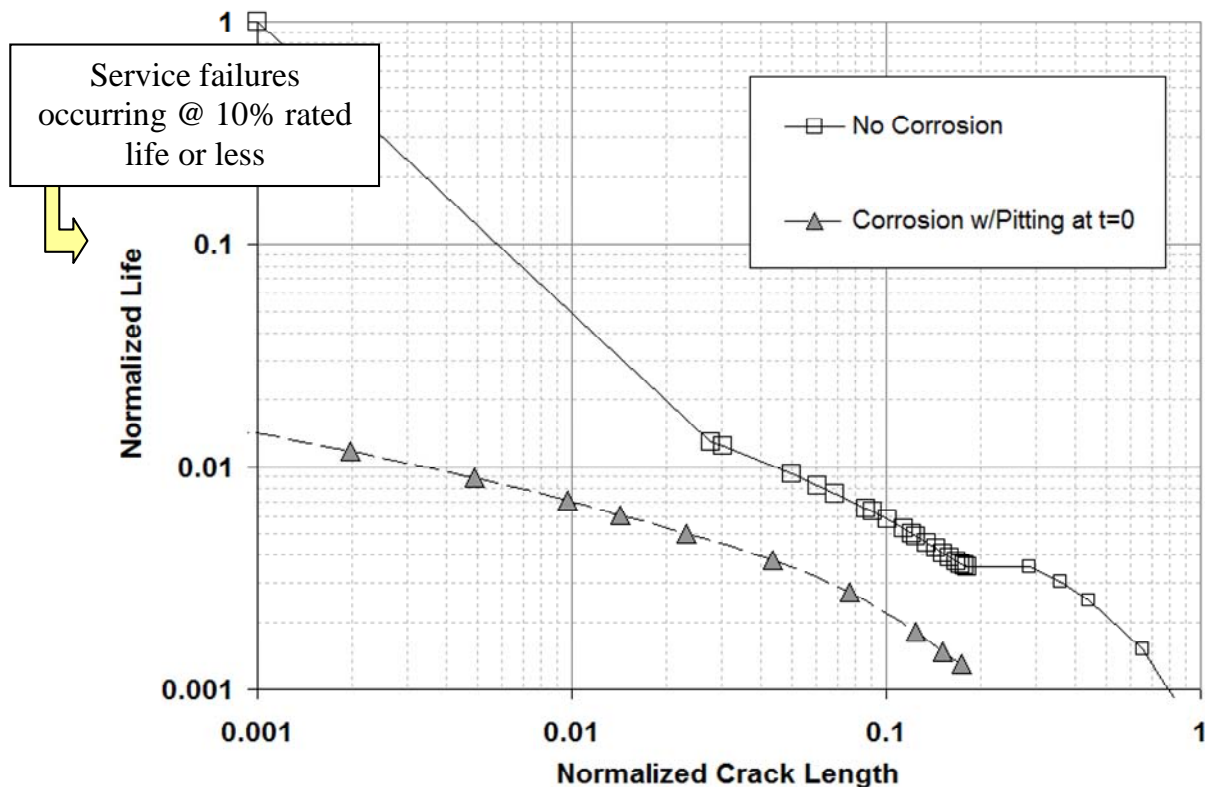


Figure 19-4: Plot of Normalized Life versus Normalized Crack Length for a Helicopter Main Rotor Component With and Without Corrosion Pitting.

Note that Figure 19-4 has been normalized where a life of “1” equals the rated safe life of the component. A crack size of “1” is equal to the critical crack size of the component.

19.3.1 Disposition

The results of these analyses, in conjunction with field experience, lead us to categorize the subject of this study as ‘corrosion-intolerant structure.’ Non-Destructive Testing (NDT) solutions were investigated, but the conclusion was that the component is so sensitive to corrosion that safety-by-inspection would simply result in a burdensome inspection frequency. While inspection is a plausible short-term solution for this type of component and situation, it is not feasible, both in terms of dollars and in terms of operational requirements, for long-term sustainment activities. Thus, more permanent and effective long-term solutions are required, such as a material substitution that exhibits greater fatigue resistance and greatly reduced susceptibility to pitting. Another promising alternative includes conducting a residual stress treatment, such as laser peening, to critical areas of the component, which when properly executed could make treated areas insensitive to violations of surface integrity caused by pitting and greatly enhance the life capability.

19.4 SUMMARY

This case study presented a holistic structural integrity analysis of a dynamically loaded helicopter component that failed due to corrosion-pitting fatigue. Fatigue analysis, including the effects of pits, suggested that in a worst case, life capability would be only 1.5% of the original certified ‘safe life’ if the pits were assumed to be present from time of manufacture. Failures in service were occurring at closer to

10% of the original certified life, which reflects the fact that the pitting occurred later during service and not at 'time zero'.

This component is best described as 'corrosion-intolerant-structure.' Furthermore, the frequency of maintenance and inspection required to keep the component safe would not only be burdensome but could also contribute to the problem through accidental breach of the coating system.

The recommended solutions to this problem include material substitution (to a material that is more fatigue and corrosion resistant) and/or treating the parts with engineered residual stresses, such as those possible through laser peening. As stated above, frequent inspection is not believed to be a supportable option, and simply replacing the components with new, original-specification parts only resets the clock. It does not eliminate the problem.

19.5 REFERENCES

- [1] Merati, A., Tsang, J., Khomusi, S., Kourline, A., Kyle, K. and Geusebroek, M., "Preliminary Report – Final Test Results for the Determination of Fatigue-Related Features of the Initial Discontinuity State (IDS) of 2024-T3 Aluminum Alloy", National Research Council-Canada Report LTR-SMPL-2002-0110, 2002.
- [2] Mills, T.B., Honeycutt, K.T., Brooks, C.L., Sharp, P.K., Loader, C. and Crawford, B., "Development and Demonstration of an Holistic Structural Integrity Process using the Initial Discontinuity State Concept for 7050-T7451 Aluminum", USAF ASIP Conference, Memphis, TN, USA, November 2004.
- [3] Mills, T.B., Honeycutt, K.T. and Brooks, C.L., "Demonstration of an Holistic Structural Integrity Process Using Corrosion/Fatigue Interactions from Laboratory Experiments and Field Experience", Proceedings, 6th International Aircraft Corrosion Workshop, Solomons, MD, USA, August 2004.



Chapter 20 – PREVENTION OF HYDROGEN EMBRITTLEMENT IN HIGH STRENGTH STEELS, WITH EMPHASIS ON RECONDITIONED AIRCRAFT COMPONENTS

R.J.H. Wanhill

National Aerospace Laboratory
Amsterdam
NETHERLANDS

S.A. Barter, S.P. Lynch and D.R. Gerrard

Defence Science and Technology Organization
Fishermans Bend, Victoria
AUSTRALIA

20.1 INTRODUCTION

Failures owing to Hydrogen Embrittlement (HE) (or hydrogen-assisted cracking) appear to be encountered more often in new components than in re-conditioned components. However, since only a small proportion of components are reconditioned, it is likely that hydrogen embrittlement failures are relatively more common for reconditioned components.

When new components fail by hydrogen embrittlement (usually after short times in service), this is mainly because the Original Equipment Manufacturers' (OEMs) specified procedures for finishing processes, such as electroplating and baking, have not been followed, resulting in significant hydrogen concentrations in the steel. On the other hand, during reconditioning it is more likely that the procedures have nominally been followed, but incorrectly, since they are more complex, involving cleaning, paint-stripping, plating removal, and restoration of worn areas, as well as re-applying the original corrosion or wear-resistant coatings. Reconditioning may also be carried out under less controlled conditions at maintenance facilities or in the field (perhaps by less specialised personnel) compared with the conditions specified by the OEMs for finishing new components.

The preceding (1985) AGARD Corrosion handbook [1] contains a chapter on hydrogen embrittlement, but not the possible problems arising from improper reconditioning. This previous chapter includes eight case histories, all with respect to cracking in high strength steel components. Seven cases were attributed to hydrogen pick-up during electroplating, and one to a surface gouge that may have occurred during re-installation of a used component.

In the present chapter the basic aspects of hydrogen embrittlement are summarised, followed by a review of the testing procedures used for assessing whether or not embrittlement is likely to be produced by finishing processes. Case histories are presented for failures involving hydrogen embrittlement owing to reconditioning of components, and also where there were concerns that embrittlement could have occurred or might occur. Several cases illustrate that improper reconditioning or reconditioning outside the normal standard conditions do not necessarily constitute a risk of hydrogen embrittlement occurring in service, although they do warrant assessment on a case-by-case basis.

Service experience, including some of the above-mentioned cases, and laboratory testing have demonstrated that hydrogen pick-up during electroplating of high strength steels is the main source or risk of hydrogen embrittlement in aircraft components when the corrosion protective scheme is adequate. However, failures of electroplated high strength steel components need not, of course, be due to hydrogen embrittlement, and can occur by Stress Corrosion Cracking (SCC), fatigue and corrosion fatigue, and combinations of these and other failure modes.

20.2 BASIC ASPECTS OF HE

20.2.1 Types of HE

There are five main types of HE in metallic materials, which are distinguished either according to the source of hydrogen or the mechanism of damage:

- 1) **Internal (Reversible) HE**, so called because it is due to the presence of solute hydrogen that can be removed by ‘baking’ at low-to-intermediate temperatures, but which otherwise diffuses to favoured sites (see Section 20.2.5) where weakening of interatomic bonds can lead to crack initiation and growth.
- 2) **Hydride-Induced Embrittlement**, which occurs in metals such as titanium, zirconium, vanadium and niobium, owing to the formation and fracture of brittle hydrides that precipitate when sufficiently high internal concentrations of hydrogen are present. Heat treatment can dissolve the hydrides and remove the resulting solute hydrogen.
- 3) **Hydrogen Environment Embrittlement**, where susceptible materials crack in the presence of external gaseous hydrogen or hydrogen sulphide.
- 4) **Internal Irreversible HE**, whereby solute hydrogen is present in such high concentrations that hydrogen gas precipitates at voids or inclusion/matrix interfaces. The resulting high gas pressures cause blistering or cracking.
- 5) **Hydrogen Attack (or Hydrogen-Reaction Embrittlement)**, whereby cracking or blistering occurs in environments containing hot hydrogen-bearing gases. The hydrogen diffuses into the metal to carbides or oxides and then produces high-pressure methane or steam.

The only type of major interest for aircraft components is Internal (reversible) HE (IHE) of high strength steels. Hydride-induced embrittlement has occasionally been observed for titanium and titanium alloy components as has IHE of specific $\alpha + \beta$ titanium alloys, but since these instances are rather rare they will not be further addressed here.

We note here that Stress Corrosion Cracking (SCC) in moist air or aqueous environments is treated as a separate phenomenon, although in many materials, including high strength steels, SCC involves hydrogen embrittlement due to hydrogen generated at crack tips.

20.2.2 Susceptibility of Materials to IHE

Structural materials with high strength are the most sensitive to IHE. The following lists groups of common aerospace materials according to their IHE susceptibility:

- 1) High and ultrahigh strength martensitic steels with yield strengths >1400 MPa (Rockwell C hardness > 38 HRC) are extremely susceptible to IHE, being embrittled by solute hydrogen concentrations as little as 1 ppm. Lower strength martensitic and ferritic steels are less susceptible and require higher hydrogen concentrations for embrittlement to occur. For martensitic steels there is a “step change” to much lower susceptibilities at yield strengths below about 1200 MPa (37 HRC) [2].
- 2) Titanium alloys with $\alpha + \beta$ microstructures are susceptible to IHE when solute hydrogen concentrations are $\geq 100 - 200$ ppm (with hydride formation not necessarily involved).
- 3) Nickel alloys, aluminium alloys, low strength ferritic steels, austenitic steels, and copper alloys, show little if any embrittlement from internal hydrogen; and if slight embrittlement does occur it is not of practical importance. Note: high strength nickel alloys are very susceptible to hydrogen environments (hot and/or high pressure gas). Such environments have caused problems with rocket motor components.

20.2.3 Important Variables for IHE

Besides steel strength and hydrogen content, already mentioned in Section 20.2.2, other important variables are:

- 1) Applied stress, stress gradients, strain-rate, stress states (plane strain or plane stress) and stress modes:
 - High triaxial stresses, which occur ahead of sharp notches under plane strain mode I (tensile) loading, are especially detrimental when the loading is sustained or takes place under slow-strain-rate conditions, see Section 20.4.
 - Tensile residual stresses, e.g., produced by abusive grinding, would obviously also be detrimental.
- 2) Temperature – maximum embrittlement usually occurs at about 20°C for high strength steels. At lower temperatures the cracking rates are reduced by lower hydrogen diffusion rates, while at higher temperatures the hydrogen adsorption kinetics decrease.
- 3) Steel composition – the presence of large inclusions and the segregation of metalloid impurities to grain boundaries is especially detrimental.

20.2.4 Sources of Internal Hydrogen

The main sources of solute hydrogen in high strength steel aircraft components are the finishing or reconditioning solutions used to clean and apply protective coatings, such as:

- 1) Electroplating solutions.
- 2) Pickling solutions.
- 3) Phosphating solutions.
- 4) Some paint-stripping solutions.
- 5) Cathodic cleaning solutions.

Corrosion of sacrificial coatings, such as cadmium, or corrosion pitting during service can also generate hydrogen, especially if the coatings are porous.

In other industries hydrogen can be introduced by:

- 1) Welding (or melting/casting the original material) in moist atmospheres or with moisture in rust, fluxes, paints or hydrocarbon contaminants.
- 2) Heat treatment in hydrogen-bearing atmospheres.
- 3) Cathodic over-protection using anodes or impressed current devices for corrosion protection.

20.2.5 Sites and Traps for Hydrogen in Steels

Solute hydrogen in steels occupies and diffuses between octahedral interstitial sites, and can be ‘trapped’ to varying degrees at other sites, viz:

- 1) Dislocation cores and dislocation strain fields.
- 2) Prior austenite and martensite-lath boundaries.
- 3) Carbide- and inclusion-matrix interfaces.
- 4) Internal voids and vacancy clusters.
- 5) Voids at interfaces between coatings and steel surfaces.

Hydrogen diffuses to and concentrates in regions of high triaxial stress because crystal lattice and hence interstitial sites are slightly expanded by such stresses. Prior austenite and lath boundaries in triaxially stressed regions are favoured crack paths since they are planar and interconnected. Cracking usually occurs preferentially along prior austenite grain boundaries because they are weakened by metalloid impurity segregation in addition to hydrogen.

Figure 20-1 illustrates a number of sites and traps. The traps do not bind the hydrogen permanently, but significantly retard its diffusion, notably at low temperatures. As mentioned in Section 20.2.1, solute hydrogen can be removed by ‘baking’ at low-to-intermediate temperatures. This is why IHE is called reversible, i.e., hydrogen can diffuse both into and out of the steel.

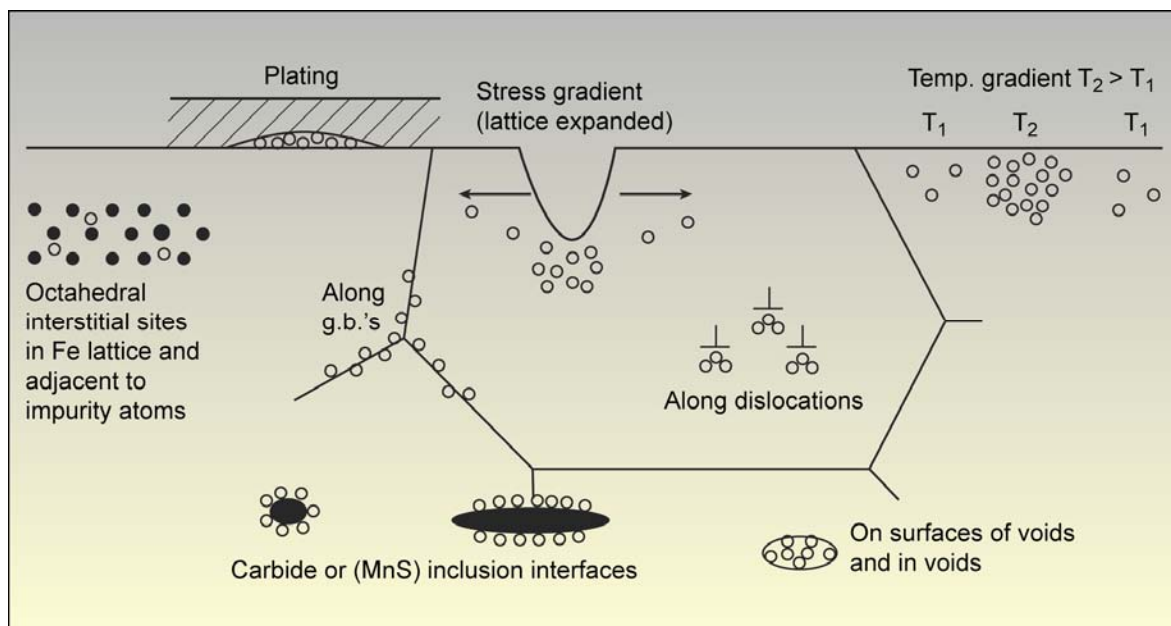


Figure 20-1: Sites and Traps for Hydrogen, Especially in Steels.

20.2.6 IHE and Hydrogen Diffusivity

Although IHE is reversible, hydrogen diffusion in steel is very variable. Measurements of the hydrogen diffusion coefficient, D , in steels shows that it depends on [3],[4]:

- 1) Strength level – D is much lower in high strength steel than in annealed steel.
- 2) Cold work – can cause large reductions in D measured during outgassing.
- 3) Temperature range – at about 200°C a break occurs in the Arrhenius plot of $\log D$ versus the reciprocal of the temperature, $1/T$, separating a low temperature region with low D values and large activation energy from a high temperature region with high D values and small activation energy.
- 4) Hydrogen diffusion into or out of the steel – D tends to be less during outward diffusion.

These phenomena are attributed to the varying degrees of trapping at different sites.

20.2.7 Minimising Hydrogen Contents

Hydrogen pick-up during electroplating can be minimised by using special conditions and solution formulations. For pickling and phosphate coating, inhibitors and depolarizers, respectively, can be added

to solutions to minimise hydrogen entry. Selecting a solution for paint-stripping should ensure that the electrode potential of the steel (or steel-plating combination) in the solution lies in the ‘water-stable’ region of the Pourbaix (E – pH) diagram (and preferably well above the $\text{H}_2\text{O} + \text{e}^- \rightarrow \text{H}_{\text{ads}} + \text{OH}^-$ line). This will minimise or prevent hydrogen ingress. This topic is of major importance in case history 20.5.4, discussed later in this chapter.

Even when hydrogen pick-up is minimised during surface finishing, removing hydrogen that has diffused into steels by subsequent baking at low temperatures ($< 205^\circ\text{C}$) is generally specified. Recommended baking times and temperatures depend on the finishing process and, for electroplated components, also on:

- 1) The type, thickness, and porosity of the plate.
- 2) The strength of the steel.
- 3) Whether components are sharply notched (or threaded), notably bolts and other fasteners.

Examples of recommended times and temperatures are:

- 1) For porous cadmium-plated high strength steels: from 23 up to 40 hours at 190°C .
- 2) For nickel- and chromium-plated steels: from 3 up to 12 hours at 190°C .
- 3) For pickled and cathodically cleaned steels: 3 to 4 hours at $175 - 205^\circ\text{C}$.

Baking specifications also indicate that it should be done as soon as possible after plating (typically 4 hours), since excessive delays (> 16 hours) between plating and baking can cause irreversible embrittlement (cracking), e.g., in ultrahigh strength 4340 steel with a tensile strength range of 260 – 280 ksi (1790 – 1930 MPa). Note also that baking at low temperatures can remove hydrogen only from interstitial sites and weak traps such as dislocations and grain boundaries. Hydrogen remaining in deep trap sites such as voids at inclusion-matrix interfaces and between steel surfaces and plating, see Figure 20-1, can diffuse into the steel when sustained tensile stresses are applied, thereby causing some embrittlement.

For some ultrahigh strength steel aircraft components electroplating is replaced by vapour deposition. The coatings are applied by evaporation of the coating species and deposition in low pressure inert gas, both with and without an applied potential. The coating species are typically cadmium or aluminium, and in both cases there is no hydrogen pick-up, although chemical cleaning procedures used prior to such processes may be a source of hydrogen pick-up.

20.2.8 Characteristics of IHE Cracking

As already mentioned, IHE cracks usually occur along prior austenite grain boundaries of high strength martensitic steels. This is evident from metallographic cross-sections, e.g., Figure 20-2.

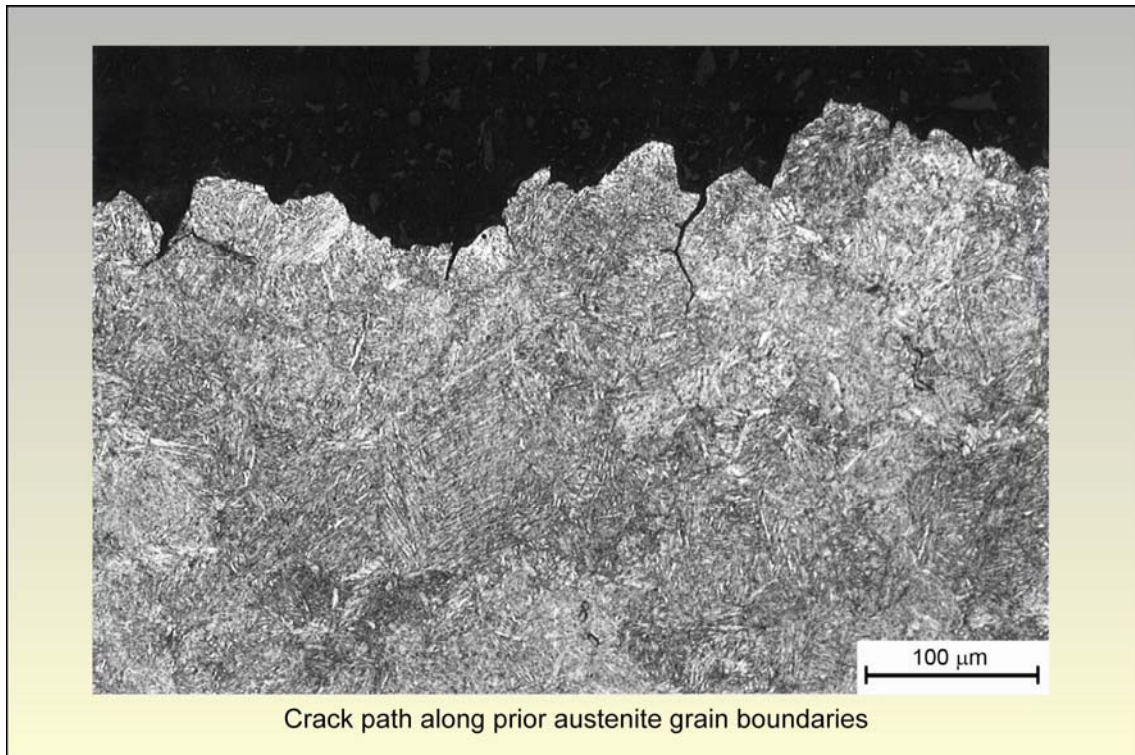


Figure 20-2: Characteristics of Internal Hydrogen Embrittlement (IHE) in High Strength Steels – I.

Figure 20-3 gives examples of IHE fracture surfaces. Using stereobinoculars (at 100 – 200 ×) the fracture surfaces generally show a bright faceted appearance, unless corroded after fracture. Scanning Electron Microscope (SEM) fractography shows intergranular facets that are generally smooth except for isolated tear ridges and dimples. Some transgranular cracking can occur and, in modern, very tough ultrahigh strength steels with low metalloids impurity contents, cracking can be completely transgranular [5].

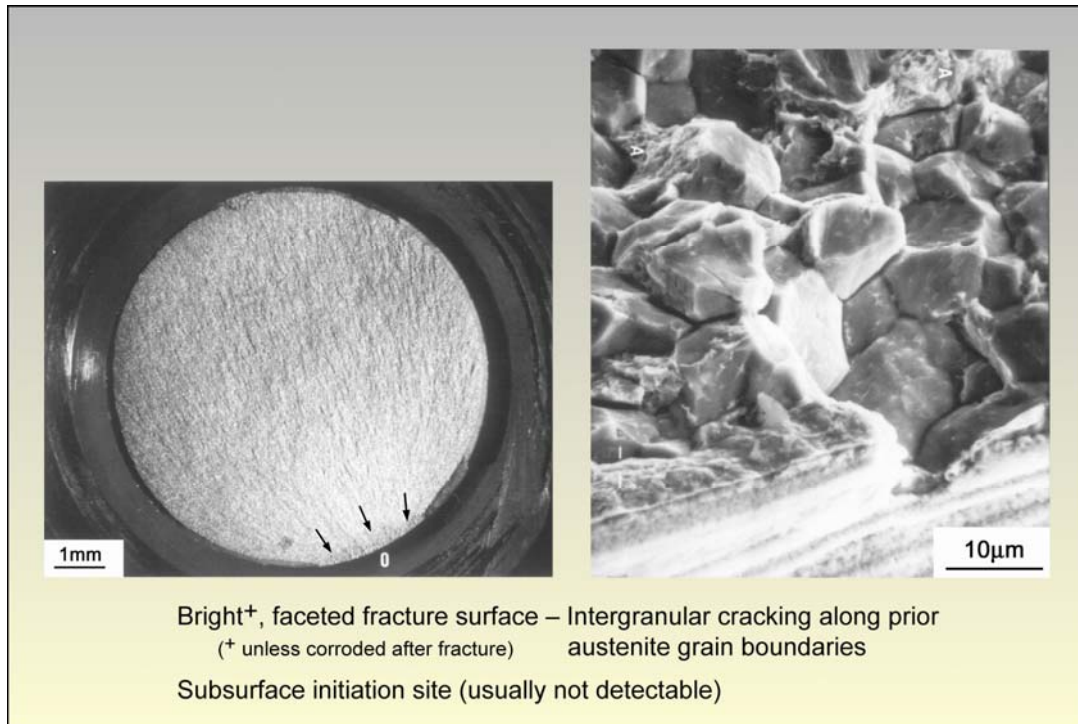


Figure 20-3: Characteristics of Internal Hydrogen Embrittlement (IHE) in High Strength Steels – II.

20.3 DISTINGUISHING IHE FROM OTHER INTERGRANULAR FRACTURE MODES

Other fracture modes that can produce cracking along prior austenite grain boundaries in high strength steels include:

- 1) Overload (fast) fracture in temper-embrittled steels.
- 2) Stress Corrosion Cracking (SCC).
- 3) Corrosion Fatigue (CF).
- 4) Liquid-Metal Embrittlement (LME).
- 5) Solid-Metal Induced Embrittlement (SMIE).
- 6) Quench Cracking.

Failures can sometimes involve several of these fracture modes, e.g., sub-critical cracking by intergranular IHE followed by intergranular overload fracture. Distinguishing between these fracture modes can be difficult, but some guidelines are:

- IHE fractures are generally bright and uncorroded, as mentioned in Section 20.2.8, but corrosion can sometimes occur after cracking. For completely fractured parts, exposure to high humidity air or aqueous environments can cause rusting (reddish hydrated ferric oxides). If components are only partly cracked by IHE, exposure of cracks to aqueous environments could produce black (magnetite) oxide films on crack surfaces.
- SCC and CF fractures produced in aqueous environments are usually covered by black oxide films or occasionally show interference colours (due to very thin oxide films produced in oxygen-depleted solutions within cracks): a probable CF fracture is shown in case history 20.5.3 later in

this chapter. However, SCC of ultrahigh strength steels can occur in moist air environments and the fracture surfaces may be bright and relatively uncorroded, closely resembling those produced by IHE.

- CF sometimes results in faint progression markings or striations on intergranular facets, but corrosion products may often obscure these details.
- SCC and CF often initiate from corrosion pits, whereas IHE initiates just beneath surfaces. However, IHE initiation in high strength steels may be so close to the surface that it appears to have begun there.
- LME usually results in thick films of the embrittling metal on fracture surfaces and within secondary cracks. These films are readily observed.
- SMIE results in thin films of the embrittling metal on fracture surfaces, but these films may not be obvious.

Examples of failures by these various modes, and more detailed discussion distinguishing between intergranular fracture modes can be found elsewhere [6]. Be that as it may, it should be evident from the foregoing discussion that much care and expertise are required when interpreting the fractographic evidence from a high strength steel component suspected to have failed by IHE.

20.4 TESTING PROCEDURES FOR ASSESSING THE DEGREE OF IHE

The OEMs usually specify that each batch of high strength steel components to be electroplated (mainly by cadmium) be accompanied by notched tensile specimens of the same material. These specimens are subsequently proof tested to verify that the components have been correctly processed. However, successful proof testing of specimens is not necessarily a guarantee that the batch of components has not been damaged by IHE, see Section 20.4.4.

The commonly accepted proof testing standard for IHE is ASTM F 519-06 [7]. In the first instance this standard is intended only for one type of high strength steel, see Section 20.4.1. There is also an ASTM standard to measure the threshold stresses and stress intensity factors for IHE in any high strength steel [8]. This standard is more of an R&D tool, though it could be used for proof testing, and is referred to in ASTM F 519-06, see Section 20.4.1. In addition, there is a military aircraft proof testing standard, NASM1312-5 [9], for externally-threaded fasteners made from any material, see Section 20.4.2.

There is also a test method based on slow Strain Rate Dynamic Tensile (SSRT) testing of ASTM F 519-06 tensile-type specimens. This test method is discussed in Section 20.4.6, and has shown promise as a relatively rapid way of assessing IHE. Two examples of the use of SSRT testing are given in case histories 20.5.5 and 20.5.6.

20.4.1 ASTM Standard Test Method F 519-06

This test method has been developed specifically to evaluate plating processes and service environments¹ with respect to their potential for hydrogen embrittlement of AISI 4340 steel with a tensile strength range of 260 – 280 ksi (1790 – 1930 MPa) corresponding to Rockwell C hardnesses of 51 – 53 HRC.

20.4.1.1 Evaluating Plating Process IHE

Three types of tests are specified for the plated and baked AISI 4340 steel:

¹ Defined as chemicals that contact bare or plated/coated steel components during manufacturing, overhaul and service life.

- 1) **Sustained Load Tests (SLT), Notched Specimens:** These must exceed 200 hours at a sustained load of 75% of the notched fracture stress.
- 2) **Sustained Load Tests (SLT), Smooth Ring Specimens:** These must exceed 200 hours at a sustained load of 92% of the tensile ultimate strength.
- 3) **Incremental Step-Load (ISL) Tests:** An accelerated incrementally increasing step-load test may be used as an alternative to SLT, if approved by the appropriate engineering authority, see Section 20.4.5.

20.4.1.2 Evaluating Service Environment IHE

These tests are for bare or plated/coated AISI 4340 steel. Different types of tests are specified for aggressive chemicals (e.g., temper etchants) or passive chemicals (cleaners and paint strippers):

- 1) **Aggressive Chemicals** – Notched and smooth specimens are immersed at 45% of the notched fracture stress for the exposure time of the relevant service specification. Then the specimens and test fixtures are neutralized per the relevant service specification, rinsed and dried. The load is then increased to 75% of the notched fracture strength for notched specimens and 92% of the tensile ultimate strength for smooth specimens. The environment is considered non-embrittling if no failures occur within 200 hours.
- 2) **Passive Chemicals** – Notched specimens are immersed at 45% or 65% of the notched fracture stress, depending on specimen type, for 150 hours. Smooth specimens are immersed at 80% of the 0.2% yield strength for 150 hours. A passive environment is considered non-embrittling if no failures occur within 150 hours.

20.4.2 National Aerospace Standard NASM1312-5

This test method applies to all types of externally threaded fasteners, made from any material, and which may be subject to any type of embrittlement. The fasteners to be tested are assembled in “test units”, which are custom-made fixtures. Loading may be applied in several ways, provided that the induced load on the fastener is 75 – 80 % of the *minimum* ultimate tensile strength [notched fracture stress] of the fastener. The loads are applied at room temperature and maintained for the time specified by the procurement document or product specification.

For evaluating IHE of high strength steels the test duration will most probably be 200 hours, as per ASTM F 519-06. There is an important reason for this, discussed in Section 20.4.3.

20.4.3 Proof Test Duration: The “No Failure in 200 Hours” Criterion

For verifying correct processing to avoid IHE, ASTM Standard F 519-06 specifies that high strength steel specimens should not fail within 200 hours at a sustained load of 75% of the notched fracture stress after plating and baking or exposure to aggressive service environments. The “no failure in 200 hours” criterion was obtained from the classic work of Troiano [10]. Figure 20-4 shows Troiano’s data for delayed failure of sharp-notched specimens of high strength AISI 4340 steel after cadmium plating and baking for various times. There are two main points to note here:

- 1) There is obviously a strong effect of baking time on the plateau failure stress level, called by Troiano the static fatigue limit.
- 2) 75% of the notched fracture stress corresponds to an applied stress of 225 ksi. From Figure 20-4 and the shapes of the delayed failure curves it may be deduced that unless baking has been done for the usual standard time of 24 hours, failure at this stress level should occur well within 200 hours.

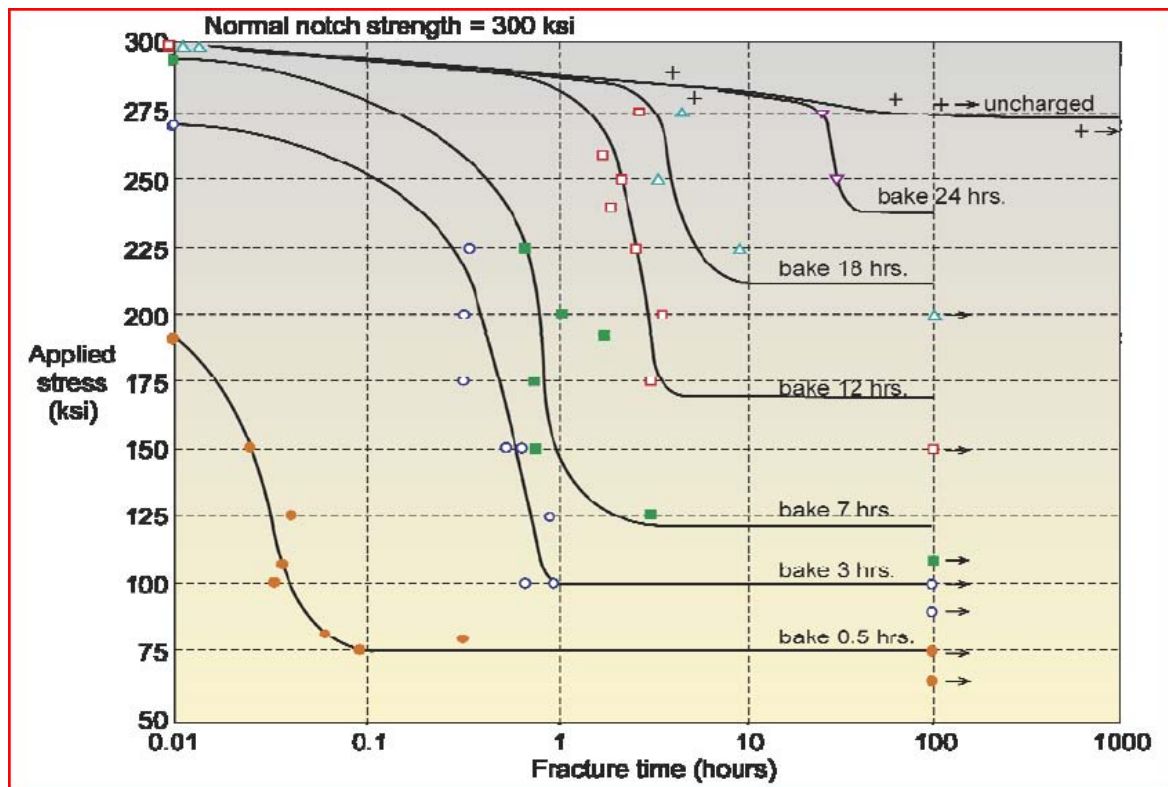


Figure 20-4: Delayed Failure Curves for Cadmium-Plated AISI 4340 Steel Containing Various Hydrogen Concentrations Corresponding to Different Baking Times at 300°F (149°C) (Notched specimens were used at the 230 ksi (1586 MPa) tensile strength level [10]).

It follows that whichever testing standard is used, ASTM F 519-06 or NASM1312-5, the evaluation of IHE for high strength steels will generally require specimens to survive 200 hours of sustained loading at a minimum of 75% of the notched fracture stress. The testing time requirement can or could be relaxed to 150 hours for specimens immersed in passive service environments. However, see conclusion (2) from case history 20.5.4.

20.4.4 Problems Not Covered by Proof Testing

As noted in Section 20.2, and as can be seen from Figure 20-4, the applied stress is a very important consideration when assessing the probability of cracking due to IHE. This is also true of residual stresses. If components containing high residual stresses are electroplated, then hydrogen pick-up may cause cracking almost immediately. Extensive tensile residual stresses can result in complete failure, which will obviously be noticed, resulting in corrective actions for similar components.

However, if tensile residual stresses are highly localised, e.g., due to local manufacturing errors such as abusive grinding and machining or cold forming without stress relief, then only local IHE cracking may occur. This local cracking will be covered by the plating, and although subsequent baking may prevent further IHE, the cracks may lead to other types of failure in service, most notably fatigue cracking. An example of this type of problem is given in case history 20.5.2.

Manufacturing errors that result in local residual tensile stresses are made all the more insidious by the inability of proof test specimens plated together with the service components to replicate this damage. Proof test specimens will typically not undergo the same manufacturing processes as service components, or may be made in batches independent of them.

Some of the above points may be equally applicable to the two tests described in the following sections (20.4.5 and 20.4.6).

20.4.5 Incremental Step Load (ISL) Tests

Incremental Step Load (ISL) testing is an accelerated test method designed to measure the IHE threshold stress within one week. The tests are standard dynamic tests specified in ASTM Standard F1624-06 [8]. This standard uses fracture mechanics specimens (similar to some of the types proposed in ASTM F519-06) loaded either in tension or four-point bending. The specimens may be manufactured from various steels being assessed for IHE.

The recommended loading procedure consists of 15 steps of 5% notched fracture stress per hour up to 75% of the notched fracture stress, and then steps of 5% notched fracture stress per 2 hours until failure. The threshold stress for IHE is determined by monitoring the loads during the hold times between load increments: if the applied load decreases during a hold period, then cracking is assumed to have occurred, and the load initially applied during this hold period is assumed to correspond to the threshold stress.

Notes:

- 1) Several tests are required to establish the maximum unembrittled fracture load for the specimen geometry being ISL-tested.
- 2) Although there is no established equivalence between the ISL and SLT test methods, it is assumed that ISL-tested specimens that sustain 90% of the notched fracture stress for 2 hours can be considered unembrittled.

Besides the above-recommended loading procedure, ASTM F1624-06 suggests a number of alternative loading protocols. These can have durations varying from 8 to 90 hours. Furthermore, the ISL test method allows flexibility in:

- a) Choosing the most appropriate number of steps and hold times; and
- b) Deciding what is a sufficient number of tests to determine the threshold stress.

The very flexibility of this test method could detract from confidence in using it, but it is nevertheless capable of giving excellent results.

20.4.6 Slow Strain Rate Tensile (SSRT) Tests

The Slow Strain Rate Tensile (SSRT) test method differs from ISL testing in three important respects:

- 1) Loading is continuous.
- 2) Only round bar notched tensile SAE E4340 specimens are used. These are similar in design to those in ASTM Standard F519-06. The steel is heat-treated to the 260 – 280 ksi level (1790 – 1930 MPa).
- 3) The cross-head displacement rate is much less than that during step loading in ISL tests. The very low displacement rate allows sufficient time for the *continuous* migration of absorbed atomic hydrogen to the triaxial stress field ahead of the notch, rather than only during the hold times in ISL tests.

Figure 20-5 shows some SSRT test rigs and the specimen configuration. The SSRT tests are carried out to failure of the specimens and provide the notched tensile strengths or fracture stresses. These data are then compared with those of identical specimens known to be unembrittled. In addition, SEM fractography

may be used to detect any brittle fractures characteristic of IHE. This test method was initially developed by Pollock [11]. He found that at cross-head displacement rates less than 2×10^{-4} mm/s the effect of IHE could be repeatedly and accurately measured and observed [11],[12].



Figure 20-5: Slow Strain Rate Tensile (SSRT) Test Rigs and Example Test Specimen.

Reductions in the SSRT fracture stress are considered to be quantitative measures of the degree of IHE. The SAE E4340 steel specimens show a reduction in notched fracture stress for even the slightest amount of IHE. Furthermore, an SSRT test can take only about 24 hours, not as quick as some ISL tests, but still much shorter than the 200 hour SLT tests.

Correlation between SSRT and SLT data has been determined [13]. This was done by cadmium electroplating notched tensile specimens of SAE E4340 steel in an embrittling solution, followed by baking groups of specimens for differing times (0 – 13 hours) at 50°C. (Thirteen hours baking was known to be sufficient to eliminate IHE.) Figure 20-6 compares the SSRT and SLT data. It is seen that the baking time for the 200 hour pass in an SLT corresponds to a notched fracture stress of about 1900 MPa for the SSRT tests.

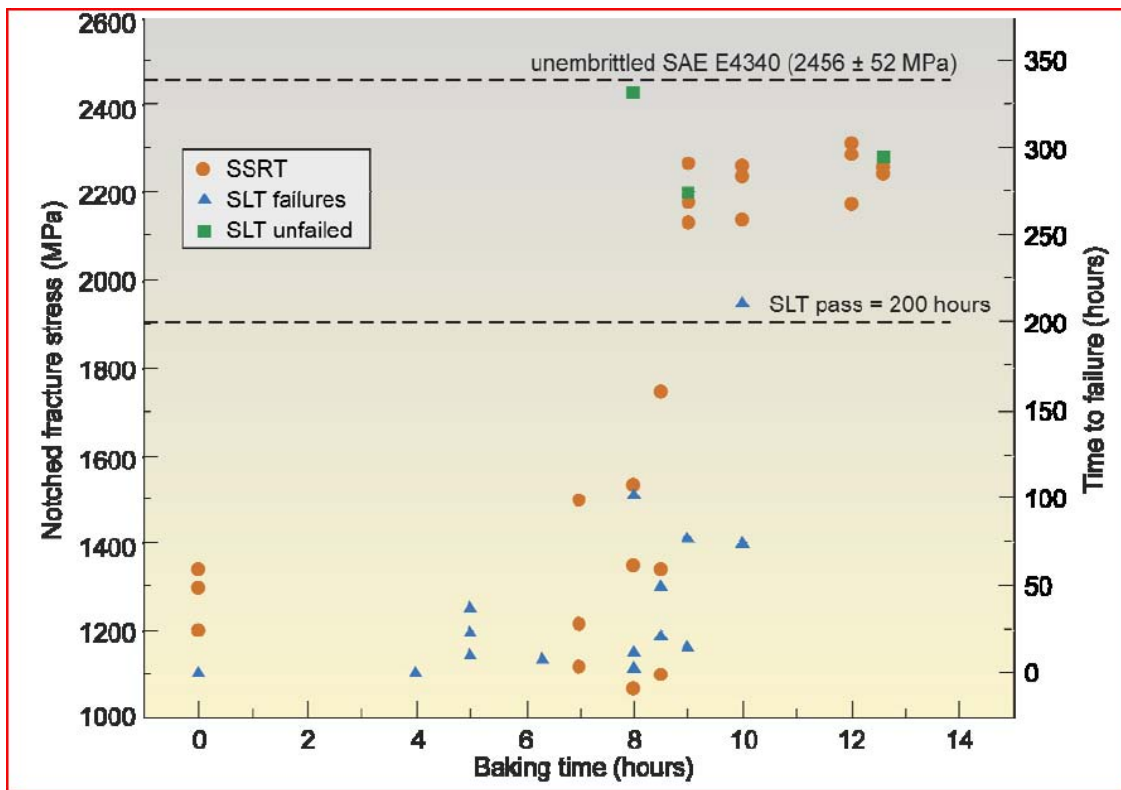


Figure 20-6: Comparison of SSRT and Sustained Load Test (SLT) Notched Fracture Stress Data for SAE E4340 Steel Specimens Cadmium Plated and Baked at 50°C for 0 – 13 Hours [13].

As a result of these tests, and taking into account the SLT acceptance criterion of 75% of the notched fracture stress in ASTM F519-06 and previous work by Pollock [11], an acceptance criterion of 1840 MPa for the SSRT notched fracture stress was proposed [13].

20.5 CASE HISTORIES: RECONDITIONED COMPONENTS

The following case histories have been selected as particularly illustrative. Case histories 20.5.1 and 20.5.2 identify IHE as the cause of cracking, but for different reasons. Case history 20.5.3 describes cracking initially suspected to be IHE, but was probably corrosion fatigue; and case histories 20.5.4 and 20.5.5 concern a perceived risk of IHE. Finally, “case history” 20.5.6 describes the development of an electroplating method that may be used *in situ* on IHE-susceptible steel and *without a baking treatment*.

Inclusion of case histories 20.5.3, 20.5.4 and 20.5.5 shows how the possibility of IHE can cause unfounded and drastic reactions that result in the wrong actions being taken. Such reactions, especially from OEMs, are understandable because IHE has resulted in catastrophic failures. On the other hand, improved knowledge about why IHE occurs, and why it may not – or will not – occur, should allow the most appropriate actions to be taken for continued operation of an aircraft fleet. Case history 20.5.6 illustrates this point very well.

20.5.1 Propeller Blade Retaining Bolts

20.5.1.1 Introduction

During the stripping of a turboprop propeller assembly at an overhaul facility, one of the four blade-retaining bolts was found to be severely cracked. Checks and information provided by the overhaul

contractor showed that this bolt was one of a batch of eight that had been previously overhauled at the same time. All eight bolts, one cracked and seven uncracked, were investigated at the Defence Science and Technology Organisation² in Melbourne, Australia. This investigation [14] comprised the following steps:

- 1) Optical examination for corrosion and mechanical damage.
- 2) Optical and Scanning Electron Microscope (SEM) fractography of the cracked bolt.
- 3) Microstructure, hardness and chemical composition of the bolt material.
- 4) Auger Electron Spectroscopy (AES) of a fresh fracture surface from a test specimen.
- 5) Slow Strain Rate Tensile (SSRT) tests and subsequent hydrogen analysis.

The bolts were specified to have been made from S99 low alloy steel heat-treated to a tensile strength of about 1380 MPa.

20.5.1.2 Investigation

20.5.1.2.1 Optical Examination for Corrosion and Mechanical Damage

All eight bolts had been bright-cadmium electroplated. There was some service-induced tarnishing of the cadmium layer, light mechanical damage to the contact areas in the threads, and rubbing damage to the bearing areas under the bolt heads. None of the mechanically damaged areas was devoid of cadmium, and consequently there was no corrosion of the steel in these areas.

20.5.1.2.2 Optical and SEM Fractography of the Cracked Bolt

Figure 20-7 shows the extent of cracking of the bolt. The crack was broken open and the fracture surfaces were examined.

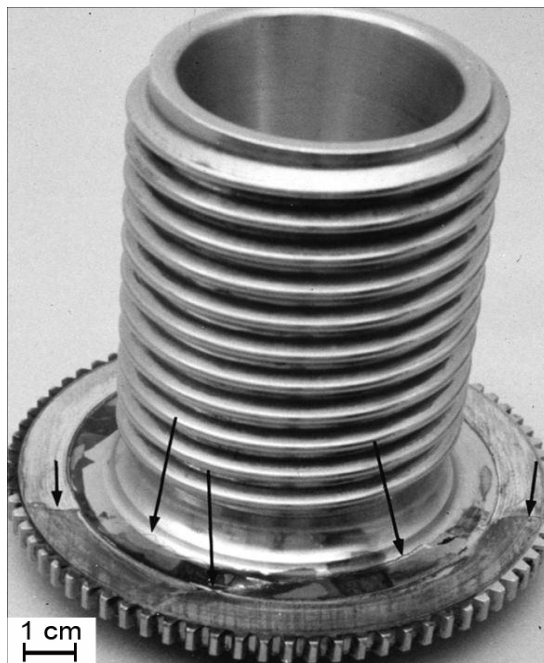


Figure 20-7: Case History 20.5.1 – The Cracked Blade-Retaining Bolt (the arrows point to the crack).

² Formerly the Aeronautical Research Laboratory (ARL).

Figure 20-8 shows the main part of the broken-open bolt. The main crack (A) initiated at O, and the two adjacent cracks (B and C) initiated at points P and Q, respectively. Note the two progression marks (arrowed) on the fracture surface of crack A. These marks are due to locally higher roughness, and may signify peak loads that occurred during service.

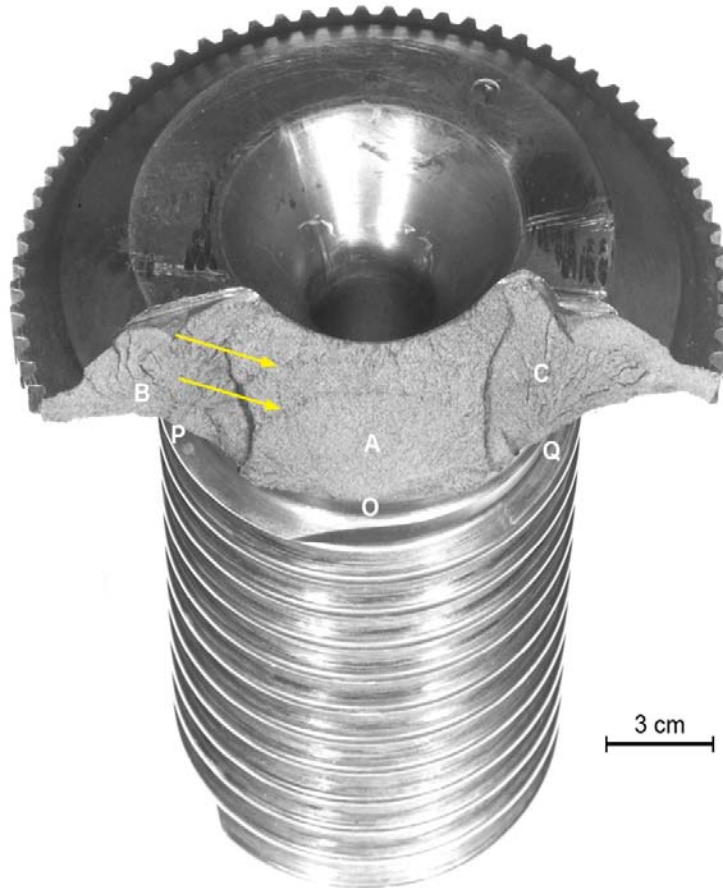


Figure 20-8: Case History 20.5.1 – Fracture Surface of the Blade-Retaining Bolt (the main crack (A) initiated at O, and the two adjacent cracks (B and C) initiated at points P and Q, respectively – note the two progression marks (arrowed)).

Optical examination showed that the three crack initiation sites O, P and Q had their origins at small pits near the radius run-out under the bolt head. The pits were surrounded by semi-circular regions having a black-brown colour. Apart from these regions, whose greatest depth was about 250 μm , most of the fracture surface was clean.

SEM fractography showed mainly clean intergranular fracture typical of IHE, e.g., Figure 20-9. However, examination of crack initiation site O showed not just the pit at the origin, Figure 20-10, but also deposits on intergranular fracture in the semi-circular region surrounding the pit, see Figure 20-11. Energy Dispersive Analysis of X-rays (EDAX) indicated that these deposits were rich in cadmium. Intergranular fractures similarly contaminated with cadmium were present in the semi-circular regions surrounding the pits at the crack initiation sites P and Q. This cadmium contamination suggests that all three semi-circular regions had been present before the last plating operation, most probably owing to IHE from the previous plating operation.

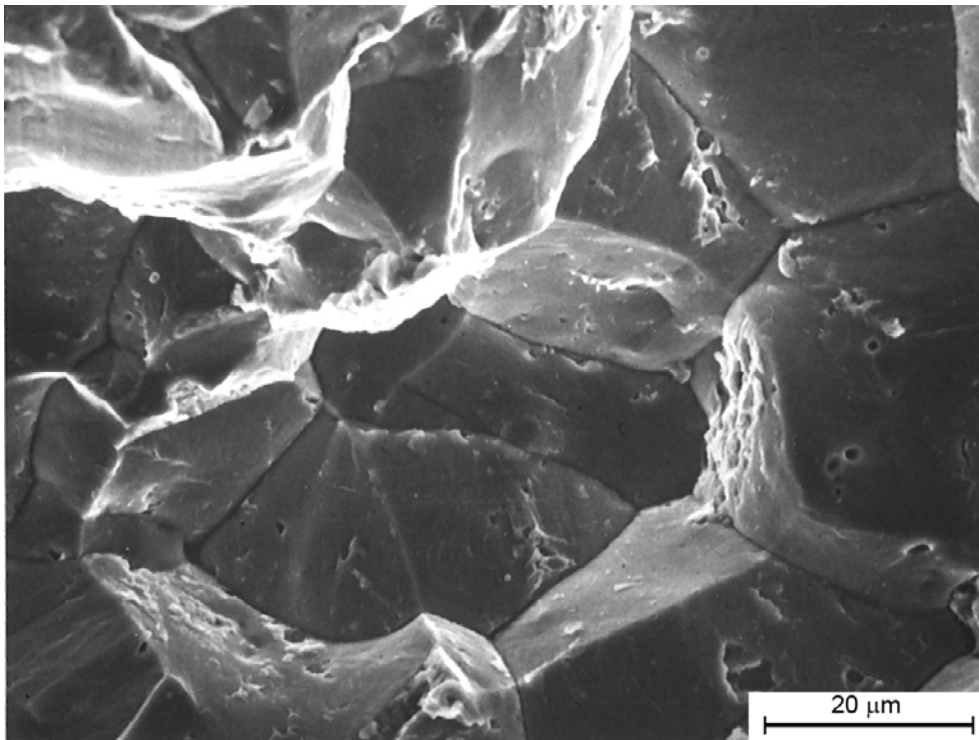


Figure 20-9: Case History 20.5.1 – Example of Clean Intergranular Fracture.

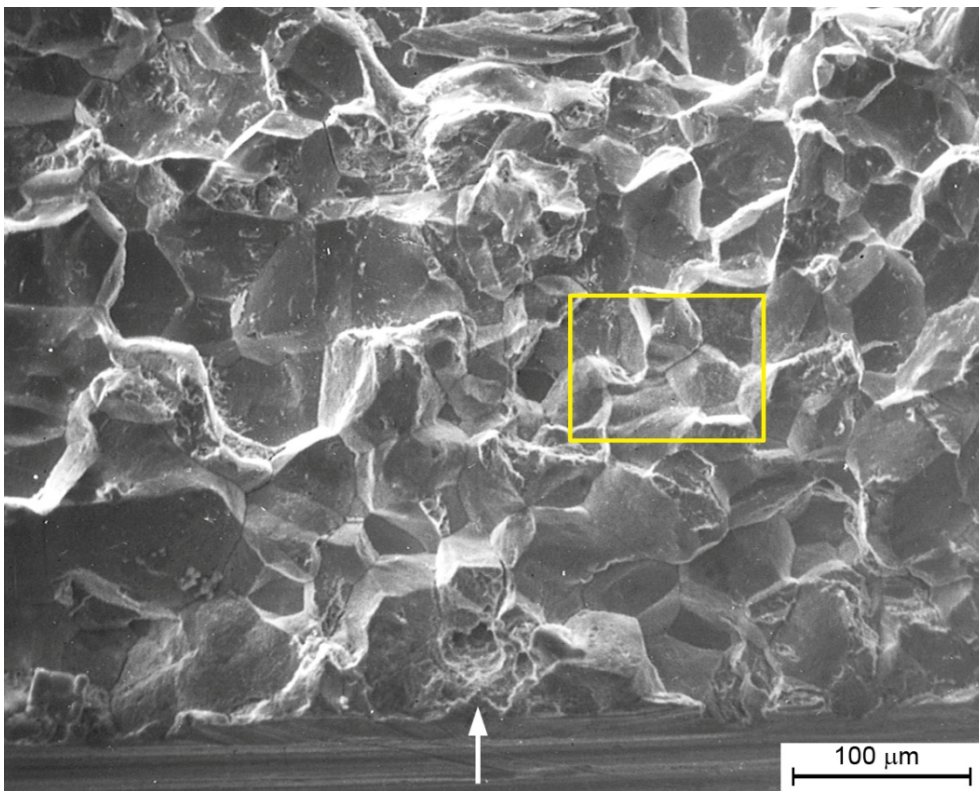


Figure 20-10: Case History 20.5.1 – Overview of Initiation Site O (the arrow points to the pit at the origin – the framed area is shown in more detail in Figure 20-11).

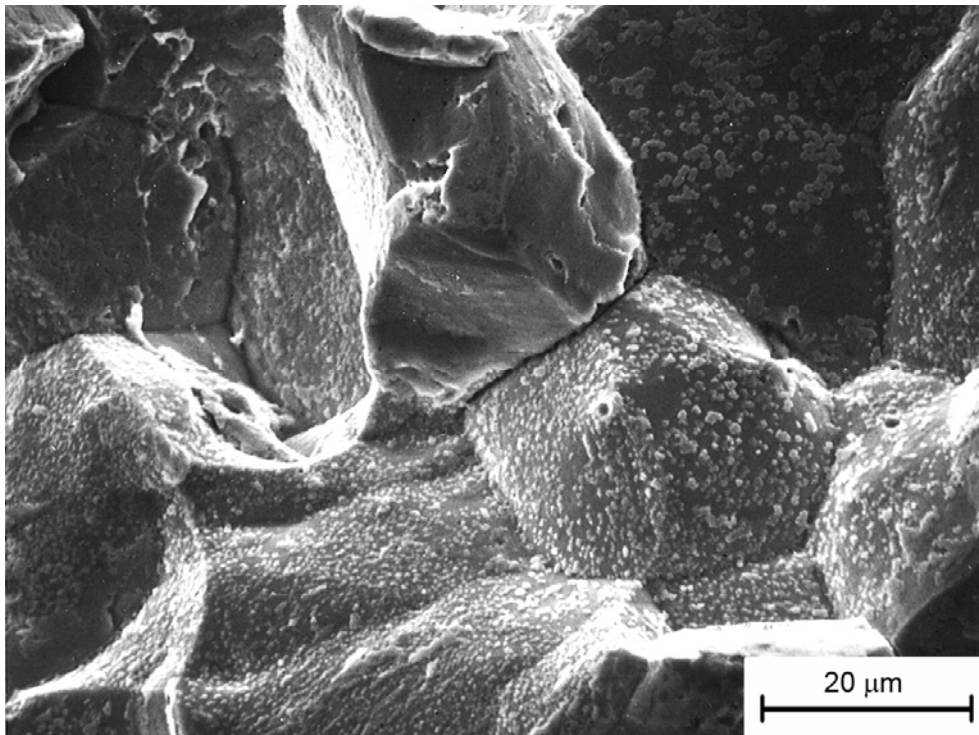


Figure 20-11: Case History 20.5.1 – Detail from Figure 20-10 Showing Deposits on the Intergranular Fracture (EDAX indicated that these deposits were cadmium-rich).

20.5.1.2.3 *Microstructure, Hardness and Chemical Composition*

Metallography showed that the cracked bolt had a tempered martensite structure, Figure 20-12, and that cracking occurred along prior austenite grain boundaries. There was slight banding (alloy segregation) containing small non-metallic inclusions. Rockwell C hardness tests on sections from the cracked bolt and three others from the same propeller assembly gave very consistent results of 42 – 45 HRC.

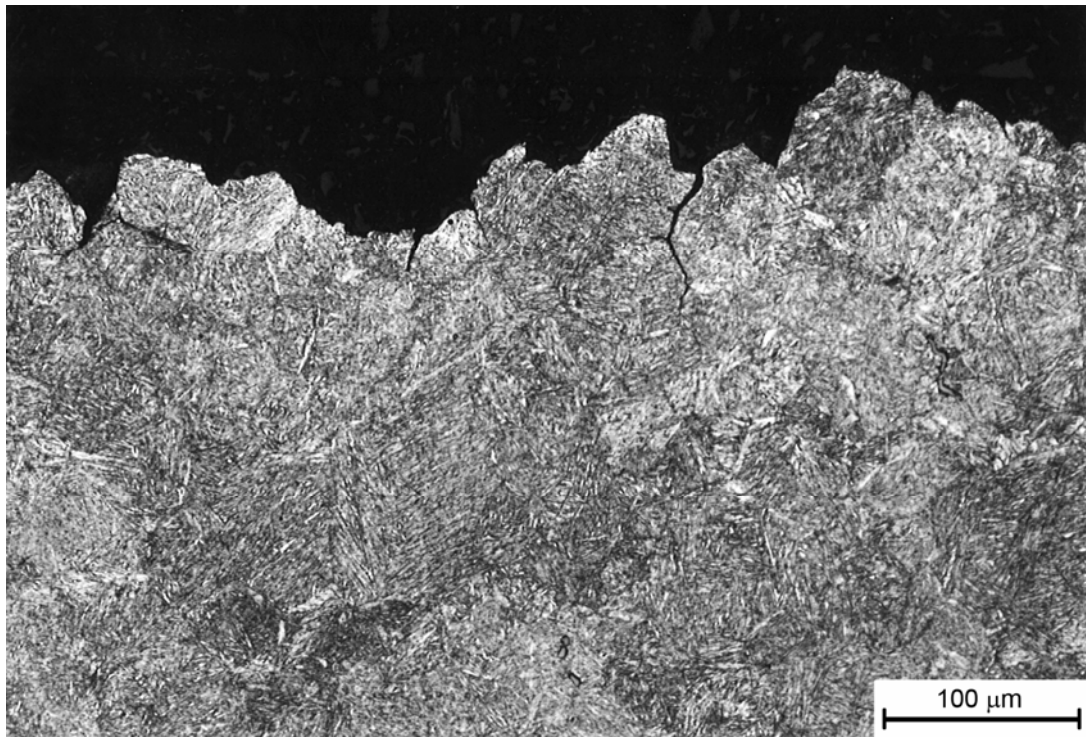


Figure 20-12: Case History 20.5.1 – Nital-Etched Metallographic Section Through Crack A (see Figure 20-8), Showing Tempered Martensite and the Intergranular Crack Path, Including Crack Branching.

Chemical analysis of the cracked bolt and another from the same propeller assembly gave the results in Table 20-1. Both bolts met the specified composition.

Table 20-1: Bolt Elemental Compositions in wt. %.

Element	C	Ni	Cr	Mn	Mo	S	P
Specification	0.36 – 0.44	2.3 – 2.8	0.5 – 0.8	0.5 – 0.7	0.45 – 0.75	0.02 max	0.02 max
Cracked Bolt	0.4	2.55	0.76	0.59	0.49	0.02	0.02
Intact Bolt	0.4	2.55	0.70	0.60	0.44	0.01	0.02

20.5.1.2.4 AES Grain Boundary Analysis

A test specimen from the cracked bolt was cathodically charged with hydrogen to ensure intergranular fracture in the Auger high-vacuum chamber. The AES results indicated that the grain boundaries were enriched in nickel (3.6 – 5 %), chromium (1.4 – 3.8 %), molybdenum (1.6 – 4.2 %) and especially phosphorus (2.5 – 8 %): compare with Table 20-1.

20.5.1.2.5 SSRT Tests and Subsequent Hydrogen Analysis

Notched tensile specimens with a stress concentration $K_t = 3.1$ were prepared from the cracked bolt and baked *in vacuo* at 200°C for 24 hours to remove any diffusible hydrogen. One specimen was left in this condition; two were bright-cadmium plated followed by either no baking or baking at 190°C for 23 hours; and the remainder were cathodically charged with hydrogen, bright-cadmium plated, and baked at 140°C for times ranging from 3 minutes to 20 hours.

The specimens were tested to failure at a cross-head displacement rate of 2.1×10^{-4} mm/s. After fracture they were immediately stored in liquid nitrogen to await hydrogen analysis *in vacuo* at 600°C. The results of the tests and analyses are shown in Figure 20-13. There are several observations to be made:

- 1) After baking to remove any diffusible hydrogen, the as-received specimen contained about 0.8 ppm of trapped hydrogen (this trapped hydrogen was removed by hydrogen analysis *in vacuo* at 600°C). The fracture stress of this specimen was 1985 MPa, and is a reference for the degree of embrittlement of the other specimens.
- 2) Baking had a beneficial effect on the fracture stress of cadmium plated specimens, and there was a concomitant decrease in hydrogen content from 2.3 ppm to 1.3 ppm.
- 3) Baking times longer than 30 minutes removed substantial embrittlement due to hydrogen charging followed by cadmium plating.

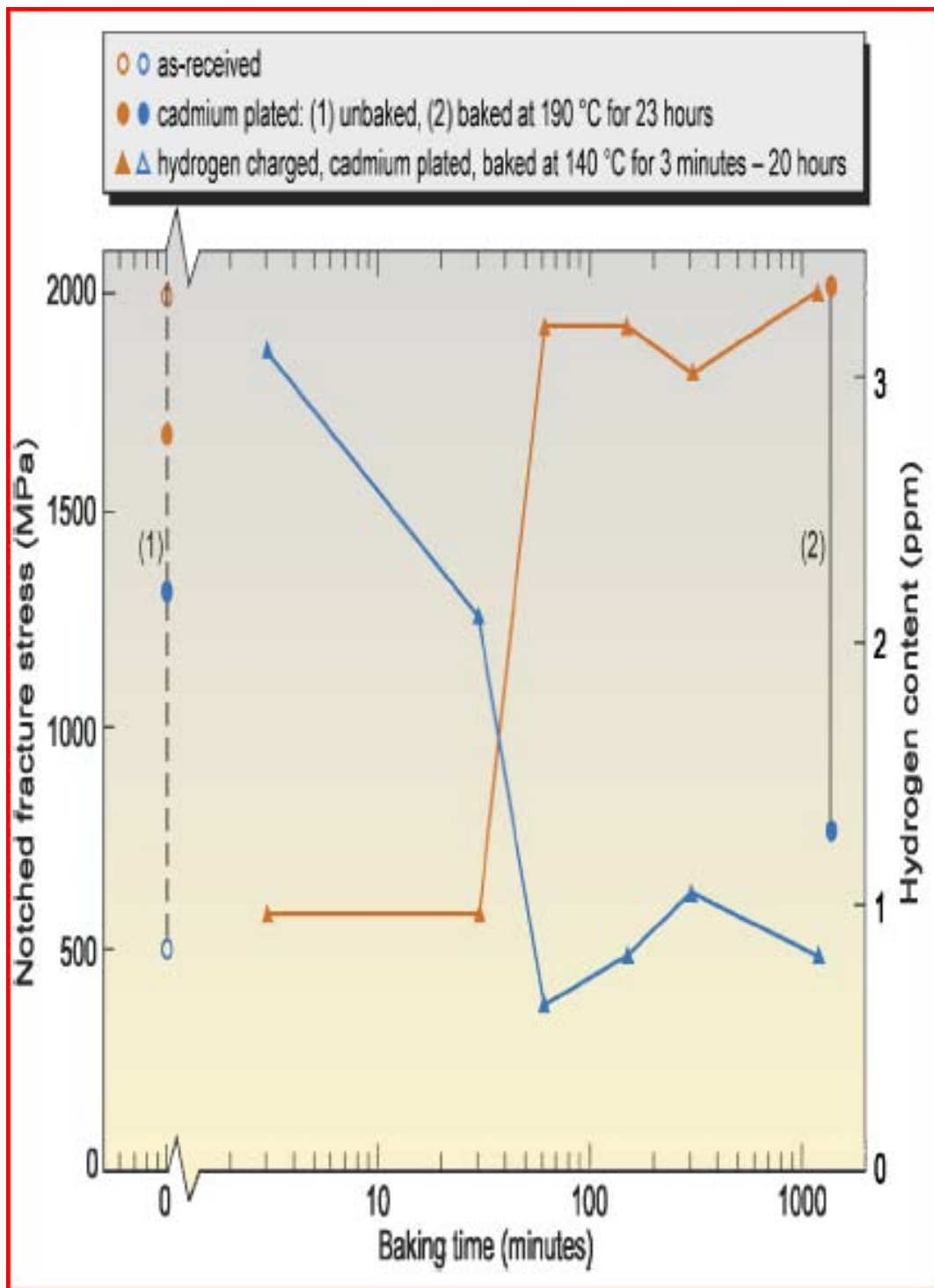


Figure 20-13: Case History 20.5.1 – Results of the Notched Tensile Tests and Hydrogen Analysis.

20.5.1.3 Conclusions

- 1) The microstructure, hardness and chemical composition results indicate that the cracked bolt was made, as specified, from S99 low alloy steel heat-treated to a tensile strength of about 1380 MPa. At this strength level such steels are known to be susceptible to hydrogen embrittlement.

- 2) During final processing (heat treatment) of the bolt there was significant segregation of phosphorus to prior austenite grain boundaries (2.5 – 8 %) compared to 0.02% in the bulk material. The phosphorus segregation would have made the bolt more susceptible to hydrogen embrittlement for a given strength level and (diffusible) hydrogen content.
- 3) At some time in the bolt's life it sustained local damage due to pitting corrosion.
- 4) Before the previous overhaul, small semi-circular regions of intergranular fracture spread from the three corrosion pits near the radius run-out under the bolt head. These intergranular fractures were most probably due to IHE from the previous plating operation.
- 5) During the previous overhaul the bolt underwent bright-cadmium electroplating, thereby absorbing hydrogen that was not entirely removed by baking, possibly because the baking process was inadequate. The electroplating also resulted in cadmium deposition on the small semi-circular regions of intergranular fracture.
- 6) After the bolt was fitted into the propeller assembly, clean intergranular fracture typical of IHE spread from the cadmium-contaminated small semi-circular regions of intergranular fracture.
- 7) By the time of the last overhaul the IHE cracking was extensive, resulting in its detection during stripping of the propeller assembly.

20.5.1.4 Remedial Actions

The initial remedial action was to recover the remaining batch of bolts, since replacement bolts were not immediately available. This recovery required stripping the cadmium and inspecting the radius regions of the bolts for pits and cracks using a high resolution magnetic particle method of Non-Destructive Inspection (NDI). If no pits or cracks were detected the bolts were re-plated, baked for an appropriate time (which was increased over the original baking time) and re-issued for service.

In parallel with this recovery procedure, the static and fatigue implications of cracks being present just below the NDI limit were assessed. It was concluded that such cracks would be very unlikely to cause failure before the next overhaul.

Since some doubt remained about the other bolts in the fleet, it was decided to inspect them with the same NDI method during their next overhaul; and as a further precaution, this next overhaul period was reduced to the minimum allowable by the fleet commitments.

20.5.2 Main Undercarriage Half-Fork Assemblies

20.5.2.1 Introduction

Following an incident involving a tactical aircraft main undercarriage half-fork assembly, an operator was advised to inspect the fleet for certain types of cracking in the hard-chromium electroplated sections of the assemblies. Numerous assemblies were found to be cracked in a potentially serious manner. Destructive examination of one of the “worst” cases showed that cracking had penetrated beyond the chromium plate and into the steel substrate. At this point the operator requested the DSTO to investigate another “worst” case. This investigation [15] comprised the following steps:

- Dye penetrant NDI of the as-received assembly.
- Chemical stripping of most of the chromium plate, dye penetrant NDI and etching of selected areas of the steel that had been below the chromium plated section.
- Metallographic cross-sections of non-stripped areas.
- Fractography of broken-open cracks.

The assembly is shown in Figure 20-14. It was made from 35NCD16 low alloy steel heat-treated to a Rockwell hardness of 51 HRC, corresponding to a tensile strength of about 1793 MPa. The nominal chemical composition in wt. % is: 0.4 C, 4.0 Ni, 1.8 Cr, 0.45 Mn, 0.45 Mo, 0.03 V, 0.3 Si.

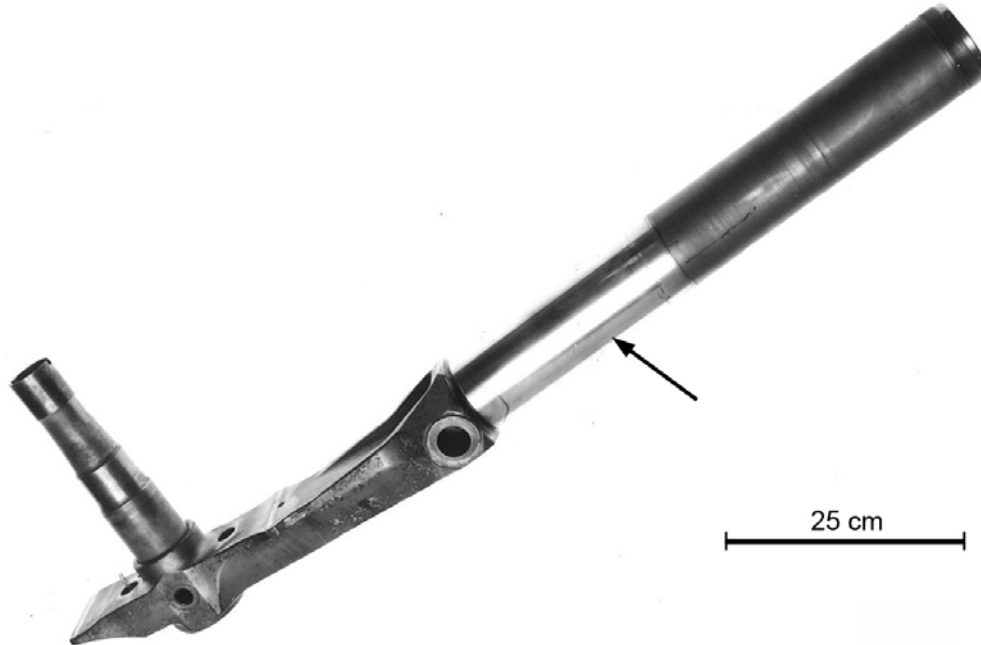


Figure 20-14: Case History 20.5.2 – Main Undercarriage Half-Fork Assembly Sent for Examination (the arrow points to the chromium plated cylindrical section).

20.5.2.2 Investigation

20.5.2.2.1 Dye Penetrant NDI of the As-Received Assembly

The arrowed cylindrical section in Figure 20-14 had been hard-chromium plated. Dye penetrant showed helically banded cracking at the lower and upper ends of the section, e.g., Figure 20-15.

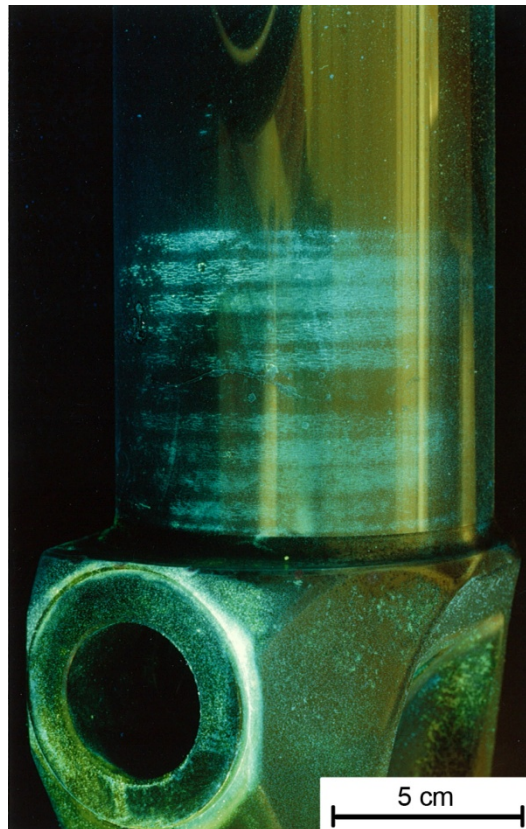


Figure 20-15: Case History 20.5.2 – Example of Helically Banded Cracking in the Hard-Chromium Plate (see Figure 20-14 for the location).

20.5.2.2.2 Chemical Stripping, Dye Penetrant NDI and Etching

The chromium plating was removed from selected areas of the cylindrical section by chemical dissolution in sodium hydroxide solution. Dye penetrant NDI of the stripped areas revealed the same pattern of helically banded cracking in the steel. Since this form of banding is characteristic of grinding damage, the steel surface was etched with nital. Helical dark etching bands confirmed the presence of grinding damage, see Figure 20-16. Discussions with the OEM suggested that this damage had occurred during overhaul of several batches of the half fork assemblies, owing to grinding conditions beyond the specified limits, i.e., abusive grinding.

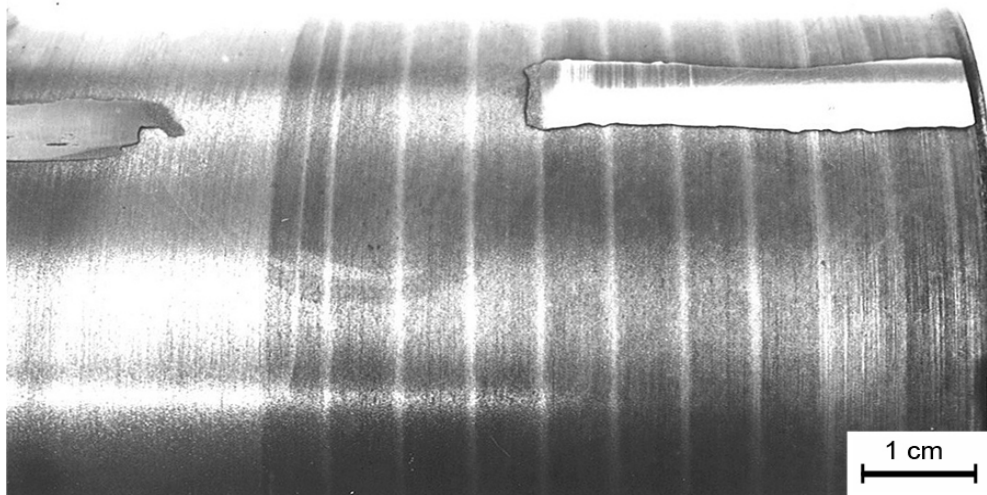


Figure 20-16: Case History 20.5.2 – Helical Dark Etching Bands Indicating Grinding Damage of the Steel Surface of the Lower Part of the Cylindrical Section (note the irregular areas with retained hard-chromium plate).

20.5.2.2.3 Metallography

Several cross-sections were made of the grinding damage in non-stripped areas. Figure 20-17 gives an example close to the lower end of the cylindrical section. There were numerous intergranular cracks in the steel, penetrating along prior austenite grain boundaries to a depth of about 130 μm . Most of these cracks were associated with cracking in the overlying chromium plate, as in Figure 20-17, but some were not. This suggests that initiation of (some) cracks in the steel may have preceded cracking of the chromium plate. Be that as it may, the initially intergranular nature of the steel cracks indicates that they were due to IHE. In turn, high tensile stresses introduced by abusive grinding could have caused IHE, and this may well have been exacerbated by hydrogen pick-up during electroplating.

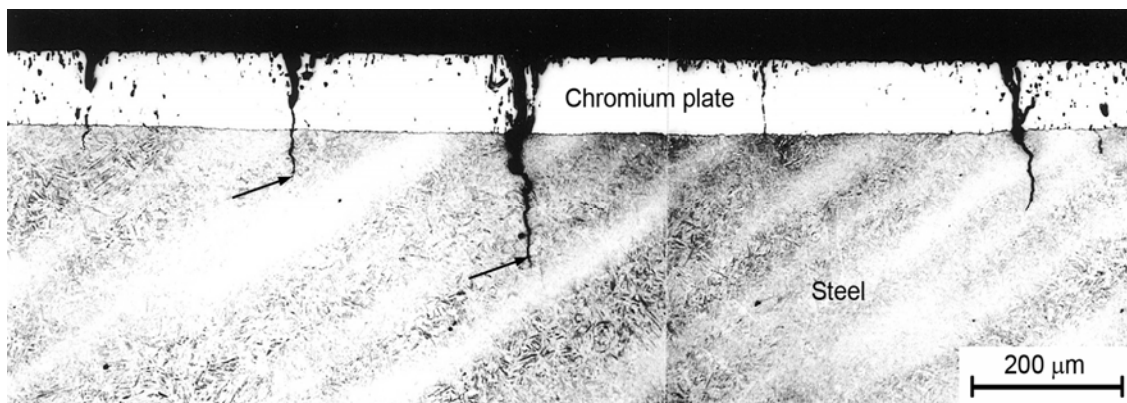


Figure 20-17: Case History 20.5.2 – Typical Cross-Section Through a Non-Stripped Area Containing Grinding Damage (the arrows point to transgranular fatigue cracks growing from intergranular crack).

The arrows in Figure 20-17 point to transgranular cracks growing into the steel from the intergranular cracks. These transgranular cracks were found only near the lower end of the cylindrical section, where the service stresses would have been highest. From their transgranular nature and location it seems most likely that these were fatigue cracks.

20.5.2.2.4 Fractography

The area containing suspected fatigue cracks was broken open. SEM fractography confirmed that fatigue cracks were growing from the intergranular cracks. An example is shown in Figure 20-18, which indicates the three successive regions of intergranular cracking, transgranular fatigue cracking, and overload fracture. More detailed observations were hindered by extensive pitting corrosion on the intergranular and fatigue fracture surfaces.

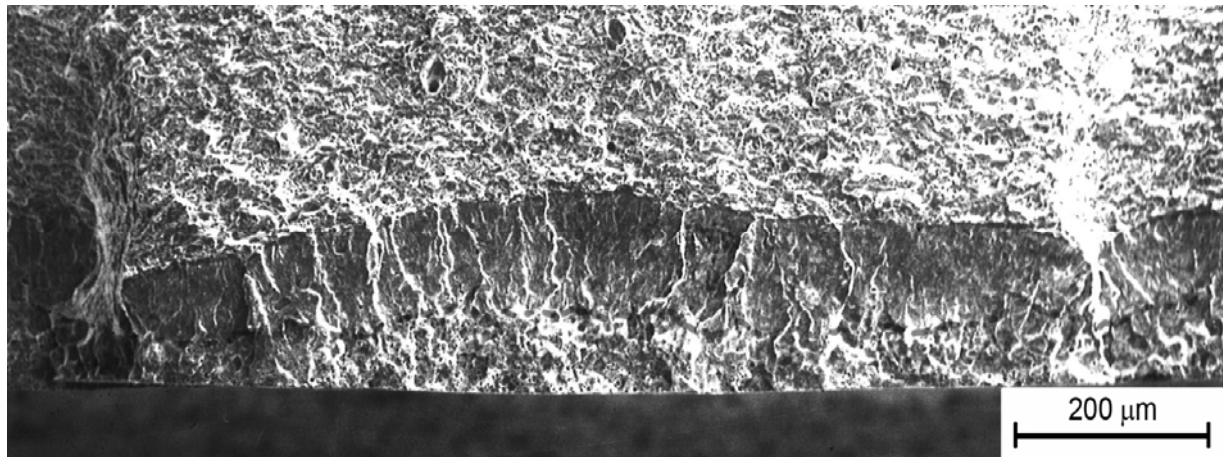


Figure 20-18: Case History 20.5.2 – A Broken-Open Crack Showing Intergranular Fracture Followed by Transgranular Fatigue Fracture and Overload Fracture.

20.5.2.3 Conclusions

Investigation of a main undercarriage half-fork assembly made from 35NCD16 low alloy steel heat-treated to 51 HRC lead to the following main conclusions:

- 1) The hard-chromium electroplating on the cylindrical section of the assembly showed helically banded cracking at the lower and upper ends of the section. The same crack pattern was present in the underlying steel.
- 2) The crack pattern in the steel suggests grinding damage. This was confirmed by etching the steel surface.
- 3) The initially intergranular nature of the steel cracks suggests that they were the result of IHE owing to high tensile stresses introduced by abusive grinding and hydrogen pick-up during electroplating.

20.5.2.4 Remedial Actions

Since the aircraft fleet to which the undercarriage half-fork assemblies belonged was very near retirement, and the lead time for replacements was likely to be longer than the remaining life required, it was decided to tolerate a particular level of cracking based on the results of the above investigation and re-inspection that was done at the DSTO and used the same dye penetrant NDI.

Half-fork assemblies that on inspection revealed extensive linked-up cracking, suggestive of fatigue, at the more highly stressed lower end of the cylindrical section were replaced with components held in stock. Assemblies with less severe cracking away from the lower end of the cylindrical section were allowed to remain in service. These mildly cracked assemblies were re-inspected at intervals conservatively based on the known time during which fatigue cracks developed in the investigated half-fork assembly.

20.5.3 Flap Carriage Assembly

The inboard carriage assembly from a transport aircraft flap fractured at the transition radius between the spindle and fork, see Figure 20-20 and Figure 20-21. The operator carried out a failure investigation, which is described in Section 20.5.3.1. The National Aerospace Laboratory (NLR) in Emmeloord, Netherlands, was requested to review the investigation and provide comments. The NLR's contribution is given in Section 20.5.3.2. The remedial actions and final conclusions are presented in Section 20.5.3.3.

20.5.3.1 Failure Investigation by the Operator

The broken carriage assembly was made from AISI 4330 M low alloy steel heat-treated to a Rockwell hardness of 53 HRC, corresponding to a tensile strength in the range 1860 – 2060 MPa. About 3 years before failure the spindle had undergone repair involving corrosion removal and nickel electroplating.

The failure investigation comprised the following steps:

- Visual examination and description.
- Optical fractography.
- Metallographic cross-sections.
- Review of the repair history.
- Conclusions.

20.5.3.1.1 Visual Examination and Description

Figure 20-19 shows the broken carriage assembly *in situ*, and Figure 20-20 gives views of the mating fracture surfaces spindle-side and fork-side. Discoloured semi-elliptical crack initiation regions are visible in both figures. The entire fracture surface of the spindle is also discoloured, but less so.

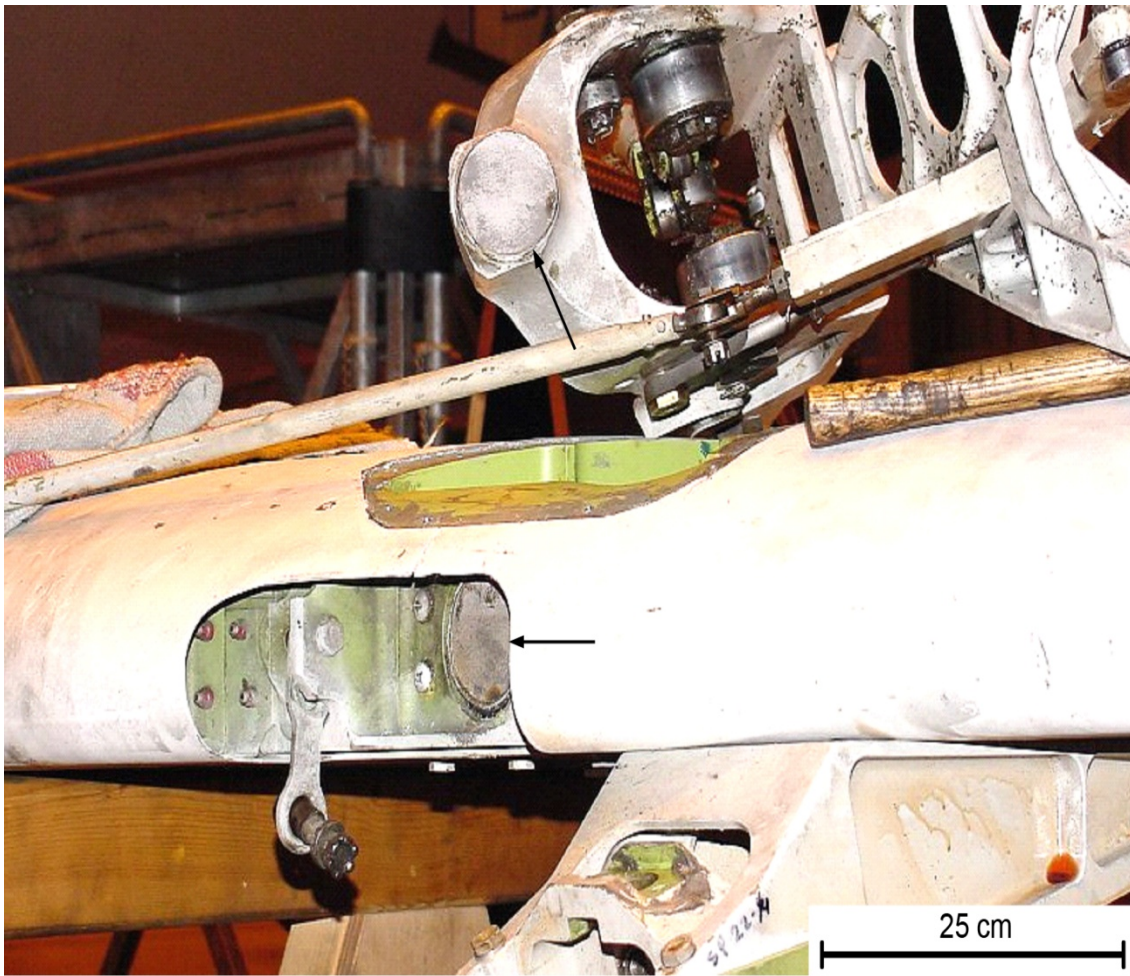


Figure 20-19: Case History 20.5.3 – Broken Inboard Carriage Assembly *In Situ* (arrows point to the fracture surfaces).



Figure 20-20: Case History 20.5.3 – Overview of the Fractured Spindle and Fork Assembly.

20.5.3.1.2 Optical Fractography

Figure 20-21 and Figure 20-22 show the fracture surfaces in more detail. There are several points to note:

- 1) Both crack initiation regions had discolorations grading from black to light brown. The spindle-side fracture surface was also discoloured by post-failure rust spots.
- 2) The spindle-side steel surface was covered by two nickel plating layers, see Figure 20-21.
- 3) Side surface corrosion was present just below the fork-side fracture surface, see Figure 20-22. This corrosion is seen in more detail in Figure 20-23, which also shows a thin remnant of nickel plating and tool marks owing to grinding away excess nickel plate.

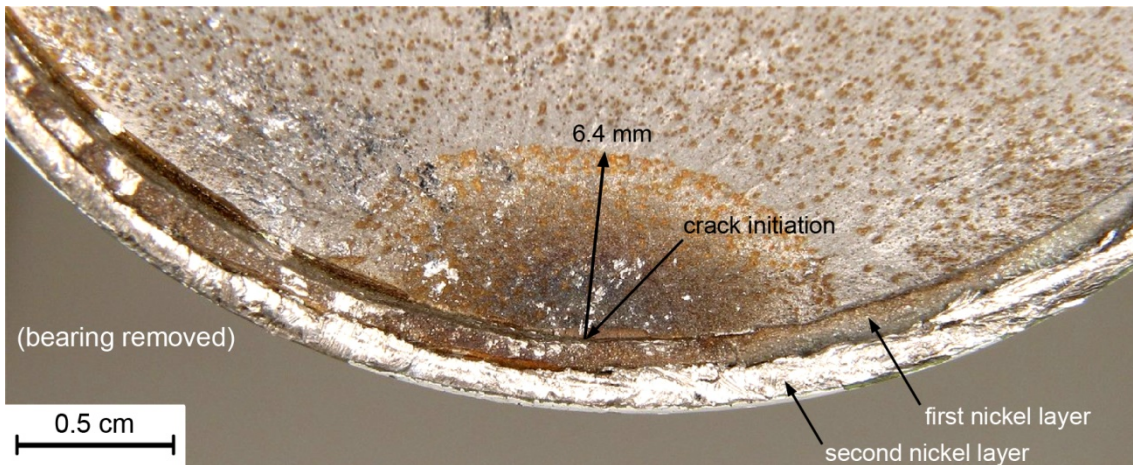
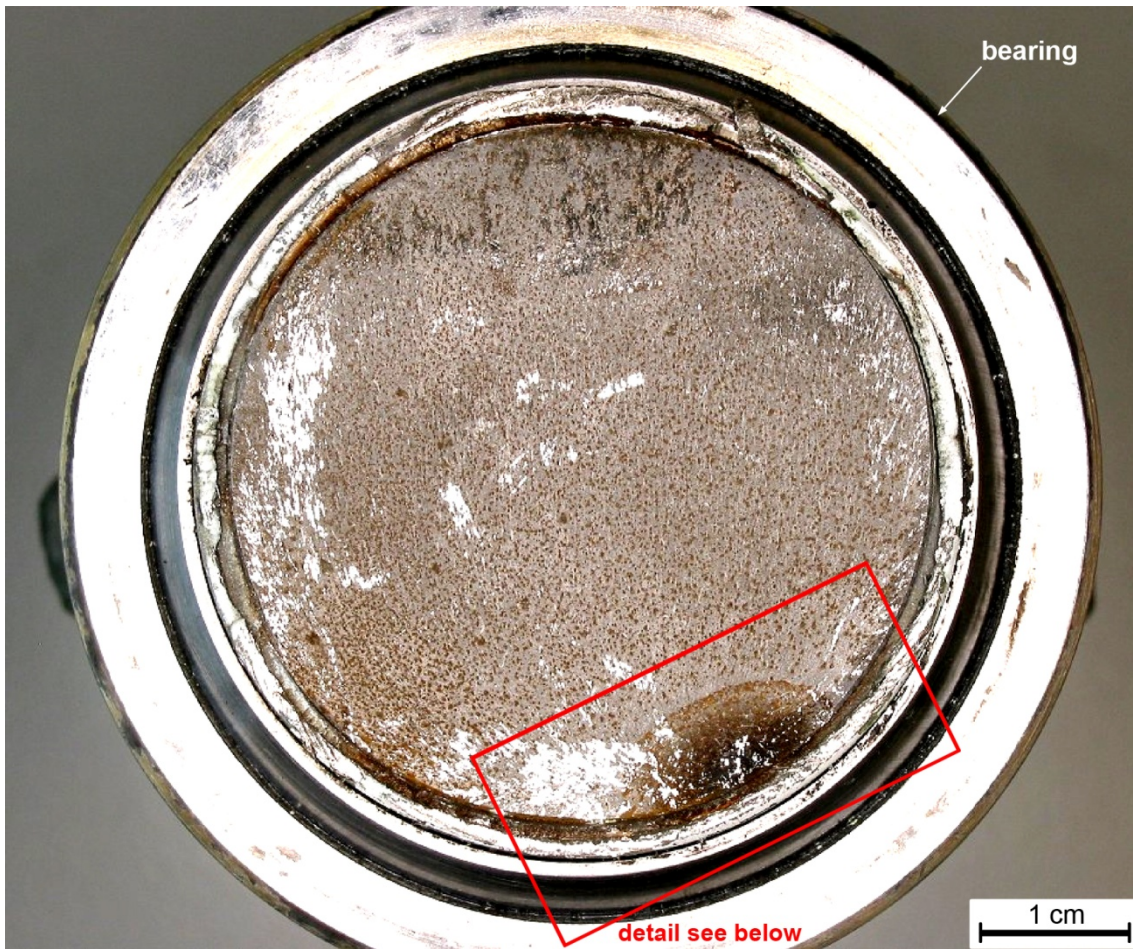


Figure 20-21: Case History 20.5.3 – Spindle-Side Fracture Surface.

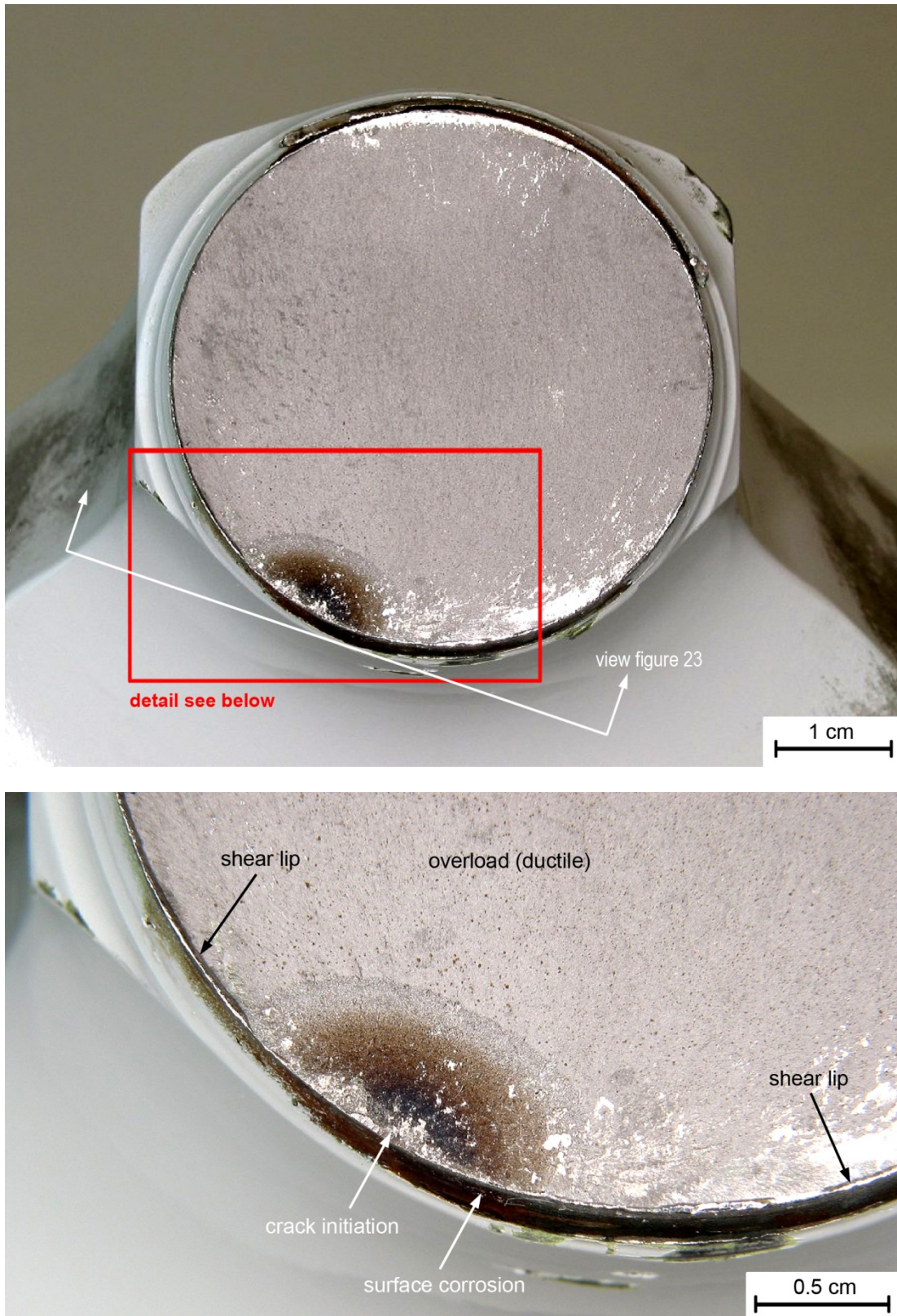


Figure 20-22: Case History 20.5.3 – Fork-Side Fracture Surface.

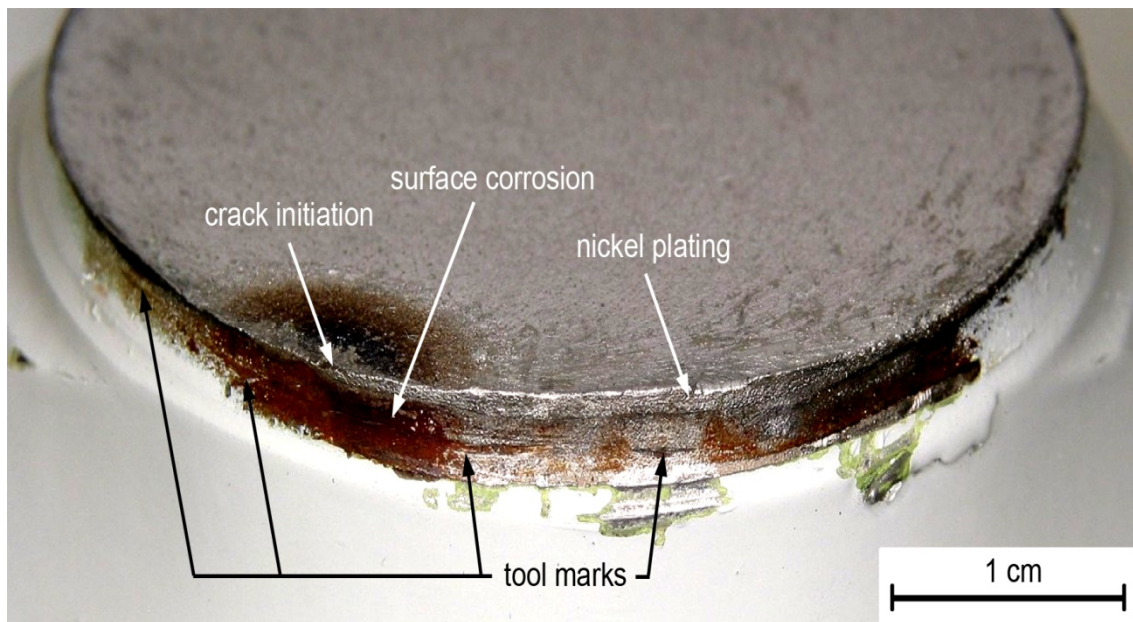


Figure 20-23: Case History 20.5.3 – Side Surface Around Fork-Side Crack Initiation Region.

From fracture surface observations using a stereobinocular at magnifications up to 80× the operator concluded that the semi-elliptical crack initiation region was the result of brittle intergranular fracture.

20.5.3.1.3 Metallography

Polished and etched cross-sections were made through the crack initiation regions. Figure 20-24 and Figure 20-25 show photomontages of the spindle-side and fork-side cross-sections. These figures present much detail, interpreted as follows:

- 1) *Spindle-Side Cross-Section*, Figure 20-24. The nickel plating was applied in two layers. The first layer was machined and blended, i.e., plating nodules were removed, before applying the second layer. The second layer was also machined, but the overhanging nodules were not removed. A thin layer of cadmium electroplate (not visible in Figure 20-24) was applied on top of the nickel plate.

A detail of the cross-section, including the crack initiation region, shows a crack in the nickel plating, corrosion products filling this crack, and a small secondary crack growing from a corrosion pit.

- 2) *Fork-Side Cross-Section*, Figure 20-25. The radius area was unprotected by electroplating and paint, and had undergone corrosion (also visible in Figure 20-23). Thin white-etching layers at the steel surface indicate untempered martensite caused by grinding.

A detail of the cross-section, including the fracture initiation region, shows remnants of nickel plating and a small secondary crack growing from a corrosion pit.

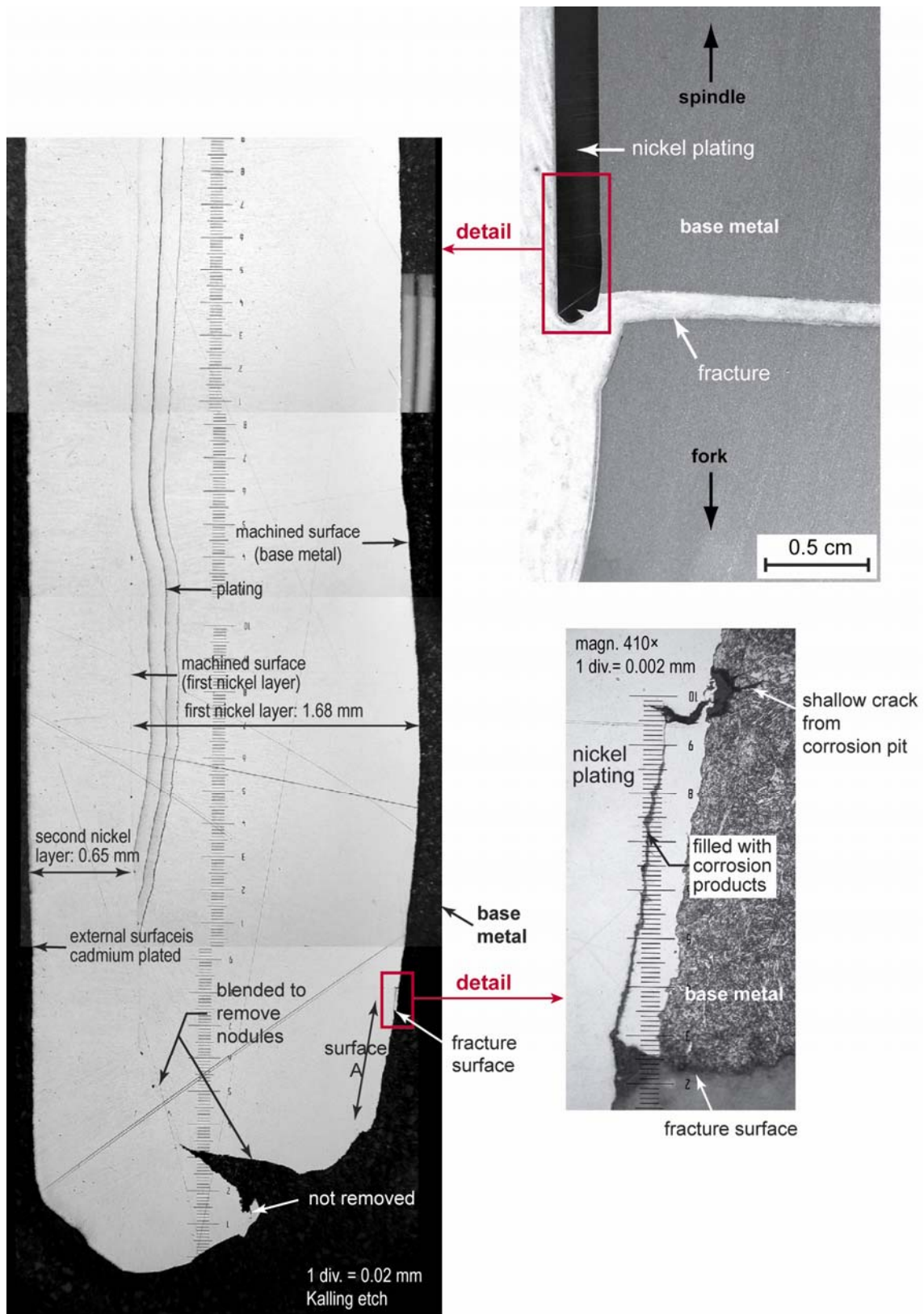
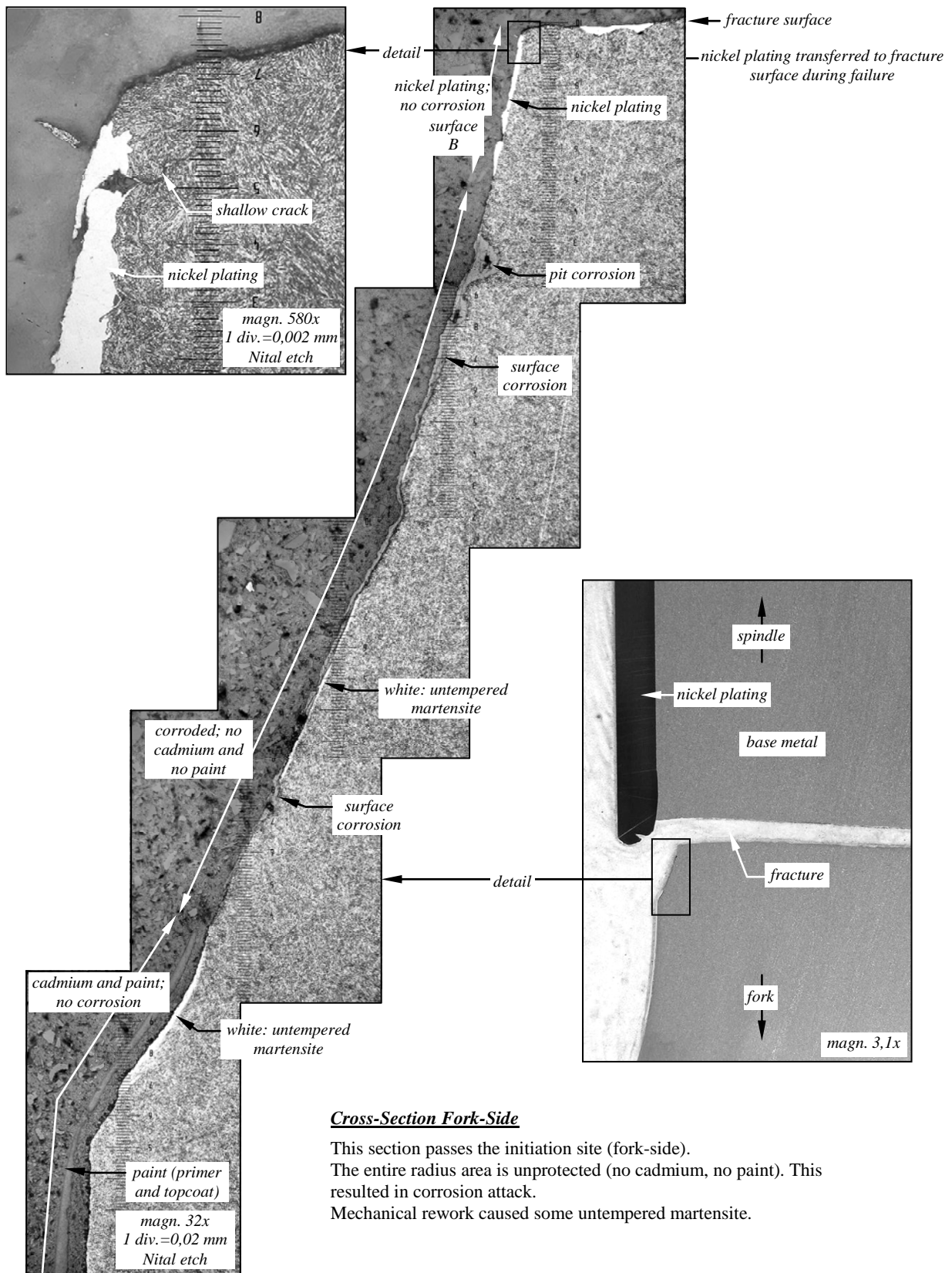


Figure 20-24: Case History 20.5.3 – Metallographic Cross-Section Through the Spindle-Side Crack Initiation Region (Note: Surface A matches surface B in Figure 20-25).



Cross-Section Fork-Side

This section passes the initiation site (fork-side). The entire radius area is unprotected (no cadmium, no paint). This resulted in corrosion attack. Mechanical rework caused some untempered martensite.

Figure 20-25: Case History 20.5.3 – Metallographic Cross-Section Through the Fork-Side Crack Initiation Region (Note: Surface B matches surface A in Figure 20-24).

Figure 20-26 summarises the metallographic observations in a detailed sketch that schematically rejoins the fracture surfaces. This sketch clearly shows the extent of the unprotected, and hence corroded, steel surface.

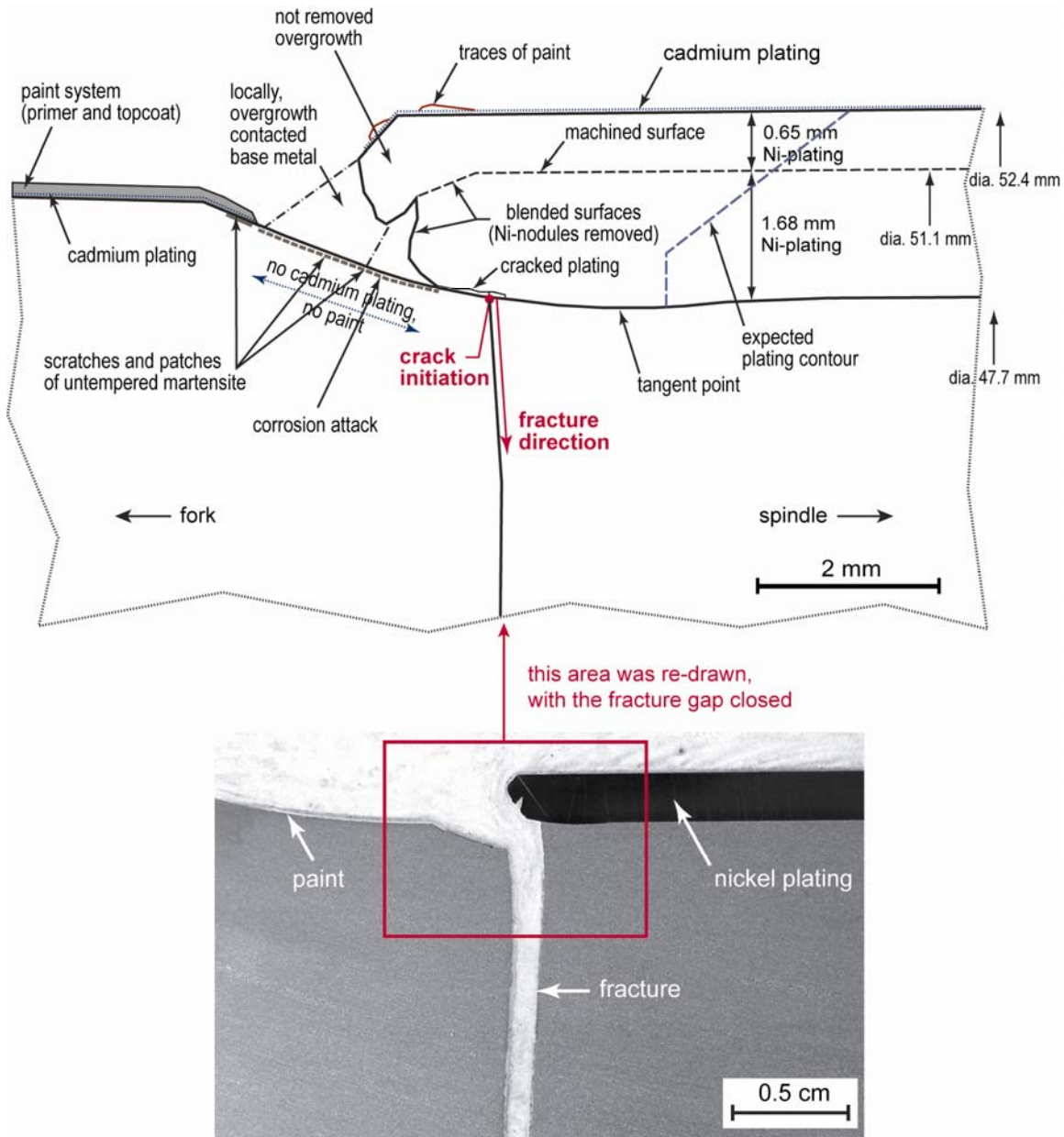


Figure 20-26: Case History 20.5.3 – Summary of the Metallographic Observation.

20.5.3.1.4 Review of the Repair History

The repair history will be reviewed with the aid of Figure 20-26. Initially, corrosion removal required machining the spindle to below the minimum repair diameter. However, the OEM issued a directive to allow repair by nickel plating and installing a sleeve. The actual repair was done solely with nickel plating. The nickel plating was applied in two layers, each followed by baking for 23 hours. The first nickel layer was machined and blended, removing nickel nodules in the radius area. This resulted in damage to the

steel surface (tool marks, see Figure 20-22, and untempered martensite, see Figure 20-25). The second nickel layer was also machined, but the overhanging nodules in the radius area were not removed.

Finally, the entire assembly was cadmium electroplated and painted.

20.5.3.1.5 Conclusions

The operator attributed failure of the carriage assembly to poor repair procedures:

- 1) The nickel plating thickness was excessive: up to 2.33 mm instead of the maximum allowable thickness of 1.5 mm. Because of this, baking for 23 hours might have been insufficient to remove all the hydrogen picked up during plating.
- 2) Near the steel crack initiation region the nickel plating was cracked and filled with corrosion products. This crack in the nickel plating could have resulted in a corrosion pit at the steel crack initiation region.
- 3) In the light of 1) and 2), cracking of the steel may have been due to a combination of stress corrosion and hydrogen embrittlement.
- 4) Corrosion in the spindle radius area occurred because overhanging nickel nodules from the second nickel plating layer prevented the final cadmium plating and painting from covering the radius area.

20.5.3.2 Review of the Operator's Investigation

The operator's report on the investigation was sent to the NLR for comments. The NLR agreed that failure of the carriage assembly was due to poor repair procedures. However, there were some comments and observations about the interpretation of cracking:

- 1) Stereobinocular fractography at magnifications up to 80 × would normally have been sufficient to determine whether brittle intergranular fracture had occurred. However, the fracture surfaces were corroded, which would have made interpretation difficult.
- 2) Figure 20-21 and Figure 20-22 show discolorations grading from black to light brown on the fracture surfaces of the crack initiation region. These discolorations are the result of progressive oxidation during crack growth, and their gradual transition from black to light brown is characteristic for both stress corrosion and corrosion fatigue in steels. On the other hand, the service loading on the carriage assembly would have been mainly cyclic (flaps in, flaps out) rather than sustained. (N.B.: See Section 20.3 2) also.)
- 3) Other features pointing to corrosion fatigue rather than IHE or a combination of IHE and stress corrosion are:
 - a) The location of the failure, which was near the root of a notch created by the end of the nickel plating and a crack in the nickel plating³;
 - b) The well-defined semi-elliptical shape of the crack initiation regions, although similar crack shapes are possible for IHE and stress corrosion, see case history 20.5.1;
 - c) The close proximity of the secondary cracks growing from adjacent corrosion pits, but not from corrosion damage further from the failure site; and
 - d) No cracks in the regions of untempered martensite, see the details in Figure 20-24 – Figure 20-26.
- 4) Nickel electroplating was most probably carried out using a sulfamate bath, a type of bath which results in only moderate hydrogen pick-up by high strength steels. More importantly, there was an unplated "window", see Figure 20-25 and Figure 20-26, through which hydrogen could have readily diffused, both during and after the baking.

³ The nickel plating would have had sufficient stiffness and strength to be load-bearing, and hence provide a notch at its end.

- 5) Figure 20-25 shows an anomaly, namely that the operator indicated nickel plate to have been transferred to the fracture surface during failure. This is most unlikely. However, the operator's report mentioned that the two fracture halves were reassembled to visualize the nickel plating transition in the radius. It is possible that this reassembly – which should not have been done! – caused smearing of some loosened or protruding nickel plate onto the fracture surface.

From the comments and observations in 1) – 4) the NLR concluded that the carriage assembly failure was most probably the result of corrosion fatigue rather than IHE.

20.5.3.3 Remedial Actions and Final Conclusions

The OEM responded to the operator's investigation by requiring all carriage assemblies with similar repair histories to be replaced. Specifically, the OEM considered that baking for 23 hours was insufficient to guarantee satisfactory long-term service. The failed and suspect carriage assemblies were replaced by new ones. However, in the light of the NLR's comments the OEM subsequently conceded that baking for 23 hours was adequate.

The operator concluded that the failed carriage assembly was an "isolated case" owing to very poor repair procedures. The cause of cracking remains uncertain, though it was most probably corrosion fatigue and not hydrogen embrittlement.

20.5.4 Wing Attachment Fitting Bolts

20.5.4.1 Introduction

During a modification programme the Wing Attachment Fitting (WAF) steel bolt assemblies from 33 tactical aircraft were cleaned in a non-approved chemical solution, a paint stripper. This removed much of the cadmium electroplating on the bolts, nuts and washers, leading to in-service superficial rusting of some bolt ends and nuts, e.g., Figure 20-27.

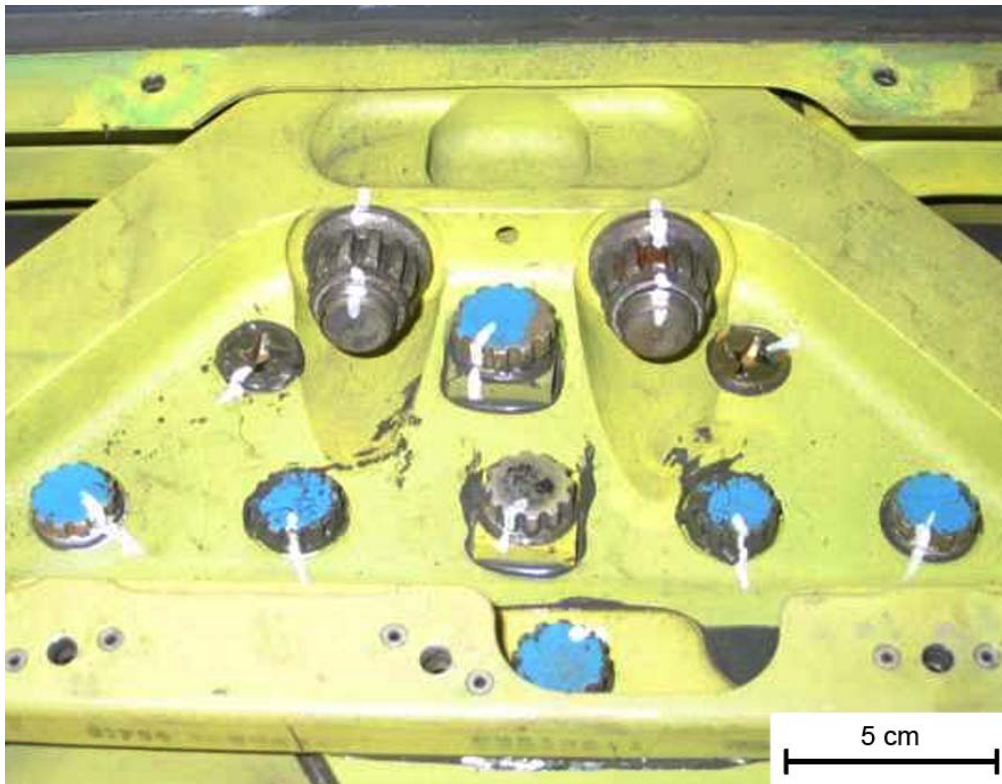


Figure 20-27: Case History 20.5.4 – Example of a Surface-Rusted WAF Bolt (R.H. bolt in photograph).

The OEM and chemical manufacturer became concerned about possible hydrogen embrittlement of the bolts owing to exposure to the paint stripper. The OEM recommended tensile testing and IHE proof testing (see Section 20.4) of some of the bolts before continuing to fly with the rest. Furthermore, the OEM stated that in-service failure of a single bolt in a WAF bolt assembly would be unacceptable for the structural integrity of the aircraft.

The operator's Crisis Management Team (CMT) then grounded all 33 aircraft. The NLR was requested to advise about the OEM's proposal and conduct a validation test programme on some of the suspect bolts to determine whether the CMT could clear the aircraft for further operation. The NLR and CMT agreed to do tensile testing only. Proof testing was considered unnecessary, for reasons discussed later in this sub-section under the heading: **The “no failure in 200 hours” criterion**. Also, SSRT testing was not considered, since the main question was whether the tensile strengths of the bolts had already been affected by IHE.

The validation programme comprised the following steps:

- Tensile tests and fractography.
- Statistical analysis of the tensile test data.
- Electrochemistry and hydrogen diffusivity considerations.
- The “no failure in 200 hours” criterion.

20.5.4.2 Examination

The bolts were specified to be made from H-11 CrMoV steel per AMS 6487, heat-treated to a minimum tensile strength of 1517 MPa. Examination of the threads showed that they had been rolled, which would

have been beneficial to their resistance to cracking, particularly if thread rolling was done after heat treatment, thereby introducing compressive residual stresses at the thread roots. (It was not determined whether heat treatment preceded the thread rolling.)

20.5.4.2.1 Tensile Tests

The NLR received 160 suspect WAF bolt assemblies from 5 aircraft (32 sets per aircraft). Table 20-2 gives information on the bolt assemblies, which were selected to provide a wide range in flight and service hours since the paint stripper treatment. Each aircraft makes between 150 – 200 flight hours per year, with an average of over 40 hours between flights, so that the minimum service hours would have been more than 200 hours.

Table 20-2: Aircraft and Suspect Bolt Assembly Information.

Aircraft	Flight Hours Since Paint Stripper Treatment
A	536.1
B	441.4
C	87.8
D	27.9
E	6.1

In addition, 4 new bolts and 4 non-suspect (cadmium-plated) used bolts were supplied for pilot tensile tests. Clamping fixtures were prepared from 17-4 PH (H900) steel to enable tensile testing of complete bolt assemblies. The tests were done in a 1 MN static machine:

- 1) *Pilot Tensile Tests.* Table 20-3 gives the result, which included one suspect bolt assembly. Note that the bolt from this assembly failed at a higher load than the new and non-suspect D10 bolts.

Table 20-3: Pilot Tensile Test Results.

Aircraft	Bolt Condition and Type*	Failure Load (kN) and Mode*
–	New D14	547: ts
–	New D14	544: ts
–	New D12	413: ts
–	New D10	295: ts
Unknown	Used D14	583: ts
Unknown	Used D14	578: ts
Unknown	Used D12	425: b
Unknown	Used D10	307: b
B	Suspect D10	312: b

* D = bolt diameter code; ts = thread-stripped; b = bolt-break

The three bolt-breaks, which occurred in the threaded parts of the shanks, were examined fractographically. The fractures were due to overload by a mixture of intergranular and

transgranular dimpled rupture, for example the SEM fractograph in Figure 20-28. This type of overload fracture has been observed for other high strength steels [6].

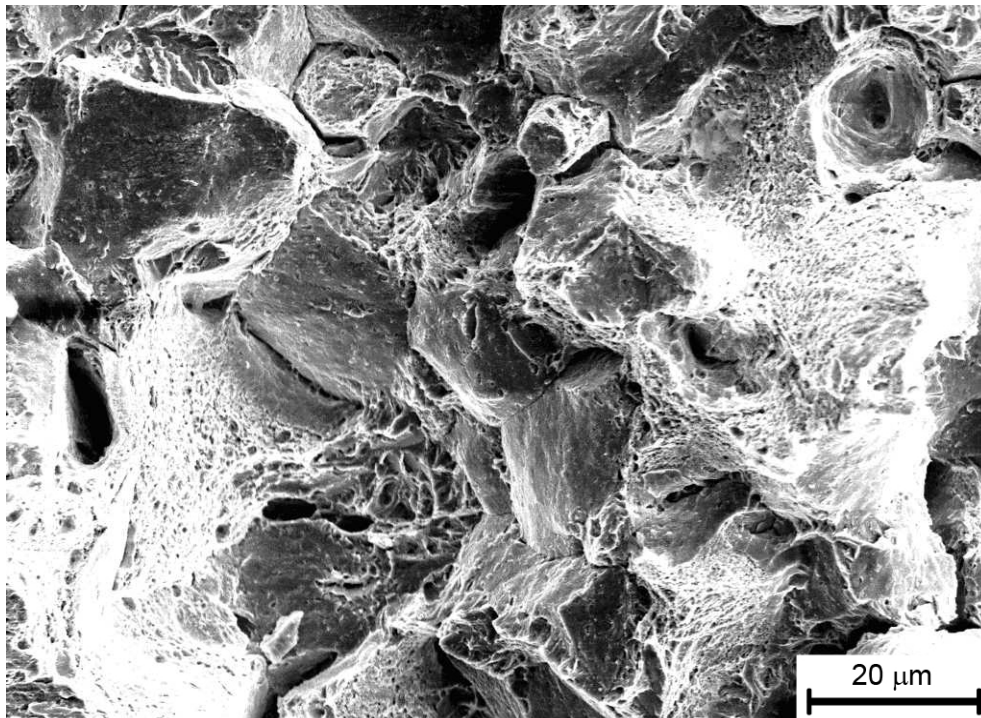


Figure 20-28: Case History 20.5.4 – Fracture Characteristics of the Non-Suspect Used D12 Bolt from the Pilot Tensile Tests.

2) *Definitive Tensile Tests.* For a reliable statistical analysis the NLR suggested testing at least 30 bolts, preferably 50, *having the same diameter.* In view of this requirement and the bolt allocations per aircraft wing, namely:

- Upper WAFs: 6 × D12 (19.05 mm), 2 × D10 (15.88 mm).
- Lower WAFs: 6 × D14 (22.23 mm), 2 × D12 (19.05 mm).

The NLR selected 10 × D12 bolt assemblies from each of the 5 aircraft listed in Table 20-2. The selection ensured that the bolt assemblies came from upper and lower WAFs, and from right and left wings. Furthermore, the selection took account of any visible rust, i.e., bolt assemblies showing service-induced rusting were preferentially selected. In fact, only bolts from aircraft A and E showed any rust, which was light and only at the bolt ends. Note from Table 20-2 that these bolts had the longest and shortest flight hours, respectively, since paint stripper treatment. Thus rusting was not necessarily a progressive in-service phenomenon.

Figure 20-29 summarises the test data in a histogram. This gives the ranges in failure loads for the two failure modes, bolt-break (19 cases) and thread-stripped (31 cases). For each of the 5 aircraft the bolt-break failure mode resulted in minimum and average failure loads at least as high as those for the thread-stripped failure mode. Also, there is no apparent relation between the failure loads and flight hours since paint stripper treatment.

All the bolt-break failures were examined fractographically. The fractures were due to overload by a mixture of intergranular and transgranular dimpled rupture, as already illustrated in Figure 20-28. There was no evidence of small semi-circular regions of IHE at the thread roots.

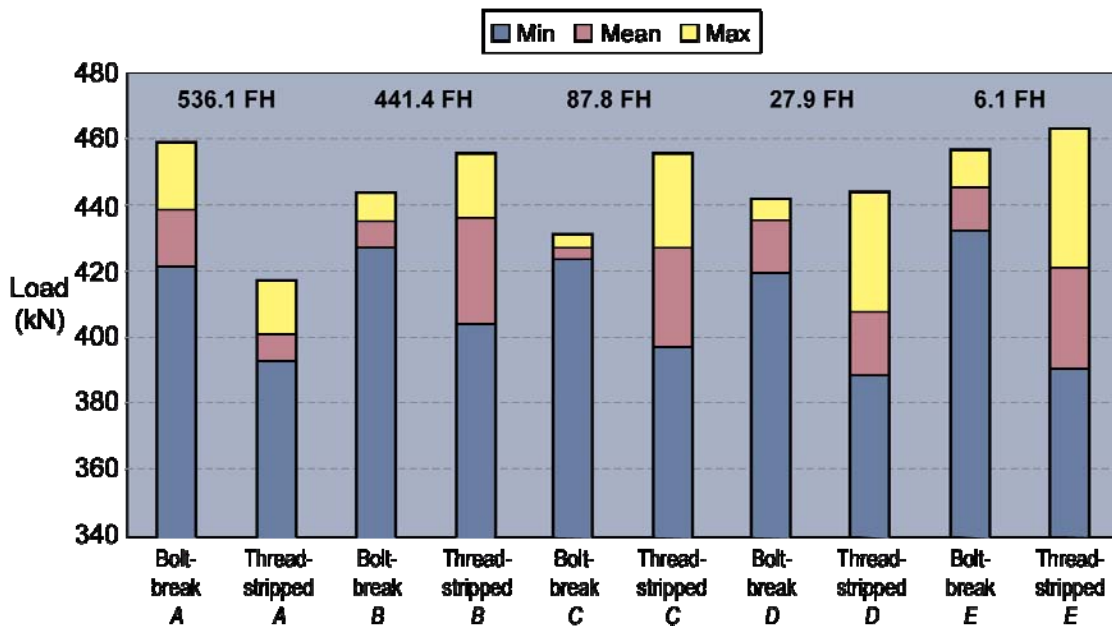


Figure 20-29: Case History 20.5.4 – Histogram of the Definitive Tensile Test Data (FH = Flight Hours since paint stripper treatment).

20.5.4.2.2 Statistical Analysis of the Test Data

The statistical analysis of the tensile test data considered the following aspects:

- Failure modes.
 - Flight hours since paint stripper treatment.
 - Minimum strength level.
 - Comparison of pilot and definitive test data.
- 1) *Failure Modes* – Statistical tests were done to determine whether the bolt-break and thread-stripped data sets could be pooled. The tests determined whether the differences in the means and variances of the data sets were statistically significant, with the level of significance set to a standard value of 0.01. A small-sample T-test on the means and a small-sample F-test on the variances showed that the differences in the means and variances were significant. Hence the data sets could not be pooled. Normal fits were made to the two data sets. Figure 20-30 and Figure 20-31 show that normal distributions fit both data sets. The goodness-of-fit was supported by the Kolmogorov-Smirnov and Hollander-Proschan test statistics [16].

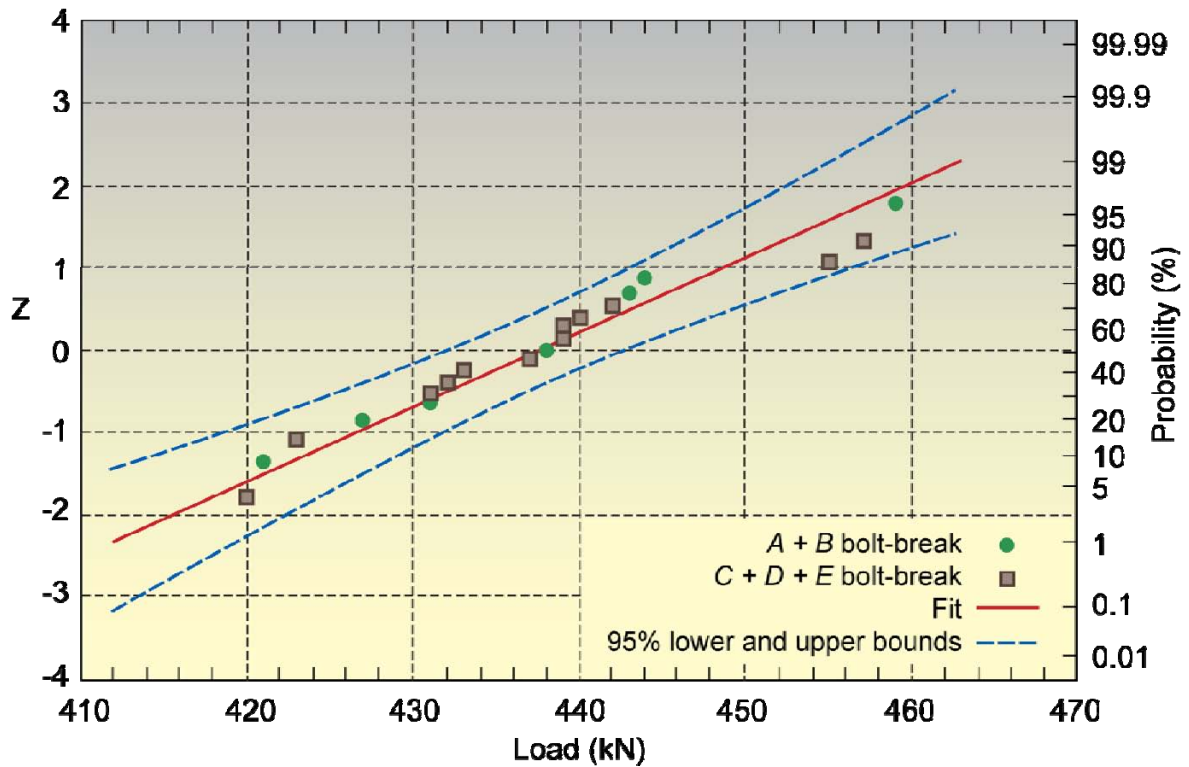


Figure 20-30: Case History 20.5.4 – Normal Fit for the Bolt-Break Failure Load Data from the Definitive Tensile Tests.

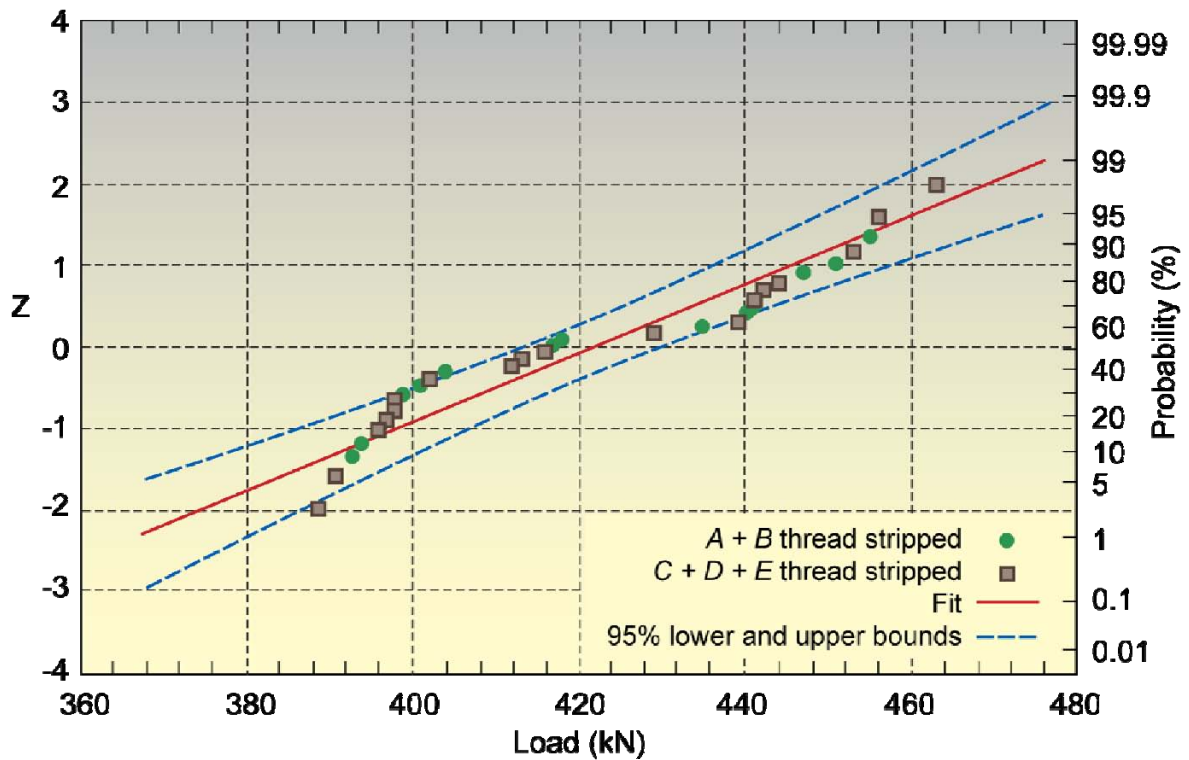


Figure 20-31: Case History 20.5.4 – Normal Fit for the Thread-Stripped Failure Load Data from the Definitive Tensile Tests.

- 2) In combining data from all 5 aircraft, it can be seen from Figure 20-30 and Figure 20-31 that the bolt-break minimum and mean failure loads were well above those for the thread-stripped failures. The mean values were 437 kN and 422 kN, respectively.
- 3) *Flight Hours since Paint Stripper Treatment* – The major differences in flight hours since paint stripper treatment (**A** and **B** versus **C**, **D** and **E** bolts) are indicated by filled and open symbols in Figure 20-30 and Figure 20-31. There is no clustering of the failure loads according to flight hours, in agreement with a lack of a trend in Figure 20-29.
- 4) *Minimum Strength Level* – Figure 20-32 depicts the same information for the bolt-break failure data as Figure 20-30, but now in terms of a Cumulative Distribution Function (CDF), together with the failure strength A- and B-values⁴. These represent the 95% confidence lower limits on the first and tenth percentiles of the property distributions, 399 kN and 415 kN, respectively. The confidence limits were determined using the Fisher information matrix [17].

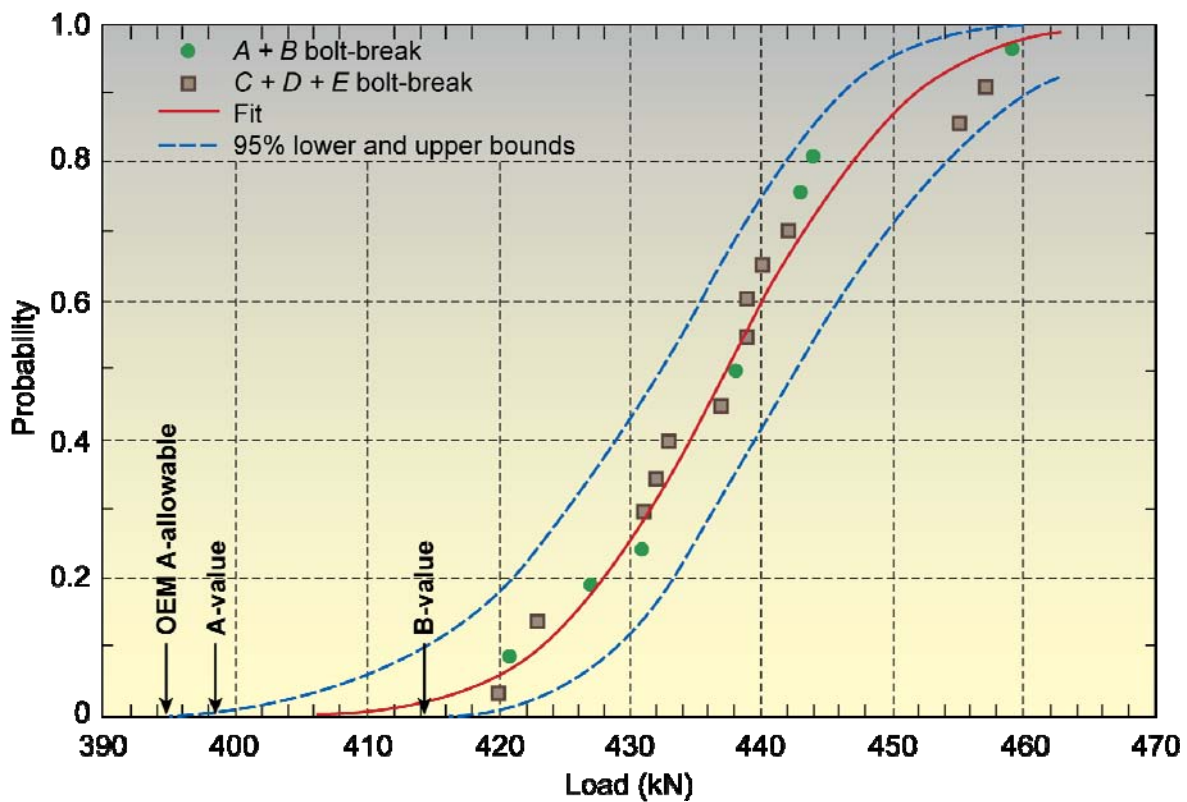


Figure 20-32: Case History 20.5.4 – Cumulative Distribution Function (CDF) for the Bolt-Break Failure Load Data from the Definitive Tensile Tests.

Figure 20-32 also shows the OEM failure strength A-allowable for D12 bolts, 395 kN. The estimated A-value from the bolt-break tests is higher, even though based on a limited data set of 19 cases. One may expect the A-value for a larger data set to be still higher.

- 5) *Comparison of Pilot and Definitive Test Data* – The failure loads for the new and non-suspect used D12 bolts in Table 20-3 were 413 kN (thread-stripped) and 425 kN (bolt-break) respectively. These values are lower than the respective mean values, 422 kN and 437 kN, for the definitive test data.

⁴ A-value (allowable) is 99% reliability with 95% confidence; B-value (allowable) is 90% reliability with 95% confidence. See MIL-HDBK 5J, Appendix A.3, 2003.

The results of the statistical analysis strongly suggested that the suspect D12 bolt assemblies had not undergone tensile failure load degradation owing to IHE caused by the paint stripper treatment. Furthermore, the fact that the bolt-break minimum and average failure loads were well above those for the thread-stripped failures suggests that the bolt shank material below the thread roots was undamaged. This is because (possible) hydrogen embrittlement of service-loaded bolts would be expected to damage the material subjected to tensile stress concentrations below the thread roots, but not the threads themselves.

20.5.4.2.3 Electrochemistry and Hydrogen Diffusivity Considerations

Figure 20-33 shows a simplified Pourbaix (E – pH) diagram for iron in water [18]. The two diagonal lines (a) and (b) bound the region of stability of water as a function of potential and pH. Above line (a) water is thermodynamically unstable with respect to the generation of oxygen gas. Between lines (a) and (b) water is thermodynamically stable. Below line (b) water is thermodynamically unstable with respect to the generation of hydrogen gas. Bubbles of hydrogen will evolve on a metal surface (acting as an electrode) in contact with water in this region.

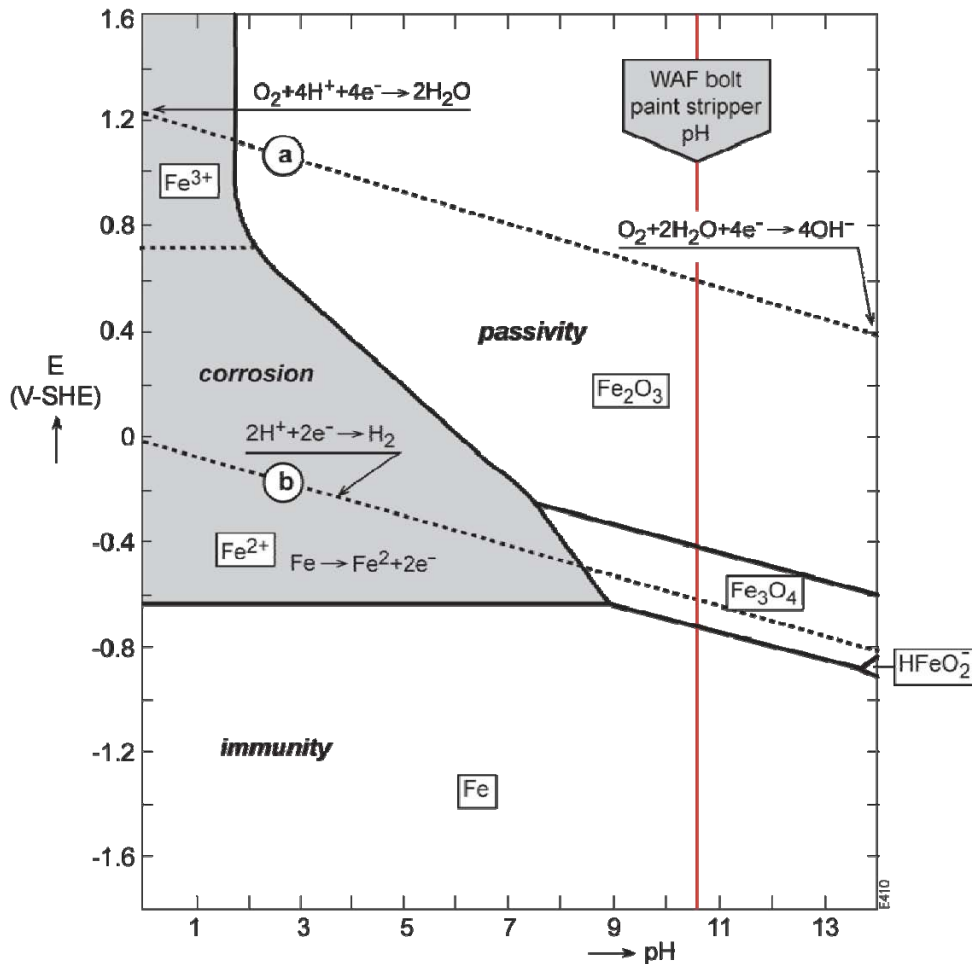


Figure 20-33: Case History 20.5.4 – Simplified E – pH Diagram for the Iron-Water System at 25°C (E is the electrode potential with respect to the Standard Hydrogen Electrode (SHE)).

The pH of the WAF bolt paint stripper is shown as a dashed vertical line in Figure 20-33. Knowing that the bolts would initially be cadmium plated, and that cadmium plating is sacrificial with respect to steel, this E – pH diagram suggests that:

- 1) Depending on the cadmium/steel galvanic coupling potential, i.e., if it would be below about -0.6 V-SHE, hydrogen gas could be liberated at the cadmium/steel interface during the anodic attack and removal of the cadmium layer by the paint stripper. *Some hydrogen could also be absorbed by the bolts*, as discussed below.
- 2) The bolts would not corrode in the paint stripper, since its pH line is well outside the corrosion region. Note that the suggestion about no corrosion of the bolts is consistent with measurements of the open-circuit potential of another low alloy steel (4340) in paint strippers having pH values ranging from 8 – 11.5 [19]. These measurements showed that the bare steel was in the water-stable (passivity) region of the E – pH diagram. In other words, even if all the cadmium plating on the WAF bolts were to be removed by anodic attack, the bolts would remain uncorroded. (In fact, as mentioned earlier, inspection of all the suspect bolts before tensile testing showed no evidence of corrosion except service-induced light rusting on some of the bolt ends from the aircraft **A** and **E**.)

With respect to 1) above, there is the question of hydrogen absorption into the WAF bolts during the anodic attack and removal of the cadmium layer by the paint stripper. This could occur only if the galvanic coupling potential was below line (b), *as may have been the case*. For example, Figure 20-34 shows the galvanic coupling potentials for cadmium and 4340 steel in several paint strippers [19], whereby it is seen that it is possible to transgress below line (b).

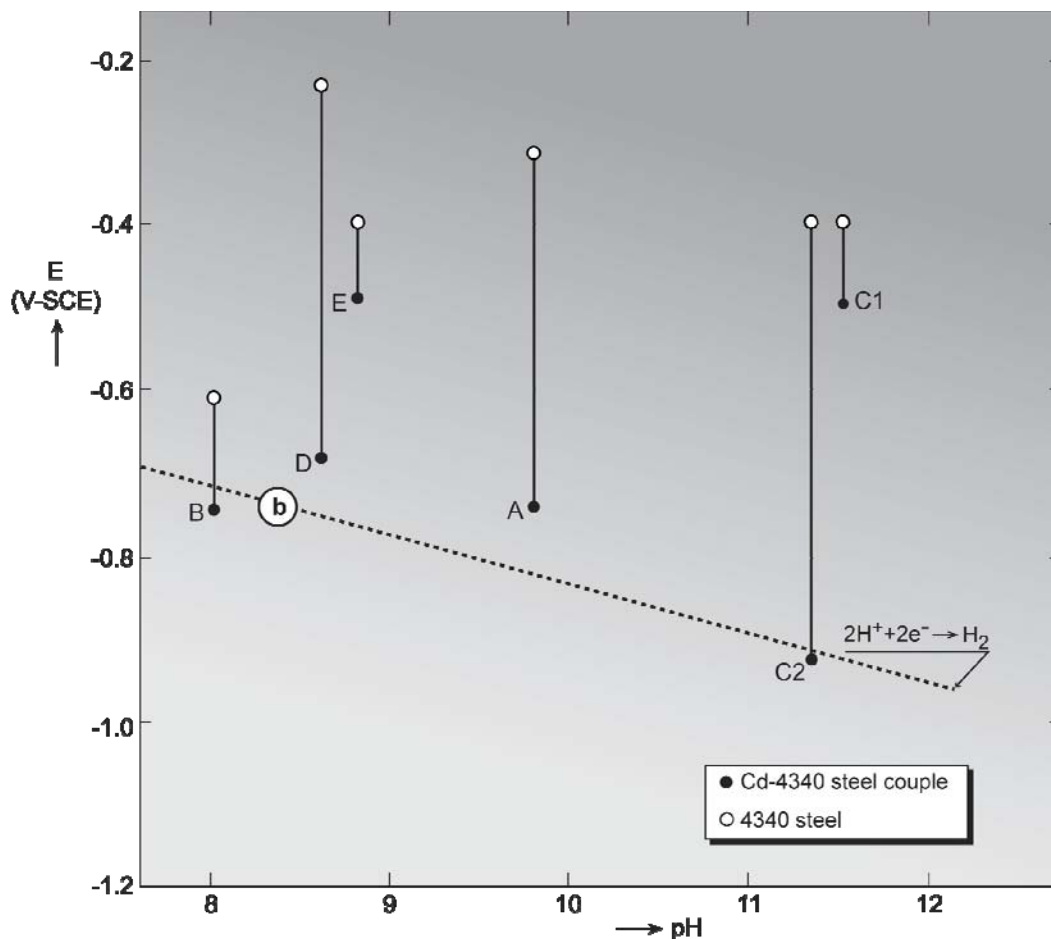


Figure 20-34: Case History 20.5.4 – E – pH Diagram for (1) Open Circuit Potentials of 4340 Steel and (2) Galvanic Couple Potentials for Cadmium and 4340 Steel in Paint Strippers [19]
 (E is the electrode potential with respect to the Saturated Calomel
 Electrode (SCE): $E(\text{SCE}) = 0.241 E(\text{SHE})$ at 25°C).

The only driving force for hydrogen absorption would be electrochemical, since the WAF bolts were not under applied tensile stresses (service loads) during paint stripper treatment and the subsequent time before reinstallation in the aircraft structure. This means that much or all of the hydrogen that *might have been* absorbed could have diffused out through the bare steel surface once the bolts were removed from the paint stripper. An estimate of the time taken for any absorbed hydrogen to diffuse out of the bolts can be made as follows.

The checks mentioned in the introduction to this case history showed that the maximum time in paint stripper would have been no more than 3 days. The diffusion distance into the steel is given by $X = \sqrt{Dt}$, where D is the diffusion coefficient for hydrogen build-up in the steel and t is the time. The diffusion coefficients for build-up and decay of hydrogen in high strength steels are $2.2 \times 10^{-7} \text{ cm}^2/\text{s}$ and $0.85 \times 10^{-7} \text{ cm}^2/\text{s}$, respectively [3]. Let X be the same distance during hydrogen build-up and decay. Then the time required for all the introduced hydrogen to diffuse out of the steel is given by:

$$t_2 = t_1 \times D_1/D_2$$

Substituting 72 hours for t_1 and $2.2 \times 10^{-7} \text{ cm}^2/\text{s}$ and $0.85 \times 10^{-7} \text{ cm}^2/\text{s}$ for D_1 and D_2 , we obtain $t_2 = 186$ hours, which is slightly less than 8 days. This is less than the time between paint stripping and reinstallation in the aircraft structure, which was 3 – 4 weeks.

Summarising, it appears unlikely that exposure of the WAF bolts paint stripper would lead to retention of any absorbed hydrogen by the time they were reinstalled in the aircraft. Nor were the bolts damaged by corrosion in the paint stripper, see point (2) above.

20.5.4.2.4 *The “No Failure in 200 Hours” Criterion*

In the introduction to this case history it was mentioned that the OEM recommended IHE proof testing as well as tensile testing. The OEM first suggested proof testing per ASTM Standard F519-06 [7] and later per NASM1312-5 [9], whereby suspect and new WAF bolts would be subjected to sustained tensile loads at 75% of the notched fracture stress for 200 hours. Survival for 200 hours would validate the suspect bolts. This is the “no failure in 200 hours criterion” obtained from Troiano’s classic data [10], see Figure 20-4, and discussed in Section 20.4.3. For the WAF bolt validation programme the most important point from Troiano’s data is that most embrittled specimens failed well within 200 hours, in fact within 10 hours. This result is relevant to the service experience of the WAF bolts after paint stripper treatment. All these bolts had survived more than 200 service hours in the fully-torqued condition, making it very unlikely that they had been embrittled. This viewpoint, without elaboration, was used in arriving at the conclusions and remedial actions below. Subsequently it was possible to be more specific in justifying this viewpoint, see the **Postscript** after the remedial actions.

20.5.4.3 **Conclusions**

- 1) The tensile test results and analysis, fractography, and a discussion of electrochemical and hydrogen diffusivity considerations and the “no failure in 200 hours” criterion, led to the NLR’s conclusion that the WAF bolt tensile failure strengths were validated as unaffected by the paint stripper.
- 2) The data in Figure 20-34 show that some paint strippers can cause hydrogen pick-up in cadmium plated high strength steels. Hence relaxation of the proof test duration from 200 hours to 150 hours in so-called passive service environments, as mentioned in Section 20.4.3, is not necessarily advisable.

20.5.4.4 **Remedial Actions**

The CMT cleared the aircraft for further operation, whereby all the remaining WAF bolt assemblies were cleaned with an approved cleaner and protected with primer. These assemblies were subsequently replaced at the latest during the next scheduled inspection.

20.5.4.4.1 *Postscript*

Information later obtained from the OEM showed that the fully-torqued condition of the suspect bolts corresponds to 60% of the OEM A-allowable. In turn, this corresponds to 54% of the mean failure load of the D12 bolt breaks shown in Figure 20-30 and Figure 20-32. At this 54% level, equivalent to 160 ksi in Figure 20-4, Troiano’s data cannot completely exclude failures of the bolts at service times beyond 200 hours, since his tests were stopped after 100 hours. However, additional data from tests up to 1000 hours [19], [20], particularly the data from Movich [20], suggest that applying more than 50% of the unembrittled failure load would have caused embrittled bolts to fail well within 100 hours.

20.5.5 Flap Tracks

20.5.5.1 Introduction

During routine maintenance a fleet of maritime patrol aircraft were fitted with refurbished SAE E4340 steel flap tracks that had been re-electroplated with cadmium. Unfortunately, it was later revealed that the electroplating solution contained a prohibited brightener additive, which would have enhanced hydrogen pick-up and inhibited its removal during baking. The tensile strength level of the flap track steel was 1380 – 1500 MPa, which meant that there was a potential risk of IHE. To determine this, a validation programme was initiated based on SSRT tests and post-test fractography.

20.5.5.2 SSRT Testing and Fractography

Notched tensile specimens were machined from several locations in a number of spare flap tracks. The machining was modified to ensure that the steel was not significantly heated, thereby minimising the loss of any absorbed hydrogen. After machining, the specimens were stored at low temperature to prevent further hydrogen loss before testing.

Specimens from various flap track locations were baked for 23 hours at 191°C and SSRT tested at a cross-head displacement rate of 2.1×10^{-4} mm/s to determine the notched fracture stress of the unembrittled steel. Specimens from leading and trailing edge locations, where IHE cracking was considered to be most likely, were SSRT tested in the unbaked condition.

All the specimen fracture surfaces were examined by SEM for the presence of intergranular cracking.

20.5.5.3 Results

Table 20-4 gives the SSRT fracture stress results. These indicate that the trailing and leading edges had not been embrittled by IHE. This was confirmed by SEM fractography, since there was no evidence of intergranular cracking.

Table 20-4: SSRT Fracture Stress Results for Flap Track Steel Specimens.

Specimen Location	Notched Fracture Stress (MPa)	
	Range	Average
Unembrittled, Various Locations	1999 – 2240	2135 ± 123
Leading Edge End	1909 – 2275	2080 ± 155
Trailing Edge End	1944 – 2249	2110 ± 99

Furthermore, all specimens had a notched fracture stress greater than the proposed acceptance criterion of 1840 MPa for SSRT testing, see Section 20.4.6, even though the flap track steel tensile strength was lower than that of the standard test material (1790 – 1930 MPa).

20.5.5.4 Conclusions and Recommendations

From the results described in Sub-Section 20.5.5.3 it was concluded that the tested and in-service flap tracks had not been embrittled by the re-electroplating process. Consequently there were no remedial actions, and it was recommended that the refurbished flap tracks remain in service.

20.5.6 *In Situ* Brush-Plating Repair of Worn Flap and Slat Tracks

20.5.6.1 Introduction

Owing to maintenance schedule problems and costs there was a requirement for *in situ* repair of worn flap and slat tracks made from an ultrahigh strength steel and used in a tactical aircraft type. The repair should use electroplated nickel and preferably avoid low temperature baking after plating. The ‘Dalic Nickel Tungsten’ brush-plating process was proposed for the repair, but it was necessary to determine firstly whether IHE could be avoided without post-plating baking, and secondly the optimum plating conditions to achieve this [21].

20.5.6.2 Experimental Details

The specified operating ranges for the Dalic Nickel Tungsten brush-plating process are as follows.

- 1) Current density: 1.00 – 1.49 A/cm²
[optimum current density of 1.18 A/cm²]
- 2) Anode/cathode movement (anode speed): 0.10 – 0.25 m/s
[optimum anode speed of 0.17 m/s].

SAE E4340 notched tensile specimens heat treated to a tensile strength range of 260 – 280 ksi (1790 – 1930 MPa) and conforming to the dimensional requirements of ASTM F519-06 were plated using various combinations of current density and anode/cathode movement covering the process manufacturer’s specifications, including the optimum current density of 1.18 A/cm² and anode speed of 0.17 m/s. The specimens were then SSRT tested at a cross-head displacement rate of 2.1×10^{-5} mm/s, which is conservatively much slower than the rates mentioned in Sections 20.4.6 and 20.5.5.

In addition:

- a) Similar specimens were SSRT tested after plating under optimum conditions and baking for 23 hours at 191°C; and
- b) Following evaluation of the SSRT results, SLT notched tensile specimens were plated using the optimum and minimum current densities and anode speeds recommended by the process manufacturer and tested *unbaked* to see whether they met the 200 hour SLT pass required by ASTM F519-06.

20.5.6.3 Results and Discussion

The SSRT results are shown in Figure 20-35 and Figure 20-36. The unembrittled notched fracture stress for SAE E4340 steel is also indicated (dashed horizontal line) to enable assessing the degree of embrittlement by any of the plating conditions, including the optimum conditions of plating and baking.

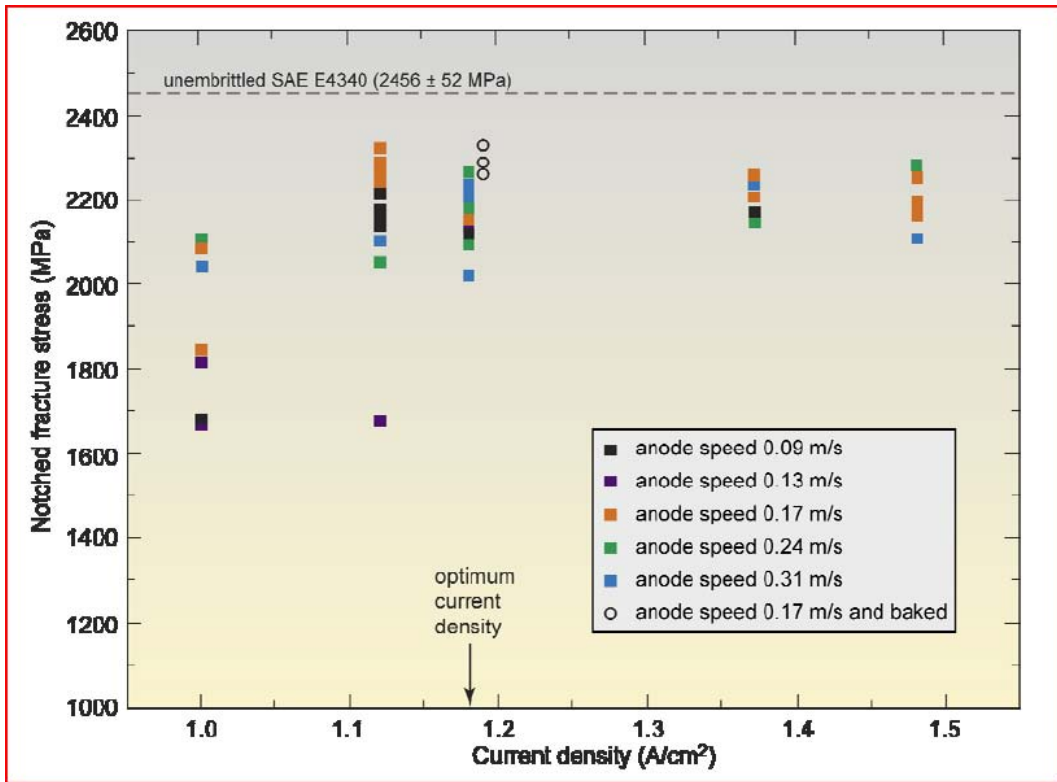


Figure 20-35: The Effect of Current Density in the Range Suggested by the Manufacturer on the Notched Fracture Stress of SAE E4340 Steel Specimens.

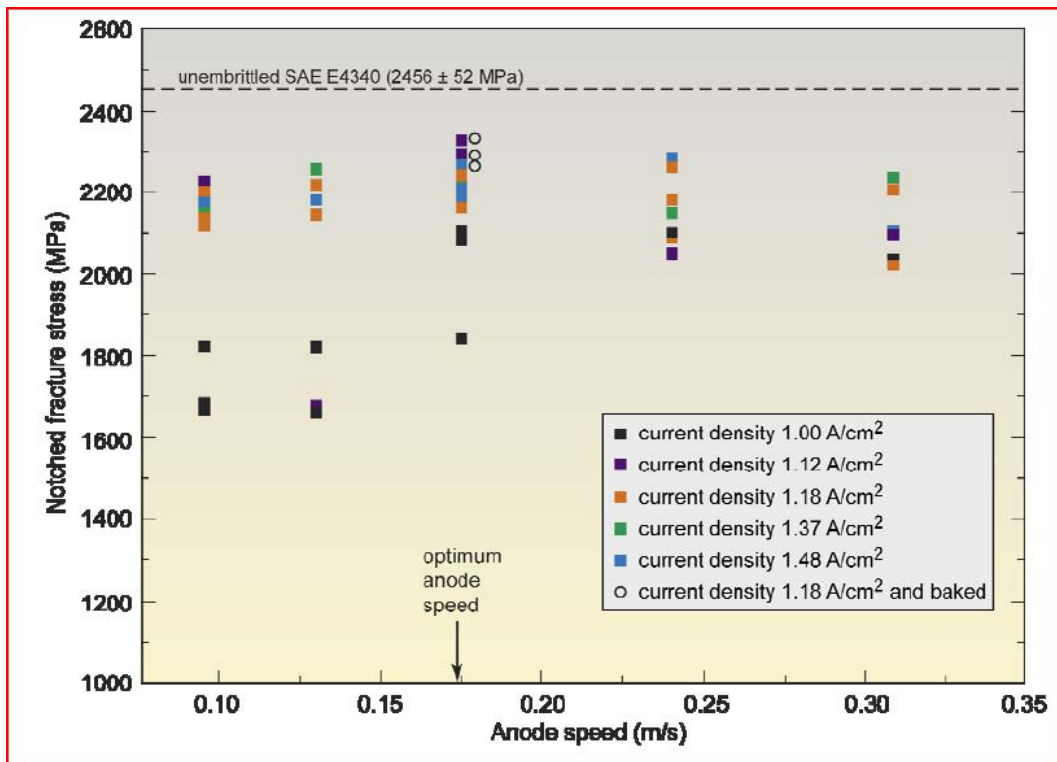


Figure 20-36: The Effect of Anode Speed on the Notched Fracture Stress of SAE E4340 Steel Specimens.

All of the SSRT specimens showed notched fracture stress reductions compared to the unembrittled fracture stress of 2456 ± 52 MPa. This was also observed in trials on Low Hydrogen Embrittlement (LHE) cadmium brush plated D6ac steel SSRT specimens [22]. More specifically, Figure 20-35 and Figure 20-36 indicate that the minimum reductions in fracture stress were obtained for SAE E4340 specimens plated under optimum conditions, whether subsequently baked or not. These results suggest that part of the fracture stress reductions may be due to some other phenomenon instead of IHE. One possibility is that the notch roots were slightly damaged by cleaning before plating.

The greatest reductions in SSRT notched fracture stresses were obtained from specimens plated with the lowest current densities and anode speeds. Some of these results were below the SSRT proposed acceptance criterion of 1840 MPa, which implies that specimens plated under these conditions might not have achieved the 200 hour SLT pass required by ASTM F519-06 (see Sections 20.4.1 and 20.4.6). This posed a potential problem for applying the Dalic Nickel Tungsten brush-plating process without subsequent baking.

To check this potential problem, SLT notched tensile specimens were plated using the process manufacturer's optimum and minimum current densities and anode speeds, and tested *unbaked* to see whether they met the 200 hour SLT pass required by ASTM F519-06. The SLT specimens plated under optimum conditions exceeded 818 hours without failure, while the specimens plated under minimum conditions exceeded 200 hours without failure. Hence it was concluded that all the plating conditions within the process manufacturer's specifications would meet the ASTM F519-06 requirements without post-plating baking.

20.5.6.4 Conclusions and Recommendation

This "case history" demonstrated that the Dalic Nickel Tungsten brush plating process can be applied to ultrahigh strength steel without baking, since a combination of SSRT and SLT results showed that the ASTM F519-06 requirements were met. Consequently this plating process was approved for *in situ* repair, without post-plating baking, of worn flap and slat tracks of the tactical aircraft type. This "case history" also shows that using more than one IHE test can be very useful when evaluating the suitability of plating processes for high and ultrahigh strength steels.

20.6 CONCLUDING REMARKS

Internal Hydrogen Embrittlement (IHE) continues to be a problem for high strength steel aircraft components. IHE is nearly always associated with finishing processes for both new and reconditioned components. It is well understood that pickling, cathodic cleaning and electroplating involve the risk of IHE, and there are strict requirements for these processes. Nevertheless, procedural errors and inadequacies still occur. The case histories described in Section 20.5 illustrate some of these errors and inadequacies for reconditioned components, namely:

- Small service-induced corrosion pits and IHE cracks undetected before re-electroplating.
- Possible inadequate baking.
- Abusive grinding during clean-up of the steel surface.
- Poor electroplating.
- Incorrect cleaning.

Some of these deficiencies can also occur for new components. Other, less frequent, errors that have been found for new components include incorrect choice of steel [23] or hardness and strength ranges [24].

20.7 ACKNOWLEDGEMENTS

We wish to acknowledge Alan Cox and Willie Pollock (DSTO), and Frank Grooteman and Anne Oldersma (NLR) for their contributions to the case histories reported in this chapter. The late Willie Pollock also made seminal contributions to developing the Slow Strain Rate Tensile (SSRT) and Incremental Step-Load (ISL) test procedures for hydrogen embrittlement testing.

20.8 REFERENCES

- [1] Wallace, W., Hoepfner, D.W. and Kandachar, P.V., “AGARD Corrosion Handbook, Volume 1, Aircraft Corrosion: Causes and Case Histories”, AGARDograph No. 278, Advisory Group for Aerospace Research and Development, Neuilly-sur-Seine, France, 1985.
- [2] Akhurt, K.N. and Baker, T., “The Threshold Stress Intensity for Hydrogen-Induced Crack Growth”, Metallurgical Transactions, A12, pp. 1059-1070, 1981.
- [3] Van Leeuwen, H.P., “A Quantitative Analysis of Hydrogen-Induced Cracking”, Doctor’s Thesis, Technical University Delft, Netherlands, June 1974.
- [4] Frank, R.C., “Time-Dependent Effects of Hydrogen in Steel”, Internal Stresses and Fatigue in Metals, Editors G.M. Rassweiler and W.L. Grube, Elsevier Publishing Company, Amsterdam, Netherlands, pp. 411- 424, 1959.
- [5] Thomas, R.L.S., Scully, J.R. and Gangloff, R.P., “Internal Hydrogen Embrittlement of Ultrahigh-Strength AERMET 100 Steel”, Metallurgical and Material Transactions A, Vol. 34A, pp. 327-344, 2003.
- [6] Lynch, S.P., “Failure of Structures and Components by Environmentally Assisted Cracking”, Engineering Failure Analysis, Vol. 1, pp. 77-90, 1994.
- [7] ASTM F 519-06, “Standard Test Method for Mechanical Hydrogen Embrittlement Evaluation of Plating/Coating Processes and Service Environments”, in: Annual Book of ASTM Standards, Section 15, Volume 15.03, ASTM International, West Conshohocken, PA, USA, 2007.
- [8] ASTM F 1624-06, “Standard Test Method for Measurement of Hydrogen Embrittlement in Steel by the Incremental Step Loading Technique”, in: Annual Book of ASTM Standards, Section 15, Volume 15.03, ASTM International, West Conshohocken, PA, USA, 2007.
- [9] National Aerospace Standard NASM1312-5, “Fastener Test Methods Method 5 Stress Durability”, Aerospace Industries Association of America, Inc., Washington, DC, USA, 1997.
- [10] Troiano, A.R., “Delayed Failure of High Strength Steels”, Corrosion, Vol. 15, pp. 207t-212t, 1959.
- [11] Pollock, W.J., “Statistical Treatment of Slow Strain Rate Data for Assessment of Hydrogen Embrittlement in Low Alloy High Strength Steel”, ARL-MAT-R-122, DSTO-AMRL, Fishermens Bend, Victoria, Australia, April 1990.
- [12] Kindermann, M.R., Cave, B. and Arnott, D.R., “A Slow Strain-Rate Tensile Testing Machine”, ARL-MAT-TM-399, DSTO – AMRL, Fishermens Bend, Victoria, Australia, 1989.
- [13] Gerrard, D.R., “The Determination of a Pass/Fail Criterion for the Slow Strain Rate Tensile (SSRT) Test for LHE Cadmium Electroplated High Strength Steel”, Milestone Report 6/02, Task AIR 99/076, DSTO, Melbourne, Australia, 2004.

- [14] Cox, A.F. and Pollock, W.J., "Investigation of the Cracking in HS748 Propeller Blade Retaining Bolts", ARL File BM2/03/17, Materials Division Ref. M89/83/AFC/WJP, DSTO, Melbourne, Australia, 1984.
- [15] Barter, S.A., "Cracking in Mirage Main Landing Gear Half Fork Assemblies", ARL File BM2/03/2, Materials Division Ref. M73/85/SAB, DSTO, Melbourne, Australia, 1986.
- [16] Dodson, B., "Weibull Analysis", ASQ Quality Press, Milwaukee, WI, USA, pp. 78-82, 1994.
- [17] Nelson, W.B., "Applied Life Data Statistics, Series in Probability and Statistics", Wiley & Sons, New York, NY, USA, pp. 370-386, 1982.
- [18] Durning, E.D.D., "Corrosion Atlas: A Collection of Illustrated Case Histories", Third, Expanded and Revised Edition, Elsevier Science Publishers B.V., Amsterdam, Netherlands, p. L [50], 1997.
- [19] Pollock, W.J. and Grey, C., "Assessment of the Degree of Hydrogen Embrittlement Produced in Plated High-Strength 4340 Steel by Paint Strippers using Slow Strain Rate Testing", Hydrogen Embrittlement: Prevention and Control, ASTM STP 962, Editor L. Raymond, American Society for Testing and Materials, Philadelphia, PA, USA, pp. 372-386, 1988.
- [20] Movich, C.R., "Notched Bar-Bending Test", Hydrogen Embrittlement Testing, ASTM STP 543, American Society for Testing and Materials, Philadelphia, PA, USA, pp. 64-73, 1974.
- [21] Gerrard, D.R., Milestone Report 3/01, "Hydrogen Embrittlement of High Strength Steels from the Dalic Nickel Tungsten Brush Plating Process", Task AIR 99/076, DSTO, 2002.
- [22] Gerrard, D.R., "Hydrogen Embrittlement of D6ac Steel from the Dalic LHE Cadmium Brush Plating Process", Milestone Report 4/01, Task AIR 99/076, DSTO, Melbourne, Australia, 2000.
- [23] Barter, S.A., "F111C Crew Module Electrical Disconnects, Locking Lug Failure", ARL File BM2/03/7, Materials Division Ref. M69/82/SAB, DSTO, Melbourne, Australia, 1984.
- [24] Barter, S.A., "Chinook Drop Stop Interposer Bolt Failures", ARL File BM2/03/11, Materials Division Ref. M49/82/SAB, DSTO, Melbourne, Australia, 1983.

Chapter 21 – NON-DESTRUCTIVE TESTING FOR CORROSION

David S. Forsyth

Texas Research International, TRI/Austin
Austin, Texas
USA

21.1 INTRODUCTION

Non-Destructive Testing (NDT) is defined by the American Society for Non-destructive Testing (ASNT) as: “The determination of the physical condition of an object without affecting that object’s ability to fulfill its intended function. Non-destructive testing techniques typically use a probing energy form to determine material properties or to indicate the presence of material discontinuities (surface, internal or concealed).” For the purpose of this article, the terms non-destructive testing, Non-Destructive Inspection (NDI), and Non-Destructive Evaluation (NDE) will be considered to be equivalent.

In the modern NDT paradigm, the uses of NDT can be broken into several categories where it plays an important role:

- Material property measurements;
- Process design for materials manufacturing;
- Online process control; and
- Quality control as various stages of manufacturing are completed.

In addition, NDT plays an important role in the continued safe operation of physical assets. For instance, NDT is being used in conventional inspections and in health monitoring, where NDT sensors are embedded or attached to the system being inspected or monitored for defects or damage. In all cases, the customer must define the requirements of the test, such as the minimum level of acceptability for the property being measured and the characteristics of the material discontinuities to be identified. Given this information, the NDT engineer or experienced technician can choose the appropriate method and develop an appropriate technique for the inspection requirements.

21.2 NON-DESTRUCTIVE TESTING METHODS

An NDT method is classified according to its underlying physical principle. For example, the common methods are:

- Visual and optical Testing (VT);
- Radiographic Testing (RT);
- Electromagnetic Testing (ET);
- Ultrasonic Testing (UT);
- Liquid Penetrant Testing (PT);
- Magnetic particle Testing (MT);
- Acoustic Emission testing (AE); and
- Infrared and thermal testing (IR).

An NDT technique defines all the parameters for the application of a specific method to a specific problem. These parameters include the instruments, probes, acceptance criteria, calibration specifications, and much more. ASNT offers a series of handbooks that are a key reference for the practical implementation of NDT. In addition, AMMTIAC (Advanced Materials, Manufacturing, and Testing Information Center) has a number of state-of-the-art reports and technology assessments that provide in-depth reviews of specific topics. A listing of these reports is available on the AMMTIAC website. The following sections will briefly describe each of the common methods listed above.

21.2.1 Visual NDT

By far, the most common NDT method is visual and optical testing. In many instances, a trained inspector armed with simple tools, such as a flashlight and magnifying glass, can perform a very effective inspection. In quality control, as well as in maintenance operations, visual testing is the first line of defence. When deciding upon whether to use visual testing, it is important to understand its potential as well as its limitations. If the visual method is not sufficient for the problem at hand, more complex methods must be considered. Using the visual inspection method for enclosed systems can be challenging and possibly ineffective. To enable a technician or engineer to inspect these difficult-to-see areas, a device known as a borescope is often used. Borescopes are essentially miniaturized cameras that can be placed on the end of a fiber optic cable. The camera can then be inserted into regions that are obstructed from direct visual inspection, and the resulting images are viewed in real-time on a video screen by the inspector.

21.2.2 Enhanced Visual/Optical NDT

There are a variety of enhanced visual/optical NDT methods available. In terms of corrosion NDT, these methods are generally used to detect and measure deformations on surfaces. These deformations may be caused by pitting on the exposed surface, or by sub-surface corrosion damage in built-up structure. There are a number of implementations of instruments based on Moire, Electronic Speckle Pattern Interference (ESPI) and digital speckle correlation [1], and holography. Other optical surface topography systems have been used for characterization of corrosion damage [2],[3]. Direct optical metrology methods such as laser interferometry and triangulation-based methods have been used in laboratory type situations for measuring pillowing caused by corrosion in thin aluminum structures [4].

21.2.3 Ultrasonic NDT

Ultrasonic testing employs an extremely diverse set of methods based upon the generation and detection of mechanical vibrations or waves within test objects. The test objects are not restricted to metals, or even to solids. The term ultrasonic refers to sound waves of frequency above the limit of human hearing. Most ultrasonic techniques employ frequencies in the range of 1 to 10 MHz. The velocity of ultrasonic waves traveling through a material is a simple function of the material's modulus and density, and thus ultrasonic methods are uniquely suited to materials characterization studies. In addition, ultrasonic waves are strongly reflected at boundaries where material properties change, and thus are often used for thickness measurements and crack detection. Recent advances in ultrasonic techniques have largely been in the field of phased array ultrasonics, now available in portable instruments. The timed or phased firing of arrays of ultrasonic elements in a single transducer allows for precise tailoring of the resulting ultrasonic waves introduced into the test object.

21.2.4 Eddy Current NDT

Electromagnetic Testing (ET), especially eddy current testing, is commonly used to inspect objects throughout their life cycle. Eddy current techniques employ alternating currents applied to a conducting coil held close to the test object. In response, the test object generates eddy currents to oppose the alternating current in the coil. The eddy currents are then sensed by the same coil, separate coils, or magnetic field

sensors. Changes in the induced eddy currents may be caused by changes to a material's electromagnetic properties and/or changes in geometry, including the abrupt changes in current flow caused by cracks. Thus ET methods are highly effective for the detection of cracks present on or below the surface of metallic objects. ET equipment has become extremely portable and is relatively inexpensive. It is the second most common method specified for NDT of aircraft. Recent advances in eddy current technology include multi-channel portable instruments, allowing faster inspections of large areas, and new magnetic sensors, such as the Giant Magnetoresistive (GMR) sensors developed for computer hard drives, instead of coils.

21.2.5 Thermographic NDT

Infrared and thermal testing methods are characterized by the use of thermal measurements of a test object as it undergoes a response to a stimulus. Thermal imaging cameras are the most common sensing method. Passive imaging of machinery or electronics may be used to detect hot spots indicative of problems. Imaging of test objects after the application of energy can be used to monitor the flow of heat in the object, which is a function of material properties as well as boundaries. Flash thermography techniques have been very successful in imaging disbonds and delaminations in composite parts, for example. The high cost of quality thermal cameras was previously a drawback of the IR method, but recently these have become significantly less expensive. Another significant recent advancement is the use of mechanical energy to stimulate localized heating at sub-surface discontinuities, such as cracks in metals, opening up a new field of application for the IR method.

21.2.6 Radiographic NDT

Historically, radiography is the next most common NDT method. Significant activity in the field occurred almost immediately after Roentgen's discovery of X-rays in 1895 [5]. Early literature notes the ability of radiographs to detect discontinuities in castings, forgings, and welds in metals. Discontinuities such as pores or inclusions in metals are readily detected in many cases. Cracks may also be detected using radiographic techniques, but attention must be paid to orientation and residual stress issues. Radiography continues to be widely used despite the expense and safety implications of the equipment. Recent advances in digital radiography have helped reduce the cost of employing this method by eliminating the use of film.

21.2.7 Additional NDT Methods

There are a number of other NDT methods that have been used for corrosion NDT. These include the Magneto-Optic Imager (MOI), a commercial device that images magnetic fields induced by a sheet current [6]. Microwave NDT methods have been used to find corrosion under paint layers [7]. Terahertz imaging is being used to find corrosion damage under thermal insulation tiles on the space shuttle [8].

Health monitoring for corrosion is a growing field, with the potential to reduce the impact of disassembly and reassembly of aircraft to enable traditional NDT. Some of the sensor types are direct evolutions of NDT methods, and are simply attached to the structure to be left in place. This topic is covered elsewhere in this book.

21.3 DATA FUSION

A simple definition of data fusion is the combination of multiple inputs into one output. Thus data fusion includes basic systems such as voting (if a majority of inputs are true, the output is true) as well as highly complex systems such as military target tracking or remote sensing using multiple band radars operating in different locations. There are three general categories used to describe the level at which data fusion takes place: Pixel level data fusion describes applications where little or no pre-processing is applied to the data,

and the fusion operation acts on the lowest level of the data. Feature level fusion refers to cases where feature extraction has been performed on the data before fusion. Finally, decision level fusion refers to the fusion of data that is carried out after feature extraction and identification on the data inputs. The results reported in this work use pixel-level fusion algorithms. Some applications of data fusion to NDI have been published, most of which are of moderate complexity (for example Gros [9],[10] and involve pixel or feature level fusion. One of the authors has previously applied simple data fusion methods on NDI results to identify and measure corrosion in aircraft structures [11], but the work presented in this paper uses NDI from commercially available inspection equipment and applies more advanced fusion techniques to yield quantitative estimates of the thicknesses of individual layers of a two-layer lap joint.

The generic steps required to perform data fusion on NDI data are:

- Inspection pre-processing;
- Registration of individual inspections on a common coordinate system; and
- Data fusion.

It is important to note that the steps of pre-processing and registration are in themselves value-added steps. Even before any data fusion operation has been performed, the NDI data from disparate sources have been brought together on one software platform, and registered on a common coordinate system. This is a significant improvement over most current practices for handling NDI data, and greatly facilitates the use of databases for maintenance planning. It also allows improved inspector interpretation by making comparison between NDI data much simpler. Often the pre-processing step can be used to transform a single NDI data source from the NDI domain to a quantitative measure; for example, Edge of Light images can be transformed from brightness levels to images of maximum pillowing deformation [12].

The final data fusion algorithm to be used will be specific to the application. Development of these algorithms will only be cost-effective for repetitive inspection situations, such as the common lap splice joint. However, the preliminary steps of data handling, pre-processing, and registration are likely to become more commonly used as fleet maintenance practices are modernized, reducing the costs of implementing data fusion in practical situations.

21.4 RELIABILITY OF NDT FOR CORROSION

When NDT is used as part of the management of risk in the life cycle maintenance of an aircraft, it is imperative to know what is the probability of finding (or equivalently of missing) discontinuities of interest in an inspection. This is usually called the Probability Of Detection (POD). The development of the POD metric was originally directed towards fatigue cracks, but it is important to note that the POD approach is not limited to cracks, and has in fact been applied to other discontinuities such as corrosion loss, impact damage, or delaminations (see for example Komorowski et al. [13], Forsyth et al. [14], Ashbaugh et al. [15], Hoppe et al. [16]. The current POD approaches present POD as a function of a single metric of damage, for example crack length, as shown in Figure 21-1 below. In cases where the corrosion damage of interest can be characterized by a single metric, the conventional POD approaches will be suitable. This may be the case for intergranular cracking and pitting on an exposed surface. In other cases, multi-dimensional damage is not well characterized by a single metric, and a number of approaches have been developed.

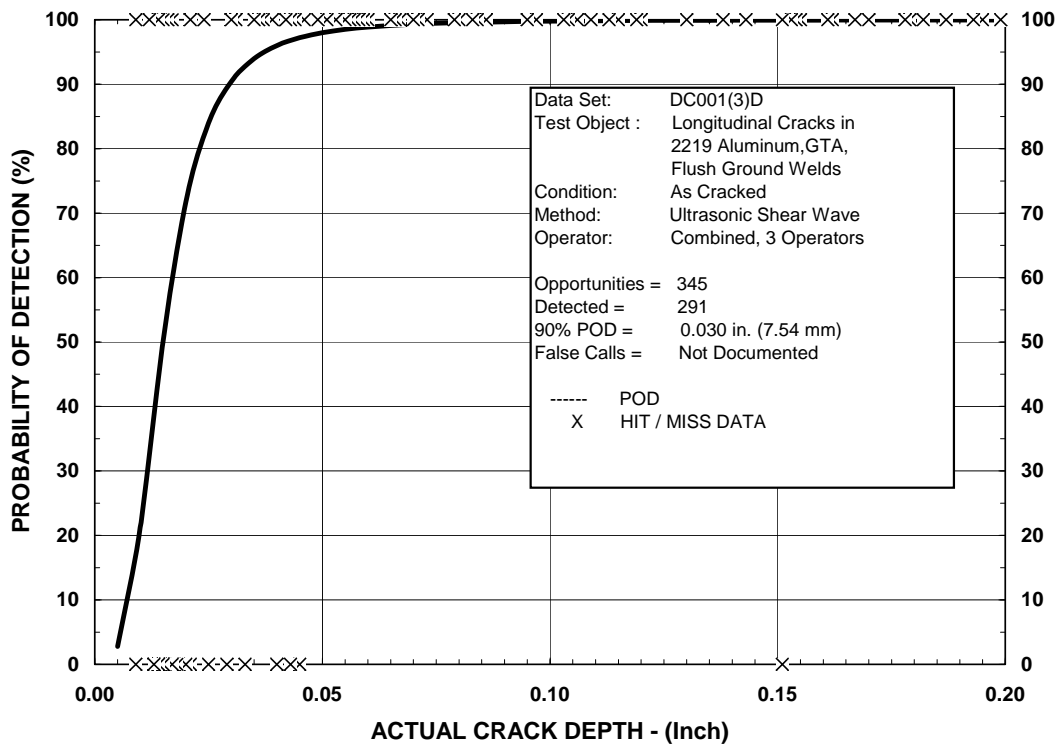


Figure 21-1: An Example of a POD Curve, from the Ultrasonic Inspection of Welds in Aluminum for Cracks (from Rummel and Matzkanin, [17], used with permission).

Both the USAF [18] and the United States Federal Aviation Agency (FAA) [19]-[21], have published guidelines that describe in detail the experiments required to estimate the POD of an inspection system. These documents are in the public domain, and can be obtained for free from the respective government agencies as well as the Department of Defense’s Advanced Materials, Manufacturing, and Testing Information Analysis Center (AMMTIAC) (see <http://ammtiac.alionscience.com>).

There are a number of useful general statements that can be made about estimating POD. The process of POD estimation requires a number of inspections to be performed:

- Using the complete, pre-defined inspection system that is being assessed including representative equipment, procedures, inspectors, and target parts;
- Using parts with discontinuities that represent the discontinuities of interest or a means to assess the difference between the two: for example, using machined notches or flat bottomed holes can provide a useful measure of capability, but should not be assumed to be representative of cracks or other natural discontinuities; and
- Using an inspection procedure and environment typical of the deployed environment. Human factors studies have shown that the relationship of factors such as environment (lighting, temperature, etc.), training, experience, motivation and others is not simple and often not intuitive.

It is key to understand the physical parameters that may affect the response of the NDT system to a discontinuity to be able to execute a representative POD estimate. If parts from service, with discontinuities arising from service, are available; this is the optimal situation. However, in most cases, this is not possible. Therefore every reasonable effort should be made to replicate the service discontinuities as close as possible, or to use engineering judgment as to whether safety factors are needed to account for the difference between the POD experiment and in-service conditions.

Unique approaches to POD for corrosion damage have been developed for the case of corrosion in the internal surfaces of aircraft skin splice joints . Ashbaugh et al. [15] showed that detection of corrosion in this case was a function of both the thickness loss and area affected (see Figure 21-2 below).

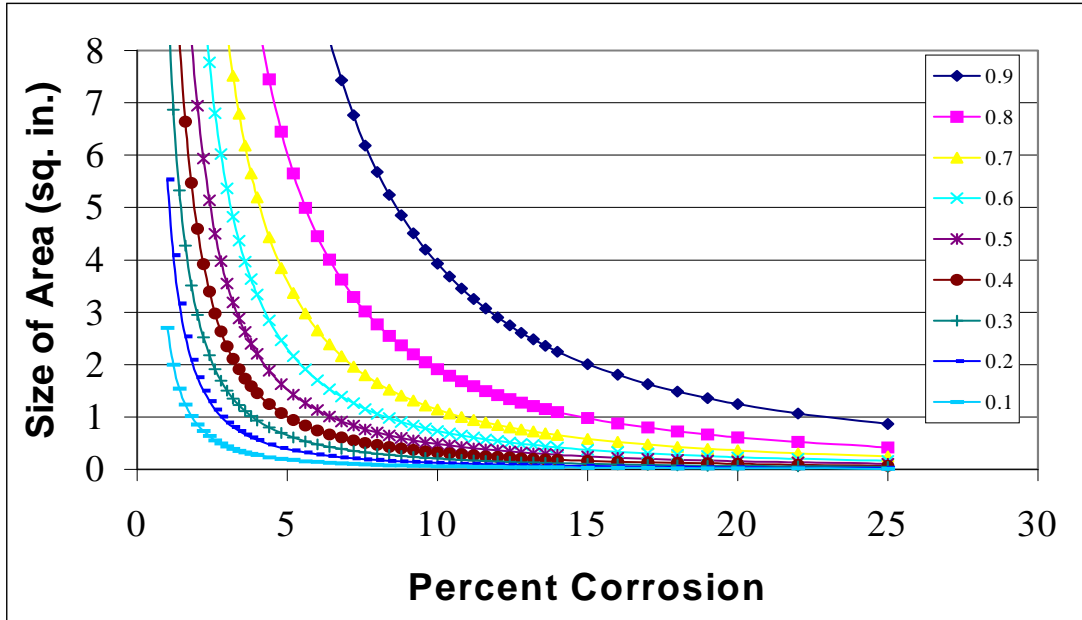


Figure 21-2: Data from Experiment, Showing Contours of POD Values as a Function of Both Area and Thickness Loss of Damage (from Ashbaugh et al. [15], used with permission).

Liao et al. [22] used the error in thickness loss measurement by NDT to calculate the effect of this error on the risk and therefore maintenance actions required, see Figure 21-3. K/C-135 lap splice joints were used as the basis of this case study. As shown in the figure below, increasing error results in increasing uncertainty about the NDT assessment, and therefore more severe maintenance actions are required as NDT error increases for the same estimated thickness loss.

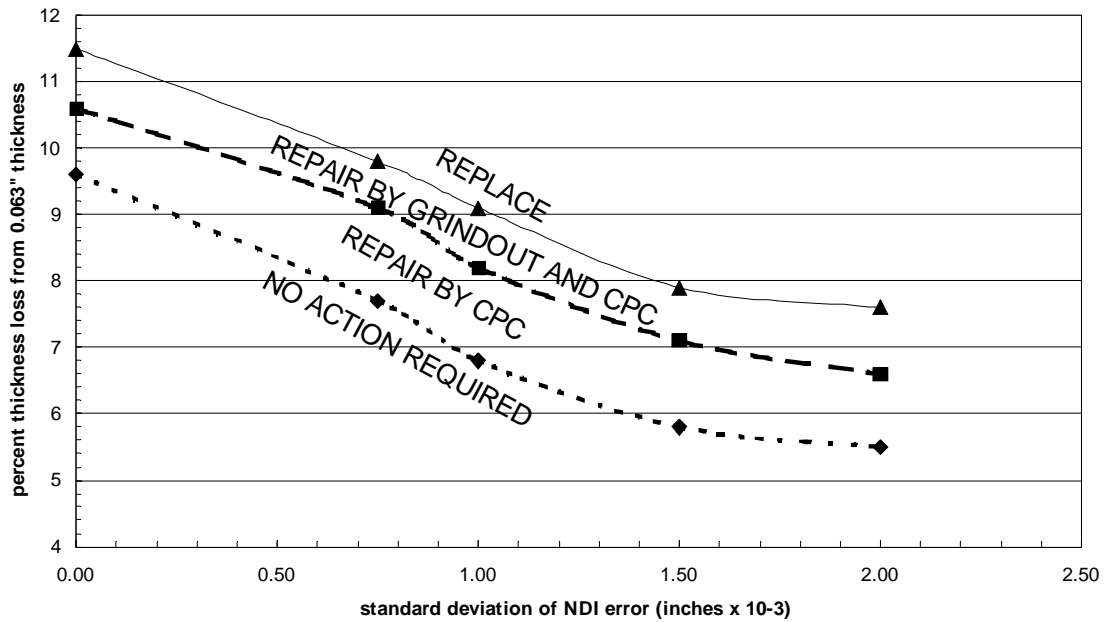


Figure 21-3: A Graph of the Effect of NDT Error on the Level of Damage and Subsequent Maintenance Actions (see Liao et al. [22]).

21.5 CASE STUDIES

21.5.1 Intergranular Corrosion in Thick Section Aluminium Structure

Typical examples of thick section structure are wing skins, ribs, and spars; and complex forgings used for fittings at locations like wing to body attachment points. These structures are commonly manufactured from 7000 series aluminum alloys, 7075-T6 being common on older aircraft. More corrosion resistant alloys are generally used in modern designs.

Because of the materials and product forms typical of these structures, intergranular corrosion attack is a common problem. This attack begins at pitting at exposed grains, and quickly becomes intergranular in nature. If sustained stresses are present, due to residual stresses or even simple “weight on wheels” loads, the phenomenon often called “stress corrosion cracking” can result.

In a number of cases, inspection may be only an interim solution, providing time for material substitution programs. Any pitting on highly loaded forgings of Al 7075-T6 or older vintage 7000 series alloys is capable of nucleating intergranular cracking. If these components are exposed for visual inspection, this may be sufficient to detect pitting and initiate any required maintenance actions. Interesting case studies include the C-130 “pork chop” fitting (see Chapter 5) and the C-141 landing gear hub [23].

Intergranular attack commonly nucleates at corrosion pits on exposed end-grains, Figure 21-4. Holes with steel fasteners are a common site, as fretting eventually wears off the coatings designed to isolate the steel from the aluminum. In severe cases, the material bulges around the fastener due to the corrosion product between multiple intergranular cracks. This is called exfoliation.

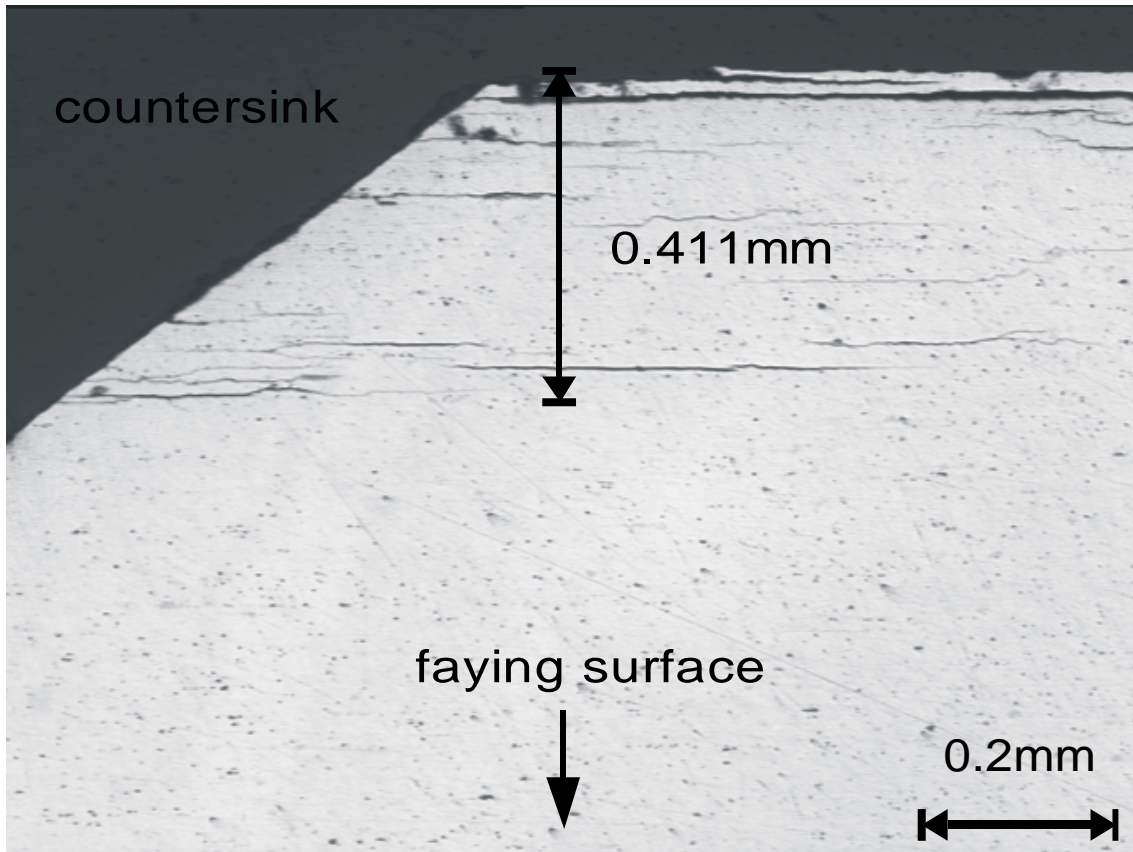


Figure 21-4: Metallographic Section Around a Fastener Hole in a Boeing 707 Wing Skin Plank, Showing Multiple Layers of Intergranular Attack from Pits in the Countersink – the material is 7178-T6 aluminum (from Forsyth et al. [24]).

This type of damage is relatively easy to detect, especially once it has progress beyond the countersink of the fastener. Even before it is visible as exfoliation, UT and IR methods can readily detect it, but will only measure the top layer and any layers beneath which extend beyond the top layer, Figure 21-5 [24].

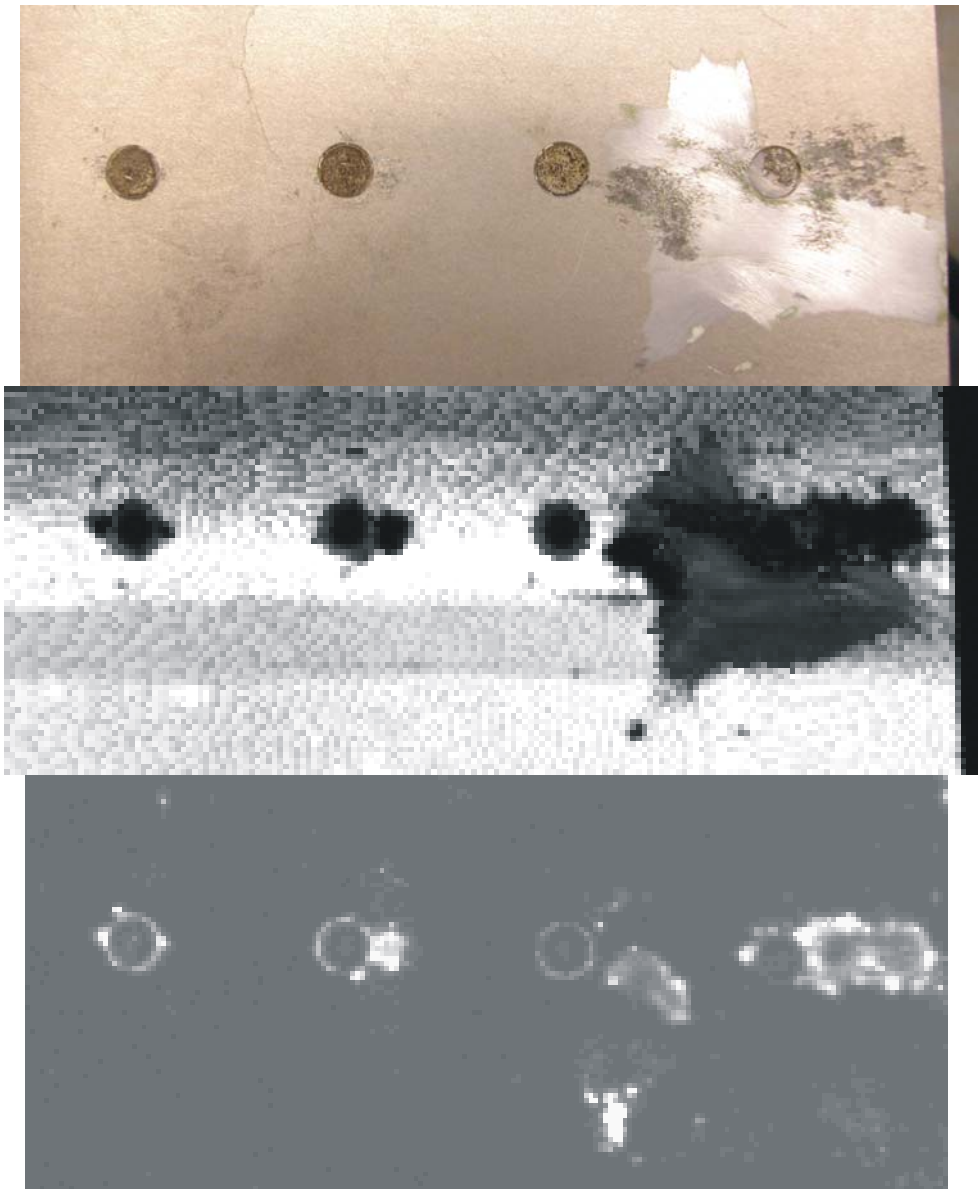


Figure 21-5: From Top to Bottom: A Photograph, a UT Image, and an IR Image of a Section of Wing Plank from a Boeing 707, Showing Exfoliation Damage and Grinding Marks from Repairs – the material is 7178-T6 aluminum (from Forsyth et al. [24]).

More advanced UT methods use surface waves or reflections to interrogate the volume obscured by fasteners, and can detect smaller areas of exfoliation. These methods are still subject to the phenomenon of top or bottom layers obscuring exfoliation occurring between them.

As described above, using UT techniques, it is relatively simple to determine the depth of the first layer of exfoliation that extends beyond fasteners. Accuracy in thick sections should be 0.127 mm (0.005”) or better in depth. More advanced UT techniques can interrogate the bottom of the fastener hole and locate the bottom layer. Accuracy of 0.254 mm (0.010”) is probably achievable under well-controlled situations.

Exfoliation that extends beyond the fastener head can be detected by simple UT and IR methods, as well as enhanced visual methods. Sizing for all these methods is limited by probe sizes and in the case of IR methods, diffusion. UT is the most accurate sizing method, and a measurement accuracy of 0.254 mm

(0.010”) should be achievable. The sensitivity of IR methods is more affected by the depth at which the exfoliation occurs, and this is not well known.

21.6 REFERENCES

- [1] Jin, F. and Chiang, F.P., “ESPI And Digital Speckle Correlation Applied To Inspection Of Crevice Corrosion On Aging Aircraft”, R. NDE., Vol. 10 (2), pp. 63-73, 1998.
- [2] Komorowski, J.P., Bellinger, N.C., Gould, R.W., Marincak, A. and Reynolds, R., “Quantification of Corrosion in Aircraft Structures with Double Pass Retroreflection”, CASJ, Vol. 42 (2), pp. 76-82, 1996.
- [3] Forsyth, D.S., Komorowski, J.P., Marincak, A. and Gould, R.W., “The Edge of Light Enhanced Optical NDI Technique”, CASJ, Vol. 43 (4), pp. 231-235, 1997.
- [4] Eastaugh, G.F., Merati, A.A., Simpson, D.L., Straznicky, P.V. and Krizan, D.V., “The Effect of Corrosion on Durability and Damage Tolerance Characteristics of Longitudinal Fuselage Skin Splices”, in USAF Aircraft Structural Integrity Program Conference 1998, San Antonio, TX, USA, 1-3 December 1998.
- [5] Bossi, R.H., Iddings, F.A., Wheeler, G.C. and Moore, P.O., “Radiographic Testing, Nondestructive Testing Handbook”, 3rd. Ed., Vol. 4, American Society for Nondestructive Testing, Columbus, OH, USA, 2002.
- [6] Thome, D.K., Fitzpatrick, G.L. and Skaugset, R.L., “Aircraft Corrosion and Crack Inspection Using Advanced MOI Technology”, in Nondestructive Evaluation of Aging Aircraft, Airports, and Aerospace Hardware, SPIE Proceedings Vol. 2945, Scottsdale, AZ, USA, pp. 365-373, 3-5 December 1996.
- [7] Hughes, D., Zoughi, R., Austin, R.K., Wood, N. and Engelbart, R., “Near-Field Microwave Detection of Corrosion Precursor Pitting under Thin Dielectric Coatings in Metallic Substrate”, in Thompson, D.O. and Chimenti, D.E., Review of Progress in Quantitative Nondestructive Evaluation: Vol. 22, AIP Conference Proceedings, 657, pp. 462-469, 2003.
- [8] Anastasi, R.F., Madaras, E.L., Seebo, J.P., Smith, S.W., Lomness, J.K., Hintze, P.E., Kammerer, C.C., Winfree, W.P. and Russell, R.W., “Terahertz NDE Application for Corrosion Detection and Evaluation Under Shuttle Tiles”, Proc. SPIE Int. Soc. Opt. Eng. 6531, 2007.
- [9] Gros, X.E., “NDT Data Fusion”, Arnold, 1997.
- [10] Gros, X.E., “Applications of NDT Data Fusion”, Kluwer Academic Publishers, 2001.
- [11] Forsyth, D.S. and Komorowski, J.P., “The Role of Data Fusion in NDE for Aging Aircraft”, in Nondestructive Evaluation of Aging Aircraft, Airports, and Aerospace Hardware IV, SPIE Proceedings Vol. 3994, pp. 47-58, 2000.
- [12] Forsyth, D.S., Gould, R.W. and Komorowski, J.P., “Correlation of Enhanced Visual Inspection Image Features with Corrosion Loss Measurements”, in Maldague X P V, TONE Volume 3: III International Workshop – Advances in Signal Processing for Non Destructive Evaluation of Materials, ASNT, Columbus, OH, USA, pp. 365-372, 1998.
- [13] Komorowski, J.P., Forsyth, D.S., Simpson, D.L. and Gould, R.W., “Corrosion Detection in Aircraft Lap Joints: Proposed Approach to Development of POD Data”, in RTO Workshop on Airframe

Inspection Reliability under Field/Depot Conditions, Brussels, Belgium, RTO-MP-10, AC/323 (AVT)TP/2, pp. 8-1 – 8-8, 13-14 May 1998.

- [14] Forsyth, D.S., Komorowski, J.P. and Gould, R.W., “Double Pass Retroreflection Versus Visual POD of Impact Damage in Composites”, Presented at RTO Workshop on Airframe Inspection under Field/ Depot Conditions, Brussels, Belgium, RTO-MP-10, AC/323(AVT)TP/2, pp.18.1 – 18.6, 13-14 May 1998.
- [15] Ashbaugh, D.M., Bode, M.D., Boyce, K.L. and Spencer, F.W., “Corrosion Structured Experiment”, in Thompson, D.O. and Chimenti, D.E, Review of Progress in Quantitative Nondestructive Evaluation: AIP Conference Proceedings, Vol. 21, p. 615, 2001.
- [16] Hoppe, W., Pierce, J. and Scott, O., “Automated Corrosion Detection Program Final Report for 07 April 1997 – 06 October 2001”, United States Air Force Report AFRL-MP-WP-TR-2001-4162, 2001.
- [17] Rummel, W.D. and Matzkanin, G.A., “Nondestructive Evaluation Capabilities Databook”, NTIAC-DR-95-02, Advanced Materials, Manufacturing, and Testing Information Center, operated by Alion Science & Technology on behalf of US DoD, Rome, NY, USA, 13440, 1996.
- [18] Anon, MIL-HDBK-1823a, United States Air Force, 2009.
- [19] Spencer, F.W., Borgonovi, G., Roach, D., Schurman, D. and Smith, R., “Reliability Assessment at Airline Inspection Facilities Volume I: A Generic Protocol for Inspection Reliability Experiments”, DOT/FAA/CT-92/12, I, 1993.
- [20] Spencer, F.W., Borgonovi, G., Roach, D., Schurman, D. and Smith, R., “Reliability Assessment at Airline Inspection Facilities Volume II: Protocol for an Eddy Current Inspection Reliability Experiment”, DOT/FAA/CT-92/12, II, 1993.
- [21] Spencer, F.W. and Schurman, D., “Reliability Assessment at Airline Inspection Facilities Volume III: Results of an Eddy Current Inspection Reliability Experiment”, DOT/FAA/CT-92/12, III, 1995.
- [22] Liao, M., Forsyth, D.S., Komorowski, J.P., Safizadeh, S., Liu, Z. and Bellinger N.C., “Risk Analysis of Corrosion Maintenance Actions in Aircraft Structures”, in the Proceedings of the 22nd Symposium of the International Committee on Aeronautical Fatigue, ICAF 2003, Lucerne, Switzerland, May 2003.
- [23] Brooks, C., Honeycutt, K., Prost-Domasky, S. and Peeler, D., “Monitoring the Robustness of Corrosion & Fatigue Prediction Models”, in 2001 United States Air Force Aircraft Structural Integrity Program (ASIP) Conference, Williamsburg, VA, USA, 11-13 December 2001.
- [24] Forsyth, D.S., Liu, Z., Hoffmann, J. and Peeler, D., “Data Fusion for Quantitative Nondestructive Inspection of Corrosion Damage in Aircraft Wing Structures”, in United States Air Force Aircraft Structural Integrity Program (ASIP) Conference, Savannah, GA, USA, 10-12 December 2002.



Chapter 22 – INSPECTION OF HELICOPTER ROTOR BLADES BY NEUTRON- AND X-RAY RADIOGRAPHY

M. Balaskó and L. Horváth
MTA KFKI Atomic Energy Research Institute
Budapest
HUNGARY

22.1 INTRODUCTION

In order to detect the presence of defects in the composite structure of helicopter rotor blades, combined neutron- and X-ray radiography investigations were performed at the Budapest Research Reactor. The rotor blades were about 10 m (or 6,5 m) long, and therefore the images were taken in several segments, and a special program was developed to reconstruct the entire radiographic image from the individual segments. Several types of defects were discovered using neutron radiation: imperfections in the honeycomb structure, resin-rich or resin-starved areas at the core-honeycomb surfaces, in-homogeneities in the adhesive filling, corrosion products behind the covering, and water percolation at the sealing interfaces of the honeycomb sections. The location and condition of structural metal parts was analysed by X-ray radiography.

A comment was once made that a helicopter was a multiple-spindle Wöhler fatigue machine. Although this is perhaps a rather unkind remark there is, nevertheless, some truth in the fact that a helicopter, by its very nature, generates large dynamic forces in its entire rotor system. Basically four constant forces are served by the rotor blades:

- Centrifugal forces;
- Lift forces;
- Flapping moment, i.e., a bending moment about horizontal axis; and
- Drag (or lag) moment, i.e., a bending moment about a vertical axis.

In addition, the rotor blades are used and stored on the airfield during both summer and winter. Altogether the huge loading and the harmful consequences of the weather reduce the life-time of the helicopter rotor blades.

The safe life testing of rotary wing aircraft is of paramount importance and especially as it applies to the rotor blades. The identification of a structural defect that can grow to the point where structural integrity is affected comprises a central challenge. In this process, the inspection of structures and the monitoring of the rate of growth of defects in relation to the total flight hours are essential. The above demands underline the necessity of testing and applying new Non-Destructive Testing (NDT) methods for inspection in service.

22.2 METHODS

Neutron- and X-ray Radiography (NR and XR) utilize transmission of radiation to obtain information on the structure and/or inner condition of a given object. The basic principle of radiography is very simple [1]. The object under examination is placed in the path of the incident radiation, and the transmitted radiation is detected by a two-dimensional imaging system, as illustrated in Figure 22-1. The radiography arrangement consists of a radiation source, a pin hole type collimator which forms the beam, and a detection system which registers the transmitted image of the investigated object.

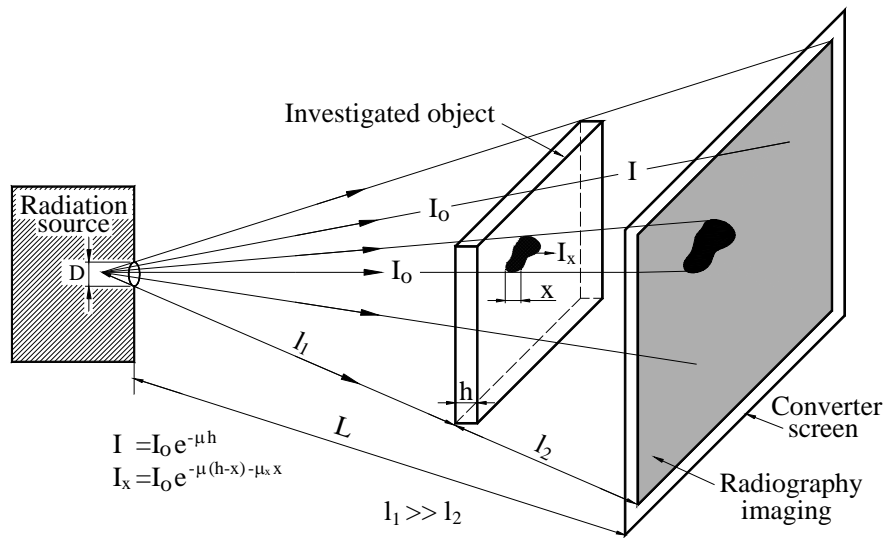


Figure 22-1: General Principle of Radiography.

The most important characteristic technical parameter of a radiography facility is the collimation ratio L/D where L is the distance between the incident aperture of the collimator and the imaging plane, D is the diameter of the aperture. This important parameter describes the beam collimation and will limit the obtainable spatial resolution by the inherent blurring independently from the properties of the imaging system. This unsharpness U_{beam} can be related to the distance between the object and the detector plane l_2 and to the L/D ratio:

$$U_{beam} = \frac{l_2}{L/D}$$

Two opposing demands have to be taken into consideration when planning a radiography arrangement: if L/D is large then the neutron flux Φ_{NR} at the imaging plane is relatively weak but the geometrical sharpness is high, and vice versa:

$$\Phi_{NR} = \frac{\Phi_s}{16(L/D)^2}$$

where Φ_s is the incident neutron flux.

In radiography imaging the attenuation coefficient μ is a crucial parameter. The transmitted intensity of the radiation, I , passing through a sample with an average transmission of μ can be written as:

$$I = I_0 e^{-\mu h}$$

where I_0 is the incident intensity and h is the thickness of the sample in the beam direction. If there is any inclusion (in-homogeneity, inner structure) in the sample of thickness x and transmission μ_x then the transmitted intensity, I_x is given as:

$$I_x = I_0 e^{-\mu(h-x) - \mu_x x}$$

If the value of μ and μ_x are different from each other then the presence of the inclusion will provide a contrast in the radiography image (dark spot in Figure 22-1).

The attenuation coefficient vs. atomic number is plotted in Figure 22-2 for neutron radiation and for gamma and X-rays. Its value depends on both the coherent and incoherent scattering and on the absorption properties of the element(s). For neutrons μ does not show any regularity as a function of atomic number, and for some of the lightest elements (H, B, Li) the attenuation coefficient is by two orders of magnitude greater than the corresponding parameter for most of the technically important elements, such as Al, Si, Mg, Fe, and Cr. This fact is of practical importance, viz. neutrons penetrate almost all metals used for construction purposes with little loss in intensity; in contrast they are considerably attenuated in passing through materials containing hydrogen, such as water, oil or several types of synthetics. On the other hand, in the case of X-ray and gamma radiation, this dependence may be characterized by more or less continuously increasing curves. This means that the radiation is absorbed to a great extent by heavy elements whereas it penetrates light materials such as hydrogen without significant loss in intensity. These differences for various radiations provide the opportunity to gain complementary information by using all three types of radiation together.

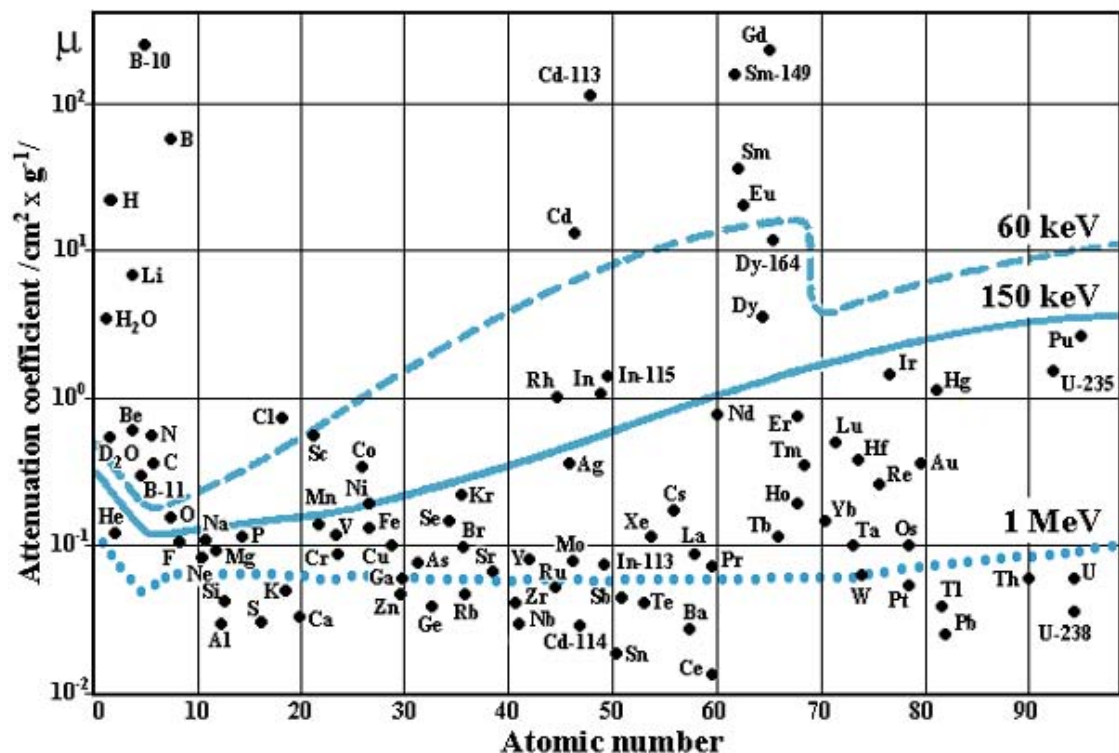


Figure 22-2: Attenuation Coefficient (note the logarithmic scale) of Elements for Neutrons (separate dots), for 1 MeV Gamma-Ray (dotted line), for 150 kV X-Ray (solid line) and for 60 kV X-Ray (dashed line).

Our imaging system detects the shading picture of the investigated object by a scintillator screen and a Low-Light-Level (LLL) CCD camera which records the light which is emitted by the scintillator. The images recorded by a CCD camera are inherently digital data and are stored by a PC. A second detection method, an Imaging Plate (IP), was used for the imaging of the plastic fiber-glass rotor blades. The IP is a new film-like radiation image sensor based on photo-excitation luminescence. It consists of a specifically designed composite structure that traps and stores the radiation energy. A polyester support film is uniformly coated with a photo-excitabile luminescent material – barium fluorobromide containing a trace amount of Eu^{2+} as a luminescence centre (BaFBr, Eu^{2+}) and it is then coated with a thin protective layer. The stored energy is stable until scanned with a laser beam whereupon the energy is released as luminescence and detected by a special multiplier. The scanner is read by a PC which provides a visual picture and allows the information to be stored electronically. After scanning and reading the IP plate will be erased prior to reuse.

22.3 INVESTIGATED OBJECTS

22.3.1 Metal Composite Structure

The majority of the helicopters, Mi-8, Mi-17 and Mi-24 types, in the Hungarian Army's inventory are several decades old and yet they are required to provide continued service. One of the most important components is the rotor blade. They are made of composite structures and contain 21 pieces of honeycomb construction with many bonded surfaces. The 21 sections of the rotor blades were divided into 4 bands horizontally and 53 field columns vertically [4]. A key part of the rotor blade comprises the aluminium alloy main spar bonded to the honeycomb structure as seen in Figure 22-3. Band "A" gives information mainly about the state of the trailing edge and the backside stringer. Band "B" shows the state of the honeycomb structure. The state of the bonded area on the aluminium-alloy spar is represented by band "C". The state of the anti-ice heater and front edge of the rotor blade are both shown by band "D". Every recorded image is identified by a capital letter, indicating the band in the rotor blade, and a two-digit number indicating the field column from which it was taken. These identifiers were used as markers during the inspections. The markers are positioned on the right-upper corner of every exposure.

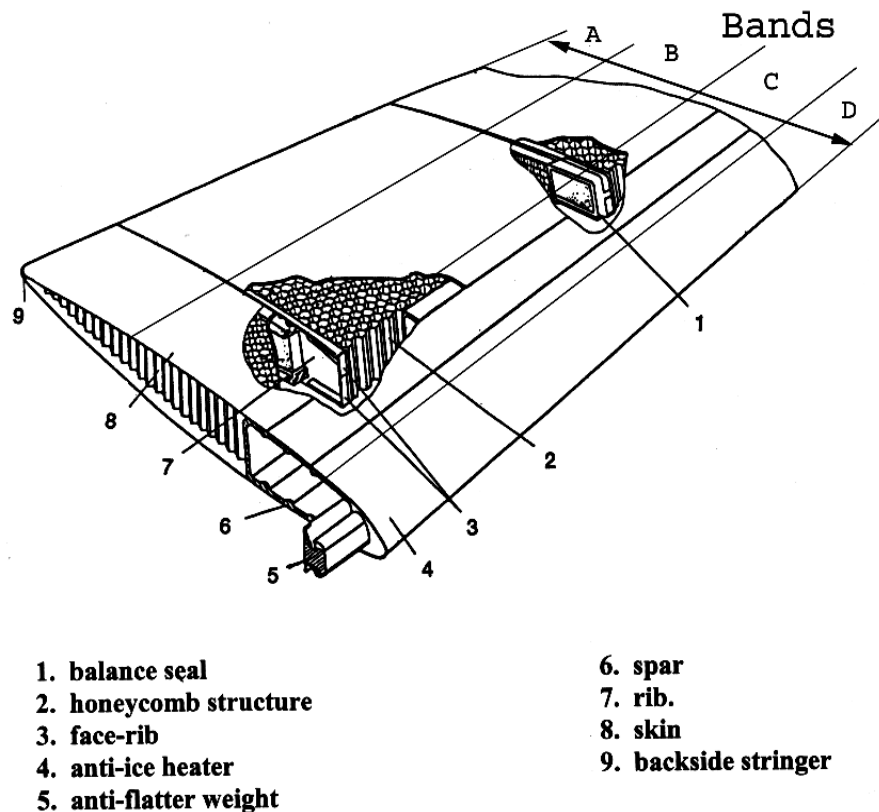


Figure 22-3: The Inner Structure of the Rotor Blade.

22.3.2 Plastic Fiber-Glass Structure

The Ka-26 type helicopters were used as reconnaissance-vehicles in the 1980's. Later they were withdrawn from military service and used for agricultural purposes. The rotor blades are made of composite structure except for the root-structure and the anti-flutter weight. The length of the rotor blade is ~ 6.5 m and its weight is ~11.5 kg. The 14 sections of the rotor blades were divided into 2 ("C" and "B") bands horizontally and 38 field columns vertically. Band "B" gives information mainly about the

state of trailing edge and the backside stringer. The state of the bonded area on the plastic fiber-glass spar is represented by band "C" with the anti-flutter weight and the anti-ice heater. These sections are filled up by cross-linked polymer foam. The inner structure of the rotor blade is shown in Figure 22-4.

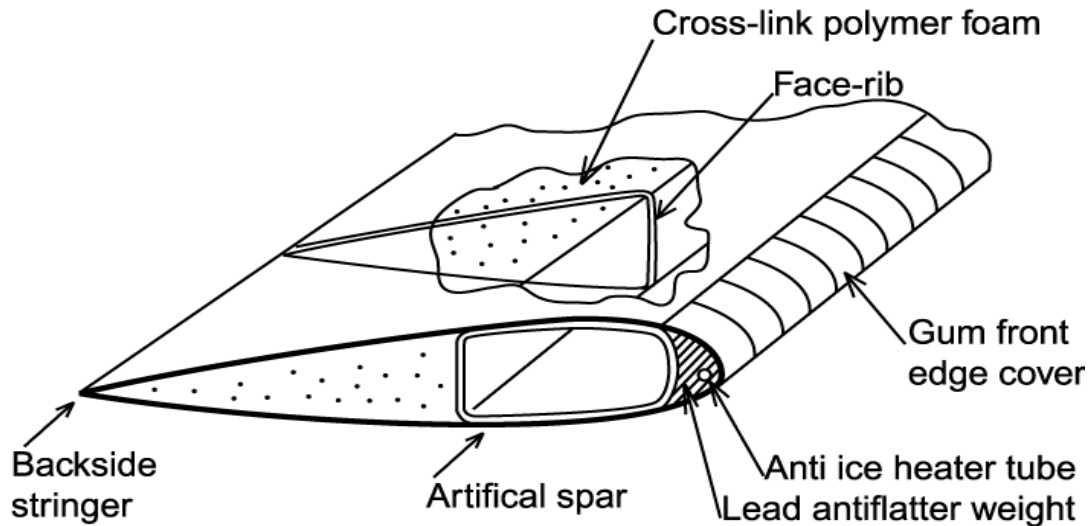


Figure 22-4: The Inner Structure of the Ka-26 Rotor Blade.

22.4 EXPERIMENTAL FACILITIES

Measurements were performed at the Dynamic Radiography Station (DRS) [2] at the 10 MW research reactor in Budapest. Its main parameters are as follows. The neutron flux is $10^8 \text{ n} \times \text{cm}^{-2} \text{ sec}^{-1}$, the collimation ratio (L/D):190, the diameter of the beam: 220 mm. The portable X-ray generator was adjusted to 150 kV and 3 mA. The radiography images were converted to optical images by a ZnS_{Ag}/Li⁶ scintillation screen (Applied Scintillation Technologies Ltd.) for NR and a ZnS type LGG400 scintillation screen was used for XR. The optical images were detected by a Low Light Level (LLL) CCD camera, which is cooled by a double Peltier system. The pictures were stored and processed by a Pentium II PC using MATROX Pulsar and Image-Pro Plus software. When the IP detector technique is applied the types of the IP plates are ND 20X25 and ND 20X40 sheets. The type of the reader is BAS 2500 and the type of the eraser is 0308.

Figure 22-5 shows the arrangement of the image system used for metal-composite blades in this work. In addition, we have two background TV cameras. One of these allows position control for the rotor blade picture by picture and the other serves as visual verification of the whole procedure. The rotor blades were moved during the experiments by an extraordinary remote control mechanism. Its weight limit was 250 kg. The surface to be scanned measures 9800 x 700 mm². The state of the rotor blades could be examined in dry and wet conditions, thus simulating complicated weather circumstances. Humidity was controlled using a "Moistening Conditioning" module with water supplied by a closed-circuit High pressure water pump system. The procedure is shown in Figure 22-6. The Moistening module is situated in the middle of the picture. The rotor blade is moved from left to right direction. In the first step, both sides of the bands A and B of the rotor blade are injected by two nozzles. In the second step the direction of movement is changed and the bands C and D are wet. After this procedure it is necessary to wait 15 minutes for the drying. The next step involves the XR measurement as shown in Figure 22-7. The portable X-ray generator is to the right of the rotor blade. The LGG 400 scintillation screen and the light shielded tube of the CCD TV camera can be seen on the left side of the picture.

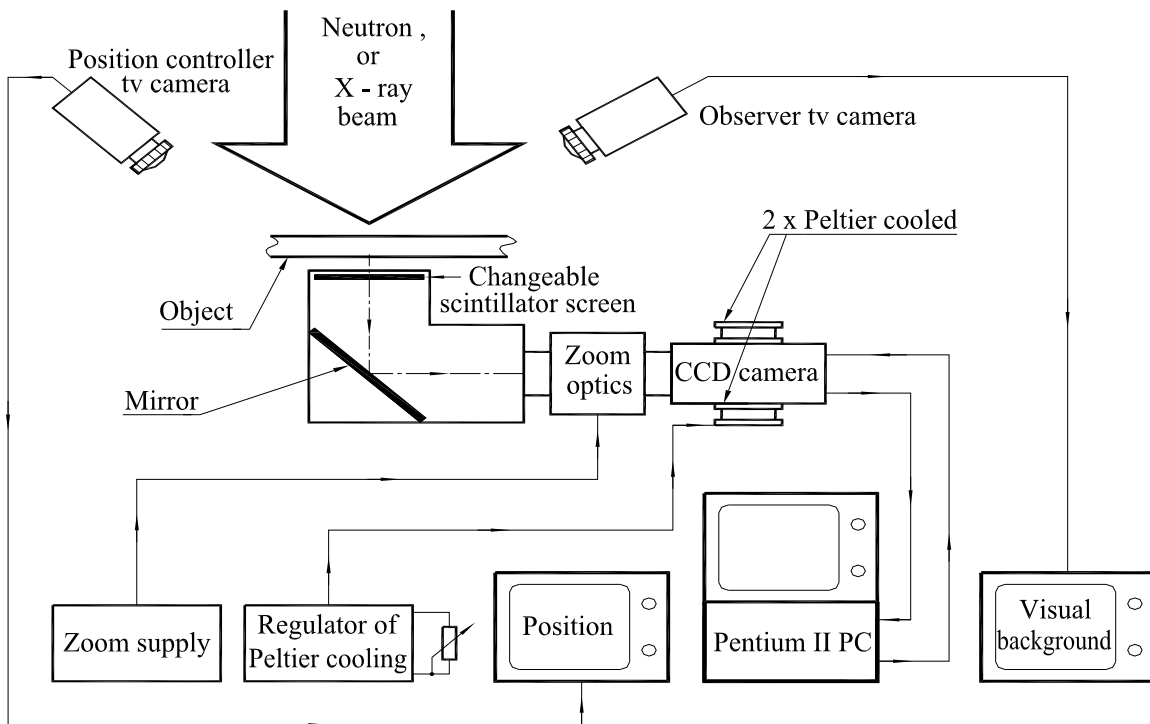


Figure 22-5: Arrangement of the Imaging System.



Figure 22-6: Mi-8 Rotor Blade Undergoing Moisture Conditioning.

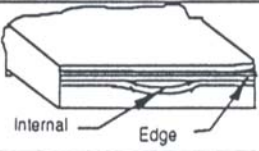
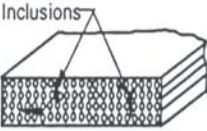
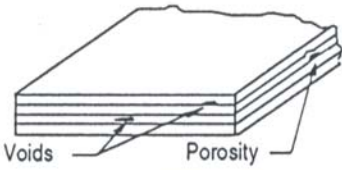
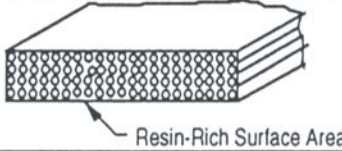
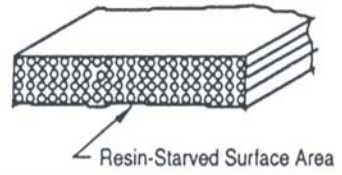

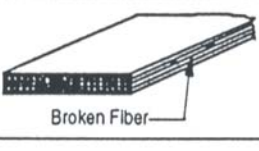
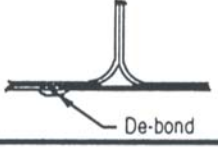


Figure 22-7: Mi-8 Type Rotor Blade Undergoing X-Ray Radiography.

22.5 CHARACTERISATION OF THE DEFECTS

Defects can be external or internal to the structure. External defects can be visually inspected, such as dimensions, finish, and warpage. Internal defects of most concern in composites are delaminations, inclusions, voids, resin-rich and starved areas, fiber misalignments, breakages, and de-bonds, as tabulated in Table 22-1. This table also includes illustrations and short descriptions of the defects [3]. Some of the most important and characteristic defects found during this investigation are presented in Table 22-1 using this classification.

Table 22-1: Descriptions of Defects in Composite Structures.

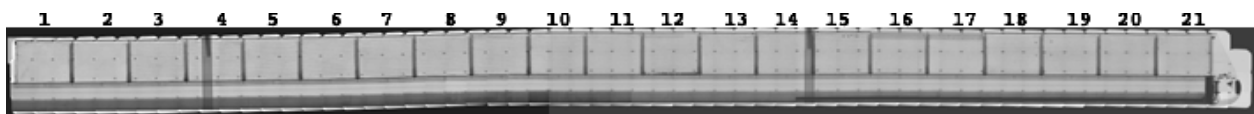
Defect	View	Description
1. Delamination		Delaminations are separations within plies of a laminate, and caused by improper surface preparation, contamination and embedded foreign matter.
2. Inclusions		Inclusions are foreign matter embedded in and between laminæ.
3. Voids and Porosity		Voids and porosity are entrapped air and gas bubbles, and are caused by volatile substances, improper flow of resin and unequal pressure distribution. Voids are clustered in the resin, while porosity are pockets within the solid material..
4. Resin-Rich Area		Resin-rich areas are localized, and filled with resin or lacking in fiber. This defect is caused by improper compaction or bleeding.
5. Resin-Starved Area		Resin-starved areas are localized with insufficient resin evident as dry spots, or having low gloss or where fibers are exposed. This defect is caused by improper compaction or bleeding.
6. Fiber Misalignment, Wrinkling, Buckling		Fiber misalignment is a distortion of the plies resulting in changes from the desired orientation, or in fiber wrinkling and buckling. These defects are due to improper lay-up and cure.
7. Fiber Breakage		Broken fibers are discontinuous or misplaced fibers due to improper handling or lay-up.
8. De-bond		De-bonds occur between different details of the built-up structure. Lack of bonding is due to contamination of the surface, excessive pressure or bad fit.

22.6 MEASUREMENTS

Strict safety precautions must be followed because of the dangerous nature of the radiations used in the study. In the schedule of inspections the first step was an NR inspection in dry conditions, the second step was the NR inspection in wet conditions, and the third step was the XR test. Twenty-eight pieces of rotor blade were verified by this procedure with no harmful effects on personnel. Because of the large dimensions

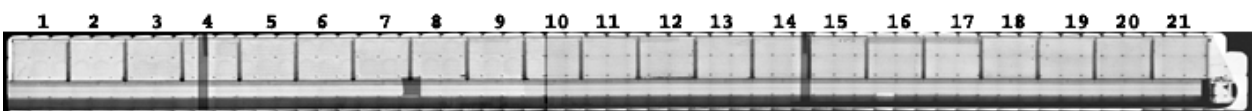
of the rotor blades (their length is almost 10 m), it was necessary to investigate the structures in two parts. The first one contains the exposure fields from the end of the blade to the symmetry axis (4×27 pictures). Then the other side of each blade was examined. The second part of the scanning procedure continued to study each blade from the driver end of the symmetry axis (4×26 pictures). The planned exposure field was $160 \times 140 \text{ mm}^2$. The simple arrangement of the 212 pictures in 4 horizontal rows and 53 vertical columns would be insufficient for a whole radiographic picture of the rotor blades with good quality. The whole image should have been composed of the small overlapping picture fields, however the fields could not be fitted to each other simply. The re-construction of the whole image was performed on the base of the markers. This procedure consists of two steps. In the first step the positions of the small picture fields were computed on the whole image. The method applied here was successful even when some markers or picture fields were missing. In the second step the whole picture was generated from the small picture fields so that the parts overlapped by two or more fields. Entire radiography pictures are shown in Figure 22-8.

Section Number:



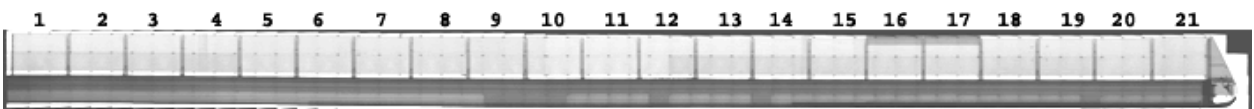
belt **8/a. Dry NR Whole Picture** belt

Section Number:



belt **8/b. Wet NR Whole Picture** belt

Section Number:



8/c. Wet XR Whole Picture

Figure 22-8: Radiography Pictures of a Mi-8 Type Helicopter Rotor Blade.

22.7 RESULTS

22.7.1 Metal Composite Structure

An important requirement of the radiography inspection was to visualize the resin-rich or resin-starved areas (defect types 4 and 5 in Table 22-1). These types of defects can be identified by the fact that they are clearly visible in the NR images due to the high neutron attenuation coefficient of hydrogen containing materials, while for X-ray radiography they are not visible. This is illustrated in Figure 22-9 which shows a resin-rich area in the honeycomb structure detected by NR. Another interesting point of this image is the well-resolved double contour lines, as they reflect the tilted position of the honeycomb elements.

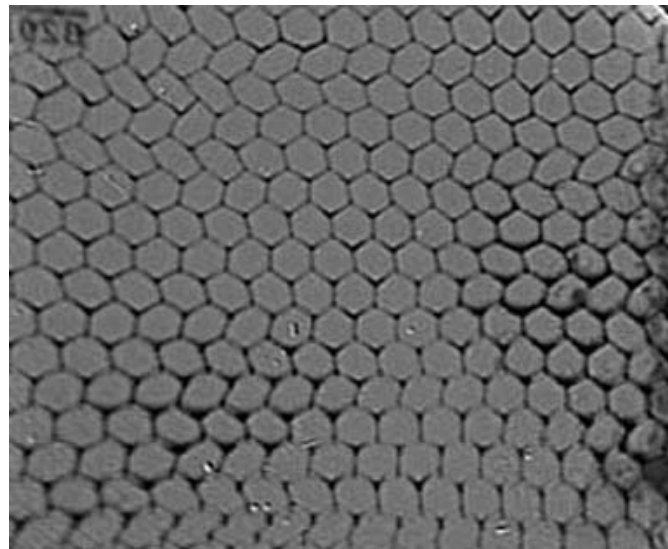


Figure 22-9: Dry NR Image of the Honeycomb Structure with Resin-Rich Areas (dark spots).

A fiber breakage (defect type 7 in Table 22-1) in the trailing edge is observable in Figure 22-10. In the same segment another type of defect was detected. Both NR and XR images show slicing of the honeycomb structure near the stiffener, however, the adhesive material can be detected only by NR. One of the most dangerous defects is when a de-bond (defect type 8) in the adhesive surface is present between the honeycomb structure and the aluminium spar. Such observations are illustrated in Figure 22-11. The double contour lines are because of the tilted position of the honeycomb elements. In this investigation one of the most important observations was the presence of cavities, holes and/or cracks in the sealant and at the border of the sections. The problems were caused by water penetrating into these places and freezing which caused damage to the surrounding structure due to the volume expansion of ice. Detection of these defects is very difficult because of the complex arrangement of the composite structure. A combination of ‘dry NR’, ‘wet NR’ and XR experiments made it possible to discover and visualize these defective areas. It was established that the most frequent locations of water penetration were at the border sections or at the honeycomb-adhesive sealant joining surfaces. These defects are visible in Figure 22-12.

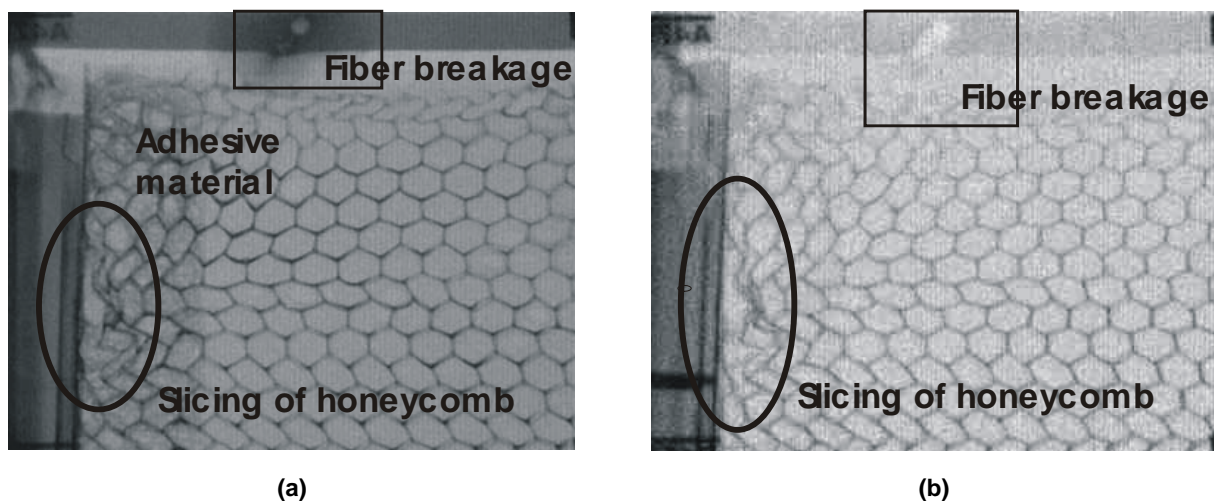


Figure 22-10: (a): Fiber Breakage and Slicing of Honeycomb and the Adhesive Material Revealed by NR; and (b): Fiber Breakage and Slicing of Honeycomb and the Adhesive Material Revealed by XR.

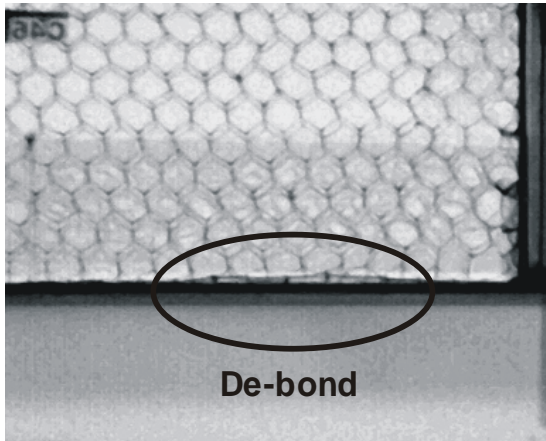


Figure 22-11: De-Bond in the Adhesive Material Between the Honeycomb and the Aluminium.

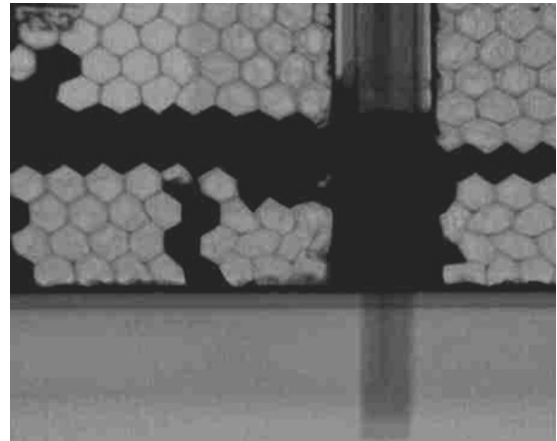


Figure 22-12: Water Percolation in the Honeycomb Structures by NR.

Damage caused by splinters may happen during flight missions (defect type 2 in Table 22-1). Our experience showed that such defects occurred during gunnery practice. Although these defects were usually repaired by the maintenance team, a small piece of splinter was not detected by them and thus it was not removed, as may be seen in Figure 22-13(a) NR and Figure 22-13(b) XR pictures. In the NR image the resin rich spots are seen to be as dark as the metal inclusion, while the XR image provides a dark contrast only for heavy elements with large X-ray attenuation.

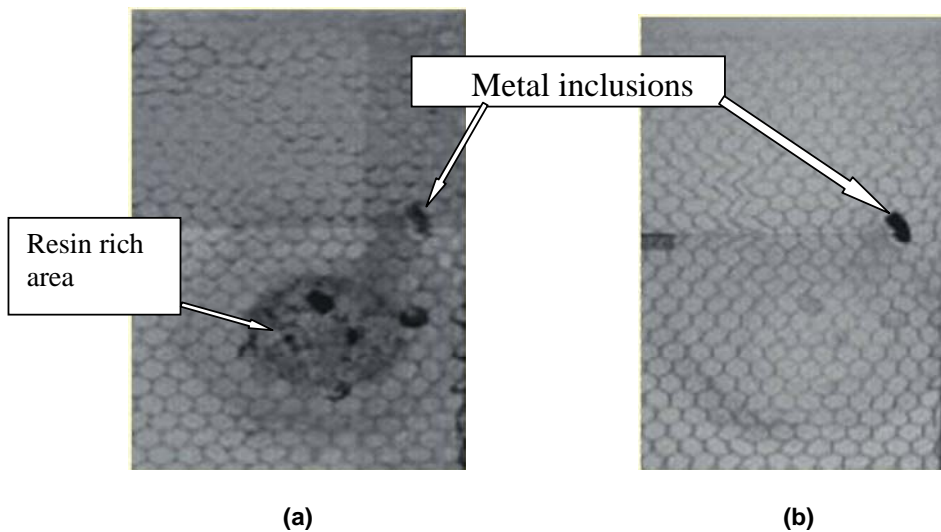


Figure 22-13: (a) NR Picture of the Repaired Area; and (b) XR Picture of the Repaired Area.

Corrosion may also cause problems, leading to possible lifetime reductions. Corrosion was detected in some of the investigated blades inside the rotor blade tail element, as shown in Figure 22-14. A resin-rich area is also shown at the bond surface of the honeycomb structure and the last stiffener. X-ray radiography is a complementary and useful tool in assessing the structural integrity of the metal parts of the blades. Figure 22-15 shows the heating element arrangements and their contacts on a blade with some corroded contacts.

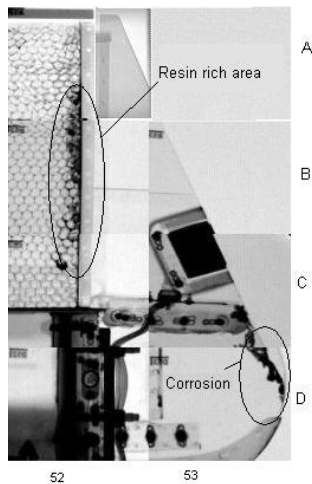


Figure 22-14: NR Picture of the Corrosion Product in the Tail of the Rotor Blade.

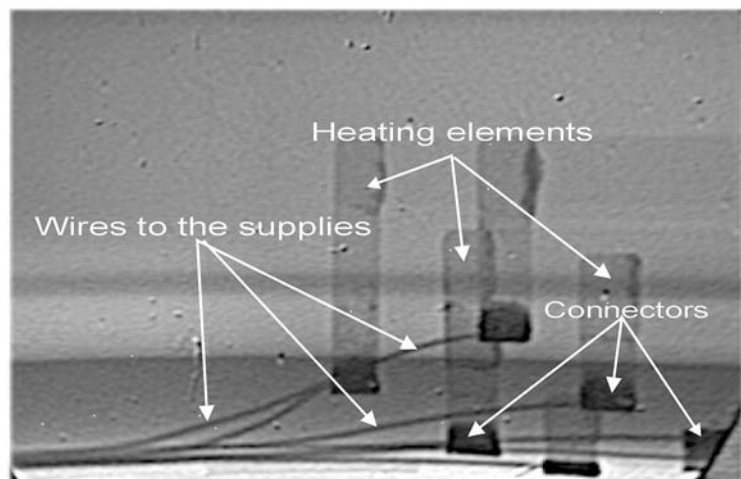


Figure 22-15: Corroded Heating Elements of the Anti-Ice Heater System Revealed by X-Ray Radiography.

22.7.2 Plastic Fiber-Glass Structure

The customer specified the use of dry state inspections of the rotor blades by neutron and X-ray radiography without inspection in the wet condition. The Imaging Plate (IP) technology, as described previously, was used to record the radiography pictures.

The structure of the plastic fiber-glass rotor blade is very different from the metal composite blade. It contains some metal parts, namely the root structure, anti-flutter weight (iron and lead bar), and some screws and adaptors. Some metal parts are visible in Figure 22-16 but the contrast of the iron and lead bars is not distinguishable by XR. A faint indication is given by the elements of the plastic fiber-glass spar. However many details of the plastic fiber-glass technology are observable in Figure 22-17. Clearly visible is the localization of the sticky material under the closing element of the blade and the border between the sections. It is easy to see that the neutron attenuation coefficient is higher for iron than it is for lead. The two complementary radiography pictures give complete information about the construction of the end element of the rotor blade. Under the blade some beam purity indicators, ASTM sensitivity indicators and step wedge indicators with holes are visible in Figure 22-17. The complementary characteristics of the XR and NR are documented in Figure 22-18 and Figure 22-19. The first one shows the perfect arrangement of the protecting aprons for the front edge. One may postulate that the form of the lead bar anti-flutter weight is intact under the protecting aprons. But this was not true because the materials of the lamination technology destroyed the lead bar. The surface of the lead bar appeared similar to the corrosion products as seen Figure 22-19. In order to study the quality of the fiber-glass bundles of the spar it was necessary to reduce the power of the X-ray generator as illustrated in Figure 22-20. In this figure one may see the perfect arrangement of the bundles. However the authors have no information about the bonding between the plastic fiber-glass spar and the cross-link polymer foam of the section.

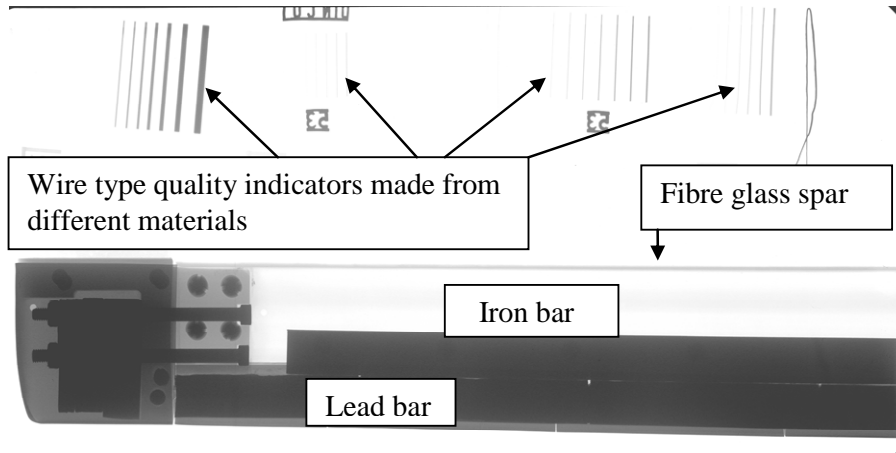


Figure 22-16: End Element of the Ka-26 Helicopter Rotor Blade by XR.

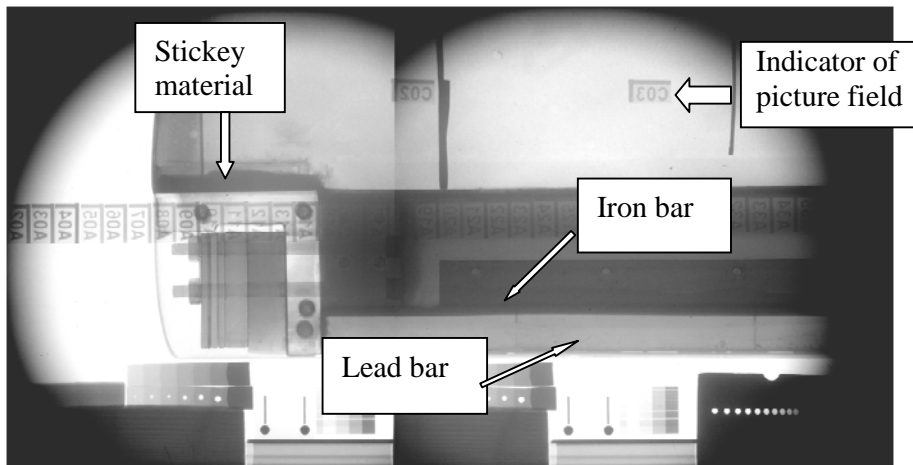


Figure 22-17: End Element of the Ka-26 Helicopter Rotor Blade Revealed by NR.

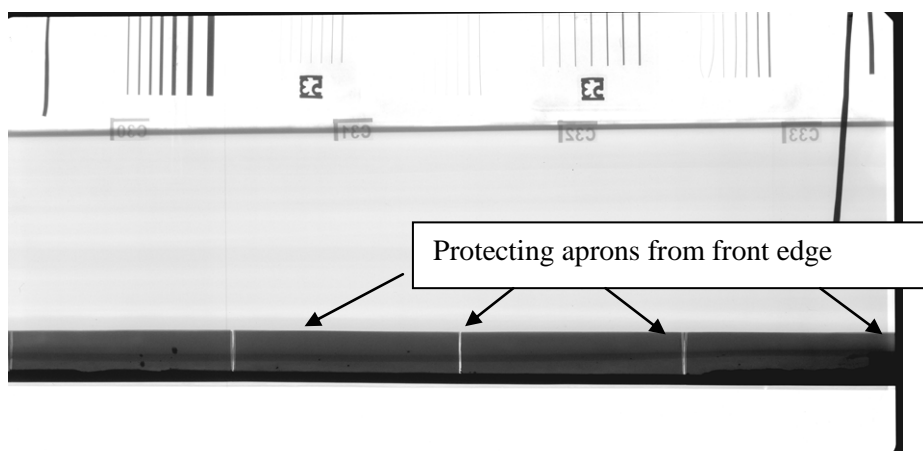


Figure 22-18: Front Edge of the Ka-26 Helicopter Rotor Blade Revealed by XR.

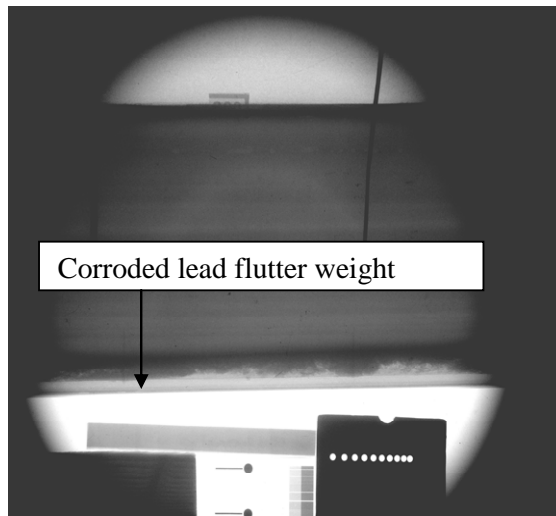


Figure 22-19: Front Edge of the Ka-26 Helicopter Rotor Blade Revealed by NR with Corrosion Products on the Anti-Flutter Weight.

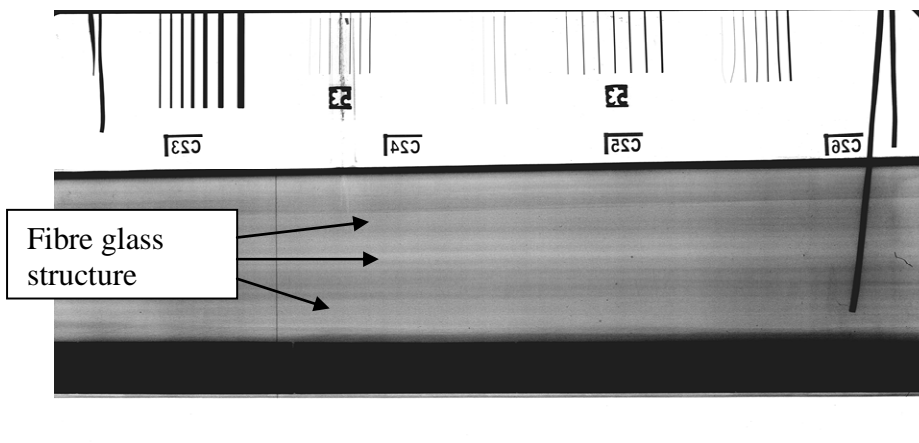


Figure 22-20: Spar in the Middle Part of the Ka-26 Helicopter Rotor Blade Revealed by XR.

The NR picture of Figure 22-21 shows two areas of de-bond between the spar and the section. In addition one can see an unequal distribution of the sticky material on the lead anti-flutter weight at the front edge of the rotor blade.

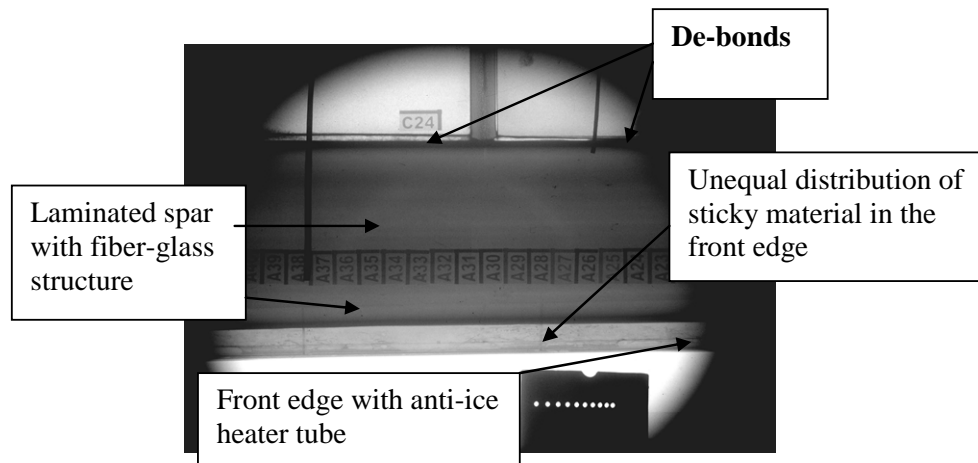


Figure 22-21: Spar in the Middle Part of the Ka-26 Helicopter Rotor Blade Revealed by NR with De-Bonds Between the Spar and the Sections.

22.8 CONCLUSIONS

This investigation revealed no really harmful effects on the helicopter rotor blades using the inspection technology. The most important points of the study were the visualisation of the possible imperfections in the honeycomb structure such as:

- Inhomogeneities of the resin materials (resin-rich or resin-starved areas) at the core-honeycomb surfaces;
- Defects at the adhesive filling (de-bond);
- Water percolation at the sealing interfaces of the honeycomb sections;
- Quality control of resin-rich repaired areas;
- Verification of the positions of metal parts (inclusions) by X-ray;
- Study the condition of the fiber-glass structure in the spar; and
- Verification of the ingress of water into the honeycomb structure and the consequent corrosion of adjacent metal structure.

22.9 REFERENCES

- [1] Domanus, J.C., "Practical Neutron Radiography", Ed. J.C. Domanus et al., Kluwer Academic Publ., Netherlands, 1992.
- [2] Balaskó, M. and Sváb, E., "Dynamic Neutron Radiography Instrumentation and Applications in Central Europe", Nucl. Instr. and Methods in Physics Research A377, pp. 140-143, 1996.
- [3] Sem, J.K. and Everett, R.A., "Structural Integrity and Aging Related Issues for Helicopters", RTO/NATO, ISBN 92-837-1051-7, pp. 5.1 – 5.21, 2000.
- [4] Balaskó, M., Endrőczi, G., Veres, I., Molnár, Gy. and Körösi, F., "Research of Extension of the Life Cycle of Helicopter Rotor Blade in Hungary", Proc. NATO Conference of Applied Vehicle Technology Panel (AVT), Manchester, England, October 7-11, RTO-MP079(II), ISBN 92-837-1089-4, pp. 1-16, 2001.



Chapter 23 – REPLACING CADMIUM AND CHROMIUM

M. Bielewski

Institute for Aerospace Research
National Research Council Canada
Ottawa, Ontario
CANADA

23.1 INTRODUCTION

Electroplated cadmium and hard chromium have been used extensively [1]-[7] and [8] as protective coatings for the most demanding aerospace applications in aggressive environments. Despite excellent technical performance and low deposition costs, these coatings are heavily regulated because both materials and/or their deposition technologies present serious health and environmental hazards. Cadmium, for example, is highly toxic in its metallic form and the plating bath contains cyanides. Thus, both the coating and the deposition process are potentially harmful. Chromium, on the other hand, is completely benign in its metallic form. However, the most common deposition process for so-called hard chromium utilizes highly toxic hexavalent chromium solutions based on chromic acid, and is the subject of strict environmental regulations. The regulatory limitations increase the life cycle cost of these materials/coatings and many countries or municipalities effectively prohibit the use of hard chromium or cadmium plating.

There is a tendency, especially evident in Europe and Japan, but also in the U.S.A. and Canada to further tighten respective environmental legislations, thus leading to a complete ban on the industrial use of cadmium and hexavalent chromium [9]-[11]. The general industry has been working under cadmium and hexavalent chromium bans for years, while the aerospace and military have been exempt from the respective regulations. However, growing legislative pressure and logistic issues are forcing aerospace and military agencies to adapt to changing standards and to look for viable alternatives. However, both cadmium and hard chromium are low-cost coatings that have unique properties making them difficult to replace on a one-to-one basis. The so-called drop-in replacements are especially sought by the aerospace industry since the required engineering changes for large numbers of component drawings would be cost-prohibitive. On the other hand, in new designs such as the Joint Strike Fighter, there is a general policy to avoid using cadmium and hard chromium coatings entirely [12].

Despite different properties and areas of applications for cadmium and hard chromium coatings, there have been some similarities in the approach to finding the cost effective and technically viable alternatives. Firstly, it became clear from the beginning that no single coating could replace either cadmium or hard chromium in all respective applications. Instead, it was realized that the protective function of the coating needed to be specifically determined for a given application, so that an alternative coating could be effectively selected. Besides technical performance, other important factors such as overall cost (from cost of deposition, through maintenance to disposal to coated parts) and wide availability of the alternative coating technology need to be considered. For the latter issue, the main concern is the dependence on proprietary technologies since this usually means limited availability and complicated logistics. Secondly, there is a general trend to replace “wet” processes, such as electroplating, with non-embrittling “dry” technologies such as thermal spraying or vacuum-based deposition techniques. This trend is a result of the hydrogen embrittlement that occurs in the wet processes. Hydrogen embrittlement is a concern for many aerospace applications where high strength steels are used (e.g., landing gear components and fasteners). Although baking can eliminate hydrogen, the process is highly energy-demanding and thus costly. Consequently, elimination of hydrogen at source from the deposition process would be advantageous for any alternative technology.

There are many potential alternatives for both hard chromium and cadmium. In recent years, several detailed reviews of cadmium and hard chromium alternative coatings for use in aircraft applications were prepared, among others [6],[7],[12] and [13]. This review provides highlights of major findings and new developments.

23.2 ENVIRONMENTAL LEGISLATION

Since the hexavalent chromium (Cr (VI)) is known human carcinogen, air emission and wastes from hard chromium plating operation must comply with environmental legislations specifying emissions standards and permissible exposure limits. In the case of cadmium the problem is even more serious and widespread since the toxic metal is carried with the plated part throughout its entire life cycle, creating hazardous conditions whenever these parts are treated or handled. The legislations in given countries (or even provinces or municipalities) are different, although the common goal is to heavily restrict the use of cadmium and hexavalent chromium, leading to complete ban.

23.2.1 Canada

In Canada, both inorganic cadmium compounds and hexavalent chromium compounds are on the Toxic Substances List that is part of the Canadian Environmental Protection Act (CEPA) [A1]. The CEPA was passed by Canadian Parliament in 1999 and came into force on March 31, 2000. Since then it has been continuously updated, with the latest revision of the Schedule 1 (Toxic Substances List) dated on December 27, 2006. Included on this list are oxidic, sulphidic and soluble inorganic nickel compounds, which may complicate the development of electrolytic hard chromium and cadmium alternatives.

23.2.2 U.S.A.

The regulatory bodies in the U.S. are the Environmental Protection Agency (EPA) and the Occupational, Safety and Health Administration (OSHA). The relevant regulations concerning cadmium, hexavalent chromium and other hazardous materials are including in the Clean Air Act (CAA) [A2] and Toxic Substance Control Act [A3].

As an example of current and incoming regulations, in February 2006, OSHA lowered Permissible Exposure Limit (PEL) for Cr(VI) in electroplating to 5 $\mu\text{g}/\text{m}^3$. The EPA, on the other hand, is now considering new rules to be issued in 2008 that may affect not only the use of cadmium and hexavalent chromium but also nickel and cobalt compounds. Interestingly, California recently issued new air rules for thermal spray operations such as HVOF that may affect one of the main technologies for hard chromium replacement.

23.2.3 Europe

For years, European Union (EU) has been driving force in setting health-protective standards in use of hazardous materials. Some of the relevant EU regulations on metal finishing include:

- End-of-Life Vehicle (ELV) – restricts the use of lead, mercury, cadmium and hexavalent chromium on new vehicles [A4];
- Waste Electrical and Electronic Equipment (WEEE) – requires producers of a wide range of products to severely restrain disposal of potentially hazardous materials and maximize recycling of affected consumer and industrial goods [A5]; and
- Restriction on the Use of Hazardous Substances (RoHS) – restricts, as of July 1, 2006, the placing on the EU market of new electrical and electronic equipment containing more than certain levels of six banned substances: lead, mercury, cadmium, hexavalent chromium, Poly-Brominated Biphenyls (PBB) or Polybrominated Diphenyl Ethers (PBDE) [A6].

23.2.4 Other Countries

Other countries are also introducing regulations similar to those in Europe. The Chinese and Korean policies are modeled on the EU rules, such as RoHS, with the same restricted materials.

There are other EU and international agreements and initiatives relevant to metal finishing such as the Stockholm Convention on Persistent Organic Pollutants (POPS) [A7], and the Convention on Long Range Transboundary Air Pollution (LRTAP) that includes Heavy Metals Protocols [A8]. Future actions under these agreements may force regulatory limitations on other materials, beyond the existing regulations on cadmium and hexavalent chromium.

23.3 CADMIUM ALTERNATIVES

The purpose of this section is to identify and briefly discuss existing alternative coatings to Electro-Deposited (ED) cadmium. A number of reference papers have already covered various aspects of this topic [12]-[21] and [22]; therefore, the present review will not attempt to discuss all the cadmium alternatives that have ever been proposed. Instead, it focuses on coatings that provide sacrificial corrosion protection for steels, coatings that are commercially available, and coatings that are environmentally acceptable. The requirement for sacrificial protection limits the range of candidate materials that could replace cadmium to aluminum and zinc and their alloys. Figure 23-1 presents anodic part of the galvanic series (data from http://www.corrosionsource.com/handbook/galv_series.htm) showing materials that are more electronegative than low alloy steels. When in contact, more electronegative material will act as an anode and will corrode preferentially.

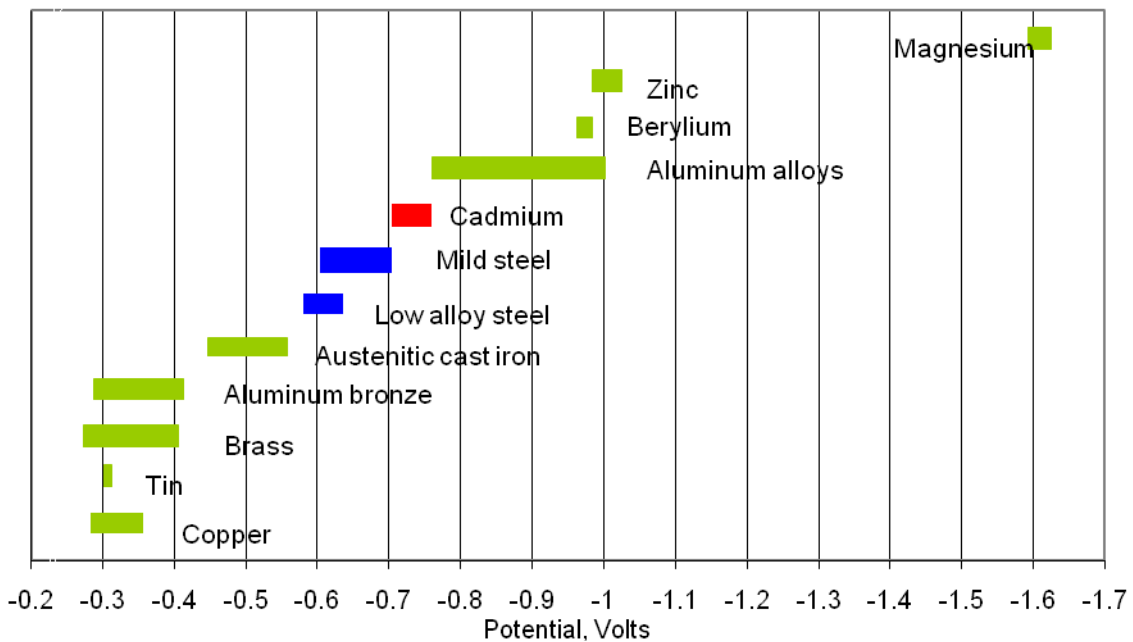


Figure 23-1: Corrosion Potentials of Selected Metals in Reference to Saturated Calomel Electrode.

The second requirement is basically about logistics, as discussed previously. The requirement for green alternatives is sometimes difficult to meet as some new materials require additional treatments that very often involve hexavalent chromium (Cr(VI)) or contain metals such as nickel or cobalt that will most likely be targeted by future environmental legislations.

REPLACING CADMIUM AND CHROMIUM

Besides sacrificial corrosion properties, important technical factors in the selection of cadmium replacement coatings are:

- a) Deposition temperature when applicable to high-strength steel substrates;
- b) The ability to coat external and internal surfaces; and
- c) The ability to produce functional coatings with thickness between 5 and 25 μm , corresponding to cadmium thickness classes specified by the ASTM Standard B 766.

The full range of tests required to qualify cadmium alternatives can be quite extensive and vary depending on coating application. The latter may include corrosion protection, lubricity for threaded hardware, electrical conductivity, and any combination of them. In the U.S.A., a test protocol was developed by the Joint Group on Pollution Prevention to validate candidate coatings [23]. A similar set of evaluation criteria was adopted in Canada [6]. Under this approach, candidate cadmium alternatives are tested under 11 general criteria to examine coating performance for all potential areas of application. Coatings that pass this screening can be further tested to produce a complete application-specific performance database. The evaluation tests proposed in the Canadian report were as follows [6]:

- 1) Corrosion resistance in neutral salt spray per ASTM B117 [A9].
- 2) Corrosion resistance in natural marine atmosphere or SO_2 salt per ASTM G85 [A10].
- 3) Coating adhesion under bend-to-break test per QQ-P-416 [A11].
- 4) Hydrogen embrittlement test per ASTM F519 [A12].
- 5) Fatigue of substrate test per ASTM E466 [A13].
- 6) Repairability: after repair, coating must pass corrosion and adhesion tests.
- 7) Lubricity: torque-tension characteristics.
- 8) Paint adhesion assessed by Plastic Media Blasting (PMB) stripping time.
- 9) Galvanic compatibility with aluminum alloys.
- 10) Compatibility with aerospace fluids such as fuels, oils and greases, and hydraulic and de-icing fluids.
- 11) Electrical contact resistance.

The present review covers three main groups of cadmium alternative coatings:

- a) Electro-deposited zinc and aluminum alloys;
- b) Vacuum-deposited aluminum and aluminum alloys; and
- c) Spray-deposited aluminum and metallic-ceramic coatings.

In addition, alternative materials to replace cadmium-plated steels on the whole are also briefly reviewed. All discussed alternative technologies and coatings are presented in Figure 23-2.

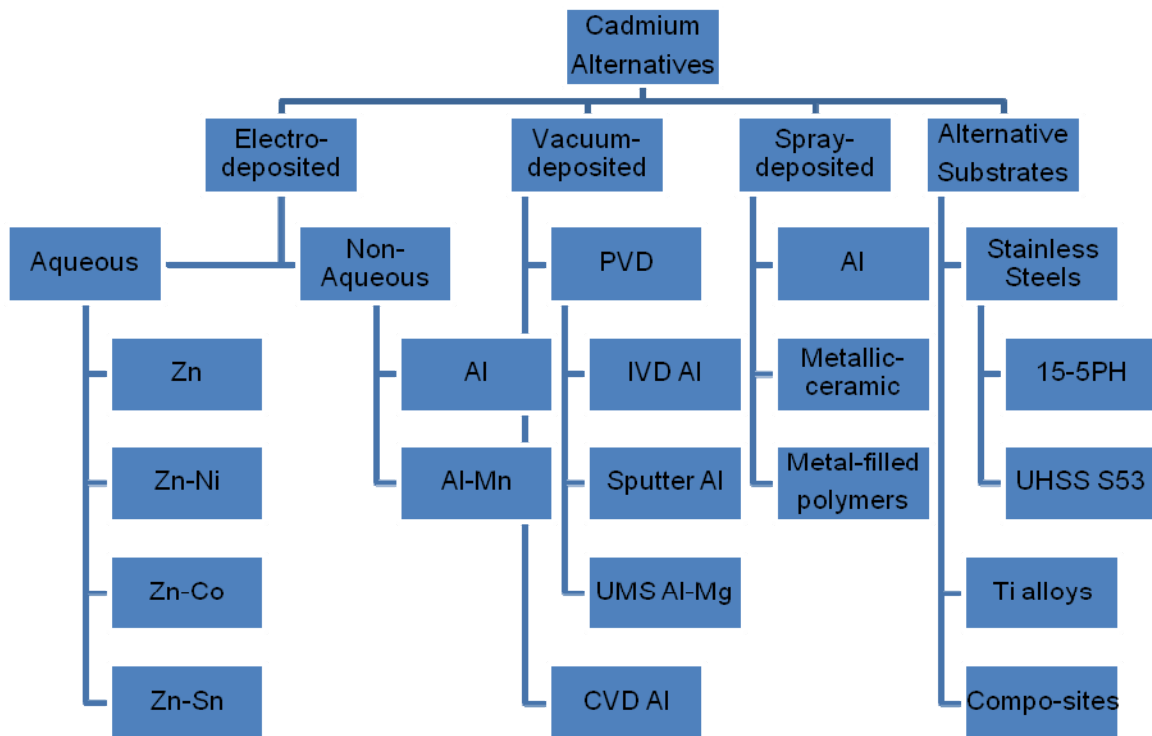


Figure 23-2: Cadmium Alternative Coatings and Materials.

23.3.1 ED Zinc-Based Coatings

Electro-deposited zinc, thanks to its general corrosion-protection properties, is the obvious choice to replace cadmium coatings on steels in many non-aerospace applications. In certain industrial atmospheres (particularly with SO₂ and CO₂), zinc performance is superior to that of cadmium [16]. However, plain zinc coatings perform rather poorly in neutral salt fog tests (less than 100 hrs to red rust) and require greater thickness plus a conversion coating in order to enhance the corrosion performance to an acceptable level. A potential problem for fasteners is the large volume of corrosion product formed and lack of galvanic compatibility with aluminum alloys [3],[15]. The latter is a common problem for all zinc alloys. Another issue is high risk of hydrogen embrittlement, thus zinc coatings are usually limited to low strength steel components.

Better performing alternatives are alloys from the zinc-nickel (Zn-Ni) system that is widely used in automotive and aerospace applications. These alloys are deposited from cyanide-free baths, which can be acid, neutral or alkaline. The acid Zn-Ni deposition process was developed by among others the Boeing Company and there are two aerospace process specifications for this alloy: BAC 5637 and AMS 2417. The acid baths produce nickel content from 10 to 14%, while alkaline baths yield about 6 to 9% Ni. In general, the acid baths produce coatings with better corrosion resistance and are more efficient than those from alkaline baths, so the risk of hydrogen embrittlement is less severe. Still, Zn-Ni coating applications in aerospace are limited to low strength steel components. The potential problem with these alloys is the need for conversion coatings (chromating of Zn-Ni alloys suppresses the dezincification process and improves the coatings' corrosion properties) and uncertain future as to the new regulations limiting the usage of nickel or some of its compounds.

Alloys of the zinc-cobalt (Zn-Co) system, like these of the zinc-nickel system, were developed to meet requirements of the automotive industry. The optimum cobalt concentration in zinc-cobalt alloys is

thought to be in the range 4 – 8 %, but for commercial reasons the level of cobalt is usually between 0.6 and 1.2 % [14]. In various tests zinc-cobalt coatings demonstrated corrosion resistance equivalent to that of cadmium [14],[16],[24]. With some topcoats Zn-Co coatings can have torque-tension characteristics comparable to that of cadmium [25]. Unfortunately, as with nickel, the future use of cobalt is uncertain due to incoming environmental regulations.

Tin-zinc (Sn-Zn) coatings were developed as a direct replacement for cadmium. They offer all the advantages of cadmium like high resistance to corrosion, lubricity, solderability and good electrical conductivity, but they do not have the toxicity of cadmium, although some deposition processes utilize cyanide baths. Compositions range from 10% Sn to 85% Sn with balance Zn, but the most common compositions are between 70% and 80% Sn. Tin-zinc can be deposited from acid, alkaline, or neutral baths, however all processes are expensive since the tin-zinc anodes must be specially cast. As is the case with all zinc alloys, tin-zinc also requires chromate (or alternative) conversion coating for best performance. Tin-zinc coatings with 70% Sn have good solderability and do not grow “whiskers” or dendritic crystals for periods up to 600 days, making them good cadmium alternatives for electrical connectors. Additionally, galvanic compatibility of tin-zinc coatings with aluminum alloys is satisfactory, and they can be applied to steel fasteners for use on aluminum alloy panels [26].

23.3.2 ED Aluminum-Based Coatings

Aluminum or aluminum alloys can be electro-deposited only from non-aqueous electrolytes. The Siemens Galvano Aluminum process (SIGAL) for deposition of pure aluminum has been known for years, but was only recently developed to the production level by AlumiPlate Inc of Minneapolis, and marketed as a new alternative for cadmium. ED aluminum from the AlumiPlate process has been found to be technically superior to other alternatives in various tests including corrosion resistance (also G85 SO₂ salt fog test), hydrogen embrittlement, and electrical conductivity. This coating is already used on a small number of military aircraft components, and has recently been qualified for F-22 landing gear components [12]. In addition, the AlumiPlate process is used on some connectors produced by Amphenol. However, the AlumiPlate process is currently available only from a single source and the process itself is very difficult to work, since it involves the use of pyrophoric aluminum compounds and flammable organic solvents such as toluene. Consequently, the plating process must be done in a sealed tank, with inert gas over the plating bath and a load-lock used to maintain an oxygen-free and water-free atmosphere.

Aluminum-manganese (Al-Mn) is a non-aqueous ED coating currently in development [12],[27]. The alloy composition is usually 13 – 25 % Mn and the process itself is quite complex, and involves molten salt baths and inert atmospheres (typically dry nitrogen). Initial results show that the Al-13Mn survived a salt spray corrosion test for 3,000 hrs with no rust, while scribed material lasted 1,000 hrs indicating good sacrificial properties. Comparing to pure aluminum, Al-Mn alloys are less electronegative, thus should have lower corrosion rates. In addition, the chemistry of the Al-Mn molten salt bath coatings is practically independent of current density, which should make it possible to plate complex shapes reproducibly. However, this process is not at the production level as yet [27].

23.3.3 Vacuum-Deposited Aluminum and Aluminum Alloys

Aluminum coatings can be very effectively deposited by Physical or Chemical Vapor Deposition (PVD or CVD) methods. Since the deposition takes place in vacuum, the risk of hydrogen embrittlement is virtually eliminated and the process is environmentally clean. The main drawbacks of PVD processes are:

- a) The limited ability to coat internal diameters owing to the line-of-sight nature of the process;
- b) Relatively low deposition rates; and
- c) The high investment cost.

The CVD process is more flexible in terms of coating small ratio internal passages, but usually the deposition temperatures are too high for high strength steels.

The Ion Vapor Deposition (IVD) process to produce aluminum coatings involves bombarding the substrate with an ionized aluminum vapor in vacuum. This process was first used by McDonnell Douglas Aircraft (now Boeing) and has been commercially available for many years. It is also recognized as a viable alternative to cadmium plating by MIL-C-83488. The IVD Al coatings show good substrate adhesion but they tend to be porous and coated components require glass-bead peening and chromating. Corrosion properties of IVD Al are good, although poorer than those of cadmium, but hydrogen embrittlement is eliminated and the effect on substrate fatigue is negligible. Obviously, IVD Al coatings on threaded hardware require dry film lubricants or equivalent top coats. The main obstacle to the wide use of IVD Al process seems to be the high cost of deposition.

Pure aluminum coatings applied by sputtering, including Unbalanced Magnetron Sputtering (UMS), offer several advantages over the IVD deposited coatings: higher density, a non-columnar structure (no need for post-deposition peening), better thickness control, and higher coating uniformity. Because of higher density, UMS Al coatings have better corrosion properties compared to IVD Al. Since the source (target) materials are not melted during the UMS process, co-deposition of dissimilar materials such as for example aluminum and magnesium or aluminum and molybdenum is possible in multi-target arrangements. Several aluminum alloys have been tried as cadmium alternatives, including aluminum magnesium (Al-Mg), aluminum molybdenum (Al-Mo), aluminum titanium (Al-Ti) and aluminum zinc (Al-Zn) [6],[14],[28]-[34] and [35]. However, none of these materials have been developed beyond the research level.

Other production coatings in the group of vacuum technologies are sputtered pure Al (plug-and-coat system developed by Marshall Labs) used for internal diameters of big landing gear components [12], and low temperature CVD Al from the LOMTM process by Liburdi [36]. The Liburdi process is used to apply a high purity aluminum coating over the exterior and internal surfaces of turbine blades. However, little information is available on the coating performance, except that it passed 600 hrs B117 (salt spray) corrosion test, thus qualifying for automotive use. Since the deposition temperature is above 260°C (500°F), CVD Al cannot be applied to many structural alloys used in aerospace [12].

23.3.4 Spray Deposited Cadmium Alternatives

There are several different aluminum-based coatings that can be deposited by spraying: aluminum and Al alloys, metallic-ceramic coatings, and Al- and Zn-filled polymers [12].

Thermal spray (flame or arc) is a very flexible and cost-effective process for deposition of pure Al, Al-Mg and Al-Zn alloys on bigger components and large structures such as bridges or communication towers where relatively high thickness (above ~75 μm or 0.003”), surface roughness and inability to coat small internal diameters (below ~ 7.5 cm or 3”) are not problems. Wire arc spray of Al and Al alloys is specified for use on some landing gear and other aircraft components (e.g., the Bombardier Dash-8 turboprop) [12]. For this type of application the spray gun can be controlled by an industrial robot to ensure uniformity and repeatability.

Metallic-ceramic coatings are a class of spray-deposited coatings consisting of metal particles (usually aluminum powder or zinc flakes) in an inorganic (usually chromate-phosphate binder) matrix [12],[18],[33]. These coatings are sprayed as slurry and subsequently cured at temperatures above 200°C. Due to the presence of the active metal particles, metallic-ceramic coatings provide good sacrificial protection for ferrous alloys. They are widely used by the aerospace sector in gas turbine applications and also as alternatives to cadmium in some applications. However, the latter appear to be problematic because of hydrogen embrittlement issues, minimum coating thickness (above 50 μm), curing temperature for some

REPLACING CADMIUM AND CHROMIUM

formulations, and common use of chromate conversion coatings [12]. Two known North American suppliers of metallic-ceramic coatings are Sermatech of Limerick, PA (Serme Tel series of coatings) and Coating for Industry of Souderton, PA (AISEAL coatings).

Metal-filled polymer coatings are widely used to provide corrosion resistance and proper torque-tension to fasteners in the automotive industry. These coatings are usually deposited either by spraying or by dip-spinning. There is a very wide variety of proprietary and non-proprietary polymer coatings that incorporate metal flakes or powders for corrosion resistance. Most commonly, the material is an epoxy with aluminum or zinc filler and a fluoropolymer (PTFE or similar) topcoat for lubricity. The methods and materials involved are commercially available and inexpensive. However, thickness control is limited and coatings require curing at temperatures up to 218°C. Applications in the aerospace industry may require tougher process control to ensure repeatability of coating properties.

23.3.5 Alternative Substrate Materials

One way to eliminate cadmium (and alternative coatings) altogether is by replacing coated steel components by corrosion resistant materials such as titanium alloys, stainless steel or composites. This is already occurring in the aerospace industry (e.g., the Boeing 787 is in large part composite, with many Ti alloy structural members) and the use of stainless steel is now standard for aircraft actuator housings and GTE fasteners [13]. Material substitution, mostly in the form of corrosion-resistant alloys, is the most common and successful approach. Most aerospace actuator rods and outer cylinders are now made from 15-5PH stainless steel rather than the older 4340 high strength steel that required cadmium plating for corrosion resistance. A new ultra high strength stainless steel, such as S53, has been recently developed and is currently being validated [13]. This steel has mechanical properties equivalent to 300 M landing gear steel (UTS = 280 ksi) and corrosion resistance similar to 15-5PH stainless steels. Note, however, that galvanic corrosion between aluminum structures and steel fasteners is still an issue for the new stainless steels. However, replacement of Al alloys by composites in aircraft fuselage solves, at least in part, the compatibility problem.

23.3.6 Summary on Cadmium Alternatives

Table 23-1 presents all discussed coatings and compares them against general requirements for cadmium alternatives. As a reference, electro-deposited cadmium features are listed as well. It is evident from the Table 23-1 that most electro-deposited coatings appear to be straightforward and non-expensive replacements for cadmium, except for ED Al and Al-Mn that are expensive and not widely available. However, the biggest problem for the ED Zn alloys is common use of conversion coatings containing hexavalent chromium. Vacuum-based PVD-UMS and CVD coatings do not have this problem, but these technologies are expensive and not widely available. The last group of spray deposited materials is very economical, but relatively large coating thickness put them out of the range for most cadmium applications. Besides, similarly to PVD processes, they are line-of-sight deposition techniques, with limited capabilities to coat Internal Diameter (ID) surfaces.

Table 23-1: General Requirements for Cadmium Alternative Coatings.

Requirement → Coating ↓	Low Dep. Temperature	OD/ID Coverage	Thickness 5 – 25 µm	Low Cost	Wide Availability	Environmental Issues
ED Zn	P	P	P	P	P	Cr(VI)
ED Zn-Ni acid	P	P	P	P	P	Cr(VI), Ni
ED Zn-Ni alkaline	P	P	P	P	P	Cr(VI), Ni
ED Zn-Co	P	P	P	P	P	Cr(VI)
ED Zn-Sn	P	P	P	?	P	Cr(VI)
ED Al	P	P	P	F	F	Toluene
ED Al-Mn	F	P	P	F	F	Wastes, fumes
IVD Al	P	F	P	F	P	Cr(VI)
Sputtered Al	P	P/F	P	F	F	None
UMS Al-Mg	P	F	P	F	F	None
CVD Al	F	P	P	?	F	Metal organics
Th. sprayed Al	P	F	F	P	P	None
Met-ceramic	P/F	?	F	P	P	Cr(VI)
Met-filled polymer	P	?	F	P	P	None
ED cadmium	P	P	P	P	F	Cd, cyanides, Cr(VI)

Legend: P = pass
 F = fail
 P/F = result depends on actual version/method, etc.
 ? = not enough data
 Cr(VI) = may contain hexavalent chromium
 Ni = contain toxic nickel compounds

Table 23-2 presents key technical requirements for discussed cadmium alternative coatings in comparison with cadmium performance. The technical requirements are related to main areas of application and based on evaluation criteria discussed in Section 23.3.

Table 23-2: Key Technical Requirements for Cadmium Alternative Coatings.

Requirement → Coating ↓	Corrosion				Hydrogen Embrittlement	Fatigue Debit	Lubricity	Compatibility with Al Alloys	Electrical Conductivity
	Salt Spray B117								
	un	sc	SO ₂	mar					
ED Zn	F	–	P	Pc	F	P	F	F	–
ED Zn-Ni acid	P	P	F	Pc	?	F	Pc	F	–
ED Zn-Ni alkaline	P	F	F	Pc	?	?	Pc	F	–
ED Zn-Co	Pc	–	–	–	–	–	Pc	F	–
ED Zn-Sn	P	–	F	–	?	P	P	P	P
ED Al	P	–	P	–	P	–	F	P	P
ED Al-Mn	P	P	P	–	P	P	P	P	–
IVD Al	Pc	Pc	Pc	–	P	P	Pc	P	Pc
Sputtered Al	P	P	P	–	P	P	Pc	P	–
UMS Al-Mg	P	–	–	P	P	–	Pc	F	–
CVD Al	F	–	–	–	P	P	F	P	–
Th. sprayed Al	–	–	–	–	P	P	–	P	–
Met-ceramic	P	F	P	–	?	?	F	–	–
Met-filled polymer	–	–	–	–	P	–	P	P	--
ED cadmium	Pc	Pc	F	Pc	Pb	P	Pc	P	Pc

- Legend:
- P = pass
 - Pc = pass if top-coated or conversion-coated
 - Pb = pass if baked out
 - F = fail
 - = not applicable or no data
 - ? = not enough data
 - un = unscribed condition
 - sc = scribed condition
 - mar = marine environment

The technical performance of electro-deposited alternatives appear to be satisfactory, however these coatings require additional treatments to improve their corrosion resistance or lubricity. In addition, the big problem for the ED Zn alloys is hydrogen embrittlement and lack of galvanic compatibility with Al alloys. Electro-deposited Al and Al-Mn have better corrosion resistance and no embrittlement problem, but similarly to other Al based coatings (except metal-filled polymers) have poor lubricity. It is also noticeable that only few alternatives are electrically conductive, thus more development in this area is needed. Most alternative coatings have acceptable fatigue debit. Since corrosion performance and hydrogen embrittlement are the

most critical performance criteria for cadmium alternatives in aerospace, aluminum based coatings appear to be preferred choice in a long run; in particular, IVD Al for big parts and external surfaces, and ED Al for small complex parts and internal diameters.

23.4 HARD CHROMIUM ALTERNATIVES

Industrial hard chromium, also known as hard chrome, is one of the most extensively used electroplated coatings in the aerospace and automotive industries [7],[13],[37] and [38]. It is used by original equipment manufacturers for wear and corrosion protection and to a lesser extent for aesthetics, and by repair and overhaul facilities to rebuilding worn parts. In the aerospace industry, the typical applications include landing gear components, hydraulic actuators, turbine engine shafts, bearings, and propeller hubs. In automotive, crankshafts, valves, hydraulic components, piston rings, and cylinder linings are typical applications. Military agencies are using hard chrome extensively for protection of inside bores of gun barrels. The main issues affecting usage of chromium plating are process toxicity (presence of hexavalent chromium Cr(VI)), low plating bath efficiency (around 15%) that leads to high energy consumption, the presence of cracks causing inconsistent corrosion performance, thickness uniformity and the necessity of post-treatment machining, and hydrogen embrittlement in steel substrates requiring post-deposition bakeout. Hard chromium alternatives are expected not only to match the chromium performance in given applications, but also address these issues with a view to gaining some improvement. All discussed here alternative technologies and coatings are presented in Figure 23-3.

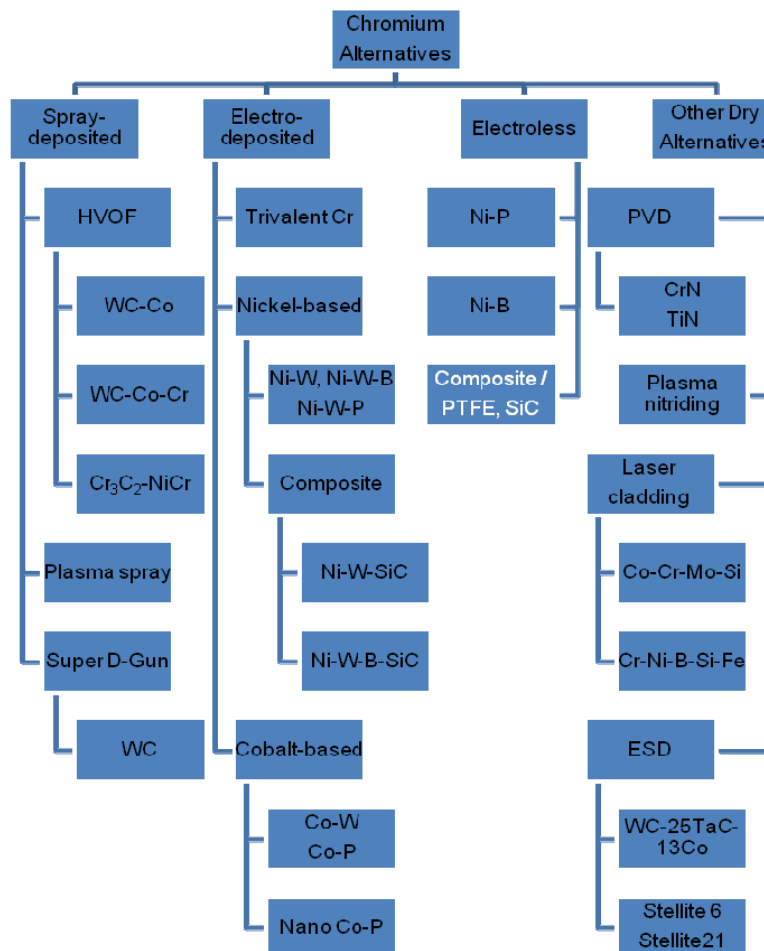


Figure 23-3: Chromium Alternative Coatings.

23.4.1 Spray Deposited Hard Chromium Alternatives

Thermal spraying is widely used in aerospace and many other industries for deposition of high quality metallic, ceramic and ceramic-metal composite coatings. There are three basic spraying technologies available as alternative technologies to hard chromium plating.

The leading technology among hard chromium alternatives is the High Velocity Oxygen Fuel (HVOF) spraying of cermets. This technology is versatile, environmentally benign, and cost effective. The coatings are most often cermets containing WC-Co, WC-Co-Cr and Cr_3C_2 -NiCr, and have been found to have physical properties equal to or better than those of hard chromium. In fact, the service temperature of typical cermets can be up to 815°C (1500°F), which is double the hard chromium capability. Deposition is completed by propelling the coating with a high velocity and high temperature flame produced through the combustion of oxygen and fuel. A significant advantage of this technology is the high deposition rate. Disadvantages include the inability to coat small and intricate parts, or parts with a small internal diameter (about 100 mm or 4"). In addition, machining is required after coating deposition due to the surface roughness and typical over-spraying. The aerospace industry has targeted the use of HVOF coatings for landing gears, flap actuators, shafts, hub propellers, and hydraulic parts [13],[37]. Other applications include industrial hydraulic and pneumatic actuators, and mill rolls used in steel, paper and plastic industries.

Plasma spraying is used to deposit similar materials and has similar applications to HVOF. However, thanks to the smaller size of the plasma gun and short standoff distance, it can be used to coat Internal Diameters (ID) not accessible to HVOF [13],[38]. Presently, the minimum ID is about 40 mm (1.6") in the case of the specially developed F-300 plasma gun from Sulzer Metco [38].

The detonation gun thermal spray process was originally developed by the Union Carbide Corporation and is now available from Praxair Surface Technologies under the name of D-Gun and Super D-Gun [39],[40]. In this technique, the powder particles suspended in the flammable gas mixture are accelerated by a detonation ignited by spark plug at the rate up to 8.6 times per second. The repeated detonation cycle produces a coating on the substrate placed 50 – 100 mm from the barrel. Super D-Gun process yields excellent coating properties particularly for tungsten carbides coatings. Bond strength is reported to reach 210 MPa (about twice the corresponding value for plasma spraying) and the coating porosity is below 1%. However, detonation gun process is strictly line-of-sight and more expensive than the other thermal spraying techniques.

23.4.2 Electrolytic Hard Chromium Alternatives

Wet technologies such as trivalent chromium and nickel depositions are in use mostly for ID applications where line-of-sight spray technologies fall short. The strong point of these processes is that the plating is well established within the industry and there is a network of suppliers and plating shops willing to adapt to the new environmental standards. The weakest point, common for all wet technologies, is the volume of wastes generated.

Electro-deposited trivalent chromium, obtained from Cr(III)-based electrolytes, is environmentally sound technology; however, physical and chemical properties of the coatings are still inferior to hexavalent hard chrome, despite years of effort [7],[13]. For now, trivalent chromium applications are limited to thin decorative coatings. Thicker coatings are suitable only for simple substrate configurations.

Electroless nickel and nickel alloys, despite all environmental concerns are still used as hard chromium alternatives. Electroless nickel-phosphorus (Ni-P) is a hardenable, corrosion resistant coating consisting of nickel alloyed with a varying percentage of phosphorus (usually 8% to 10%). It offers good thickness uniformity and control. The coating properties are largely determined by coating composition, with 8% phosphorus coating being harder and 10% phosphorus coating being more corrosion resistant. Electroless

Ni-P composite coatings are available with additions such as Silicon Carbide (SiC) for wear resistance or teflon (PTFE) for lubricity. Thanks to the ability to cover parts of complex geometry, typical applications of electroless Ni-P include hydraulic valves, pump components, moulding dies and fuel injector plates. Electroless nickel-boron (Ni-B) coating exhibits better wear resistance, lower friction, higher hardness but lower corrosion resistance compared to hard chrome. In addition, Ni-B coatings are expensive to produce, not widely available and plating bath contains lead or thallium that are toxic materials. Typical areas of application include jet engine components, glass manufacturing, foundry molds, gears, shafts, knife blades and drills.

There are a number of electroplated alloys considered as drop-in replacements for hard chromium [7],[13]. They are based either on nickel (Ni-W, Ni-W-B, Ni-W-P, Ni-W-SiC and Ni-W-B-SiC) or cobalt (Co-W and Co-P). However, nickel (or some of its compounds) already faces increased environmental scrutiny and cobalt's future is also uncertain. To complicate things even further, cobalt is more expensive than nickel. Nevertheless, worth mentioning here is nanocrystalline Cobalt-Phosphorus (Co-P) coating recently developed by Integran Technologies [41]. Thanks to better microstructure and low residual stress, the nanocrystalline Co-P coatings are more corrosion resistant than hard chromium. The process is not embrittling, although the fatigue effect on the substrate is not known. In general, electroplated alloys surpass hard chromium in many respects and may be used in selected applications as a direct replacement. However, environmental restrictions (nickel compounds in plating bath) and problems with process control (e.g., SiC particles in composite coatings) may limit or even eliminate their application in the future.

23.4.3 Other “Dry” Alternatives

In principle, any hard coating can be considered as a hard chromium alternative [7]-[9] and [43]. The candidate “dry” alternatives can be deposited by vacuum-based PVD methods, laser techniques, and micro-welding. In addition, surface modifications that do not create coatings but improve surface properties, such as ion implantation, plasma nitriding and thermo-chemical treatment, can also be considered. The techniques that have been considered as hard chromium replacement are discussed next. However, comparing to spray technologies and plating, they have only niche applications.

PVD deposition techniques are relatively well-known alternatives for hard chromium plating. Included in this category are sputtering and cathodic arc deposition that produce thin coatings (below 10 μm), and Electron Beam-PVD (EB-PVD) techniques which can produce coatings up to hundreds of μm in thickness. Two of the most important features of PVD coatings, relevant to hard chromium applications, are the high deposition rate and compressive residual stresses in the coatings after deposition. The high deposition rate of EB-PVD allows for significant thickness build-up and can be used for refurbishment purposes as well as for net shape forming [42]. The compressive residual stresses, characteristic of all PVD coatings, improve the corrosion resistance of the coating. A variation of PVD technique, Ion-Beam Assisted Deposition (IBAD), is a combination of low energy ion bombardment and a physical vapor deposition. This process produces high-density coatings with excellent adhesion and controllable residual stresses. Among PVD coatings considered as hard chromium alternative are CrN, TiN and Metal containing Diamond-Like Carbon (Me-DLC) coatings that can be deposited by magnetron sputtering or cathodic arc evaporation [43]. Overall, PVD methods are environmentally clean and offer high quality coatings. Although the capital cost for PVD equipment can be high, this can be offset by mass production.

Ion technologies such as ion implantation or plasma nitriding use energetic ion bombardment to modify surface properties of the material [7]. Since no coating is produced, there is no change to part dimensions, no problems with adhesion, and residual stresses are negligible. One of the newest developments, Plasma Source Implantation is a low-cost and non-line-of-sight technique, most often used for nitriding. So-called plasma nitriding can be used in combination with physical vapor deposition or electro-deposition. For those parts that already have hard chromium coating plated, the application of nitriding leads to the

formation of CrN phases on the surface. This increases the wear resistance and service life of chromium coated parts. Although not the ideal solution, ion technologies can provide a versatile means to enhance chromium coatings already in use and thus contribute to the lower life cycle cost of coated parts. The latter translates into longer times between refurbishments, resulting in less environmental impact.

Laser Cladding (LC), which is also known as laser plating or hard facing, is another technology with potential as a chromium plating alternative [44],[45]. The cladding process consists of melting the coating, which is usually in the powder form, together with the surface layer of the substrate. The coefficient of mixing is usually 0.1 indicating that there is little mixing with the substrate. LC produces a strong metallurgical bond and preserves the unique properties of the coating material and the substrate. Among the varieties of materials used, Co-Cr-Mo-Si and Cr-Ni-B-Si-Fe compositions are known to provide good combinations of wear and corrosion resistance. In comparison to hard chromium, the advantages of cladding processes include: absence of micro-cracking, low energy consumption, low heat input, and coating composition flexibility. Similar to chromium plating, post-deposition machining is required.

Electro-Spark Deposition (ESD) is in principle a pulsed-arc micro-welding process that uses short duration, high current electrical pulses to deposit, with very low heat input, a consumable electrode material on a metallic substrate [46],[47]. The process is environmentally benign, cost-effective and requires no special chambers, or operator protection. This commercially available technology offers a wide selection of coating materials, and portability of coating equipment. In addition, ESD can be applied to inside diameters as small as 7.6 mm (0.30"). In principle, any electrically conductive material can be deposited, but for the purpose of hard chromium replacement, tungsten carbides such as WC-25TaC-13Co, and cobalt-base alloys such as Stellite 6 and Stellite 21 have been successfully used. Characterization of the ESD coatings showed that compared to hard chromium, the ESD coatings have comparable corrosion performance, and slightly lower hardness and wear resistance. Fatigue testing, however, revealed that in the case of high-strength steel substrates (e.g., 4340) the loss of fatigue life could reach 20%. The low deposition rates may also be a concern, but ESD can play a significant role in on-site repairs of original materials and chromium coatings.

23.4.4 Summary on Hard Chromium Alternatives

Table 23-3 and Table 23-4 present all discussed alternative coatings and compare them against relevant properties of Electro-deposited Hard Chromium (EHC). Since deposition temperature and service temperature are not problematic for alternatives considered in this review, they are not listed in Table 23-3 as a requirement.

Table 23-3: General Requirements for Hard Chromium Alternative Processes and Coatings.

Requirement → Process/Coating ↓	Low Cost	Rebuild Capacity	Post-Deposition Machining	ID Coverage (min dia)	Environment Issues	Availability and Fit with OEM/MRO
EHC	Yes	Yes	Needed	Yes	Cr(VI)	Yes
HVOF WC-Co WC-Co-Cr Cr ₃ C ₂ -NiCr	P	P	P	100 mm	?	P
Plasma spray	P	P	P	40 mm	None	P
Super D-gun	F	P	P	F	None	F
ED trivalent Cr	P	F	None	P	None	?
Electroless Ni-P	P	P	?	P	Ni	P
Electroless Ni-B	F	P	?	P	Ni, Tl, Pb	P
Electroless Ni-P-SiC	P	P	?	P	Ni, SiC	P
ED Ni-W	P	P	?	P	Ni	P
ED Ni-W-B	P	P	?	P	Ni	P
ED Ni-W-P	P	P	?	P	Ni	P
ED Ni-W-SiC	P	P	?	P	Ni, SiC	P
ED Ni-W-B-SiC	P	P	?	P	Ni, SiC	P
ED Co-W	F	P	?	P	None	P
ED Co-P	F	P	?	P	None	P
ED nano Co-P	F	P	?	P	None	?
PVD CrN	F	F	None	F	None	F
PVD TiN	F	F	None	F	None	F
PVD Me-DLC	F	F	None	F	None	F
Plasma nitriding	P	F	None	P	None	P
LC Co-Cr-Mo-Si Cr-Ni-B-Si-Fe	P	P	P	F	None	F
ESD WC-TaC-Co Stellite 21	P	P	P	7.6 mm	None	P

Legend: P = pass (same as EHC or better)

F = fail

? = not enough data

OEM/MRO = Original Equipment Manufacturer / Maintenance Repair and Overhaul facility

REPLACING CADMIUM AND CHROMIUM

Table 23-4: Technical Requirements for Hard Chromium Alternative Processes and Coatings.

Requirement → Process/Coating ↓	Hardness HV	Wear Resistance	COF	Corrosion Resistance	Hydrogen Embrittlement	Fatigue Debit
EHC	800 – 1000	High	0.12	F (cracks)	Needs bake out	F
HVOF WC-Co	P	P	–	?	P	?
WC-Co-Cr	P	P	–	P	P	?
Cr ₃ C ₂ -NiCr	P	P	–	P	P	–
Plasma spray	P	P	–	P	P	P
Super D-gun	P	P	–	P	P	P
ED trivalent Cr	F	F	–	?	–	–
Electroless Ni-P	P	P	–	P	–	–
Electroless Ni-B	P	P	P	F	–	–
Electroless Ni-P-SiC	P	P	–	P	–	–
ED Ni-W	P	P	P	P	–	–
ED Ni-W-B	P	P	P	–	P	F
ED Ni-W-P	P	P	–	P	–	–
ED Ni-W-SiC	P	P	–	–	–	P
ED Ni-W-B-SiC	P	P	–	–	–	P
ED Co-W	F	P	–	P	–	–
ED Co-P	P	P	–	–	–	–
ED nano Co-P	P	F	F	P	P	?
PVD CrN	P	P	F	P	P	P
PVD TiN	P	P	F	P	P	P
PVD Me-DLC	P	P	P	P	P	P
Plasma nitriding	P	P	–	–	P	P
LC Co-Cr-Mo-Si Cr-Ni-B-Si-Fe	P	P	–	P	P	P
ESD WC-TaC-Co	P	P	–	P	P	P
Stellite 21	F	F	–	P	P	F

Legend: P = pass (same as EHC or better)

F = fail

? = not enough data

– = not applicable or no data

As evident from Table 23-3, all thermal spray processes and laser cladding have proven rebuilding capabilities, and as a consequence, post-deposition machining is typically required. It is also noticeable that most of “wet” ED and Electroless coatings have variety of potential environmental problems, the most serious in the case of Electroless Ni-B, relating to nickel, lead (Pb) and thallium (Tl) contents. In addition, all composite coatings have problems with air emission of SiC particles. On the other hand, all wet coatings have good OD/ID coverage. This property is lacking from the “dry” alternatives, where PVD, LC and Super D-Gun technologies are strictly line-of-sight, while HVOF and plasma spraying have quite serious limitations as to minimum diameter that could be coated. The PVD and laser technologies are not widely available at service depots and PVD in particular can be expensive, especially on small scale production.

With few exceptions, hard chromium alternatives have no problem with meeting the hardness and wear resistance criteria. Also the corrosion resistance is not an issue. Since hydrogen embrittlement is critical only for high-strength substrates, suitable alternative can be found for most of applications. Overall, when combining general requirements (with the low cost as a go / no go criteria) and technical requirements, the spray technologies (HVOF and Plasma) and laser cladding appear to be the best alternatives for big components and mostly external surfaces, while variety of electro-deposited and electroless coatings can be applied to coat ID's. However, future environmental restrictions concerning nickel compounds may complicate this picture, as Ni-based coatings cover most ID applications. Plasma nitriding may replace hard chromium in applications on some small and complex components, while Electro-Spark Deposition of carbides may be used for field repairs.

23.5 CONCLUSIONS

There are many potential alternatives for both hard chromium and cadmium. In the case of hard chromium, HVOF and plasma spraying of cermets has been the leading process of choice for most applications. However the electrolytic Ni-based coatings are still needed for internal surfaces. Laser cladding, plasma nitriding and Electro-Spark Deposition processes may also play a role in specific applications. In the case of cadmium, however, the situation is more complicated and serious concessions are needed. First of all, there is no leading technology, and electro-deposition of zinc- and aluminum-based alloys is competing with other techniques like PVD, CVD and thermal spray technologies. However, the big problem for the ED Zn alloys is hydrogen embrittlement and lack of galvanic compatibility with Al alloys that make most of structural component in aerospace. Electro-deposited Al and Al-Mn do not have these problems, but similarly to other Al-based coatings have poor lubricity that complicates applications to threaded hardware. Another problem is that only few cadmium alternatives are electrically conductive, thus more development in this area is needed. Since corrosion performance and hydrogen embrittlement are the most critical performance criteria for cadmium alternatives in aerospace, aluminum based coatings, despite higher cost, appear to be preferred choice in a long run; in particular, IVD Al for big parts and external surfaces, and ED Al for small complex parts and internal diameters. Sputtered Al may also find niche applications. In other areas than aerospace, selection of suitable cadmium alternative appears to be not that critical.

23.6 REFERENCES

- [1] Morrow, H., “The Environmental and Engineering Advantages of Cadmium Coatings”, Proceedings of the OECD Cadmium Workshop in Stockholm, Sweden, 1995.
- [2] Safranek, W.H., “Cadmium Plating”, Plating and Surface Finishing, Vol. 82, No. 8, pp. 46-47, 1995.
- [3] Marce, R.E., “Cadmium Plating”, Metals Handbook, American Society for Metals, Ninth Edition, Vol. 5, pp. 256-269, 1982.
- [4] Stevens, K., “Hard Chrome Plating – A Clean Bill of Health”, Trans. IMF, 75(2), B33, 1997.

- [5] Debarro, J.A., “Hard Chromium Coatings Outdated?”, Sulzer Technical Review, Vol. 79, No. 1, pp. 20-23, 1997.
- [6] Bielawski, M. and Holt, R.T., “A Review of Sacrificial Coatings to Replace Cadmium”, National Research Council Canada, Institute for Aerospace Research, Technical Report LTR-ST-2174, March 1999.
- [7] Bielawski, M., “Hard Chromium Alternative Coatings for Aerospace Applications”, National Research Council Canada, Institute for Aerospace Research, Technical Report LTR-ST-2176, November 1998.
- [8] Bielawski, M., Dudzinski, D., Au, P. and Patnaik, P.C., “Environmentally Compliant Alternatives to Hard Chrome and Cadmium for Aerospace Applications”, Proceedings of the COM 2002, Canadian Institute of Mining, Montreal, Quebec, Canada, pp. 83-96, 2002.
- [9] Council Directive of 18 June 1991, (91/338/EEC), “Official Journal of the European Communities”, No. L 186, pp. 59-63, 12.7.1991.
- [10] “Canadian Environmental Protection Act”, Minister of Supply and Services Canada 1994, Catalogue No. En 40-215/40E, ISBN 0-662-22046-3, 1994.
- [11] Hartle, S.J. and Stephens, B.T.I., “US Environmental Trends and Issues Affecting Aerospace Manufacturing and Maintenance Technologies”, Proceedings of the 83rd Meeting of the AGARD Structures and Material Panel on “Environmentally Compliant Surface Treatments of Materials for Aerospace Applications”, Florence, Italy, AGARD R-816, p. 7, 1996.
- [12] Legg, K., “Cadmium Replacement Alternatives for the Joint Strike Fighter”, Rowan Technology Group, Libertyville, IL, USA, Report No. 3105JSF3, 18 December 2000.
- [13] Legg, K. and Pellerin, C., “SERDP/ESTCP Metal Finishing Workshop Summary”, SERDP & ESTCP Program Office, Washington, DC, USA, Available at ESTCP Online Library, 2006, <http://www.estcp.org/>.
- [14] Baldwin, K.R. and Smith, C.J.E., “Advances in Replacements for the Cadmium Plating of Aerospace Fasteners and Components”, Wire Industry, pp. 667-677, November 1997.
- [15] Groshart, E., “Finishing in the Green – Cadmium Replacements”, Metal Finishing, pp. 79-81, February 1997.
- [16] Gabe, D.R., “Surface Finishing and the Environment: Alternatives to Cadmium as a Surface Coating”, Special Publications of the Royal Society of Chemistry, Vol. 126, pp. 215-224, 1993.
- [17] Matz, C.W., “Corrosion Prevention with Environmentally Compliant Materials – a Design Challenge”, Proceedings of the 79th Meeting of the AGARD Structures and Material Panel, October Seville, Spain, AGARD-CP-565, p. 15, 1994.
- [18] “Environmentally Acceptable Alternatives to Cadmium Plating: Performance Testing”, Ocean City Research Corporation, Arlington, VA, USA, Final Report for Naval Sea Systems Command Corrosion Control Division (Code 03M1), 10 October 1995.
- [19] Vaessen, G. et al., “Cadmium Substitution on Aircraft”, Proceedings of the 83rd Meeting of the AGARD Structures and Material Panel, Florence, Italy, AGARD R-816, p. 15, 1996.
- [20] Roberts, M., “Environmentally Compliant Electroplating Alternatives”, Proceedings of the 83rd Meeting of the AGARD Structures and Material Panel, Florence, Italy, AGARD R-816, p. 20, 1996.

- [21] Cuntz, J.M. et al., "Procedes de Protection et Environnement Problemes et Solutions", Proceedings of the 83rd Meeting of the AGARD Structures and Material Panel, Florence, Italy, AGARD R-816, p. 2, 1996.
- [22] Smith, C.J.E., "Advances in Protective Coatings and Processes for Aerospace Applications", Aircraft Engineering and Aerospace Technology, Vol. 67, No. 5, pp. 13-16, 1995.
- [23] "Joint Test Protocol BD-P-1-1 for Validation of Alternatives to Electrodeposited Cadmium for Corrosion Protection and Threaded Part Lubricity Applications", Joint Group on Pollution Prevention (JG-PP), Contract No. DAAA21-93-C-0046, 30 June 1999.
- [24] Thomson, M.D., "Zinc Alloys – the Boeing Alternative to Cadmium", Trans. IMF, Vol. 74, No. 3, pp. 3-5, 1996.
- [25] Ingle, M.W. et al., "Evaluation of Environmentally Acceptable Multi-Layer Coating Systems as Direct Substitutes for Cadmium Plating on Threaded Fasteners", Tri-Service Committee on Corrosion, Wright-Patterson AFB, OH, USA, 1994.
- [26] Budman, E. and Sizelove, R.R., "Zinc Alloy Plating", Metal Finishing, Vol. 99, Supplement 1, pp. 334-339, doi:10.1016/S0026-0576(01)85294-6, January 2001.
- [27] Beck, E. et al., "Final Report Aluminum Manganese Molten Salt Plating", WP 9903, Naval Air Systems Command Materials Engineering Division, Patuxent River, Maryland, USA, ESTCP, June 2006, Online Library <http://www.estcp.org/>.
- [28] Bates, R.I., and Arnell, R.D., "Microstructure of Novel Corrosion-Resistant Coatings for Steel Components by Unbalanced Magnetron Sputtering", Surface & Coatings Technology, Vol. 89, No. 3, pp. 204-212, 1997.
- [29] Baldwin, K.R. et al., "Aluminum-Magnesium Corrosion Resistant Coatings", Special Publications of the Royal Society of Chemistry, Vol. 206, pp. 119-131, 1997.
- [30] Baldwin, K.R. et al., "Aluminum-Magnesium Alloys as Corrosion Resistant Coatings for Steel", Corrosion Science, Vol. 38, No. 1, pp. 155-170, 1996.
- [31] Arnell, R.D. and Bates, R.I., "The Deposition of Highly Supersaturated Metastable Aluminum-Magnesium Alloys by Unbalanced Magnetron Sputtering from Composite Targets", Vacuum, Vol. 43, pp. 105-109, 1992.
- [32] Abu-Zeid, O.A. and Bates, R.I., "Friction and Corrosion Resistance of Sputter Deposited Supersaturated Metastable Aluminum-Molybdenum Alloys", Surface & Coatings Technology, Vol. 86, Pt. 2, pp. 526-529, 1996.
- [33] Smith, C.J.E. and Baldwin, K.R., "Some Cadmium Replacements for Use on Aircraft Components", Product Finishing, Vol. 45, pp. 12-18, 1992.
- [34] Teer, D.G. and Abu-Zeid, O.A., "Al-Zn Coatings for the Corrosion Protection of Steel", Thin Solid Films, Vol. 72, pp. 291-296, 1980.
- [35] Bielawski, M., "Development of Unbalanced Magnetron Sputtered Al-Mo Coatings for Cadmium Replacement", Surface and Coatings Technology, Vol. 179, pp. 10-17, 2004.
- [36] Liburdi Engineering, Dundas, Ontario, Canada, <http://www2.liburdi.com/liburditurbine/index.php>.

- [37] Sartwell, B.D. et al., “Validation of HVOF WC/Co, WC/CoCr and Tribaloy 800 Thermal Spray Coatings as a Replacement for Hard Chrome Plating on C-2/E-2/P-3 and C-130 Propeller Hub System Components”, Naval Research Laboratory, Washington, DC, USA, May 2003, ESTCP Online Library <http://www.estcp.org/>.
- [38] Legg, K.O. et al., “Investigation of Plasma Spray Coatings as an Alternative to Hard Chrome Plating on Internal Surfaces”, SERDP Project WP-1151, Final Report, June 2006, ESTCP Online Library <http://www.estcp.org/>.
- [39] Binfield, M.L. and Eyre, T.S., “The Tribological Characteristics of a Detonation Gun Coating of Tungsten Carbide under High Stress Abrasion”, Special Publication of the Royal Society of Chemistry, Vol. 206, pp. 203-216, 1997.
- [40] Super D-Gun Coating Process, Hard Facts, Praxair S.T. Technology Inc., 2005, [http://www.praxair.com/praxair.nsf/d63afe71c771b0d785256519006c5ea1/2471692e3b79f13485256ef600676b10/\\$FILE/Super%20D-Gun%20Coating%20Process.pdf](http://www.praxair.com/praxair.nsf/d63afe71c771b0d785256519006c5ea1/2471692e3b79f13485256ef600676b10/$FILE/Super%20D-Gun%20Coating%20Process.pdf).
- [41] McCrea, J.L., Marcoccia, M. and Limoges, D., “Electroformed Nanocrystalline Coatings: An Advanced Alternative to Hard Chromium Electroplating”, SERDP, Final Report, November 2003, ESTCP Online Library <http://www.estcp.org/>.
- [42] Singh, J., Wolfe, D.E. and Quli, F., “Electron Beam-Physical Vapor Deposition Technology – Present and Future Applications”, Publication of Applied Research Laboratory, Pennsylvania State University, University Park, PA, USA.
- [43] van der Kolk, G.J. et al., “PVD Coatings as Replacement of Chromium Electroplating”, Galvanotechnik, Vol. 92, Issue 11, pp. 3058-3066, September 2001.
- [44] Burakowski, T. and Wierzchon, T., “Surface Engineering of Metals”, CRC Press LLC, Boca Raton, FL, USA, 1999.
- [45] Carter, D.M. and Taylor, B., “Laser Cladding vs. Chrome Plating”, Proceedings (CD) of Cadmium, Chromium and Nickel Alternatives Information Exchange, Organized by Concurrent Technologies Corporation, Seven Springs Mountain Resort, Champion, PA, USA, 25-27 September 2000.
- [46] Johnson, R.N., Bailey, J.A. and Goetz, J.A., “Electro-Spark Deposited Coatings for Replacement of Chrome Electroplating”, SERDP Project PP-1147, Final Report, June 2005, ESTCP Online Library <http://www.estcp.org/>.
- [47] Sartwell, B.D. et al., “Electrospark Deposition for Depot- and Field-Level Component Repair and Replacement of Hard Chromium Plating”, ESTCP Final Report, September 2006, ESTCP Online Library <http://www.estcp.org/>.

23.7 ADDITIONAL REFERENCES

- [A1] “Canadian Environmental Protection Act”, http://www.ec.gc.ca/CEPARRegistry/the_act/.
- [A2] “Clean Air Act”, 42 U.S.C. §§ 7401 et seq.
- [A3] “Toxic Substance Control Act”, 15 U.S.C. §§ 2601 et seq.
- [A4] “End-of-Life Vehicle”, EU Directive 2000/53/EC, http://ec.europa.eu/environment/waste/elv_index.htm.

- [A5] “Waste Electrical and Electronic Equipment”, EU Directive 2002/96/EC, http://ec.europa.eu/environment/waste/weee/index_en.htm.
- [A6] “Restriction on the Use of Hazardous Substances”, EU Directive 2002/95/EC, <http://www.rohs.eu/english/index.html>.
- [A7] “Stockholm Convention on Persistent Organic Pollutants”, <http://www.pops.int/>.
- [A8] Convention on Long Range Transboundary Air Pollution, <http://www.unece.org/env/lrtap/welome.html>.
- [A9] ASTM B117, “Standard Practice for Operating Salt Spray (Fog) Testing Apparatus”, American Society for Testing and Materials, 1997.
- [A10] ASTM G85, “Standard Practice for Modified Salt Spray (Fog) Testing”, American Society for Testing and Materials, 1994.
- [A11] QQ-P-416, “Plating, Cadmium (Electrodeposited)”, Federal Specification, 1991.
- [A12] ASTM F519, “Standard Method for Mechanical Hydrogen Embrittlement Evaluation of Plating Processes and Service Environments”, American Society for Testing and Materials, 1997.
- [A13] ASTM E466, “Standard Practice for Conducting Force Controlled Constant Amplitude Axial Fatigue Tests of Metallic Materials”, American Society for Testing and Materials, 1996.



Chapter 24 – MATERIALS REPLACEMENT FOR AGING AIRCRAFT

Ali Merati

Structures and Materials Performance Laboratory, Institute for Aerospace Research
National Research Council Canada
Ottawa, Ontario
CANADA

24.1 INTRODUCTION

The criteria for the selection of materials for aircraft structure have evolved over the years. When the Wright brothers used the first cast aluminum engine block on the Flyer, the main drivers for material selection were weight and static strength. The main airframe materials were wood with fabric covering. Wood is a natural composite with long fibers of cellulose held together in a weaker matrix of lignin, which illustrates that using composite airframes is not a new idea. After development of precipitation hardening and the method to protect the surface of aluminum by cladding and anodizing, aluminum has been the primary material for airframe structures. Aluminum has been established in the aerospace industry, due to very high specific strength (strength/density), high toughness, ease of manufacture (major advantage being extrusion), long term performance, no low temperature brittle fracture, readily joinable by welding or mechanical riveting, and easily recyclable. Although pressure is increasing from composite fiber reinforced plastics, the latter three or four advantages seem to keep aluminum at the leading edge.

In the campaign for the position of “dominant material”, aluminum producers are trying to reduce weight. Introduction of new designs, aluminum-lithium alloys, and rivet replacement with laser welding or Friction Stir Welding (FSW) can be cited as examples. However, the main thrust of polymer based composites producers is to develop low cost manufacturing methods. The dominance of aluminum received a serious blow when Boeing designed the 787 with almost 50% polymer based composite in its structure. Nevertheless, aluminum remains a highly attractive material from which to make aircraft and space vehicles. Its recycling and low weight advantages are essential considerations, as they are in the automotive industry.

Corrosion control in the aerospace industry has always been important, but is becoming more so with the ageing of the aircraft fleet. The new approach of “care free” structures suggests that optimized structures should be designed for minimum life cycle cost [1], which translates to crack-free long life, minimum corrosion and repair, and reduced inspection costs. Today combinations of low weight, fatigue resistance, durability, damage tolerance, reliability, manufacturability, maintainability, corrosion resistance, low manufacturing costs and low assembly costs are needed to satisfy the required operating costs and safety of aircraft. Winning products need to be light in weight as well as low in manufacturing costs and processing methods (e.g., friction stir welded fuselage panel using improved Al-Li alloys). In a case study by Airbus, wing ribs were manufactured using friction stir welding of 2050 alloy. The lower density and high modulus of the aluminum lithium alloys provided the weight saving, and low cost manufacturing was achieved by friction stir welding as opposed to machining [2],[3].

Since the earliest days of the aircraft industry, alloy selection has seen different methodologies such as safe life, fail safe, and damage tolerance (fail-safe + periodical inspection) designs. Aluminum alloys such as 7079 and 7075 were developed for high static strength, but failed to provide adequate toughness and corrosion resistance. Later, alloys such as 7475, 7050, and 7010 were among the first alloys developed to satisfy the fracture toughness requirements of new damage tolerance designs.

With current high fuel costs, use of more expensive low density materials such as Al-Li, Metal Matrix Composite (MMC), polymer (epoxy) based composites (PMC), and Fiber Metal Laminate (FML) such as

Glare is predicted [4],[5]. However, introducing these newer materials as substitutes for older aluminum alloys in existing aircraft structures is not usually an option because of the profound implications on structural integrity and airworthiness. In fact even the simple replacement of one aluminum alloy with another must be approached with extreme caution because of unexpected negative consequences.

The focus of this chapter is mainly on aluminum alloys for airframe structures, however engines are also witnessing great innovation, for example with increased use of newer forms of the nickel-based superalloys such as directionally solidified and single crystal blades and vanes [6],[7].

The average age of aircraft in the USAF fleet, which is the largest fleet of aging military aircraft, is estimated to be 26 years and the average age of KC-135 tankers is now 50 years [8]. Civil aircraft operators have chosen to replace their older fleets; however most military aircraft operators choose to extend service life by more frequent inspection and repair. This has led to higher maintenance costs and workload, and reduced availability of aircraft. It should be noted that military aircraft reliability is still based on usage rates, which largely reflect flying hours with less emphasis on absolute chronological age when the time-dependent effects of corrosion would become significant.

24.2 AGING (LEGACY) ALUMINUM ALLOYS

High strength is the priority requirement for upper wing and fuselage stiffeners, while for lower wing alloys and fuselage skins damage tolerance is key [9],[10]. Most of the older aircraft were manufactured with Alclad 2024-T3 or 7075-T6 aluminum, both of which are precipitation hardenable alloys and hence can be heat treated to achieve high static strength. They are typical of many alloys developed in the late 1930s through to the late 1950s and early 1960s. Dealing with corrosion and fatigue problems of these legacy alloys (2024 and 7075) is the main source of cost in older aircraft. The alloy 2024 has served the aerospace industry since 1935. For the lower wing skin, 2024 was favored because of its higher fracture toughness. Alloy 7075-T651 was introduced in 1944 and has been used for upper wing structures or where high strength is needed in many of the older aircraft. In contrast to 7075-T6, the lower strength 2024-T3 is much more damage tolerant.

There are many parameters considered in the selection of materials for aircraft. However, as aircraft age reliability and maintainability gain considerable importance. There is a high probability of interaction between corrosion and fatigue, and the probability increases as an aircraft ages. In most cases of life extension, the alloys are replaced with the same but unused materials. Parameters influencing the corrosion and fatigue performance of the legacy alloys, such as heat treatment, constituent particles, and surface treatment, are discussed in the following sections.

24.2.1 Heat Treatment

Alloys 2024-T3 and 7075-T6 are both susceptible to exfoliation (Figure 24-1), intergranular corrosion, Stress Corrosion Cracking (SCC), and pitting [11]-[15]. These alloys in general have been the subject of extensive research since their development.

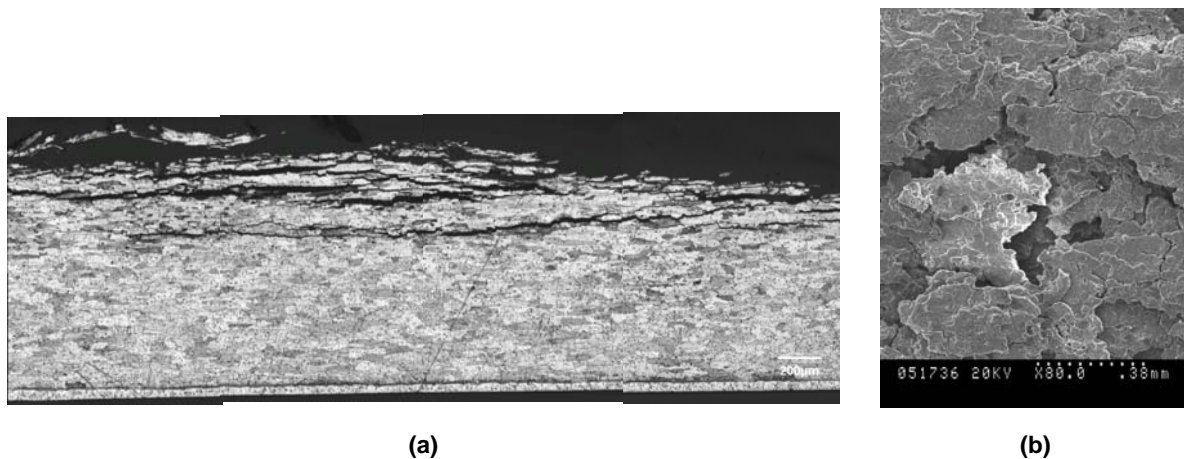


Figure 24-1: The Top Skin of a Severely In-Service Corroded B727 Lap Splice (Faying Surface) Made from One-Side Clad 2024-T3 – (a) Optical micrograph of exfoliation corrosion and a thickness loss of approximately 40%. The sample was taken from (b) SEM micrograph of top view of faying surface [11].

Inadequate corrosion resistance of 7000 series alloys in the T6 temper, particularly in the case of SCC and exfoliation have been the source of many service failures. SCC resistance is extremely important in thick sections. 7075 in the T6 temper and even 2024-T3 for thick products are found to be susceptible to SCC when stressed in the short transverse direction. Unlike general corrosion, the amount of deformation and the degree of observable corrosion accompanying SCC is small and could go undetected using most conventional NDI methods.

SCC in some 7000 series alloys can be overcome by the application of a T7 overaging heat treatment but typically by sacrificing 10 – 20 % strength. The aging treatments such as Retrogression and Re-Ageing (RRA) and T77, however, provide the resistance without considerable sacrifice in strength [16]-[19].

RRA is a multi-stage artificial ageing process and has been demonstrated to improve SCC resistance of 7075-T6 alloys. However, the quench sensitivity of the alloy, apparently due to the chromium-containing grain refinement used, prevents RRA from becoming a common commercial treatment for 7075. By contrast, alloys that are grain refined by zirconium, such as 7050, 7150, and 7055, respond well to the heat treatment which is designated as T77 type. The proprietary T77 temper, developed by Alcoa, is also a multi-step aging treatment that produces a higher strength with matching or better damage tolerance than T76 [8]. Further information on the RRA treatment and variants of it are provided in Chapter 25 [19].

In addition to susceptibility to SCC and exfoliation, the core alloys of 7075-T6 and 2024-T3 are prone to selective corrosion such as pitting along with intergranular corrosion. The fatigue and corrosion failure processes exploit the weakest links within the material, which act as nucleation sites for the fatigue cracks and corrosion (Figure 24-2). For improvement in resistance to localized corrosion, surface treatments such as cladding and anodizing are applied. However, it is found that the benefits gained in terms of corrosion protection by cladding and anodizing could be offset by detrimental effects on fatigue performance [15], [20],[21].

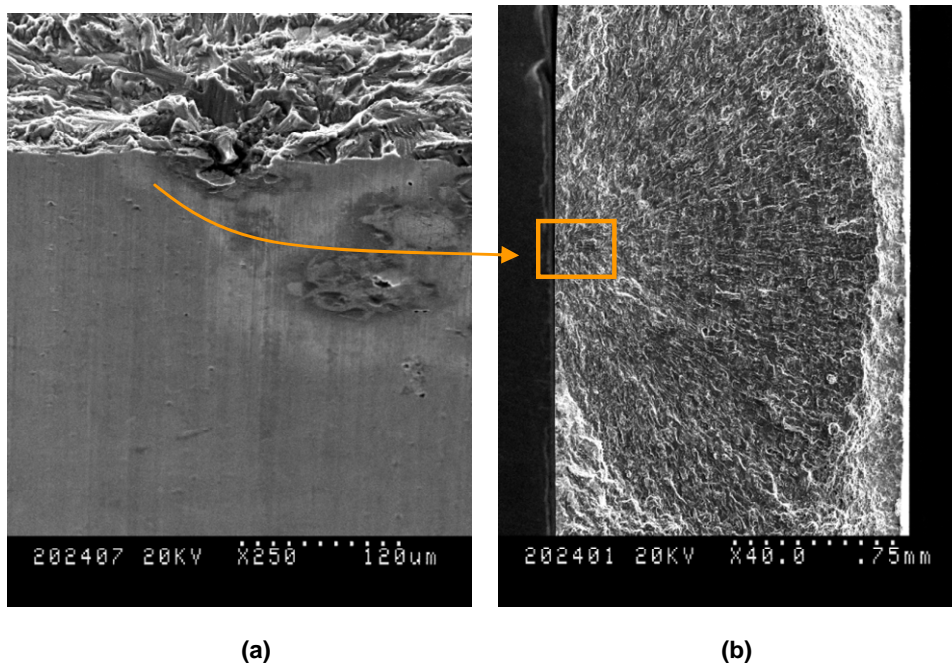


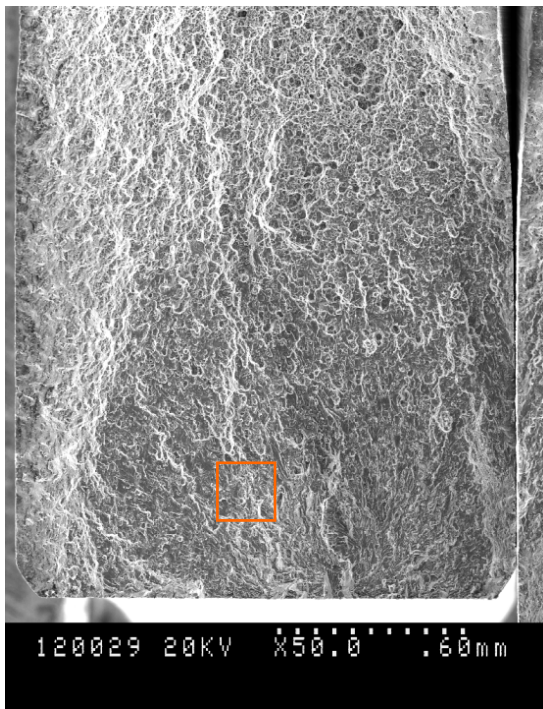
Figure 24-2: Localized Corrosion (Pitting) Due to Discontinuity at the Surface of an Unclad 1.6 mm 2024-T351 Sheet which Acted as Fatigue Crack Nucleation Site [12]. The fatigue coupon was made from a mildly corroded sheet: (a) Tilted view; and (b) Fracture face with window indicating to the nucleation site.

From the post fracture analysis in these studies, the microstructural features and discontinuities found to be associated with fatigue crack origins in the 7000 and 2000 series materials studied were in order of decreasing severity:

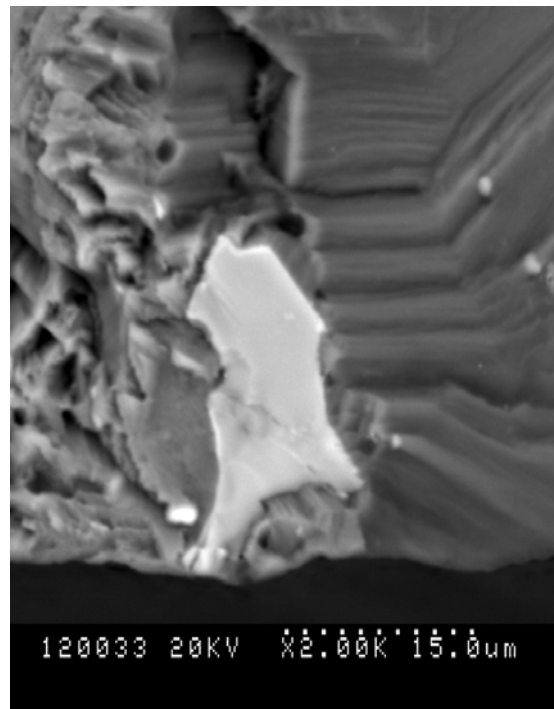
- a) Anodizing;
- b) Cladding;
- c) Constituent particles; and
- d) Scratches and machining marks.

24.2.2 Particles

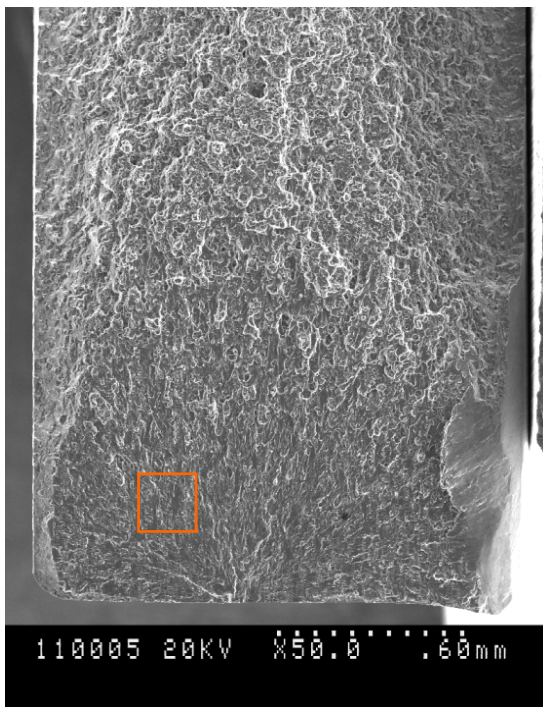
The center of the ingot is the last region to solidify during casting. Porosity and insoluble constituent particles form in this region. Given enough mechanical work in thin gauge sheets, the porosity will generally heal. However, the constituent particles remain and often lie in stringers in the rolling direction of the sheet. Among the major discontinuities that limit corrosion and fatigue performance of the two legacy alloys are constituent particles in the microstructure. Studies have shown that fatigue crack nucleation sites for bare (i.e., no cladding/anodized layer) coupons with acceptable machined surfaces are normally in the vicinity of large constituent particles (Figure 24-3) [15],[22],[23]. The detrimental effects of large constituent particles on the fracture toughness and crack nucleation have also been documented by many other investigators [24]-[29].



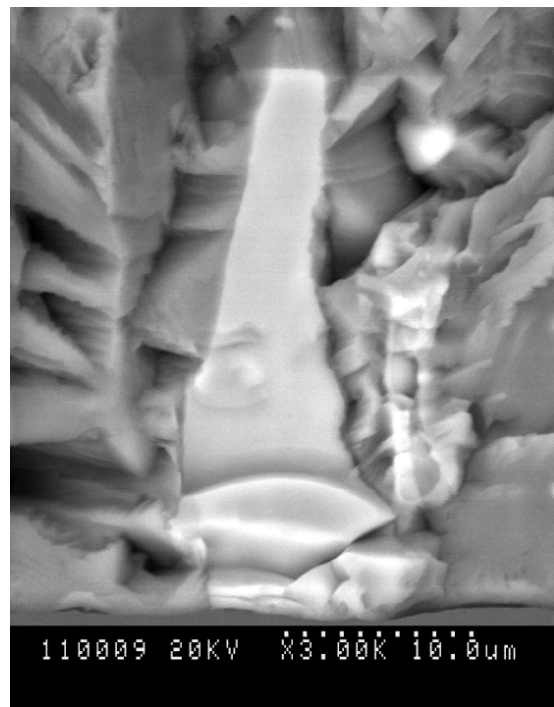
(a)



(b)



(c)



(d)

Figure 24-3: SEM Micrographs of Fracture Surfaces of Fatigue Coupons of 2024-T3 and 7075-T6 Sheets, Indicating Constituent Particles as Crack Origins – (a) Low magnification view of fracture surface for 2024 specimen; (b) High magnification, backscatter view of the (window) nucleation site; (c) Low magnification view of fracture surface for 7075 specimen; and (d) High magnification, backscatter view of the (window) nucleation site [15],[22],[23].

Studies suggest that there are two physically and chemically distinguishable types of constituent particles in these alloys. Larger and more angular particles have considerable amounts of iron, whereas the smaller, spherical particles do not. The chemical composition of the constituent particles from EDX studies taken from a metallographic section was compared with the chemical composition of the particles that were associated with the crack nucleation sites in the failed fatigue coupons. All of the spectra from the fatigue crack nucleating particles were identical to those from analysis of large particles found in metallographic sectioning, as shown in Figure 24-4. It was also evident that the particles that acted as crack origins in fatigue testing were at the high end of the particle size distribution obtained through metallography. Again, large particles only represent a very small fraction of the particle population. According to the ASM Metals handbook [30], the main intermetallic phase for the larger particles associated with crack nucleation is Al_7Cu_2Fe (β -phase).

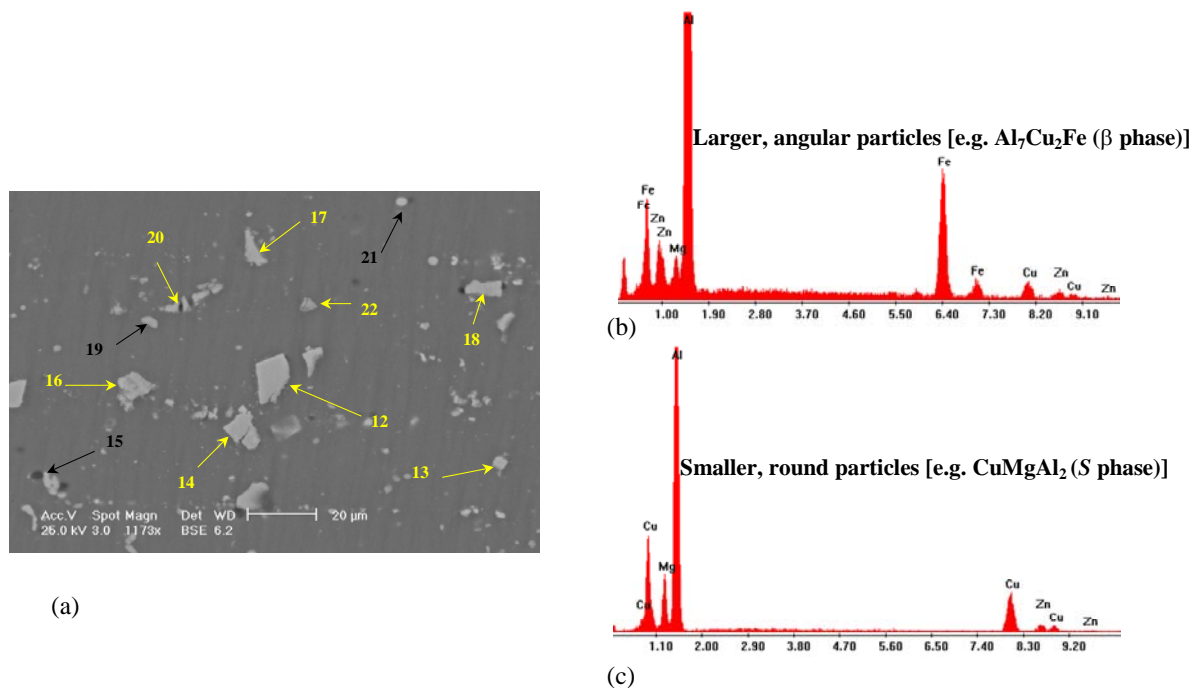


Figure 24-4: (a) SEM Micrograph of Typical Constituent Particles in a 2024-T3 Alloy. EDX results showed that (b) larger and more angular particles have considerable amounts of iron, whereas (c) the smaller, spherical particles do not. The spectra from the fatigue crack nucleating particles were identical to those from analysis of large particles found in metallographic sectioning [22].

Spherical particles seem to be mainly of the $CuMgAl_2$ (S-phase) type. They do not appear to be as harmful as iron bearing β -phase particles to fatigue performance. However, when these alloys are exposed to corrosive solutions, S-phase type particles appeared to be the weak link of the microstructure in terms of initiating pitting corrosion (Figure 24-5).

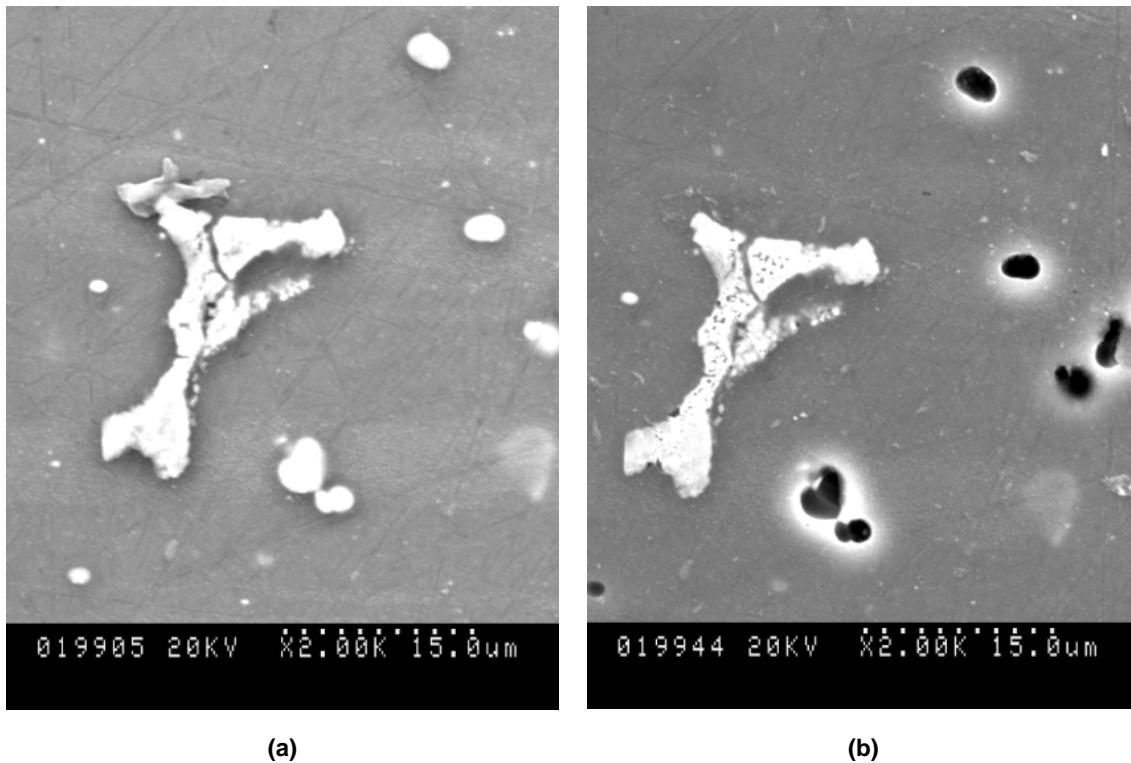


Figure 24-5: Constituent Particles – (a) Prior to corrosion; and (b) After 2 hours in corroding solution. Although, spherical particles did not seem to be harmful to fatigue performance, they appeared to be the weak link of the microstructure in terms of initiating pitting corrosion [22].

The key ingredients of the fatigue nucleating particles in aluminum alloys are impurities such as iron and silicon. Studies strongly suggest that modification of chemical composition and minimizing the volume fraction and size of intermetallic constituent particles can result in improvements in corrosion and fatigue performance. As will be discussed in the following sections, the new derivatives of these alloys have better control of alloy impurities such as Fe and Si, and could be used as replacement alloys.

24.2.3 Cladding/Anodizing

Cladding and anodizing are widely applied surface treatments for the legacy alloys and in general for aging aerospace aluminum alloys to enhance the corrosion performance.

In order to improve corrosion resistance, sheet materials are often clad with more anodic pure aluminum. The role of cladding is to protect the high strength core from localized corrosion attack. The thickness of the cladding layer is generally less than 5% of the overall thickness (~50 μm). The thin clad layer corrodes rather mildly and uniformly to protect the core alloy (Figure 24-6(a)). The yield stress of cladding is very low (10% of core metal); therefore, even under normal operating conditions for core materials, the yield stress of the cladding is likely to be exceeded and induce many cracks (Figure 24-6(b)). These multiple surface cracks in the cladding will assist the earlier nucleation of fatigue cracks and propagation into the core material. They could also raise local mean stress in the core metal because the clad layer carries very little load. It is well known that nucleation and/or early (small) crack growth comprises the major portion (e.g., up to 80%) of the fatigue life [31]-[36]. Therefore, acceleration of the nucleation process would significantly decrease the fatigue life. Studies by Hunter and Edwards [37],[38] showed that on clad specimens, the first crack could be detected as early as 1% of the fatigue life.

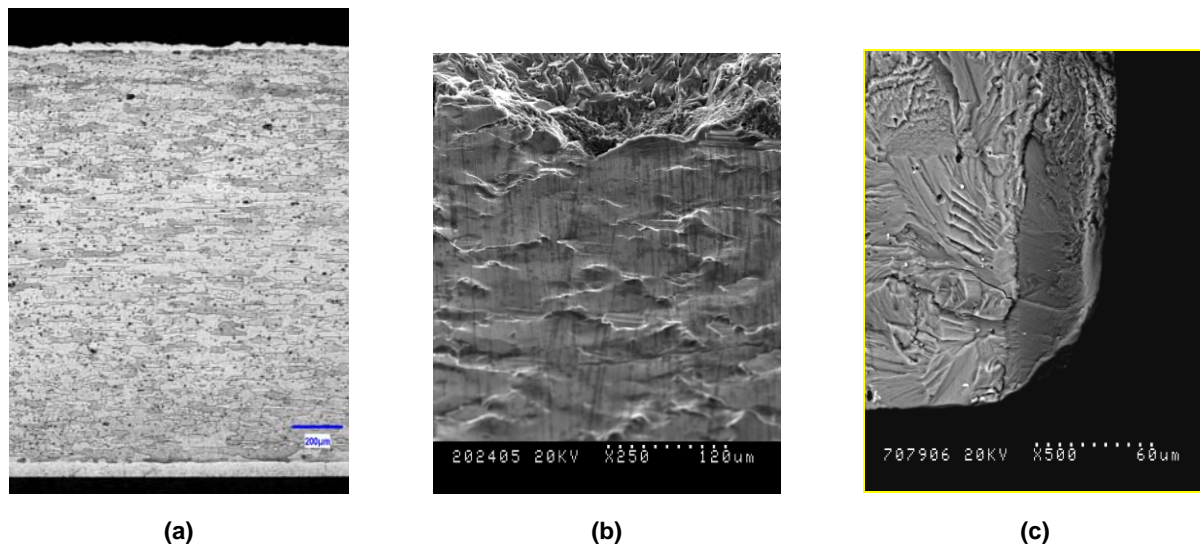


Figure 24-6: The Thin Clad Layer Corrodes Rather Mildly and Uniformly to Protect the Core Alloy – (a) General corrosion of clad layer at the exterior surface of fuselage skin (top surface) from B727; (b) Tilted image crack nucleation site as indication of severe deformation and cracking at clad layer at the surface of 2024 core alloy which failed in fatigue testing; and (c) Fracture surface showing the clad layer (~ 50 μm) at the right side [15].

Since the clad layer is soft and provides poor adhesion for paint, sometimes an anodic coating is grown on top of the cladding. Anodized coatings are commonly applied to aluminum alloys to provide resistance to corrosion and wear. They are also used as pre-treatments for adhesive bonding and painting [39]. Coatings for corrosion resistance are typically either the thin Type I (1 – 3 μm) or the moderately thick Type II (3 – 25 μm). For wear resistance, thicker hard anodizing (Type III up to 100 μm) is applied [40]. The two main anodizing treatments to achieve corrosion and wear resistance are chromic acid anodizing and sulfuric acid anodizing. The electrolytic process of anodizing produces a controlled columnar growth of amorphous aluminum oxide on the surface of aluminum alloys where the thickness of the oxide film is much greater than those formed naturally.

Anodizing also harms the fatigue life in various ways, with the main effect again being the encouragement of crack nucleation. The anodizing process produces a brittle and hard oxide film with inherent pores, which would readily crack when deformed. The presence of defects in the oxide film facilitates the early nucleation of fatigue cracks (Figure 24-7). The fatigue life of anodized specimens is also affected by the formation of so called “etch pits”. A long etching time (deoxidizing) prior to anodizing could result in pitting, particularly in the vicinity of chemically active regions such as grain boundaries and intermetallic particles at the surface [41],[42].

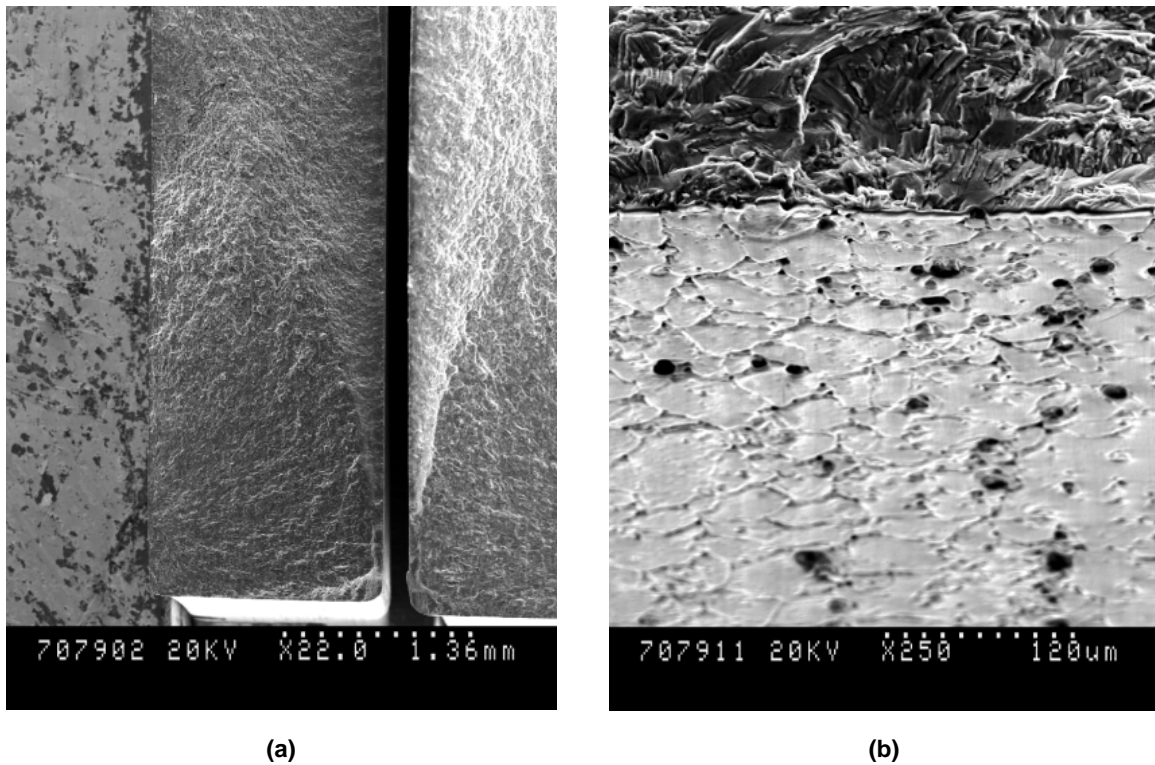


Figure 24-7: Fatigue Fracture Surface of Coupons Made of Anodized 1.6 mm Thick 7079-T6 Alloy. The sheet was removed from a retired C-5 fuselage skin – (a) Fracture surface of fatigue coupon with window showing the nucleation site; and (b) Tilted SEM image represents a close up view of nucleation site (the window) indicating a brittle and hard oxide film anodized layer with inherent pores and tiny cracks [13].

24.3 NEW REPLACEMENT MATERIALS

In reaction to the many service failures of the legacy alloys and cost burden on ageing aircraft, there is a continuing demand for better fatigue and corrosion performance. The appeal of aircraft manufacturers to materials scientists has been to manufacture alloys with combinations of good properties such as high strength of 7075-T6, good fracture toughness of 2024-T3, and high corrosion resistance of 7XXX series alloys in the T7 temper. In response to the demand (in particular for thick products), alloy manufacturers have produced new derivatives of 2000 and 7000 series and more recent alloys as shown in Table 24-1. As it was mentioned, the weak links of materials in terms of fatigue and corrosion performance have been constituent particles. Also because of low corrosion resistance of core alloys, they had to be coated (clad/anodized) at the expense of fatigue performance. Impurity elements, in particular iron and silicon are the damaging ingredients of the fatigue nucleating particles in aluminum alloys, and their reduction is the main modification in chemical composition observed. For instance, modified chemical compositions and reduced volume fraction of intermetallic constituent particles resulted in the development of 2524 alloy and 7475 as derivatives of 2024 and 7075 respectively. As indicated by Table 24-1, these new derivatives have much lower Fe and Si contents (up to 4 to 10 times). Table 24-2 compares and contrasts the mechanical properties of older and newer alloys and materials that might be used as replacements.

MATERIALS REPLACEMENT FOR AGING AIRCRAFT

Table 24-1: Chemical Composition of Alternative Materials.

Aerospace Al Alloys											
2000 Series	Cu	Zn	Mg	Mn	Fe	Si	Cr	Zr	Ti		
2024	4.4	–	1.5	0.6	≤0.5	≤0.5	0.1	–	0.15		
2026	3.6 – 4.3	0.1	1.0 – 1.6	0.3 – 0.8	0.07	0.05	–	0.05 – 0.25	0.06		
2224	4.1	–	1.5	0.6	≤0.15	≤0.12	–	–	–		
2324	3.8 – 4.4	0.25	1.2 – 1.8	0.3 – 0.9	0.12	0.1	0.1	–	0.15		
2524	4.0 – 4.5	0.15	1.2 – 1.6	0.45 – 0.7	0.12	0.06	0.05	–	0.1		
6000 Series	Cu	Zn	Mg	Mn	Fe	Si	Cr	Zr	Ti		
6013	0.6 – 1.1	0.25	0.8 – 1.2	0.2 – 0.8	0.5	0.6 – 1.0	0.1	–	0.1		
7000 Series	Cu	Zn	Mg	Mn	Fe	Si	Cr	Zr	Ti		
7010	1.5 – 2.0	5.7 – 6.7	2.1 – 2.6	0.1	0.15	0.12	0.05	0.1 – 0.16	0.06		
7049	1.2 – 1.9	7.2 – 8.2	2.0 – 2.9	0.2	0.35	0.25	0.1 – 0.22	–	0.1		
7050	2.3	6.2	2.25	–	≤0.15	≤0.12	–	0.1	–		
7055	2.0 – 2.6	7.6 – 8.4	1.8 – 2.3	0.05	0.15	0.1	0.04	0.08 – 0.25	0.06		
7075	1.2 – 2.0	5.1 – 6.1	2.1 – 2.9	0.3	0.5	0.4	0.18 – 0.28	–	0.2		
7079	0.6	4.3	3.2	0.2	≤0.4	≤0.3	0.15	–	–		
7085	1.3 – 2.0	7.0 – 8.0	1.2 – 1.8	≤0.04	≤0.08	≤0.06	≤0.04	0.08 – 0.15	≤0.06		
7150	1.9 – 2.5	5.9 – 6.9	2.0 – 2.7	0.1	0.15	0.12	0.04	0.08 – 0.15	0.06		
7178	1.6 – 2.4	6.3 – 7.3	2.4 – 3.1	0.3	0.5	0.4	0.18 – 0.28	–	0.2		
7249	1.3 – 1.9	7.5 – 8.2	2 – 2.4	0.1	0.12	0.1	0.12 – 0.18	–	0.06		
7475	1.2 – 1.9	5.2 – 6.2	1.9 – 2.6	0.06	0.12	0.10	0.18 – 0.25	–	0.06		
Al-Li Alloys	Li	Cu	Zn	Mg	Mn	Fe	Si	Cr	Zr	Ti	Other
2050	0.7 – 1.3	3.2 – 3.9	0.25	0.2 – 0.6	0.2 – 0.5	0.1	0.08	0.05	0.06 – 0.14	0.1	0.2-0.7 Ag
2090	1.9 – 2.6	2.4 – 3.0	0.1	0.25	0.05	0.12	0.10	0.05	0.08 – 0.15	0.15	–
2098	0.8 – 1.3	3.2 – 3.8	0.35	0.25 – 0.8	0.35	0.15	0.12	–	0.04 – 0.18	0.1	0.25-0.6 Ag
2099	1.6 – 2.0	2.4 – 3.0	0.4 – 1.0	0.1 – 0.5	0.1 – 0.5	0.07	0.05	0.1 – 0.5	0.05 – 0.12	0.1	0.0001Be
2199	1.4 – 1.8	2.0 – 2.9	0.2 – 0.9	0.05 – 0.4	0.1 – 0.5	0.07	0.05	–	0.05 – 0.12	0.1	0.0001Be
8090	2.2 – 2.7	1.0 – 1.6	0.25	0.6 – 1.3	0.1	0.30	0.20	0.10	0.04 – 0.16	0.1	–

Table 24-2: Mechanical Properties of Alternative Materials.

Aerospace Al Alloys	UTS (MPa)	Yield Strength (MPa)	Fracture Toughness, K_{Ic} (MPa*m ^{1/2})	Elongation (%)	Applications
2024-T351	428	324	37	21	Lower wing, skin and stringer, high damage tolerance
2026-T3511	496	365	NA	11	Lower wing, fuselage stringer
2050-T84	540	500	43 (LT)	NA	Thick products, spars, ribs
2090-T83	531	483	43.9	3	Lower wing
2098-T82	503	476	NA	6	Sheet or thin plate
2099-T83	543	520	30 (LT) 27 (TL)	7.6	Floor beams, seat tracks
2199-T8	400	345	42 (LT) 36 (TL)	8	Lower wing skin
2224-T39	476	345	53	10	Lower wing, fuselage stringer
2324-T39	475	370	38.5 – 44.0	8	Lower wing skin
2524-T3	434	306	40 (TL)	24	Fuselage skin
6013-T6	379 359	359	46 (LT)	8	Fuselage skin
7010-T73651	525	455	41 (LT), 33 (TL) 26 (SL)	12	Upper wing skin and stringer, thick products
7049-T73	517	448	33 (LT) 24 (TL)	12	Thick products
7050-T7351	552	490	35 (LT) 31 (TL)	11	Thick products e.g., spars, ribs, landing gear
7055-T7751	614	593	26	7	Upper wing, skin, stringer
7075-T651	572	503	22	6	Upper wing skin and stringer
7079 – T651	540	470	45 (TL)	14	Wing panels, bulkhead
7085-T7651	519	468	29 (LT)	8	Thick products, wing spars
7150-T7751	579	538	24	8	Upper wing, skin, stringer
7178 – T6	590	521	23 (LT)	11	Upper wing skin
7249-T6	592	532	37	11	Extrusion, thick products, wing
7475-T7351	545	476	42 (LT) 37 (TL)	12	Fuselage skin
8090-T851	500	455	33 (LT), 30 (TL) 12.4 (SL)	12	Fuselage skin, stringer, frame
ARALL-1	800 (L) 386 (L+45)	641 (L) 341 (LT)	NA	0.7 (L) 7.1 (LT)	
ARALL-2	717 (L) 317(L+45)	359 (L) 228 (LT)	NA	1.4 (L) 12.0 (LT)	
ARALL-3	828 (L) 373 (L+45)	587 (L) 317 (LT)	NA	1.0 (L) – (LT)	
ARALL-4	731 (L) 338 (L+45)	373 (L) 317 (LT)	NA	1.4 (L) 3.9 (LT)	
Carbon Composite (Typical)	655 (L) 276 (L+45)	–	NA	0.5	
CF/PEEK Composite (unidirectional)	1507 (L) 88 (T)	NA	NA	NA	
GLARE (cross-ply)	717 (L) 716 (T)	305 (L) 283 (T)	NA	4.7	
GLARE (uni-directional)	1282 (L) 352 (T)	545 (L) 333 (T)	NA	4.2 (L) 7.7 (T)	

In the search for improved materials Alcoa developed 7050-T7, as well as 7049, 7249 and 7010 alloys, but among these four alloys the former appears to have the most favourable combination of properties. Alloy 7050 was also developed in response to lower strength of 7075-T73 and for the retrofit of 7079-T6 that showed very low resistance to SCC. In response to demand for higher strength (as high as 7178-T6), the more recent product 7150-T77 was developed, which has higher strength and damage tolerance when compared with 7050-T76 [43]. Another new alloy; 7055-T77 has even higher strength than 7150-T6 alloy. High compression strength, combined with good fracture toughness and good corrosion resistance has made 7055 a good replacement of 7075 for the upper wing skin.

However for lower wing structures where predominantly tensile loading conditions prevail, even the major improvements of the newer 7000 series alloys are not considered adequate and they are not recommended. Where 2024-T3 was the dominant alloy, today alloys 2324 and 2224 are favoured for lower wing skins due to their higher tensile strengths and fracture toughness values and improved fatigue performance. For fuselage applications, 2024 has been replaced by 2524 due to excellent fracture toughness and good tensile strength [44],[45].

Alloy 2524-T3 has approximately 15 – 20 % improvement in fracture toughness and twice the fatigue crack growth resistance when compared with 2024-T3. The improvement helped in the elimination of tear-strap reinforcements in a weight efficient manner on the Boeing 777 [8],[45]-[47].

The 6000 series alloys, and in particular 6013-T6, have been considered to replace 2024 on a number of US Navy programs. They are weldable and less expensive, and do not need cladding. Nevertheless, they are still susceptible to intergranular corrosion similar to 2024-T3 [48],[49].

Under pressure from competing polymer-based composite for structural applications, Al-Li has been a new thrust for the aluminum industry. The aerospace industry saw the benefits of a high strength metallic alloy since it allowed use of the same tooling and assembly techniques as the more conventional Al alloys. It also involved lower risk, requiring no new repair and maintenance methodologies and avoided the recycling issues of composites. Both Li and Be are exceptions among other elements in that despite being lighter than Al, they increase the stiffness of the aluminum. Al-Li alloys are lighter in weight and higher in stiffness compared to conventional aluminum alloys. Al-Li began with high promise, and since high stiffness is one of the major design factors for airframes, there were good opportunities for Al-Li. The second generations of these alloys with 2 – 3% lithium, such as 2090 and 8090 have been used in the MIG 29 and Cormorant (EHI) Helicopter. However, these early versions of Al-Li in particular, did not live up to their initial promise and until now have seen only limited use in airframes. Their major shortcomings were delamination and lack of ductility. The third generation alloys with much lower lithium content (2098, 2099 extrusion and 2199 sheet) are claimed to eliminate the problems with high planar anisotropy, poor ST properties, and low fracture toughness [50]. It is believed that the new generation of Al-Li alloys will find widespread usage in future commercial aircraft. The other new alloy, although with much higher cost, is Al-Mg-Sc which has excellent corrosion resistance and can be used as skin requiring minimum maintenance [60].

Titanium alloys also can be used where there is a need for much better resistance to corrosion (almost immune to exfoliation) and where there is a need for physically smaller components, for example landing gear components of the B777. They are even good replacements for high strength steel due to elimination of the risk of hydrogen embrittlement and need no protective coating. Ti alloys also exhibit good galvanic compatibility and nowadays are extensively used for attaching aluminum to carbon fiber composites for repair purposes. In construction of new hybrid structures, the use of Ti fittings is generally recommended.

24.4 LESSONS LEARNED

It is often best to review past examples of important developments and misjudgments to provide guidance for the future. The objectives for introducing new materials are to improve performance, reduce the cost

(both the purchase cost and the maintenance cost), extend service life, and reduce environmental impact. There is always interaction among these factors that have to be balanced to reach an overall improved performance.

For example if stiffness were the main limiting factor for a component, honeycomb structure would be ideal. However, not all of the materials can be fabricated this way and also there is a tendency for corrosion to occur in this type of construction. Metal Matrix Composites (MMC), either aluminum based or titanium based, with SiC (or Al_2O_3) particles also provide high stiffness, but low ductility in the current product forms has limited their application.

Another example is the development of the very highly alloyed 7178-T6 in 1951 as a replacement for 7075-T6. The increased demand in the aircraft industry for higher strength-to-weight ratio material led to a record peak in strength from this aluminum alloy. It was used for the upper wing skins of aircraft in both extruded and rolled forms and was used on Boeing 707 aircraft and lower wing skin of KC-135 [8],[51]. However, due to the lack of damage tolerance and the need for high fracture toughness and high mechanical reliability, this alloy was gradually withdrawn from use. High strength 7055 has been a good replacement for 7178, with much improved fracture toughness [43].

It is also important that new materials achieve maturity before being used in aircraft. Experience with alloys in service, perhaps in aircraft secondary structures or non-aeronautical applications or simulated service behavior concerning corrosion, inspection, long term performance, etc. should be known prior to use in aircraft primary structure. A good lesson from the past is the launch of the high strength alloy 7079 in T6 temper for thick products. The alloy was introduced as a replacement for 7075-T6 to improve SCC performance in the short transverse direction. Laboratory tests in 3.5% NaCl solution by alternate immersion showed superior performance to the alloys in use at the time. Despite the good resistance predicted by the accelerated testing, service failures of alloy 7079-T6 showed it to be by far the most SCC susceptible alloy and temper among the commonly used high strength aluminum alloys available at that time. Although it was resistant to nucleation of SCC cracks, the rate of growth of SCC was orders of magnitude faster than that of the other alloys. The pre-cracked SCC test was not a standard test at the time in early 1950s. Figure 24-8 shows the nature of the crack paths for EAC in aluminum alloys which are almost exclusively intergranular [14]. Widespread service failures resulted in recommendations that 7079-T6 be replaced with alternative materials such as 7475-T7 [10].

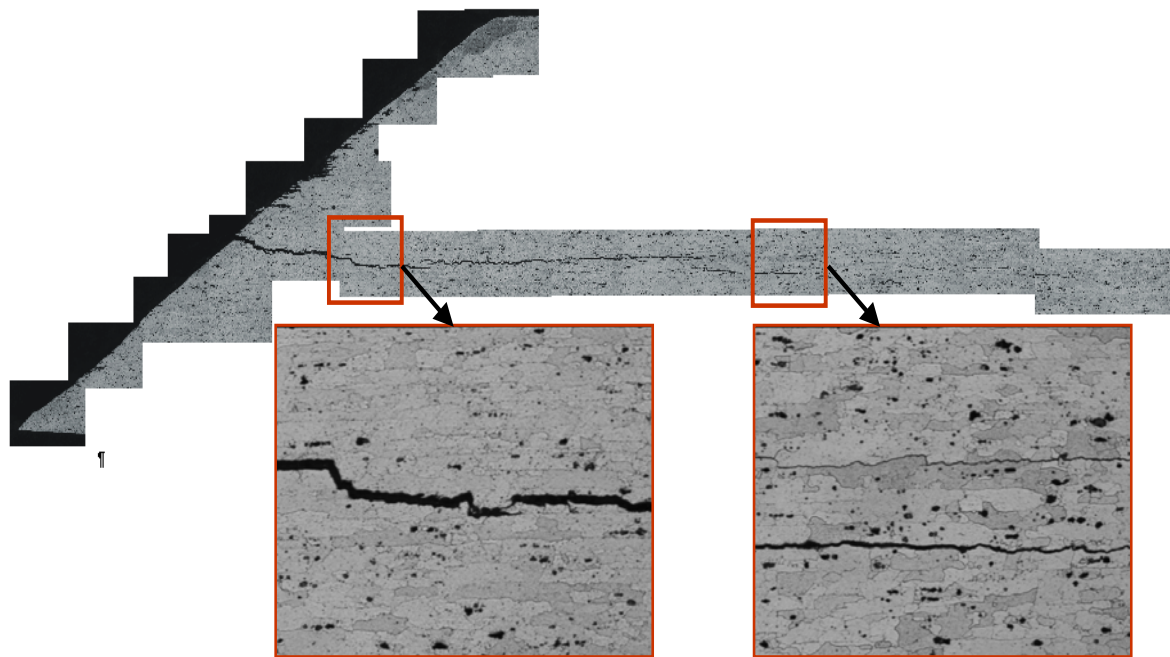


Figure 24-8: SCC Failures During Service at Mid Thickness of a Sheet Made of Alloy 7079-T6. Section of rivet hole, displaying a 4 mm (0.157") long crack. Crack at fastener hole on a fuselage panel near the troop door of C141 Starlifter [14].

Introducing new replacement materials should not be done in a radical way. New materials should be derivative alloys that have been developed by gradual changes in composition or temper. Brand new materials will face qualification and certification issues, high substitution risk and higher manufacturing costs. For instance, although polymer matrix composites are used in Airbus and Boeing (777 & 787) aircraft, they are not generally recommended as replacements for conventional aluminum airframe materials. They could alter the load distributions in the airframe, center of gravity, and affect vibration signatures of the structures.

Other examples of hasty introduction of materials into service are Metal Matrix Composites (MMC) in the form of discontinuous or continuous reinforcement, along with aluminum lithium alloys. The first few versions of these products had very limited success when incorporated into aircraft due to lack of ductility. The next generations of these materials have had fewer problems; however, the earlier bad experiences discouraged their widespread use and they have never achieved their full potential as structural alloys. Long term performance, substitution risk, prior in-service experience, results of full scale testing and life cycle costs of the new replacement material have to be considered before any attempt can be made to insert them into service.

The low density and good mechanical properties of Al-Li alloys make them attractive for many structural applications. Known applications of Al-Li alloys in military and civilian aviation are: EH101/CH149 structure; F-16 bulkheads and fuselage structure; hydrogen tank of NASA's space shuttle; and fuselage skins of Russian BE-103 amphibious aircraft and Tupolev business class aircraft [52]-[55].

In the case of the CH149 Cormorant Search and Rescue Helicopter, 8090 Aluminium-Lithium (Al-Li) alloys in different product forms and tempers have been used to replace most of the conventional aircraft alloys such as 7075-T6 and 2024-T3 [56]. This is because of their low density and high elastic modulus. Although the Cormorant is in the early stages of its life cycle, signs of premature material failure are raising concerns about long-term durability. The fracture surfaces of a number of in-service failed Al-Li parts indicate that brittle intergranular fracture is the most common mode of failure (Figure 24-9).

The study also points out the possibility of embrittlement of Al-Li over time when exposed to temperatures between 30°C and 160°C which is within the operational envelope. Table 24-3 outlines where the Al-Li alloys are used in aircraft and the conventional alloys they replaced [57].

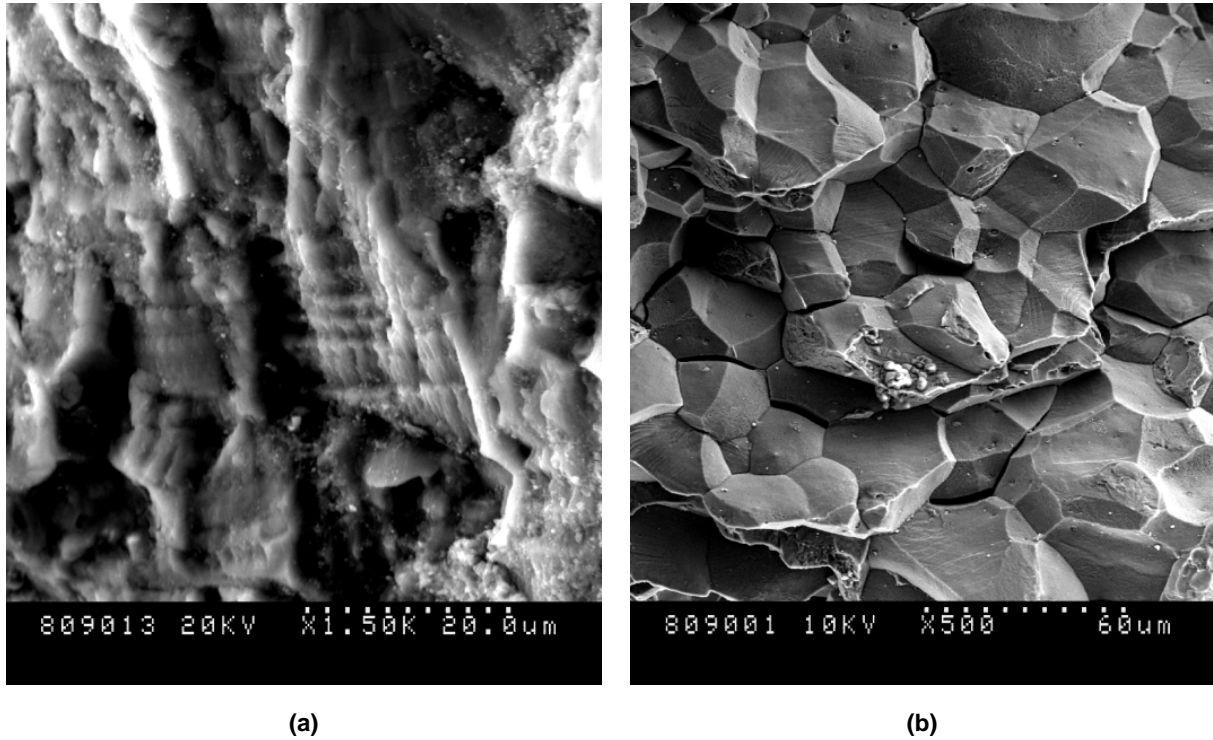


Figure 24-9: Typical Fracture Feature Found During Maintenance Inspection of the CH149 Cormorant at the Secondary Structures (Under-Floor Z-Stiffeners) After Only a Few Years of Service. The most common failure mode observed was (a) small area of fatigue followed by (b) major part of fracture as brittle intergranular failure. The part is made of 8090-T8 aluminum lithium [56].

Table 24-3: Al-Li Alloys Used in the CH149 Cormorant [52].

Product Form	Temper	Substitute For	Applications
<i>Sheet</i>	8090-T3 (as-received)	–	Floor installations, brackets, stiffeners, frames, spars, stringers, longerons, ribs, bulkheads, tail cone skin
	8090C-T8 (medium-strength)	2014-T6	Flying control system and avionics bay structures, nose cap, cabin roof frames
	8090C-T81 (damage-tolerant)	2024-T3, 2024-T42	Flying control system structure, skin panels (in lower fuselage), cabin roof frames, flat roof panels
	8090-T84 (medium-strength)	–	Z-stiffeners
	8090C-T621 (damage-tolerant)	2024-T42	Sponsons, repairs
<i>Forging</i>	Cold compressed 8090-T852 (medium-strength)	7010-T7451	Cabin roof and side frames (frames, stringers, joints, intercostals)
	Non-cold compressed 5091-H112 (medium/high-strength)	7075-T73, 7010-T7451/T74	Landing gears
<i>Extrusion</i>	8090-T8511 (medium-strength)	7075-T7351/ T73510/T37511	Frames, brackets, stringers, bulkheads, door rails, seat tracks

The 8090 alloy may have only been evaluated using small-scale coupons, since this author has found no evidence in the literature of component or full-scale tests of these alloys. The manufacturers of Cormorant conducted the large-scale tests and prototype flight trials using the original materials (2XXX and 7XXX series alloys).

As a result of their high stiffness, Al-Li components can alter load paths and distributions within the aircraft's structure, affecting the inherent vibration signature and creating several new, unexpected fatigue-susceptible areas (e.g., in the nose under the pilot seat structure). The more recent (third generation) alloys with much lower lithium content (2098, 2099 extrusion, 2199 sheet) are claimed to be more isotropic, have better ST properties, and improved fracture toughness.

In addition, replacing the old materials with new ones could affect center of gravity for the vehicle, change vibration signature, and increase the probability of galvanic corrosion due to incompatibility with adjacent materials.

Airbus has considered a more evolutionary approach, which is preferred since past experience has shown that every technology has some initial technical problems. Application of any new material in primary structure such as carbon fiber reinforced plastics, fiber metal laminates (Glare and ARALL) and glass thermoplastics requires the establishment of a good materials and design database.

24.5 COMPOSITE MATERIALS

Material and assembly costs (first costs), maintenance costs, and performance are three main drivers for material selection. For instance, polymer based composites and hybrid materials such as Glare have high first cost but are excellent in damage tolerance and corrosion resistance which translates to low maintenance and high performance. For instance the B787 with 50% composite is promising twice as long operation time

between scheduled maintenance intervals of the B767 it replaces [4]. Polymer matrix composites use glass, carbon, aramid, or boron fibers as the reinforcement, with the matrix being either thermoplastic or thermosetting. They outperform aluminum alloys in specific strength, modulus and fatigue; however initial cost of the material can be as much as 10 to 20 times higher than that of aluminum alloys. In general, advanced or new materials are offered at higher costs compared to the existing materials.

The most common matrix resins are thermosetting epoxy resins, which can be used to temperatures as high as 175°C and are compatible with all common reinforcements. These also possess fatigue strengths significantly superior to aluminum alloys. Bismaleimides and other thermosetting polyimides offer increasing temperature capability from 250 – 315 °C. Thermoplastics such as PEEK (polyether ether ketone) are processed beyond their melting points and are tougher than the thermosets, but soften at higher temperatures because of the lack of cross-linking. Many are also less resistant to environmental effects. The cost of processing polymer matrix composites is significantly higher than equivalent metal structures. Lower-cost processes such as resin transfer molding have been improved to allow a high volume fraction of fiber than in previous generations of liquid molding processes. The embedding of smart sensors and actuators adds an additional dimension to the use of composite materials in terms of health monitoring of structures made of such materials.

Laminates of aluminum and polymer composites provide exceptional fatigue-crack-growth resistance and damage tolerance at high specific strength. Although earlier predictions on the increase in use of Al-Li alloys, intermetallics, and ceramics have often been overly optimistic, hybrid laminates of titanium alloys, aluminum alloys, and reinforced polymers are considered to provide combinations of properties beyond the capabilities of the current materials.

24.6 PROCESSING TECHNOLOGIES

One of the ways for the aluminum industry to compete against the composite challenge is to integrate design concepts and advanced manufacturing technologies. Casting and new robust joining techniques for similar and dissimilar materials will enhance such an integration process by eliminating the need for mechanical fastening of separately manufactured parts.

Although cost reduction is a primary reason for use of castings for aircraft structures, by reducing the number of joints, benefits such as improved corrosion resistance can also be realized. However, the poor reproducibility and inconsistency in mechanical properties of conventional castings has introduced the concept of the casting factor as a safety measure. However, by improvements in processing, use of aluminum castings is being increased even in primary structures, e.g., Airbus cargo and passenger doors [58].

Almost all engineered products are made from a number of components. Choosing the best way to joint them together is essential. The combination of new design, advanced manufacturing processes such as Friction Stir Welding or laser welding, and new materials (extruded Al-Li) is capable of producing integrally stiffened panels that offer significant cost and weight savings. One of the shortcomings associated with the use of Al alloys relates to the problems encountered in their joining. Riveting adds unnecessary weight, and fusion welding processes can introduce solidification defects such as porosity and solidification cracking. Friction Stir Welding (FSW) is one of the most promising processes to replace riveting [59]. The process can be used to join aluminum alloys that have traditionally been considered non-weldable. It can also be used to join dissimilar metals.

24.7 CONCLUSIONS

Aging aircraft are increasingly experiencing fatigue and corrosion related cracking problems that pose significant challenges in terms of keeping air operations safe, reliable and economic. The aging materials

and structures have to be repaired or replaced. Since the early fleets entered service, significant progress has occurred in alloy development and manufacturing processes. Combination of the new materials and the new assembly processes could reduce the maintenance burden and sustain vehicle airworthiness.

Tighter control on composition, fabrication processes and heat treatment has enabled alloy manufacturers to achieve superior microstructures which lead to optimum tailored properties. Alloys are being developed that have inherent corrosion resistance and which are less critically dependent on supplementary corrosion protection such as via cladding and anodizing. One example is the weldable and corrosion resistant aluminum-magnesium-scandium alloy [60].

Solid state friction stir joining with its low heat input allows for a higher portion of base metal strength to be retained. Friction stir and laser beam welding can be used as repair processes or as alternatives to riveting process.

24.8 REFERENCES

- [1] Hinrichsen, J., "Requirements for Care-free Aircraft Structures and Expected Benefits from Hybrid Structures/Materials", SAWE Paper 3387, 65th Annual Conference of Society of Allied Weight Engineers, Valencia, CA, USA, May 2006.
- [2] Lequeu, P. and Maziarz, R., "High Performance Friction Stir Welded Structures Using Advanced Alloys", ASM International AeroMat Conference, 2006, https://www.entrepreneur.com/tradejournals/article/156577633_2.html.
- [3] Kroninger, H. and Reynolds, A., "R-Curve Behavior of Friction Stir Welding in Aluminum-Lithium Alloy 2195", in Fatigue and Fracture of Engineering Materials and Structures, Vol. 25, pp. 283-290, 2002.
- [4] Fredell, R., Gunnink, J., Bucci, R.J. and Hinrichsen, J., "Carefree Hybrid Wing Structures for Aging USAF Transports", in Proceeding, First Int. Conference on Damage Tolerance of Aircraft Structures, Edited by R. Benedictus, J. Schijve, R. Alderliesten, J. Homan, TU Delft, Netherlands, 2007.
- [5] Hinrichsen, J., "Airbus A3xx: Design Features and Structural Technologies Review", 28th Workshop: Advanced Design Problems in Aerospace Engineering: Galileo Galilei Celebrations, Sicily, Italy, July 1999.
- [6] Green, K. and Furrer, D., "Advanced Turbine Engine Materials", in Advanced Materials and Processes, ASM International, pp. 21-23, March 2009.
- [7] Backman, D. and Williams, J., "Advanced Materials for Aircraft Engine Applications", in Science, Vol. 255, Frontiers in Materials Science, pp. 1082-1087, downloaded from <http://www.sciencemag.org>.
- [8] Bucci, R.J., Warren, C. and Starke, Jr., E.A., "The Need for New Materials in Aging Aircraft Structures", RTO MP-25, RTO AVT Workshop on "New Metallic Materials for the Structure of Aging Aircraft", Corfu, Greece, April 1999.
- [9] Starke, Jr., E.A. and Staley, J., "Application of Modern Aluminum Alloys to Aircraft", in Journal of Progress in Aerospace Sciences, Vol. 32, No. 2-3, pp. 131-172, 1996.
- [10] Staley, J., "History of Wrought Aluminum Alloy Development", Edited by A. Vasudevan, and R. Doherty in "Aluminum Alloys-Contemporary Research and Applications", Treaties on Materials Science and Technology, Vol. 31, pp. 4-29, 1989.

- [11] Kourline, A. and Merati, A., “Corrosion Characterization and Metallographic Examination of B727 Lap Splice, Sample DT1-B727, Task L – Corrosion Fatigue Structural Demonstration (CFSD) Program”, IAR-NRC Internal Report, LM-SMPL-2002-0127, National Research Council Canada, June 2002.
- [12] Merati, A. and Gasser, L., “Initial Discontinuity State and Results of Fractographic Analysis of Clad and Unclad 0.063” AA2024 Sheets”, IAR-NRC Internal Report LTR-SMPL-2006-0073, National Research Council Canada, June 2006.
- [13] Merati, A., Tsang, J., Chang, C., Khomusi, S., Kourline, A., Kyle, K. and Eastaugh, G., “Final Report – Test Results for the Determination of Fatigue-Related Features of the Initial Discontinuity State (IDS) of 7075-T6 and 7079-T6 Aluminum Alloys”, IAR-NRC Internal Report LTR-SMPL-2003-0002, National Research Council Canada, March 2003.
- [14] Merati, A., Lepine, B., Geusebroek, M. and Rogé, B., “Analysis of Fuselage Fastener Holes with Environmentally Assisted Cracks”, IAR-NRC Internal Report LTR-SMPL-2002-0178, National Research Council Canada, August 2002.
- [15] Merati, A. and Eastaugh, G., “Fatigue Related Discontinuity State of 7000 Series of Aerospace Aluminum Alloys”, in *Journal of Engineering Failure Analysis*, Vol. 14, Issue 4, pp. 673-685, 2007.
- [16] Cina, B. and Gan, R., “Reducing the Susceptibility of Alloys, Particularly Aluminum Alloys, to Stress Corrosion Cracking”, US Patent No. 3856584, 1974.
- [17] Wallace, W., Raizenne, M. and Ankara, A., “Techniques of Improved Surface Integrity of Aerospace Aluminum Alloys”, in *Surface Engineering*, pp. 218-227, 1990.
- [18] Holt, R., Parameswaran, V. and Wallace, W., “RRA Treatment of 7075-T6 Aluminum Components”, in *Canadian Aeronautics and Space Journal*, Vol. 42, pp. 83-87, 1996.
- [19] Raizenne, M.D., Wu, X., Sjoblom, P., Rondeau, R. and Kuhlman, S., “Corrosion Control Using Retrogression and Reaging”, Chapter 25 – this publication, 2010.
- [20] Cree, A.M. and Weidmann, G.W., “Effect of Anodized Coatings on Fatigue Crack Growth Rates in Aluminium Alloy”, in *Journal of Surface Engineering*, Vol. 13, No. 1, pp. 51-55, 1997.
- [21] Hartman, A., “The Effect of Anodizing on the Fatigue Strength of 2024-T3 Alclad Specimens Notched by an Open Hole”, National Aerospace Laboratory NLR, Netherlands, NLR-TR-68080-U, 1968.
- [22] Merati, A., “A Study of Nucleation and Fatigue Behavior of an Aerospace Aluminum Alloy 2024-T3”, in *International Journal of Fatigue*, Vol. 27, pp. 33-44, 2005.
- [23] Merati, A., Tsang, J. and Eastaugh, G., “Final Report – Test Results for the Determination of Fatigue-Related Features of the Initial Discontinuity State (IDS) of 2024-T3 Aluminum Alloy”, IAR-NRC Internal Report, LTR-SMPL-2003-0001, National Research Council Canada, March 2003.
- [24] Hoepfner, D.W., “Model for Prediction of Fatigue Lives Based Upon a Pitting Corrosion Fatigue Process”, in *Fatigue Mechanisms*, ASTM STP 675, 1979.
- [25] Owen, C.R., Bucci, R.J. and Kegarise, R.J., “An Aluminum Quality Breakthrough for Aircraft Structural Reliability”, in *Journal of Aircraft*, Vol. 2, Proceedings ICOSSAR’89, American Society of Civil Engineers, NY, USA, pp. 1467-1474, 1989.

- [26] Magnusen, P.E., Hinkle, A.J., Kaiser, W., Bucci, R.J. and Rolf, R.L., “Durability Assessment Based on Initial Material Quality”, in *Journal of Testing and Evaluation*, Vol. 18, No. 6, pp. 439-445, November 1990.
- [27] Magnusen, P.E., Hinkle, A.J., Rolf, R.L., Bucci, R.J. and Lukasak, D.A., “Methodology for the Assessment of Material Quality Effects on Airframe Fatigue Durability”, in *Fatigue 90*, Vol. II, Proc. Fourth Int. Conf. on Fatigue and Fatigue Thresholds, Materials and Components Engineering Publications Ltd., pp. 2239-2244, 1990.
- [28] Schijve, J. and Jacobs, F.A., “Fatigue Tests on Un-Notched and Notched Specimens of 2024-T3 Alclad and 7178-T6 Extruded Material”, National Aerospace Laboratory NLR, Netherlands, NLR-TR-68017U, 1968.
- [29] Rooke, D.P., Gunn, N.J.F., Ballett, J.T. and Bradshaw, J.T., “Crack Propagation in Fatigue – Some Experiments with DTD 5070 Aluminum Alloy Sheet”, RAE-TR-No. 64025, Royal Aircraft Establishment, United Kingdom, October 1964.
- [30] *Metals Handbook Ninth Edition, Metallography and Microstructures, Volume 9*, American Society for Metals, Metals Park, OH, USA, pp. 355-357, 2004.
- [31] Laz, P.J. and Hillberry, B.M., “Fatigue Life Prediction From Inclusion Initiated Cracks”, in *International Journal of Fatigue*, Vol. 20, No. 4, pp. 263-270, 1997.
- [32] Kung, C.Y. and Fine, M.E., “Fatigue-Crack Initiation and Microcrack Growth in 2024-T4 and 2124-T4 Aluminum Alloys”, in *Metallurgical Transactions A*, Vol. 10A, pp. 603-610, May 1979.
- [33] Starke, Jr., E.A. and Lutjering, G., “Cyclic Plastic Deformation and Microstructure”, in *Fatigue and Microstructure*, ASM, Metals Park, OH, USA, pp. 205-243, 1979.
- [34] Richie, R.O. and Suresh, S., “Mechanics and Physics of the Growth of Small Cracks”, in *Behavior of Short Cracks in Airframe Components*, AGARD Conf. Proc. No. 328, 1-1, Neuilly-sur-Seine, France, 1983.
- [35] Miller, K.J., “The Behavior of Short Fatigue Cracks and Their Initiation, Part II, A General Summary”, in *Fatigue and Fracture of Engineering Materials and Structures*, Vol. 10, No. 2, p. 93, 1987.
- [36] Newman, Jr., J.C. and Edwards, P.R., “Short Crack Growth Behavior in an Aluminum Alloy”, An AGARD Cooperative Test Programme, AGARD Report 732, Neuilly-sur-Seine, France, 1988.
- [37] Hunter, M.S. and Fricke, W.G., “Metallographic Aspects of Fatigue Behavior of Aluminum” in *Proceedings, ASTM*, Vol. 54, pp. 717-736, 1954.
- [38] Edwards, P.R. and Earl, M.G., “A Comparative Study of the Fatigue Performance of Notched Specimens of Clad and Unclad Aluminium Alloy, With and Without a Pre-Stress”, in *RAE Technical Report of Aeronautical Research Council*, Farnborough, United Kingdom, CP. No. 1361, 1977.
- [39] Wanhill, R.J.H., “Effects of Cladding and Anodizing on Flight Simulation Fatigue of 2024-T3 and 7475-T761 Aluminium Alloys”, in *Fatigue Prevention and Design; Proceedings, International Conference at Amsterdam*, Netherlands, pp. 323-332, 21-24 April 1986.
- [40] Rateick, Jr., R.G., Binkowski, T.C. and Boray, B.C., “Effect of Hard Anodize Thickness on the Fatigue of AA6061 and C355 Aluminium”, in *Journal of Materials Science Letters*, Vol. 15, No. 15 pp. 1321-1323, August 1996.

- [41] Abramovici, E., Leblanc, P. and Weaver, B., "The Influence of Etch Pits on the Fatigue Life of Anodized Aluminum Alloys: Fractographic Examination", in Proceedings, Int. Conference and Exhibits on Failure Analysis, Montreal, Quebec, Canada, pp. 21-32, 8-11 July 1991.
- [42] Merati, A. and Gagnon, A., "Microstructural Features of 7050-T7452 Die Forged Aluminum – Case Study of Shear Tie Lug", IAR-NRC, LM-SMPL-2007-0009, National Research Council Canada, 2007.
- [43] Brown, S., Whitehead, J., Williams, T. and Tenney, D., "New Alloy Development for the P-3 Service Life Extension Program", P-3C Service Life Assessment Program (SLAP), Lockheed Martin Corporation, September 2001.
- [44] Bray, G., Bucci, R.J., Kulak, M., Warren, C., Grandt, A., Golden, P. and Sexton, D., "Benefits of Improved Fuselage Skin Sheet Alloy 2524-T3 in Multisite Damage Scenarios", Light Metal Age, pp. 20-28, December 1998.
- [45] Williams, J. and Starke, Jr., E.A., "Progress in Structural Materials for Aerospace Systems", Acta Materialia, Vol. 51, No. 19, pp. 5775-5799, 2003.
- [46] Colvin, E., Petit, J., Westerlund, R. and Magnusen, P., "Damage Tolerant Aluminum Alloy Products Useful for Aircraft Applications Such as Skin", US Patent NO. 5213639, 1993.
- [47] Quist, W.E., "Effect of Composition on the Fracture Properties of Aluminum Alloy 7178", MSc Thesis, University of Washington, USA, 1993.
- [48] Hyatt, M., Caton, R. and Lovell, D., "Advanced Materials Development in Commercial Aircraft", AIAI 89-2127, AIAI/AHS/ASEE Aircraft Design, Systems and Operations Conference, Seattle, WA, USA, August 1989.
- [49] Bechet, D., Warner, T. and Ribes, H., "6056-T78: A Corrosion Resistant Copper-Rich 6XXX Alloy for Aerospace Applications", in Proceedings ICAA6, Tokyo, Japan, the Japan Institute of Light Metals, 1998.
- [50] Giummarra, G., Thomas, B. and Rioja, R., "New Aluminum Lithium Alloys for Aerospace Applications", in Proceedings of the Light Metals Technology Conference, Bombardier Aerospace and Alcoa Trade Study, 2007.
- [51] Merati, A., Chang, C. and Bellinger, N., "Fatigue Results for the Determination of Fatigue-Related Features of the Initial Discontinuity State of AA7178-T6 Aluminum Alloy", Corrosion Effect on Structural Integrity (CESI) Program, IAR-NRC, LTR-SMPL-2003-0180, National Research Council Canada, August 2003.
- [52] Quist, W.E. and Narayanan, G.H., "Aluminium-Lithium Alloys," in Aluminium Alloys – Contemporary Research and Applications, Eds. A.K. Vasudevan, R.D. Doherty, San Diego: Academic Press Inc., Vol. 31, pp. 219-250, 1989.
- [53] Abdel-latif, A.M., Beaudet, J.F.P., Roth, M., Steffen, A.A., Fraser, I. and Yanishevsky, M., "Literature Survey: A Review of the Properties of Aluminium-Lithium (Al-Li) Alloy Systems," in Suitability of Aluminium-Lithium Alloys in the NSA Primary and Secondary Structures, Annex A of National Defence Report 11500 NSA-104 Quality Engineering Test Establishment (QETE), Canada, 1988.
- [54] James, R.S., "Aluminium-Lithium Alloys," in Metals Handbook Tenth Edition, Vol. 2 Properties and Selection: Nonferrous Alloys and Special-Purpose Materials, ASM International, the Materials Information Society, Metals Park, OH, USA, pp. 178-199, 1990.

- [55] Chaturvedi, M.C. and Mukhopadhyay, A.K., “A Critical Review of Aluminium-Lithium Technology and its Impact on Aircraft Structural Design, Manufacture and Maintenance, Part I”, Prepared for Structures and Materials Laboratory, National Aeronautical Establishment, NAE-CR-3, Canada, 1989.
- [56] Merati, A., Awatta, H. and Yanishevsky, M., “Aluminum Lithium Alloys – Long Term Durability Concerns of the CH149 Cormorant”, IAR-NRC, LTR-SMPL-2005-0159, National Research Council Canada, August 2005.
- [57] Smith, A.F., “An Overview of the Use of Aluminium-Lithium Alloys on the EH101”, in Research and Development on Aluminum-Lithium Alloys, Defence Research Establishment Pacific (DREP) Report 93-1, J. Morrison, Canada, pp. 43-72, 1993.
- [58] Rendings, K., “Metallic Structures Used in Aerospace During 25 years and Prospects”, In: Back to the Future, Proceedings of the 15th Int. European Chapter Conference of the Society for the Advance of Material and Process Engineering, Toulouse, France, pp. 49-65, SAMPE, 1994.
- [59] Corral, J., Trillo, E., Li, Y. and Murr, E., “Corrosion of Friction-Stir Welded Aluminum Alloys 2024 and 2195”, in Journal of Materials Science Letters, Vol. 19, No. 23, pp. 2117- 2122, 2000.
- [60] Røyset, J. and Ryum, N., “Scandium in Aluminium Alloys”, International Materials Reviews, Vol. 50, No. 1, pp. 19-44, 2005.

Chapter 25 – CORROSION CONTROL USING RETROGRESSION AND RE-AGING (RRA)

D. Raizenne and X. Wu

Institute for Aerospace Research
National Research Council of Canada
Ottawa, Ontario
CANADA

P. Sjöblom, R. Rondeau and S. Kuhlman

University of Dayton Research Institute
Dayton, Ohio
USA

ABSTRACT

Stress Corrosion Cracking (SCC) of primary structural components manufactured from Al 7075-T6 forgings, extrusions and plate products continues to plague aging aircraft. A two-step heat treatment, Retrogression and Re-Aging (RRA), applied to 7XXX series aluminum alloys in the T6 temper has been shown to greatly enhance the SCC resistance of these materials with minimal trade-off in strength. The RRA technology has reached a level of technical maturity where it can be transitioned to actual aircraft components. There are two ways that the RRA heat treatment process can be carried out. The shop RRA process utilizes conventional heat-treating equipment such as oil bath and furnace. The in-situ RRA process uses state-of-the-art hot bonder heat conduction technology coupled with real-time dissolution kinetics algorithms to heat treat selected areas of large parts. This paper describes the development of both the shop and in-situ RRA processes.

25.1 INTRODUCTION

The aluminum alloy 7075 in the peak aged T6 heat treatment condition has been widely used for aircraft structural applications. Corrosion damage in the form of Stress Corrosion Cracking (SCC), exfoliation and pitting is often the reason why 7075-T6 components are replaced. When improved corrosion resistance is required, alloy Al 7075 is often used in the over-aged temper T73, but in comparison to 7075-T6, there is a strength penalty of 10 to 15%, which precludes the use of the T73 temper when material substitution is considered. An alternative is to perform a retrogression and re-aging heat treatment on parts in the T6 condition. The RRA process has been shown to improve corrosion resistance to levels approaching those of the T73 condition. An RRA heat treatment will however result in a five to seven percent reduction in tensile strength from the T6 temper. An RRA heat treatment involves two steps: a **retrogression** step in the preferred temperature range of 180 to 200°C for 30 to 40 minutes, followed by a **re-aging** step at 120°C for 24 hours. The RRA process was first developed by Cina and Gan [1],[2] in the mid 1970s and was further developed at the National Research Council of Canada (NRC) by Wallace et al. [3]-[9] to the more practical time and temperature combinations described above. The RRA process has been successfully applied to extrusions and aircraft components up to 0.75 inch (20 mm) thick [10]. A comprehensive review of RRA work is provided in Reference [11].

The RRA process is illustrated through a series of metallurgical transformations in Figure 25-1. Starting in the T6 condition, retrogression is applied in the range 180 – 200°C to cause hardness and yield strength to fall rapidly through Stage 1 as Guinier-Preston (G-P) zones dissolve and the solid solution is enriched in the strengthening elements. Stage 2 is a transient period of hardness recovery as the remaining η' grows to a near optimum size distribution, but it begins to fall again as this η' coarsens excessively and begins

transforming to η . In Figure 25-1, it is important to note that the electrical conductivity and corrosion resistance increase steadily with hold time at the retrogression temperature. Therefore, if the goal is to increase corrosion resistance with minimal loss of original strength, then retrogression should be carried out to point D in Figure 25-1. The recovery of strength during re-aging may be due to the reformation of G-P zones or the formation of additional η' directly from the supersaturated solid solution or via the initial formation of G-P zones. The net result of the RRA process is a material with a strength slightly below that of a single step aged T6 material together with resistance to environmentally assisted cracking equivalent to that of an over-aged T73 material. Temperatures at the low end of the range quoted above require longer times to reach the optimum microstructural condition, which make it easier to achieve temperature uniformity in thicker section parts and greater uniformity of properties.

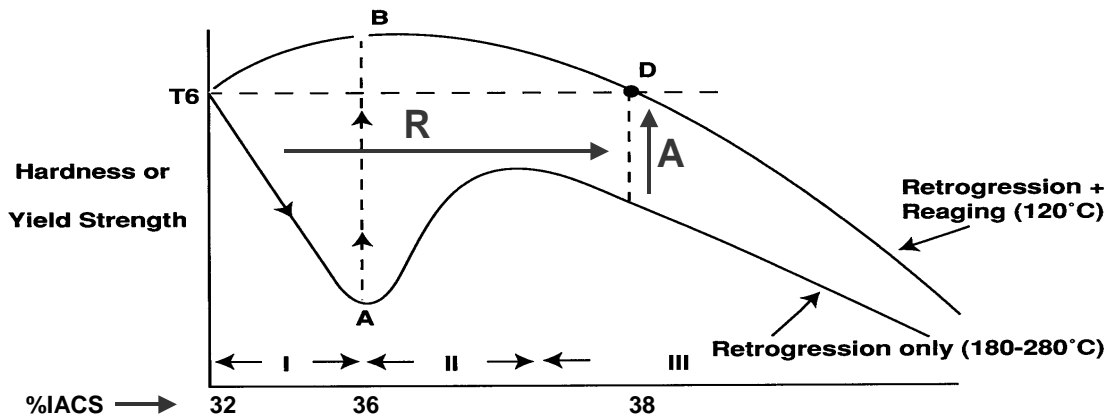


Figure 25-1: Schematic of the Retrogression and Re-Aging Process.

From 1999 to 2005 the USAF (through UDRI), the Canadian Department of National Defence and NRC carried out a joint program to further develop the RRA process so that it could be applied to service components that were particularly susceptible to stress corrosion cracking. Al 7075-T6 extrusions and forgings with histories of SCC damage were identified on the C-130 and C-141 aircraft as ideal candidates for the RRA process [12]-[18].

25.2 KINETICS MODELLING OF THE PRECIPITATION PROCESS IN 7000 SERIES ALUMINUM ALLOYS

The 7000 series aluminum alloys are precipitation hardenable alloys. The peak strength is developed through the T6 temper while the T73 temper produces superior corrosion resistance. These temper specific properties are controlled by the following precipitation sequence [19]:

Solid Solution →	Guinier-Preston (GP) Zones →	η' →	η →	T	(1)
	Metastable	Metastable	Pseudostable	Equilibrium	
Particle Size	35 Å	200x50 Å	500 Å	----	
Solvus	150°C	250°C	370°C	190°C	

G-P zones are essentially coherent spherical solute clusters of Zn, Mg and Cu, while η' , $MgZn_2$ or more correctly $Mg(ZnCuAl)_2$ appears as discrete platelet particles that are semi-coherent with the matrix and η is a non-coherent form of the same phase appearing as rods or plates. Other phases such as Tau- $Mg_{32}(AlZn)_{49}$

may appear at longer aging times while primary S-phase (Al₂CuMg) may appear in some of the newer alloys such as Al 7050 with high Cu and Mg contents.

Let x_1 , x_2 and x_3 denote the relative phase fraction of G-P zones, η' and η precipitates, the above precipitation sequence, Equation (1) (neglecting formation of the T phase), can be reasonably well described by a set of differential equations, based on the first-order reaction kinetics, as:

$$\frac{dx_i}{dt} = k_{if} \left(1 - \sum_{j=i}^3 x_j\right) - k_{id} x_i \quad (i = 1,2,3) \quad (2)$$

where k_{if} and k_{id} are the formation and dissolution rate constants for the i -th precipitate type ($i = 1, 2, 3$) respectively. This set of kinetics equations recognizes the order of thermodynamic stability of each precipitate. For each precipitate, the formation rate is set to null above its solvus temperature.

Equation (2) allows us to evaluate the total phase content in a 7XXX aluminum alloy at different heat treatment conditions, and thus to find optimized phase fractions that can yield a good combination of strength and stress corrosion resistance. The set of fraction numbers (G-P zone dissolution and η' and η formation) can then be used to control the actual retrogression and re-aging heat treatment in ‘real time’ to ensure that the desired properties are obtained in practice. The key to this process is monitoring the part’s temperature during the RRA process.

Depending upon the part’s as-received electrical conductivity, threshold levels of η' and η are used to determine the optimum time for a retrogression treatment [20]. Each retrogression treatment is thus optimized for strength and corrosion resistance. This is illustrated in Figure 25-2 where the heat-up profiles are shown for three parts of similar shape heated in three different air-recirculating ovens. Optimized retrogression treatments (ramp to retrogression temperature, hold and cool to 50°C) ranged from 50.5 to 72.5 minutes. It is very important to understand the role of convective and conductive heat transfer – thus the requirement to monitor the temperature of each part using a device such as a thermocouple.

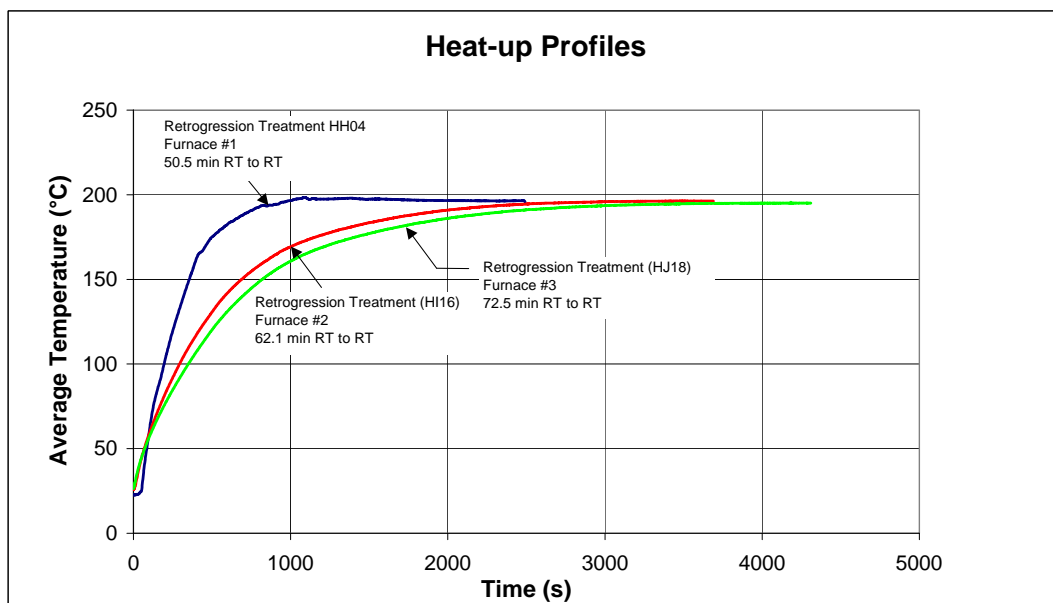


Figure 25-2: Comparison of Heat-Up and Retrogression Times for C-130 Sloping Longeron Sections in Three Different Air-Recirculating Furnaces. By using real-time kinetics modelling, the three sections were optimized for strength and corrosion resistance.

25.3 MATERIAL TEST PROGRAM

The objectives of the RRA material test program were twofold. The first objective was to verify the improvement in corrosion resistance through exfoliation and stress corrosion cracking tests. The second objective was to ensure that the drop in static strength caused by the RRA process did not lead to strength below minimum specified levels:

- Increase the electrical conductivity from 32 – 34 % IACS to a minimum of 38% IACS;
- Improve exfoliation corrosion rating to EXCO A;
- Improve SCC resistance to the T73 temper;
- Meet MIL-HDBK-5H A-Basis allowables for tensile strength, yield strength and ductility;
- Maintain T6511 temper fracture toughness; and
- Maintain T6511 temper fatigue crack growth rates.

For the material test program 2000 tests were carried out. They include corrosion tests, tensile tests, compression tests, bearing tests, fracture and fatigue tests, warpage and distortion tests, electrical conductivity and hardness tests. The effect of the RRA process on protective coatings such as anodizing was also evaluated.

25.4 RRA PROCESS DEVELOPMENT

Two RRA treatment processes were developed. The first, an immersion process, developed at UDRI, used an oil bath to carry out RRA treatments on small parts such as the C-130 Paratrooper Door Longeron (PDL). The second is an ‘*in situ*’ process developed at NRC and UDRI. The in-situ process shown in Figure 25-3 uses a 16 zone hot bonder that is coupled with the ‘real-time’ dissolution kinetics algorithms described above to heat treat ‘selected’ areas of large parts such as the C-130 sloping longeron and the C-141 landing gear main frame.

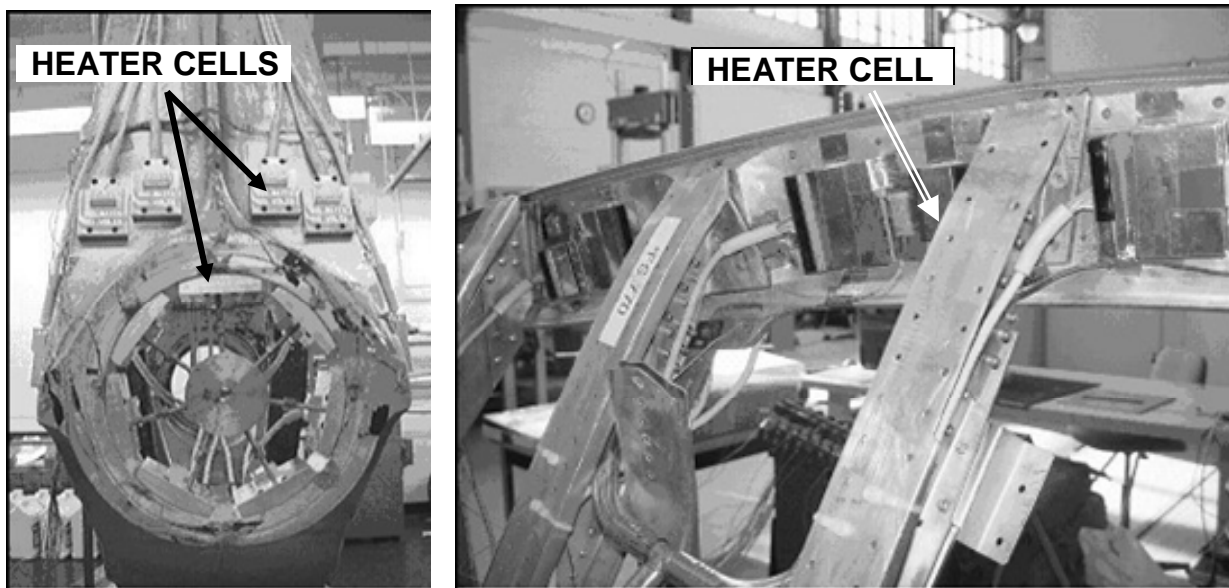


Figure 25-3: *In Situ* RRA Process on C-141 Landing Gear Main Frame and C-130 Sloping Longeron Using Zimac Heater Cells.

Detailed processing specifications for the two RRA processes were developed. For the *in situ* RRA process, the processing specification addresses the following areas:

- Closed form thermal analysis to determine heat transfer requirements.
- Preparation of drawings for heater cell, thermocouple and active cooling placement.
- Electrical conductivity for screening the material's initial condition.
- Retrogression treatment at 195°C using dissolution kinetics modeling for optimized retrogression time.
- Re-aging treatment at 120°C for 24 hours.
- Electrical conductivity and hardness surveys to determine the material's final condition.

25.5 CERTIFICATION REQUIREMENTS

No formal exercise to generate A and B basis allowables for the RRA process was undertaken. The USAF certification approach focused on strength reduction rather than on meeting MIL-HDBK-5H static strength allowables. What this means in practice is that the USAF was satisfied with no greater than a seven percent reduction in 'as-received' static strength. Typically the 'as-received' static strength for extruded product such as the C-130 sloping longeron is at least seven percent greater than the MIL-HDBK-5H A-Basis static strength allowable. Because each component will be screened using electrical conductivity before an RRA treatment is carried out, the process specification ensures that the component's final static strength will meet the MIL-HDBK-5H A-Basis static strength allowable. In addition, the USAF also have access to the Lockheed Martin design data for the C-130 and they have determined that for those candidate RRA parts the seven percent knockdown in static strength is within the static margin-of-safety for those specific components.

25.6 C-130 SLOPING LONGERON

The C-130 sloping longeron (Figure 25-4) is an Al 7075-T6511 extrusion 26 ft (7.9 m) in length with a maximum section thickness of 0.78 in. (19.6 mm). C-130 sloping longerons are replaced on a regular basis during depot level maintenance because of pitting corrosion and stress corrosion cracking damage. Corrosion damage is limited to two sections of the longeron between fuselage stations FS770 and FS835. For the sloping longeron 8 of the 26 feet were in-situ RRA treated starting at FS737 and extending to FS835. The RRA qualification trials were carried out as follows:

- 1) Service exposed longeron material was used for:
 - a) Corrosion, static strength, fatigue and fracture coupon tests;
 - b) Dissolution kinetics model optimization; and
 - c) Heat transfer hardware and software development.
- 2) New extruded Al-7075-T6511 material was then used to ensure that the service exposed longeron material did not influence the coupon test results and the RRA process parameters. A processing specification was written for the in-situ RRA process as applied to the sloping longeron.
- 3) Two new sloping longerons were then purchased. The first sloping longeron was in-situ RRA treated following the processing specification. The longeron was then sectioned for tensile strength verification. The second sloping longeron was then in-situ RRA treated.

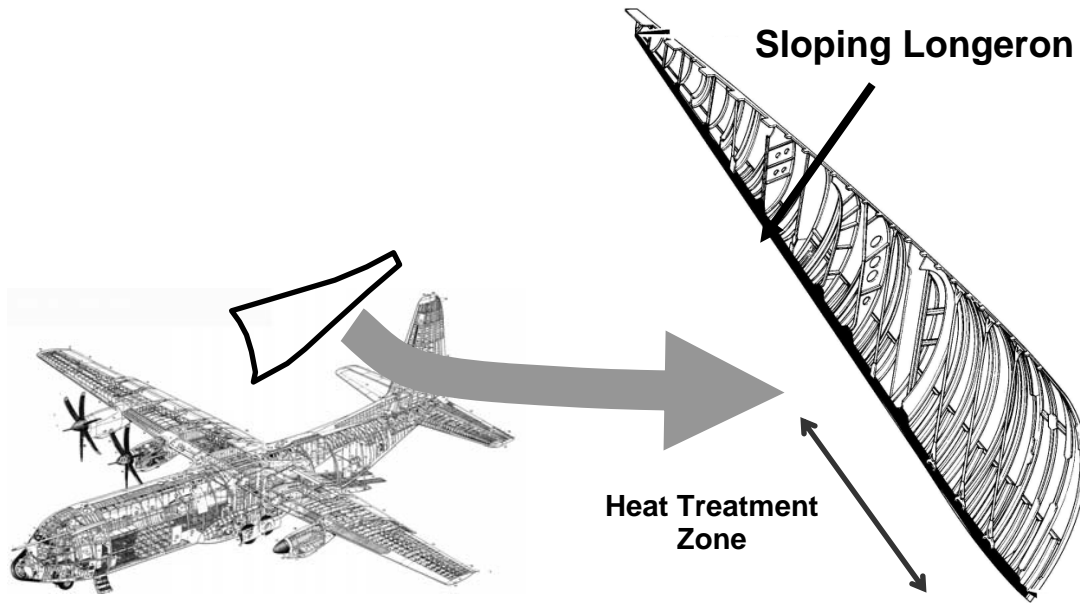
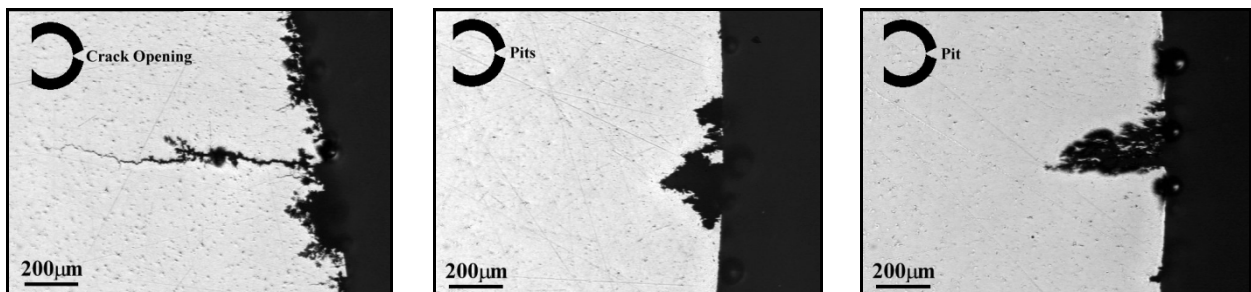


Figure 25-4: C-130 Showing Location of 26 ft Long Sloping Longeron and Heat Treatment Zone.

25.6.1 Sloping Longeron Corrosion Results

Exfoliation corrosion tests were conducted in accordance with ASTM Standard G 34. The RRA treated specimens improved the exfoliation corrosion resistance of as-received Al 7075-T6511 sloping longeron specimens from an EXCO rating of ED (severe separation of metal into layers) to a rating of P (discrete pits).

Stress corrosion cracking tests were conducted in accordance with ASTM Standards G 38 and G 44. The C-ring specimen was chosen because of the limited material thickness available in the S-T orientation. The specimens were pre-stressed to 45 and 54 ksi and placed in an alternate immersion tank where they were exposed to a 10 minute immersion in a 3.5% NaCl solution followed by 50 minutes of drying time. According to Federal Specification Sheet QQ-A-200/11E [21], the test duration is to be 20 days and specimens lasting until the end of 20 day period are considered to have SCC resistance equivalent to the T73 temper. The RRA treated specimens successfully completed the 20 day exposure period without developing evidence of intergranular cracks. Figure 25-5 shows polished x-sections of typical T6511, T73511 and T6RRA C-ring specimens.



T6 Specimen SK29
(16 days to failure)

T73 Specimen SL03
(20+ days)

T6RRA Specimen SK01
(20+ days)

Figure 25-5: C-Ring SCC Comparison with 54 ksi (372 MPa) Pre-Stress Level.

A more extensive series of stress corrosion tests were conducted with four inch thick new Al 7075-T6511 and Al7075-T73511 extrusions. For this work ASTM Standard G-139 was used. Figure 25-6 is a comparison of residual strength averages in Box-Cox metric shows comparable performance between the T73 temper and the T6RRA processed material.

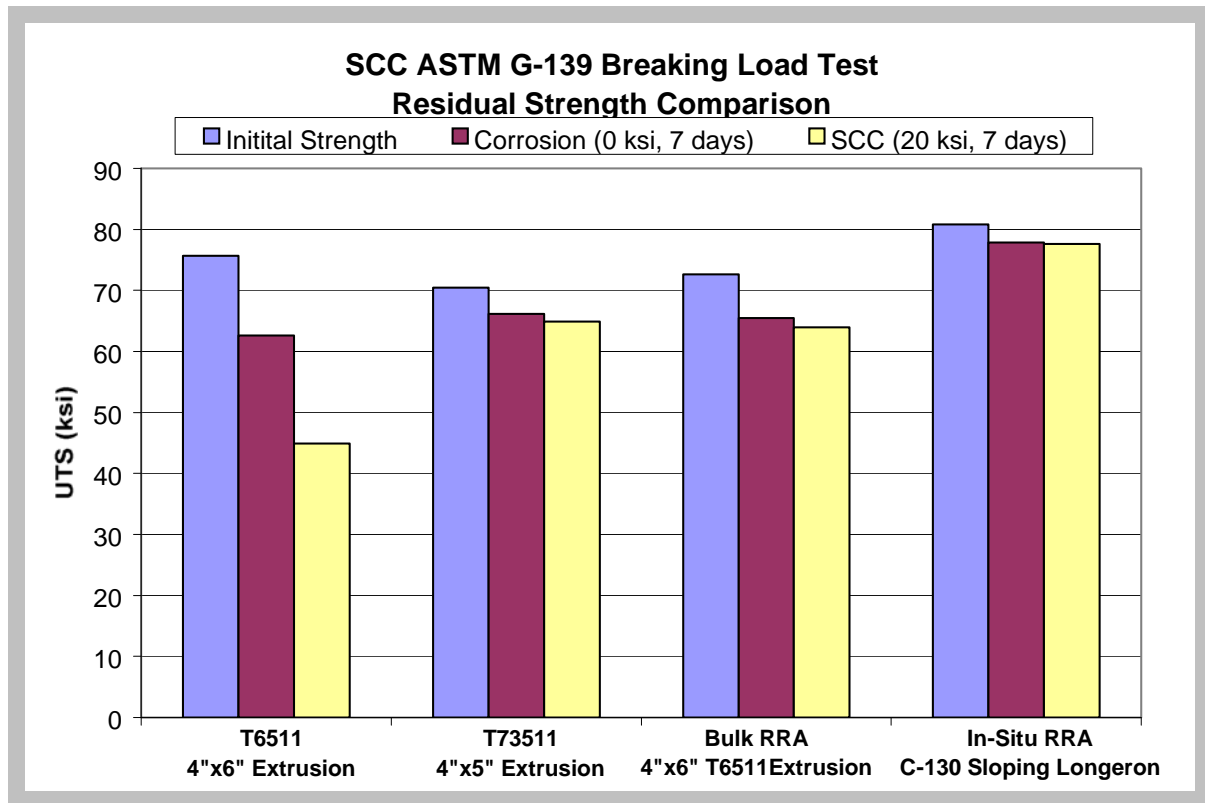


Figure 25-6: Breaking Load SCC Test Results Using Box-Cox Metric (ASTM G 139).

25.6.2 Sloping Longeron Tensile Test Results

Tensile testing was conducted in accordance with ASTM Standard B 557. Tensile specimens in the L direction were cut from as-received and RRA treated material. The average results for 84 RRA treated specimens (Table 25-1) show that the mean strength values exceeded the MIL-HDBK-5H A-Basis tensile strength allowable (the target value for minimum strength reduction). If a normal distribution for the tensile data is assumed, the mean value minus three standard deviations for the optimized RRA treatments also exceeds the MIL-HDBK-5H A-Basis allowable.

Table 25-1: C-130 Sloping Longeron Tensile Strength Results.

	Yield (ksi)	Ultimate (ksi)	Elongation (%)
As-received Al 7075-T6511	83.6 (576 MPa)	90.7 (625 MPa)	10.6
RRA Treated Material	77 (530 MPa)	84.5 (583 MPa)	9.6
MIL-HDBK-5H A-Basis	72 (496 MPa)	81 (558 MPa)	7

25.6.3 Sloping Longerons Electrical Conductivity Results

For Al 7075-T6, there is a correlation between electrical conductivity and corrosion resistance. If the electrical conductivity of RRA treated Al 7075-T6 material is increased beyond 38% IACS, the exfoliation corrosion rating will improve to EXCO A or greater and the SCC resistance will improve to that of the T73 temper. There is not an established correlation between electrical conductivity and static strength. However, for the C-130 material test program, electrical conductivity measurements were taken on each tensile specimen. The results for the L-direction tensile data are shown in Figure 25-7. The results indicate that electrical conductivity values between 38 and 40% IACS will consistently produce tensile strength results above the MIL-HDBK-5H A-Basis allowable. This finding is important because electrical conductivity measurements are non-intrusive, accurate and repeatable. For quality control purposes, electrical conductivity can be used in a highly reliable fashion to evaluate the as-received and the RRA condition (corrosion resistance and static strength) of a sloping longeron.

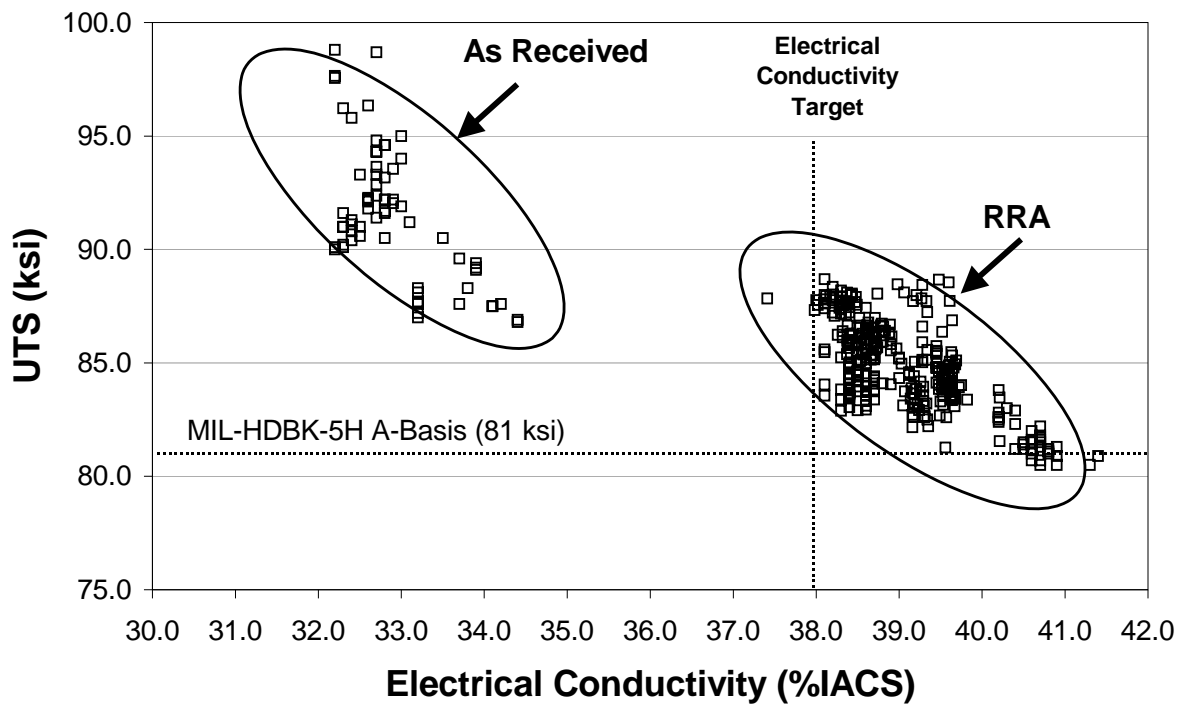


Figure 25-7: UTS vs. Conductivity Data for Sloping Longerons Material.

25.7 C-130 PARATROOPER DOOR LONGERON

The forged Al 7075-T6 Paratrooper Door Longerons (PDL) of the C-130 have been affected by pitting and exfoliation corrosion damage. The lower longitudinal attachment of the fitting on the outboard side is an area on the PDL that is particularly susceptible to exfoliation and pitting corrosion. The current off-the-aircraft repair method permits grinding away the corrosion to specific limits based on where the corrosion is found on the longeron. Once the grind-out limits have been reached, replacement of the longeron is mandated. For the PDL the RRA process was developed as a shop process using an oil bath. This is an easier heat treatment process to carry out than the in-situ RRA process developed for the C-130 sloping longeron and the C-141 landing gear mainframe. The retrogression phase is carried out for a specific period of time with no monitoring of part temperature or use of ‘real-time’ dissolution kinetics.

25.7.1 PDL Test Results

The results for stress corrosion cracking and static strength tests are presented in Table 25-2 and Table 25-3. The alternate immersion stress corrosion cracking testing was carried out using C-ring specimens in accordance with ASTM Standard G 38. All C-ring specimens were pre-stressed to 45 ksi (310 MPa). Tensile strength testing was carried out in accordance with ASTM Standard E 8.

Table 25-2: C-130 PDL Tensile Strength Results.

	Ultimate Strength (ksi)
Service Exposed Al 7075-T6	85 (586 MPa)
Service Exposed RRA	81 (558 MPa)
New Al 7075-T6	94.5 (650 MPa)
New Material RRA	87 to 93 (600 to 640 MPa)

Table 25-3: C-130 PDL Stress Corrosion Cracking Results (ASTM G 38).

	Electrical Conductivity (%IACS)	Duration (days)
Service Exposed Al 7075-T6	32.9	5 to 9
New Material RRA	38.5	20+

The corrosion and tensile results for the forged Al 7075 PDL material are similar to those presented for the C-130 sloping longeron extrusions. The RRA process can therefore be applied to either extruded or forged Al 7075 T6 aircraft components.

25.8 CONCLUSIONS

- Retrogression and re-aging of Al 7075 in the T6 temper significantly improves the material’s resistance to corrosion without compromising static strength properties.
- RRA tensile data in the L-direction indicated that tensile strength, yield strength and percent elongation were consistent with the A-Basis allowables from MIL-HDBK-5H.
- The exfoliation test results indicate that the RRA process raises the resistance to exfoliation corrosion from AD (severe exfoliation) to EA (superficial exfoliation) / P (pitting).
- Stress corrosion tests showed no evidence of intergranular cracking after 20 days of alternate immersion exposure. This corrosion resistance is equivalent to the T73 temper.
- The retrogression phase has been optimized using computer controlled ‘real-time’ dissolution kinetics to ensure that for an RRA treated component:
 - 1) The electrical conductivity is raised to at least 38% IACS; and
 - 2) The static strength properties remain above MIL-HDBK-5H A-Basis allowables.

- The RRA process can be carried out using two heat transfer mediums. The first is an oil bath, ideally suited for small components such as the C-130 paratrooper door longeron. The second is an in-situ conduction process that is applied to selected areas of larger components such as the C-130 sloping longeron and the C-141 landing gear mainframe.
- For C-130 Al 7075-T6511 extrusions no greater than 0.75 inches thick (20 mm), a consistent trend between electrical conductivity and static strength was established. This correlation will be useful as a tool to assess the as-received static strength and the post RRA static strength.

25.9 ACKNOWLEDGEMENTS

This work was carried out with funding from the United States Air Force, the Canadian Department of National Defence and the National Research Council of Canada.

25.10 REFERENCES

- [1] Cina, B. and Gan, R., "Reducing the Susceptibility of Alloys, Particularly Aluminum Alloys, to Stress Corrosion Cracking", United States Patent 3856584, 24 December 1974.
- [2] Cina, B. and Zeidess, F., "Advances in the Heat Treatment of 7000 Type Aluminum Alloys by Retrogression and Re-Aging", Materials Science Forum, Vol. 102-104, 1992.
- [3] Wallace, W., Beddoes, J.C. and de Malherbe, M.C., "A New Approach to the Problem of Stress Corrosion Cracking in 7075-T6 Aluminum", Canadian Aeronautics and Space Journal, Vol. 27, No. 3, 1981.
- [4] Rajan, K., Wallace, W. and Beddoes, J.C., "Microstructural Study of a High Strength Stress Corrosion Resistant 7075 Aluminum Alloy", Journal of Material Science and Technology, Vol. 17, 1982.
- [5] Wallace, W. and Beddoes, J.C., "Microstructural Study of a High Strength Stress Corrosion Resistant 7075 Aluminum Alloy," Journal of Material Science, Vol. 17, 1982.
- [6] Danh, N.C., Rajan, K. and Wallace, W., "A TEM Study of Microstructural Changes During Retrogression and Re-Aging in 7075 Aluminum", Metallurgical Transactions, Vol. 14A, 1983.
- [7] Islam, M.U. and Wallace, W., "Retrogression and Re-Aging Response of 7475 Aluminum Alloy", Metals Technology, Vol. 10, 1983.
- [8] Holt, R.T., Parameswaran, V.R. and Wallace, W., "RRA Treatment of 7075-T6 Aluminum Components", Canadian Aeronautics and Space Journal, Vol. 42, No. 2, 1996.
- [9] Wallace, W., Holt, R.T., Butler, C. and DuQuesnay, D.L., "Retrogression and Re-Aging Revisited", Key Engineering Materials, Vols. 145-149, Part 2, 1998.
- [10] Holt, R.T., Raizenne, M.D. and Wallace, W., "RRA Heat Treatment of Large Al 7075-T6 Components", NATO/RTA AVT, Corfu, Greece, 1999.
- [11] Wu, X.J., Raizenne, D.M., Poon, C., Chen, W. and Wallace, W., "Thirty Years of Retrogression and Re-Aging (RRA)", Presented at 23rd Congress of International Council of Aeronautical Science, Toronto, Ontario, Canada, 2002.

- [12] Raizenne, D.M., Wu, X.J., Whitehouse, M. and Poon, C., “In-Situ Retrogression and Re-Aging of a C-130 Al 7075-T6511 Sloping Longerons”, USAF Aircraft Structural Integrity Program Conference, San Antonio, TX, USA, December 2000.
- [13] Raizenne, D.M., Sjöblom, P., Snide, J., Peeler, D.T. and Hunter, C., “In-Situ Retrogression and Re-Aging of C-130 Al 7075 T6511 Sloping Longerons”, Presented at AEROMAT 2001 Conference, Long Beach, CA, USA, June 2001.
- [14] Raizenne, D.M., Wu, X. and Poon, C., “In-Situ Retrogression and Re-Aging of Al 7075-T6 Parts”, 5th FAA/DoD/NASA Conference on Aging Aircraft, Orlando, FL, USA, September 2001.
- [15] Raizenne, D., Sjöblom, P., Rondeau, R. and Peeler, D.T., “Transitioning of the Retrogression and Re-Aging (RRA) Process to USAF Hardware”, USAF Aircraft Structural Integrity Program Conference, Williamsburg, VA, USA, December 2001.
- [16] Raizenne, D.M., Sjöblom, P., Rondeau, R., Snide, J. and Peeler, D.T., “Retrogression and Re-Aging of New and Old Aircraft Parts”, 6th FAA/DoD/NASA Conference on Aging Aircraft, San Francisco, CA, USA, September 2002.
- [17] Rondeau, R., “Retrogression and Re-Aging (RRA) of 7075-T6 Corrosion Prone Parts”, USAF Report ASC-TR-2005-0001, January 2005.
- [18] Peeler, D.T., Raizenne, D., Sjöblom, P., Rondeau, R., Kuhlman, S. and Snide, J., “Retrogression and Re-Aging (RRA) of Aluminum 7075-T6 Aircraft Components”, Tri-Service Corrosion Conference, Las Vegas, NV, USA, November 2003.
- [19] Wu, X.J., Kou, A.K. and Zhao, L., “A New Approach to Heat Damage Evaluation for 7XXX Aluminum Alloy”, Canadian Aeronautics and Space Journal, Vol. 42, 1996.
- [20] Hunt, W.H., Stiffler, R.C. and Green, J., “The Use of Electrical Conductivity for Heat Treatable Aluminum Alloys”, 18th ASM Heat Treating Society Conference, Rosemont, IL, USA, 1998.
- [21] Federal Specification Sheet QQ-A-200/11E, November 1993.



Chapter 26 – ENVIRONMENTAL SEVERITY ASSESSMENT AND AIRCRAFT WASH OPTIMIZATION

Pierre R. Roberge

Royal Military College, Department of National Defence
Kingston, Ontario
CANADA

26.1 INTRODUCTION

Removing salt deposits on aircraft is an important component of a successful corrosion maintenance program and this is particularly true for equipment operated in marine environments. Both rinsing and washing aim at preventing corrosion damage by reducing the surface concentration of corrosive agents on aircraft exterior surfaces. While rinsing is a relatively simple operation typically carried out by taxiing through a “bird bath” upon returning from a mission, as illustrated in Figure 26-1, the washing process is much more complex and often carried out in special hangars.



Figure 26-1: A C-130J Hercules is Cleaned Up in the New “Bird-Bath” System at Keesler Air Force Base, Biloxi, Mississippi. Aircraft from the Air Force Reserve fly many hours over the Gulf of Mexico. Salt and moisture could lead to corrosion if aircraft are not kept clean. (U.S. Air Force photo / Tech Sgt. Jame Pritchett).

The question of how frequently to wash aircraft is one of the many management decisions on minimizing the total cost of asset maintenance. Washing an aircraft directly incurs costs while not washing an aircraft indirectly incurs costs from future corrosion damage. Reducing the period between washes may reduce the cost of corrosion damage but increases the cost of washing.

26.2 ENVIRONMENTAL SEVERITY ASSESSMENT

26.2.1 USAF Environmental Severity Index (ESI)

An environmental assessment scheme based on atmospheric parameters has been developed for the United States Air Force (USAF) by Summitt and Fink as early as 1980 [1]. The scheme, code named PACER LIME, was constructed on the parametrically fitted corrosion behaviour of aircraft materials such as uncoated aluminum, steel, titanium and magnesium alloys. The ESI rankings were based on four parameters: proximity to the sea, total particulate level, sulphur dioxide concentration and amount of rainfall. An important advantage of this approach was that required data were typically available at most weather stations. The section of the Corrosion Damage Algorithm (CDA) presented in Figure 26-2, for example, considers distance to salt water, leading either to the very severe AA rating or lesser ratings based on a consideration of moisture factors. An algorithm for aircraft washing based on similar corrosivity considerations is presented in Figure 26-3.

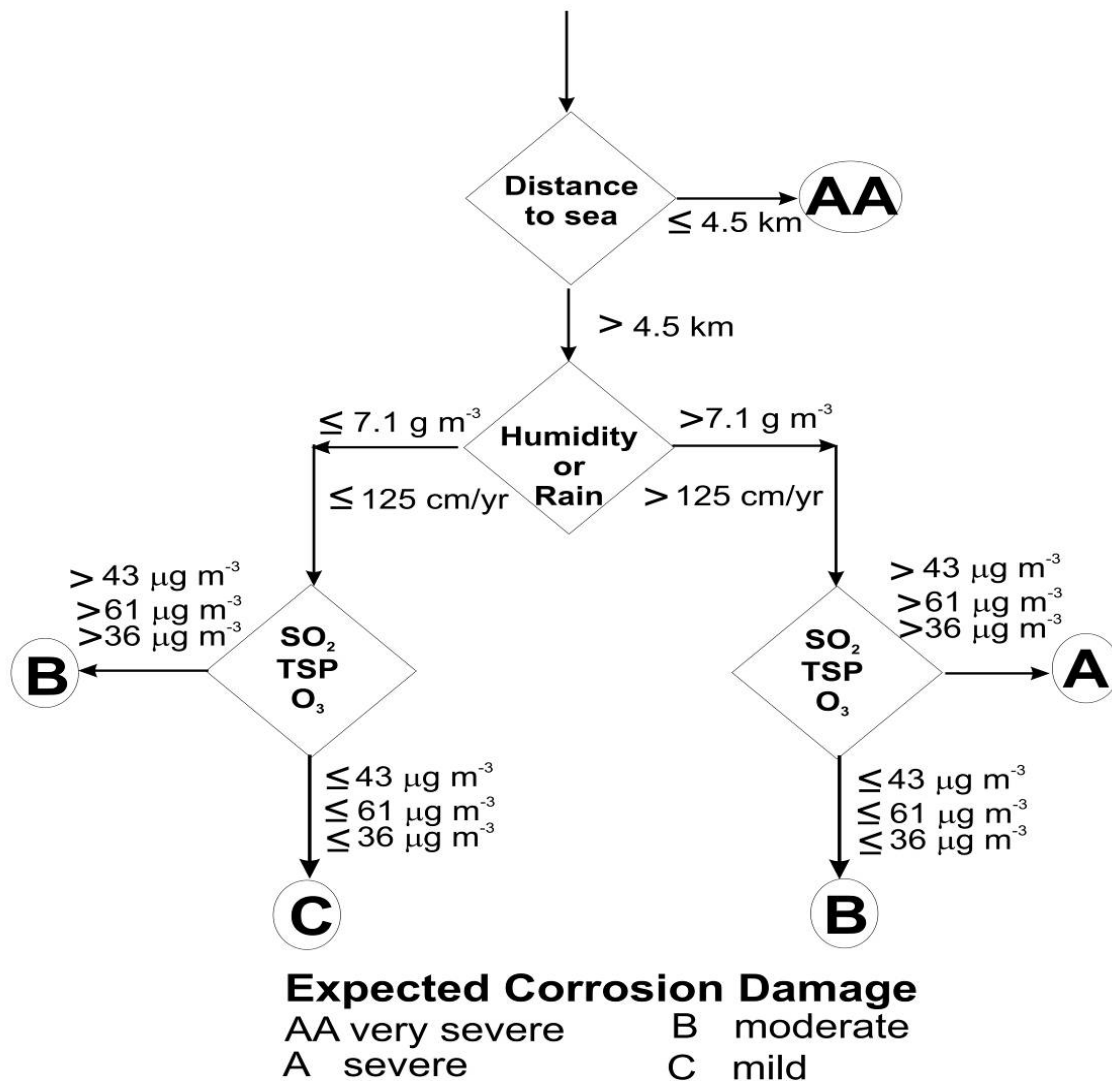


Figure 26-2: Section of the Corrosion Damage Algorithm that Considers Distance to Salt Water, Leading Either to the Very Severe AA Rating or a Consideration of Moisture.

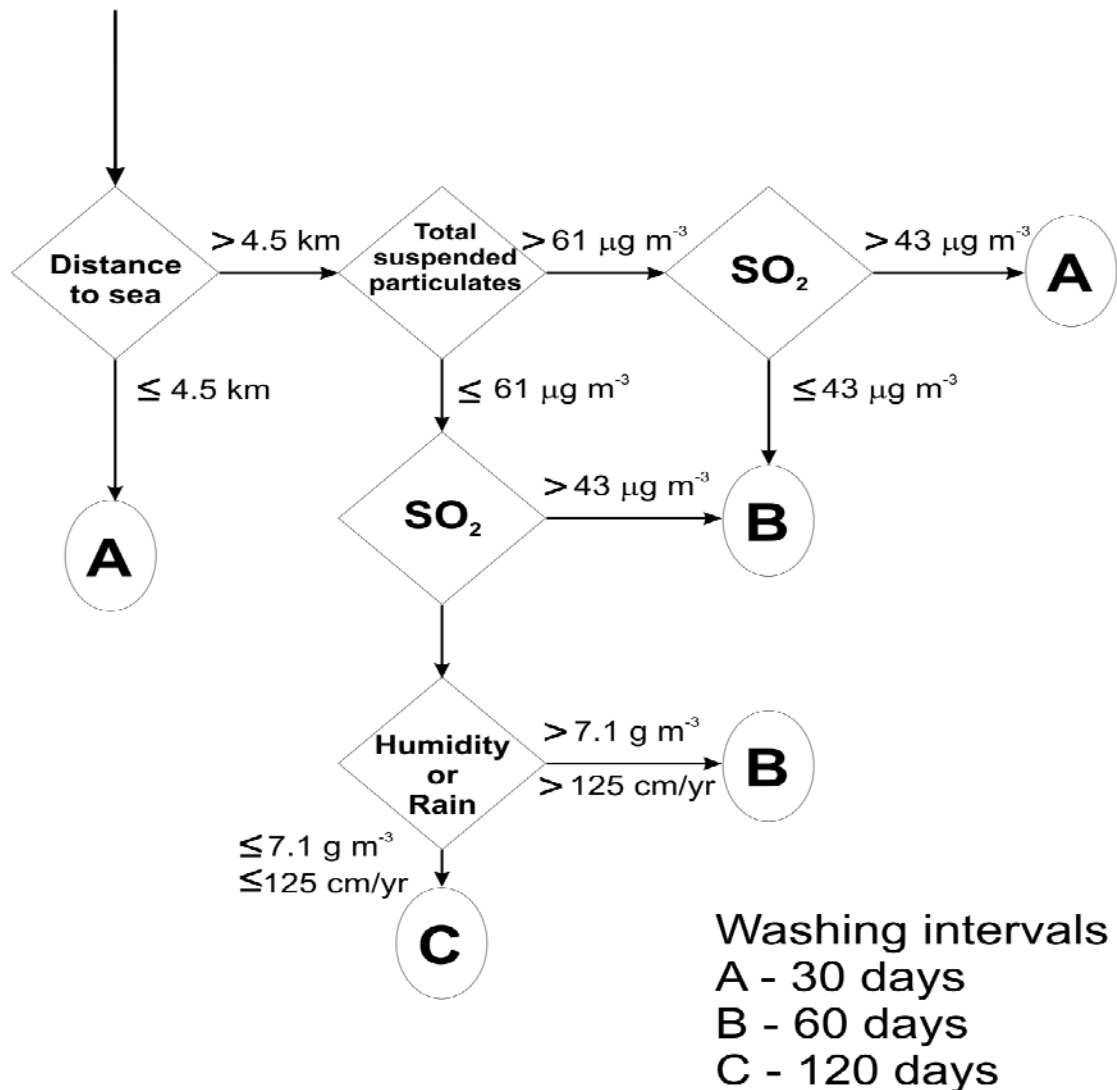


Figure 26-3: Section of the Corrosion Damage Algorithm for Planning a Washing Schedule.

The environmental corrosivity, predicted from the CDA algorithm, of six marine air bases has been compared to the actual corrosion maintenance effort expended at each base. Considering the simplicity of the algorithms and simplifying assumptions in obtaining relevant environmental and maintenance data the correlation obtained was considered to be reasonable. However, subsequent attempts to enhance the PACER LIME algorithm by using the results obtained from broad based corrosion testing programs failed to provide enough differentiation between moderately corrosive environments [2].

In order to remedy the deficiencies in the CDA scheme, Battelle was tasked to monitor the atmospheric corrosivity of Air Force and other sites worldwide [3]. The database describing the relative corrosive severity levels of different locations and actual corrosion rates of a variety of metals has now grown to more than 100 sites worldwide. The following metals were included in that study: three aluminum alloys (A92024, A96061, and A97075), copper, silver and steel.

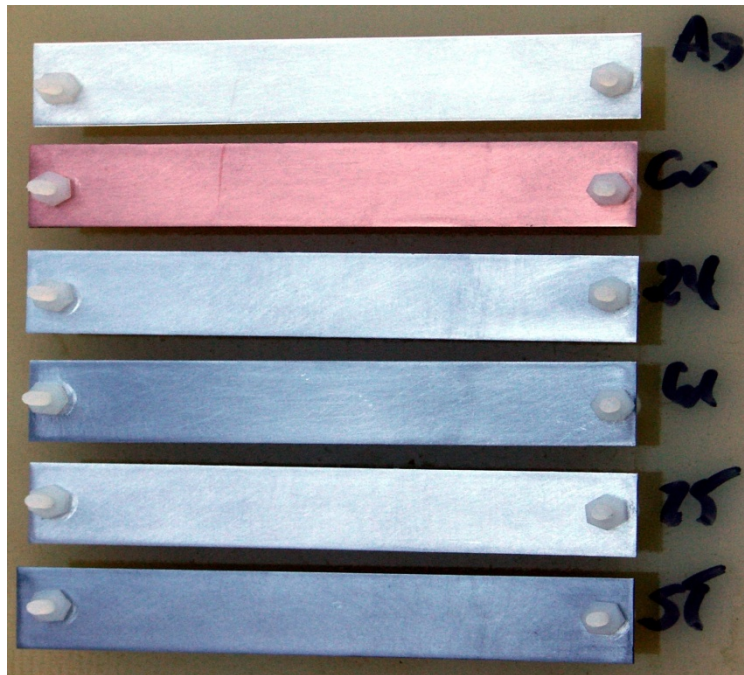
Data have been collected for metals directly exposed to the outdoor environment in a standard sample mounting configuration and test package. A typical plastic test rack with its metallic coupons is shown in

Figure 26-4 besides a CLIMAT coupon¹ exposed at the Kennedy Space Center (KSC) beach corrosion test site, a test site renowned for having the highest corrosivity in the continental United States [6]. Figure 26-5(a) shows a close-up view of the coupons before exposure. Once exposed to the environment for a given period of time the corroded metal strips (Figure 26-5(b)) are sent back to the laboratory for mass loss measurements following standard methods [7] and further analysis.

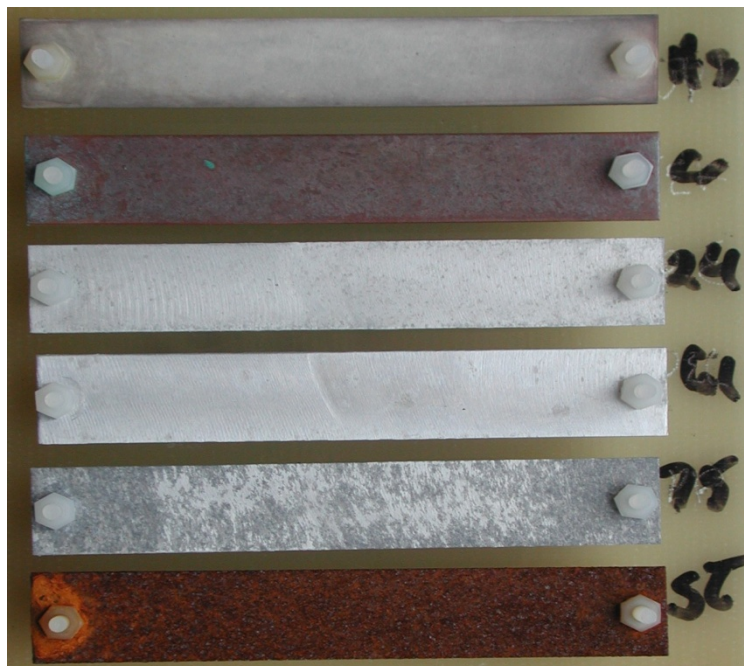


Figure 26-4: Metal Coupons in a Plastic Test Rack Exposed at the Kennedy Space Center Beach Corrosion Test Site Besides a CLIMAT Coupon (Courtesy of Battelle).

¹ The use of bimetallic specimens in which a helical A91100 aluminum wire is wrapped around a coarsely threaded bolt is described as the Classify Industrial and Marine Atmospheres (CLIMAT) coupon [4],[5].



(a)



(b)

Figure 26-5: Metal Coupons Before Exposure to the Environment (a) and After a Three Month Exposure in a Rural Environment (b) (Courtesy of Battelle).

These efforts established a correlation between the corrosivity of various Air Force Base environments and the costs associated with the maintenance of various aircraft. Figure 26-6 summarizes three years of corrosion data compared to maintenance records taken directly from the Air Force database (REMIS). It has now been shown that there is a relatively good correlation between base level ESI values and base

level corrosion related maintenance [3]. Not only is the correlation surprisingly good, but it also appears to be intuitively correct to show a definite effect of size of the aircraft and surface area.

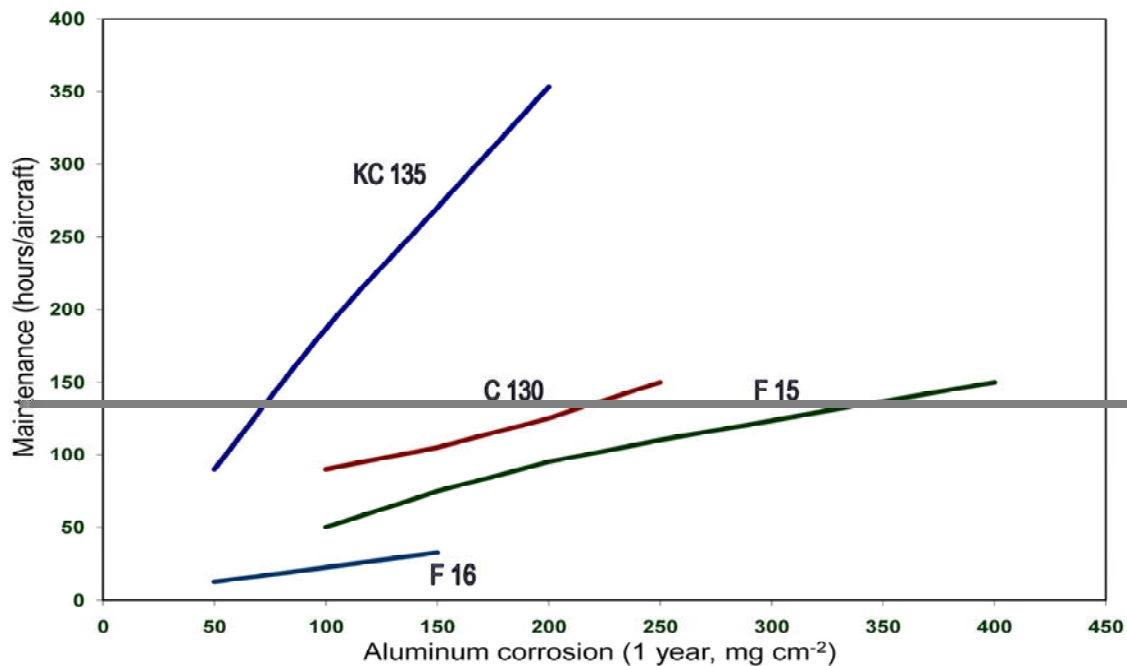


Figure 26-6: Maintenance Costs for Various Aircraft as a Function of the Corrosivity of Air Force Base Environments Towards the Corrosion of Aluminum (KC 135 is the re-fueling support aircraft; CC130 is the Hercules airlift mission aircraft; F15 and F16 are fighter aircraft).

26.2.2 International Organization for Standardization (ISO) Classification Scheme

A scheme widely accepted by architects and designers for the classification of outdoor environments has been developed by a Working Group (WG 4) of the International Organization for Standardization (ISO) corrosion Technical Committee (TC 156) [8].

In the program nicknamed ISO CORRAG, specially prepared coupons of steel, copper, zinc, and aluminum were exposed for 1, 2, 4, and 8 years at 51 sites located in 14 nations in order to generate the necessary data for predicting atmospheric corrosivity from commonly available weather data [9]. Triplicate specimens were used for each exposure. The program was initiated in 1986 and terminated in 1998. After a planned exposure, each specimen was sent to the laboratory that had done the initial weighing for cleaning and evaluation. Based on these data, a simple classification scheme of five corrosivity classes was established for each metal (Table 26-1). The environmental and weather data gathered in this program were based on SO₂, and Cl⁻ deposition rates combined with Time Of Wetness (TOW)² measurements at each site. These five corrosivity categories can be roughly translated into five outdoor situations in the following decreasing order of corrosivity, i.e., industrial, tropical marine, temperate marine, urban, and rural.

² Time spent above 80% relative humidity (RH). TOW is typically expressed in number of hours above 80% RH in one month or in one year.

Table 26-1: ISO 9223 Corrosion Rates After One Year of Exposure Predicted for Different Corrosivity Classes.

Corrosion Category	Steel (g/m ² year)	Copper (g/m ² year)	Aluminum (g/m ² year)	Zinc (g/m ² year)
C1	= 10	= 0.9	Negligible	= 0.7
C2	11 – 200	0.9 – 5	= 0.6	0.7 – 5
C3	201 – 400	5 – 12	0.6 – 2	5 – 15
C4	401 – 650	12 – 25	2 – 5	15 – 30
C5	651 – 1500	25 – 50	5 – 10	30 – 60

26.2.3 Seasonal and Local Variations

While the data gathered for the development of these two classification schemes are from relatively well characterized locations, the actual information on topographical or other local variables is not considered in the general assessment. Similarly no effort is spent in these general schemes to include seasonal variations that may also vary greatly at each location.

In a study focused on the shielding effects due to buildings in a marine environment, the directional impact of marine aerosols was revealed by comparing the level of patina on copper rods of CLIMAT coupons exposed for three winter months at a facility on the Pacific coast [10],[11]. What became evident in that study was that the pattern of the bluish-green patina attributed to the corrosion product $\text{CuCl}_2 \cdot 2\text{H}_2\text{O}$ was not uniformly distributed around the circumference of each copper rod.

A template with the sixteen points of the compass was placed on the outside of each boldly exposed coupon in order to visually quantify the intensity of the bluish-green color. The relative degree of corrosion for each compass point was assessed by assigning a number between zero and ten with zero corresponding to zero bluish-green patina and ten corresponding to 100% coverage of the coloured corrosion product. The average corrosion index for each of the sixteen points of the compass for the copper rods is shown in Figure 26-7. One attempt to correlate the directional corrosivity observed on the copper rods with weather data was to plot the fraction of time that winds came from the sixteen points of the compass during the three-month exposure period. The dominant direction was the north to north-east. However, the pattern of corrosion product did not correspond to the most frequent wind direction but did correspond to the direction with the highest wind speeds, which were in the west to south quadrant at this particular site (Figure 26-7).

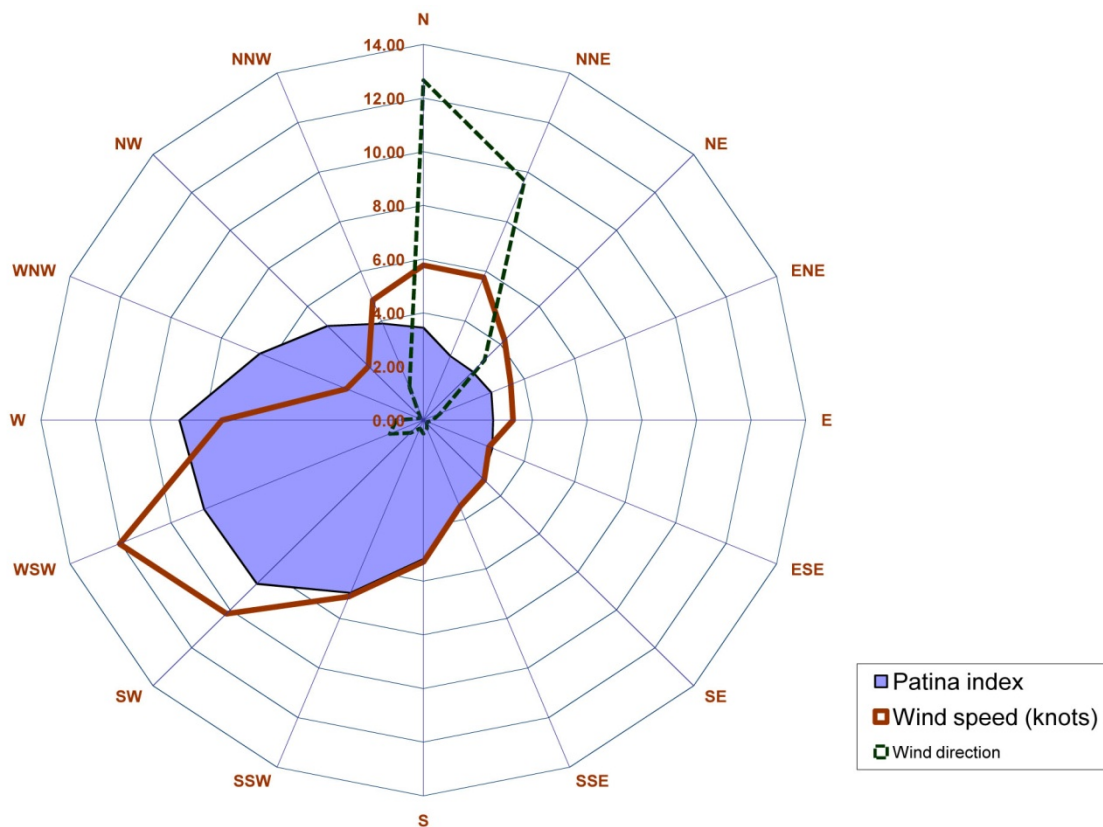


Figure 26-7: Average Corrosion Index for the Copper Rods Exposed on the Rooftop and the Average Wind Speed Recorded at the Local Weather Station as a Function of the Sixteen Points of the Compass.

This is consistent with observations made by others that a minimum wind speed or threshold of approximately 11 km h^{-1} is required for the entrainment of marine aerosols over a salt-water body [12].

26.3 WASH COSTS OPTIMIZATION

The conclusions of an experimental study on the effects of wash intervals on corrosion indicate that the relative benefit of washing increases with increasing severity of the environment [13]. One recommendation of the study was also that while wash intervals in severe environments should not be relaxed and maintained at a minimum of 30 days, wash cycles in mild environments on the other hand could be relaxed beyond 120 days. Following this study, each air base was assigned an Environmental Severity Index (ESI), i.e., either mild, moderate or severe. The wash period and certain maintenance work was then scheduled according to the ESI. Some wash periods currently assigned to a sample of air bases by the USAF are shown in Table 26-2 [14].

Table 26-2: Wash Periods Assigned to Sample of Bases According to Environmental Severity.

Air Base Name and Location	Wash Period by Severity		
	Severe (One Month)	Moderate (Three Months)	Mild (Four Months)
Aj Taif, SA			X
Allen C. Thompson Fld., Jackson, MS			X
Altus AFB, OK			X
As Sulayyil, SA			X
Anderson AFB, GU	X		
Anchorage IAP, AK			X
Bagram AB, Afghanistan		X	
Bahrain	X		
Bangor IAP, ME			X
Barksdale AFB, Shreveport, LA			X

Determining an optimal aircraft wash interval requires combining a model for damage due to atmospheric corrosion and economic factors. Cumulative metal loss under atmospheric conditions is generally found to follow a power law or bi-logarithmic relationship with exposure time [15],[17]:

$$C = Kt^n \tag{1}$$

where C is the cumulative metal loss, t is the exposure time, K is a constant specific to a location and n is an exponent. The fitted value of the exponent is a rough indicator of the corrosion mechanism. An exponent of 0.5 is consistent with the corrosion rate being dependent on diffusion through a protective film that grows as corrosion proceeds. An exponent of unity is consistent with a corrosion rate that is independent of corrosion products accumulated on a surface. Typically, the exponent is between 0.5 and unity [15]. The rate constant, K, depends on the atmospheric corrosivity [16],[17]. If one assumes that corrosion-related maintenance required on aircraft follows the law of equation (1), a cumulative metal loss may now be expressed as equation (2):

$$M = kt^n \tag{2}$$

where M is the corrosion-related maintenance required and k is a constant, analogous to K in equation (1). M is expected to increase with time until periodic maintenance brings accumulated damage down to a lower level. As washing was shown to decrease the cumulative corrosion damage of coupons [13], aircraft washing is expected to decrease required maintenance. Figure 26-8 illustrates these concepts qualitatively.

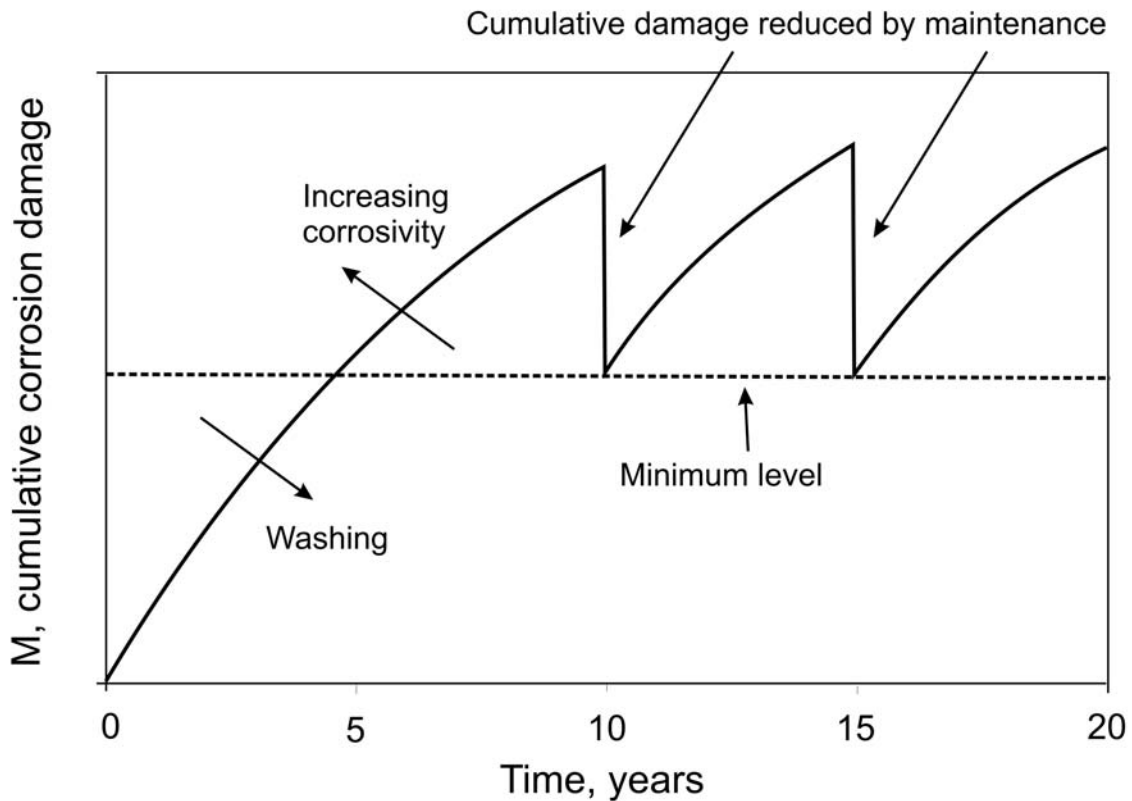


Figure 26-8: Schematic of Cumulative Corrosion Damage on Aircraft as a Function of Time.

The data available for M , and thus for estimating k and n , is limited to periodic maintenance records. The maintenance records of three phases for a fleet of marine patrol aircraft are listed in Table 26-3. Each phase corresponds to a Depot Level Inspection and Repair (DLIR). There was no corrosion-related maintenance at phase 1 DLIR for any aircraft. The number of flight hours, months since the last DLIR, number of non-corrosion related man-hours required and the number of corrosion-related man-hours are listed for each of eighteen aircraft. The parameters for modeling the level of required maintenance may be extracted from such data with the following assumptions:

- 1) Each periodic maintenance effort brings the overall level of required maintenance down to a lower level as shown in Figure 26-8.
- 2) The exponent, n , is assumed to be between 0.5 and unity.
- 3) The rate constant is assumed to increase with atmospheric corrosivity and wash interval as expressed in equation (3):

$$k = k_M c T_{wash} \quad (3)$$

where c is a measure of atmospheric corrosivity, T_{wash} is the wash interval and k_M is a characteristic maintenance rate constant.

Table 26-3: Periodic Inspection and Repair Records for Marine Air Patrol Fleet.

No.	Flt Hrs	Months Since Last Phase	Non-Corrosion Hrs	Corrosion Hrs
Phase 2				
1	4918	50	6239	656
2	5311	55	4706	729
3	5779	61	8249	3550
4	5531	56	5864	847
5	4665	52	5165	684
6	5374	57	7044	977
7	3339	35	6737	546
8	4487	43	6272	1010
9	4652	53	6576	585
10	5111	54	6154	651
11	5041	50	6736	737
12	5591	59	6888	723
13	4771	54	7210	1218
14	5194	59	12277	1856
15	5043	54	8145	1481
16	5432	57	6300	1145
17	5129	52	5182	341
18	5648	60	5984	824
Phase 3				
1	4674	52	7824	1455
2	4449	50	7681	1681
3	3269	37	5308	1107
4	4324	48	5379	1704
5	4266	49	6818	1425
6	3812	48	5653	1010
7	4766	51	5948	1326
8	4680	54	10171	3479
9	5001	50	6274	1472
10	3093	41	5493	689
11	4321	50	5175	1189
12	3055	39	8160	1155
13	5021	54	6763	1690
14	3343	41	6444	1647
15	2995	42	7622	1429
16	3704	51	7956	1609
17	4384	52	6156	1297
18	2954	41	6980	1022

No.	Flt Hrs	Months Since Last Phase	Non-Corrosion Hrs	Corrosion Hrs
Phase 4				
1	3479	53	7682	1109
2	3119	59	12949	2129
3	3732	57	9940	1746
4	3652	58	11452	1377
5	3723	54	6838	951
6	–	–	–	–
7	4124	60	8931	1231
8	3849	55	7316	1204
9	3445	55	7314	1046
10	–	–	–	–
11	3688	58	9091	1841
12	–	–	–	–
13	3428	58	11760	1961
14	3083	61	12558	2955
15	–	–	–	–
16	–	–	–	–
17	3712	57	6525	987
18	–	–	–	–

With these assumptions, k_M can be extracted by combining equations (2) and (3) for each phase and each aircraft according to equation (4):

$$k_M = \frac{M - M_{\text{acceptable}}}{cT_{\text{wash}}T_{\text{DLIR}}^{0.75}} \quad (4)$$

where T_{DLIR} is the number of months in each phase between DLIR and $M - M_{\text{acceptable}}$ is the amount of maintenance applied at a DLIR phase as measured in man-hours. This method requires a measure of atmospheric corrosivity, c , that the planes are exposed to. Any method will do as long as the same method is used for calculating the wash interval as described below.

In the present study, the ground-level corrosivity has been measured for several years using CLIMAT coupons at the home base for this fleet. Figure 26-9 shows the monthly corrosivity at CFB Greenwood, Nova Scotia averaged over three years. As indicated in Figure 26-10, the airfield at CFB Greenwood is only eight km from the Bay of Fundy and downwind from the highest speed winds of winter.

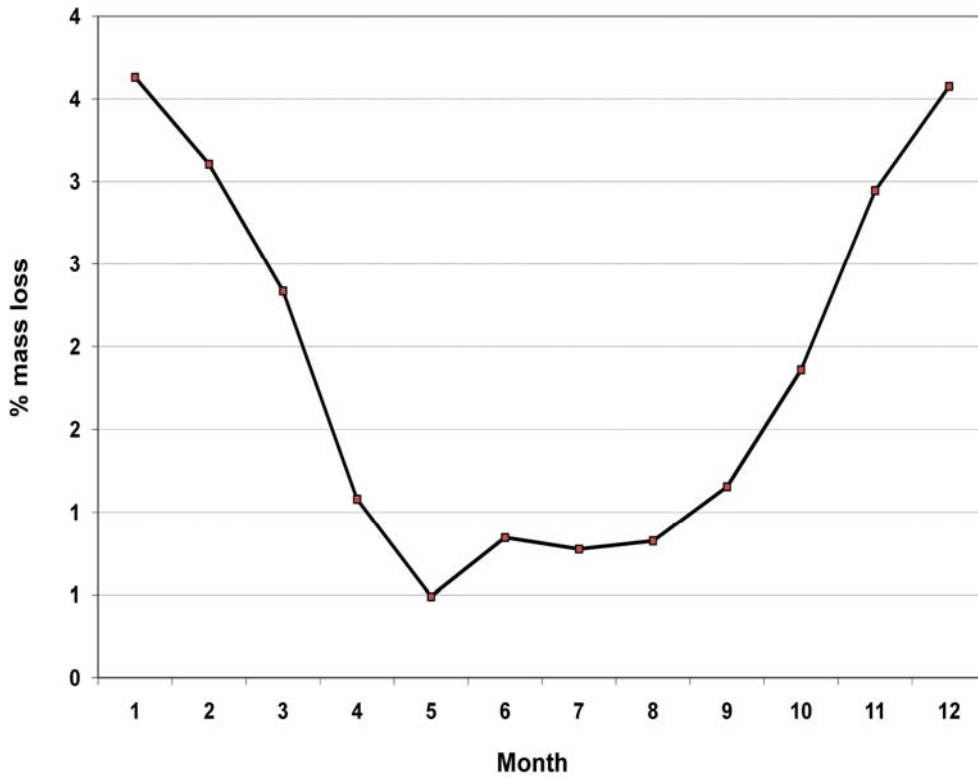


Figure 26-9: Monthly Corrosivity at Canadian Forces Base (CFB) Greenwood, Nova Scotia, as Mass Loss of CLIMAT Coupons Between 2002 and 2006.

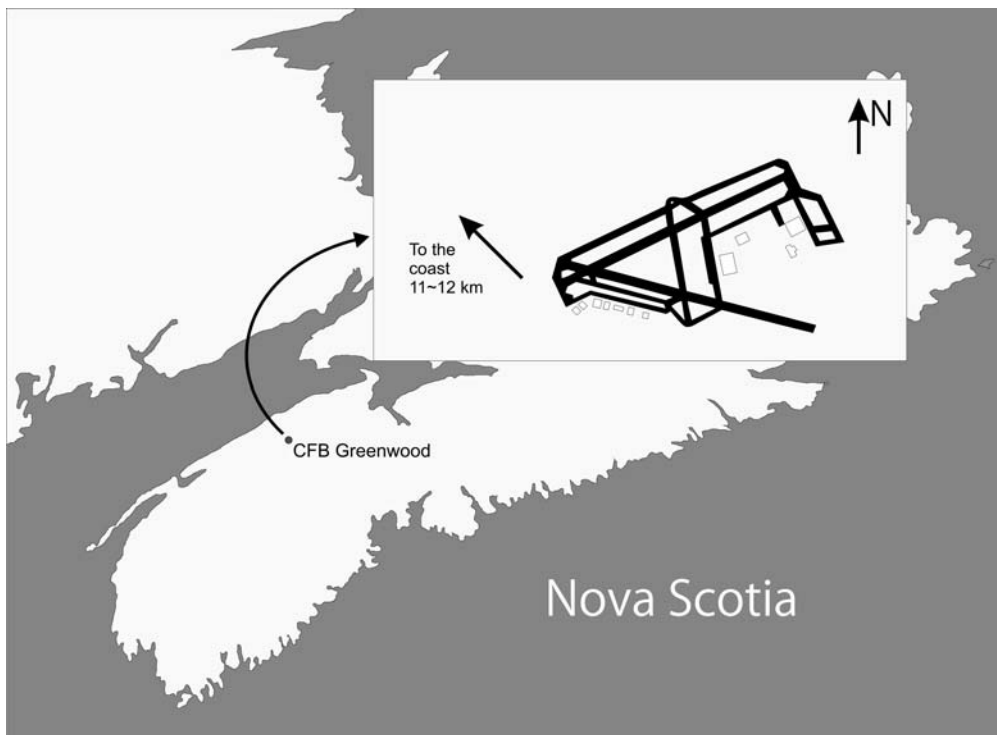


Figure 26-10: Geographical Position of CFB Greenwood in Nova Scotia and in Relation to the Sea.

Month 1 and month 12 in Figure 26-9 correspond respectively to January and December. The corrosivity is highest in the winter and lowest in the summer. The units of k_M with CLIMAT coupons as the measure of corrosivity are man-hours/(CLIMAT mass loss x month^{1.75}) or man-hours’.

The maintenance factor, k_M , for each aircraft after each phase is listed in Table 26-4. The average CLIMAT corrosivity of 1.69% and the wash interval was 1 month. The 95% confidence intervals for the average k_M are 21 – 40, 40 – 55 and 36 – 51 man-hours’ for Phases 2, 3 and 4 respectively.

Table 26-4: Estimates for Time Averaged k_M Based on Periodic Inspection and Repair Records in Table 26-3 and Equation (3).

	Phase 2	Phase 3	Phase 4
Plane	k_M, Man-Hours’	k_M, Man-Hours’	k_M, Man-Hours’
1	20.6	44.5	33.4
2	21.3	52.9	59.2
3	96.2	43.7	49.8
4	24.5	55.3	38.8
5	20.9	45.5	28.2
6	27.9	32.8	
7	22.4	41.1	33.8
8	35.6	103.3	35.3
9	17.6	46.3	30.6
10	19.3	25.2	
11	23.2	37.4	51.8
12	20.1	43.8	
13	36.2	50.2	55.2
14	51.6	60.1	80.1
15	44.0	51.2	
16	32.6	49.9	
17	10.4	39.6	28.2
18	22.6	37.3	
Average	30.4	47.8	43.7
Std Deviation	19.3	16.2	15.8
95% Confidence	21.3 – 39.5	40.1 – 55.4	36.2 – 51.1

*Also included are the average, standard deviation and 95% confidence interval for the average.

The maintenance factor for another fleet was calculated from a different but limited set of data. This fleet was stationed at an inland base at Trenton, Ontario. The average yearly corrosivity as measured by CLIMAT coupons was 0.3%. The average number of man-hours at a DLIR after a phase of 66 months from three aircraft was 4473 man-hours for corrosion related maintenance. Given an average wash interval of 13 months, the maintenance factor was 50 man-hours’. The closeness of this value to that for the marine patrol fleet, even with much different values for corrosivity and wash interval, hints that this range of values for k_M may have some general applicability.

In order to develop a model for calculating an optimal wash interval, the cost of corrosion-related maintenance over a DLIR phase may be formulated in equation (5):

$$C_T = \frac{N_M}{T_{wash}} [C_W + C_U] + r_M k_M c T_{wash} N_M^{0.75} \quad (5)$$

where:

- C_T = total cost of washes and DLIR maintenance
- T_{wash} = wash interval, months
- C_W = cost per wash
- C_U = cost of aircraft unavailability during washes
- r_M = charge rate for maintenance work, dollars/hour
- N_m = number of months between DLIR

The first term in equation (5) is the cost of washes during the DLIR phase and the second term is the cost of corrosion-related maintenance during DLIR. The wash interval that minimizes the total cost, T_{min} , can be obtained by differentiating equation (5) with respect to T_{wash} , setting dC_T/dT_{wash} to zero and solving for T_{wash} . The wash period, T_{Min} , that minimizes the total cost is expressed in equation (6):

$$T_{min} = \sqrt{\frac{N_M^{2.5} (C_W + C_U)}{r_M k_M c}} \quad (6)$$

Figure 26-11 shows the optimal wash interval, according to equation (6), as a function of atmospheric corrosivity within reasonable limits for k_M (i.e., 25 to 55 man-hours'). The values for the other parameters used in this equation were typical for a marine patrol fleet in North America, i.e., $C_W = \$4000$, $C_U = \$1000$, $r_M = \$85/\text{hour}$ and $N_M = 55$ months. It is obvious then that the uncertainty in k_M produces uncertainty in estimating T_{min} , which is about 1 month at the lower end of corrosivity (0.5% CLIMAT mass loss) and about 0.4 months at the upper end of corrosivity (4% CLIMAT mass loss).

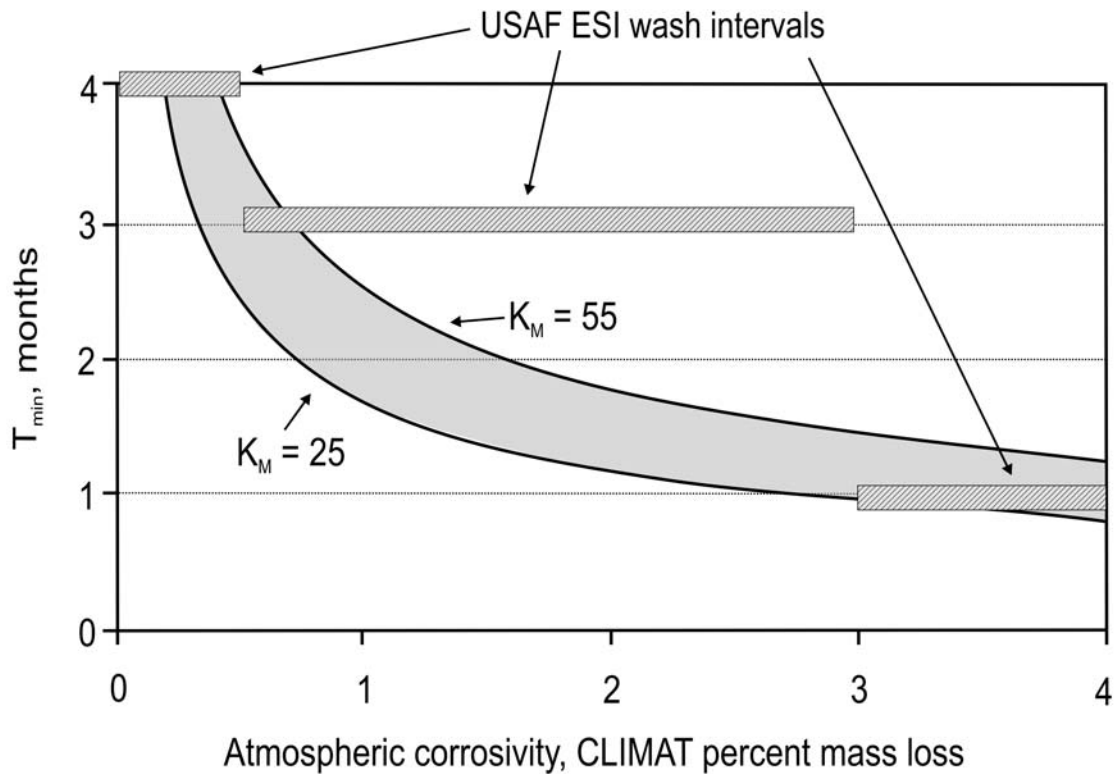


Figure 26-11: Predicted Wash Interval as Function of Corrosivity as Measured by CLIMATs Within Reasonable Limits for k_M (i.e., 25 – 55 man-hours') – Other parameters were: $C_W = \$4000$, $C_U = \$1000$, $r_M = \$85/h$, $N_M = 55$ months.

These results indicate that the optimal wash interval for the maritime patrol fleet is 1 – 1.4 months during the winter and 2.7 – 4.0 months during the summer. Given that the current practice at CFB Greenwood is to wash marine patrol aircraft once per month, stretching out the wash interval during three seasons, i.e., spring, summer, and fall, will result in significant savings on a fleet-wide basis.

Also shown in Figure 26-11 are the wash intervals recommended by the new USAF ESI algorithm after correcting for the differences in the atmospheric corrosivity scales between the USAF ESI and ISO 9223. A mildly corrosive environment would therefore correspond to a CLIMAT mass loss of less than about 0.5%, a severely corrosive environment to a CLIMAT mass loss greater than about 3% and a moderately corrosive environment with a value between 0.5% and 3%. The USAF algorithm and T_{min} according to equation 5 are similar for the mild and severe environments but differ significantly for the moderate environments.

26.4 SUMMARY

The USAF ESI algorithm for setting wash intervals is based on an environmental severity rating and an implied set of economic assumptions. A maintenance factor approach was introduced for setting wash intervals based on corrosion maintenance records, an atmospheric corrosion model and an explicit set of economic parameters. The maintenance records required are the number of man hours required to repair corrosion related damage and the number of months since the last repair. The atmospheric corrosion model assumed a bilogarithmic or power law relationship between cumulative damage and exposure time. It was also assumed that atmospheric severity increases corrosion damage whereas washing decreases it. The economic parameters are the cost per wash, the cost of aircraft unavailability during a wash and the

charge-out rate for aircraft maintenance. This approach requires a measure of atmospheric corrosivity that is not restricted to any particular method as long as one processes the maintenance data and calculates the optimal wash interval with the same method.

26.5 REFERENCES

- [1] Summitt, R. and Fink, F.T., "PACER LIME: An Environmental Corrosion Severity Classification System", AFWAL-TR-80-4102 Part I, Air Force Wright Aeronautical Laboratories, Wright-Patterson Air Force Base, OH, USA, 1980.
- [2] Dean, S.W., "Corrosion Testing of Metals Under Natural Atmospheric Conditions", In: Baboian, R., Dean, S.W., Eds., Corrosion Testing and Evaluation, Silver Anniversary Volume, Philadelphia, PA, USA, ASTM, pp. 163-76, 1990.
- [3] Abbott, W.H. and Kinzie, R., "Corrosion Monitoring in Air Force Operating Environments", U.S. Department of Defense, 2003 Tri-Service Corrosion Conference, 17 November 2003.
- [4] Doyle, D.P. and Wright, T.E., "Rapid Method for Determining Atmospheric Corrosivity and Corrosion Resistance", In: Ailor, W.H., Ed., Atmospheric Corrosion, New York, NY, USA, John Wiley and Sons, pp. 227-243, 1982.
- [5] "Standard Practice for Conducting Wire-on-Bolt Test for Atmospheric Galvanic Corrosion", ASTM G116-99 Edn, West Conshohocken, PA, USA, American Society for Testing of Materials, 1999.
- [6] Coburn, S., "Atmospheric Corrosion", In: Korb, L.J., Ed., Metals Handbook, 9th Ed, Vol. 1, Properties and Selection, Carbon Steels, Metals Park, OH, USA, American Society for Metals, p. 720, 1978.
- [7] "Standard Practice for Preparing, Cleaning, and Evaluating Corrosion Test Specimens", G1-03, Vol. 03.02, West Conshohocken, PA, USA, American Society for Testing of Materials, 2003.
- [8] Knotkova, D., F.N. Speller Award Lecture: "Atmospheric Corrosion – Research, Testing, and Standardization", Corrosion, Vol. 61, pp. 723-738, 2005.
- [9] Leygraf, C. and Graedel, T.E., "Atmospheric Corrosion", New York, NY, USA, John Wiley and Sons, 2000.
- [10] Klassen, R.D., Roberge, P.R., Lenard, D.R. and Blenkinsop, G.N., "Corrosivity Patterns Near Sources of Salt Aerosols", Townsend, H.E. [ASTM STP 1421], 19-33, West Conshohocken, PA, USA, American Society for Testing and Materials, Outdoor and Indoor Atmospheric Corrosion, 2002.
- [11] Roberge, P.R., "Corrosion Engineering: Principles and Practice", New York, NY, USA, McGraw-Hill, 2008.
- [12] Morcillo, M., Chico, B., Mariaca, L. and Otero, E., "Salinity in Marine Atmospheric Corrosion: Its Dependence on the Wind Regime Existing in the Site", Corrosion Science, Vol. 42, pp. 91-104, 2000.
- [13] Kinzie, R. and Abbott, W.H., "An Experimental Study of the Effects of Wash-Rinse Intervals on Corrosion", U.S. Department of Defense, 9th Joint FAA/DoD/NASA Conference on Aging Aircraft, March 6-9, Atlanta, GA, USA, 2006.
- [14] Technical Manual – "Cleaning and Corrosion Prevention and Control, Aerospace and Non-Aerospace Equipment", TO 1-1-691, Robins AFB, GA, USA, Warner Robins Air Logistics Center, 2006.

- [15] Veleva, L. and Kane, R.D., “Atmospheric Corrosion”, In: Cramer, D.S., Covino, B.S., Eds., Volume 13A, Corrosion: Fundamentals, Testing, and Protection, Metals Park, OH, USA, ASM International, pp. 196-209, 2003.
- [16] Feliu, S., Morcillo, M. and Feliu, Jr., S., “The Prediction of Atmospheric Corrosion from Meterological and Pollution Parameters-I Annual Corrosion”, Corrosion Science, Vol. 34, pp. 403-414, 1993.
- [17] Feliu, S., Morcillo, M. and Feliu, Jr., S., “The Prediction of Atmospheric Corrosion from Meterological and Pollution Parameters-II Long-term forecasts”, Corrosion Science, Vol. 34, pp. 415-422, 1993.

Chapter 27 – REPAIRING CORROSION DAMAGE

Ronald W. Gould

Structures and Materials Performance Laboratory, Institute for Aerospace Research
National Research Council Canada
Ottawa, Ontario
CANADA

27.1 INTRODUCTION

Repair of corrosion damage requires that suspect structure can be accessed and inspected non-destructively so that the damage can be detected and quantified in terms of severity. Chapter 21 of this publication describes some of the inspection methods available as well as the quantitative success of most of these methods. This chapter illustrates how some of these methods are used in practice and the complications that arise when dealing with multi-layer, built up structure. It also reviews some of the methods available for repairing corrosion damaged structure as well as work performed at the National Research Council to develop a library of specimens of corroded aircraft structures.

27.2 REPAIRING CORROSION DAMAGE

27.2.1 Standard Practice

All aircraft must be periodically inspected for corrosion. During visual inspections an inspector looks for surface features that indicate the presence of corrosion. One such feature is known as corrosion pillowing, which occurs when corrosion products are present at the faying surfaces of lap joints or in areas of multi-layer construction. Service bulletins and maintenance manuals state that if corrosion is visually detected, then eddy current equipment should be used to estimate the percentage of thickness loss. In general, if the thickness loss in a single skin is greater than 10% [1] the joint must be repaired. This entails:

- Removing the rivets in the affected area;
- Wedging open the skins;
- Removing the corrosion products and any visible damage (e.g., pits) [2];
- Applying doublers to the affected skins; and
- Returning the aircraft to service.

For a thickness loss of less than 10% the required action varies depending on the aircraft. For some aircraft repair is not mandatory, but there must be regular inspections until the joint is repaired. However, for other aircraft the service bulletins state that if the corrosion is within specified limits, prior to flight, it, and any other visible damage, must be removed, e.g., by blending out.

The standards for safe corrosion damage repair have been developed from years of accumulated experience. The guidelines for these best practices are set out in training and repair manuals and the work is carried out by skilled personnel. Nevertheless, the nature of the work does sometimes result in unwitting damage being done, and the time spent carefully exploring the extent of the corrosion damage could be wasted if the end result is that the part must be scrapped and replaced.

Paint systems are still removed from aircraft structures before inspections are made for corrosion and fatigue damage, since there is as yet no acceptance that available NDI techniques can detect such damage

through the protective coatings [3]. To illustrate that hazards exist during paint stripping, the FAA recently added an Airworthiness Directive for B757s to the previous warning for B737s¹ [4]. These ADs followed the discovery of procedural errors (use of metal tools, resulting in scratches) when some airframes were being paint-stripped for inspection prior to maintenance. Not only are scratches a concern for fatigue damage but they are potential sites for corrosion initiation. Blending out of such scratches should be followed by the application of a protective coating since the blending (grinding/hand sanding) may extend through the original protective cladding layer.

27.2.2 Inspection Methods and Examples

Typical line inspection of operational aircraft relies on the human inspector's ability to view the surface and visually recognize faults such as 'pillowing', cracks and loose or failed fasteners. NDI techniques are not typically applied to the interrogation of individual fasteners. On the aircraft such damage is usually noticed only when the fastener head has fallen out. Often the fastener is replaced from the exterior only (blind or pop-rivet type) owing to access difficulties. This means that the condition of the inner structure is not properly assessed. Structures receiving this type of maintenance have sometimes been found to have non-existent or severely compromised inner structure. The end result can be a filled hole in the outer layer with no mechanical connection to the sub-structure. The inability of normal visual inspections to detect hidden corrosion damage has led to enhanced visual inspections, see below, and sometimes to X-radiography.

27.2.2.1 D Sight Aircraft Inspection System (DAIS)

This inspection system enables enhanced visual inspections of intact joints [5]. Figure 27-1 is a DAIS image of a lap joint that illustrates the stages in corrosion growth, detection and repair:

- Green line: this area is undamaged (green line) and shows the normal skin deformations in joints resulting from manual assembly: note also that the deformations along the body frames are typical.
- Yellow line at left: corrosion was detected and assessed to exceed the damage limits (>10% thickness loss), thereby requiring local disassembly, clean-up between the skins and application of an external doubler. The mechanical deformations resulting from this repair mean that this area can no longer be assessed simply by visual inspection of the outer surface.
- Orange line at right: a lower level of corrosion was detected (<10% loss) and the repair involved local disassembly, clean-up and reassembly with larger diameter protruding head rivets. Drilling for these rivets completely removed the countersinks in the outer skin of the original flush-head rivets. The large size of the protruding rivet heads and their spacing make future visual and NDI inspections very difficult. There is very little room to slide an eddy current probe around between the heads.
- Red line: this area suffered un-repaired corrosion damage, visible as pillowing. Either this damage had occurred since the repairs were carried out or it was present at the time and was missed by the inspection techniques employed. At the next D-check the external doubler repair (solid yellow line) was removed and replaced with a larger doubler that covered the expanded repair area, as indicated by the dotted yellow line.

¹ FAA AD 2007-19-07 for certain Boeing Model 757-200, 200PF, and -200CB series airplanes. This AD requires inspections to detect scribe lines and cracks of the fuselage skin, lap joints, circumferential butt splice strap, and external and internal approved repairs; and related investigative/corrective actions if necessary. This AD results from reports of scribe lines adjacent to the skin lap joints. We are issuing this AD to detect and correct cracks, which could grow and cause rapid decompression of the airplane.

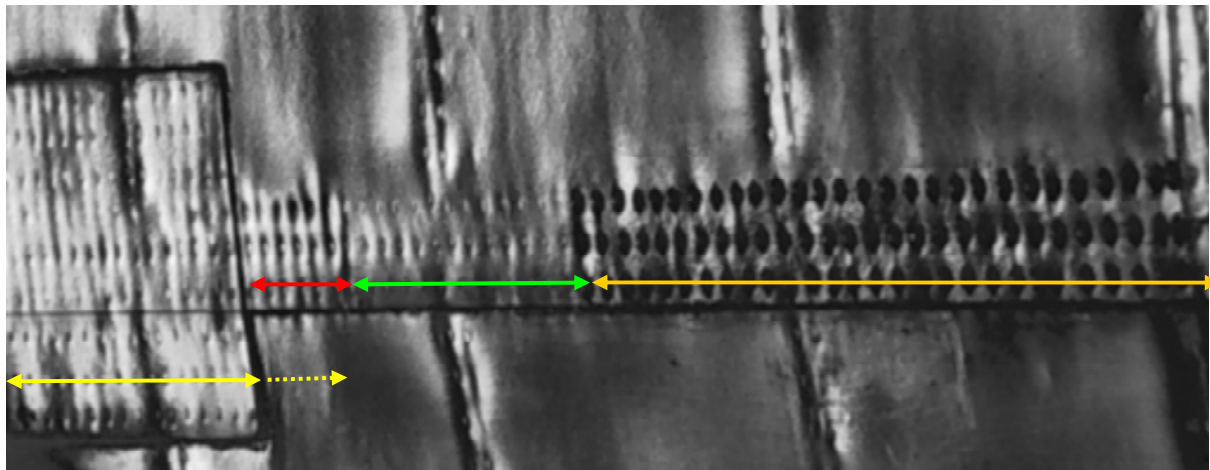
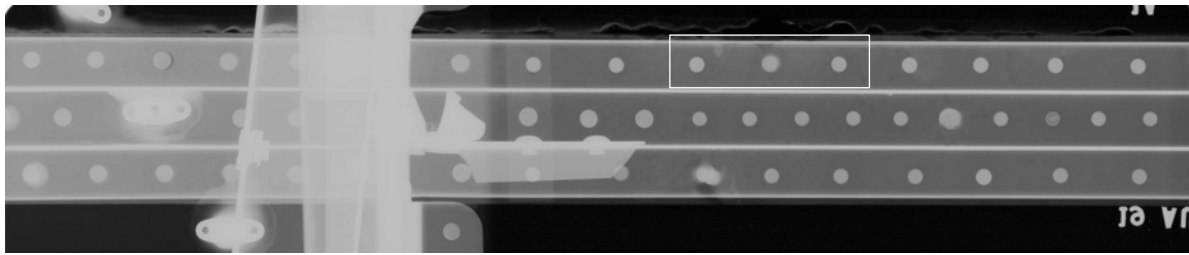


Figure 27-1: Lap Joint Corrosion and Repairs.

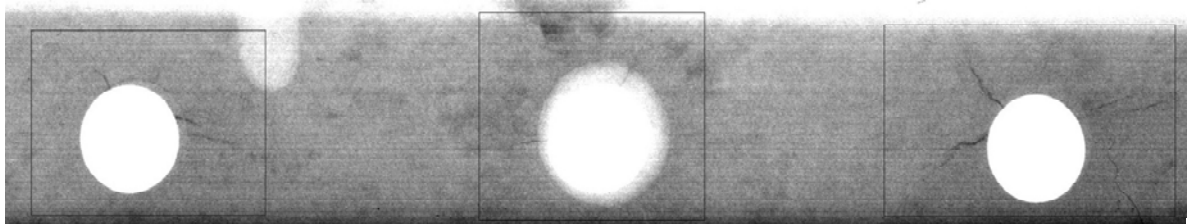
In the above illustration the rivet-to-rivet and row spacings in the joint were nominally equal, which caused the pillowing response when the skins were deformed by the accumulation of corrosion products between the fasteners restraining them. However, each manufacturer has invested heavily in the understanding of their proprietary joint designs and chosen specific rivet / rivet row spacings. These spacings directly affect the corrosion pillowing response and inspectability. For example, Airbus and Lockheed L1011 joints do not pillow, they make waves. Douglas DC-10 joints also make waves, but the view is complicated by the use of ‘beauty strips’ (external butt joint doublers). Douglas DC-9 longitudinal joints do not appear to pillow or make waves unless they are viewed perpendicular to the joint rather than along it as in Figure 27-1. The reason is that the DC-9 has closely spaced rivets in widely spaced rows, and corrosion product accumulation results in wave-like distortions parallel to the joint. These are almost impossible to detect when viewed along the joint.

27.2.2.2 X-Ray Inspection

X-radiography is not typically used for corrosion detection, as is mentioned also in Part 2 of this chapter. However, the pillowing forces generated by the corrosion activity in multi-layer structures can lead to tensile forces sufficient to nucleate cracks which are detectable by X-ray, Figure 27-2.



(a) Typical x-ray film of intact joint.

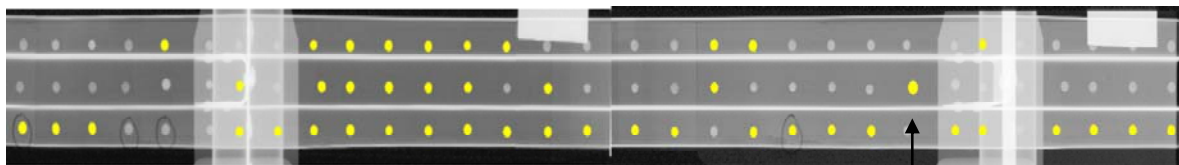


(b) Non-surface breaking cracks (enlargement of area in white box).

Figure 27-2: Corrosion-Induced Pillowing Cracks.

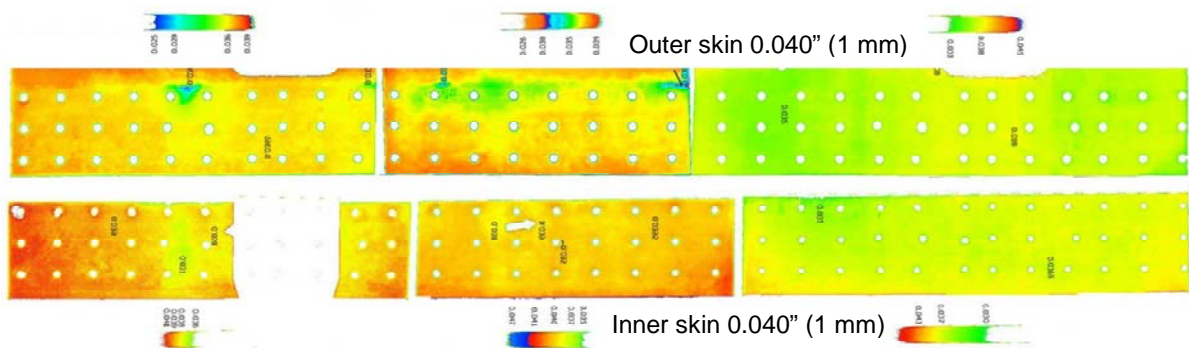
27.2.2.3 Examples of Damage Undetectable Without Detailed Inspections

Skin thickness loss and cracked rivets – Figure 27-3 shows X-ray inspection results for an intact and disassembled lap joint. The skins of the lap joint suffered only 3 – 4% combined thickness loss yet 43 of the 93 rivets in the joint, a total of 47%, were *subsequently* (during teardown) found to be fractured, including a larger diameter replacement rivet in the middle row. Fractured rivets were those that easily broke into two during teardown of the joint (shop heads machined off and rivets pressed out).



Larger diameter replacement rivet also fractured

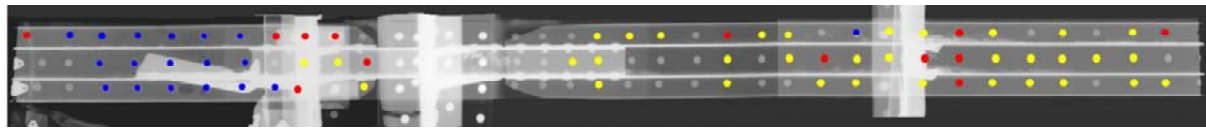
(a) Rivet condition: Yellow – fractured.



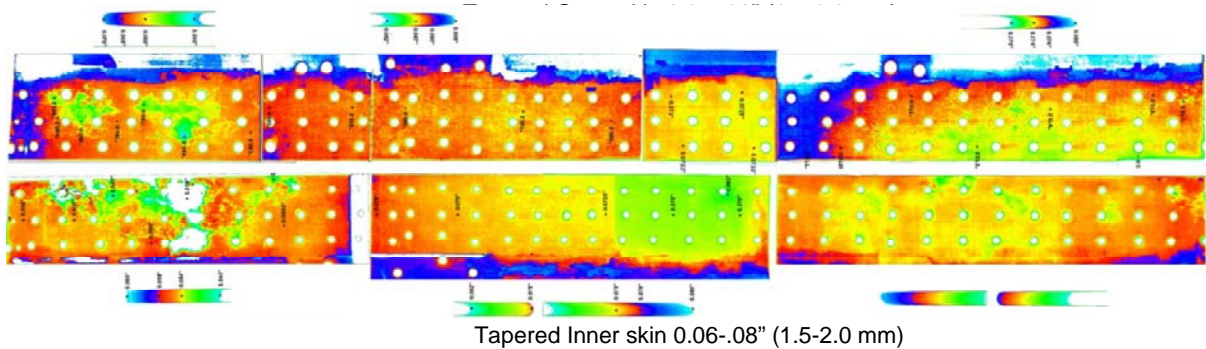
(b) False-color digitized X-ray thickness loss (calibration ramps adjacent to sections).

Figure 27-3: X-Ray Inspection Results for (a) Intact and (b) Disassembled Joint.

Figure 27-4 gives another example of X-ray inspection results for an intact and disassembled lap joint. The upper X-ray was taken before the joint was disassembled and cleaned of paint, primer, sealants and corrosion product to facilitate the thickness loss mapping of the separate skins. Both skins had been taper-machined: the outer skin from 0.07 to 0.09 inch (1.78 – 2.28 mm) and the inner skin from 0.06 to 0.08 inch (1.52 – 2.03 mm). Disassembly allowed detection of the thickness loss due to corrosion.



(a) Rivet condition: Red – Failed-in-place, Yellow – Fractured, Blue – Replaced.



(b) False-color digitized X-ray thickness loss (calibration ramps adjacent to sections).

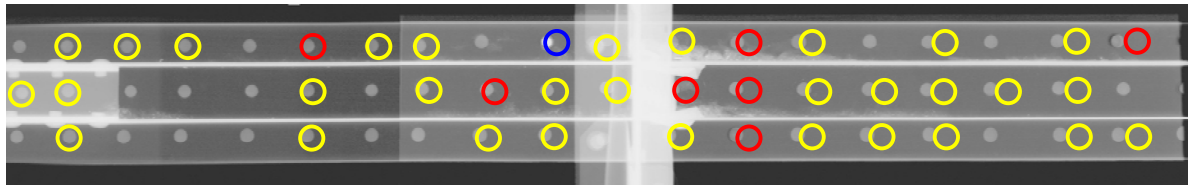
Figure 27-4: X-Ray Inspection Results for (a) Intact and (b) Disassembled Joint.

However, neither X-ray nor eddy current inspections before disassembly showed differences between intact and cracked rivets. Disassembly showed that of the 108 fasteners in the lap joint, 13 had failed, 31 were fractured, and 18 had been previously replaced – but 17 of these were installed into the severely exfoliated second layer skin and stringer (left end). A total of 57% of the fasteners in this section of lap joint were either failed or distressed.

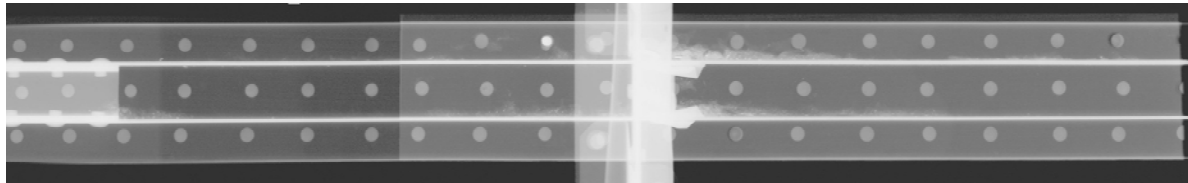
Figure 27-5 provides a closer assessment of the fasteners at the right end of the joint shown in Figure 27-4. The key for the colored circles applied to the X-ray image of the joint in Figure 27-5(a) is:

- Red – cracked around base of rivet head or head missing.
- Yellow – partially cracked.
- Blue – replacement for previously failed rivet.

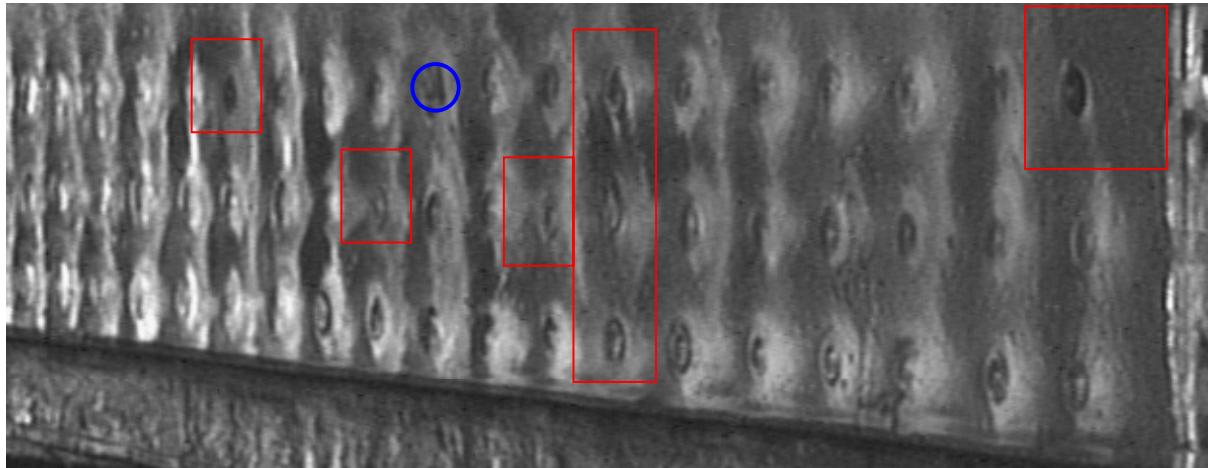
REPAIRING CORROSION DAMAGE



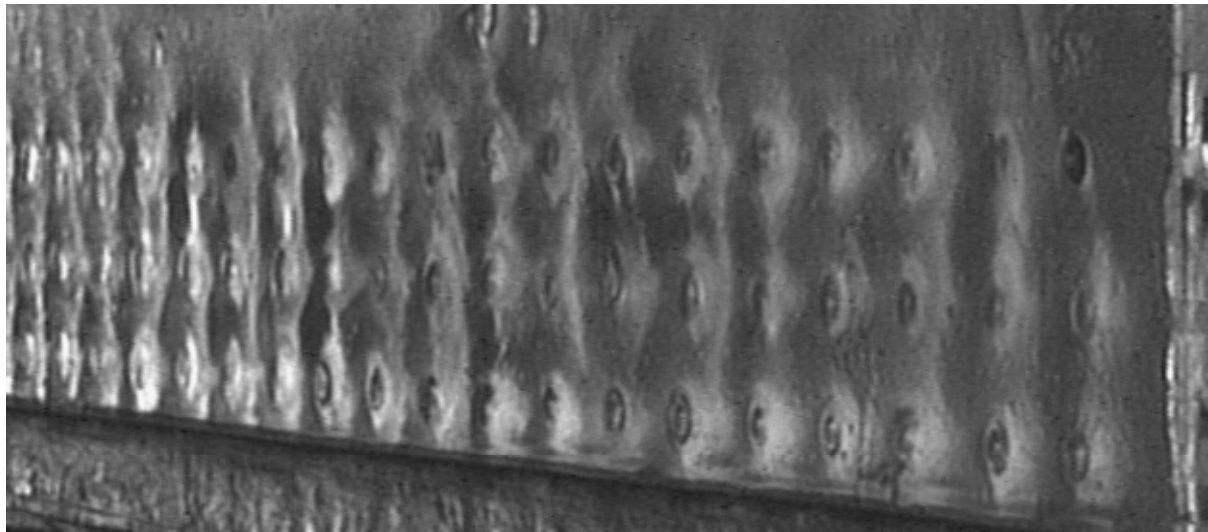
(a) Rivet damage assessment on X-Ray of intact joint.



(b) X-Ray of intact joint (same as 'a').



(c) Replaced rivet (blue circle), fractured rivets (red).



(d) DAIS view of LH end of lap joint (same as 'c').

Figure 27-5: DAIS and X-Ray Images of Left End of Joint (Figure 27-4) Showing Failed Rivets *In Situ*.

In yet another example (not shown), a lap joint with a combined average of only 8.8% thickness loss had 4 failed rivets, and a further 32 of the 48 rivets were cracked. Hence 75% of the fasteners in the lap joint section were distressed.

27.2.2.4 Corrosion Pillowing and Cracked Rivets

Figure 27-6 shows an unpainted longitudinal lap joint. One rivet head in the top row was missing (arrow) and this visible damage contributed to the selection of this joint for study. An automated eddy current scan of the joint was carried out before teardown. Scanning of the entire intact joint required the application of Teflon tape to prevent wear of the eddy current probe. After the scan the tape was peeled off, and this resulted in two additional rivet heads being released (circled). Observation of the parts of these two failed rivets showed that they had cracked and ultimately failed owing to the force created by corrosion pillowing. There was only minor corrosion on the rivet surfaces.

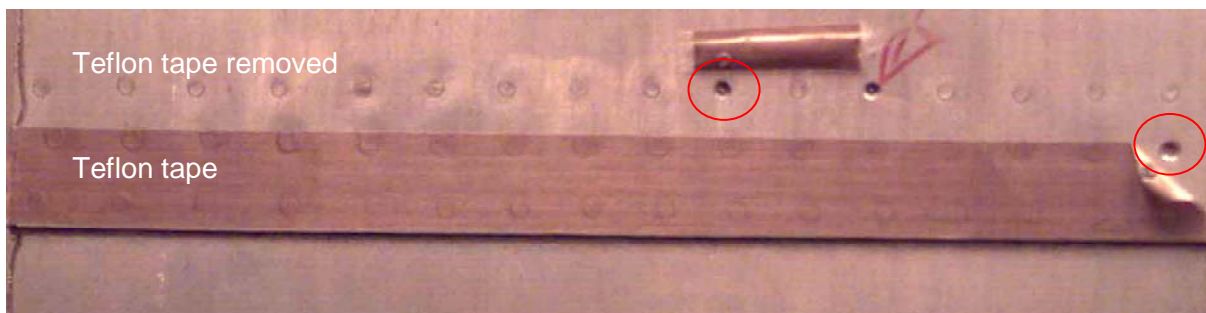


Figure 27-6: Corrosion Pillowing Induced Failure-in-Place of Rivets Discovered by Tape Peel.

During many similar eddy current scans, often on painted joints, there were numerous cases where Teflon tape removal also resulted in the discovery of rivets failed *in situ*. Neither X-ray nor eddy current inspections of the intact joints indicated any difference between undamaged, cracked or failed rivets.

27.2.3 Repair Philosophy

With increased understanding of the fatigue and corrosion behavior of a specific joint design the move can be made from the current “find and fix” philosophy to a “predict and manage” philosophy. Corrosion removal activities must balance the need to remove all detectable damage, blend the excavated area to avoid stress concentrations, permit spliced repair sections and doublers in the space available, not impede drainage, and meet OEM guidelines for minimum thickness allowables.

At times the thickness loss will be found to exceed the minimum thickness allowables and the offending part must be replaced. This is relatively straightforward. However, repair rather than replacement tends to cause the most trouble:

- 1) Much effort can be expended before it is discovered that the damage exceeds the allowables and the whole part will need to be replaced.
- 2) The real hazard with trying to save an installed part is the natural tendency to cover the repaired area in sealant, with the thought that this will prevent corrosion from reappearing. What typically happens is that not all the corrosion is removed, and so it starts again. This restart is difficult to determine because the area is totally obscured from visual or instrumented damage inspection. The sealant also forms a barrier to any future effective applications of Corrosion Prevention Compounds (CPC). Any repair must therefore consider that the conditions that led to damage were not unique, and that the repaired area is most likely to see the same environmental conditions

REPAIRING CORROSION DAMAGE

that led to the original damage. Drainage paths must be re-established, not blocked or rerouted, or new problems will occur. Visual and NDI records of the repair should be made for later comparison and assessment of any changes during further service.

- 3) Drilling out rivets always has the potential to cause elongated fastener holes. Figure 27-7 gives an example where not only were the fastener holes enlarged to the maximum size but they were almost all elongated. In addition, the skin was found to be corroded and the removal process thinned the skin by up to 37% (white areas). In this case it was deemed appropriate to attach a new skin to this damaged skin, match-drilled into the same elongated fastener holes. On the other hand, one might well consider that enlarging the replacement skin sheet size and also shifting the joint to the next stringer on the remaining original sheet should eliminate such a compromised joint.

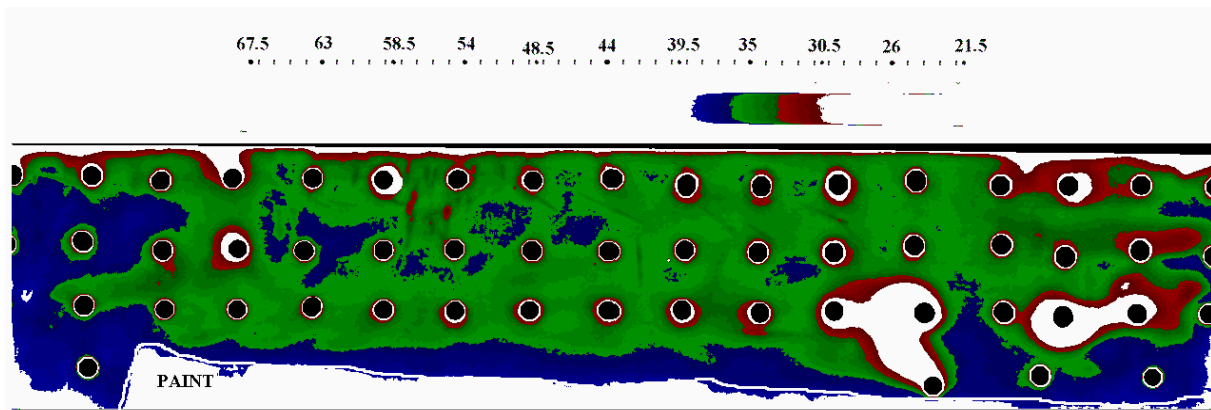


Figure 27-7: Elongated Holes from Rivet Removal and Skin Thinned by Corrosion Removal.

27.2.4 Repair and Repair Problems

Service repair instructions state that corrosion detected between layers in a joint should be removed. This is done mechanically. However, the access to accomplish this task is often limited to de-riveting a short length of joint and wedging the skins apart. This means that the maintenance operator cannot properly observe the clean-up, which will necessarily err on the side of removing too much material, i.e., including sound metal. Besides this conservatism, an incomplete understanding of the corrosion process can lead to using clean-up techniques that actually cause more damage than corrosion removal. Some examples of the problems that occur are given here.

27.2.4.1 Faying Surface Grinding Around Rivet Holes

Because corrosion product build-up permanently deforms the skins of a joint (at 6% thickness loss the forces are sufficient to exceed the yield strength of the skin material), and because of the fastener clamp-up, the deformation will occur away from the fastener holes. This means that the first contact of any corrosion removal process will be with the material closest to the fastener holes.

As shown schematically in Figure 27-8, corrosion product removal by grinding, i.e., with rigid abrasive power tools, can cause serious damage to the faying surfaces. This damage could cause high stress concentrations, increasing the risk of premature cracking. Also, if cracks have *already* initiated at the faying surfaces owing to pillowing forces (as predicted by Finite Element Analysis and found during teardowns) then grinding could smear the cracks closed and obscure them from visual and X-ray inspections. Thus faying surface corrosion products are better removed by chemical cleaning.

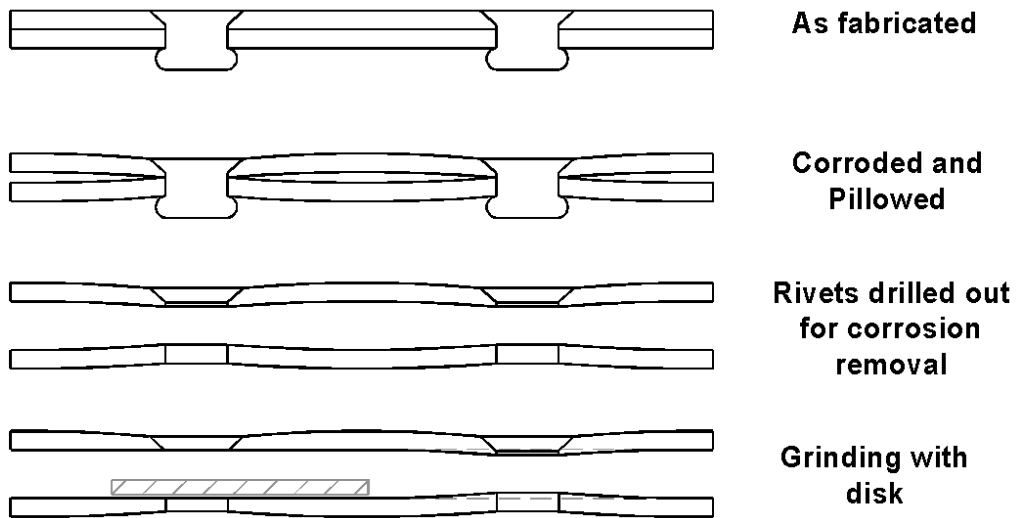
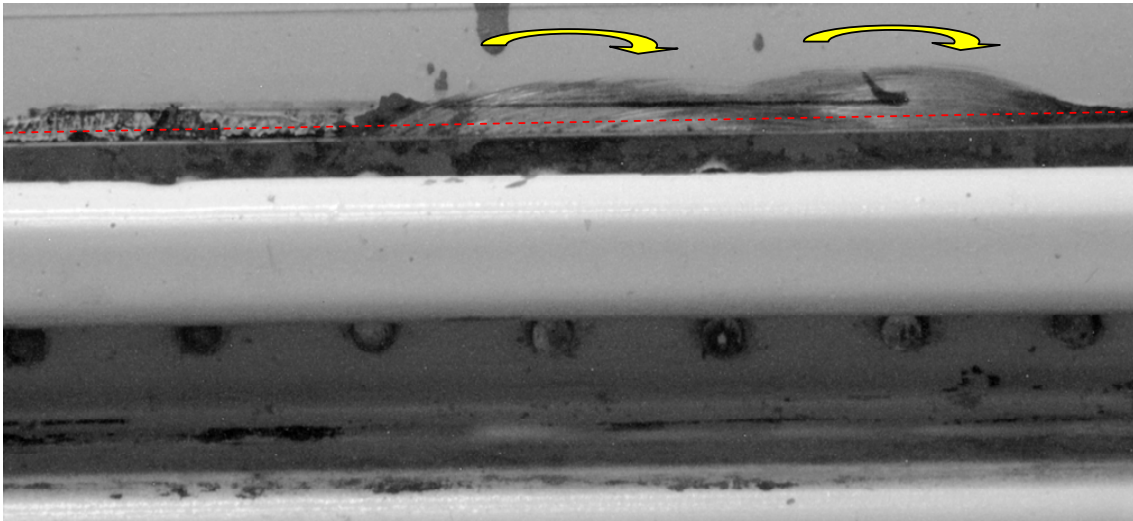
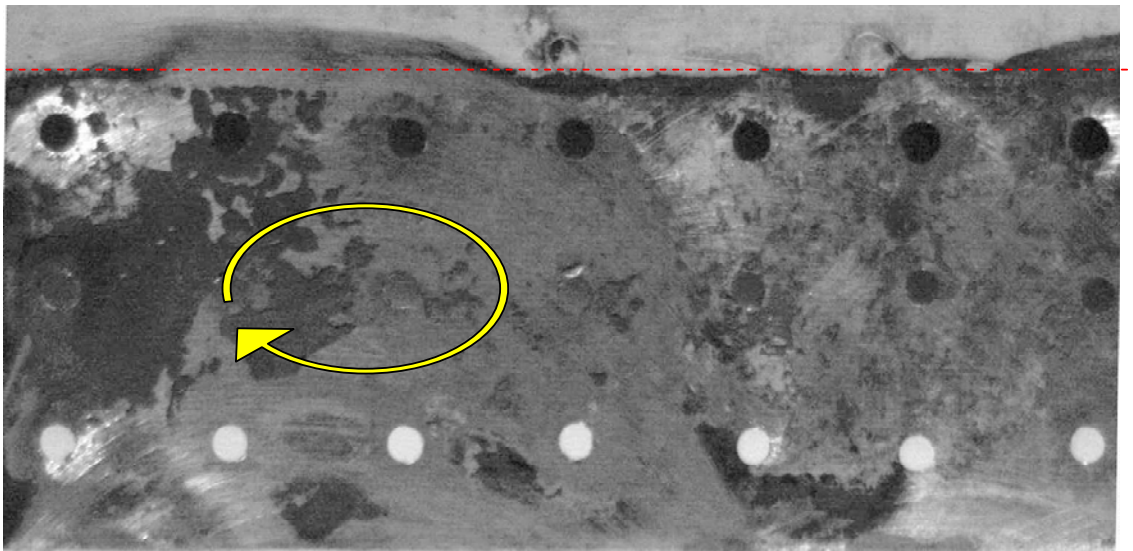


Figure 27-8: Scenario Showing how Grinding Could Remove Excessive Amounts of Material from Around Rivet Holes.

Evidence of the use of a rigid abrasive disc to remove faying surface corrosion is visible extending above the top edge of the inner skin on the inboard surface of the outer skin (red line) of the previously repaired and re-assembled joint shown in Figure 27-9(a).



(a) Rear surface of joint rebuilt after grinding for corrosion removal. Red line – Top of inner skin.



(b) First layer skin, inboard surface, disassembled, showing grinding marks. Red line denotes top of inner skin (removed).

Figure 27-9: Evidence of Grinding on Re-Assembled and Disassembled Joints.

Figure 27-9(b) shows the faying surface of the outer skin from the disassembled joint. The grinding marks indicate that the joint had been previously opened for corrosion removal, and that this was done using a motor driven rigid abrasive disc. The limited access and visibility mentioned above makes it understandable that motor driven discs of a diameter large enough to span the joint might be preferred to manual scraping/sanding tools. This is despite the fact that there are written warnings that powered grinding operations can generate temperatures sufficient to affect the temper of the aluminum. The only recommended powered corrosion removal tools are rotary files, flap brushes (both impractical in this instance) and *flexible* abrasive discs, see the FAA and Airbus guidelines after Figure 27-10. The point often missed here is ‘flexible’. The danger is the unintended damage done as a result of employing non-recommended tools and procedures owing to the difficult accessibility.

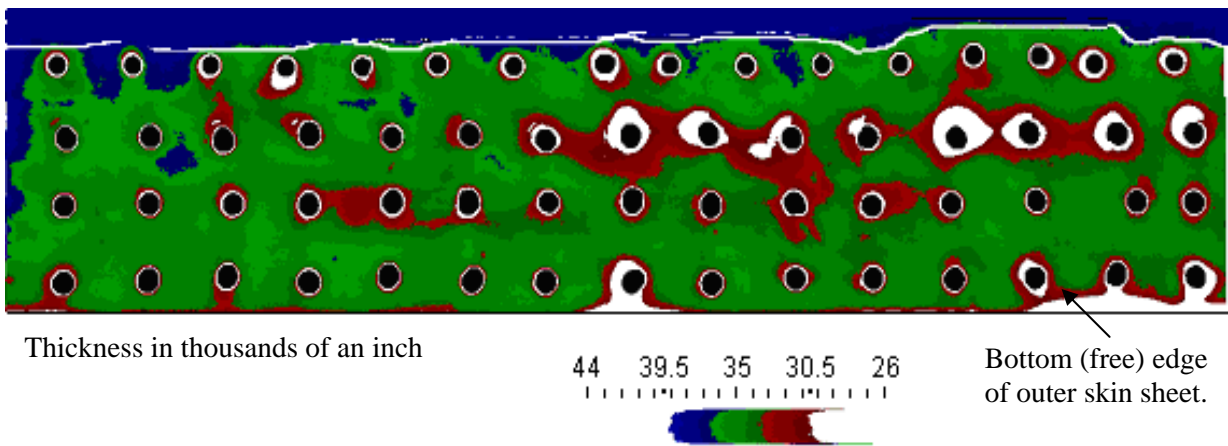


Figure 27-10: Digitized and Colorized X-Ray Thickness Loss Map for Outer Skin.

The selected removal technique, rigid abrasive disc grinding, resulted in significant skin thickness loss and produced knife-edges at fastener holes and at the free edge of the 0.038 inch (0.96 mm) thick sheet. These effects are illustrated by the digitized and false-colored X-ray thickness loss map shown in Figure 27-10: red indicates a range of 20 – 25% loss and white indicates a loss beyond the range of the calibration master. The minimum measured thickness was 0.026 inch (0.66 mm) at the bottom edge, a 34% loss.

27.2.4.2 FAA and Airbus Guidelines for Corrosion Removal

- FAA Advisory Circular AC 43.13-1B Large AC. Acceptable Methods, Techniques, and Practices – Aircraft Inspection and Repair. 9/27/01 Section 6 Corrosion Removal procedures, Pages 6-18:

“Do not abrade or scratch any surface unless it is an authorized procedure. If surfaces are accidentally scratched, the damage should be assessed and action taken to remove the scratch and treat the area.”
- Airbus A-310 STRUCTURAL REPAIR MANUAL Dec 01/97 51-74-10 Corrosion Removal Techniques – General
 - 1) Abrasion by hand with paper or pads is only suitable for removing light corrosion and finish work after heavy corrosion removal by other means.
 - 2) Wire bushing by hand or motor driven is acceptable but only with stainless steel or aluminum oxide coated brushes.
 - 3) Grinding is not suitable for use on aluminum alloys and high temperatures may be generated that may change the mechanical properties of the materials.
 - 4) Hand held rotary files are the only rigid cutting tool permitted for motorized use to remove heavy corrosion on aluminum structures. Otherwise hand scraping is prescribed.
 - 5) Abrasive blasting can be used to remove heavy corrosion but it is not recommended for use inside the airframe. The choice of blast media and the number of applications may be restricted.

27.2.4.3 Exterior Grinding

Exterior surface corrosion damage may be exacerbated when addressed with rigid abrasive tools and a lack of appreciation for the damage that can quickly be done. In the case illustrated in Figure 27-11 the effort to remove filiform corrosion damage around rivets succeeded only in grinding the heads off the rivets and thinning the adjacent skin, in some cases completely through the thickness. The minor damage and appearance issues were thus transformed into a completely ruined joint. As with the faying surface

REPAIRING CORROSION DAMAGE

corrosion removal situation, the outer surfaces are pillowed by the internal build up of corrosion products, and attempts to remove exterior surface damage must recognize the danger of removing sound material before the damaged area is cleaned up. Fortunately, this example was seen in an aircraft graveyard, but on the other hand the aircraft must have been flown to get it there.



Figure 27-11: Exterior Spot Grinding.

Figure 27-12 shows a DAIS view of another lap joint that was ground externally while also suffering faying surface corrosion with resulting pillowing. The pillowing complicated the grinding action and the DAIS image illustrates the damage and thickness loss to the skin. Not only was the skin thinned, but more importantly the heads of the rivets were also damaged, in this case most notably in the middle rivet row and as shown in a normal view in Figure 27-13. Clearly, either the grinding should be done after the rivets have been removed or the rivets should be replaced after the surface has been ground.

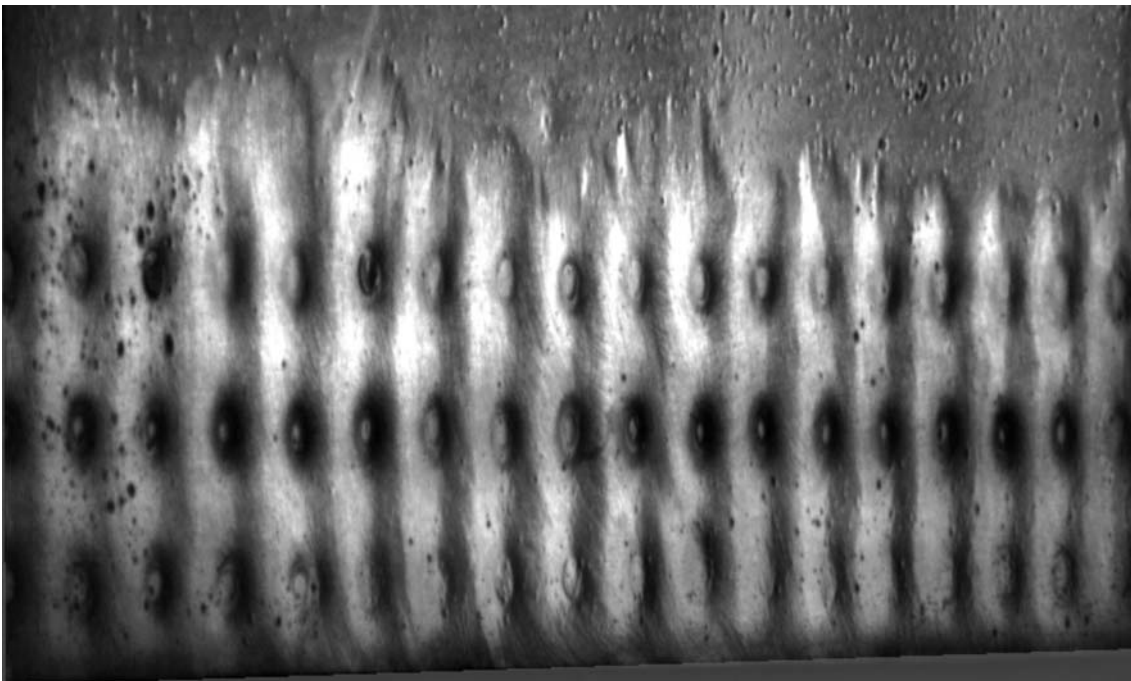


Figure 27-12: DAIS View of Pillowed Skin Suffering Surface Grinding.

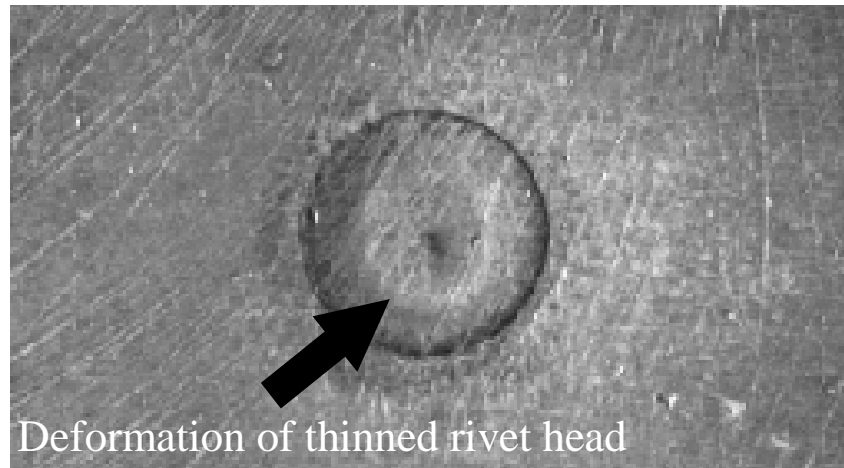


Figure 27-13: Close-Up of Grinding Damage to Rivet Head, Middle Row Rivet, Joint Shown in Figure 27-12.

27.2.4.4 Exfoliation Corrosion Removal

Wing skins machined from rolled aluminum plate tend to suffer exfoliation corrosion at edges such as stepped thickness changes and fastener holes, where the ends of the elongated grains are exposed. Following the inspection of numerous aged aircraft wings it has been noted that exfoliation damage is not always confined to these physical locations. Apart from grain and constituent particle directionality, aluminum alloys are assumed to be more or less homogeneous. However, many cases of exfoliation damage have appeared in areas well away from any fastener holes or machined edges. In two cases (KC-135 and A-300B4) the occurrence could be referred directly back to a common batch of plate material. The alloy must have contained non-uniform inclusions that became active corrosion sites when the protective coating systems degraded in service.

Figure 27-14 gives an example where severe exfoliation corrosion was removed from an upper wing skin plank. Unfortunately, the material removal and blending at two fastener holes (circled) went far beyond the allowed minimum thickness, and this resulted in the entire wing plank having to be replaced.



Figure 27-14: Upper Wing Skin with Exfoliation Corrosion Damage at Fastener Holes.

Another example is given in Figure 27-15. At great expense in time and effort almost every fastener site on the upper wing skin has been ground and blended-out to remove the exfoliation corrosion.

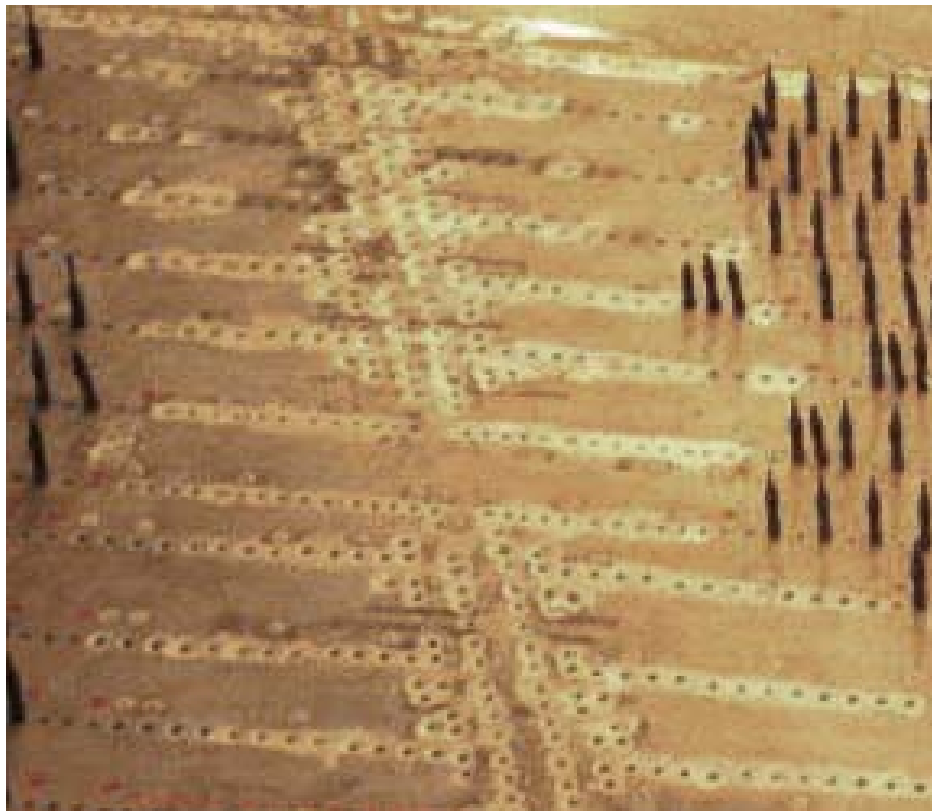


Figure 27-15: Upper Wing Skin with Multiple Sites Ground for Exfoliation Corrosion.

Testing [7] of upper wing skin material with similar levels of damage that has not been re-worked has shown that there is no decrease in load capacity or durability (compression-dominant fatigue). One might consider that more damage may be done to the structure by completely removing this form of corrosion; and that it would be better to surface grind to restore aerodynamic smoothness, followed by re-application of the protective coatings and institution of an NDI monitoring plan. This would probably be sufficient to extend the life of the part without the expense of extensive reworking.

27.2.5 Post-Repair Inspection

It seems often to be assumed that once a repair is done then no further corrosion damage will occur and thus there is no need for a follow-up inspection or monitoring program. Be that as it may, the addition of doublers and sealants to the repair makes inspection and detection more difficult.

Nevertheless, there is great value in repeated inspections specific to the repaired area to confirm corrosion abatement. Part of the above assumption is that the damaged and repaired area has been returned to a 'zero time' condition. This is incorrect, since not only has the structure been changed by material removal, fastener replacement, possible reinforcing doublers and the addition of sealants, but the disassembly and reassembly operations are bound to have caused some mechanical deformation. In addition, the stiffness of the repaired area will have changed, and flight loads will therefore affect the structure in ways other than expected.

A major point is to thoroughly document a repair. Yet repairs are rarely documented for their post-repair appearance or NDI response, both of which should serve as baselines for future inspections. Some examples of continuing problems after corrosion repairs are given in the remainder of this sub-section. These problems all involve sealants.

27.2.5.1 Inside Surface Corrosion

Figure 27-16 shows inside surface corrosion of an upper skin from a lap joint. This occurs more often and more severely than one might expect, for reasons given below.



Figure 27-16: View of Surface Corrosion on INBD Side of Upper Skin at Lap Joint.

On the outside of the fuselage the lapping of sheets top-over-bottom seems sensible if you are concerned with shedding rainfall. The exterior joint edge is given a bead of sealant to restrict moisture entry, and the integrity of that sealant is easy enough to check and replace. But what about the ‘rain’ inside? Internal moisture condenses, collects, and runs down the inside of the skin sheets until it hits the ledge formed by the top edge of the inner skin. This edge also receives a bead of sealant but it is only seen on rare occasions, like D Checks, and age plus pressure cycling eventually defeats these edge seals.

If lap joints were oriented the other way (as some lower lobe KC-135 joints are) the moisture running down the inside would not have a ledge to collect on; and if the lower edge of the inner skin is not caulked, then any breakdown in the outer sealant bead and /or faying surface sealant layer would naturally drain (until the easily accessible outer sealant breach is fixed). Alternatively, deleting the outer sealant bead on the lower edge of a standard lap would allow drainage of moisture that has entered the joint.

27.2.5.2 Widespread Inside Corrosion

In response to the heightened awareness of how important corrosion can be for the integrity of ageing aircraft lap joints, some manufacturers mandated a comprehensive sealant program where every internal joint and fastener was potted or received additional sealant. Even the upper and lower edges of the stringer were sealed. This succeeded in only one thing: the moisture that was already in the joint was locked in, and inside corrosion was inevitable. Figure 27-17 is an example: sealants were comprehensively applied to exclude moisture intrusion in an attempt to avoid the development of crevice corrosion. The result was that every section harvested from the fuselage of this retired aircraft suffered corrosion inside the joints.



(a) Lap joint top row fasteners and stringer sealant application.



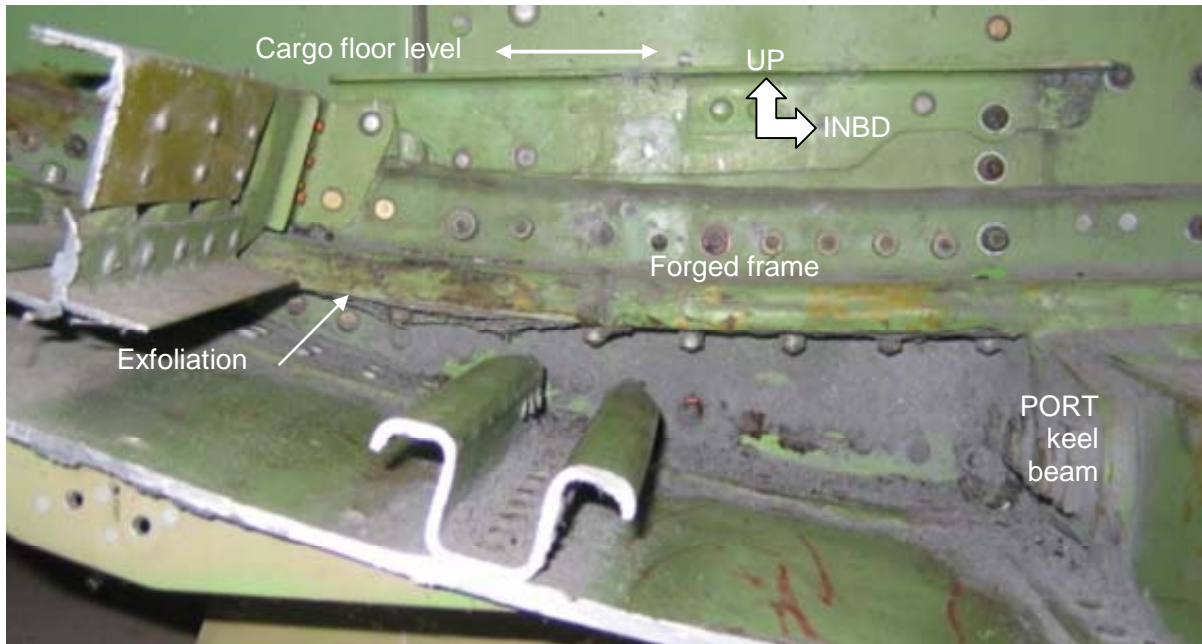
(b) View along lower surface of stringer on lap joint and body station frame attachment.

Figure 27-17: Rivet Shop Head and Stringer Edge Sealant Applications.

27.2.5.3 Exfoliation Corrosion

Figure 27-18(a) is a view of the port side of a bilge area in a fuselage where a heavy forged frame passes close to the bottom. The bottom surface of the frame has begun to exfoliate. This is a difficult location to inspect, since it is under the cargo floor and below the flange of the frame.

Figure 27-18(b) is the view of the starboard side of the frame. As may be inferred, exfoliation corrosion of the frame had been discovered previously, and following (any) remedial actions the frame was liberally covered with sealant. This prevented any later assessment of ongoing corrosion and the integrity of the frame. In fact, the area suffered significant further damage: large pieces of the frame could be pulled out from below, although the sealant was in good condition.



(a) View of area below cargo floor at fuselage frame, PORT.



(b) View of area below cargo floor at fuselage frame, STBD.

Figure 27-18: Views of Exfoliated Frame Treated with Sealant.

27.2.5.4 Other Problems with Sealants

Maintenance procedures for corrosion damage removal end with the requirement that surface protective coatings be re-applied to the cleaned area (wash primer, primer and possibly paint). There is no mention of encasing the area in sealant. Besides the problems illustrated in Figure 27-16 – Figure 27-18, the sealant would also act as a barrier thus preventing any benefit from CPC applications.

REPAIRING CORROSION DAMAGE

On the other hand, a sealant layer is required to be between the inner and outer fuselage skins in order to prevent fretting and achieve pressurization requirements. Care must be taken in applying a thin even layer (recommended 0.02 inch (0.5 mm) thick) otherwise the joined sheets may be deformed by any excess sealant, see Figure 27-19 and Figure 27-20. This deformation will confuse subsequent exterior visual inspections for corrosion pillowing unless the repairs are documented and subsequently referred to before re-inspection.

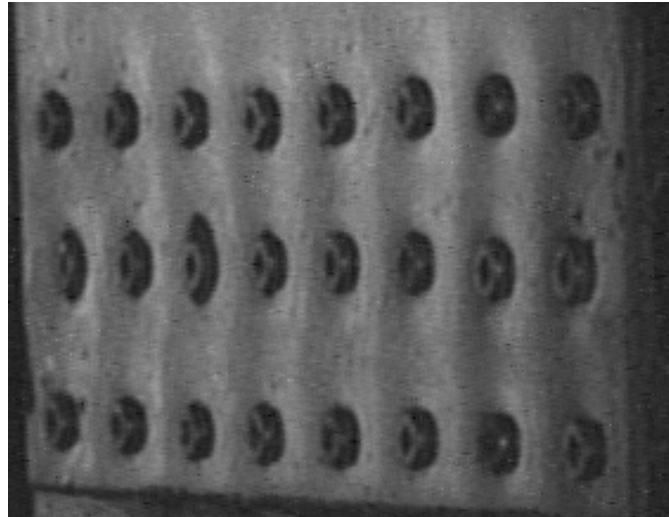


Figure 27-19: Surface Deformations from Excess Sealant in Laboratory Test Lap Joint (Non-Aerospace Fasteners).



Figure 27-20: Surface Deformations from Excess Sealant in Repaired On-Aircraft Lap Joint.

27.2.6 Issues Related to New Materials and Techniques

Standard practices of material removal and replacement/reinforcement have not changed for many years, but they will have to be modified and augmented owing to the growing acceptance of bonded repairs and the substitution of composites and fiber-metal laminates for traditional patching materials.

Surface preparation is the key to successful and enduring bonding of new surfaces and will be even more of a challenge with corroded surfaces. Composite patch faying surface and edge conditions will have heightened importance because they must remain sealed and galvanically insulated from the metallic substrate.

27.2.6.1 Composite Patching

The Graphite Epoxy (Gr/Ep) framed / aluminum skinned structure shown in Figure 27-21 had the standard glass fiber insulating layer for galvanic corrosion protection. There was also a fillet seal to prevent moisture entering from the outside. However, internal corrosion took place, basically because the edge of the Gr/Ep spar was not sealed, i.e., the glass fiber layer was not wrapped around the trimmed Gr/Ep edge. The corrosion mechanism is as follows: although there was no direct contact between the graphite and aluminum, moisture accumulated internally and bridged between the ends of the graphite fibers and any scratches through the protective coatings on the aluminum skin, thereby completing the electrical circuit.

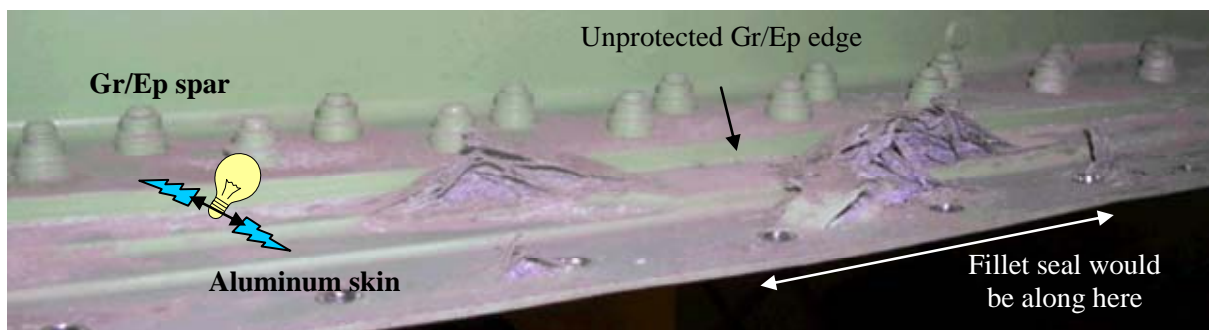


Figure 27-21: Graphite to Aluminum Connection Produces Corrosion.

The lessons are that:

- a) Any graphite fiber patch repairs on metallic surfaces would have to be similarly insulated and edge sealed to prevent similar occurrences of corrosion; and
- b) Routine inspections would have to include condition assessments of these features of the repairs.

27.2.6.2 Fiber-Metal Laminates

Manufacturers are looking to optimize structural weight. Lighter materials such as Glare® sheet material are being employed as replacements for aluminum sheet. Glare is a fiber-metal laminate, whereby thin sheets of aluminum are bonded to layers of glass fibers with an adhesive. Glare panels can be manufactured to large dimensions, and are used in the Airbus A380.

Glare is considered to be resistant to corrosion because the damage should penetrate only the outer aluminum layer and then stop at the adjacent fiber/epoxy layer. However, once damaged, the outer surface will become an aerodynamic smoothness issue and someone will try to clean this up, also for cosmetic reasons, see Figure 27-22.



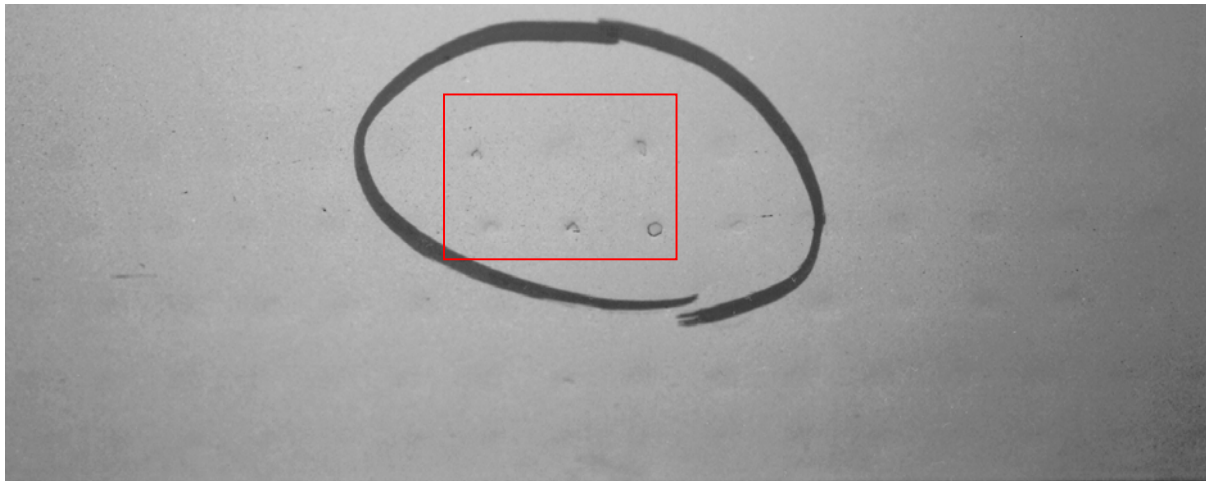
Figure 27-22: Corrosion Damage on Outer Surface of Glare Lap Joint.

Corrosion repair on the outer aluminum surfaces will require great care (no power tools!) because the metal layers are very thin, typically only 0.016 inch (0.4 mm). With such thin aluminum layers there is an increased possibility of damaging the thin fiber/epoxy layer. Epoxies will absorb moisture over time, and if the outer surface is not resealed the adhesive bond will eventually degrade and the next aluminum layer will be corroded. The protective coating systems applied to the surfaces and edges of Glare panels will have to be carefully maintained to prevent corrosion initiation.

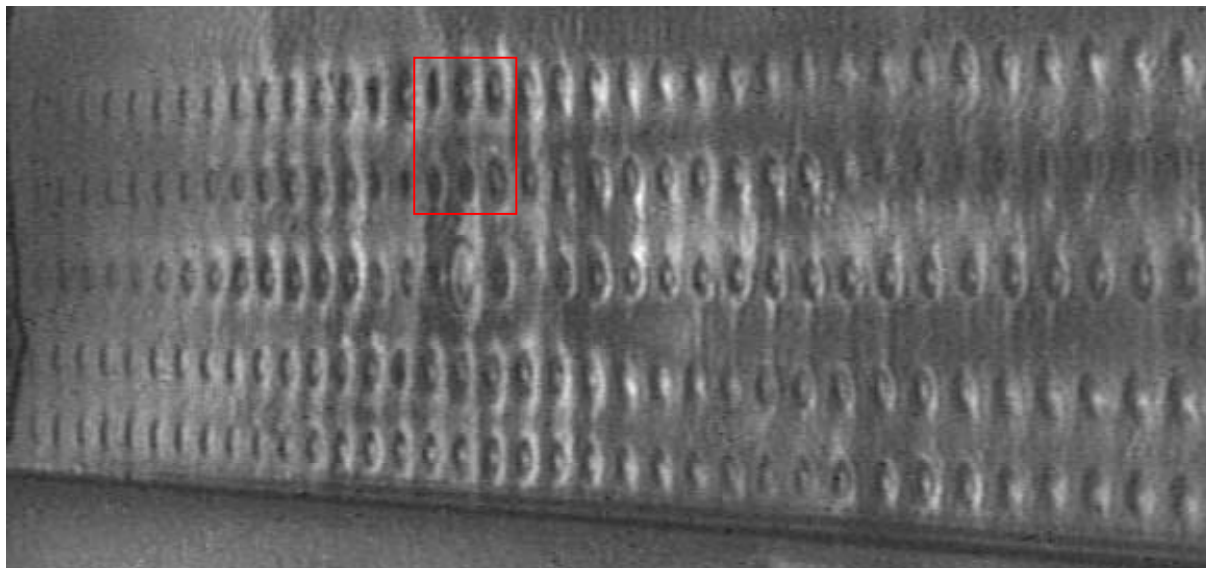
27.2.6.3 Welding

In the past, spot welding has been used (B707, KC-135 and Dassault Falcon jet) to mechanically fasten fuselage structures. Spot welding has a poor reputation – indeed, until recently any kind of welding in aluminum alloy aircraft structures was generally considered less than desirable.

In corrosion situations spot-welded structures fail differently to riveted ones. Owing to pillowing forces, cracks occur in the spot welds and grow towards the surface. The corroded and cracked areas may not be easily visible, even with enhanced techniques such as DAIS, Figure 27-23(b), until the cracks have reached the surface and gone on to crack the paint, see Figure 27-23(a). Dye penetrant or magnetic particle inspections are required to detect the surface-breaking cracks in their early stages. Besides corrosion clean-up, if feasible and necessary, repairs are made by drilling out the cracked spot welds and installing rivets.



(a) Normal view. Cracked paint aids visual detection.



(b) DAIS view shows only subtle difference between normal deformation and corrosion pillowing.

Figure 27-23: Corroded KC-135 Spot Welded Lap Joint with 4 Fractured Welds (Inside Red Boxes).

27.2.6.4 Friction-Stir Welding (FSW)

FSW is beginning to replace traditional mechanically fastened constructions especially for fuselage stringers. FSW will enable significant reduction in aircraft assembly time and may replace the installation of thousands of rivets. As an example; the use of FSW will replace 60% of the rivets that would have been required on major assemblies of the Eclipse 500 jet including the cabin, aft fuselage, wings and engine mounts.

Figure 27-24 shows a development FSW stringer to skin joint. Unlike a riveted joint FSW joining cannot tolerate traditional protective coatings already being in place. Any coatings and sealants will have to be applied to the skin, stringer and joint edges after the weld is formed. By incorporating intermittent non-welded areas the joint would allow the egress of any moisture that accumulated between the stringer and skin.

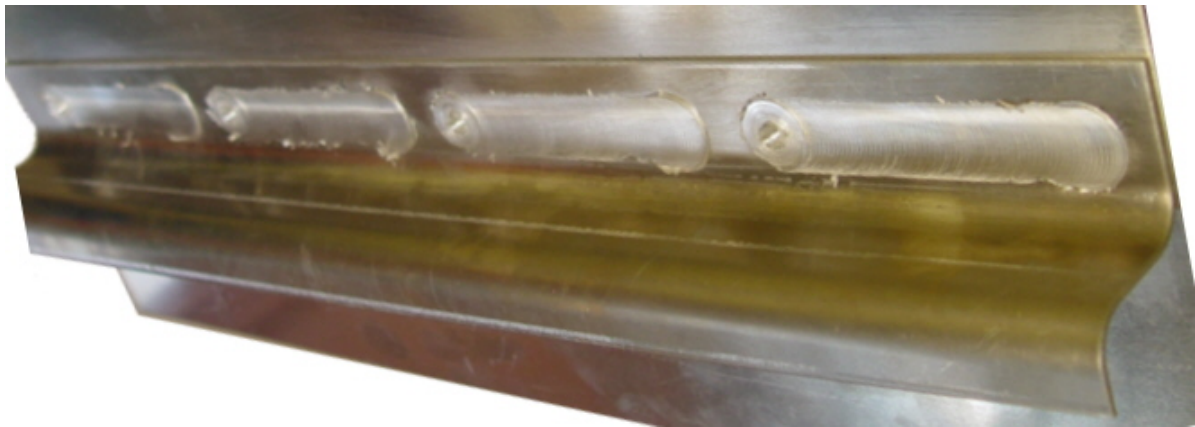
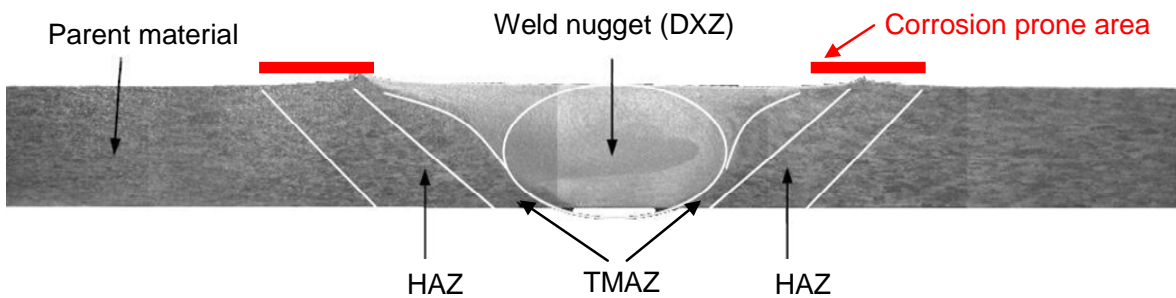


Figure 27-24: Friction Stir Welded Stringer and Skin.

A friction-stir weld is typically characterized as being comprised of three primary zones: the Heat-Affected Zone (HAZ), the Thermomechanically Affected Zone (TMAZ), and the Dynamically Recrystallised Zone (DXZ) or weld nugget. Tensile failure in transverse tensile tests most often occurs within the HAZ or the section between the HAZ and the TMAZ. Due to the change in precipitate morphology, this region is also generally susceptible to corrosion (red lines in Figure 27-25). One way to potentially improve the resulting corrosion properties is through post-weld heat ageing treatments. Another would be to coat the susceptible surface area with another, more resistant, alloy.



(a) Cross section through joint identifying regions of the weld zone.



(b) Outer surface showing exfoliation corrosion (ASTM G-34).

Figure 27-25: FSW Joint Structure and Corrosion Damage.

The main concerns that will require additional study and testing of FSW are currently related to corrosion properties, damage tolerance properties (fracture toughness), residual stresses and the long-term stability of the joints. With respect to corrosion maintenance, simply grinding to remove the corrosion will not end

the problem. As mentioned above, it may be possible to improve the corrosion resistance of susceptible areas by re-ageing or coating following corrosion removal, although it would obviously be better and easier to use these options on new structure. On-aircraft repairs will have to be done using riveted aluminum patches, since field repair FSW will not be possible.

27.2.6.5 Laser Welding

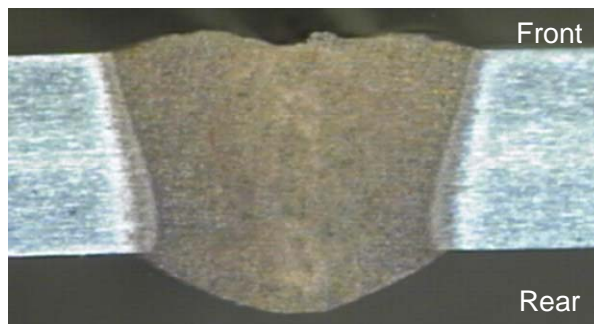
A development laser welded skin butt joint of two equal thickness sheets is shown in Figure 27-26.



(a) Front surface.



(b) Rear surface.



(c) Cross-section.

Figure 27-26: Laser Welded Skin Butt Joint.

Laser welding may eliminate lap joints by enabling butt welds. As with FSW, there may corrosion-prone areas adjacent to the laser weld, owing to microstructural differences relative to the parent material. The welds are quite narrow, and early detection of corrosion and fatigue damage will therefore require the use of sophisticated inspection equipment. Repairs will have to be done using riveted aluminum patches, since field repair laser welding will not be possible.

27.3 CORROSION TEARDOWN METHODS

A teardown is complete disassembly of a structure in a controlled, stepwise manner that allows detailed intermittent inspections. It is necessary to know and understand the steps to be followed, and also the most

suitable inspection techniques, in order to obtain the desired information before it is lost or destroyed by the disassembly process. The real value of a technically rigorous teardown is to validate the Non-Destructive Inspections (NDI) and to provide information to aid in residual strength assessment. Sample selection for teardowns requires knowledge of the problem areas and can be aided by the damage history. Much of this information can be acquired from surveying the “Service Difficulty Reports, Notice of Proposed Rule Making and Airworthiness Directives”. These can also be useful in planning the teardowns and inspections of candidate structures. In addition, some information for sample selection may be obtainable from maintenance records, if available.

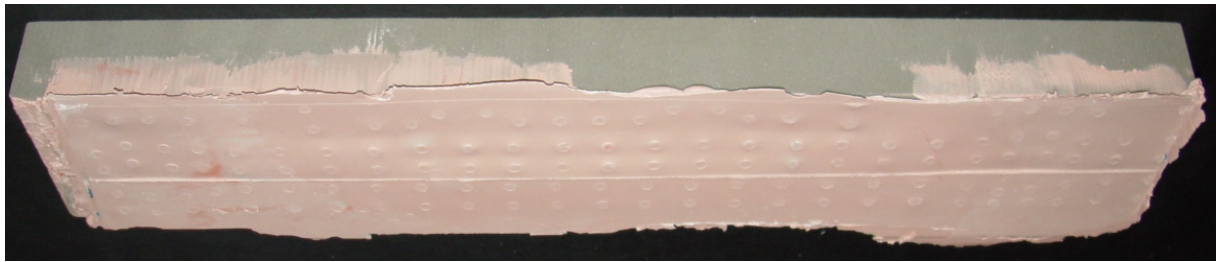
Once samples have been selected, removing them from the overall structure without additional (mechanical) damage requires suitable support equipment and skilled operators.

27.3.1 Pre-Teardown

27.3.1.1 Initial Assessment and Records

Typical means of documenting the condition of a structure are photographic records and written descriptions from initial close visual inspections. Recent advances in the precision and portability of 3-D laser measuring systems indicate their potential to quickly add metrics to the documentation, thereby enabling virtual replicas of the sample surfaces.

Physical replicas of the entire sample surfaces are impractical, and measurement data would still have to be collected. Hence surface replication is done on a smaller scale, for example parts of lap joints. Both rigid and flexible (but dimensionally stable) replicas can be, and have been, made. These provide surface topography records, e.g., Figure 27-27, which are available for investigation after teardown. For example, after disassembly it might be found useful to relate corrosion-induced pillowing (a surface topography effect) directly to internal corrosion product accumulation and any permanent deformation of the skin material.



(a) Surface replica of joint discussed in Post Teardown (Figure 27-38 – Figure 27-40).



(b) Replica of a replica recreates surface for further analysis.

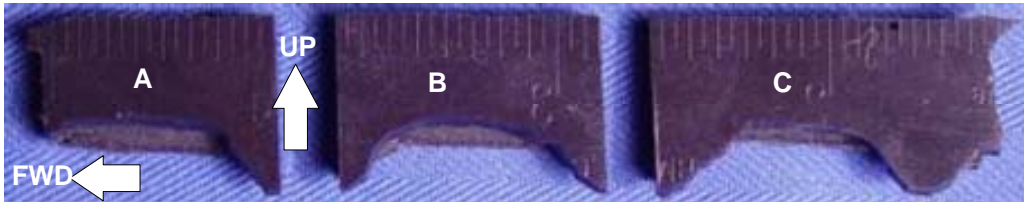
Figure 27-27: Replicas on Rigid Foam Backing of Damaged Fuselage Joints.

Some samples may have accessible fracture surfaces before teardown. In such cases replicas of the fracture surfaces can be made, or indeed have to be made, since sometimes it is not allowed to cut out and examine the originals if they are part of an accident investigation. Also, using replicas for detailed investigation avoids sectioning and mounting the originals for Optical and Scanning Electron Microscope (SEM) fractography. Depending on the results, which might be compromised by resolution limitations and artifacts from the replication process, one can still decide to examine the original fracture surfaces. (This will obviously be necessary if metallographic cross-sections are required.) Figure 27-28 provides an example of a fracture surface replica, its sectioning for SEM investigation, and details from this investigation.

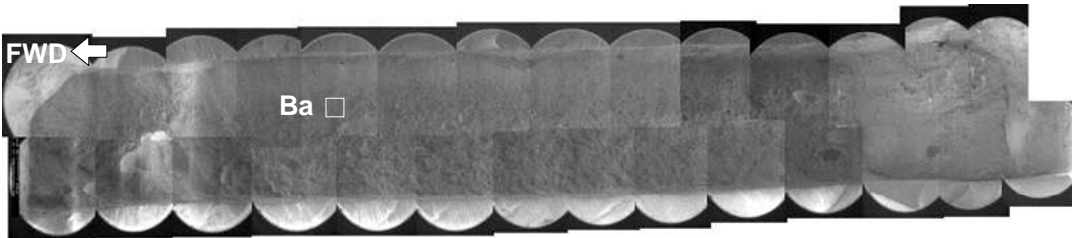
REPAIRING CORROSION DAMAGE



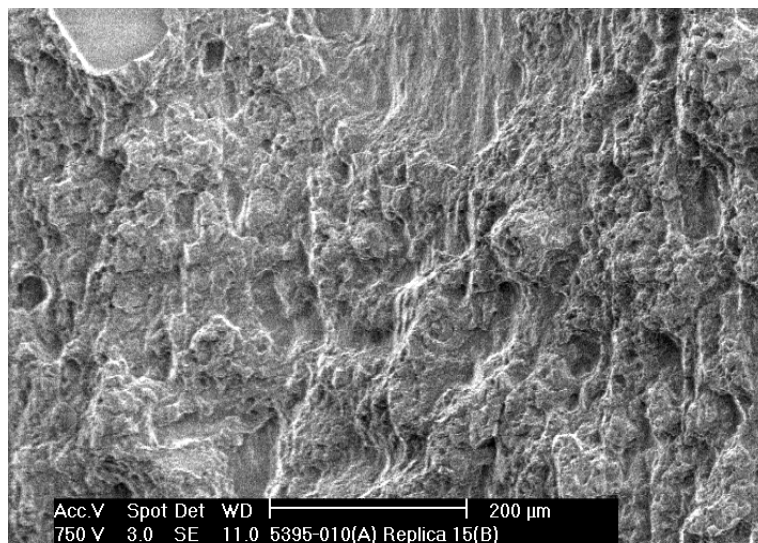
(a) Side view of replica from a fractured skin edge showing fracture surface.



(b) Skin fracture replica sectioned to fit into SEM.



(c) SEM image montage for replica section B. Note selected site Ba.



(d) SEM image of fracture surface at site Ba from failed fuselage skin replica B.

Figure 27-28: Fracture Surface Replica Analysis.

27.3.1.2 Paint and Sealant Removal

Paint and primer systems are removed either by chemical or mechanical means. Chemical strippers have been reformulated to make them more environmentally friendly. In some cases this results in lower effectiveness and increased time and effort to completely remove coatings, especially if they are multi-layered.

Dry particle blast stripping systems have advantages with respect to environmental and health considerations, and also layer by layer removal control. They are typically restricted on metallic materials to sheet greater than 0.032 inch thick (0.8 mm) and must be closely monitored. Repeat applications may be restricted to exclude damaging the surface. Sealants may mask corrosion damage and their presence will interfere with NDI inspections. Sealants are best removed by a combination of mechanical and chemical stripping. After most of the sealant has been removed mechanically, the remainder is removed by chemical softening and final mechanical removal with non-marring tools. Air-assisted hand tools have been developed to expedite bulk and final mechanical removal without damaging the substrate. These tools are especially useful for stripping sealants from inside wing fuel tanks.

27.3.1.3 Alloys and Coatings

A small sample of metallic material may be excised and used to verify the alloy and determine the presence of a protective coating (oxide or metal). This sample may also show whether the coating has deteriorated owing to mechanical damage caused by polishing or previous paint system removal.

There may be issues regarding the protective coatings on rivets, depending on their manufacture and age. For example, Alodine coated rivets have sometimes been chosen instead of anodized rivets, owing to improved electrical contact during lightning strikes. However, Alodine coatings have given paint adhesion problems (“rivet rash”). They have also been implicated in degrading NDI, specifically the reliability of sliding probe Eddy Current (EC) inspection for cracks at fastener holes [7],[8],[9]. This is because the conductivity of Alodine coated rivets could be sufficient to mask some cracks. In the light of these issues it may be prudent, during teardown, to remove some rivets with the additional goal of determining the type of coating used, since rivet types may have been mixed due to repair actions.

Corrosion Prevention Compounds (CPCs) are applied internally to large areas of ageing aircraft structures. Inspections cannot be completed with these coatings in place because they accumulate dirt and debris and obscure direct viewing of the surfaces. These will often have had multiple applications of CPCs, which bind the dirt and debris in place, and the CPCs become increasingly difficult to remove as they harden with age. Another disadvantage is that the dirt-collecting nature of CPCs discolors white-painted bilges, see Figure 27-29. This discoloration reduces the visibility of corroded areas.



(a) White paint over primer (corrosion circled).



(b) White paint coated with CPC.

Figure 27-29: Bilge Areas Below Cargo Floor (Floor Panels and Insulation Blankets Removed).

27.3.1.4 Non-Destructive Inspection

Whenever possible, reference standards for setting up and calibrating NDI techniques are made using the same alloys and material thicknesses as those in the structures to be inspected. However, this is not necessarily sufficient. A typical example is the mechanical removal of material to simulate thickness losses owing to corrosion of one or more layers of a built-up structure. Machining cannot represent the rough topography of a corrosion-damaged surface, and this may lead to difficulties in the detection and quantification of damage to the specimen. Ideally, reference standards should be developed with surface topography representative of corrosion damage and also with the inclusion of corrosion products and associated pillowing or exfoliation, if present in the specimen. This is no easy task, however.

NDI techniques are selected for their applicability to the materials and structures involved and the suspected damage. In contrast to the spot inspections made in the field on operational aircraft, samples subject to complete teardown can be inspected using automated scanning systems to produce complete Eddy Current (EC), Ultrasonic (UT) or similar maps of the parts or areas of interest. In addition, the samples can be inspected with new techniques, to aid in their development and add the results to the NDI knowledge base.

Enhanced optical systems can provide increased sensitivity for damage assessment (2 – 3 % thickness loss) and act as a control for the traditionally manual visual inspection process. For example, laser topographical mapping can quickly capture the surface deformations and, if the entire part is scanned, produce accurate 3-D models.

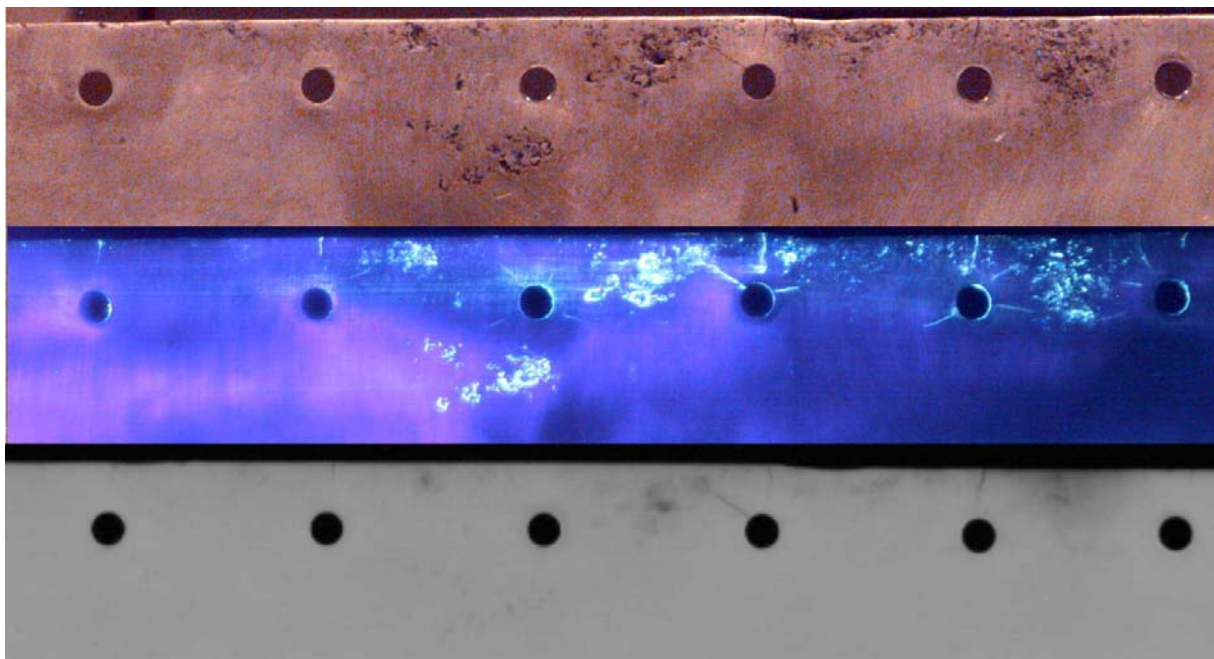
Eddy current techniques should be tolerant of air gaps when applied to multi-layer structures with suspected corrosion damage. Frequency mixing is one technique that removes the effects of any spaces between layers.

Through-transmission UT C-scan inspection can be used if samples can tolerate immersion or if a couplant squirter system is available. This technique is used primarily on wing skin samples to determine the exfoliation corrosion damage area and depth. If a sample comes from a wet wing design, the internal sealant must be removed because it attenuates the signal and may mask any corrosion damage.

X-ray inspection is not typically used for corrosion detection. However, the pillowing forces generated by corrosion in multi-layer structures may lead to tensile forces sufficient to nucleate cracks, and these can be detectable by X-rays. Both fatigue and stress corrosion cracks can occur in some structures, so more detailed investigation (part of the teardown) is often needed.

Dye penetrant inspections for cracks are affected by the presence of paint systems and sealants. Although dye penetrant is often used on in-service components and structures, the paint systems and sealants on samples must be removed. However, mechanical removal of surface corrosion products should be avoided, since the cracks may become obscured by being partially filled-in.

Figure 27-30 is an illustration of crack detection in a chemically cleaned corroded skin that contained pillowing cracks. These cracks were small and non-surface-breaking, i.e., they did not reach the outer surface of the skin. Careful disassembly and cleaning allowed these small cracks to be detected, notably by dye penetrant. Mechanical removal of corrosion products would probably have reduced the number of cracks detected by this technique.



Top: Optical, Middle: Dye penetrant, Bottom: X-ray.

Figure 27-30: Three Views of Inner Surface of a Chemically Cleaned Corroded Skin Exhibiting Pillowing Cracks.

Non-surface-breaking cracks like those illustrated in Figure 27-30 have been predicted by Finite Element Modeling (FEM) of fuselage joint designs. These radiating cracks are caused by tensile forces induced in

the skin faying surfaces when sufficient corrosion products build up between them, causing pillowing. The cracks initiate outside the fastener holes and then grow both towards and away from the holes.

27.3.2 Teardown

As stated at the beginning of this section, a teardown is disassembly in a controlled, stepwise manner. Before disassembly all measurements, documentation and non-destructive inspections that depend on, or benefit from, intact specimens should have been carried out. It is necessary to know and understand the disassembly steps to be followed, and also the most suitable inspection techniques, in order to obtain the desired information before it is lost or destroyed by the ongoing disassembly process.

27.3.2.1 Fasteners

Teardown begins with the careful removal of fasteners and visually examining their condition before and after cleaning. This can provide very useful information, because damaged fasteners on an aircraft are usually noticed only when they are severely corroded or have fallen out. Furthermore, in-service replacement typically results in damaged fasteners being destroyed by drilling out (rivets) or being discarded after disassembly (nuts and bolts).

The condition and integrity of mechanical fasteners deserves more attention. Corrosion or fretting damage on rivets, bolts and nuts controls and directs their replacement, but the source of their degradation should also be sought. For example, rivets have been found that at first sight showed corrosion on their surfaces, but with the corrosion cleaned off they were seen to have cracking problems as well, see Figure 27-31. This damage was detected only because the prescribed teardown required the upset heads to be machined off and the rivets pressed out instead of being drilled out.

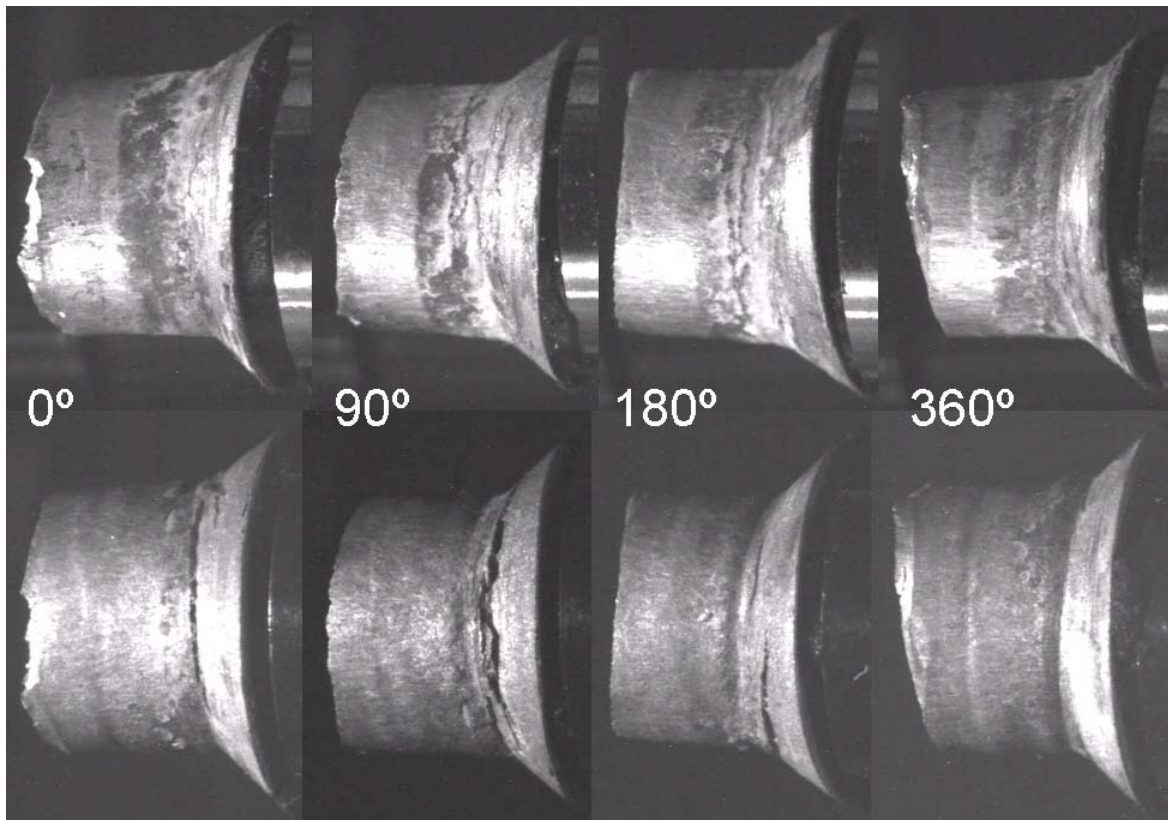


Figure 27-31: Corrosion Pillowing Induced Cracks in a Rivet (Top: As removed; Bottom: Cleaned).

27.3.2.2 Adhesives and Sealants

Structural adhesives or gap-filling sealants are often applied to the faying surfaces of fuselage skin joints. Disassembly requires care since the parts may be damaged and deformed by the tools and forces needed to wedge the layers apart. All traces of the adhesives or sealants must be removed before the exposed surfaces can be examined for damage. This removal is best accomplished by mechanically removing the bulk of the material followed by chemical dissolution and final removal with non-marring tools, as mentioned earlier. Mechanical actions that might contact the surfaces should be avoided to prevent metal smearing and obscuring any cracks from detection.

27.3.2.3 Corrosion Removal

In a teardown for corrosion damage the steps are:

- a) Document the total thickness loss in the structural sample;
- b) Validate the results of NDI techniques; and
- c) Prepare the remaining base material for detailed analysis (coupon selection and removal).

The method of corrosion product removal should be chosen to ensure that no additional damage is done to the structure. This is especially true if cracks are to remain undisturbed. It has been proven that corrosion product removal by chemical dissolution is greatly assisted by ultrasonic vibration in an immersion tank, for example Figure 27-32.



Ultra Kleen is a mild cleaning solution designed for cleaning corrosion products off aluminum. The solution has the following composition:

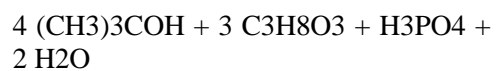


Figure 27-32: Ultrasonic Immersion Corrosion Cleaning Tank.

Rather than filling the tank with the chemical cleaning solution, the samples are placed in solution-filled bags which are then suspended in water in the tank. This minimizes the amount of cleaning solution required. Various chemical solutions can be used. To verify the selected chemical removal process, long exposure tests are required to demonstrate that no damage is done to the remaining base material, see Figure 27-33.

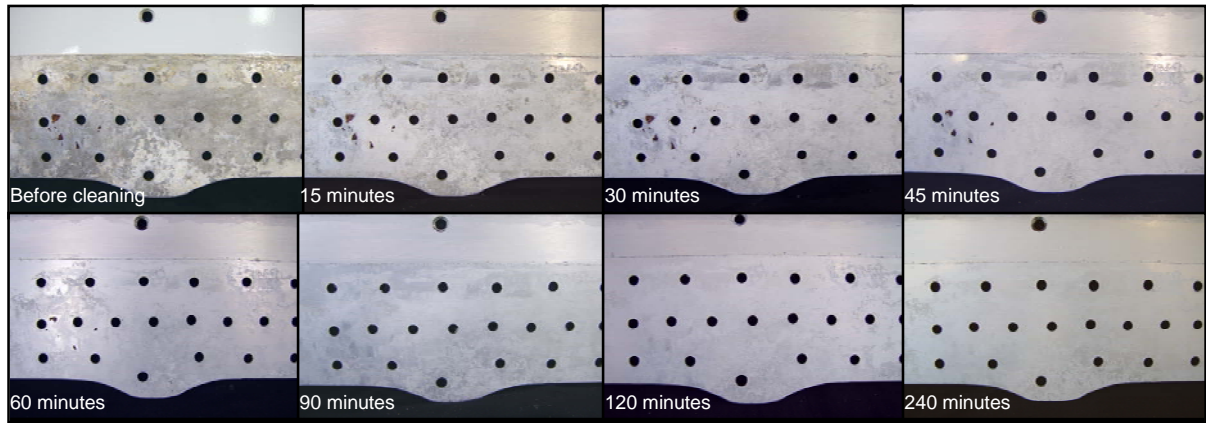


Figure 27-33: Views of Skin Surface Before and During Long Exposure Chemical/Ultrasonic Corrosion Cleaning for Corrosion Removal.

27.3.2.4 Thickness Loss

Figure 27-34 is an example of corrosion-induced pillowing from the teardown investigation of a lap joint outer skin. The pillowing was made visible by the D Sight Aircraft Inspection System (DAIS) [10], which enables enhanced visual inspections of intact joints. It was known that the joint had undergone maintenance because of corrosion. This maintenance had included removing the original flush-head rivets and re-installing with protruding-head rivets.

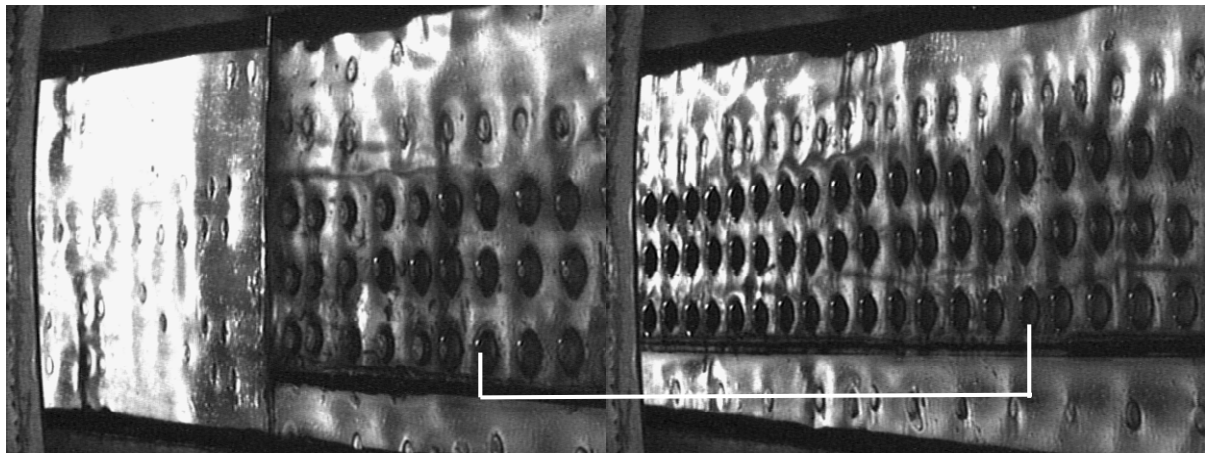


Figure 27-34: DAIS Lap Inspections on the Intact Joint (White Line Shows Specimen in Figure 27-35).

The protruding-head rivets made it impossible to inspect the intact joint by eddy current NDI. Consequently the rivets were drilled out to separate the outer and inner skins. Figure 27-35 shows the rear surface of the outer skin. The black and gray areas are the remains of faying surface sealant from the prior maintenance, which had also included applying a primer. Significantly, there was no visual evidence of corrosion at the time of the teardown. This means that the pillowing observed in the DAIS inspection, Figure 27-34, was due to corrosion product accumulation up until the maintenance action, and that the subsequent visible persistence of pillowing was due to permanent deformation of the skin.



Figure 27-35: Rear Surface of Outer Skin.

The outer skin inner surface shown in Figure 27-35 was cleaned chemically to remove the sealant and primer. This was followed by X-radiography that included a ramped master calibration tool to enable thickness measurements. The NRC/IAR NDI Analysis™ software was used to obtain the calibration and skin thickness measurements from the digitized image file of the X-ray film, Figure 27-36.

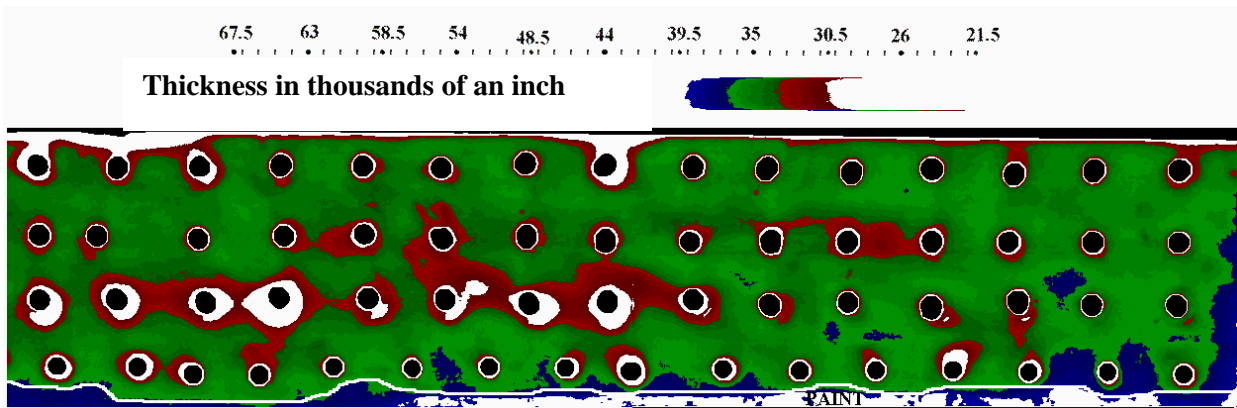


Figure 27-36: X-Ray Thickness Loss Map (Calibration Ramp at Top).

Figure 27-37 shows mechanically made thickness measurements taken nominally midway between fastener holes and also where thinning was beyond the lower limit of the X-ray calibration. The maximum thickness was 0.038 inch. The minimum thickness between fastener holes was 0.030 inch [24% loss], and the minimum thickness at the free edge was 0.026 inch [34% loss]. These losses and the pattern of losses, especially around fastener holes, compromised the skin and would have made it more prone to fatigue damage.

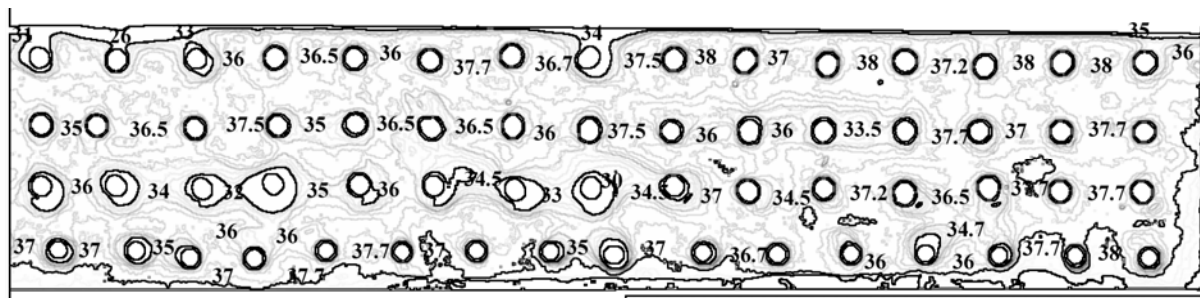


Figure 27-37: Thickness Measurement Map.

27.3.3 Post-Teardown

Acquisition, inspection and teardown information must be recorded to document the investigative methods employed. The information that is collected is rarely in a convenient format, either for archiving or presentation. A searchable database makes the job easier. It facilitates the recording of image and text information on the history, metrics, condition and teardown findings for each specimen. An example is the NRC/IAR NDI Analysis™ software used for X-radiography.

A disciplined approach is required to fully exploit the opportunities for damage assessment. A methodology is needed that accounts for the capability of each step in the teardown process and defines the sequence of steps to ensure that information is not inadvertently destroyed. The teardown process should be governed by a set of decisions and authorization procedures that include knowledge of the consequences for not following the prescribed order of events. Finally, all this must be fully understood by everyone involved in the teardown process.

27.3.3.1 When It All Goes Wrong – C141 “Corroded” Joint

Field inspection of a C-141 airframe located classic visual evidence for corrosion induced pillowing at the joint on Stringer 32 Right, see the left-hand photograph in Figure 27-38. The skin was buckled between the steel fasteners (Hi-Lok® HL19, 100°, Reduced Flush, shear bolts), and some fastener heads were being pulled through the outer skin. Furthermore, this damage was at a known corrosion site, below the sewage access port for the hospitality pallet. The right-hand photograph in Figure 27-38 shows that sealant had been added to the original protection scheme on the inner surface, indicating maintenance for corrosion damage.



Figure 27-38: A Visual Inspection of the Exterior Surface Indicated Corrosion Pillowing (left) While the Interior Showed Sealant Added (red) Indicating Maintenance for Same (right).

Laboratory DAIS and UT inspections gave the results shown in Figure 27-39. The DAIS inspection indicates corrosion-induced pillowing, and the UT inspection apparently indicates corrosion product build-up along two fastener rows below the access port. However, teardown revealed something totally different. Figure 27-40 shows that a shim had been placed along one bolt row, presumably during maintenance. Tightening of the steel bolts caused the outer skin to buckle, and where it was unsupported by the shim the fastener heads tended to be pulled through the skin. The resulting incomplete clamp-up confused the UT inspection, since air gaps were interpreted as corrosion build-up.

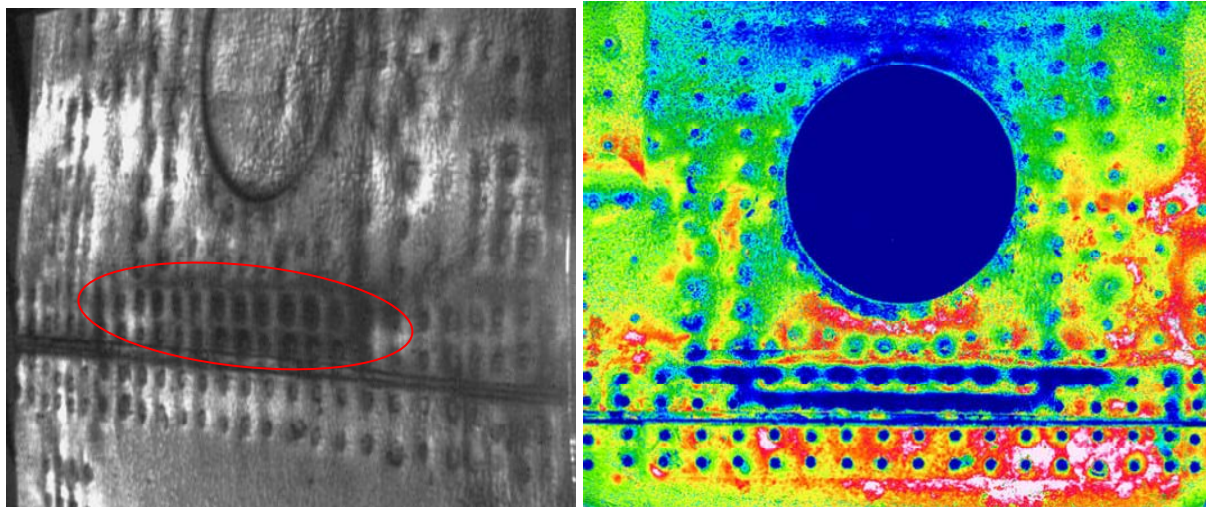


Figure 27-39: Laboratory Inspections Preceding Teardown Both DAIS (left) and UT (right) Indicated Damage in the Upper Skin of the Butt Joint.



Figure 27-40: A 0.080 Inch (2.03 mm) Thick Shim In-Situ (left, circled), Enlarged (right).

27.4 CORRODED COMPONENTS AVAILABILITY

When corrosion is discovered on airframe components, it is usually assessed, more or less quantitatively, by Non-Destructive Inspection (NDI). Ideally this should enable well-founded decisions about repairing or replacing the affected parts. If repair appears to be possible, e.g., by attaching replacement materials (inserts) and/or reinforcements (doublers), the first maintenance action is to remove the damage mechanically. If the damage is assessed or turns out to be too severe, the components are removed and disposed of.

These customary procedures for repair or replacement make it virtually impossible to investigate and collect examples of as-found corrosion damage. This is unfortunate, since such examples can be valuable for:

- a) Verifying NDI techniques, thereby facilitating decisions about repairs or replacements; and
- b) Determining the underlying causes of corrosion.

The non-optimal alternative is to do corrosion tests on simulated structural details in artificial environments.

There is an additional problem. As aircraft fleets age there can be, and have been, situations where the original materials for some components have gone out of production, therefore being no longer available

REPAIRING CORROSION DAMAGE

for repair or replacement, or for serving as baselines for corrosion test evaluations of substitute materials. Collected examples of pristine original structures can provide these baselines.

Some research organizations, operators and maintenance contractors have recognized the above-mentioned usefulness of collecting examples of typical aircraft structures. By doing so, they benefit from having assemblies of the original materials, surface treatments, protective coatings, sealants, paint systems and fasteners.

If possible, both naturally damaged and pristine structures are collected. The usual sources for these original components have been wrecks and airframes Withdrawn From Use (WFU), see Figure 27-41 and Figure 27-42. Operators of new designs have been known to purchase additional airframes intended as immediate sources of spare parts, but these can also serve as sources for materials and assemblies.

A chance phone call resulted in a rush across three states to capture some of the last available B707 wings, made with discontinued 7178-T6, just days before they would have been lost to the scrap metal smelter.



Figure 27-41: Aircraft Graveyards have been Valuable Sources of Corrosion Samples.



Figure 27-42: Cut-Outs Show where Fuselage Structure was Harvested from WFU Airframes.

Note from Figure 27-42 that these WFU aircraft are parked in desert environments. Actually, deserts are *not* the best places to store aircraft that have been in service. It has been assumed that the arid climate minimizes corrosion activity. This may be true for the exterior surfaces, but experience has shown that the closed-off internal environments still support corrosion processes, and the high daytime temperatures may well accelerate them. Consequently, desert storage areas have proven to be productive sources of examples of service and post-service corrosion, Figure 27-43 and Figure 27-44.



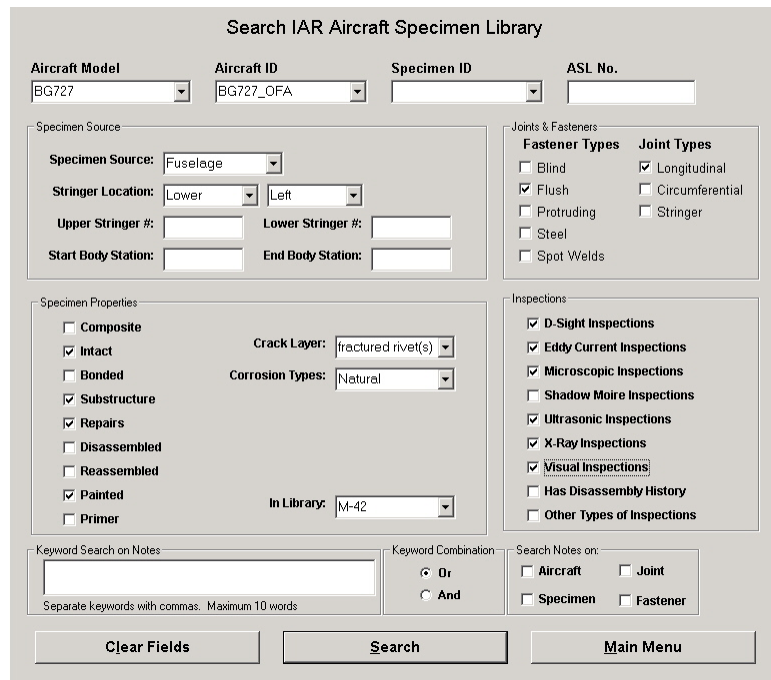
Figure 27-43: Stringer and Frame Corrosion in the Crown of a Stored Fuselage Due to Moisture Remaining in Insulation Blankets (Removed).



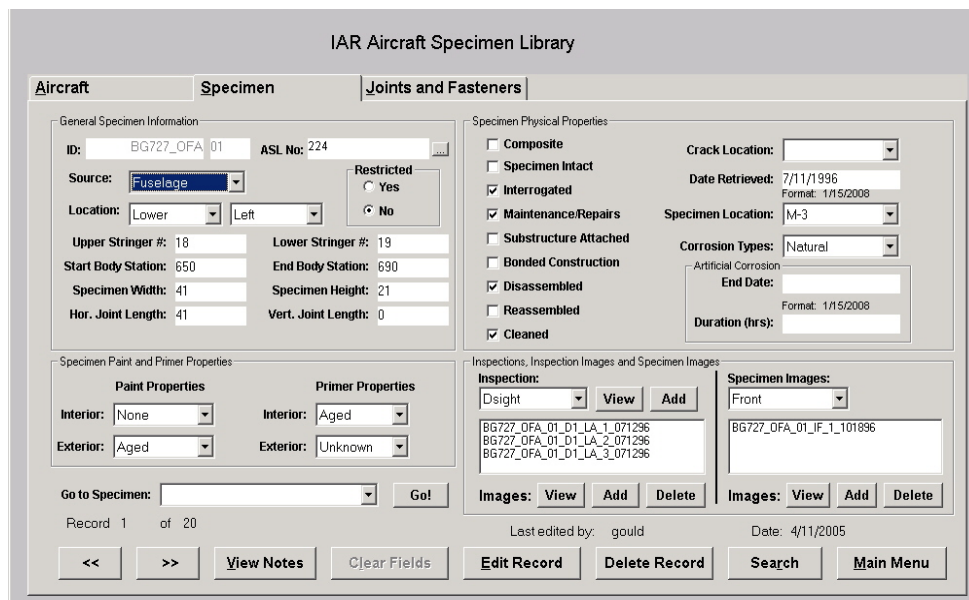
Figure 27-44: Lower Window Frame Corrosion Due to Moisture Accumulating Between Seal and Structure of Stored Airframe.

From nose to tail and top to bottom the materials, structural elements and assemblies of transport aircraft fuselages generally remain the same. The upper and lower wing skins are usually made from different alloys (7XXX upper skin, 2XXX lower skin) and they vary in thickness from root to tip. However, apart from these differences both fuselage and wing structures can be sampled for collection, i.e., it is not necessary to obtain entire airframes. Figure 27-42 illustrates that the samples can be relatively small.

Storage space is always an issue, especially when the use of collected samples is uncertain. Linking collections via databases could enable users to avoid a heavy storage burden, but still have the benefit of access to representative material, available when the need arises. Figure 27-45 shows details from a database set up by the NRC/IAR in Canada.



(a) Search pick-list has 27 parameters to choose from.



(b) Information on the parent aircraft, the condition of each specimen and detailed inspection results are all accessible through the database.

Figure 27-45: NRC/IAR Aircraft Specimen Library Database.

There are very few known collections of aircraft structure. Those that exist have been used successfully to support NDI equipment and technique verification, repair scheme development, damage characterization, and human factors studies. Figure 27-46 shows cut-outs where natural corrosion damage specimens have been extracted from a WFU aircraft wing. The labels show where even more specimens are to be harvested. Thus instead of disappearing into the “recycle-bin” the components and samples in these libraries continue to educate and serve their fleets.

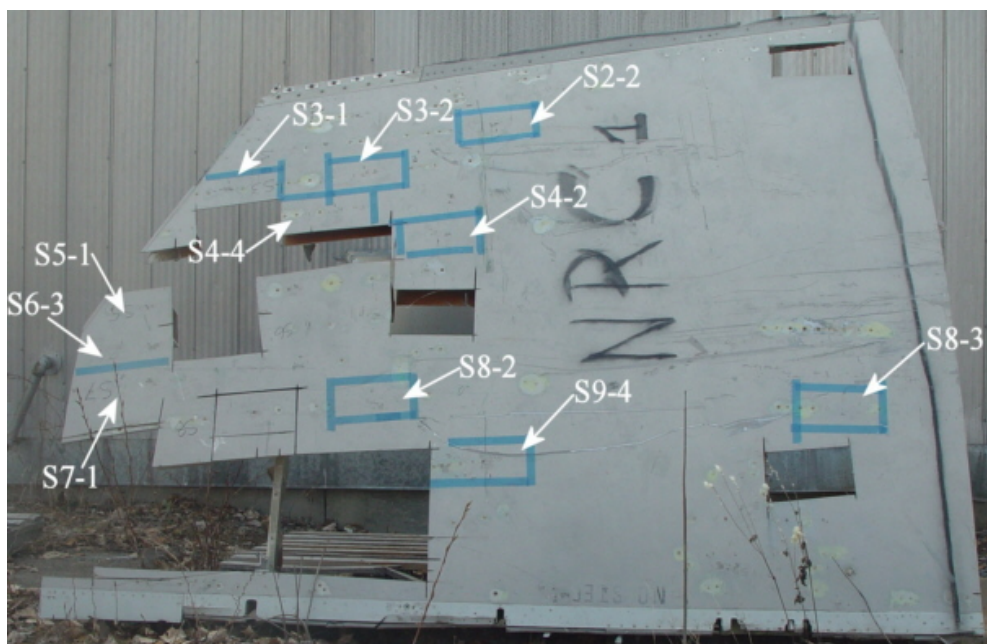


Figure 27-46: Upper Wing Section Being Harvested for Corroded and Undamaged Material.

27.5 REFERENCES

- [1] Thompson, J.G., "Subsurface Corrosion Detection in Aircraft Lap Splices Using a Dual Frequency Eddy Current Inspection Technique", *Material Evaluation*, Vol. 51, No.12, December 1993.
- [2] Boeing Service Bulletin 737-53A1039.
- [3] Blackshire, J., Buynak, C., Steffes, G. and Marshall, R., "Nondestructive Evaluation Through Aircraft Coatings: A State-of-the-Art Assessment", Air Force Research Laboratory, Materials and Manufacturing Directorate, Nondestructive Evaluation Branch, 9th Joint FAA/DoD/NASA Conference on Aging Aircraft, 6-9 March 2006.
- [4] Flight Standards Information Bulletin for Airworthiness (FSAW) FSAW 03-10B (Amended) Fuselage Skin "Scribe Mark" Damage on Boeing 737 Aircraft AMENDED 2004-31-03.
- [5] Bellinger, N.C., Komorowski, J.P. and Gould, R.W., "Corrosion Pillowing in Aircraft Fuselage Lap Joints", 46th AIAA/ASME/ASCE/AHS/ASC Structures, Structural Dynamics & Materials Conference, 19 April 2005.
- [6] Bellinger, N.C., Foland, T. and Carmody, D., "Structural Integrity Impacts of Aircraft Upper Wing Exfoliation Corrosion and Repair Configurations", Published in the Proceedings of the Seventh Joint DoD/FAA/NASA Conference on Aging Aircraft, New Orleans, LA, USA, September 2003.
- [7] Kollgaard, J., "Effect of Rivet Treatment", 7th Joint DoD/FAA/NASA Conference on Aging Aircraft, Session 28, September 2003.
- [8] Boeing, Environmental Technotes, Volume 8, No. 3, August 2003.
- [9] FAA supersedes AD 90-26-10 with AD 2006-24-02, effective 27 December 2006.

- [10] Bellinger, N.C., Komorowski, J.P. and Gould, R.W., "Corrosion Pillowing in Aircraft Fuselage Lap Joints", 46th AIAA/ASME/ASCE/AHS/ASC Structures, Structural Dynamics & Materials Conference, 19 April 2005.



REPORT DOCUMENTATION PAGE																					
1. Recipient's Reference	2. Originator's References	3. Further Reference	4. Security Classification of Document																		
	RTO-AG-AVT-140 AC/323(AVT-140)TP/346	ISBN 978-92-837-0125-5	UNCLASSIFIED/ UNLIMITED																		
5. Originator	Research and Technology Organisation North Atlantic Treaty Organisation BP 25, F-92201 Neuilly-sur-Seine Cedex, France																				
6. Title	Corrosion Fatigue and Environmentally Assisted Cracking in Aging Military Vehicles																				
7. Presented at/Sponsored by	This AGARDograph has been sponsored by the Applied Vehicle Technology Panel of RTO.																				
8. Author(s)/Editor(s)	Multiple		9. Date March 2011																		
10. Author's/Editor's Address	Multiple		11. Pages 434																		
12. Distribution Statement	There are no restrictions on the distribution of this document. Information about the availability of this and other RTO unclassified publications is given on the back cover.																				
13. Keywords/Descriptors	<table style="width: 100%; border: none;"> <tr> <td style="width: 33%;">Aging aircraft</td> <td style="width: 33%;">Crack nucleation</td> <td style="width: 33%;">Pillowing</td> </tr> <tr> <td>Cadmium replacement</td> <td>Environmentally assisted cracking</td> <td>Pitting</td> </tr> <tr> <td>Chromium replacement</td> <td>Exfoliation</td> <td>Retrogression</td> </tr> <tr> <td>Corrosion</td> <td>High strength steel</td> <td>Simulation</td> </tr> <tr> <td>Corrosion fatigue</td> <td>Hydrogen embrittlement</td> <td>Stress-Corrosion Cracking (SCC)</td> </tr> <tr> <td>Crack growth</td> <td>Modeling</td> <td>Wash optimization</td> </tr> </table>			Aging aircraft	Crack nucleation	Pillowing	Cadmium replacement	Environmentally assisted cracking	Pitting	Chromium replacement	Exfoliation	Retrogression	Corrosion	High strength steel	Simulation	Corrosion fatigue	Hydrogen embrittlement	Stress-Corrosion Cracking (SCC)	Crack growth	Modeling	Wash optimization
Aging aircraft	Crack nucleation	Pillowing																			
Cadmium replacement	Environmentally assisted cracking	Pitting																			
Chromium replacement	Exfoliation	Retrogression																			
Corrosion	High strength steel	Simulation																			
Corrosion fatigue	Hydrogen embrittlement	Stress-Corrosion Cracking (SCC)																			
Crack growth	Modeling	Wash optimization																			
14. Abstract	<p>This AGARDograph provides a comprehensive and updated state-of-the-art on corrosion fatigue and environmentally assisted cracking.</p> <p>The interest of the NATO community in this specific subject can be dated back some decades ago, as shown by the publication of the AGARDograph AG-278 issued in 1985, the "AGARD Corrosion Handbook Vol. 1 – Aircraft Corrosion: Causes and Case Histories", where this issue was also jointly covered with the many other aspects of aircraft corrosion.</p> <p>A long time, however, has elapsed since then and the whole scenario in which the military platforms are now operated and maintained, as well as the materials and the tools available, have completely changed. These changes have resulted in the generation of a new AGARDograph, fully devoted to this specific area – undoubtedly one of the most important among the corrosion-related phenomena; and whose consequences may seriously affect the reliability and the availability of military fleets.</p> <p>This report has collected the most relevant experiences within the NATO community, accumulated over the years, on how to deal with this never ending problem. It also offers useful tools in the new fields of the modeling and the simulation.</p>																				





BP 25

F-92201 NEUILLY-SUR-SEINE CEDEX • FRANCE
Télécopie 0(1)55.61.22.99 • E-mail mailbox@rta.nato.int



DIFFUSION DES PUBLICATIONS
RTO NON CLASSIFIEES

Les publications de l'AGARD et de la RTO peuvent parfois être obtenues auprès des centres nationaux de distribution indiqués ci-dessous. Si vous souhaitez recevoir toutes les publications de la RTO, ou simplement celles qui concernent certains Panels, vous pouvez demander d'être inclus soit à titre personnel, soit au nom de votre organisation, sur la liste d'envoi.

Les publications de la RTO et de l'AGARD sont également en vente auprès des agences de vente indiquées ci-dessous.

Les demandes de documents RTO ou AGARD doivent comporter la dénomination « RTO » ou « AGARD » selon le cas, suivi du numéro de série. Des informations analogues, telles que le titre et la date de publication sont souhaitables.

Si vous souhaitez recevoir une notification électronique de la disponibilité des rapports de la RTO au fur et à mesure de leur publication, vous pouvez consulter notre site Web (www.rto.nato.int) et vous abonner à ce service.

CENTRES DE DIFFUSION NATIONAUX

ALLEMAGNE

Streitkräfteamt / Abteilung III
Fachinformationszentrum der Bundeswehr (FIZBw)
Gorch-Fock-Straße 7, D-53229 Bonn

BELGIQUE

Royal High Institute for Defence – KHID/IRSD/RHID
Management of Scientific & Technological Research
for Defence, National RTO Coordinator
Royal Military Academy – Campus Renaissance
Renaissancelaan 30, 1000 Bruxelles

CANADA

DSIGRD2 – Bibliothécaire des ressources du savoir
R et D pour la défense Canada
Ministère de la Défense nationale
305, rue Rideau, 9^e étage
Ottawa, Ontario K1A 0K2

DANEMARK

Danish Acquisition and Logistics Organization (DALO)
Lautrupbjerg 1-5, 2750 Ballerup

ESPAGNE

SDG TECEN / DGAM
C/ Arturo Soria 289
Madrid 28033

ETATS-UNIS

NASA Center for AeroSpace Information (CASI)
7115 Standard Drive
Hanover, MD 21076-1320

FRANCE

O.N.E.R.A. (ISP)
29, Avenue de la Division Leclerc
BP 72, 92322 Châtillon Cedex

GRECE (Correspondant)

Defence Industry & Research General
Directorate, Research Directorate
Fakinos Base Camp, S.T.G. 1020
Holargos, Athens

HONGRIE

Hungarian Ministry of Defence
Development and Logistics Agency
P.O.B. 25
H-1885 Budapest

ITALIE

General Secretariat of Defence and
National Armaments Directorate
5th Department – Technological
Research
Via XX Settembre 123
00187 Roma

LUXEMBOURG

Voir Belgique

NORVEGE

Norwegian Defence Research
Establishment
Attn: Biblioteket
P.O. Box 25
NO-2007 Kjeller

PAYS-BAS

Royal Netherlands Military
Academy Library
P.O. Box 90.002
4800 PA Breda

POLOGNE

Centralna Biblioteka Wojskowa
ul. Ostrobramska 109
04-041 Warszawa

PORTUGAL

Estado Maior da Força Aérea
SDFA – Centro de Documentação
Alfragide
P-2720 Amadora

REPUBLIQUE TCHEQUE

LOM PRAHA s. p.
o. z. VTÚLaPVO
Mladoboleslavská 944
PO Box 18
197 21 Praha 9

ROUMANIE

Romanian National Distribution
Centre
Armaments Department
9-11, Drumul Taberei Street
Sector 6
061353, Bucharest

ROYAUME-UNI

Dstl Knowledge and Information
Services
Building 247
Porton Down
Salisbury SP4 0JQ

SLOVAQUIE

Akadémia ozbrojených síl gen.
M.R. Štefánika, Distribučné a
informačné stredisko RTO
Demänová 393, Liptovský Mikuláš 6
031 06

SLOVENIE

Ministry of Defence
Central Registry for EU and
NATO
Vojkova 55
1000 Ljubljana

TURQUIE

Milli Savunma Bakanlığı (MSB)
ARGE ve Teknoloji Dairesi
Başkanlığı
06650 Bakanlıklar
Ankara

AGENCES DE VENTE

NASA Center for AeroSpace Information (CASI)

7115 Standard Drive
Hanover, MD 21076-1320
ETATS-UNIS

The British Library Document Supply Centre

Boston Spa, Wetherby
West Yorkshire LS23 7BQ
ROYAUME-UNI

Canada Institute for Scientific and Technical Information (CISTI)

National Research Council Acquisitions
Montreal Road, Building M-55
Ottawa K1A 0S2, CANADA

Les demandes de documents RTO ou AGARD doivent comporter la dénomination « RTO » ou « AGARD » selon le cas, suivie du numéro de série (par exemple AGARD-AG-315). Des informations analogues, telles que le titre et la date de publication sont souhaitables. Des références bibliographiques complètes ainsi que des résumés des publications RTO et AGARD figurent dans les journaux suivants :

Scientific and Technical Aerospace Reports (STAR)

STAR peut être consulté en ligne au localisateur de ressources
uniformes (URL) suivant: <http://www.sti.nasa.gov/Pubs/star/Star.html>
STAR est édité par CASI dans le cadre du programme
NASA d'information scientifique et technique (STI)
STI Program Office, MS 157A
NASA Langley Research Center
Hampton, Virginia 23681-0001
ETATS-UNIS

Government Reports Announcements & Index (GRA&I)

publié par le National Technical Information Service
Springfield
Virginia 2216
ETATS-UNIS
(accessible également en mode interactif dans la base de
données bibliographiques en ligne du NTIS, et sur CD-ROM)



BP 25

F-92201 NEUILLY-SUR-SEINE CEDEX • FRANCE
Télécopie 0(1)55.61.22.99 • E-mail mailbox@rta.nato.int



DISTRIBUTION OF UNCLASSIFIED RTO PUBLICATIONS

AGARD & RTO publications are sometimes available from the National Distribution Centres listed below. If you wish to receive all RTO reports, or just those relating to one or more specific RTO Panels, they may be willing to include you (or your Organisation) in their distribution.

RTO and AGARD reports may also be purchased from the Sales Agencies listed below.

Requests for RTO or AGARD documents should include the word 'RTO' or 'AGARD', as appropriate, followed by the serial number. Collateral information such as title and publication date is desirable.

If you wish to receive electronic notification of RTO reports as they are published, please visit our website (www.rto.nato.int) from where you can register for this service.

NATIONAL DISTRIBUTION CENTRES

BELGIUM

Royal High Institute for Defence – KHID/IRSD/RHID
Management of Scientific & Technological Research
for Defence, National RTO Coordinator
Royal Military Academy – Campus Renaissance
Renaissancelaan 30
1000 Brussels

CANADA

DRDKIM2 – Knowledge Resources Librarian
Defence R&D Canada
Department of National Defence
305 Rideau Street, 9th Floor
Ottawa, Ontario K1A 0K2

CZECH REPUBLIC

LOM PRAHA s. p.
o. z. VTÚLaPVO
Mladoboleslavská 944
PO Box 18
197 21 Praha 9

DENMARK

Danish Acquisition and Logistics Organization (DALO)
Lautrupbjerg 1-5
2750 Ballerup

FRANCE

O.N.E.R.A. (ISP)
29, Avenue de la Division Leclerc
BP 72, 92322 Châtillon Cedex

GERMANY

Streitkräfteamt / Abteilung III
Fachinformationszentrum der Bundeswehr (FIZBw)
Gorch-Fock-Straße 7
D-53229 Bonn

GREECE (Point of Contact)

Defence Industry & Research General Directorate
Research Directorate, Fakinos Base Camp
S.T.G. 1020
Holargos, Athens

HUNGARY

Hungarian Ministry of Defence
Development and Logistics Agency
P.O.B. 25
H-1885 Budapest

ITALY

General Secretariat of Defence and
National Armaments Directorate
5th Department – Technological
Research
Via XX Settembre 123
00187 Roma

LUXEMBOURG

See Belgium

NETHERLANDS

Royal Netherlands Military
Academy Library
P.O. Box 90.002
4800 PA Breda

NORWAY

Norwegian Defence Research
Establishment
Attn: Biblioteket
P.O. Box 25
NO-2007 Kjeller

POLAND

Centralna Biblioteka Wojskowa
ul. Ostrobramska 109
04-041 Warszawa

PORTUGAL

Estado Maior da Força Aérea
SDFA – Centro de Documentação
Alfragide
P-2720 Amadora

ROMANIA

Romanian National Distribution
Centre
Armaments Department
9-11, Drumul Taberei Street
Sector 6, 061353, Bucharest

SLOVAKIA

Akadémia ozbrojených síl gen.
M.R. Štefánika, Distribučné a
informačné stredisko RTO
Demänová 393, Liptovský Mikuláš 6
031 06

SLOVENIA

Ministry of Defence
Central Registry for EU & NATO
Vojkova 55
1000 Ljubljana

SPAIN

SDG TECEN / DGAM
C/ Arturo Soria 289
Madrid 28033

TURKEY

Milli Savunma Bakanlığı (MSB)
ARGE ve Teknoloji Dairesi
Başkanlığı
06650 Bakanlıklar – Ankara

UNITED KINGDOM

Dstl Knowledge and Information
Services
Building 247
Porton Down
Salisbury SP4 0JQ

UNITED STATES

NASA Center for AeroSpace
Information (CASI)
7115 Standard Drive
Hanover, MD 21076-1320

SALES AGENCIES

NASA Center for AeroSpace Information (CASI)

7115 Standard Drive
Hanover, MD 21076-1320
UNITED STATES

The British Library Document Supply Centre

Boston Spa, Wetherby
West Yorkshire LS23 7BQ
UNITED KINGDOM

Canada Institute for Scientific and Technical Information (CISTI)

National Research Council Acquisitions
Montreal Road, Building M-55
Ottawa K1A 0S2, CANADA

Requests for RTO or AGARD documents should include the word 'RTO' or 'AGARD', as appropriate, followed by the serial number (for example AGARD-AG-315). Collateral information such as title and publication date is desirable. Full bibliographical references and abstracts of RTO and AGARD publications are given in the following journals:

Scientific and Technical Aerospace Reports (STAR)

STAR is available on-line at the following uniform resource
locator: <http://www.sti.nasa.gov/Pubs/star/Star.html>
STAR is published by CASI for the NASA Scientific
and Technical Information (STI) Program
STI Program Office, MS 157A
NASA Langley Research Center
Hampton, Virginia 23681-0001
UNITED STATES

Government Reports Announcements & Index (GRA&I)

published by the National Technical Information Service
Springfield
Virginia 2216
UNITED STATES
(also available online in the NTIS Bibliographic Database
or on CD-ROM)